

Plant and fungal extracts and metabolites in neurotherapy: exploring their pharmacology and potential clinical uses

Edited by

Jian Hao, Igor Lavrov and Xianhu Zhou

Published in

Frontiers in Pharmacology

Frontiers in Neuroscience



FRONTIERS EBOOK COPYRIGHT STATEMENT

The copyright in the text of individual articles in this ebook is the property of their respective authors or their respective institutions or funders. The copyright in graphics and images within each article may be subject to copyright of other parties. In both cases this is subject to a license granted to Frontiers.

The compilation of articles constituting this ebook is the property of Frontiers.

Each article within this ebook, and the ebook itself, are published under the most recent version of the Creative Commons CC-BY licence. The version current at the date of publication of this ebook is CC-BY 4.0. If the CC-BY licence is updated, the licence granted by Frontiers is automatically updated to the new version.

When exercising any right under the CC-BY licence, Frontiers must be attributed as the original publisher of the article or ebook, as applicable.

Authors have the responsibility of ensuring that any graphics or other materials which are the property of others may be included in the CC-BY licence, but this should be checked before relying on the CC-BY licence to reproduce those materials. Any copyright notices relating to those materials must be complied with.

Copyright and source acknowledgement notices may not be removed and must be displayed in any copy, derivative work or partial copy which includes the elements in question.

All copyright, and all rights therein, are protected by national and international copyright laws. The above represents a summary only. For further information please read Frontiers' Conditions for Website Use and Copyright Statement, and the applicable CC-BY licence.

ISSN 1664-8714
ISBN 978-2-8325-6387-8
DOI 10.3389/978-2-8325-6387-8

About Frontiers

Frontiers is more than just an open access publisher of scholarly articles: it is a pioneering approach to the world of academia, radically improving the way scholarly research is managed. The grand vision of Frontiers is a world where all people have an equal opportunity to seek, share and generate knowledge. Frontiers provides immediate and permanent online open access to all its publications, but this alone is not enough to realize our grand goals.

Frontiers journal series

The Frontiers journal series is a multi-tier and interdisciplinary set of open-access, online journals, promising a paradigm shift from the current review, selection and dissemination processes in academic publishing. All Frontiers journals are driven by researchers for researchers; therefore, they constitute a service to the scholarly community. At the same time, the *Frontiers journal series* operates on a revolutionary invention, the tiered publishing system, initially addressing specific communities of scholars, and gradually climbing up to broader public understanding, thus serving the interests of the lay society, too.

Dedication to quality

Each Frontiers article is a landmark of the highest quality, thanks to genuinely collaborative interactions between authors and review editors, who include some of the world's best academicians. Research must be certified by peers before entering a stream of knowledge that may eventually reach the public - and shape society; therefore, Frontiers only applies the most rigorous and unbiased reviews. Frontiers revolutionizes research publishing by freely delivering the most outstanding research, evaluated with no bias from both the academic and social point of view. By applying the most advanced information technologies, Frontiers is catapulting scholarly publishing into a new generation.

What are Frontiers Research Topics?

Frontiers Research Topics are very popular trademarks of the *Frontiers journals series*: they are collections of at least ten articles, all centered on a particular subject. With their unique mix of varied contributions from Original Research to Review Articles, Frontiers Research Topics unify the most influential researchers, the latest key findings and historical advances in a hot research area.

Find out more on how to host your own Frontiers Research Topic or contribute to one as an author by contacting the Frontiers editorial office: frontiersin.org/about/contact

Plant and fungal extracts and metabolites in neurotherapy: exploring their pharmacology and potential clinical uses

Topic editors

Jian Hao — The Second Affiliated Hospital of Guangzhou Medical University, China

Igor Lavrov — Mayo Clinic, United States

Xianhu Zhou — The Second Affiliated Hospital of Guangzhou Medical University, China

Citation

Hao, J., Lavrov, I., Zhou, X., eds. (2025). *Plant and fungal extracts and metabolites in neurotherapy: exploring their pharmacology and potential clinical uses*.

Lausanne: Frontiers Media SA. doi: 10.3389/978-2-8325-6387-8

Table of contents

- 05 Editorial: Plant and fungal extracts and metabolites in neurotherapy: exploring their pharmacology and potential clinical uses
Jian Hao, Igor Lavrov and Xianhu Zhou
- 08 Topical application of daphnetin hydrogel for traumatic brain injury
Yuanhao Ma, Yu Liu, Jianqiang Guo, Zhongjun Chen, Zongren Zhao and Jinyu Zheng
- 21 Plant medicine metabolite Yulinzhu treating neurological disorder causing polycystic ovary syndrome: a systematic review and a meta-analysis
Beibei Jiao, Ruilin Chen, Si Chen, Jian Zhang, Peijuan Wang, Huaijun Zhou and Weibo Zhao
- 35 Isoliquiritigenin ameliorates abnormal oligodendrocyte development and behavior disorders induced by white matter injury
Dong Wu, Wenjuan Zhou, Jingyi Du, Tiantian Zhao, Naigang Li, Fan Peng, Anna Li, Xinyue Zhang, Meihua Zhang and Aijun Hao
- 52 Oleuropein enhances proteasomal activity and reduces mutant huntingtin-induced cytotoxicity
Zih-Ning Huang, Sin-Yi Lee, Jie-Mao Chen, Zih-Ting Huang and Lu-Shiun Her
- 69 Eucalyptus essential oil exerted a sedative-hypnotic effect by influencing brain neurotransmitters and gut microbes via the gut microbiota-brain axis
Xuejiao Li, Yuanyi Zhang, Qian Zhang, Aizhi Cao and Jie Feng
- 82 Meta-analysis of the effect of *sophora flavescens* on tumor metastasis-induced bone neuropathic pain
Cheng Chang, Di Sun, Zhilei Zhang, Lei He, Qiang Wang, Yingchao Shen, Hengzhou Zhu and Donghua Fan
- 95 Anti-neuropathic effects of astaxanthin in a rat model of chronic constriction injury: passing through opioid/benzodiazepine receptors and relevance to its antioxidant and anti-inflammatory effects
Boshra Hashemi, Sajad Fakhri, Amir Kiani, Fatemeh Abbaszadeh, Shahram Miraghaee, Mohammad Mohammadi and Javier Echeverría
- 110 Neuroprotective effects of ethanol extraction from *Rubia yunnanensis* Diels on chronic cerebral hypoperfusion: modulation of the System Xc-/GSH/GPX4 axis to alleviate oxidative stress and ferroptosis
Jianghao Cheng, Xiaoxia Ma, Jie Tao, Xiaoli Jiang, Pu Chen and Xiaohua Duan

- 132 **Exploring the potential anti-senescence effects of soybean-derived peptide Soymetide in mice hippocampal neurons via the Wnt/ β -catenin pathway**
Asmita Garg, Jyotshana Saroj, Saurabh Tiwari, Uttara Das, Neetu Shukla, Jimut Kanti Ghosh and Sanghamitra Bandyopadhyay
- 148 **Zingerone alleviates inflammatory pain by reducing the intrinsic excitability of anterior cingulate cortex neurons in a mice model**
Yuanyuan Wang, Lang Dong, Shu Han, Yuehan You, Mingrui Zhang, Bingjing Sun, Hong Ni, Rongjing Ge, Jianhong Liu and Jiandong Yu
- 160 **Pelargonidin improves functional recovery and attenuates neuropathic pain following spinal cord injury in rats: relevance to its neuroprotective, antioxidant, and anti-inflammatory effects**
Leila Kooshki, Sajad Fakhri, Fatemeh Abbaszadeh, Amir Kiani, Mohammad Hosein Farzaei, Ehsan Mohammadi-Noori and Javier Echeverria



OPEN ACCESS

EDITED AND REVIEWED BY
Michael Heinrich,
University College London, United Kingdom

*CORRESPONDENCE
Jian Hao,
✉ haojian@gzhmu.edu.cn

RECEIVED 30 March 2025
ACCEPTED 07 April 2025
PUBLISHED 06 May 2025

CITATION
Hao J, Lavrov I and Zhou X (2025) Editorial: Plant and fungal extracts and metabolites in neurotherapy: exploring their pharmacology and potential clinical uses.
Front. Pharmacol. 16:1602574.
doi: 10.3389/fphar.2025.1602574

COPYRIGHT
© 2025 Hao, Lavrov and Zhou. This is an open-access article distributed under the terms of the [Creative Commons Attribution License \(CC BY\)](https://creativecommons.org/licenses/by/4.0/). The use, distribution or reproduction in other forums is permitted, provided the original author(s) and the copyright owner(s) are credited and that the original publication in this journal is cited, in accordance with accepted academic practice. No use, distribution or reproduction is permitted which does not comply with these terms.

Editorial: Plant and fungal extracts and metabolites in neurotherapy: exploring their pharmacology and potential clinical uses

Jian Hao^{1*}, Igor Lavrov^{2,3} and Xianhu Zhou¹

¹Orthopedics Department, The Second Affiliated Hospital, Guangzhou Medical University, Guangzhou, China, ²Department of Neurology, Mayo Clinic, Rochester, MN, United States, ³Department of Physiology and Biomedical Engineering, Mayo Clinic, Rochester, MN, United States

KEYWORDS

central nervous system disorders, phytochemicals, neuroprotection, ethnopharmacology, traditional medicine

Editorial on the Research Topic

[Plant and fungal extracts and metabolites in neurotherapy: exploring their pharmacology and potential clinical uses](#)

Central nervous system (CNS) disorders—including Alzheimer's disease, Parkinson's disease, spinal cord injury (SCI), stroke, and traumatic brain injury (TBI)—continue to impose profound clinical and societal burdens (Tsai et al., 2024). Despite decades of research and significant advancements in neuroscience, most therapeutic interventions remain largely palliative, addressing symptoms rather than altering the underlying course of disease progression (Gao et al., 2020). The multifactorial and heterogeneous nature of CNS pathologies presents considerable challenges to developing effective disease-modifying therapies.

This therapeutic gap has catalyzed growing scientific interest in naturally derived bioactive metabolites, particularly phytochemicals and fungal metabolites. Long valued in traditional medical systems across diverse cultures, these metabolites are now being systematically explored for their neuroprotective, anti-inflammatory, antioxidant, and neuromodulatory properties (Koshak et al., 2017; Khazdair et al., 2019). Their multi-target pharmacological profiles, combined with favorable safety, make them compelling candidates for CNS drug discovery and development. This Research Topic features a curated Research Topic of studies that rigorously examine the therapeutic potential of plant- and fungus-derived metabolites across a range of CNS disease models, integrating ethnopharmacological knowledge with contemporary neuropharmacological approaches and methodologies.

Several studies featured in this Research Topic focus on cognitive impairment and proteinopathies within neurodegenerative contexts. Chang et al. evaluated an ethanol extract of *Rubia yunnanensis* Diels (Rubiaceae) in a rat model of chronic cerebral hypoperfusion. Their findings revealed activation of the System Xc-/GSH/GPX4 antioxidant pathway and inhibition of ferroptosis, resulting in improved cognitive outcomes (Chang et al.). Similarly, Huang et al. demonstrated that *Olea europaea* L. (Oleaceae), a polyphenol metabolite extracted from olives, enhanced the proteasomal degradation of mutant huntingtin protein aggregates in Huntington's

disease cell models, independent of autophagy pathways (Huang et al.). These studies underscore the potential of phytochemicals to modulate oxidative stress and proteostasis—key processes implicated in the pathogenesis of neurodegenerative diseases.

CNS trauma, including SCI and TBI, represents another major focus within this Research Topic. Kooshki et al. reported that *Pelargonium × hortorum* L.H.Bailey (Geraniaceae), an anthocyanin metabolite, significantly improved motor function and alleviated neuropathic pain in a rat model of SCI, primarily through antioxidant and anti-inflammatory mechanisms (Kooshki et al.). In a parallel study, Ma et al. developed a hydrogel-based drug delivery system for *Daphne odora* Thunb. (Thymelaeaceae), a coumarin metabolite with neuroprotective activity. In a murine TBI model, this system enhanced *D. odora* Thunb. (Thymelaeaceae) bioavailability, leading to improved spatial memory and reduced neuroinflammation (Ma et al.). These studies highlight the value of innovative formulation strategies in optimizing the efficacy of natural metabolites for acute CNS injuries.

Additional insights into SCI therapeutics are provided by Hao et al. (2019) who investigated the neuroprotective effects of rhein lysinate (RHL) (Hao et al., 2019). In SCI rats, RHL administration significantly improved motor function, increased the activity of endogenous antioxidant enzymes (SOD and GSH-Px), and reduced lipid peroxidation, as indicated by lower MDA levels. Mechanistically, RHL inhibited activation of the p38 MAPK signaling pathway, thereby attenuating neuronal apoptosis. These findings suggest that RHL promotes neuroprotection through the modulation of oxidative stress and apoptotic pathways.

In a subsequent study, the same group demonstrated that *Syringa vulgaris* L. (Oleaceae), a lignan metabolite, facilitates functional recovery following SCI by activating the UBE4B/AKT signaling pathway. In glutamate-induced neurotoxicity models using SH-SY5Y cells, *S. vulgaris* L. (Oleaceae) upregulated UBE4B expression and enhanced AKT phosphorylation, resulting in reduced neuronal apoptosis. The protective effects were abolished by either UBE4B knockdown or AKT inhibition, confirming the critical role of this signaling axis (Hao et al., 2024). These findings reinforce the therapeutic relevance of the UBE4B/AKT pathway and underscore the broader potential of lignan metabolites in CNS repair and regeneration.

Pain management, particularly for chronic and neuropathic pain, is another area where phytotherapeutics offer considerable promise. Wang et al. showed that *Zingiber officinale* Roscoe (Zingiberaceae), a bioactive metabolite derived from Zingiber officinale (ginger), mitigated inflammatory pain by suppressing neuronal excitability in the anterior cingulate cortex, suggesting a central mechanism of analgesia (Wang et al.). Complementarily, Hashemi et al. reported that *Haematococcus pluvialis* Flotow (Haematococcaceae), a marine carotenoid metabolite, alleviated neuropathic pain in a chronic constriction injury model. Its mechanism of action involved both oxidative stress reduction and modulation of opioid and benzodiazepine receptor pathways, reflecting its multi-target pharmacological properties (Hashemi et al.).

Age-related cognitive decline and neuronal senescence were explored by Garg et al., who investigated *Glycine max* (L.) Merr.

(Fabaceae), a soybean-derived oligopeptide. In a doxorubicin-induced hippocampal aging model, *Glycine max* (L.) Merr. (Fabaceae) activated the Wnt/ β -catenin signaling pathway, suppressed senescence markers such as p16INK4a and p21, and improved memory performance (Garg et al.). Similarly, Wu et al. assessed the effects of *Glycyrrhiza uralensis* Fisch. ex DC. (Fabaceae) in a neonatal white matter injury model. The metabolite promoted oligodendrocyte maturation and reduced microglial activation through inhibition of histone deacetylase 3 (HDAC3), suggesting that phytochemicals may exert neuroprotective effects via epigenetic modulation (Wu et al.).

Sleep and mood disturbances, commonly observed in neurodegenerative and psychiatric disorders, were addressed by Li et al. using *Eucalyptus globulus* Labill. (Myrtaceae) (EEO) (Li et al.). Their study demonstrated that EEO increased the levels of inhibitory neurotransmitters, including GABA and glycine, and modulated the composition of gut microbiota. These findings support the hypothesis that EEO exerts its sedative-hypnotic effects through gut–brain axis interactions, offering a novel mechanistic perspective on plant-based interventions for sleep disorders.

Clinical evaluations of traditional botanical drug formulations were also featured. Chang et al. conducted a meta-analysis on the use of *Sophora flavescens* Aiton (Fabaceae) in patients experiencing bone neuropathic pain secondary to tumor metastasis. The analysis revealed significant reductions in pain severity and improvements in functional outcomes, validating its therapeutic potential in oncology-related pain management (Chang et al.). Jiao et al. investigated the Yulinzhu botanical drug formula in women with polycystic ovary syndrome (PCOS), a condition involving neuroendocrine dysregulation (Jiao et al.). Their findings demonstrated improvements in ovulation rates and hormonal profiles, indicating potential modulation of the hypothalamic–pituitary–gonadal axis. These results emphasize the systemic therapeutic potential of CNS-targeted phytomedicine in broader physiological contexts.

Collectively, the contributions in this volume offer a comprehensive overview of recent progress in plant- and fungus-derived metabolites for CNS disorders. These studies address a wide spectrum of conditions—from neurodegeneration and trauma to chronic pain, neurodevelopmental injury, and neuroendocrine dysfunction—highlighting the ability of natural metabolites to influence key pathological processes such as oxidative stress, inflammation, apoptosis, proteostasis imbalance, and epigenetic dysregulation.

Critically, while the studies in this volume have advanced our understanding of the therapeutic potential of plant- and fungus-derived metabolites, several limitations remain. Many investigations rely on preclinical models that do not fully capture the complexity of human CNS disorders, and standardized methodologies for the development of botanical drugs are still lacking. Moreover, the pharmacokinetic profiles and long-term safety of several metabolites have not been comprehensively evaluated.

Future research should therefore prioritize the design and execution of robust clinical trials to validate these preclinical findings. Additionally, more in-depth mechanistic studies are

needed to elucidate the molecular targets of these metabolites, and efforts should be made to optimize extraction, purification, and standardization protocols for botanical drugs. Interdisciplinary approaches that integrate ethnopharmacology, neurobiology, and advanced drug delivery systems will be crucial to translating these promising findings into effective therapeutic interventions. Such research topics will not only help bridge the gap between preclinical promise and clinical application but will also set the scene for further developments in CNS pharmacotherapy.

Author contributions

JH: Writing – original draft, Writing – review and editing, Conceptualization. IL: Formal Analysis, Writing – review and editing. XZ: Writing – review and editing.

Funding

The author(s) declare that no financial support was received for the research and/or publication of this article.

References

- Gao, W., Wilson, R., Hepgul, N., Yi, D., Evans, C., Bajwah, S., et al. (2020). Effect of short-term integrated palliative care on patient-reported outcomes among patients severely affected with long-term neurological conditions: a randomized clinical trial. *JAMA Netw. Open* 3, e2015061–e2015061.
- Hao, J., Li, Z., Xie, L., Yu, B., Ma, B., Yang, Y., et al. (2024). Syringaresinol promotes the recovery of spinal cord injury by inhibiting neuron apoptosis via activating the ubiquitination factor E4B/AKT Serine/Threonine kinase signal pathway. *Brain Research* 1824, 148684. doi:10.1016/j.brainres.2023.148684
- Hao, J., Wang, P., Pei, D., Jia, B., and Hu, Q. (2019). Rhein lysinate improves motor function in rats with spinal cord injury via inhibiting p38 MAPK pathway. *Kaohsiung J. Med. Sci.* 35, 765–771. doi:10.1002/kjm2.12123
- Khazdair, M. R., Anaeigoudari, A., Hashemzahi, M., and Mohebbati, R. (2019). Neuroprotective potency of some spice herbs, a literature review. *J. tradit. complement. med.* 9, 98–105.
- Koshak, A., Wei, L., Koshak, E., Wali, S., Alamoudi, O., Demerdash, A., et al. (2017). Nigella sativa Supplementation Improves Asthma Control and Biomarkers: A Randomized, Double-Blind, Placebo-Controlled Trial. *Phytother. Res.* 31, 403–409. doi:10.1002/ptr.5761
- Tsai, M.-H., Wu, C.-Y., Wu, C.-H., and Chen, C.-Y. (2024). The current update of conventional and innovative treatment strategies for Central Nervous System Injury. *Biomedicines* 12, 1894.

Conflict of interest

The authors declare that the research was conducted in the absence of any commercial or financial relationships that could be construed as a potential conflict of interest.

Generative AI statement

The author(s) declare that Generative AI was used in the creation of this manuscript. Language editing, grammar correction, and typo detection were performed using the GPT-4o version of ChatGPT during the manuscript preparation process.

Publisher's note

All claims expressed in this article are solely those of the authors and do not necessarily represent those of their affiliated organizations, or those of the publisher, the editors and the reviewers. Any product that may be evaluated in this article, or claim that may be made by its manufacturer, is not guaranteed or endorsed by the publisher.



OPEN ACCESS

EDITED BY

Ping Zheng,
The University of Melbourne, Australia

REVIEWED BY

Zheng Yuan,
China Academy of Chinese Medical Sciences,
China

Hanxiao Sun,
University of Texas Health Science Center at
Houston, United States

Weini Li,
Cedars Sinai Medical Center, United States

*CORRESPONDENCE

Zongren Zhao

✉ zhaozongrenking@163.com

Jinyu Zheng

✉ guanr80@163.com

[†]These authors have contributed equally to
this work

RECEIVED 16 June 2024

ACCEPTED 29 July 2024

PUBLISHED 07 August 2024

CITATION

Ma Y, Liu Y, Guo J, Chen Z, Zhao Z and
Zheng J (2024) Topical application of
daphnetin hydrogel for traumatic brain injury.
Front. Neurosci. 18:1450072.
doi: 10.3389/fnins.2024.1450072

COPYRIGHT

© 2024 Ma, Liu, Guo, Chen, Zhao and Zheng.
This is an open-access article distributed
under the terms of the [Creative Commons
Attribution License \(CC BY\)](#). The use,
distribution or reproduction in other forums is
permitted, provided the original author(s) and
the copyright owner(s) are credited and that
the original publication in this journal is cited,
in accordance with accepted academic
practice. No use, distribution or reproduction
is permitted which does not comply with
these terms.

Topical application of daphnetin hydrogel for traumatic brain injury

Yuanhao Ma^{1,2,3†}, Yu Liu^{1,3†}, Jianqiang Guo^{1,3†}, Zhongjun Chen¹,
Zongren Zhao^{1*} and Jinyu Zheng^{1*}

¹Department of Neurosurgery, Affiliated Huaian Hospital of Xuzhou Medical University, Huaian, China,

²Department of Neurosurgery, Huzhou Central Hospital, Huzhou, China, ³Xuzhou Medical University, Xuzhou, China

Background: Traumatic brain injury (TBI) causes neuronal cell damage and dysfunction. According to previous studies, daphnetin (Dap) has a protective effect in neurological injury. However, the *in vivo* bioavailability of daphnetin is not high. The purpose of this study was to determine whether administering daphnetin directly into the site of injury via a hydrogel drug carrier could improve its therapeutic impact.

Methods: Tripalmitolein monostearates / daphnetin (TM/Dap) hydrogels were prepared and characterised using water bath heating, scanning electron microscopy (SEM) and small animal *in vivo* imaging techniques. The TBI model was established using the Feeney free fall impact method. Using the Morris water maze test, the mNSS neurological deficit rating scale, haematoxylin-eosin staining, and liver and kidney function tests, the therapeutic benefit of TM/Dap and its toxic side effects were assessed. The therapeutic effects of TM/Dap were further investigated using wet and dry gravimetric methods, Evans blue staining, protein immunoblotting, immunofluorescence staining techniques and ELISA.

Results: The efficacy of the TM/Dap hydrogel in gradually releasing daphnetin in the context of traumatic brain damage was shown by both *in vitro* and *in vivo* tests. Behavioral experiments showed that the learning and spatial memory abilities of TM/Dap hydrogel treated mice were significantly improved in the water maze experiment. And TM/Dap hydrogel has high biosafety for organisms. The results of the therapeutic mechanism of action showed that TM/Dap hydrogel showed more significant efficacy in reducing the neuroinflammatory response caused by TNF- α , IL-6 and other factors, as well as promoting the recovery of post-traumatic neurological function.

Conclusion: The use of hydrogel as a drug carrier for daphnetin showed more significant efficacy in reducing neuroinflammatory response, protecting nerve tissue and promoting post-traumatic neurological recovery compared with traditional drug delivery methods.

KEYWORDS

daphnetin, hydrogel, traumatic brain injury, drug carrier, bioavailability

1 Introduction

Globally, traumatic brain injury (TBI) is one of the main causes of mortality and disability (Yuan et al., 2020; Jha and Ghewade, 2022). It is commonly caused by falls, traffic accidents, and slips or falls. In addition, TBI is also observed in explosions or industrial accidents, both of which stem from trauma caused by direct or indirect violence to the head. A large number of patients with craniocerebral trauma still die from injuries secondary to TBI, and the lethality of TBI is also high (Cheng et al., 2020; Piatt, 2020). Secondary injuries arise subsequent to primary injuries and exert a noteworthy influence on the patient's deteriorating condition. Mechanisms of injury comprise disruptions of the blood–brain barrier, cerebral metabolic disturbances, aberrant energy metabolism, cerebral oedema, and excitotoxicity, all of which are changes linked to an inflammatory response (Yuan et al., 2020; Jin et al., 2023; Liu et al., 2023). Recent studies have indicated that stem cell transplantation, bioscaffolds, and exosomes demonstrate efficacy in the treatment of cranial trauma (Zhang et al., 2017; Hade et al., 2021). However, the efficient transportation of stem cells to regions of traumatic brain injury, as well as the adverse impacts of scaffold-based therapy, continue to pose technical difficulties. There aren't any therapies available right now that can stop the original harm from spreading later on. Consequently, there is an urgent need to develop new and effective treatment approaches for traumatic brain injury.

When a traumatic brain injury occurs, a series of immune responses are initiated by the body in an attempt to repair the damaged tissue and safeguard the brain against further harm. This response involves multiple cell types, signaling molecules and biological processes. First, astrocytes and microglia around the brain injury are activated to respond (Liu et al., 2020; Matejuk and Ransohoff, 2020). These cells maintain the stability of the brain environment and remove harmful substances. Second, after injury, cells release a variety of inflammatory cytokines (TNF- α , IL-1 β , IL-6, etc.) as well as chemokines (CXCL1) (Mishra et al., 2021), which perform a crucial function in the inflammatory response, but excessive release can lead to aggravation of the injury. The inflammatory response also increases vascular permeability (Hazy et al., 2020), allowing blood and fluid to leak into the tissues, potentially causing oedema. In addition, during the inflammatory response, leukocytes and macrophages gather at the site of injury to help remove dead cells and tissue debris. Although the inflammatory response after TBI contributes to some tissue repair, an excessive inflammatory response can lead to neuronal cell damage, disruption of the blood–brain barrier, oedema and further cell death (Schimmel et al., 2017). Therefore, controlling the inflammatory response in patients with TBI is critical.

The active component, daphnetin (Dap), is taken from the Daphne Korean Nakai plant, which belongs to the Daphne genus. It is a subject-specific compound that has been extracted from this particular plant. The first new drug in China, its chemical name is 7,8-dihydroxycoumarin, which is mainly found in plants of the daphnetin family. Numerous biological activities are displayed by daphnetin, such as anti-inflammatory, antitumor, antibacterial, antiviral, anticoagulant, and immunomodulatory properties (Albiero et al., 2020; Garg et al., 2020; Bhattarai et al., 2021; Han and Hyun, 2023). Daphnetin has shown multiple effects in neurological injury, including amelioration of blood–brain barrier disruption, attenuation of cerebral oedema and enhancement of anti-inflammatory effects

(Wang et al., 2020; Singh et al., 2021). Despite its good therapeutic effects in neurological injuries, daphnetin is metabolized too quickly in the body, so its bioavailability in the organism is not high. This may be due to its lower solubility, intestinal absorption efficiency, etc. (Fang et al., 2021; Hussain et al., 2022; Javed et al., 2022). To overcome these limitations and improve therapeutic efficacy, the selection of an appropriate drug delivery system to encapsulate daphnetin is critical.

In recent years, hydrogel research and application has increased. Hydrogel materials are able to fill the lesion area and mimic the porous three-dimensional structure of the natural extracellular matrix and nutrients that allow cell proliferation, and hydrogels are also highly biocompatible (Lantigua et al., 2020; Qu et al., 2021; do et al., 2022). The physical properties of hydrogels make them ideal for drug delivery, allowing for sustained release of the encapsulated drug (Ilochonwu et al., 2020; Zhang et al., 2020; Zou et al., 2020; Hu et al., 2021). The hydrogel can maintain a high local drug concentration over an extended period of time through an appropriate release mechanism. The blood–brain barrier (BBB) is an important biological barrier located between the cerebral vascular system and the brain tissue that limits the entry of harmful substances into the brain tissue while preventing the free passage of most drugs through the vessel walls into the brain tissue. After TBI, *in situ* injection of the encapsulated drug through a hydrogel at the site of injury can significantly improve drug utilization.

Triglycerol monostearate (TM), also known as glycerol monostearate, is an FDA-approved hydrogel agent that encapsulates hydrophobic molecules through van der Waals forces to form hydrogels (García et al., 2018). Even low levels of traumatic brain injury can activate matrix metalloproteinases (MMPs) (Lima et al., 2020; Qian et al., 2021). In contrast, TM has an ester bond that is enzymatically unstable and can be cleaved in an inflammatory environment containing matrix metalloproteinases (MMPs) (Bassiouni et al., 2021). Therefore, the selection of TM hydrogel as a drug carrier for the treatment of TBI will greatly enhance the therapeutic effect of drugs.

This study employed TM hydrogel encapsulated with daphnetin to treat traumatic brain injury in TBI-injured mice by injecting TM/Dap hydrogel into their mouth. The objectives of injecting TM/Dap hydrogel directly into the mouth of a TBI injury are as follows. (1) To improve drug accumulation and get over the restrictions of the blood–brain barrier, the TM/Dap hydrogel can be injected straight into the trabecular area of traumatic brain injury. (2) After traumatic brain injury, the TM/Dap hydrogel allows continuous delivery of Dap in a matrix metalloproteinase environment. (3) The released Dap will continue to exert its therapeutic effects. In a word, this study aims to propose a new mode of administration to enhance the therapeutic efficacy of daphnetin.

2 Materials and methods

2.1 Construction and physicochemical properties of hydrogel

2.1.1 Preparation of TM/Dap hydrogel

100 mg of TM was added to a glass vial containing a mixture of 800 μ L deionised water and 200 μ L DMSO, the cap was closed and 45 mg of Dap was added. Place the vial in a water bath at 65°C until

dissolution is complete and the mixture is homogeneous. The vials are removed and placed on a table at room temperature and allowed to cool naturally, the mixture will gradually turn into a thick gel.

2.1.2 Micromorphology of TM/Dap hydrogel

Hydrogel micromorphology was characterized by high resolution scanning electron microscope (HR-SEM) (Zeiss Merlin High resolution SEM) with the following procedures. Samples were quickly frozen in liquid nitrogen at -210°C after being deposited in the sample stage's wells. To sublime the samples for 3 min, the temperature of the sample preparation chamber was progressively raised from -140°C to 90°C . Next, the sample's surface was treated with the spray coating process for 50 s. Finally, a scanning electron microscope was used to photograph and record the materials.

2.1.3 *In vitro* drug-release of TM/Dap hydrogel

Cerebrospinal fluid (CSF) samples were collected by lumbar puncture after TBI at Huai'an Hospital of Xuzhou Medical University with the approval of the Ethics Committee of Huai'an Hospital of Xuzhou Medical University (Ethics No. HEYLL202118) and the informed consent of the patients' families. To assess the sustained release of Dap from TM/Dap hydrogels, TM/Dap hydrogel samples (200 μL) were placed in 15 mL centrifuge tubes and suspended in 10 mL of phosphate buffer solution (PBS). To these samples, PBS (10 mL, control), CSF (10 mL, control), matrix metalloproteinase-2 (MMP-2) (100 ng mL^{-1} , 10 mL), MMP-2 (100 ng mL^{-1} , 10 mL) + inhibitor (1 $\mu\text{mol L}^{-1}$, 10 mL), CSF (10 mL + MMP-2) (100 ng mL^{-1} , 10 mL) + inhibitor (1 $\mu\text{mol L}^{-1}$, 10 mL). What we used the inhibitor we used was CP-471471 (Sigma), which is a broad-spectrum inhibitor of MMPs. The tubes were closed and incubated at 37°C with a shaking speed of 150 rpm. At each time point, an aliquot (100 μL) was taken from the was taken from the PBS reservoir, the solid was dissolved in 200 μL DMSO and the concentration of Dap was determined by spectrophotometric analysis.

2.1.4 Experimental animals and grouping

All animal experiments were conducted in accordance with the Xuzhou Medical University Policy on Animal Welfare and were approved by the Xuzhou Medical University. Healthy male ICR mice weighing 15–20 g and 6–8 weeks old were acquired for this investigation from the Experimental Animal Centre of Xuzhou Medical University. To stop them from fighting, they were housed separately in separate cages. In order to mimic natural light, mice were placed in an environment with a temperature of $24 \pm 2^{\circ}\text{C}$. Five groups of mice were randomly assigned: the sham group, the TBI group, the TM group, the ip Dap group and the TM/Dap group.

The sham group only removed the scalp, did not open the bone window and did not deliver a traumatic blow. The TBI group served as a blank control group, receiving only trauma blow modelling. The TM group was the group treated with blank hydrogel. The ip Dap group was a comparison group for TM/Dap by intraperitoneal injection of daphnetin. The TM/Dap group is the treatment group containing hydrogel-coated Dap.

2.1.5 TBI animal models

The article describes the establishment of weight drop injury (WDI) using a modified version of Feeney's weight-drop method, as previously reported (Feeney et al., 1981; Marmarou et al., 1994). The steps are as follows: (1) Inhalation anaesthesia was given to the mice

by adding isoflurane to a small animal gas anaesthesia machine. (2) The anaesthetized mice were fixed to the stereotaxic apparatus and the wounds sterilized with iodine. (3) The scalp was incised along the midline of the mouse's head for about 1.5 cm to expose the skull. (4) The skull was windowed using a small animal skull brick of approximately (5 mm) diameter to expose the parietal lobe, taking care to protect the dura mater during surgery. (5) The impact parameters were set to simulate a moderate TBI (hammer mass 40 g, drop 7.5 cm, impact depth 1.5 mm). (6) At the end of the procedure, the wound was carefully cleaned and approximately 20 μL of hydrogel was applied topically to the strike zone. (7) The incised scalps of the mice were carefully sutured and, after they had awakened from anaesthesia, they were carefully returned to their original feeding cages.

2.1.6 Degradation studies *in vivo*

Two groups were obtained using the above modelling method: the sham group and the TBI group. TM/Dap hydrogel containing 1,1-diiododecyl-3,3,3-tetramethylindotricarbocyanine iodide (DiI) was injected into the injury and mice were imaged with a small animal imager at 1 day, 3 days and 7 days post surgery to determine the rate of hydrogel degradation based on fluorescence intensity on a daily basis.

2.2 Evaluation of therapeutic effect and side effects of TM/Tap hydrogel

2.2.1 Morris water maze

The experiment was conducted consecutively from 14 days to 19 days after TBI, using a black pool of approximately 1.2 m in diameter divided into four quadrants and four different shapes as spatial navigation cues. A small platform is hidden in the pool and the mice must use their learning and memory skills to find the platform in the pool and remember where it is in the pool. In each experiment, mice entered the pool once from each quadrant and had 90 s to swim each time, and the duration of the mice's search for the platform was recorded. If the mice do not find the platform within 90 s, the experimenter will use a stick to guide them to the platform. On the sixth day of the test, we would remove the platform and record the mice's course of action and how long they stayed in each area. To exclude mice that cannot swim, the animals must be placed in water for observation before the experiment. The position of the graph and the platform remained constant throughout the experiment.

2.2.2 mNSS score (modified degree of nervous system injury)

The degree of neurological damage in the mice was assessed using the modified Neurological Severity Scale (mNSS) on day 19 after establishment of the mouse TBI model. This assessment covers balance, sensory, motor and reflex functions, with scores derived from indicators such as the tail-lift test, sensory test, abnormal movement and reflex test. If all indicators were normal, the composite score was 0. If there were abnormal indicators, the score was based on the scale criteria, with a maximum deficit score of 18.

2.2.3 Detection and analysis of toxic and side effects in ICR mice

H&E staining: First, 3 ICR mice were randomly selected from each subgroup and anaesthetized by intraperitoneal injection. A

surgical incision was then made in the left side of the mouse chest and the exposed left apical portion of the heart was punctured with a needle to a depth of 4–6 mm and fixed. The vessels were then rinsed with 0.9% NaCl solution and perfused with 4% paraformaldehyde for 600 s.

After that, the samples were preserved in a 4% paraformaldehyde solution. After dehydration, multi-organ paraffin blocks were prepared. The paraffin block was cut into thin slices and flattened against the center of the slide. It was then degreased with xylene and stained with H&E.

The specific procedure was as follows: The sections were soaked in hematoxylin water for 180–300 s and then cleaned repeatedly with tap water; then the sections were placed in acidic water and ammonia of differentiation solution, stained sequentially for a few seconds, and then cleaned repeatedly with tap water for 60 min; the sections were reblued with rebluing solution and washed repeatedly under tap water again; then the sections were placed in graded alcohols of 85 and 95% sequentially. Then the sections were dehydrated in graded alcohols of 85 and 95% for 300 s and then stained with eosin stain for 300 s. Finally, the sections were immersed in gradient concentrations of anhydrous ethanol I for 300 s, anhydrous ethanol II for 300 s, anhydrous ethanol III for 300 s, xylene solution I for 300 s, and xylene solution II for 300 s, sequentially, and then washed repeatedly in tap water; the sections were air dried and then sealed with a transparent neutral resin; the results were observed under a microscope and recorded.

Liver and kidney function tests: When the therapy was over, three mice were chosen at random from each group. The tail is first exposed and can be wiped with warm water to fully reveal the blood vessels. A scalp needle attached to a syringe was then used to inject a dilution of heparin to prevent clotting. After puncturing the tail vein, a blood sample is taken using negative pressure. When blood collection is complete, slowly remove and sterilize the needle. Finally, blood samples were tested and the results analyzed.

2.3 Study on the therapeutic effect of TM/Dap hydrogel

2.3.1 Detection of BBB integrity

The experimental steps were as follows (1) 2% Evans blue solution was prepared; (2) Evans blue solution was injected into the tail vein of mice 3 days after injury (at a dose of 2 mL/kg); (3) 2 h later, mice were over-anaesthetized with 10% chloral hydrate and brain tissue was removed by saline perfusion; (4) the damaged cerebral hemispheres were removed and their weights measured; (5) the samples obtained using a tissue homogeniser were mixed with 4 mL of 1 M potassium hydroxide solution using a tissue homogeniser; (6) a 0.2 M extract was prepared using phosphoric acid and acetone in a ratio of 5:13; (7) 1 mL of tissue suspension was centrifuged with 5 mL of the mixed extract at 4°C and 3,000 rpm for 30 min; (8) absorbance values of the supernatant at 323 nm were detected using an enzyme marker and the Evans blue content.

2.3.2 Determination of brain water content

The peak of cerebral oedema is reached around 3 days after TBI. To measure the degree of cerebral oedema, experiments were performed on mice 3 days after TBI. The mice were anaesthetized intraperitoneally with 10% chloral hydrate, the brains were removed by decapitation and

the damaged lateral cerebral hemisphere was isolated. Blood and excess water were thoroughly removed from the surface of the brain samples using filter paper and placed on dried aluminium foil. The samples were weighed using a precision electronic analytical balance after subtracting the weight of the aluminium foil. They were then dried in an oven at 80°C for 72 h. The brain tissue's dry weight (minus the weight of the aluminium foil) was measured, and the water content was calculated as (wet weight - dry weight)/wet weight x 100%.

2.3.3 Immunofluorescence staining

Traumatic brain injury can cause damage to brain tissue and an inflammatory response that activates astrocyte and microglial responses (Mira et al., 2021). Glial fibrillary acidic protein (GFAP) is a major structural protein of astrocytes and its expression level can be used as an indicator of astrocyte activity. Ionized calcium binding adapter molecule (Iba-1) is the signature protein of microglia, which also increase in number and activity after TBI. The degree of neuroinflammatory response and recovery of brain tissue after TBI can be assessed by detecting the expression of GFAP and Iba-1 using immunofluorescence techniques. The specific experimental steps are as follows.

2.3.3.1 Preparation of paraffin sections

After deep anaesthesia, the mice were perfused with PBS until a clear and transparent fluid was obtained. The intact brain tissue was then immersed in 4% paraformaldehyde for 24 h and then rinsed with fresh water for 24 h. The brain tissues were dehydrated with 75, 85, 90, 95, 95 and 100% ethanol, in that order, for 1 h. They were then immersed in ethanol-xylene for 40 min, then in xylene I for 25 min and finally in xylene II for 15 min to make the sections transparent. Finally, the specimens were placed at 65°C for three times to immerse the wax until it was completely encapsulated.

2.3.3.2 Immunofluorescence staining

The brain tissue paraffin sections were heated to 60°C in an oven and treated with dimethylbenzene at 15-min intervals, three times. The sections were heated to 60°C in an oven and treated with dimethylbenzene three times, every 15 min. Then, for 2 min each, they received treatments with 100, 100, 95, 95, and 85% alcohol. After that, the sections were cleaned with 0.01 mol/L phosphate buffered solution (PBS) and rinsed with tap water. Following a 10-min immersion in a 3% H₂O₂ solution, they were washed with distilled water. The sections were microwave repaired for 15 min at 95°C in sodium citrate buffer, cooled, and then cleaned with 0.01 mol/L PBS. The slices were blocked with immunofluorescence blocking solution for 2 h after being incubated in 0.1 mol/L PBS. The sections were placed in a dark box and incubated at 4°C for the entire night after a dilution of the fluorescent primary antibody was applied. After a PBS-Tween wash the next day, a diluted secondary fluorescent antibody was dropwise applied to the sections. After that, the sections were left to incubate for 2 h at ambient temperature without any light. Add 5 μ L of anti-fluorescence attenuating solution to the slide, then cover it with a coverslip to make it ready. Observe the slide under a fluorescence microscope while protecting it from light. Image Pro Plus software was used to analyze areas of positive fluorescent staining.

2.3.4 Bioinformatics analysis

In GSE173975, the investigators used the moderate lateral fluid percussion (LFP) approach to fabricate a TBI model to identify

differentially expressed genes (DEGs) in the acute phase of TBI. By analyzing DEGs in GSE173975 and reviewing TBI-related literature, we found that NF- κ B plays an important role in the acute phase of TBI. Differently expressed genes in the two groups were analyzed using the R software (version 4.3.1) loaded with the “edgeR” package (conditions: $\text{fdrFilter} = 0.05$, $\text{logFCfilter} = 1$), and these differentially expressed genes were used to perform enrichment analyses for possible pathways.

2.3.5 Western blotting

Studies have revealed the critical role of nuclear transcription factor- κ B (NF- κ B) in the production of inflammatory mediators and cytokines. Pro-inflammatory factors that contribute to the inflammatory response are produced when NF- κ B is activated. These factors include TNF- α (tumor necrosis factor) and IL (Kalra et al., 2022). NF- κ B consists of five members, RelA (p65), RelB, c-Rel, NF- κ B1 (p50) and NF- κ B2 (p52) (Iacobazzi et al., 2023). The most prevalent heterodimer and the primary mode of NF- κ B activity expression is p65/p50. RelA (p65), RelB, c-Rel, NF- κ B1 (p50), and NF- κ B2 (p52) are the five members of NF- κ B. The most prevalent heterodimer and the primary source of NF- κ B activity is p65/p50. The immunoblotting assay for p65 and p50 was performed as follows.

2.3.5.1 Sampling

On day 7 after TBI modelling, mice were anaesthetized and blood was collected via the heart using a 1 mL syringe to rapidly remove brain tissue from the injured side of the mice. Blood was collected in EP tubes and rapidly frozen in liquid nitrogen for protein extraction.

2.3.5.2 Protein extraction

After being taken out of the -80°C refrigerator, frozen tissue blocks were ground into a powder in a mortar using liquid nitrogen. The powdered brain tissue was then placed in a centrifuge tube for further storage. A fresh 1.5 mL centrifuge tube was filled with a little amount of brain powder, 300 μL of RIPA protein lysate containing phenylmethanesulfonyl fluoride (PMSF), and it was shaken and mixed before being put on ice for half an hour. Following the addition of two iron beads, the tissue was crushed three times at a frequency of 50 Hz for 15 s each; the centrifuge tube was then set on ice, inserted inside the ultrasonic crusher probe, and ultrasonically sonicated three times for 5 s each; The freezing centrifuge was then used to place the centrifuge tube. It was pre-cooled to 4°C and centrifuged for 10 min at 13,000 rpm. The supernatant was then collected, and the protein concentration was determined using the bicinchoninic acid (BCA) technique. All samples were then processed based on the protein concentration. The BCA method was used to determine the protein concentration. All of the samples were levelled in accordance with the protein concentration, and then $4\times$ loading buffer was added. The samples were then placed on the heating module to denature the proteins for 10 min at 100°C . Afterward, the proteins were quickly cooled on ice before being used in Western blot experiments.

2.3.5.3 Immunoblotting

10% SDS-PAGE gel was prepared, and a 15-well comb was used to make the sample wells, 70 μg of extracted protein was added to each well, and the voltage in the running buffer was run at 80 V until the marker separated, then it was changed to 120 V to continue running the gel; the gel run was stopped when the marker was run to the lowest

part of the gel, and the PAGE gel was removed and placed on a piece of PVDF membrane moistened with methanol. The PAGE gel was removed and placed on a 0.22 μm PVDF membrane moistened with methanol to ensure that the gel was in full contact with the membrane, covered with filter paper and foam pads, and the air bubbles were removed with a small roller in the transfer buffer, and then placed in the transfer tank to transfer the membrane at 100 V for 90 min; the transferred membrane was removed and then incubated with 5% BSA for 1 h at room temperature, and then p-p65 (1:1,000) diluted with 1% BSA, p65 (1:1,000) and GAPDH (1:5,000) primary antibodies diluted with 1% BSA and incubated overnight at 4°C ; the membrane was washed three times with TBST for 5 min each time. After that, the corresponding secondary antibody (1:3,000) was added according to the antibody source and incubated for 1 h at room temperature. Finally, the membrane was washed three times with TBST for 5 min each time. For color development, the membrane was immersed in the ultrasensitive chemiluminescent reagent for 10–30 s and photographed. Each indicator was repeated more than twice to complete the run. The greyscale values of all bands were read in ImageJ software.

2.3.6 Detection of TNF- α , IL-1 β , IL 6, and CXCL1 content

On day 7 post-injury, mice were anaesthetized and then brain tissue was harvested. Brain tissue samples were weighed, homogenised and centrifuged, and the levels of CXCL1, IL-1 β , IL-6 and TNF- α were detected by ELISA kits (Bost Biotech, Wuhan, China). Levels of TNF- α were determined according to the manufacturer's instructions. All results were quantified using the BCA Protein Assay Kit (Boster Biotechnology, Wuhan, China).

2.4 Data analysis

Software such as SPSS 27.0 and GraphPad Prism 8.0.2 were used to conduct statistical analysis. Statistical analysis of data was performed with the Student's *t*-tests or one way ANOVAs, *p* values <0.05 was considered to be statistically significant. The results were expressed as mean \pm SD in the figures (ns = non-significance, $*p < 0.05$, $**p < 0.01$, $***p < 0.001$, $****p < 0.0001$).

3 Results

3.1 TM/Dap hydrogel preparation and characterisation

According to previous reports, TM/Dap was successfully prepared (Figures 1Aa,b) (Gajanayake et al., 2014; Joshi et al., 2018). To simulate traumatic brain injury, we established a TBI model using the Feeney method (Figure 1Ba) and injected the TM/Dap hydrogel into the wound cavity (Figure 1Bb). Using a scanning electron microscope, it can be clearly seen that the TM/Dap hydrogel has a loose and porous mesh structure inside (Figure 1C), which can achieve efficient encapsulation and drug release.

MMPs are zinc-dependent proteases that degrade extracellular matrix molecules. They play a crucial role in various biological processes, such as vascular regeneration and inflammatory responses.

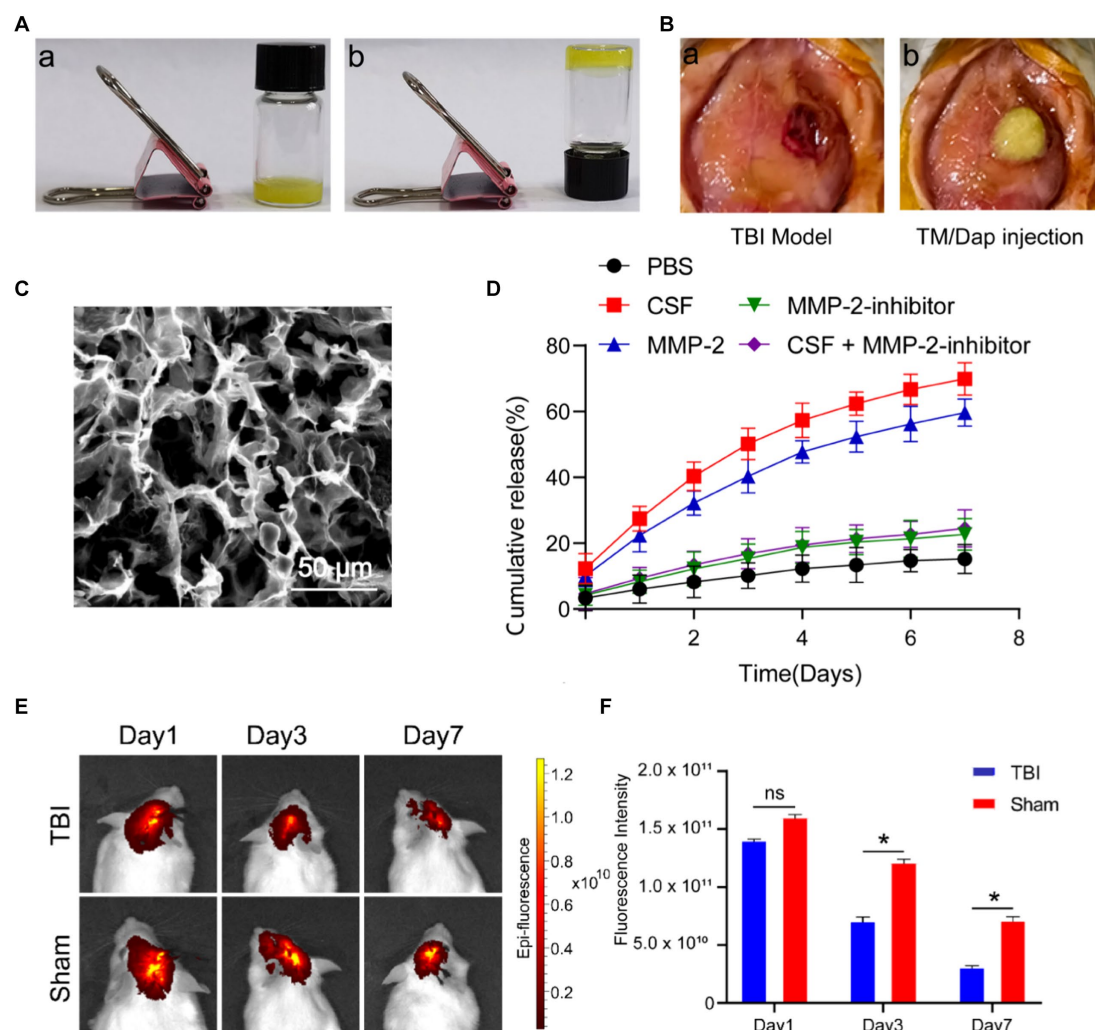


FIGURE 1

The formation and characteristics of the hydrogel TM/Dap. (A) TM/Dap hydrogel gelation both before (a) and after (b) cooling. (B) (a) Make a midline incision, cut the brain tissue, and open a cranial window. (b) TM/Dap hydrogel is inserted into the operative cavity. (C) TM/Dap hydrogel SEM image. There is a 50 μ m scale bar. (D) Data are shown as mean \pm SEM, $n = 5$, for the Dap release profile of TM/Dap hydrogel in PBS at 37°C with mild stirring under MMP-2, MMP-2 + inhibitor, CSF, and CSF + inhibitor conditions. (E) Fluorescence signals after intracranial injection of TM/Dap hydrogel in mice on days 1, 3 and 7. (F) Quantitative analysis of DiR fluorescence signals of mice ($n = 5$).

Among these, MMP-2 is a matrix metalloproteinase that is widely implicated in a variety of pathophysiological processes, including blood–brain barrier disruption, modulation of inflammatory responses, damage repair and extracellular matrix remodeling after TBI. To evaluate the ability of TM/Dap hydrogels to release daphnetin in TBI, we used cerebrospinal fluid to simulate drug release in the TBI environment. As shown in Figure 1D, all groups of TM/Dap hydrogels were able to release daphnetin within 7d in the MMP-2 and CSF environments of the traumatic brain injury setting. At day 7, the final release rates were $59.62 \pm 4.11\%$ and $69.84 \pm 4.92\%$ in the MMP-2 and CSF groups, respectively, whereas the drug release rates were $15.21 \pm 4.44\%$, $22.65 \pm 4.74\%$ and $24.44 \pm 5.69\%$ in the PBS, MMP-2 inhibitor and CSF + MMP-2 inhibitor groups, respectively. When the MMP-2 group, CSF group and PBS group were compared, the drug release rate increased significantly and the difference was statistically significant ($p < 0.05$). Meanwhile, drug release was significantly

inhibited in the CSF + MMP-2 inhibitor group compared with the CSF group, and in the MMP-2 inhibitor group compared with the MMP-2 group ($p < 0.05$). The experimental results indicated that the TM/Dap hydrogel was able to release more daphnetin in the presence of MMP-2 and CSF after TBI to exert therapeutic effects. To test the biodegradability of TM/Dap hydrogel, we implanted TM/Dap hydrogel containing fluorescent dye DiR into the trabecular space of mice after TBI to monitor the degree of degradation. The experimental results showed (Figures 1E,F) that the fluorescence intensity of the fluorescent dye DiR gradually decreased at 1, 3 and 7 days postoperatively, and the degradation rate was significantly higher than that of the control group ($p < 0.05$). This indicates that the hydrogel can effectively adapt to the *in vivo* trauma microenvironment, continuously release drugs to maintain the relative stability of drug concentration, and avoid fluctuations in drug concentration to affect the therapeutic effect.

3.2 TM/Dap hydrogel promotes functional recovery after traumatic brain injury

The Morris water maze test was used to measure the recovery of learning and memory abilities in TBI mice on day 19 following TBI in order to examine the therapeutic efficacy of TM/Dap hydrogel (Othman et al., 2022). Each group of mice was trained on a standing platform on days 14–18 following TBI, and the results were noted on day 5. The study's conclusions demonstrated that the mice in the TM/Dap group were more accurate in their ability to locate compared to the other groups (Figure 2A). On day 19, day 6 of the Morris water maze experiment, a spatial memory test was performed and trajectories were recorded. The results showed that the TM/Dap group was relatively more focused, whereas the other groups were more

dispersed relative to the standing platform (Figure 2B). Higher scores indicate more severe neurological abnormalities. The mNSS score is a widely used tool to evaluate the degree of neurological deficits in animal investigations. Additionally, by day 19, the TM/Dap group's composite scores were considerably lower than those of the other groups' mice (Figure 2C, $p < 0.05$), indicating that these groups had a positive impact on the TBI mice's ability to regain neurological function. The distance to the platform and the decrease in platform search time were indicators of the mice treated with TM/Dap hydrogel having significantly improved their learning ability during the first 5 days of training, as Figures 2D,E illustrates. Compared to the other experimental groups, mice in the TM/Dap group spent more time in the target quadrant and crossed the platform more frequently throughout the spatial exploration experiment (Figures 2F–I, $p < 0.05$).

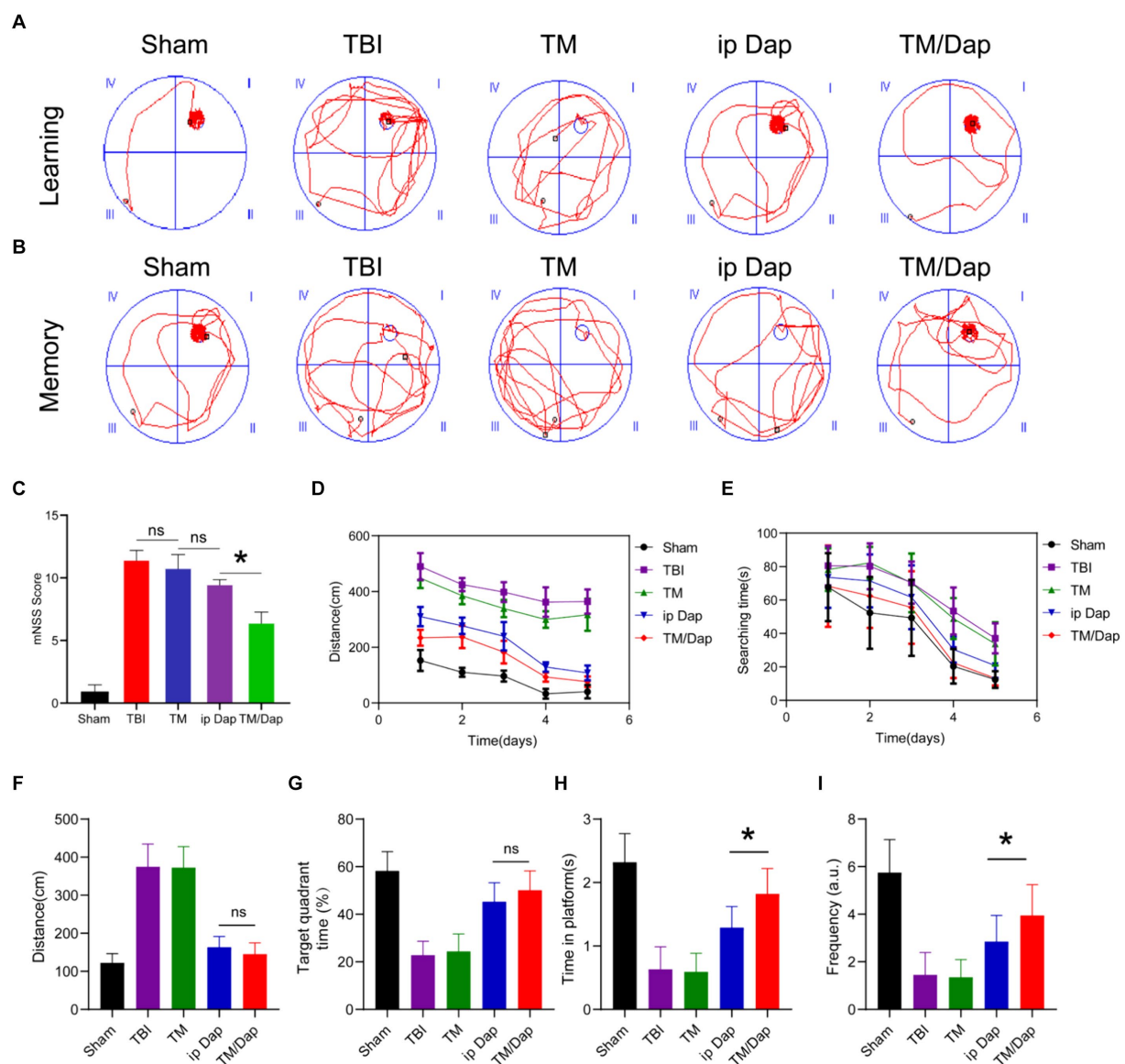


FIGURE 2

Morris water maze test and mNSS score were used to assess functional recovery 19 days following traumatic brain injury. (A,B) swimming trajectories printed out on a computer during the memory and learning phases. mNSS score was examined (C). During the 5 days of training, (D) is the swimming distance to the platform and (E) is the amount of time spent searching for the platform distance at the last trial. Distance swum to the platform (F), time spent in the target quadrant (G), time spent on the platform (H), and frequency on the platform (I).

In conclusion, TM/Dap hydrogel can greatly aid in TBI mice's recovery of their cognitive and memory functions.

3.3 *In vivo* biocompatibility

We assessed typical liver and kidney function indices, such as AST, ALT, BUN, and CREA, and looked at H&E-stained sections of the major organ tissues of the heart, liver, spleen, lung, and kidney to evaluate the biosafety of TM/Dap hydrogel. The heart, liver, spleen, lung, and kidney tissue sections in all groups did not exhibit any appreciable tissue damage or morphological or structural alterations, according to the results of the H&E section staining (Figure 3A, $p > 0.05$). There were no statistically significant differences between the findings of each index ($p > 0.05$) for the liver and kidney function tests (Figure 3B). Therefore, the TM/Dap hydrogel showed no obvious toxic side effects in mice, demonstrated good biocompatibility and provided a guarantee of the safety of the hydrogel in clinical applications.

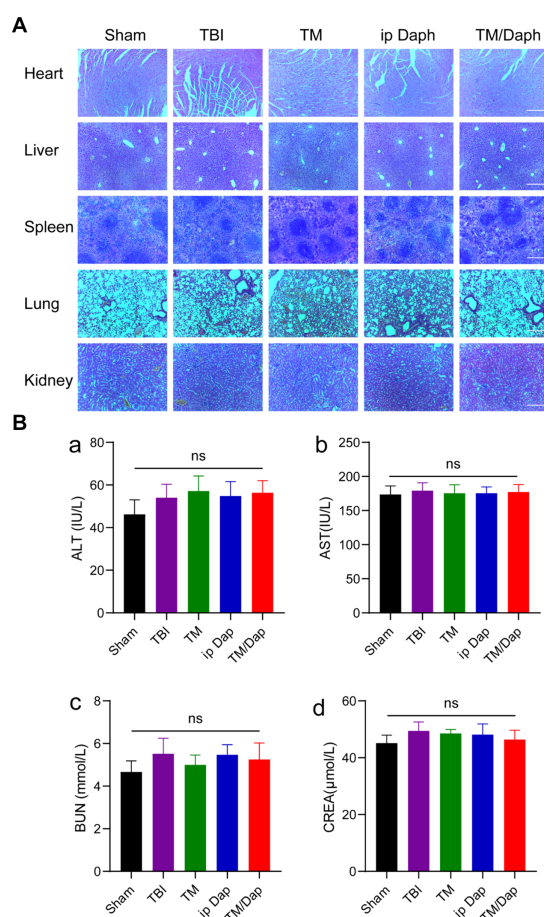


FIGURE 3
Therapeutic efficacy and biological safety of TM/Dap hydrogel. (A) Heart, liver, spleen, lung, and kidney treated with Sham, TBI, TM, ip Dap, and TM/Dap were stained with H&E. Scale bar = 200 μm. (B) Evaluation of TM/Dap hydrogel's toxicity to the liver and kidneys. (a) alanine aminotransferase (ALT), (b) aspartate aminotransferase (AST), (c) blood urea nitrogen (BUN), (d) creatinine (CREA).

3.4 TM/Dap hydrogel protects the blood–brain barrier and reduces cerebral oedema

The blood–brain barrier was damaged following traumatic brain injury (TBI). In order to determine if TM/Dap hydrogel could successfully mitigate the extent of this disruption, the blood–brain barrier's permeability following TBI was measured using Evans blue dye exudation. As seen in Figures 4A,B, the BBB permeability of the injured lateral hemisphere was significantly reduced in both ip Dap and TM/Dap hydrogel treatment groups compared with the TBI and TM groups, and the TM/Dap hydrogel treatment group significantly suppressed the Evans blue leaking, limiting the area of leakage to the site of the primary focus. The results showed that TM/Dap hydrogel effectively protected the integrity of the blood–brain barrier. Disruption of the blood–brain barrier leads to the formation of cerebral oedema, which further exacerbates traumatic brain injury. The water content of normal rat brain is relatively stable, and the water content of rat brain was determined by the dry and wet weight method, and the severity of brain oedema can be reflected by the change in the average brain water content, which indirectly reflects the treatment effect. As illustrated in Figure 4C, TM/Dap hydrogel could effectively inhibit brain oedema ($p < 0.05$) and had the most obvious protective and restorative effect on the central nervous system.

3.5 Enhanced anti-inflammatory effect of TM/Dap hydrogel

The synthesis of pro-inflammatory cytokines (TNF- α , IL-1 β , and IL-6) and chemokines (CXCL1) increases significantly following traumatic brain injury (TBI), which has a major impact on the prognosis of TBI patients. One of the main transcription factors expressed by cytokines and inflammatory mediators is nuclear transcription factor-kB (NF-kB). NF-kB activation can produce pro-inflammatory factors like IL and tumor necrosis factor- α (TNF- α), which can contribute to the inflammatory response. The GEO database is a bioinformatics resource for storing and sharing gene expression and genetic variation data to facilitate global collaboration and data sharing in biological and medical research. Data on the evolution of transcriptional pathology over time following impact traumatic brain injury (TBI) in the lateral fluid of the rat hippocampus were collected in GSE173975. The corresponding data were divided into two groups according to sham and TBI, as well as the genes that exhibited differential expression between the two groups were obtained by loading the “edgeR” package using the R software (with the setting conditions of $\text{fdrFilter} = 0.05$ and $\text{logFCfilter} = 1$) (Figure 5A). Meanwhile, the corresponding pathways were obtained according to the differentially expressed genes (Figure 5B), which further confirmed the crucial part of NF-kB in TBI.

NF-kB consists of five members, RelA (p65), RelB, c-Rel, NF-kB1 (p50) and NF-kB2 (p65/p50 is the most common heterodimer and the major form of NF-kB activity). The results of immunoblotting experiments for p65 and p50 showed that the TM/Dap hydrogel group had the lowest protein expression levels of p65 and p50 compared to the TBI, TM and ip Dap groups (Figures 5C–E). In order to corroborate the TM/Dap hydrogel's anti-inflammatory properties, we measured the production of pro-inflammatory chemokines (CXCL1) and cytokines (TNF- α , IL-1 β , and IL-6). Once more, TBI

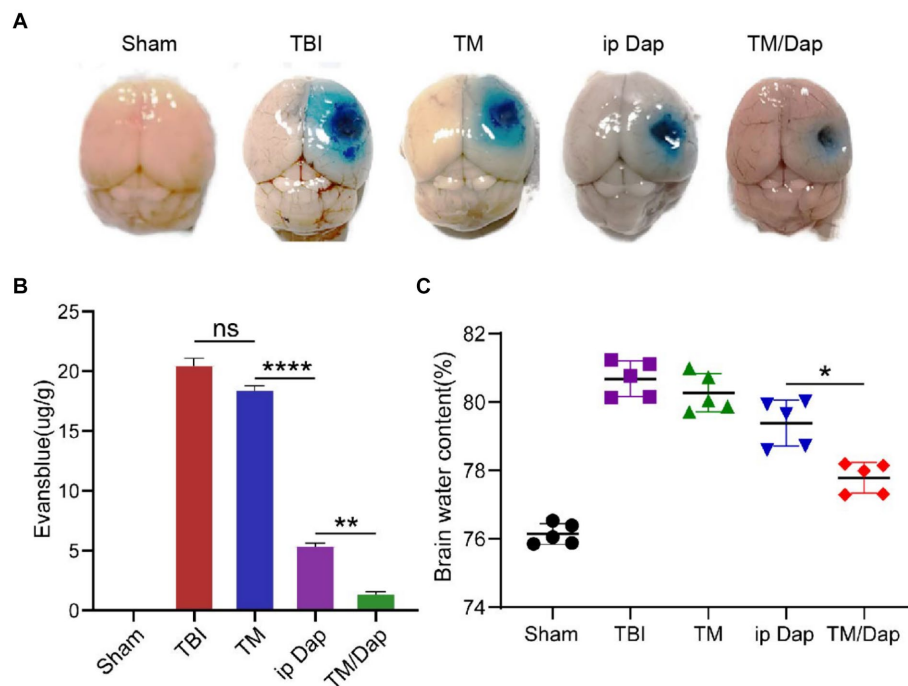


FIGURE 4

TM/Dap hydrogel decreased cerebral edema and preserved the BBB. (A) Representative images of EB extravasation in different groups' right brains on day three following traumatic brain injury ($n = 5$). (B) Numerical evaluation of EB leakage ($n = 5$). (C) Brain water content. Values are the mean \pm SEM. ($n = 5$).

mice given TM/Dap hydrogel exhibited the lowest amounts of chemokines and inflammatory cytokines, indicating that the hydrogel amplifies the anti-inflammatory response following TBI (Figures 5F–I).

Following traumatic brain injury, astrocytes and microglia were widely dispersed in the damaged cortex's periphery, creating a unique zone of glial cell activity. To look into how TBI affects microglial and astrocyte activation, the severity of the inflammatory response was reflected by the detection of astrocyte and microglial activation markers, GFAP and Iba-1, on days 7 and 14 after injury. The outcomes demonstrated that in the marginal zone of the traumatized area, all groups showed different degrees of cell activation, with the TBI group showing the most pronounced inflammatory response with the maximum quantity of positive cells. In contrast to the other cohorts, the number of positive cells in the TM/Dap group was all the lowest and statistically significant (Figures 6A,B, $p < 0.05$), indicating that the hydrogel in the TM/Dap group had the best inhibitory effect on the inflammatory response, providing favorable conditions for nerve tissue recovery.

4 Discussion

For patients of all ages, traumatic brain injury (TBI) is the primary cause of mortality and disability (Kureshi et al., 2021; Giner et al., 2022). Today, preventing further injuries is crucial to treating traumatic brain injury (TBI) (Keating and Cullen, 2021; Rakhit et al., 2021). Some studies have shown that daphnetin can effectively reduce neurological damage (Singh et al., 2021), but clinical application is limited by the low bioavailability of

daphnetin *in vivo* and the presence of the blood–brain barrier. Therefore, an effective solution is desperately required. In this investigation, we used TM hydrogel to deliver Dap for the therapy for traumatic brain injuries and to stop the subsequent deterioration following a traumatic brain injury. Dap encapsulated in TM hydrogel could be directly injected *in situ* at the site of TBI, and the loose and porous reticular microstructure could be observed by scanning electron microscopy. Due to the unstable ester linkages of TM, it can be cleaved in an inflammatory environment with matrix metalloproteinase (MMP-2) mimicry, resulting in efficient release of the encapsulated Dap. In addition, the rate of Dap release is significantly higher under patient cerebrospinal fluid, whereas the release of Dap can be very low when the gels are in PBS solution. Thus, local administration of TM/Dap hydrogels can provide sustained drug release at the site of injury and neuroprotection at the site of injury in TBI-injured mice. It may be possible to turn medications with bad pharmacokinetic characteristics into successful medications by using this targeting strategy.

The neuroprotection that Dap offers is another crucial role of the TM/Dap hydrogel in TBI. It is generally believed that the function and number of neuronal cells are destroyed after TBI, leading to significant neurological dysfunction. In the present study, except for the sham group, the mNSS scores of mice in the TM/Dap hydrogel treatment group were the lowest, suggesting that TM/Dap hydrogel had a more pronounced therapeutic effect on TBI mice. The water maze index also showed that the treatment effect of the TM/Dap group was better than that of the other groups, suggesting that spatial learning memory recovery was better in the TM/Dap treatment group. This suggests that by using TM hydrogel as a drug carrier, Dap can achieve sustained

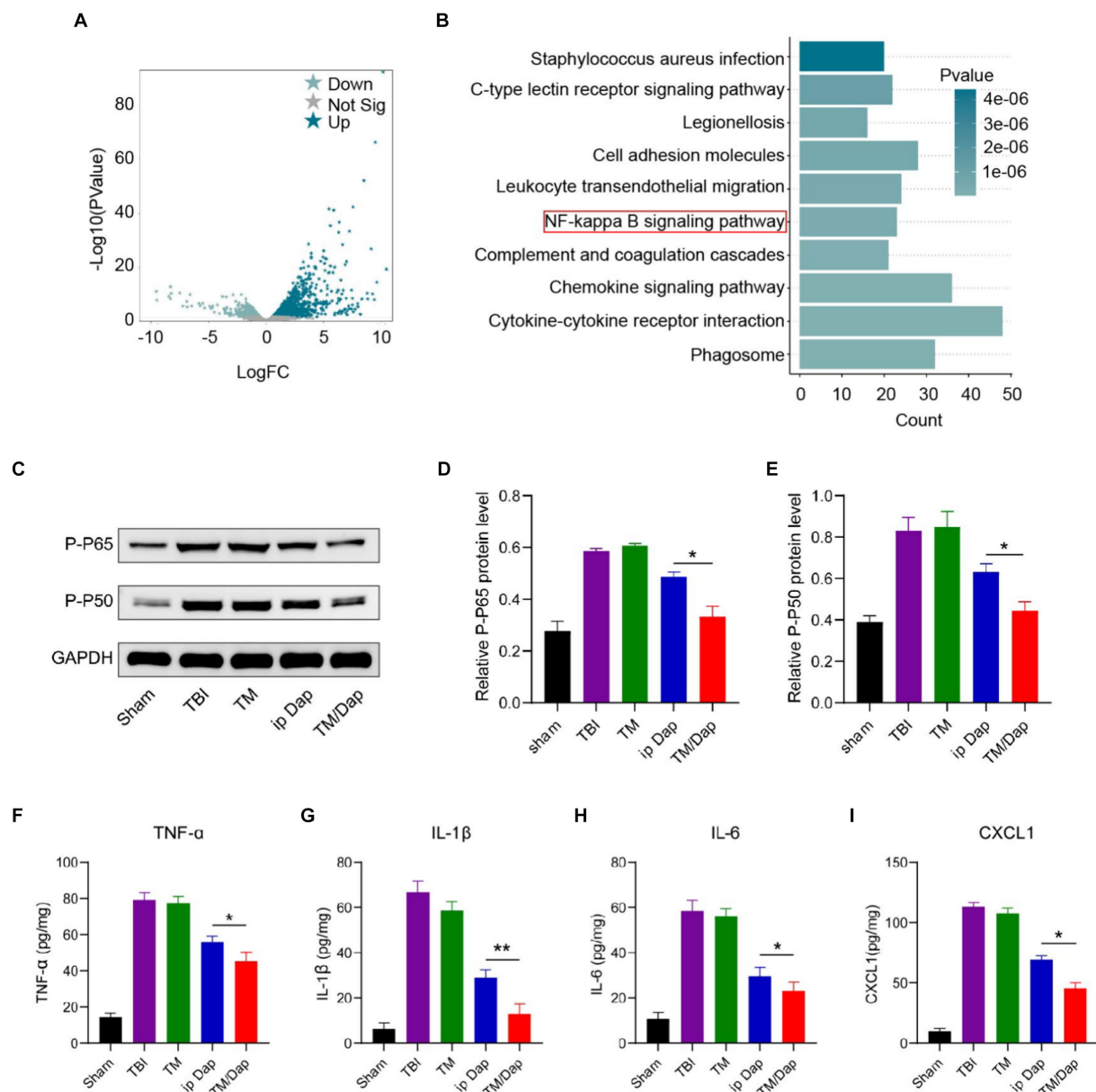


FIGURE 5

Inflammatory pathways and factors after TBI. (A,B) Volcano mapping (A) and enrichment analysis (B) of differentially expressed genes in the Sham and TBI groups in GSE173975. (C) P-P65 and P-P50 protein expression levels. (D) Analysis of P-P65 quantitatively. (E) Analysis of P-P50 quantitatively. (F–I) Injured tissue's levels of TNF-α, IL-1β, IL-6, and CXCL1 12 h after a traumatic brain injury.

release of the encapsulated drug, thus maximizing the therapeutic effect of Dap.

In order to clarify whether TM/Dap hydrogel would have toxic side effects on major organs *in vivo*, we investigated the biosafety of TM/Dap hydrogel by the experimental methods of H&E staining and liver and kidney functions. The primary organs of the mice in each group were stained with H&E, which revealed no visible morphological or tissue damage and indicated that the hydrogel TM/Dap was not obviously biotoxic to the organism. The liver and renal function data further ruled out the harmful effects of the TM/Dap hydrogel since they revealed no significant variations in the groups' liver (AST, ALT) or kidney (CREA, BUN).

Disruption of the blood–brain barrier as a result of TBI can lead to and exacerbate the development of cerebral oedema. The blood–brain

barrier integrity following TM/Dap treatment was the best in this investigation, with the least amount of Evans Blue exudation, which may maximally limit the region of leakage to the site of the principal foci. These findings were based on the results of the EB extravasation test. In addition, TM/Dap hydrogel could effectively inhibit brain oedema after treatment, further suggesting that TM/Dap hydrogel could lessen the dissemination of supplementary harm and thus protect the blood–brain barrier. In conclusion, TM/Dap hydrogel may also play a useful neuroprotective function in traumatic brain injury.

Both astrocytes and microglia are major cells mediating neuroinflammation (Bhusal et al., 2023), and activation of NF-κB and a dramatic increase in the production of tissue inflammatory cytokines (TNF-α, IL-1β and IL-6) and chemokines (CXCL1) are important contributors to secondary brain damage. After TM/Dap hydrogel

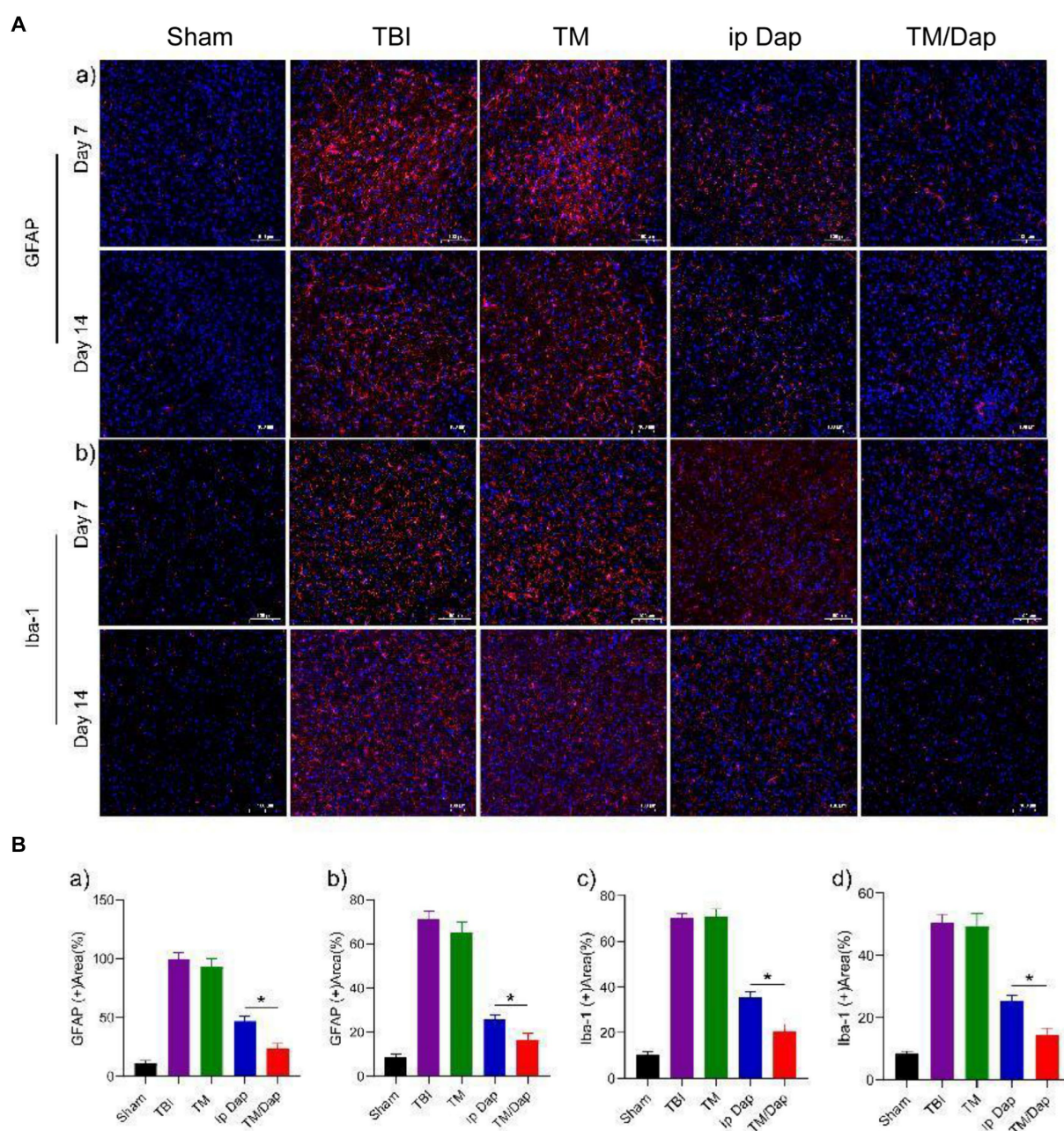


FIGURE 6

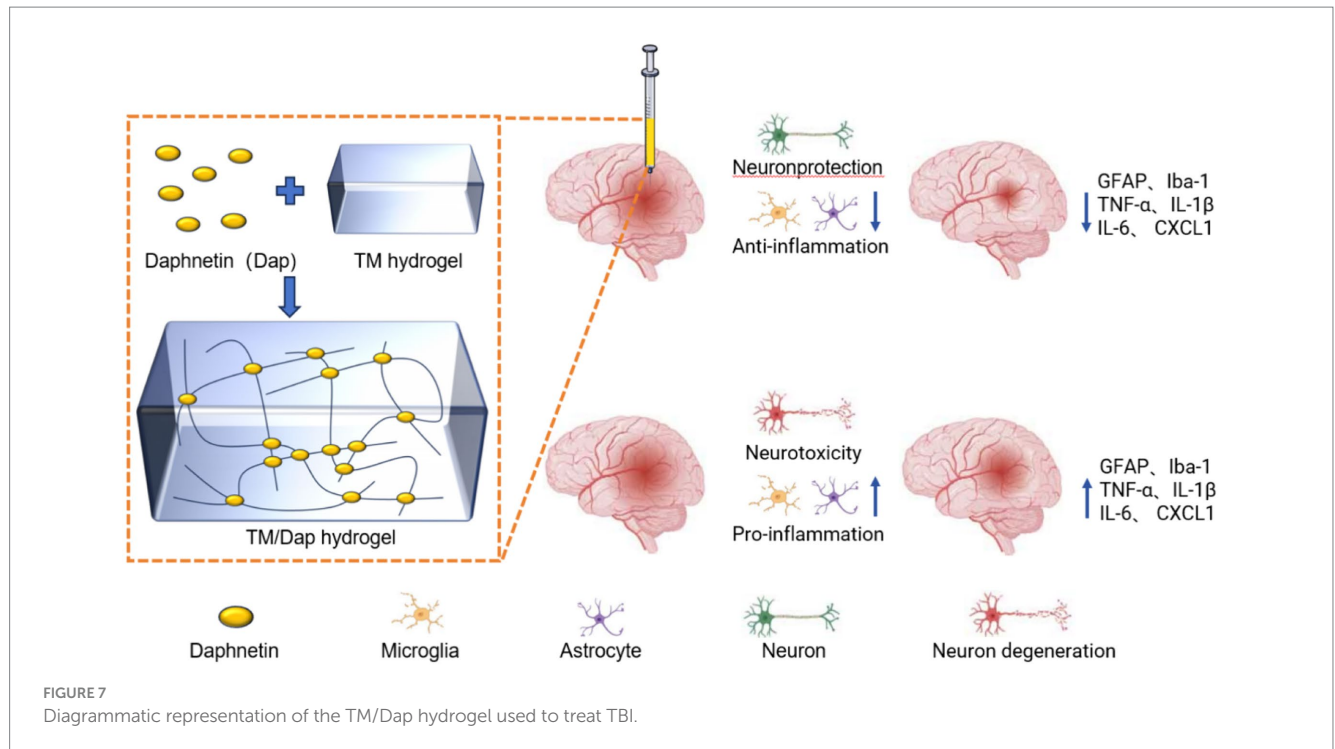
TM/Tab hydrogel enhanced the anti-inflammatory activity after traumatic brain injury. **(A)** Expression of GFAP (a) in astrocytes and Iba-1 (b) in microglia of the injured tissue at 7 and 14 days subsequent to a traumatic brain injury. **(B)** (a) Analysis of GFAP levels quantitatively 7 days following a traumatic brain injury. (b) Quantitative analysis of GFAP levels 14 days after traumatic brain injury. (c) Analysis of Iba-1 levels quantitatively 7 days after traumatic brain injury. (d) Analysis of Iba-1 levels quantitatively 14 days after traumatic brain injury.

treatment, astrocyte, microglial and NF- κ B activity was reduced, and levels of inflammatory cytokines and chemokines in brain tissue were decreased.

To verify these ideas, we used immunofluorescence, WB experiment and ELISA. The immunofluorescence staining results showed that astrocytes and microglia were active in the brains of mice in the TBI group. And the expression of GFAP and Iba-1 was significantly reduced in mice treated with TM/Dap hydrogel. Meanwhile, the TM/Dap hydrogel also led to the inhibition of NF- κ B activation and reduced the levels of inflammatory cytokines and chemokines compared to the TBI group (Figure 7).

5 Conclusion

In conclusion, our delivery of Dap using hydrogel as a drug carrier can compensate for the deficiencies in the *in vivo* bioavailability of Dap and further enhance the therapeutic effect of Dap, thus halting the subsequent dissemination of injury. After TBI, the concentration of Dap could be increased by injecting TM/Dap hydrogel directly into the surgical cavity. TM/Dap hydrogel could effectively protect the blood-brain barrier and ameliorate cerebral oedema. TM/Dap hydrogel treatment in TBI mice resulted in a reduction of the inflammatory response, which promoted neuronal regeneration and



restored neurological dysfunction. This provides a new idea for Dap treatment of secondary damage in TBI.

Data availability statement

The original contributions presented in the study are included in the article/supplementary material, further inquiries can be directed to the corresponding authors.

Ethics statement

The animal study was approved by the Affiliated Huaian Hospital of Xuzhou Medical University. The study was conducted in accordance with the local legislation and institutional requirements.

Author contributions

YM: Writing – original draft, Writing – review & editing. YL: Writing – review & editing. JG: Writing – review & editing. ZC: Writing – review & editing. ZZ: Writing – original draft, Writing – review & editing. JZ: Writing – original draft, Writing – review & editing.

References

Albiero, L. R., de Andrade, M. F., Marchi, L. F., Landi-Librandi, A. P., de Figueiredo-Rinhel, A. S. G., Carvalho, C. A., et al. (2020). Immunomodulating action of the 3-phenylcoumarin derivative 6, 7-dihydroxy-3-[3', 4'-methylenedioxyphenyl]-coumarin in neutrophils from patients with rheumatoid arthritis and in rats with acute joint inflammation. *Inflamm. Res.* 69, 115–130. doi: 10.1007/s00011-019-01298-w

Funding

The author(s) declare that financial support was received for the research, authorship, and/or publication of this article. The Hua'an Science and Technology Plan (Project No. HA235816) provided funding for this work.

Conflict of interest

The authors declare that the research was conducted in the absence of any commercial or financial relationships that could be construed as a potential conflict of interest.

Publisher's note

All claims expressed in this article are solely those of the authors and do not necessarily represent those of their affiliated organizations, or those of the publisher, the editors and the reviewers. Any product that may be evaluated in this article, or claim that may be made by its manufacturer, is not guaranteed or endorsed by the publisher.

Bassiouni, W., Ali, M. A. M., and Schulz, R. (2021). Multifunctional intracellular matrix metalloproteinases: implications in disease. *FEBS J.* 288, 7162–7182. doi: 10.1111/febs.15701

Bhattarai, N., Kumbhar, A. A., Pokharel, Y. R., and Yadav, P. N. (2021). Anticancer potential of Coumarin and its derivatives. *Mini Rev. Med. Chem.* 21, 2996–3029. doi: 10.2174/1389557521666210405160323

- Bhusal, A., Afridi, R., Lee, W.-H., and Suk, K. (2023). Bidirectional communication between microglia and astrocytes in Neuroinflammation. *CN* 21, 2020–2029. doi: 10.217/4/1570159X21666221129121715
- Cheng, P., Li, R., Schwebel, D. C., Zhu, M., and Hu, G. (2020). Traumatic brain injury mortality among U.S. children and adolescents ages 0–19 years, 1999–2017. *J. Saf. Res.* 72, 93–100. doi: 10.1016/j.jsr.2019.12.013
- do, N. H. N., Truong, Q. T., Je, P. K., and Ha, A. C. J. C. P. (2022). Recent developments in chitosan hydrogels carrying natural bioactive compounds. *Carbohydr. Polym.* 294:119726. doi: 10.1016/j.carbpol.2022.119726
- Fang, C.-Y., Lou, D.-Y., Zhou, L.-Q., Wang, J.-C., Yang, B., He, Q.-J., et al. (2021). Natural products: potential treatments for cisplatin-induced nephrotoxicity. *APS* 42, 1951–1969. doi: 10.1038/s41401-021-00620-9
- Feeney, D. M., Boyeson, M. G., Linn, R. T., Murray, H. M., and Dail, W. G. (1981). Responses to cortical injury: I. Methodology and local effects of contusions in the rat. *Brain Res.* 211, 67–77. doi: 10.1016/0006-8993(81)90067-6
- Gajanayake, T., Olariu, R., Leclère, F. M., Dhayani, A., Yang, Z., Bongoni, A. K., et al. (2014). A single localized dose of enzyme-responsive hydrogel improves long-term survival of a vascularized composite allograft. *STM* 6:249ra110-249ra110. doi: 10.1126/scitranslmed.3008778
- García, M., Aloisio, C., Onnainty, R., and Ullio-Gamboa, G. (2018). Unidad de Investigación y Desarrollo en Tecnología Farmacéutica-UNITEFA (CONICET-UNC). Córdoba, Argentina.
- Garg, S. S., Gupta, J., Sharma, S., and Sahu, D. (2020). An insight into the therapeutic applications of coumarin compounds and their mechanisms of action. *Eur. J. Pharm. Sci.* 152:105424. doi: 10.1016/j.ejps.2020.105424
- Giner, J., Mesa Galán, L., Yus Teruel, S., Guallar Espallargas, M. C., Pérez López, C., Isla Guerrero, A., et al. (2022). Traumatic brain injury in the new millennium: new population and new management. *Neurologia* 37, 383–389. doi: 10.1016/j.nrleng.2019.03.024
- Hade, M. D., Suire, C. N., and Suo, Z. J. C. (2021). Mesenchymal stem cell-derived exosomes: applications in regenerative medicine. *Cells* 10:1959. doi: 10.3390/cells10081959
- Han, H., and Hyun, C. J. P. (2023). Acenocoumarol, an anticoagulant drug, prevents Melanogenesis in B16F10 melanoma cells. *Pharmaceuticals* 16:604. doi: 10.3390/ph16040604
- Hazy, A., Kowalski, E., Groot, N., and Theus, M. (2020). Peripheral immune response following traumatic brain injury, advancement and new understanding in brain injury. *IntechOpen*, 1–26. doi: 10.5772/intechopen.93597
- Hu, Y., Hu, S., Zhang, S., Dong, S., Hu, J., Kang, L., et al. (2021). A double-layer hydrogel based on alginate-carboxymethyl cellulose and synthetic polymer as sustained drug delivery system. *Sci. Rep.* 11:9142. doi: 10.1038/s41598-021-88503-1
- Hussain, Z., Thu, H. E., Khan, S., Sohail, M., Sarfraz, R. M., Mahmood, A., et al. (2022). Phytonanomedicines, a state-of-the-art strategy for targeted delivery of anti-inflammatory phytochemicals: a review of improved pharmacokinetic profile and therapeutic efficacy. *J. Drug Deliv. Sci. Technol.* 77:103895. doi: 10.1016/j.jddst.2022.103895
- Iacobazzi, D., Convertini, P., Todisco, S., Santarsiero, A., Iacobazzi, V., and Infantino, V. J. B. (2023). New insights into NF- κ B signaling in innate immunity: focus on immunometabolic crosstalks. *Biology* 12:776. doi: 10.3390/biology12060776
- Ilochonwu, B. C., Urtti, A., Hennink, W. E., and Vermonden, T. (2020). Intravitreal hydrogels for sustained release of therapeutic proteins. *J. Control. Release* 326, 419–441. doi: 10.1016/j.jconrel.2020.07.031
- Javed, M., Saleem, A., Xaveria, A., and Akhtar, M. F. (2022). Daphnetin: a bioactive natural coumarin with diverse therapeutic potentials. *FPHAR* 13:993562. doi: 10.3389/fphar.2022.993562
- Jha, S., and Ghewade, P. (2022). Management and treatment of traumatic brain injuries. *Cureus* 14:e30617. doi: 10.7759/cureus.30617
- Jin, Y., Li, S., Yu, Q., Chen, T., and Liu, D. J. M. (2023). Application of stem cells in regeneration medicine. *Cell Prolif.* 4:e291. doi: 10.1002/mco2.291
- Joshi, N., Yan, J., Levy, S., Bhagchandani, S., Slaughter, K. V., Sherman, N. E., et al. (2018). Towards an arthritis flare-responsive drug delivery system. *Nat. Commun.* 9:1275. doi: 10.1038/s41467-018-03691-1
- Kalra, S., Malik, R., Singh, G., Bhatia, S., al-Harrasi, A., Mohan, S., et al. (2022). Pathogenesis and management of traumatic brain injury (TBI): role of neuroinflammation and anti-inflammatory drugs. *Inflammopharmacology* 30, 1153–1166. doi: 10.1007/s10787-022-01017-8
- Keating, C. E., and Cullen, D. K. (2021). Mechanosensation in traumatic brain injury. *Neurobiol. Dis.* 148:105210. doi: 10.1016/j.nbd.2020.105210
- Kureshi, N., Erdogan, M., Thibault-Halman, G., Fenerty, L., Green, R. S., and Clarke, D. B. (2021). Long-term trends in the epidemiology of major traumatic brain injury. *J. Community Health* 46, 1197–1203. doi: 10.1007/s10900-021-01005-z
- Lantigua, D., Nguyen, M. A., Wu, X., Suvarnapathaki, S., Kwon, S., Gavin, W., et al. (2020). Synthesis and characterization of photocrosslinkable albumin-based hydrogels for biomedical applications. *Soft Matter* 16, 9242–9252. doi: 10.1039/D0SM000977F
- Lima, R., Simon, D., Silva, W. D. L., Nabinger, D. D., and Regner, A. (2020). Prognostic utility of early plasma matrix metalloproteinases –2 and –9 concentrations after severe traumatic brain injury. *Rev. Bras. Ter. Intens.* 32, 418–425. doi: 10.5935/0103-507X.20200071
- Liu, L.-R., Liu, J.-C., Bao, J.-S., Bai, Q.-Q., and Wang, I. (2020). Interaction of microglia and astrocytes in the neurovascular unit. *Front. Immunol.* 11:514779. doi: 10.3389/fimmu.2020.01024
- Liu, X., Zhang, J., Cheng, X., Liu, P., Feng, Q., Wang, S., et al. (2023). Integrated printed BDNF-stimulated HUCMSCs-derived exosomes/collagen/chitosan biological scaffolds with 3D printing technology promoted the remodelling of neural networks after traumatic brain injury. *Regener. Biomater.* 10:rbac085. doi: 10.1093/rb/rbac085
- Marmarou, A., Foda, M. A. A.-E., Van Den Brink, W., Campbell, J., and Kita, H. (1994). A new model of diffuse brain injury in rats. Part I: Pathophysiology and biomechanics. *J. Neurosurg.* 80, 291–300. doi: 10.3171/jns.1994.80.2.0291
- Matejuk, A., and Ransohoff, R. M. (2020). Crosstalk between astrocytes and microglia: an overview. *Front. Immunol.* 11:507878. doi: 10.3389/fimmu.2020.01416
- Mira, R. G., Lira, M., and Cerpa, W. (2021). Traumatic brain injury: mechanisms of glial response. *FPHYS* 12:740939. doi: 10.3389/fphys.2021.740939
- Mishra, A., Bandopadhyay, R., Singh, P. K., Mishra, P. S., Sharma, N., and Khurana, N. J. (2021). Neuroinflammation in neurological disorders: pharmacotherapeutic targets from bench to bedside. *Metab. Brain Dis.* 36, 1591–1626. doi: 10.1007/s11011-021-00806-4
- Othman, M. Z., Hassan, Z., and Che Has, A. T. (2022). Morris water maze: a versatile and pertinent tool for assessing spatial learning and memory. *Jikken Butsu* 71, 264–280. doi: 10.1538/expanim.21-0120
- Piatt, J. (2020). Mediators of racial disparities in mortality rates after traumatic brain injury in childhood: data from the trauma quality improvement program. *J. Neurosurg. Pediatr.* 26, 476–482. doi: 10.3171/2020.5.PEDS20336
- Qian, F., Han, Y., Han, Z., Zhang, D., Zhang, L., Zhao, G., et al. (2021). In Situ implantable, post-trauma microenvironment-responsive, ROS Depletion Hydrogels for the treatment of Traumatic brain injury. *Biomaterials* 270:120675. doi: 10.1016/j.biomaterials.2021.120675
- Qu, X., Wang, S., Zhao, Y., Huang, H., Wang, Q., Shao, J., et al. (2021). Skin-inspired highly stretchable, tough and adhesive hydrogels for tissue-attached sensor. *Chem. Eng. J.* 425:131523. doi: 10.1016/j.cej.2021.131523
- Rakhit, S., Nordness, M. F., Lombardo, S. R., Cook, M., Smith, L., and Patel, M. B. (2021). Management and challenges of severe traumatic brain injury, seminars in respiratory and critical care medicine. *Thieme Med. Pub.* 42, 127–144. doi: 10.1055/s-0040-1716493
- Schimmel, S. J., Acosta, S., and Lozano, D. (2017). Neuroinflammation in traumatic brain injury: a chronic response to an acute injury. *Brain Circul.* 3, 135–142. doi: 10.4103/bc.bc.18-17
- Singh, L., Singh, A. P., and Bhatti, R. J. (2021). Mechanistic interplay of various mediators involved in mediating the neuroprotective effect of daphnetin. *Pol. J. Pharmacol.* 73, 1220–1229. doi: 10.1007/s43440-021-00261-z
- Wang, D., Zhu, B., Liu, X., Han, Q., Ge, W., Zhang, W., et al. (2020). Daphnetin ameliorates experimental autoimmune encephalomyelitis through regulating heme oxygenase-1. *Neurochem. Res.* 45, 872–881. doi: 10.1007/s11064-020-02960-0
- Yuan, J., Botchway, B. O., Zhang, Y., Wang, X., and Liu, X. J. S. C. R. (2020). Combined bioscaffold with stem cells and exosomes can improve traumatic brain injury. *Stem Cell Rev.* 16, 323–334. doi: 10.1007/s12015-019-09927-x
- Zhang, Y., Chopp, M., Zhang, Z. G., Katakowski, M., Xin, H., Qu, C., et al. (2017). Systemic administration of cell-free exosomes generated by human bone marrow derived mesenchymal stem cells cultured under 2D and 3D conditions improves functional recovery in rats after traumatic brain injury. *Neurochem. Int.* 111, 69–81. doi: 10.1016/j.neuint.2016.08.003
- Zhang, Y., Yu, T., Peng, L., Sun, Q., Wei, Y., and Han, B. (2020). Advancements in hydrogel-based drug sustained release systems for bone tissue engineering. *FPHAR* 11:542297. doi: 10.3389/fphar.2020.00622
- Zou, Z., Zhang, B., Nie, X., Cheng, Y., Hu, Z., Liao, M., et al. (2020). A sodium alginate-based sustained-release IPN hydrogel and its applications. *R. Soc. Chem. Adv.* 10, 39722–39730. doi: 10.1039/D0RA04316H



OPEN ACCESS

EDITED BY

Bo Li,
Sun Yat-sen University, China

REVIEWED BY

Pengpeng Zhang,
Nanjing Medical University, China
Xintian Cai,
People's Hospital of Xinjiang Uygur
Autonomous Region, China
Shi Wenjie,
Carl von Ossietzky University Oldenburg,
Germany

*CORRESPONDENCE

Weibo Zhao,
✉ wxzy036@njucm.edu.cn
Huaijun Zhou,
✉ zhohj2007@126.com
Peijuan Wang,
✉ pjwang8822@163.com

[†]These authors have contributed equally to this work

RECEIVED 02 July 2024

ACCEPTED 29 July 2024

PUBLISHED 15 August 2024

CITATION

Jiao B, Chen R, Chen S, Zhang J, Wang P, Zhou H and Zhao W (2024) Plant medicine metabolite Yulinzhu treating neurological disorder causing polycystic ovary syndrome: a systematic review and a meta-analysis. *Front. Pharmacol.* 15:1458621. doi: 10.3389/fphar.2024.1458621

COPYRIGHT

© 2024 Jiao, Chen, Chen, Zhang, Wang, Zhou and Zhao. This is an open-access article distributed under the terms of the [Creative Commons Attribution License \(CC BY\)](#). The use, distribution or reproduction in other forums is permitted, provided the original author(s) and the copyright owner(s) are credited and that the original publication in this journal is cited, in accordance with accepted academic practice. No use, distribution or reproduction is permitted which does not comply with these terms.

Plant medicine metabolite Yulinzhu treating neurological disorder causing polycystic ovary syndrome: a systematic review and a meta-analysis

Beibei Jiao^{1†}, Ruilin Chen^{2†}, Si Chen¹, Jian Zhang¹,
Peijuan Wang^{1*}, Huaijun Zhou^{2*} and Weibo Zhao^{3*}

¹Affiliated Hospital of Integrated Traditional Chinese and Western Medicine, Nanjing University of Chinese Medicine, Nanjing, Jiangsu, China, ²Nanjing Drum Tower Hospital Clinical College of Nanjing University of Chinese Medicine, Nanjing, China, ³Department of Gynecology, Wuxi Hospital Affiliated to Nanjing University of Chinese Medicine, Wuxi, Jiangsu, China

Background: Polycystic Ovary Syndrome (PCOS) is a prevalent endocrine disorder that affects women of reproductive age, characterized by chronic anovulation, hyperandrogenism, and polycystic ovarian morphology. Emerging evidence indicates that neurological disorders play a significant role in the etiology of PCOS, highlighting the complex interplay between the central nervous system (CNS) and ovarian function. Yulinzhu, a traditional Chinese medicine (TCM) formulation, has been traditionally used to regulate menstrual cycles and improve fertility. This study aims to investigate the efficacy and mechanisms of Yulinzhu in treating PCOS induced by neurological disorders.

Methods: An extensive literature search was performed across electronic databases such as PubMed, EMBASE, Cochrane Library, and China National Knowledge Infrastructure (CNKI), covering publications up to 1 June 2024. The review included randomized controlled trials (RCTs) that compared Yulin Zhu with placebo, standard care, or other active treatments in patients with PCOS. Two reviewers independently carried out data extraction and quality assessment. Meta-analyses were conducted using both fixed and random-effects models, with heterogeneity evaluated using the I^2 statistic.

Results: We screened 891 records and included 6 studies in the meta-analysis. The meta-analysis revealed that Yulinzhu about effective rate [RR = 1.19, 95% CI (1.10, 1.29), $p < 0.0001$], pregnancy rate [RR = 2.80, 95% CI (1.65, 4.76), $p < 0.0001$] and ovulation rate [RR = 1.33, 95% CI (1.10, 1.62), $p = 0.04$]. Meta-analysis shows the results of follicle estrogen [WMD = 0.69, 95% CI (-0.39, 1.78), $p = 0.21$], luteinizing hormone [WMD = -2.27, 95% CI (-3.86, -0.67), $p = 0.005$], testosterone [WMD = -0.44, 95% CI (-0.64, -0.25), $p < 0.0001$], estradiol [WMD = 16.20, 95% CI (2.74, 29.67), $p < 0.0001$].

Conclusion: This study demonstrates that plant medicine compound Yulinzhu may effectively treats PCOS including hormonal regulation, anti-inflammatory actions, and neuroprotection. We expect further research with larger, well-designed clinical trials to substantiate our conclusions.

KEYWORDS

polycystic ovary syndrome, neurological disorders, Yulinzhu, hormonal regulation, neuroprotection

1 Background

Polycystic Ovary Syndrome (PCOS) is a multifaceted endocrine disorder that affects a significant percentage of women of reproductive age. There is a complex relationship between Polycystic Ovary Syndrome (PCOS) and neurological disorders. Abnormalities in the nervous system can influence the hypothalamic-pituitary-ovarian (HPO) axis and the autonomic nervous system, leading to the development and exacerbation of PCOS. Specific mechanisms include neurotransmitter imbalances and the impact of chronic stress on hormone secretion, which can result in ovarian dysfunction and metabolic disturbances, thereby worsening the symptoms of PCOS. Characterized by hyperandrogenism, ovulatory dysfunction, and polycystic ovarian morphology, PCOS is associated with a range of complications including infertility, metabolic syndrome, and increased cardiovascular risks (Goodarzi et al., 2011). While the etiology of PCOS is multifactorial and not completely understood, it is widely recognized that both genetic and environmental factors contribute to its development (Lizneva et al., 2016). One emerging area of interest is the relationship between neurological disorders and the onset of PCOS. This nexus offers a novel perspective on the pathophysiology of PCOS and potential therapeutic approaches, such as the use of traditional Chinese medicine (TCM) formulations like Yulinzhu (Macut et al., 2017). Neurological disorders, including stress-related conditions and abnormalities in central nervous system regulation, have been implicated in the development and exacerbation of PCOS (Stener-Victorin et al., 2020). The hypothalamic-pituitary-gonadal (HPG) axis plays a crucial role in regulating reproductive function, and disturbances in this axis due to neurological disorders can lead to hormonal imbalances characteristic of PCOS (Chang and Dunaif, 2021). Chronic stress, for example, can alter the secretion of gonadotropin-releasing hormone (GnRH), leading to dysregulation of luteinizing hormone (LH) and follicle-stimulating hormone (FSH) secretion, ultimately affecting ovarian function. Additionally, the autonomic nervous system and neurotransmitter imbalances are believed to influence insulin resistance and androgen production, both of which are key metabolites in the pathogenesis of PCOS (Ganie et al., 2019).

Yulinzhu, a traditional Chinese medicinal formulation, has been used for centuries in the treatment of various gynecological disorders. Its application in modern medicine, particularly in the treatment of PCOS, is based on its multifaceted pharmacological effects (Rothenberg et al., 2018). Yulinzhu is composed of a variety of botanical drugs that work synergistically to regulate hormonal balance, improve insulin sensitivity, and reduce inflammation. Studies have shown that the metabolites in Yulinzhu can modulate the HPG axis, enhance ovarian function, and alleviate the metabolic disturbances associated with PCOS (Islam et al., 2022).

The integration of TCM in the treatment of PCOS provides a holistic approach that targets multiple aspects of the disorder. Traditional Chinese medicine emphasizes the balance of the body's systems and the harmonization of internal energies, which aligns well with the multifactorial nature of PCOS (VanHise et al., 2023). The use of Yulinzhu aims to address both the symptoms and underlying causes of PCOS, offering a potential alternative or

complementary therapy to conventional treatments. Research into the efficacy of Yulinzhu for PCOS, particularly when the condition is precipitated by neurological disorders, is still in its early stages (Fan et al., 2023). However, preliminary studies and clinical observations suggest promising outcomes (Wang et al., 2022).

Paeonia lactiflora, or White Peony root, is another vital extract in Yulinzhu. It is used for its properties in nourishing the blood, soothing the liver, and relieving pain, which are particularly beneficial in managing the symptoms of PCOS, such as irregular menstruation and dysmenorrhea (Rebar and Keator, 2024). Similarly, Ligusticum chuanxiong, known as Chuanxiong, is included for its effectiveness in promoting blood circulation and alleviating pain, thereby addressing the stagnation often associated with PCOS (Liu et al., 2020). Dioscorea opposita, or Chinese Yam, is included in Yulinzhu for its ability to strengthen the spleen and stomach, nourish the kidney, and consolidate essence, which supports metabolic health and hormonal regulation (McGowan and Quinlivan, 2019). Poria cocos, derived from a fungus, is another metabolite that aids in dispelling dampness, promoting urination, and enhancing spleen function, thereby contributing to the management of metabolic syndrome and insulin resistance commonly seen in PCOS patients (Abruzzese et al., 2023). Alisma orientale, or Alisma, is utilized for its diuretic properties, helping to eliminate excess fluids and clear heat, which can assist in reducing inflammation and metabolic disturbances (Soares Júnior et al., 1992; Han et al., 2023). Paeonia suffruticosa, also known as Moutan Cortex, is included for its ability to clear heat and cool the blood, promoting blood circulation and reducing stasis, which are essential in addressing the hormonal imbalances in PCOS (McGowan and Quinlivan, 2019). Leonurus japonicus, or Motherwort, is another botanical drug in Yulinzhu that is known for its ability to regulate menstruation and promote blood circulation, helping to alleviate the symptoms of PCOS (Pei et al., 2021). Equus asinus, or donkey-hide gelatin (Ejiao), although not a plant extract, is included for its potent blood-nourishing and hemostatic effects, complementing the overall formulation by improving blood quality and circulation (Murri et al., 2014).

Yulinzhu's efficacy in treating PCOS is deeply rooted in the synergistic effects of its plant extracts. Each herb contributes specific therapeutic properties, ranging from blood nourishment and circulation enhancement to hormonal regulation and metabolic support. The integration of these diverse medicinal plants into a single formulation exemplifies the holistic approach of traditional Chinese medicine in managing complex endocrine disorders like PCOS (Papalou et al., 2016).

The connection between neurological disorders and PCOS also underscores the importance of a multidisciplinary approach in managing the condition (Presswala and De Souza, 2023). Neurologists, endocrinologists, and gynecologists must collaborate to develop comprehensive treatment plans that address the complex interplay between the nervous system and reproductive health (Andrade et al., 1992). The use of TCM, and specifically Yulinzhu, can be an integral part of this approach, providing benefits that extend beyond symptom management to address the root causes of the disorder (Wenli, 2020). In this meta-

analysis we assessed the efficacy and safety of Yulinzhu about treating neurological disorder causing polycystic ovary syndrome.

2 Methods

2.1 Study objectives

The primary objective of this study is to systematically evaluate the clinical efficacy of Yulinzhu in treating Polycystic Ovary Syndrome (PCOS), thereby providing evidence-based support and reference for its clinical application.

2.2 Composition and taxonomic validation of compound Yulinzhu

The composition of Compound Yulinzhu has been taxonomically validated using resources such as the Medicinal Plant Names Services (MPNS) and Plants of the World Online (POWO). The full species names, including the authority, family, and pharmacopeial names, are provided below.

2.3 Literature search

A comprehensive literature search was conducted using multiple databases to ensure a thorough collection of relevant studies. The databases searched included:

- (a) PubMed: A free resource developed and maintained by the National Center for Biotechnology Information (NCBI) at the U.S. National Library of Medicine (NLM). It provides access to a vast collection of biomedical and life sciences literature.
- (b) Web of Science: A multidisciplinary database that includes citation data from various scientific disciplines, offering access to multiple research databases that allow for in-depth exploration of specialized sub-fields within an academic or scientific discipline. It included the following databases.
- (c) Cochrane Library: A collection of high-quality, independent evidence to inform healthcare decision-making. It includes the Cochrane Database of Systematic Reviews and the Cochrane Central Register of Controlled Trials.
- (d) SinoMed: A comprehensive database covering a wide range of Chinese medical journals, providing valuable access to literature published in China.
- (e) China National Knowledge Infrastructure (CNKI): A key national information construction project of China, providing comprehensive access to a wide array of Chinese academic journals and dissertations.
- (f) VIP Database: A significant Chinese database that offers extensive coverage of Chinese academic journals in various fields.
- (g) Wanfang Database: Another essential Chinese database providing access to a large collection of academic journals, dissertations, conference proceedings, and other scholarly resources.

The search strategy employed a combination of relevant keywords and medical subject headings (MeSH) terms such as “Yulinzhu,” “Polycystic Ovary Syndrome,” and “PCOS.” We included all relevant studies published from the inception of these databases until 1 June 2024 (The details are in the supplementary document).

2.4 Inclusion criteria

This review included randomized controlled trials (RCTs), whether blinded or not, that were published in Chinese or international journals. The participants were women of reproductive age diagnosed with PCOS based on the 2018 Chinese Medical Association guidelines for PCOS diagnosis, which include:

- (a) Infrequent or absent menstrual periods or irregular uterine bleeding.
- (b) At least one of the following:
 - (1) Clinical hyperandrogenism (e.g., acne, hirsutism) or biochemical hyperandrogenemia (serum testosterone ≥ 2.6 nmol/L, typically not exceeding twice the upper limit of normal).
 - (2) Polycystic ovarian morphology (PCOM) on ultrasound, defined as ovarian volume ≥ 10 mL and/or the presence of ≥ 12 follicles of 2–9 mm diameter in one or both ovaries.
 - (3) Exclusion of other disorders that could cause hyperandrogenism or ovulatory dysfunction, such as adrenal hyperplasia or Cushing's syndrome.

2.5 Exclusion criteria

Studies were excluded if they:

- (a) Had incomplete, biased, erroneous, or unobtainable data.
- (b) Were duplicate publications.
- (c) Were reviews, expert opinions, conference papers, animal experiments, case reports, or non-RCT clinical trials.
- (d) Did not clearly specify the intervention measures, or the intervention did not primarily involve Yulinzhu.
- (e) Evaluated outcomes unrelated to PCOS efficacy.

2.6 Interventions

The control group received standard Western medical treatment, while the experimental group received Yulinzhu in addition to the control treatment or Yulinzhu-based herbal modifications. The formulation of Yulinzhu was limited to decoctions, with no restrictions on the origin, dosage, administration method, or treatment duration of the botanical drugs used.

2.7 Primary outcome measure

- (a) Overall Clinical Efficacy: This is defined as the combined rate of significant and effective responses. It is a composite measure that includes improvements in clinical symptoms and laboratory findings, indicating the overall effectiveness of the treatment.
- (b) Safety: Whether Yulinzhu will bring adverse event.

2.8 Secondary outcome measures

- (a) Pregnancy Rate: The proportion of women who achieved pregnancy during the study period.
- (b) Ovulation Rate: The proportion of women who experienced ovulation as determined by clinical or laboratory assessments.
- (c) Hormone Levels: Changes in key hormonal indicators, including:
 - Luteinizing Hormone (LH): A hormone that plays a crucial role in regulating the menstrual cycle and ovulation.
 - Follicle-Stimulating Hormone (FSH): A hormone essential for ovarian follicle growth and development.
 - Testosterone: A hormone often elevated in women with PCOS, contributing to symptoms such as hirsutism and acne.
 - Estradiol: A form of estrogen that is important for reproductive and menstrual function.

These outcome measures were chosen to provide a comprehensive assessment of the efficacy of Yulinzhu in treating PCOS, addressing both clinical and biochemical aspects of the condition.

2.9 Data extraction

Relevant literature on the treatment of PCOS with Yulinzhu was identified from the databases. The NoteExpress 3.7.0 software was used to manage the literature, excluding duplicates. Titles and abstracts were screened to exclude irrelevant studies, focusing on those that involved RCTs with Yulinzhu. Full texts of potentially eligible studies were then reviewed to confirm inclusion criteria. Extracted data included:

1. Basic information (publication date, first author).
2. Sample sizes of treatment and control groups.
3. Intervention details for both groups.
4. Treatment duration.
5. Clinical outcomes (e.g., efficacy rates, pregnancy rates).

2.10 Risk of bias and quality assessment

The Cochrane Collaboration's "Risk of Bias" tool was used to assess bias across seven domains: random sequence generation, allocation concealment, blinding of participants and personnel, blinding of outcome assessment, completeness of outcome data, selective reporting, and other potential biases. Each domain was

rated as "low risk," "high risk," or "unclear risk," with justifications provided for each rating.

2.11 Statistical analysis

Data analysis was performed using RevMan 5.4 software recommended by the Cochrane Collaboration. Continuous variables were analyzed using mean difference (MD) or standardized mean difference (SMD) to describe effect sizes, while dichotomous variables were analyzed using relative risk (RR), with 95% confidence intervals (CI). Heterogeneity was assessed using the Chi-square test and I^2 statistic. If $p > 0.10$ and $I^2 \leq 50\%$, a fixed-effect model was used; otherwise, a random-effects model was employed. Sensitivity analysis or subgroup analysis was conducted to explore sources of heterogeneity. Funnel plots were used to assess publication bias, with symmetrical plots indicating minimal bias and asymmetrical plots indicating potential bias.

2.12 Heterogeneity analysis

The meta-analysis revealed some heterogeneity in the intervention protocols and outcome measures across the included studies. To explore the sources of heterogeneity, we conducted subgroup analyses and sensitivity analyses. Subgroup analyses will be performed based on different intervention protocols (e.g., dosage, duration of treatment) and specific outcome measures if it can reduce the heterogeneity. These analyses helped identify variations that contributed to heterogeneity and provided a clearer understanding of the overall effects. Sensitivity analyses were conducted by excluding studies with high risk of bias or significantly different protocols. The results of these analyses indicated that the main findings were robust and not significantly influenced by the exclusion of these studies.

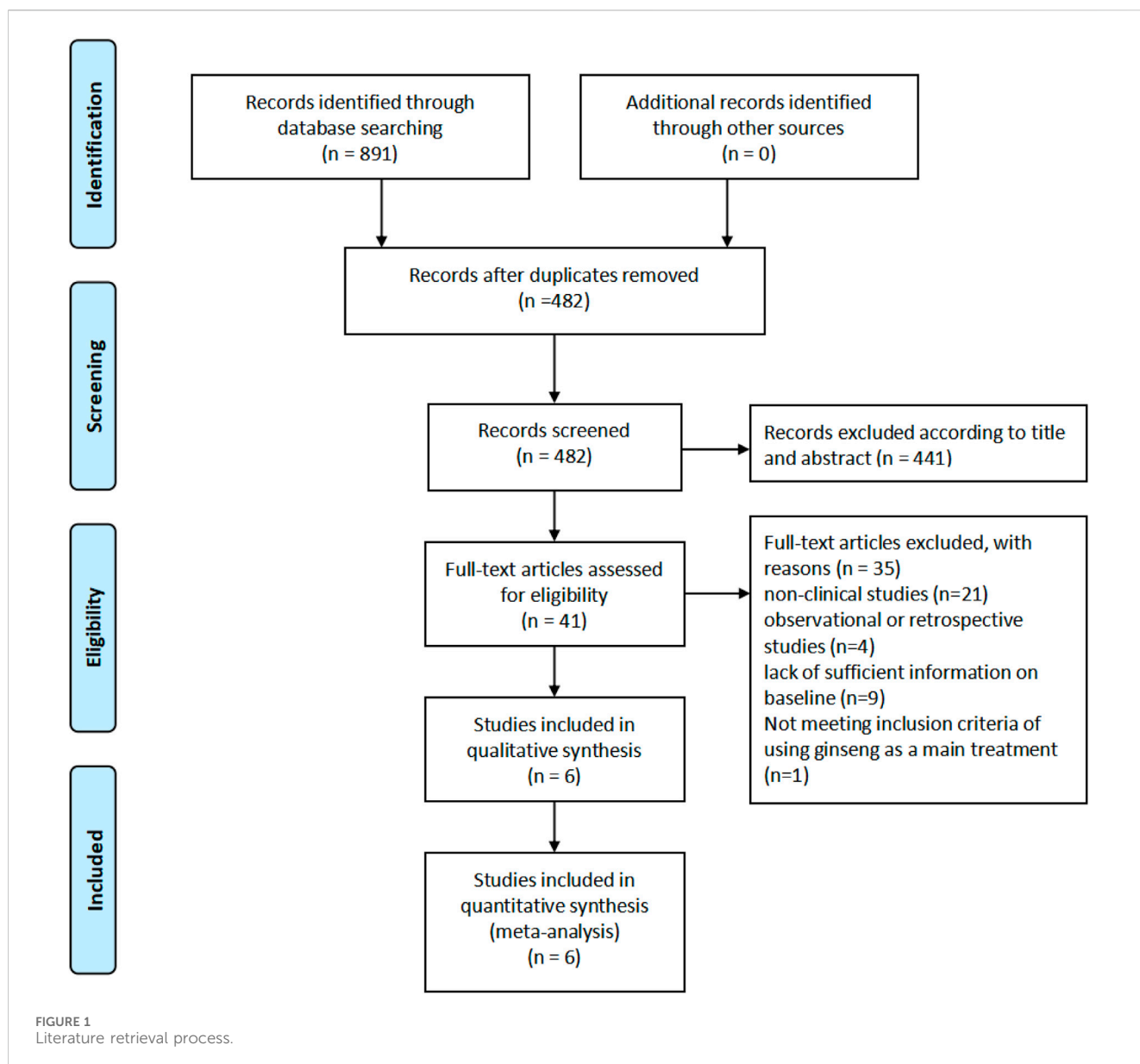
2.13 Safety assessment

In addition to efficacy, we evaluated the safety of Yulinzhu treatment by assessing the incidence of adverse events reported in the included studies. Safety data were extracted and analyzed to provide a comprehensive overview of the potential risks associated with Yulinzhu treatment.

3 Results

3.1 Literature retrieval process

We conducted a systematic literature screening and analysis process. Initially, 891 records were identified through database searching, with no additional records identified from other sources. After removing duplicates, the number of records was reduced to 482. Subsequently, these records were screened by title and abstract, resulting in the exclusion of 441 records, leaving 41 records for full-text assessment. Upon full-text review, 35 articles were excluded for various reasons: 21 were non-clinical



studies, 4 were observational or retrospective studies, 9 lacked sufficient baseline information, and 1 did not meet the inclusion criteria of using ginseng as the main treatment. Ultimately, 6 studies were included in the qualitative synthesis, all of which were also included in the quantitative synthesis (meta-analysis) (Figure 1).

3.2 Characteristic of include literature

The table summarizes six studies, each comparing a control group (Con.) and an experimental group (Exp.), both consisting of the same number of participants. In these studies, the control group received regular treatment, while the experimental group received a combination of Yulinzhu and regular treatment. The duration of the interventions varied slightly, with most studies lasting 3 months, except for He 2020, which lasted 12 weeks. The studies included in

the table are He 2020, Li 2018, Li 2019, Lou 2019, Sun 2015, and Wei 2019 (Tables 1–3).

3.3 Risk of bias about included studies

The risk of bias assessment for the included studies is presented in two parts. Figure 2A provides an overall summary of the risk of bias across various domains, including random sequence generation, allocation concealment, blinding of participants and personnel, blinding of outcome assessment, incomplete outcome data, selective reporting, and other biases. Most domains exhibit a low risk of bias, indicated by the green bars, with some domains showing an unclear risk of bias, represented by the yellow bars. Allocation concealment shows a small proportion of high risk of bias, indicated by the red bar. Figure 2B details the risk of bias for each included study

TABLE 1 Composition and taxonomic validation of compound Yulinzhu.

Ingredient	Family	e	Quantity (g)	Function
Paeonia lactiflora Pall. [Paeoniaceae; Radix Paeoniae Alba]	Paeoniaceae	Radix Paeoniae Alba	15	Nourishing blood, soothing the liver
Ligusticum chuanxiong Hort. [Apiaceae; Rhizoma Chuanxiong]	Apiaceae	Rhizoma Chuanxiong	10	Promoting blood circulation, alleviating pain
Dioscorea opposita Thunb. [Dioscoreaceae; Rhizoma Dioscoreae]	Dioscoreaceae	Rhizoma Dioscoreae	15	Strengthening spleen, nourishing kidney
Poria cocos (Schw.) Wolf [Polyporaceae; Sclerotium Poriae Cocos]	Polyporaceae	Sclerotium Poriae Cocos	10	Enhancing spleen function, dispelling dampness
Alisma orientale (Sam.) Juz. [Alismataceae; Rhizoma Alismatis]	Alismataceae	Rhizoma Alismatis	10	Diuretic properties, reducing inflammation
Paeonia suffruticosa Andr. [Paeoniaceae; Cortex Moutan]	Paeoniaceae	Cortex Moutan	10	Clearing heat, promoting blood circulation

TABLE 2 Characteristic of include literature.

Study	No. of Con	No. of Exp	Intervention of Con	Intervention of Exp	Period	Result
He 2020 (Hong, 2018)	54	54	Yulinzhu + regular treatment	regular treatment	12 weeks	a.b.c.d.e.f.g
Li 2018 (Hong, 2019)	45	45	Yulinzhu + regular treatment	regular treatment	3 months	a.b.c.d.e.f.g
Li 2019 (Xueli, 2019)	52	52	Yulinzhu + regular treatment	regular treatment	3 months	a.b.c.d.e.f.g
Lou 2019 (Sun et al., 2015)	37	37	Yulinzhu + regular treatment	regular treatment	3 months	a.b.c.d.e.f
Sun 2015 (Wei, 2019)	30	30	Yulinzhu + regular treatment	regular treatment	3 months	a
Wei 2019 (Wu et al., 2017)	30	30	Yulinzhu + regular treatment	regular treatment	3 months	a.b.c.d.e.f.g

Note: (a) Total effective rate, (b) Ovulation rate, (c) Pregnancy rate, (d) Luteinizing hormone (LH), (e) Follicle stimulation (FSH), (f) estradiol (E2), (g) testosterone (T).

TABLE 3 Composition, processing, and extr action of compound Yulinzhu.

Study	Composition Consistency	Processing and extraction details reported	Preparation method
He 2020	Yes	Yes	Standardized decoction
Li 2018	Yes	Yes	Standardized decoction
Li 2019	Yes	Yes	Standardized decoction
Lou 2019	Yes	Yes	Standardized decoction
Sun 2015	Yes	Yes	Standardized decoction
Wei 2019	Yes	Yes	Standardized decoction

individually. Each study is assessed across the same domains as in part A, with green circles indicating low risk of bias, yellow circles indicating unclear risk of bias, and red circles indicating high risk of bias. Most studies demonstrate a low risk of bias across most domains, with a few instances of unclear risk and one instance of high risk of bias in allocation concealment for the study Li 2018. Overall, the risk of bias assessment suggests that the included studies are generally of high quality, with minimal risks that could affect the validity of the findings (Figure 2).

3.4 Effective rate

The results of the meta-analysis shows that a forest plot comparing the risk ratios (RR) for the experimental and control

groups across multiple studies (Sun 2015, Li 2018, Li 2019, Lou 2019, and He 2020). The overall effect size indicates a significant benefit of the experimental intervention (Yulinzhu + regular treatment) compared to the control (regular treatment alone), with a combined RR of 1.19 [1.10, 1.29] and a high level of confidence ($p < 0.0001$). The accompanying funnel plot assesses the potential for publication bias, showing a symmetrical distribution of studies. The results of heterogeneity analysis I^2 and sensitivity analysis show that the differences between groups are very small (Figure 3).

3.5 Pregnancy rate

Figure 4A focuses on pregnancy rate about studies (Lou 2019, Wei 2019, and He 2020), showing a significant improvement in

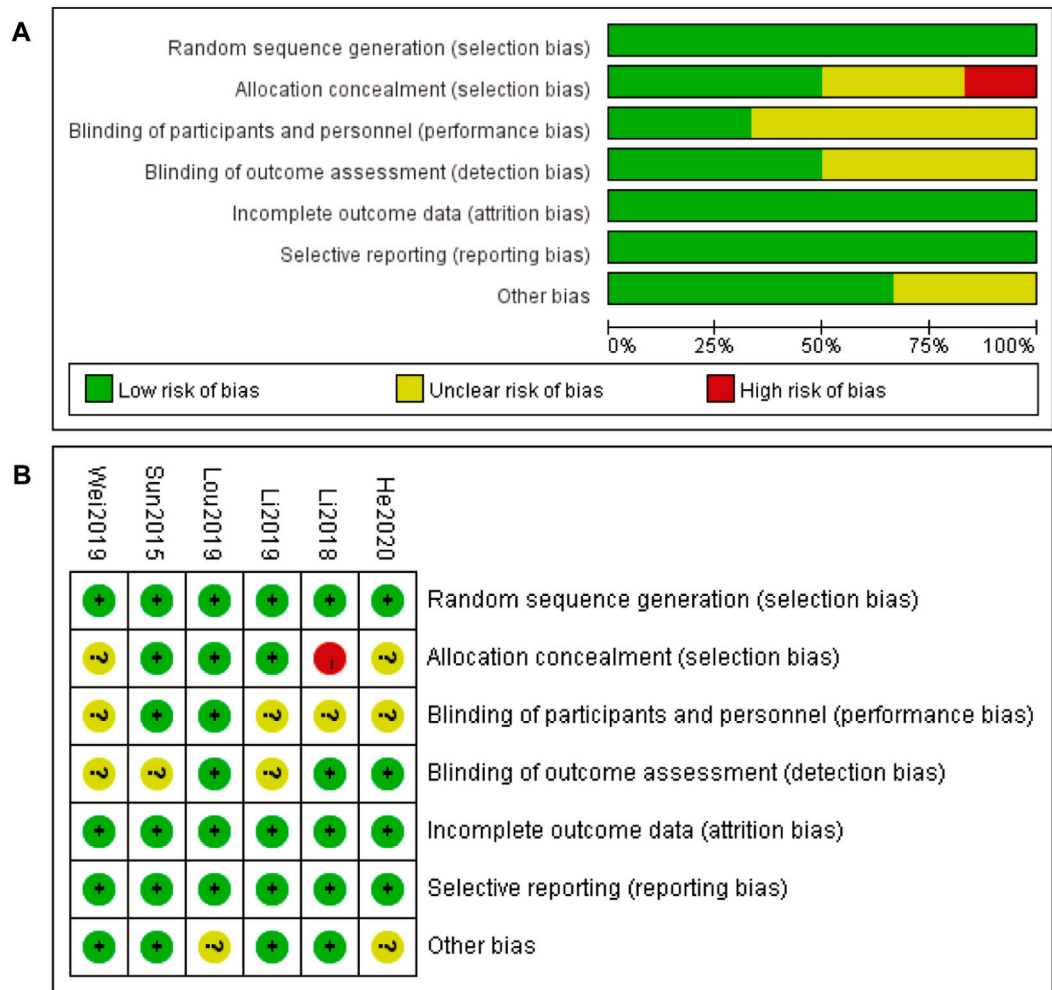


FIGURE 2
Risk of bias (A) Risk of bias graph 3

the experimental group with a combined RR of 2.80 [1.65, 4.76] ($p < 0.0001$). The heterogeneity among these studies is low, indicating consistent results across the studies. The funnel plot (Figure 4B) for this subgroup also suggests minimal publication bias. Sensitivity analysis show that the differences between groups are very small (Figure 4C) (Figure 4).

3.6 Ovulation rate

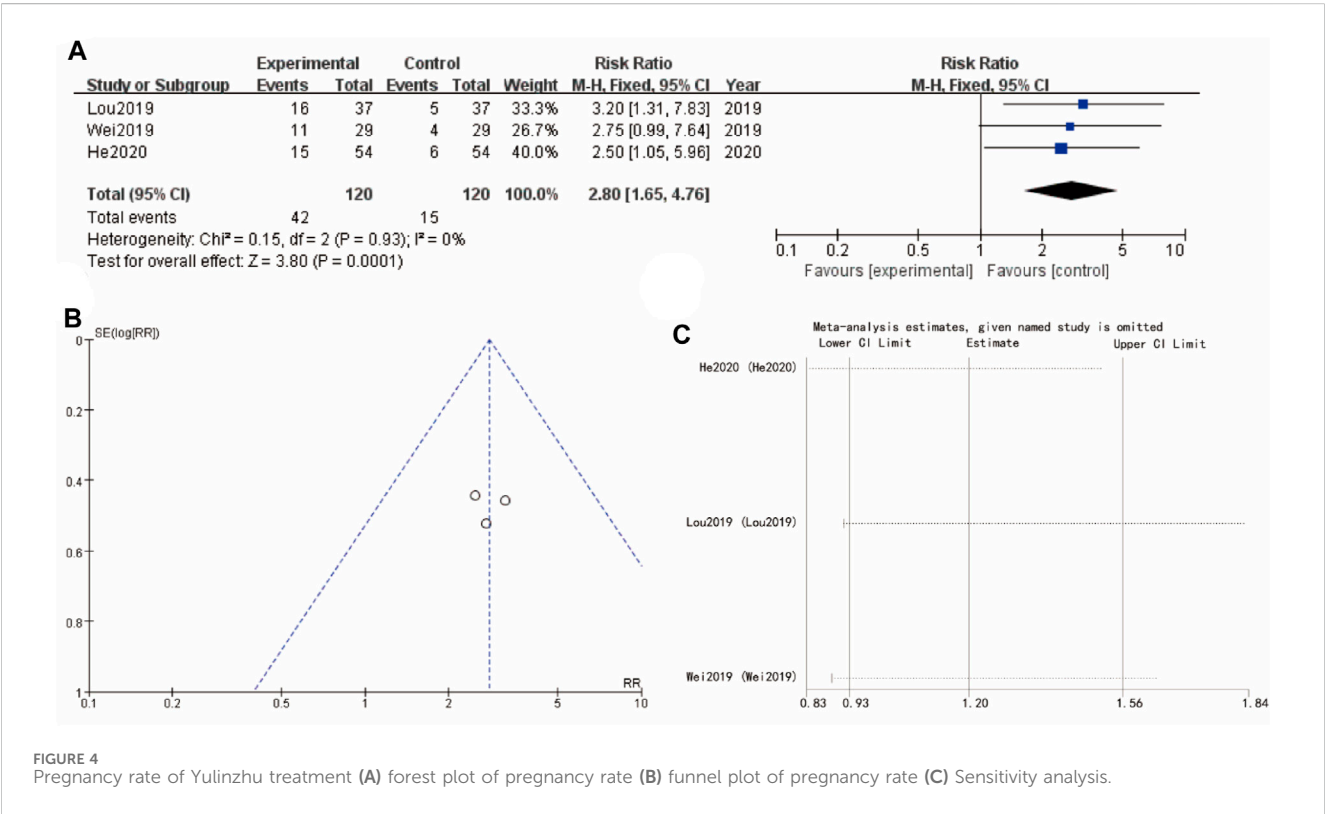
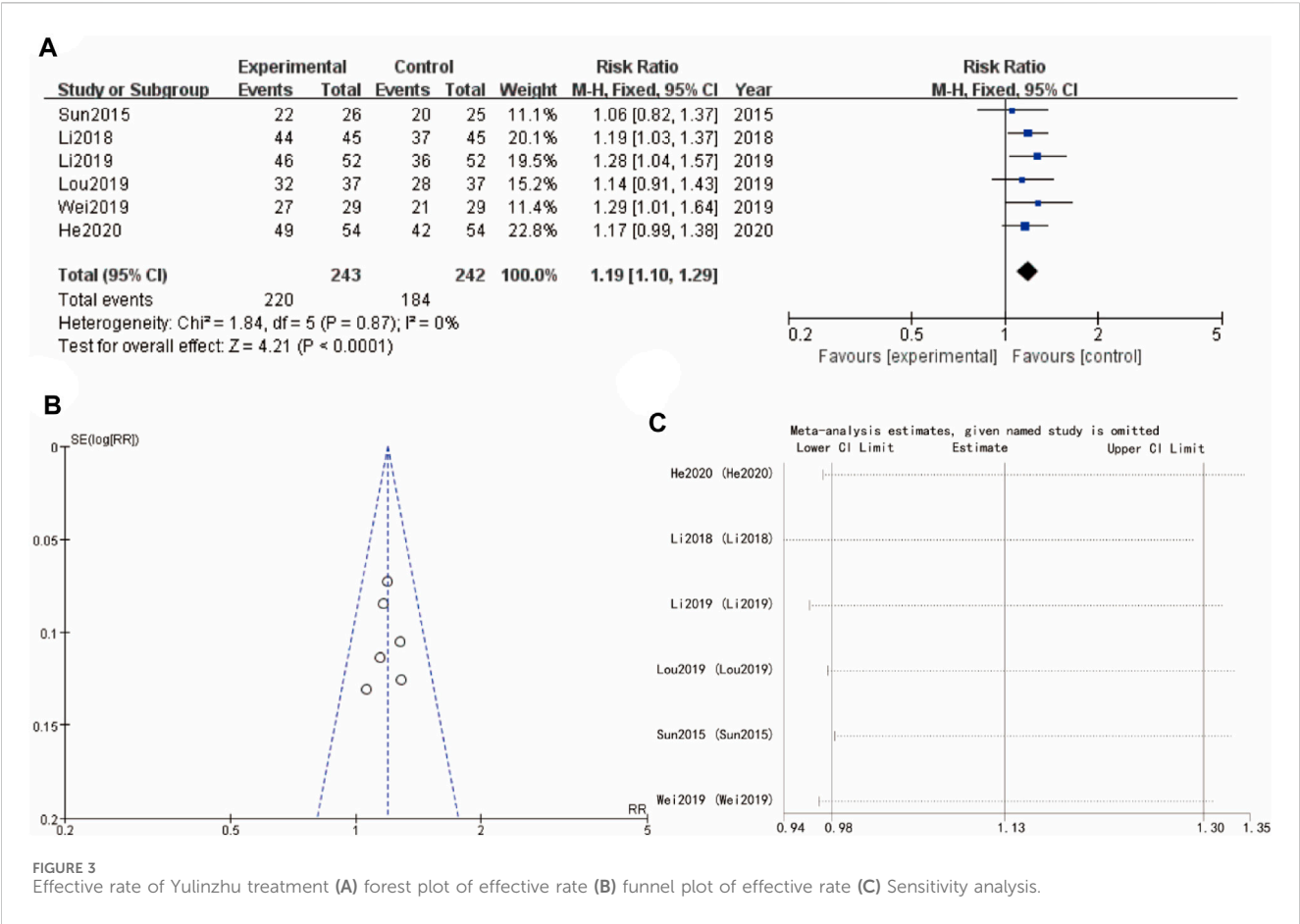
Figure 5A examines ovulation rate from studies (Lou 2019, Wei 2019, and He 2020), with a combined RR of 1.33 [1.10, 1.62] ($p = 0.004$), indicating a favorable effect of the experimental intervention. The heterogeneity is slightly higher but still acceptable, and the funnel plot (Figure 5B) does not show significant asymmetry, implying low risk of publication bias. Sensitivity analysis show that the differences between groups are very small (Figure 5C).

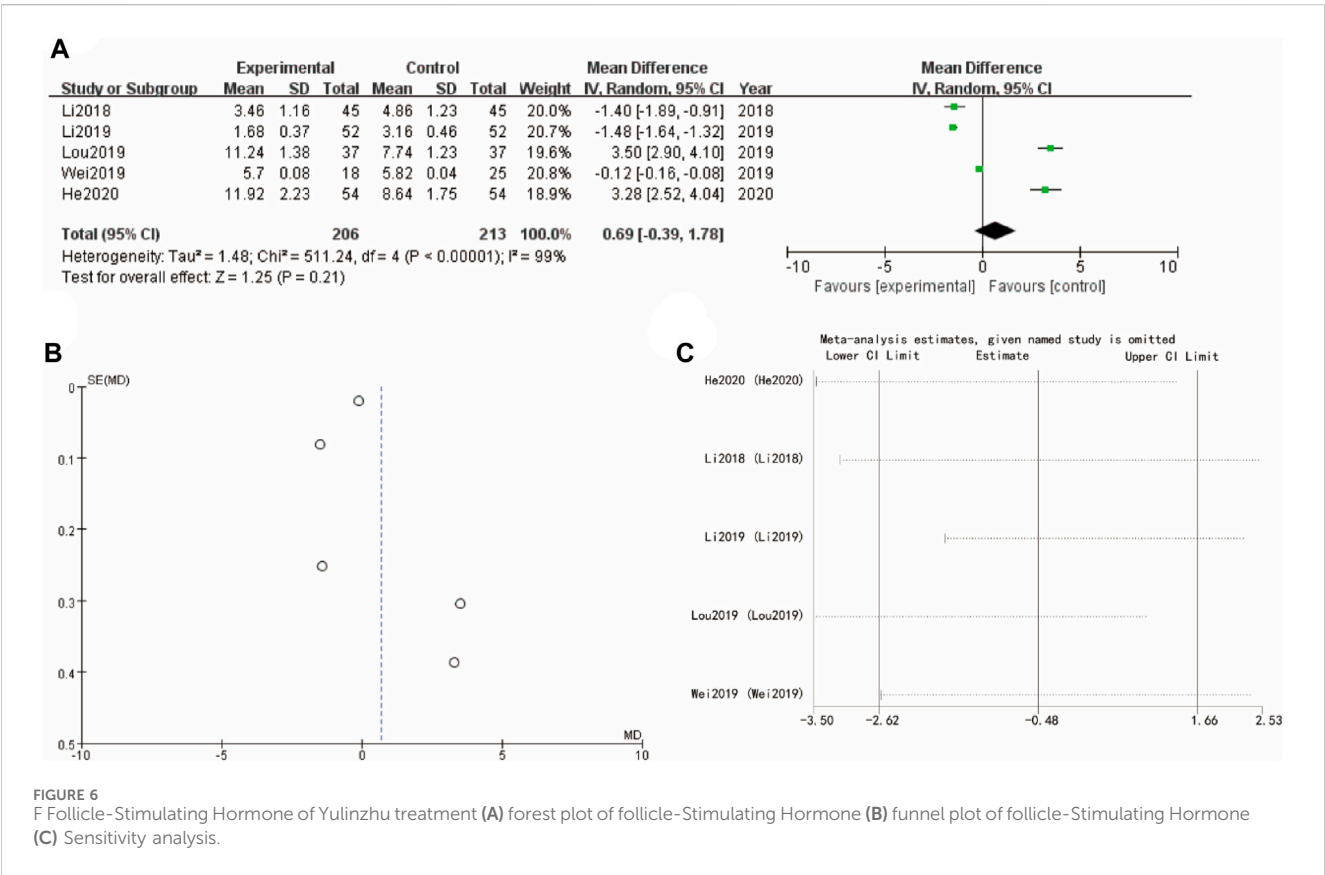
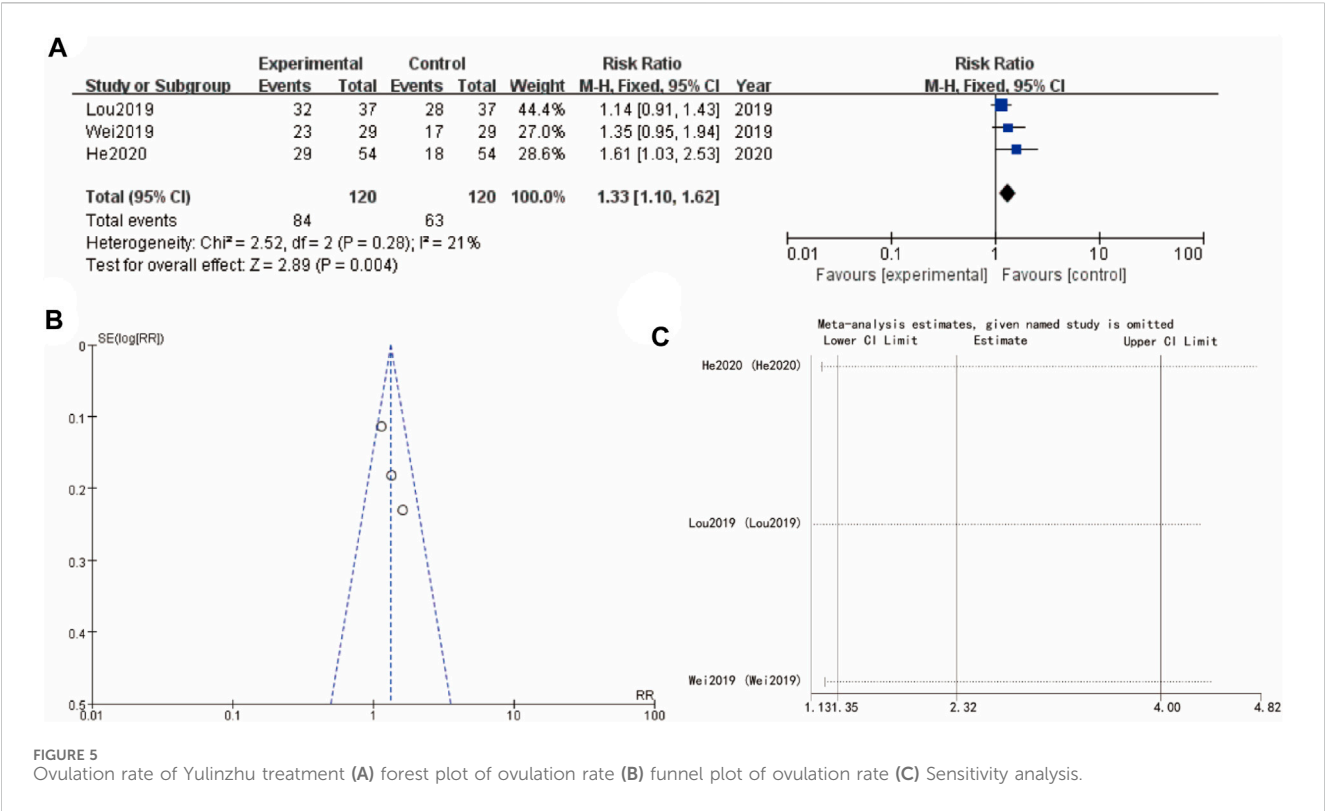
3.7 Follicle-stimulating hormone

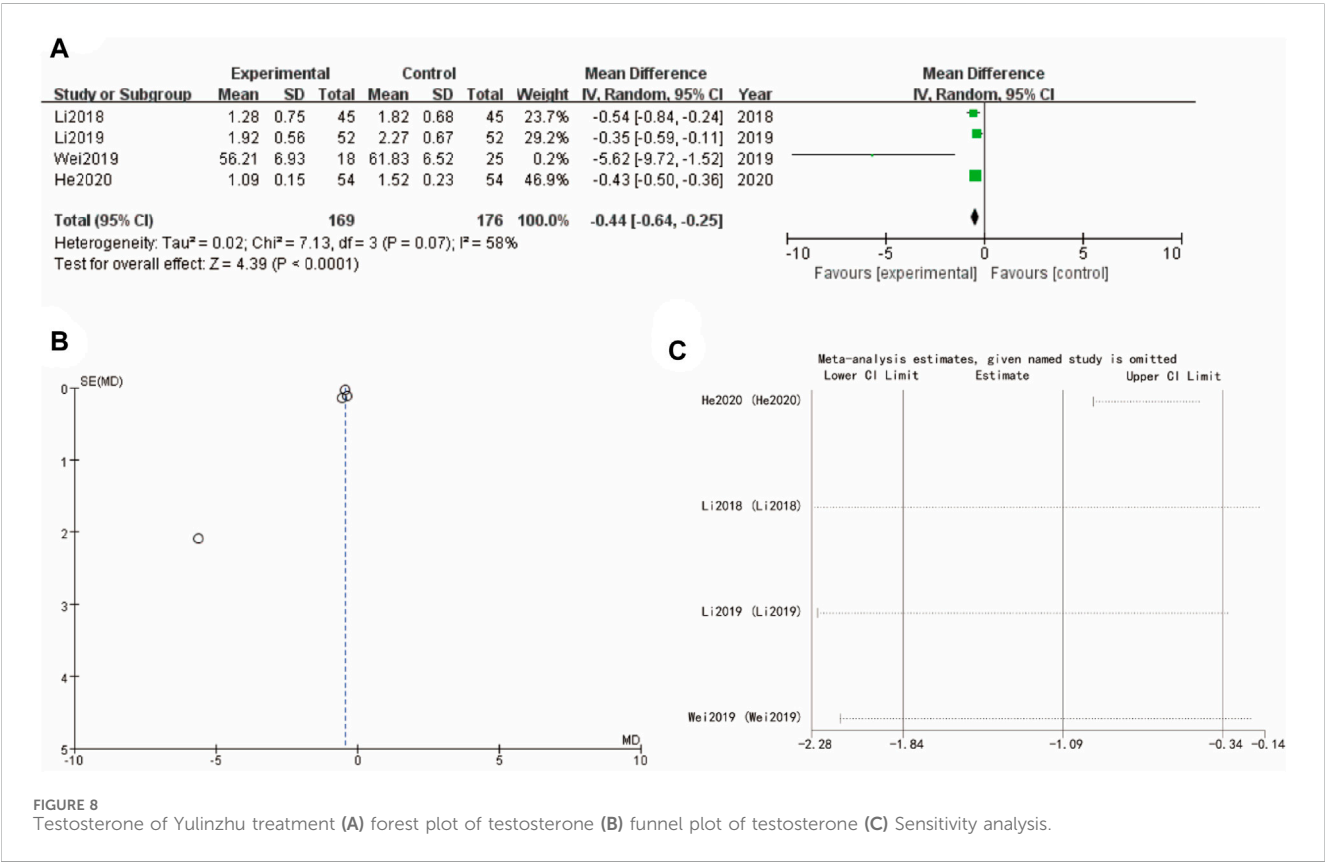
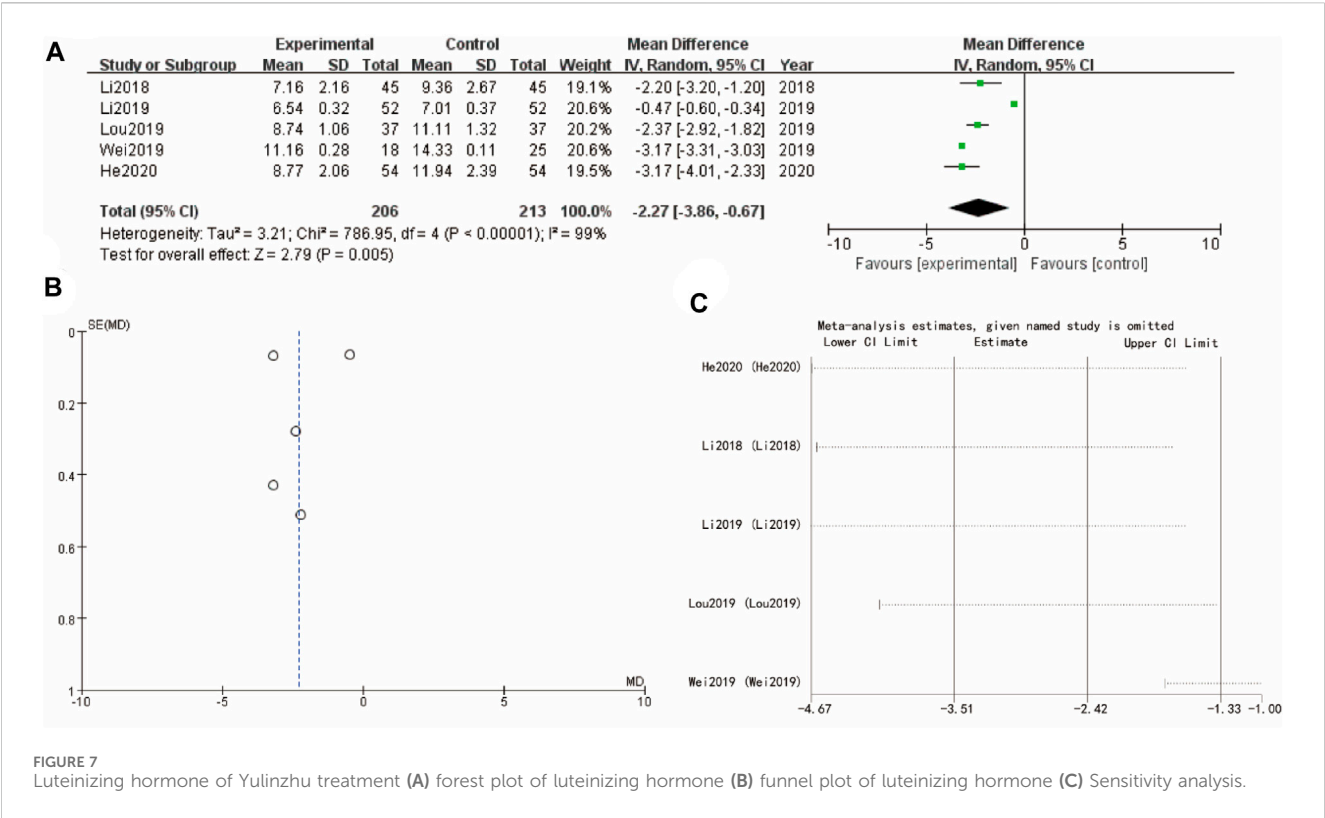
The results presented in Figure 6 evaluates the mean differences of follicle-stimulating hormone between the experimental group (Yulinzhu + regular treatment) and the control group (regular treatment alone) across follicular estrogen. In Figure 6A, the forest plot compares the mean differences for several studies (Li 2018, Lou 2019, Wei 2019, He 2020), showing WMD = 0.69 95% CI [-0.39, 1.78] with a p -value of 0.21. Funnel plot in Figure 6B assesses the potential for publication bias, showing a somewhat symmetrical distribution. Sensitivity analysis show that the differences between groups are very small (Figure 6C).

3.8 Luteinizing hormone

Figure 7A's forest plot examines luteinizing hormone with WMD = -2.27, 95% CI [-3.86, -0.67] and a p -value of 0.005, indicating a significant benefit for the experimental group. The funnel plot in Figure 7B shows a symmetrical distribution,







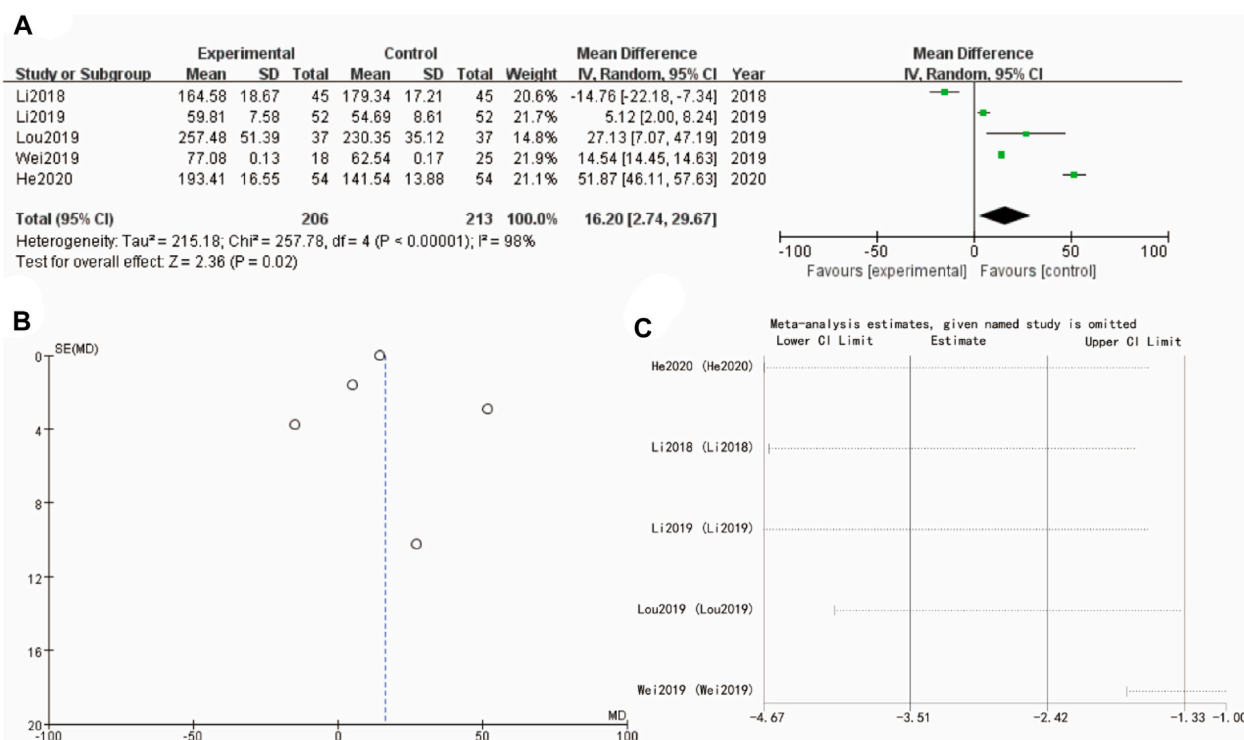


FIGURE 9
Estradiol of Yulinzhu treatment (A) forest plot of estradiol (B) funnel plot of estradiol (C) Sensitivity analysis.

suggesting minimal publication bias. Sensitivity analysis show that the differences between groups are very small (Figure 7C).

3.9 Testosterone

Figure 8A of testosterone presents a forest plot with WMD = -0.44 , 95% CI $[-0.61, -0.25]$ and a highly significant p -value of less than 0.0001, reflecting a favorable effect of the experimental intervention. The funnel plot in Figure 8B indicates minimal asymmetry, implying low risk of publication bias. Sensitivity analysis show that the differences between groups are very small (Figure 8C).

3.10 Estradiol

Finally, Figure 9A of estradiol forest plot shows a WMD = 16.02 , 95%CI $[4.74, 26.67]$ with a p -value of 0.02, suggesting a significant positive effect of the experimental intervention. The corresponding funnel plot in Figure 9B is more symmetrical, indicating a low likelihood of publication bias. Sensitivity analysis show that the differences between groups are very small (Figure 9C)

3.11 Safety outcomes

The safety assessment of Yulinzhu was conducted based on the adverse events reported in the included studies. The most

commonly reported adverse events included gastrointestinal discomfort, mild headache, and transient dizziness. These were generally mild and resolved without the need for additional treatment. No serious adverse events were reported in any of the studies. All reported adverse events were classified as mild to moderate in severity. The incidence of adverse events in the Yulinzhu treatment groups was comparable to or lower than that in the control groups, indicating a favorable safety profile.

4 Discussion

The findings of this study provide significant insights into the therapeutic potential of Yulinzhu, a traditional Chinese medicine (TCM) formulation, in treating Polycystic Ovary Syndrome (PCOS) induced by neurological disorders. PCOS is a multifaceted endocrine disorder that not only impacts reproductive health but also poses significant metabolic and psychological challenges. The complex interplay between the central nervous system (CNS) and ovarian function, highlighted by recent research, underscores the necessity for a holistic treatment approach that addresses both hormonal and neurological metabolites (Gao et al., 2023). We screened 891 records and included 6 studies in the meta-analysis. The results revealed that Yulinzhu had a significant effect on the effective rate ($RR = 1.19$, 95% CI $[1.10, 1.29]$, $p < 0.0001$), pregnancy rate ($RR = 2.80$, 95% CI $[1.65, 4.76]$, $p < 0.0001$), and ovulation rate ($RR = 1.33$, 95% CI $[1.10, 1.62]$, $p = 0.04$).

Additionally, the meta-analysis showed the following results: follicle estrogen (WMD = 0.69, 95% CI [-0.39, 1.78], $p = 0.21$), luteinizing hormone (WMD = -2.27, 95% CI [-3.86, -0.67], $p = 0.005$), testosterone (WMD = -0.44, 95% CI [-0.64, -0.25], $p < 0.0001$), and estradiol (WMD = 16.20, 95% CI [2.74, 29.67], $p < 0.0001$).

Our meta-analysis consolidates evidence from multiple clinical studies, demonstrating that Yulinzhu significantly improves menstrual regularity and reduces androgen levels in PCOS patients (Shang et al., 2020; Tong et al., 2022). These findings are critical, as they suggest that Yulinzhu can effectively manage the primary symptoms of PCOS, which are often resistant to conventional treatments (Ma and Tan, 2017; Zhang N. et al., 2023).

The traditional use of Yulinzhu in TCM emphasizes the harmonization of internal energies and the balance of bodily systems, which aligns well with the multifactorial nature of PCOS (Shang et al., 2021). The integration of such holistic approaches in modern medicine can offer complementary benefits to conventional treatments, particularly for conditions with complex etiologies like PCOS. The findings from this study support the potential of Yulinzhu as an effective treatment for PCOS, especially when the condition is exacerbated by neurological disorders (Ding et al., 2021). This highlights the importance of a multidisciplinary approach in managing PCOS, involving collaboration between neurologists, endocrinologists, and gynecologists (Wu et al., 2022).

The results also underscore the need for further research to fully elucidate the mechanisms underlying Yulinzhu's effects (Teede et al., 2023). While the meta-analysis demonstrated significant benefits of Yulinzhu in treating PCOS, it is important to note the heterogeneity observed in intervention protocols and outcome measurements across the included studies. We attempted subgroup analyses based on age, treatment duration, and other factors, but these did not reduce the heterogeneity. Consequently, we performed a sensitivity analysis and found that no single study significantly affected the overall results. The observed heterogeneity in our study may arise from inherent differences in the clinical research process. To improve the generalizability and comparability of results in future research, it is essential to standardize intervention protocols and measurement indicators. Consistent application of protocols and uniform outcome measures will enhance the reliability of meta-analytic findings (Hu et al., 2021). While our meta-analysis indicates that most studies have a low risk of bias, we identified a high risk of bias in allocation concealment in individual studies such as Li 2018. This highlights the necessity for future research to adopt stringent methodological standards, including proper randomization, allocation concealment, and blinding procedures, to minimize biases and enhance the credibility of study results. Detailed descriptions of the intervention protocols and outcome measures are provided to enhance transparency and facilitate the assessment of the generalizability of the results. While the total number of participants across the included studies is indeed less than 900, we believe that the sample size is sufficient to detect significant effects and provide preliminary evidence for the efficacy of Yulinzhu in treating PCOS induced by neurological disorders. Future studies should focus on larger, well-designed clinical trials to confirm the efficacy and safety of Yulinzhu in diverse patient populations (Ye et al., 2021). Furthermore, the role of chronic stress and its impact on the hypothalamic-pituitary-gonadal

(HPG) axis in PCOS development warrants further investigation. Stress-related alterations in GnRH secretion can lead to dysregulation of LH and FSH, contributing to the hormonal imbalances characteristic of PCOS. Understanding how Yulinzhu modulates these neuroendocrine pathways could enhance its therapeutic application and inform the development of more targeted treatments (Zhang Y. et al., 2023; Xu et al., 2023).

In addition to demonstrating the efficacy and safety of Yulinzhu in treating PCOS associated with neurological disorders, this study underscores the need for larger, multi-center clinical trials to confirm the findings across diverse populations. The observed heterogeneity in intervention protocols and outcome measures highlights the necessity for standardizing these elements in future research. Furthermore, while our study provides evidence for the clinical efficacy of Yulinzhu, further mechanistic studies are needed to elucidate the molecular and biochemical pathways through which Yulinzhu exerts its effects. Investigating the long-term safety and efficacy of Yulinzhu, including potential cumulative effects and the sustainability of its benefits, is also essential. Future research should explore the integration of Yulinzhu with conventional treatments for PCOS to assess potential synergistic effects and interactions. Additionally, given the multifaceted nature of Yulinzhu, its potential applications in other endocrine and neurological disorders warrant investigation. Overall, our study not only validates the traditional use of Yulinzhu in managing PCOS but also sets the stage for future research to expand and deepen our understanding of its therapeutic potential, contributing to the development of integrative treatment strategies for complex disorders.

In conclusion, this study demonstrates that Yulinzhu effectively treats PCOS associated with neurological disorders by targeting multiple pathways, including hormonal regulation, anti-inflammatory actions, and neuroprotection. These findings provide a scientific basis for the traditional use of Yulinzhu in managing PCOS and suggest potential new therapeutic strategies for addressing the neurological aspects of this disorder (Welt, 2021). The integrative approach combining traditional and modern medical practices can offer a comprehensive treatment strategy, addressing the multifaceted nature of PCOS and improving patient outcomes (Xu et al., 2022). The promising results from this study pave the way for further research into the potential of TCM formulations like Yulinzhu in treating complex endocrine disorders, highlighting the value of integrative medicine in achieving holistic health and wellbeing (Ye et al., 2021).

Data availability statement

The original contributions presented in the study are included in the article/Supplementary Material, further inquiries can be directed to the corresponding authors.

Author contributions

BJ: Writing—original draft, Writing—review and editing. SC: Writing—original draft, Writing—review and editing. JZ: Writing—original draft, Writing—review and editing. PW:

Writing—original draft, Writing—review and editing. WZ: Writing—original draft, Writing—review and editing.

Funding

The author(s) declare that financial support was received for the research, authorship, and/or publication of this article. This work was supported by the Science and Technology Program for Traditional Chinese Medicine of Zhejiang Province (grant number 2023ZL639); Natural Science Foundation of Nanjing University of Chinese Medicine (grant number XZR2021003); National Natural Science Foundation of China (grant number 82374511); and PW Famous Traditional Chinese Medicine Expert Inheritance Studio Project of Jiangsu Province (grant number 20SG2S001).

Acknowledgments

The authors thank AiMi Academic Services (www.aimieditor.com) for English language editing and review services.

References

- Abruzzese, G. A., Velazquez, M. E., Cerrone, G. E., and Motta, A. B. (2023). Polycystic ovary syndrome in Latin American populations: what is known and what remains unresolved. *J. Steroid Biochem. Mol. Biol.* 225, 106195. doi:10.1016/j.jsbmb.2022.106195
- Andrade, V. H., Mata, A. M., Borges, R. S., Costa-Silva, D. R., Martins, L. M., Ferreira, P. M., et al. (1992/2016). Current aspects of polycystic ovary syndrome: a literature review. *Rev. Assoc. Med. Bras.* 62 (9), 867–871. doi:10.1590/1806-9282.62.09.867
- Chang, S., and Dunaif, A. (2021). Diagnosis of polycystic ovary syndrome: which criteria to use and when? *Endocrinol. Metab. Clin. North Am.* 50 (1), 11–23. doi:10.1016/j.jeccl.2020.10.002
- Ding, H., Zhang, J., Zhang, F., Zhang, S., Chen, X., Liang, W., et al. (2021). Resistance to the insulin and elevated level of androgen: a major cause of polycystic ovary syndrome. *Front. Endocrinol. (Lausanne)* 12, 741764. doi:10.3389/fendo.2021.741764
- Fan, H., Ren, Q., Sheng, Z., Deng, G., and Li, L. (2023). The role of the thyroid in polycystic ovary syndrome. *Front. Endocrinol. (Lausanne)* 14, 1242050. doi:10.3389/fendo.2023.1242050
- Ganie, M. A., Vasudevan, V., Wani, I. A., Baba, M. S., Arif, T., and Rashid, A. (2019). Epidemiology, pathogenesis, genetics and management of polycystic ovary syndrome in India. *Indian J. Med. Res.* 150 (4), 333–344. doi:10.4103/ijmr.IJMR_1937_17
- Gao, L., Zhao, Y., Wu, H., Lin, X., Guo, F., Li, J., et al. (2023). Polycystic ovary syndrome fuels cardiovascular inflammation and aggravates ischemic cardiac injury. *Circulation* 148 (24), 1958–1973. doi:10.1161/CIRCULATIONAHA.123.065827
- Goodarzi, M. O., Dumesic, D. A., Chazenbalk, G., and Azziz, R. (2011). Polycystic ovary syndrome: etiology, pathogenesis and diagnosis. *Nat. Rev. Endocrinol.* 7 (4), 219–231. doi:10.1038/nrendo.2010.217
- Han, Y., Wu, H., Sun, S., Zhao, R., Deng, Y., Zeng, S., et al. (2023). Effect of high fat diet on disease development of polycystic ovary syndrome and lifestyle intervention strategies. *Nutrients* 15 (9), 2230. doi:10.3390/nu15092230
- Wenli, H. (2020). Modified Yulinzhu decoction for the treatment of 54 cases of polycystic ovarian syndrome with kidney deficiency and blood stasis type. *Zhejiang J. Traditional Chin. Med.* 55 (04), 266–267.
- Hu, M., Zhang, Y., Ma, S., Li, J., Wang, X., Liang, M., et al. (2021). Suppression of uterine and placental ferroptosis by N-acetylcysteine in a rat model of polycystic ovary syndrome. *Mol. Hum. Reprod.* 27 (12), gaab067. doi:10.1093/molehr/gaab067
- Islam, H., Masud, J., Islam, Y. N., and Haque, F. K. M. (2022). An update on polycystic ovary syndrome: a review of the current state of knowledge in diagnosis, genetic etiology, and emerging treatment options. *Womens Health (Lond.)* 18, 17455057221117966. doi:10.1177/17455057221117966
- Hong, L. (2018). The effect of modified Yulinzhu decoction combined with metformin on the levels of Leptin, IGF-1, and SHBG in polycystic ovary syndrome. *World J. Integr. Traditional Chin. West. Med.* 13 (12): 1723–1726.
- Hong, L. (2019). The effect of Yulinzhu decoction combined with tamoxifen on blood lipids and adipokines in patients with polycystic ovary syndrome. *Tradit. Chin. Med. Inf.* 36 (05), 92–96.
- Liu, Q., Jiang, J., Shi, Y., Mo, Z., and Li, M. (2020). Apelin/Apelin receptor: a new therapeutic target in Polycystic Ovary Syndrome. *Life Sci.* 260, 118310. doi:10.1016/j.lfs.2020.118310
- Lizneva, D., Suturina, L., Walker, W., Brakta, S., Gavrilova-Jordan, L., and Azziz, R. (2016). Criteria, prevalence, and phenotypes of polycystic ovary syndrome. *Fertil. Steril.* 106 (1), 6–15. doi:10.1016/j.fertnstert.2016.05.003
- Ma, Q. W., and Tan, Y. (2017). Effectiveness of co-treatment with traditional Chinese medicine and letrozole for polycystic ovary syndrome: a meta-analysis. *J. Integr. Med.* 15 (2), 95–101. doi:10.1016/S2095-4964(17)60320-0
- Macut, D., Bjekić-Macut, J., Rahelić, D., and Doknić, M. (2017). Insulin and the polycystic ovary syndrome. *Diabetes Res. Clin. Pract.* 130, 163–170. doi:10.1016/j.diabres.2017.06.011
- McGowan, L., and Quinlivan, J. (2019). Polycystic ovary syndrome (PCOS): moving from characterization to interventions. *J. Psychosom. Obstet. Gynaecol.* 40 (4), 249. doi:10.1080/0167482X.2019.1672337
- Murri, M., Insenser, M., and Escobar-Morreale, H. F. (2014). Metabolomics in polycystic ovary syndrome. *Clin. Chim. Acta.* 429, 181–188. doi:10.1016/j.cca.2013.12.018
- Papalou, O., Victor, V. M., and Diamanti-Kandarakis, E. (2016). Oxidative stress in polycystic ovary syndrome. *Curr. Pharm. Des.* 22 (18), 2709–2722. doi:10.2174/1381612822666160216151852
- Pei, C. Z., Jin, L., and Baek, K. H. (2021). Pathogenetic analysis of polycystic ovary syndrome from the perspective of omics. *Biomed. Pharmacother.* 142, 112031. doi:10.1016/j.biopha.2021.112031
- Presswala, B., and De Souza, L. R. (2023). The diagnostic experience of polycystic ovary syndrome: a scoping review of patient perspectives. *Patient Educ. Couns.* 113, 107771. doi:10.1016/j.pec.2023.107771
- Rebar, R. W., and Keator, C. S. (2024). Polycystic ovary syndrome: consider the entire spectrum. *Fertil. Steril.* 121 (6), 934–936. doi:10.1016/j.fertnstert.2024.02.008
- Rothenberg, S. S., Beverley, R., Barnard, E., Baradaran-Shoraka, M., and Sanfilippo, J. S. (2018). Polycystic ovary syndrome in adolescents. *Best. Pract. Res. Clin. Obstet. Gynaecol.* 48, 103–114. doi:10.1016/j.bpobgyn.2017.08.008
- Shang, Y., Zhou, H., He, R., and Lu, W. (2021). Dietary modification for reproductive health in women with polycystic ovary syndrome: a systematic review and meta-analysis. *Front. Endocrinol. (Lausanne)* 12, 735954. doi:10.3389/fendo.2021.735954
- Shang, Y., Zhou, H., Hu, M., and Feng, H. (2020). Effect of diet on insulin resistance in polycystic ovary syndrome. *J. Clin. Endocrinol. Metab.* 105 (10), dgaa425. doi:10.1210/clinem/dgaa425

Conflict of interest

The authors declare that the research was conducted in the absence of any commercial or financial relationships that could be construed as a potential conflict of interest.

Publisher's note

All claims expressed in this article are solely those of the authors and do not necessarily represent those of their affiliated organizations, or those of the publisher, the editors and the reviewers. Any product that may be evaluated in this article, or claim that may be made by its manufacturer, is not guaranteed or endorsed by the publisher.

Supplementary material

The Supplementary Material for this article can be found online at: <https://www.frontiersin.org/articles/10.3389/fphar.2024.1458621/full#supplementary-material>

- Soares Júnior, J. M., Baracat, M. C., Maciel, G. A., and Baracat, E. C. (1992)2015). Polycystic ovary syndrome: controversies and challenges. *Rev. Assoc. Med. Bras.* 61 (6), 485–487. doi:10.1590/1806-9282.61.06.485
- Stener-Victorin, E., Padmanabhan, V., Walters, K. A., Campbell, R. E., Benrick, A., Giacobini, P., et al. (2020). Animal models to understand the etiology and pathophysiology of polycystic ovary syndrome. *Endocr. Rev.* 41 (4), bnaa010. doi:10.1210/edrv/bnaa010
- Sun, X., Ding, C., and Xin, Y. (2015). Etc clinical observation on the treatment of non obese type 67 polycystic ovarian syndrome with Yulinzhu combined with chaihushugan san Zhejiang. *J. Integr. Traditional Chin. West. Med.* 25 (01), 52–54.
- Teede, H. J., Tay, C. T., Laven, J., Dokras, A., Moran, L. J., Piltonen, T. T., et al. (2023). Recommendations from the 2023 international evidence-based guideline for the assessment and management of polycystic ovary syndrome. *Fertil. Steril.* 120 (4), 767–793. doi:10.1016/j.fertnstert.2023.07.025
- Tong, C., Wu, Y., Zhang, L., and Yu, Y. (2022). Insulin resistance, autophagy and apoptosis in patients with polycystic ovary syndrome: Association with PI3K signaling pathway. *Front. Endocrinol. (Lausanne)* 13, 1091147. doi:10.3389/fendo.2022.1091147
- VanHise, K., Wang, E. T., Norris, K., Azziz, R., Pisarska, M. D., and Chan, J. L. (2023). Racial and ethnic disparities in polycystic ovary syndrome. *Fertil. Steril.* 119 (3), 348–354. doi:10.1016/j.fertnstert.2023.01.031
- Wang, Y., Teng, X., and Liu, J. (2022). Research progress on the effect of traditional Chinese medicine on signal pathway related to premature ovarian insufficiency. *Evid. Based Complement. Altern. Med.* 2022, 7012978. doi:10.1155/2022/7012978
- Wei, L. (2019). *Clinical observation of Yulinzhu combined with clomiphene in the treatment of PCOS infertility with kidney deficiency and blood stasis syndrome [D]*. world traditional Chinese medicine: Guangxi University of Traditional Chinese Medicine.
- Welt, C. K. (2021). Genetics of polycystic ovary syndrome: what is new?. *Endocrinol. Metab. Clin. North Am.* 50 (1), 71–82. doi:10.1016/j.ecl.2020.10.006
- Wu, X. K., Stener-Victorin, E., Kuang, H. Y., Ma, H. L., Gao, J. S., Xie, L. Z., et al. (2017). Effect of acupuncture and clomiphene in Chinese women with polycystic ovary syndrome: a randomized clinical trial. *JAMA* 317 (24), 2502–2514. doi:10.1001/jama.2017.7217
- Wu, Y. X., Yang, X. Y., Han, B. S., Hu, Y. Y., An, T., Lv, B. H., et al. (2022). Naringenin regulates gut microbiota and SIRT1/PGC-1 α signaling pathway in rats with letrozole-induced polycystic ovary syndrome. *Biomed. Pharmacother.* 153, 113286. doi:10.1016/j.biopha.2022.113286
- Xu, Y., Cao, Z., Chen, T., and Ren, J. (2023). Trends in metabolic dysfunction in polycystic ovary syndrome: a bibliometric analysis. *Front. Endocrinol. (Lausanne)* 14, 1245719. doi:10.3389/fendo.2023.1245719
- Xu, Y., Zhou, Z. Y., Pan, J. X., and Huang, H. F. (2022). Associations between asthma and polycystic ovary syndrome: current perspectives. *Front. Endocrinol. (Lausanne)* 13, 936948. doi:10.3389/fendo.2022.936948
- Xueli, L., Chen Yu A clinical study on the modified treatment of ovulatory dysfunction infertility in polycystic ovary syndrome with Yulin Zhu and Guizhi Fuling Pills [J] *New Tradit. Chin. Med.*, 2019, 51 (11): 43–47.
- Ye, W., Xie, T., Song, Y., and Zhou, L. (2021). The role of androgen and its related signals in PCOS. *J. Cell Mol. Med.* 25 (4), 1825–1837. doi:10.1111/jcmm.16205
- Zhang, N., Liao, Y., Zhao, H., Chen, T., Jia, F., Yu, Y., et al. (2023a). Polycystic ovary syndrome and 25-hydroxyvitamin D: a bidirectional two-sample Mendelian randomization study. *Front. Endocrinol. (Lausanne)* 14, 1110341. doi:10.3389/fendo.2023.1110341
- Zhang, Y., Lu, D., Guo, V. Y., Wang, Y., Qiu, S., Zhang, J., et al. (2023b). Association between maternal polycystic ovary syndrome and attention-deficit/hyperactivity disorder in offspring aged 3–6 years: a Chinese population-based study. *Front. Public Health* 10, 1032315. doi:10.3389/fpubh.2022.1032315



OPEN ACCESS

EDITED BY

Jian Hao,
The Second Affiliated Hospital of Guangzhou
Medical University, China

REVIEWED BY

Zheng Yuan,
China Academy of Chinese Medical Sciences,
China
Ruiheng Wang,
Cedars Sinai Medical Center, United States

*CORRESPONDENCE

Meihua Zhang,
✉ meihua2013@163.com
Aijun Hao,
✉ aijunhao@sdu.edu.cn

RECEIVED 30 July 2024

ACCEPTED 26 August 2024

PUBLISHED 11 September 2024

CITATION

Wu D, Zhou W, Du J, Zhao T, Li N, Peng F, Li A,
Zhang X, Zhang M and Hao A (2024)
Isoliquiritigenin ameliorates abnormal
oligodendrocyte development and behavior
disorders induced by white matter injury.
Front. Pharmacol. 15:1473019.
doi: 10.3389/fphar.2024.1473019

COPYRIGHT

© 2024 Wu, Zhou, Du, Zhao, Li, Peng, Li, Zhang,
Zhang and Hao. This is an open-access article
distributed under the terms of the [Creative
Commons Attribution License \(CC BY\)](#). The use,
distribution or reproduction in other forums is
permitted, provided the original author(s) and
the copyright owner(s) are credited and that the
original publication in this journal is cited, in
accordance with accepted academic practice.
No use, distribution or reproduction is
permitted which does not comply with these
terms.

Isoliquiritigenin ameliorates abnormal oligodendrocyte development and behavior disorders induced by white matter injury

Dong Wu^{1,2}, Wenjuan Zhou², Jingyi Du², Tiantian Zhao²,
Naigang Li², Fan Peng², Anna Li¹, Xinyue Zhang², Meihua Zhang^{1*}
and Aijun Hao^{1,2*}

¹Key Laboratory of Maternal and Fetal Medicine of National Health Commission of China, Shandong Provincial Maternal and Child Health Care Hospital Affiliated to Qingdao University, Jinan, China, ²Key Laboratory for Experimental Teratology of Ministry of Education, Shandong Key Laboratory of Mental Disorders, Department of Anatomy and Histoembryology, School of Basic Medical Sciences, Cheeoloo College of Medicine, Shandong University, Jinan, China

Background: White matter injury is a predominant form of brain injury in preterm infants. However, effective drugs for its treatment are currently lacking. Previous studies have shown the neuroprotective effects of Isoliquiritigenin (ISL), but its impact on white matter injury in preterm infants remains poorly understood.

Aims: This study aimed to investigate the protective effects of ISL against white matter injury caused by infection in preterm infants using a mouse model of lipopolysaccharide-induced white matter injury, integrating network pharmacology as well as *in vivo* and *in vitro* experiments.

Methods: This study explores the potential mechanisms of ISL on white matter injury by integrating network pharmacology. Core pathways and biological processes affected by ISL were verified through experiments, and motor coordination, anxiety-like, and depression-like behaviors of mice were evaluated using behavioral experiments. White matter injury was observed using hematoxylin-eosin staining, Luxol Fast Blue staining, and electron microscopy. The development of oligodendrocytes and the activation of microglia in mice were assessed by immunofluorescence. The expression of related proteins was detected by Western blot.

Results: We constructed a drug-target network, including 336 targets associated with ISL treatment of white matter injury. The biological process of ISL treatment of white matter injury mainly involves microglial inflammation regulation and myelination. Our findings revealed that ISL reduced early nerve reflex barriers and white matter manifestations in mice, leading to decreased activation of microglia and release of proinflammatory cytokines. Additionally, ISL demonstrated the ability to mitigate impairment in oligodendrocyte development and myelination, ultimately improving behavior disorders in adult mice. Mechanistically, we observed that ISL downregulated HDAC3 expression, promoted histone acetylation, enhanced the expression of H3K27ac, and regulated oligodendrocyte pro-differentiation factors.

Conclusion: These findings suggest that ISL can have beneficial effects on white matter injury in preterm infants by alleviating inflammation and promoting oligodendrocyte differentiation.

KEYWORDS

isoliquritigenin, anxiety, depression, white matter injury, oligodendrocytes, microglia, HDAC3

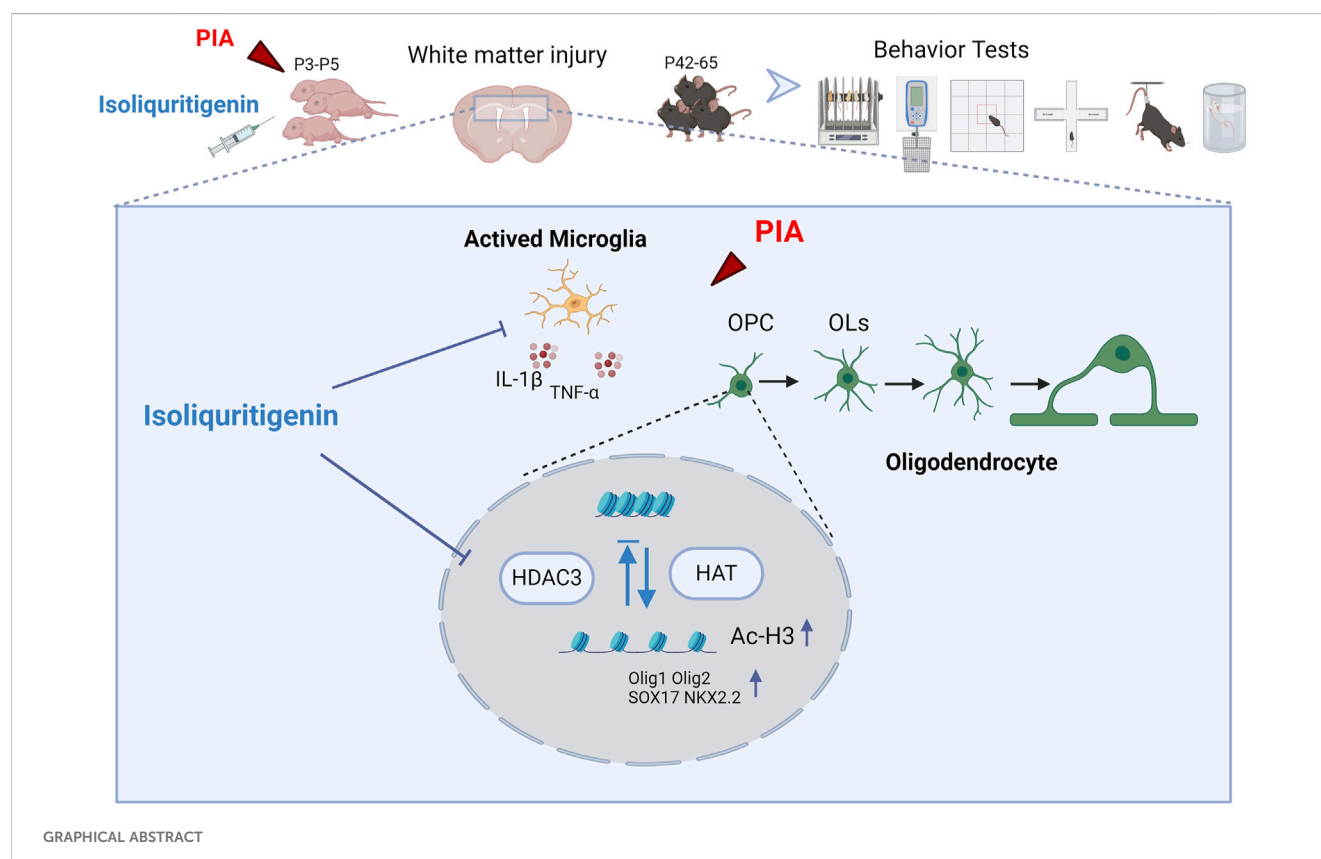
1 Introduction

According to the World Health Organization (WHO), approximately 15 million preterm babies are born every year, accounting for about one in ten live births. Preterm birth poses a significant international public health concern due to its close association with high rates of mortality and morbidity (Liu et al., 2016). Despite significant advances in preterm care that have greatly improved survival rates, there has been a concurrent rise in chronic neurological dysfunction among preterm infants (Wilson-Costello et al., 2005). Research indicates that a range of severe abnormalities in motor function, cognition, and emotion are present in 5–10 percent of preterm infants (Soria-Pastor et al., 2008; Volpe et al., 2011). It is important to recognize that brain injury in preterm infants not only detrimentally impacts their health and quality of life, but also imposes a significant economic burden on families and society (Kruse et al., 2009).

White matter injury is the primary form of brain injury observed in preterm infants (Volpe, 2009). Perinatal infection is widely recognized as one of the most significant risk factors for white

matter injury (Edwards and Tan, 2006; Ledger, 2008). Infection-induced proinflammatory cytokines easily cross the blood-brain barrier and enter the brain parenchyma, subsequently activating microglia and initiating a detrimental cascade (Malaeb and Dammann, 2009; Kuypers et al., 2012). During the period of preterm birth, late oligodendrocyte progenitor cells (OPCs) are vulnerable to selective degeneration caused by adverse stimuli (Segovia et al., 2008). This damage disrupts the normal processes of oligodendrocyte maturation and myelination through aberrant regenerative and repair mechanisms (Back, 2017). Therefore, improving the inflammatory response of microglia and preserving the normal development of oligodendrocytes are critical therapeutic targets for white matter injury.

Isoliquritigenin (ISL) is a compound extracted from licorice that possesses a chalcone structure. Numerous studies have demonstrated the diverse biological and pharmacological activities of ISL, including anti-inflammatory, antioxidant, and anti-tumor properties (Yadav et al., 2011; Peng et al., 2015). Notably, ISL exhibits notable neuroprotective effects (Shi et al., 2020). Research has revealed that ISL can inhibit the release of



mitochondrial apoptosis-inducing factors, Bcl-2 and Bax, into the cytoplasm, suppress glutamate-induced reactive oxygen species (ROS) production, mitigate glutamate-induced damage to mitochondria, and prevent hippocampal neuronal death (Yang et al., 2012). Moreover, ISL has demonstrated the ability to enhance or maintain the antioxidant capacity of mice while inhibiting neuroinflammation (Zhu et al., 2019). Nevertheless, the role of ISL in white matter injury of the nervous system remains unexplored. This study aims to explore the therapeutic effects of ISL on white matter injury. First, network pharmacology will be used to predict the potential mechanisms by which ISL may treat white matter injury. Subsequently, an experimental model of white matter injury in premature infants will be established to verify whether ISL can reduce white matter injury and related neurobehavioral disorders, and to elucidate its specific mechanisms.

2 Material and methods

2.1 Animals and white matter injury mice model

The experiment was conducted using Kunming mice pups ($n = 111$). Approval for all animal procedures was obtained from the Ethics Committee on Animal Experiments of the Medical School of Shandong University. The dams and pups, with 9–11 pups per litter, were housed in animal facilities maintained at a constant temperature of $22^{\circ}\text{C} \pm 2^{\circ}\text{C}$, and subjected to a 12-h light/dark cycle. They were provided unlimited access to food and water. The day of birth was designated as postnatal day 1 (P1). In order to establish a white matter injury model, the mice were intraperitoneally injected with lipopolysaccharide (LPS) for three consecutive days, starting from P3.

2.2 Drug treatment

The experiment was conducted following previous studies (Pang et al., 2012; Fan et al., 2013; Xie et al., 2016). The experimental design and drug treatment schedule are presented in Figure 2A. The experimental animals were divided into three groups: the Control group (treated with vehicle solution), the LPS group (treated with LPS at a dosage of 1 mg/kg/24 h), and the LPS + ISL group (treated with LPS at a dosage of 1 mg/kg/24 h, and ISL at a dosage of 4 mg/kg/24 h). At the end of the experiment, the mice were euthanized in accordance with institutional guidelines and approved protocols. The euthanasia was carried out using carbon dioxide (CO_2) inhalation, followed by cervical dislocation to ensure death. CO_2 was introduced into the chamber at a rate that displaced 10%–30% of the chamber volume per minute. The animals were monitored for cessation of respiration and lack of a heartbeat before proceeding with the subsequent procedures. All efforts were made to minimize animal suffering and to ensure a humane endpoint. The brain was removed, and the corpus callosum was collected and quickly stored at -80°C until further use. Some of the mice were used in the behavioral experiments. The LPS (*Escherichia coli* strain O111:B4) used in the experiments was purchased from Sigma-Aldrich (St. Louis, MO, United States) and prepared in saline

solution (0.9% NaCl). ISL (98.07% purity) was purchased from MCE (Shanghai, China) and dissolved in sterile saline with 1% dimethyl sulfoxide (Solarbio, Beijing, China). The chosen dosage of the drug was based on the results of our study (Supplementary Figure 1A, B) and consistent with previous literature demonstrating the neuroprotective effects of the agent (Liu et al., 2019; Wang et al., 2020).

2.3 Behavioral tests

Behavioral tests of mice were conducted between P42 and P56. Every behavioral experiment was conducted in an individual, dark chamber, devoid of unwanted external light and sound. During the experiment, the operator was blinded to the mice in the different treatment groups. Mice were moved there at least 30 min in advance before the experiment to adapt to the environment. After each mouse experiment, the behavioral device was cleaned with 75% ethanol. After each experiment, the mice rested for 24 h, waiting for the next experiment. A tracking system (TopScan 3.0) was used to record, measure and analyze all behavioral experiments.

2.3.1 Righting reflex

The mice were placed on the surface of the table with gentle pressure applied to both sides of their heads and hind limbs. Once released, the time taken by the mice to roll over and make contact with the table using all four limbs was recorded.

2.3.2 Negative geotaxis

The mice were positioned with their heads facing downward on a 45° incline. The time required for the mice to rotate and lift their heads was observed and recorded. If the mice did not complete the task within 60 s, the test was terminated.

2.3.3 Tail suspension test (TST)

The mice were suspended by their tails for 6 min and monitored using a video tracking system to assess escape-related behavior. The duration of immobility during the 6-min suspension period was recorded.

2.3.4 Forced swim test (FST)

This test aimed to assess depression-like behavior in the mice. The forced swim tests were conducted in a cylindrical glass tank measuring 30 cm in height and 18 cm in width, filled with fresh water at a temperature of $25^{\circ}\text{C} \pm 2^{\circ}\text{C}$ and a depth of 20 cm. The total immobility duration was recorded over a 6-min period, with immobility defined as the time when the mouse made minimal movements to keep its head above the water surface.

2.3.5 Elevated plus maze (EPM)

This experiment aimed to evaluate anxiety-like behavior in mice. The apparatus used in this experiment consisted of two open arms and two closed arms. The dimensions of the open arms were 40×5 cm, while the dimensions of the closed arms were the same. All arms were surrounded by walls measuring 19 cm in height. The apparatus was positioned 50 cm above the ground. The mice were placed on the central platform of the maze, which measured 5×5 cm, facing towards an open arm. They were given 6 min to explore

the maze, with locomotion data being collected using a video-tracking system.

2.3.6 Open field test (OFT)

The mice were placed in a 40 cm × 40 cm field and allowed to move freely for a duration of 10 min. They were initially situated in the center of the arena, with the center region defined as the 20 cm × 20 cm area located at the center. The activities of the mice were observed and recorded using an overhead video camera. The total distance moved and the time spent in the center were analyzed using an animal behavioral tracking system. After each mouse's test, the open field apparatus was thoroughly cleaned with a 75% ethyl alcohol solution.

2.3.7 Grip strength

Grip strength was measured using a computerized grip strength meter. The apparatus comprised a metal bar connected to a force transducer. To measure the grip strength of the mouse's whole body and fore paws, the experimenter held the mice at the base of the tail, enabling them to grip the metal bar with all four paws or just the fore paws. The experimenter pulled the mice backwards by their tails until they lost their grip. The peak force of each measurement was automatically recorded in grams (g) by the device. Three measurements of grip strength were taken in each mouse.

2.3.8 Rotating rod test

In the first 2 days of training, mice were placed on a rotating rod that underwent linear acceleration, reaching a minimum speed of 10 RPM and a maximum speed of 40 RPM at a rate of 9.9 RPM/s. They were then maintained at a constant speed of 40 RPM for an additional 5 min. On the third day, the mice were placed on a rotating rod at a fixed speed of 40 RPM to assess motor function and coordination based on the latency to fall.

2.4 Luxol fast blue (LFB) staining

Cryosections selected from each group were rinsed with distilled water for 5 min and dehydrated using an ascending ethanol series. The sections were then stained with preheated (55°C) luxol fast blue stain (LFB; 0.1 g LFB in 100 mL of 90% ethanol with 0.5 mL of 10% glacial acetic acid) for an extended period. Finally, the sections were sealed using neutral balsam and examined under a microscope.

2.5 Transmission electron microscope

The brain tissue of mice 21 days after birth was cut into 1 mm³ and fixed with 3% glutaraldehyde at 4°C for 2 h. The fixed tissue was washed 3 times with phosphate-buffered saline (PBS). The tissue was then fixed in 1% OsO₄ at 4°C for 2 h. The tissues were dehydrated with ethanol gradient and infiltrated with 100% epoxy resin: acetone (1:3, 1:1, 3:1) for 1 h, 4 h, and 12 h, respectively. Finally, the tissues were embedded in fresh epoxy resin and polymerized at 37°C for 12 h, 45°C for 12 h, and 60°C for 1 h. The ultra-thin slices were supported on a grid (150 nm) and stained at room temperature for 20 min with uranyl acetate and 20 min with lead citrate. Images were captured using a Talos F200C transmission electron microscope (FEI Company).

2.6 Immunofluorescence

The mice were anesthetized and then perfused with a 4% paraformaldehyde solution. Subsequently, the brain tissue was removed and fixed for frozen sectioning. The brain tissue sections were washed three times with PBS. Next, they were blocked with a mixture of 10% goat serum and 0.3% Triton X-100 for 3 h, followed by incubation with the primary antibody overnight at 4°C. The primary antibodies used were anti-Iba1 (1:200, Abcam), anti-PDGFR-α (1:20, CST), and anti-APC (1:50, Beyotime Biotechnology). Then, the cells or sections were incubated with fluorescently conjugated secondary antibodies (AbBkine-488 and AbBkine-594) for 1 h. The nuclei were stained with DAPI (Sigma-Aldrich Corp). The images were acquired using an IX71 Olympus fluorescence microscope.

2.7 Immunohistochemical staining

The tissues were fixed using a 4% paraformaldehyde solution, dehydrated, embedded in paraffin, and then sectioned. Following dewaxing and hydration, the sections were immersed in a 3% hydrogen peroxide solution for 10 min. Subsequently, they were blocked with either 10% normal goat serum or 10% normal donkey serum, and incubated overnight at 4°C with the primary antibody (Anti-MBP antibody was used at a dilution of 1:600, CST). After washing with PBS, the samples were incubated with a horseradish peroxidase (HRP)-conjugated secondary antibody for 1 h. Following that, they were stained with 3,3'-diaminobenzidine (DAB) and photographed.

2.8 Primary microglia isolation and cell culture

Neonatal mice were sacrificed on postnatal day 3 (P3), and the brain tissue was removed, and the cerebellum, olfactory bulb, hippocampus and meninges were stripped. The rest of the brain tissue was then digested using 0.25% trypsin. The mixed glial single-cell suspension was further resuspended in Dulbecco's Modified Eagle Medium (DMEM) supplemented with 10% fetal bovine serum (FBS) and 1% Penicillin/Streptomycin/Amphotericin B (P/S/A) (100X). The cells were seeded into poly-lysine coated culture flasks at a density of approximately 5 × 10⁶ cells/mL. On day 7, floating microglia were collected by gently tapping the culture flask. The isolated primary microglia were then seeded in either 6-well plates or 96-well plates for subsequent experiments. The cells were cultured in a humidified chamber at 37°C with 5% CO₂.

2.9 Cell counting kit-8 (CCK-8) assay

The Cell Counting Kit-8 (CCK-8) assay (K1018, APExBIO) was performed to assess the impact of ISL on cell viability. Microglia were cultured in 96-well plates and exposed to varying concentrations of ISL for 24 h. Prior to testing, 100 μL of CCK-8 solution was added to each well of the culture plate and incubated in a CO₂ incubator at 37°C for 2 h. The optical density at a wavelength of 450 nm was measured using a Microplate Reader (BIO-RAD iMark).

TABLE 1 Primer sequences used for q-PCR experiments.

q-PCR primer sequence (mouse)		
Actin	Forward	CGTTGACATCCGTAAAGACCTC
	Reverse	CCACCGATCCACACAGAGTAC
IL-1β	Forward	GCAACTGTTCTGAACTCAACT
	Reverse	ATCTTTGGGGTCCGTCAACT
TNF-α	Forward	GACGTGGAAGTGGCAGAAGAG
	Reverse	TTGGTGGTTTGTGAGTGTGAG
HDAC1	Forward	CAGACTCAGGGCACCAAGAGGAAA
	Reverse	GGGTGCCCTTGTCCATAATAGTAG
HDAC2	Forward	AGACAAATCCAAGGACAATAGTGGT
	Reverse	CAAATTCAAGGGTTGCTGAGTTGT
HDAC3	Forward	CAATCTCAGATTCGAGGACATG
	Reverse	GCAACATTTTCGGACAGTGTAGCC
HDAC8	Forward	CAATCCGAAGCGAGTGGTT
	Reverse	GCCAGCTGCCACTGTAGG
Olig1	Forward	TCTTCCACCGCATCCCTTCT
	Reverse	CCGAGTAGGGTAGGATAACTTCG
Olig2	Forward	TCCCCAGAACCGATGATCTT
	Reverse	CGTGGACGAGGACACAGTC
TCF4	Forward	CGAAAAGTTCTCCGGGTTTG
	Reverse	CGTAGCCGGGCTGATTCAT
NKX2.2	Forward	AAGCATTTCAAACCGACGGA
	Reverse	CCTCAAATCCACAGATGACCAGA
ID2	Forward	ATGAAAGCCTTCAGTCCGGTG
	Reverse	AGCAGACTCATCGGGTCGT
ID4	Forward	CAGTGCATATGAACGACTGC
	Reverse	GACTTCTTGTGGCGGGAT
SOX17	Forward	GATGCGGGATACGCCAGTG
	Reverse	CCACCACCTCGCCTTTCAC
SOX9	Forward	GAGCCGATCTGAAGAGGGA
	Reverse	GCTTGACGTGTGGCTGTTC
SOX10	Forward	AGCCCAGGTGAAGACAGAGA
	Reverse	CCCCTCTAAGGTCTGGGATAG

2.10 RNA isolation and real-time quantitative PCR

Mouse brain tissues were used to extract total RNA with TRIZOL reagent (Invitrogen). The purity and concentration of the total RNA were determined using a spectrophotometer (Thermo NanoDrop 2000). Subsequently, the cDNA was synthesized using the RevertAidTM First Strand cDNA Synthesis Kit (Thermo Fisher Scientific). Real-time PCR was performed with

the SYBR Green Real-Time PCR Master Mix (TOYOBO CO., Ltd., Japan). β-actin expression served as the normalized control, and changes in gene expression were calculated using the 2^{-ΔΔCT} method. The primer sequences are provided in Table 1.

2.11 Western blot

The corpus callosum tissue was lysed in RIPA buffer at 4°C for 30 min. Following centrifugation, the supernatant was collected, and the total protein concentration was measured using the BCA method. Equal amounts of protein from each sample were then separated using 8%–15% SDS-PAGE gel electrophoresis and transferred onto PVDF membranes with pore sizes of either 0.22 or 0.45 μm (Millipore). Subsequently, the PVDF membrane was blocked using TBST buffer containing 5% milk and incubated overnight at 4°C with the primary antibody. The secondary antibody, either goat anti-mouse IgG or rabbit IgG conjugated to HRP, was used. Finally, the bands were visualized using the enhanced chemiluminescence (ECL) detection kit (Merck Millipore), and the analysis was performed using ImageJ software (Version 1.46r). Primary antibodies were used at the following dilutions: rabbit anti-HDAC1 (1:500, Proteintech), rabbit anti-HDAC2 (1:500, Proteintech), rabbit anti-HDAC3 (1:500, Proteintech), rabbit anti-HDAC8 (1:500, Proteintech), rabbit anti-H3 (1:500, CST), rabbit anti-H3K18ac (1:500, CST), rabbit anti-H3K9/14ac (1:500, CST), rabbit anti-H3K27ac (1:500, CST), rabbit anti-ACh3 (1:1000, CST), mouse anti-β-actin (1:2000, CST).

2.12 Chromatin immunoprecipitation assay

Enzymatic chromatin immunoprecipitation (ChIP) was conducted using the SimpleChIP® Enzymatic Chromatin IP Kit (CST). Formaldehyde fixation was performed on the tissue, followed by lysis and partial digestion of chromatin using Micrococcal Nuclease provided in the kit. This digestion process resulted in fragments ranging from 200–500 base pairs. The chromatin was immunoprecipitated overnight at 4°C using the specific antibody anti-HDAC3 or the control antibody (anti-IgG). The DNA was subsequently purified using a DNA purification centrifuge column, and after protein-DNA uncross-linking according to the manufacturer’s instructions, it was analyzed using real-time PCR. The primer sequences used for the PCR analysis can be found in Table 2.

2.13 Access to potential targets for ISL and white matter injury

The chemical structure and specification of ISL smile was downloaded from PubChem (<https://pubchem.ncbi.nlm.nih.gov/>). Importing the information into the PharmMapper server (<https://www.lilab-ecust.cn/pharmmapper/>) and Swiss Target Prediction (<http://www.swisstargetprediction.ch/>) allowed identification of ISL related targets. Potential targets for white matter injury were identified using “white matter injury” as a search term in the Genetic Society database (<https://www.genecards.org/>). Subsequently, the intersection of ISL and WMI targets was identified by analyzing the two sets of targets using Venny software (<https://bioinfogp.cnb>

TABLE 2 Primer sequences used for ChIP-qPCR experiments.

ChIP-qPCR primer sequences (mouse).		
Olig1-#1	Forward	GGTGTCCAAGGAGCGATGT
	Reverse	CCCTGCCAGTGGGTGAGTT
Olig1-#2	Forward	CCATCGGTGTTCGGACTTAC
	Reverse	GCCCAACTCCGTTACTTTA
Olig2-#1	Forward	TGAGGAGGCAGGAGATTAG
	Reverse	GGGTCATTGTTCCCATTT
Olig2-#2	Forward	ATGGGCTCCACTTCCTCA
	Reverse	TCCCTCTATTGGGTTTCG
NKX2.2-#1	Forward	TATCTGCCTTGGA CTGCG
	Reverse	AAATTGCTTGGTCGCTAA
NKX2.2-#2	Forward	TCTTTCCTCCCACTTCT
	Reverse	CATAAACATCTGGCTTCAC
SOX17-#1	Forward	CAGGGCAGTTGTGAGGGT
	Reverse	GAAAGCCAGGCTGAAGAT
SOX17-#2	Forward	TCCAGGATTGAAAGGTGT
	Reverse	GAGGGAAGAGTTAGGAAGC

csic.es/tools/venny/). The STRING database (<https://cn.string-db.org/cgi/input.pl>) can provide network visualization. Based on the STRING database, the interaction genes between ISL and WMI targets were analyzed (confidence data >0.4).

2.14 Bioinformatics analysis

Kyoto Encyclopedia of Genes and Genomes (KEGG) and Gene Ontology (GO) pathway enrichment analyses were performed on an online bioinformatics platform (<https://www.genedenovo.com/>) to elucidate key signaling pathways and identify biological functions associated with potential therapeutic targets for ISL.

2.15 Statistical analysis

The data are presented as the mean ± standard error of the mean (SEM). Statistical analysis was performed using one-way analysis of variance (ANOVA) followed by Tukey’s test. Statistically significant differences were defined as *p* values <0.05.

3 Results

3.1 Network pharmacology predicts the targets of ISL effect on white matter injury

A total of 362 potential targets for ISL were predicted using the Swiss Target Prediction and PharmMapper databases (Figures 1A, B; Supplementary Table 1). Of these,

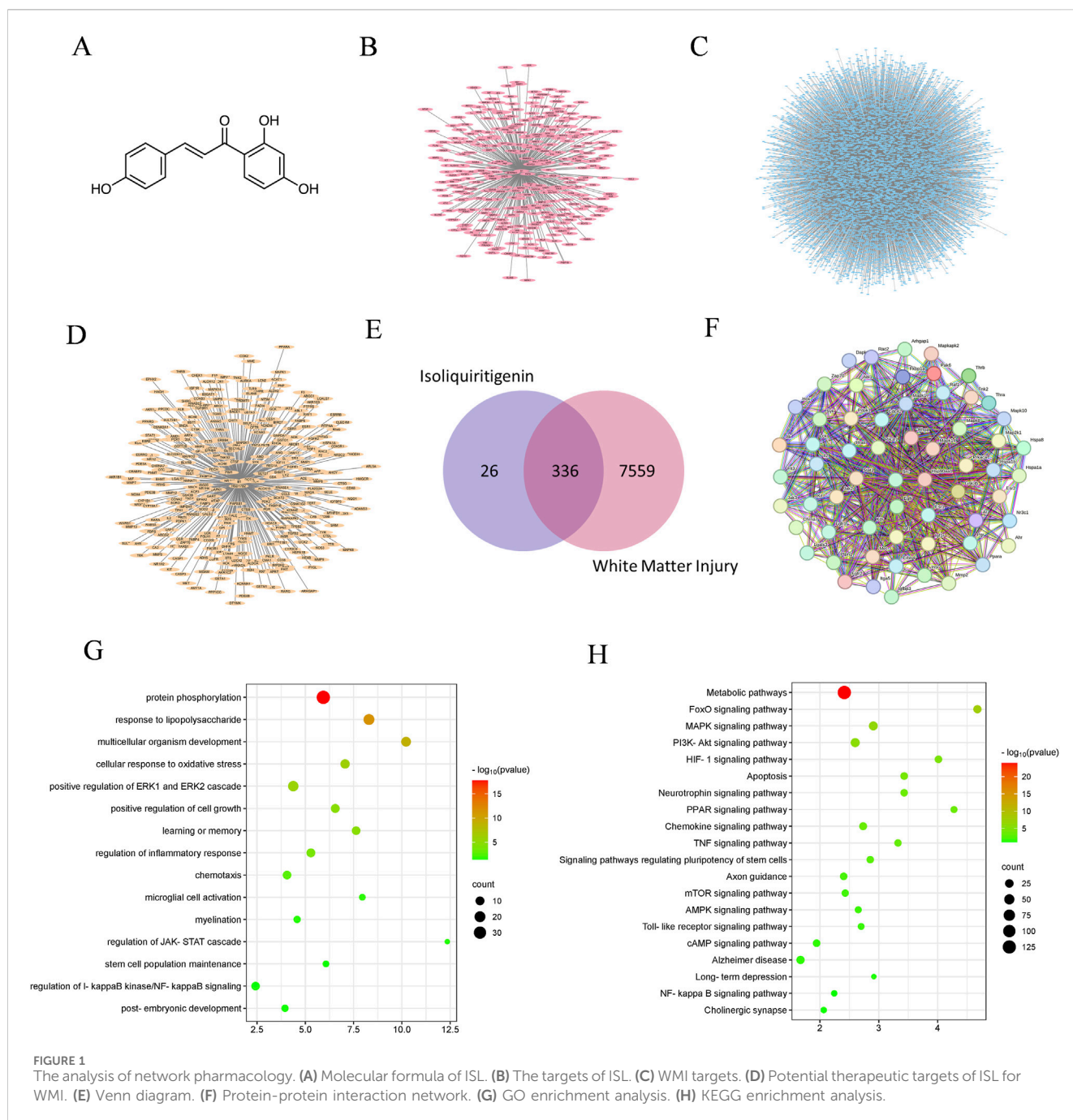
336 therapeutic targets were identified by intersecting with 7,895 WMI-related targets (Figures 1C–E; Supplementary Tables 2, 3). Results from STRING analysis show that there are 321 targets in the PPI network, including 113 nodes and 3,445 edges, with an average node degree of 21.5 (Figure 1F). To analyze the role of these targets, GO enrichment analyses were performed to assess the biological functions of ISL targets (Figure 1G). The results indicated significant associations with inflammation, microglia cell activation, and myelination, which are important mechanisms of ISL treatment for WMI. Additionally, KEGG enrichment analysis suggested that ISL may affect WMI through multiple signaling pathways, including the MAPK signaling pathway, PI3K-Akt signaling pathway, Toll-like receptor signaling pathway, and NF-κB signaling pathway (Figure 1H).

3.2 ISL attenuates weight loss and motor coordination

To investigate the potential of ISL in improving behavioral abnormalities in mice with white matter injury, we initially assessed body weight and early neural reflexes (Figure 2A). The righting reflex and negative geotaxis are commonly used neurobehavioral tests in rodent research, which we utilized to assess early motor coordination function in mice development. Compared to the control group, mice subjected to LPS-induction exhibited significant reductions in body weight and early neurobehavioral deficits. ISL treatment significantly improved the body weight loss (Figure 2B). The righting reflex and negative geotaxis experiments showed that ISL treatment shortened the latency (Figures 2C, D). Furthermore, we conducted the rotary rod and grip tests in mice at P42 to evaluate the impact of ISL treatment on mice motor function. The findings demonstrated that ISL treatment significantly enhanced motor coordination impaired by LPS induction (Figure 2E) and grip reduction in mice (Figure 2F).

3.3 ISL ameliorates depressive- and anxiety-like behaviors in adult mice

To further explore the enduring impacts of ISL treatment, we analyzed the effect on emotional behavior in mice. We conducted the open field test (OFT) to assess anxiety-like behavior. Mice in the LPS group spent less time in the center, indicating increased anxiety. ISL treatment increased center time, suggesting reduced anxiety (Figures 3A, B). Additionally, the elevated plus maze (EPM) confirmed higher anxiety levels in the LPS group, with reduced time in open arms. ISL-treated mice spent more time in open arms, indicating decreased anxiety (Figures 3C, D). We evaluated depressive-like behavior using the forced swim test (FST) and tail suspension test (TST). LPS group mice showed longer immobility periods, indicative of increased depressive-like behavior. ISL treatment significantly reduced immobility time in both tests, suggesting an antidepressant effect (Figures 3E, F). These findings collectively demonstrate the potential of ISL treatment to mitigate emotional deficits in mice.



3.4 ISL improves LPS-induced white matter injury in mice

The abnormal structure of white matter may lead to impaired or disrupted neural signal transmission, thereby affecting emotional regulation and motor coordination. Therefore, we conducted a pathological examination of the brain tissue. HE staining revealed that the LPS group exhibited subcortical and periventricular white matter lesions compared to the control group. The ISL group showed a noticeable improvement in the periventricular white matter looseness and nerve fiber disorder, with some white matter structures returning to normal (Figure 4A). Neonatal white matter injury can result in impaired myelination. Myelin

basic protein (MBP) is a critical component of the myelin sheath, playing an essential role in the process of myelination. MBP is crucial for maintaining the structural integrity and function of myelin, and its expression levels are often used as an indicator of myelination status in the central nervous system. Immunohistochemical staining of MBP revealed a decrease in MBP expression within the corpus callosum of the LPS group compared to the control group. The ISL group exhibited increased expression of MBP compared to the LPS group (Figure 4B). Furthermore, Western blot analysis indicated that ISL treatment was able to reverse the decreased expression of MBP induced by LPS (Figures 4C, D). The density of LFB-staining myelin in the callosum was significantly increased upon

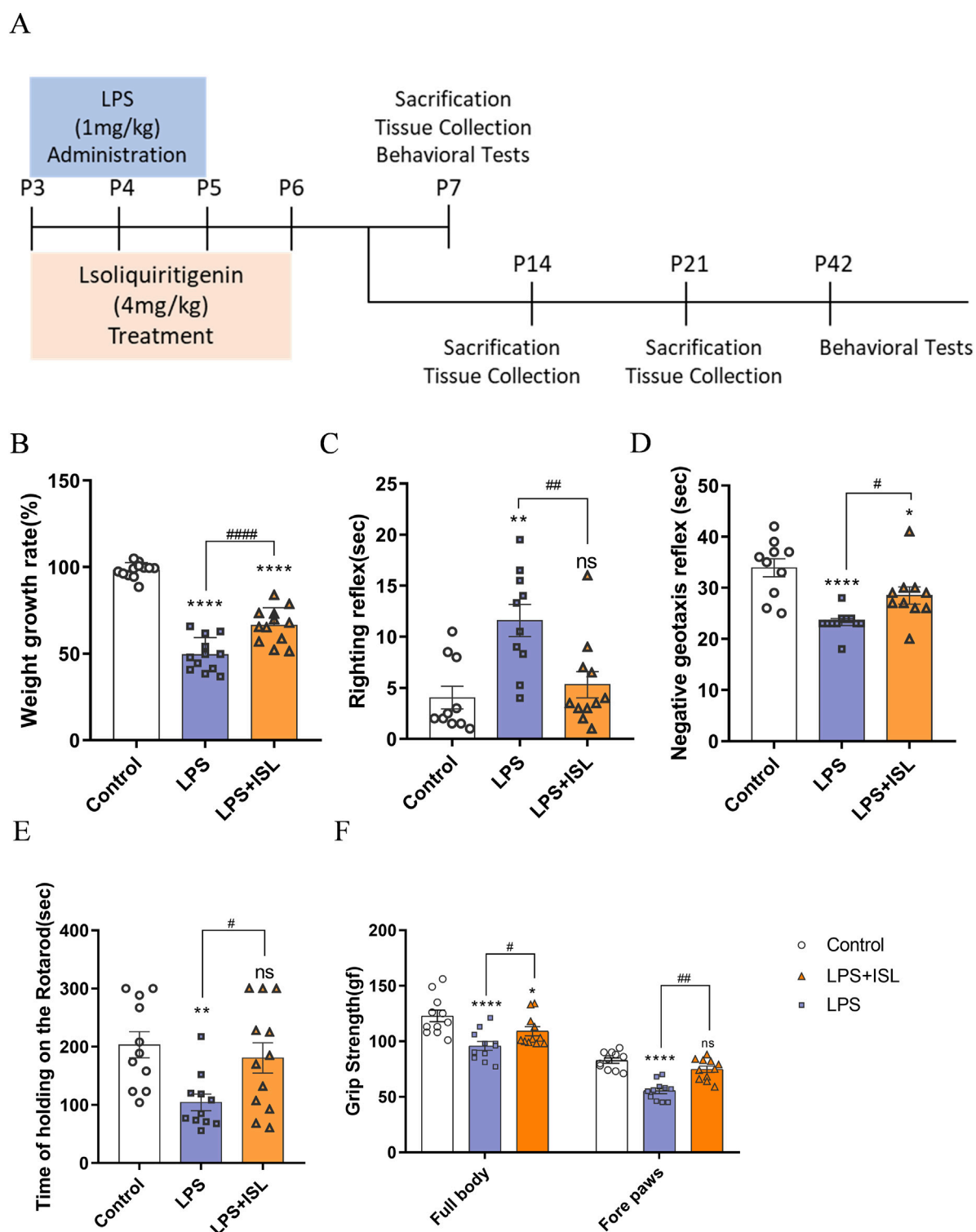


FIGURE 2

Isoliquritigenin attenuated body weight loss and motor capacity in mice. (A) Schematic representation of the early induction of systemic inflammation. (B) The increase in body weight of the pups at day 7 compared with day 3 after birth (%) ($n = 12$). (C,D) Performance of righting reflex and negative geotaxis ($n = 10-11$). (E) Rotating rod test for the motor coordination evaluation of each group ($n = 11$). (F) Grip Strength test for the whole body and forelimb of each group ($n = 11$). The results are shown as the mean \pm SEM, and analyzed by one-way ANOVA followed by *post hoc* Turkey test. * $p < 0.05$, ** $p < 0.01$, *** $p < 0.001$, **** $p < 0.0001$ compared with the control group. # $p < 0.05$, ## $p < 0.01$, ### $p < 0.001$, #### $p < 0.0001$ compared with the LPS group. "ns" indicates not significant.

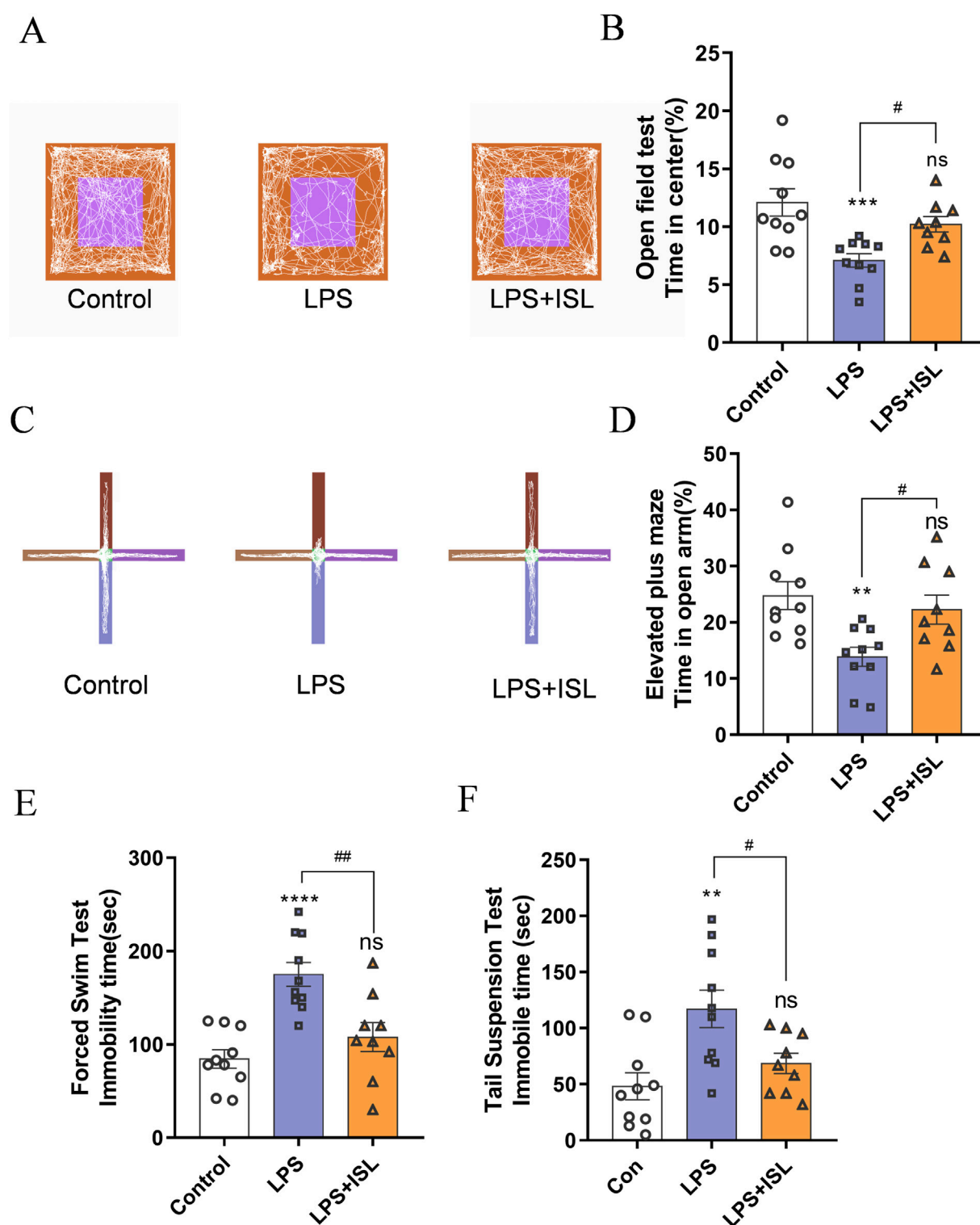


FIGURE 3

Isoliquiritigenin ameliorates anxiety-like behavior and depressive-like behavior. (A) Representative trajectory of mice in the open field test. Blue line square represents the center zone. (B) The percentage of time spent in the central region of the open field test ($n = 9-10$). (C) Representative trajectory of mice in the elevated plus maze test. (D) The duration (%) of stay in the open arm region in elevated plus maze test ($n = 9-10$). (E) The immobility time of different treatment groups in forced swimming test ($n = 8$). (F) The immobility time of different treatment groups in tail suspension test ($n = 8$). The results are shown as the mean \pm SEM, and analyzed by one-way ANOVA followed by *post hoc* Turkey test. $*p < 0.05$, $**p < 0.01$, $***p < 0.001$, $****p < 0.0001$ compared with the control group. $\#p < 0.05$, $\##p < 0.01$, $\###p < 0.001$, $\####p < 0.0001$ compared with the LPS group. "ns" indicates not significant.

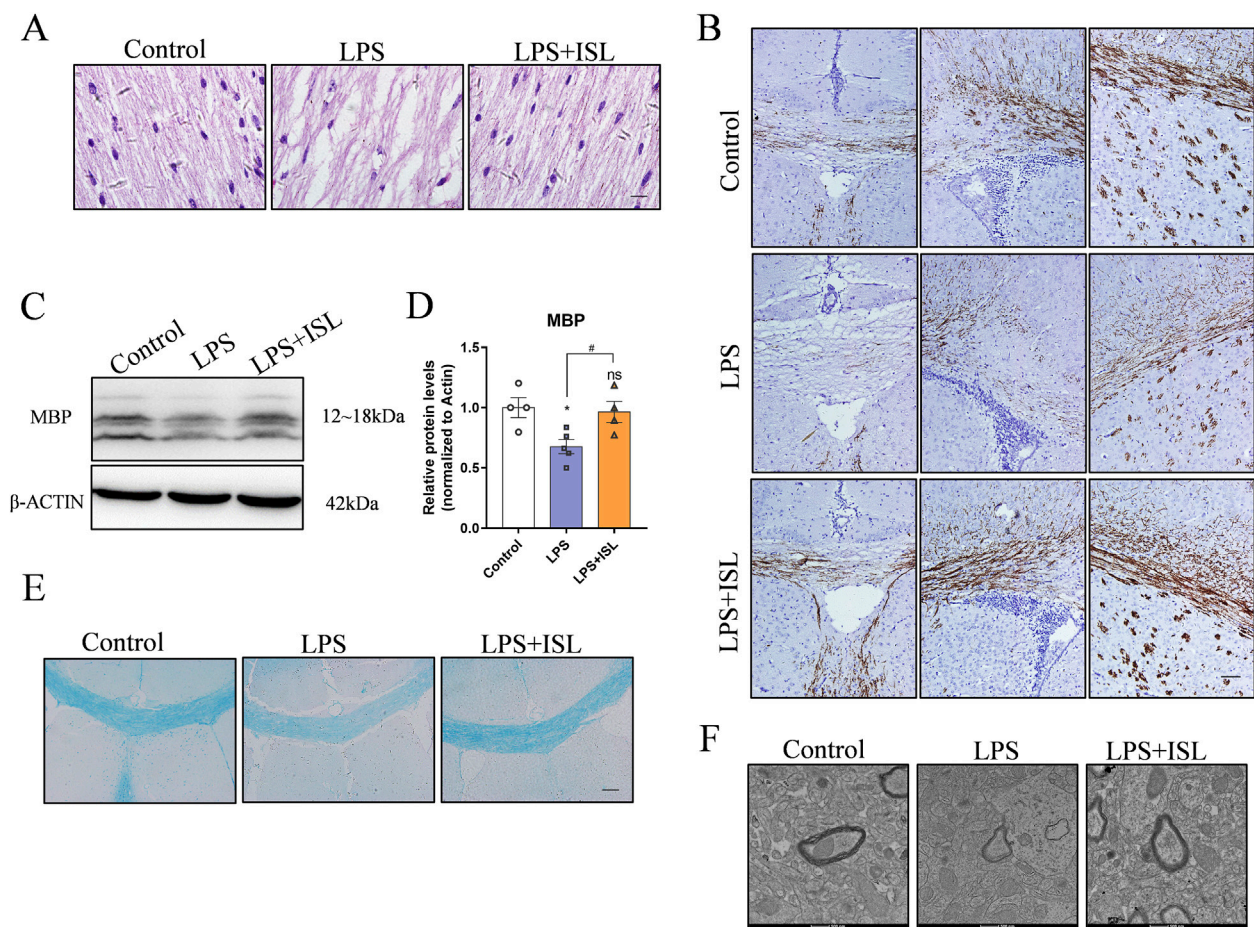


FIGURE 4

ISL alleviated white matter injury in the neonatal mouse brain. **(A)** Representative images of hematoxylin and eosin (HE) staining of corpus callosum and cingulate. scale bar = 10 μ m. **(B)** Representative images of immunohistochemistry and relative quantification analysis of the expression of MBP in the corpus callosum, cingulate and corpus striatum. **(C,D)** Representative Western blot images and quantification of MBP expression of the callosum. **(E)** Representative Luxol Fast Blue staining of the corpus callosum. Scale bar = 100 μ m. **(F)** Representative images of myelin ultrastructure. Scale bar = 100 nm. $n = 3-4$ for each group. The results are shown as the mean \pm SEM, and analyzed by one-way ANOVA followed by *post hoc* Turkey test. $*p < 0.05$, $**p < 0.01$, $***p < 0.001$, $****p < 0.0001$ compared with the control group. $\#p < 0.05$, $##p < 0.01$, $###p < 0.001$, $####p < 0.0001$ compared with the LPS group. "ns" indicates not significant.

ISL treatment, as observed in Figure 4E. The results of myelin transmission electron microscopy scanning showed that there were fewer myelinated axons in the corpus callosum of the LPS group, with irregular myelin shape and loose structure, while the myelinated axons in ISL group were significantly improved (Figure 4F). Collectively, our data strongly suggest that ISL has the potential to ameliorate neonatal white matter injury and prevent myelination defects.

3.5 ISL inhibits microglial activation and pro-inflammatory gene expression

GO analysis showed that ISL treatment was associated with microglial activation and inflammatory response. Microglia-mediated neuroinflammation plays a crucial role in white matter injury. We aimed to assess the potential of ISL in regulating the inflammatory response in a model of LPS-induced white matter injury. We examined the quantity and morphology of microglia in

the corpus callosum region, as well as the mRNA expression levels of classical inflammatory factors secreted by microglia. In Figures 5A, B, the number of Iba1+ microglia (green) in the LPS group was higher compared to the control group, indicating that systemic LPS exposure activated microglia. Conversely, the number of Iba1+ microglia (green) in LPS + ISL treated mice was significantly reduced (Figure 5B). The mRNA expression analysis also confirmed that ISL can reduce the upregulation of LPS-induced inflammatory cytokines IL-1 β (Figure 5C) and TNF- α (Figure 5D). We additionally assessed the impact of ISL on LPS-induced microglia activation *in vitro*. When microglia were treated with different concentrations of ISL, it was found that 40 μ M of ISL did not significantly affect microglia viability (Supplementary Figure 2A). Increasing the dose of ISL significantly decreased microglia viability. Based on the results of CCK8, a dose of 40 μ M was chosen for subsequent experiments. Immunofluorescence staining of microglia revealed that ISL treatment significantly improved their activation state (Supplementary Figure 2B). Furthermore, qPCR results

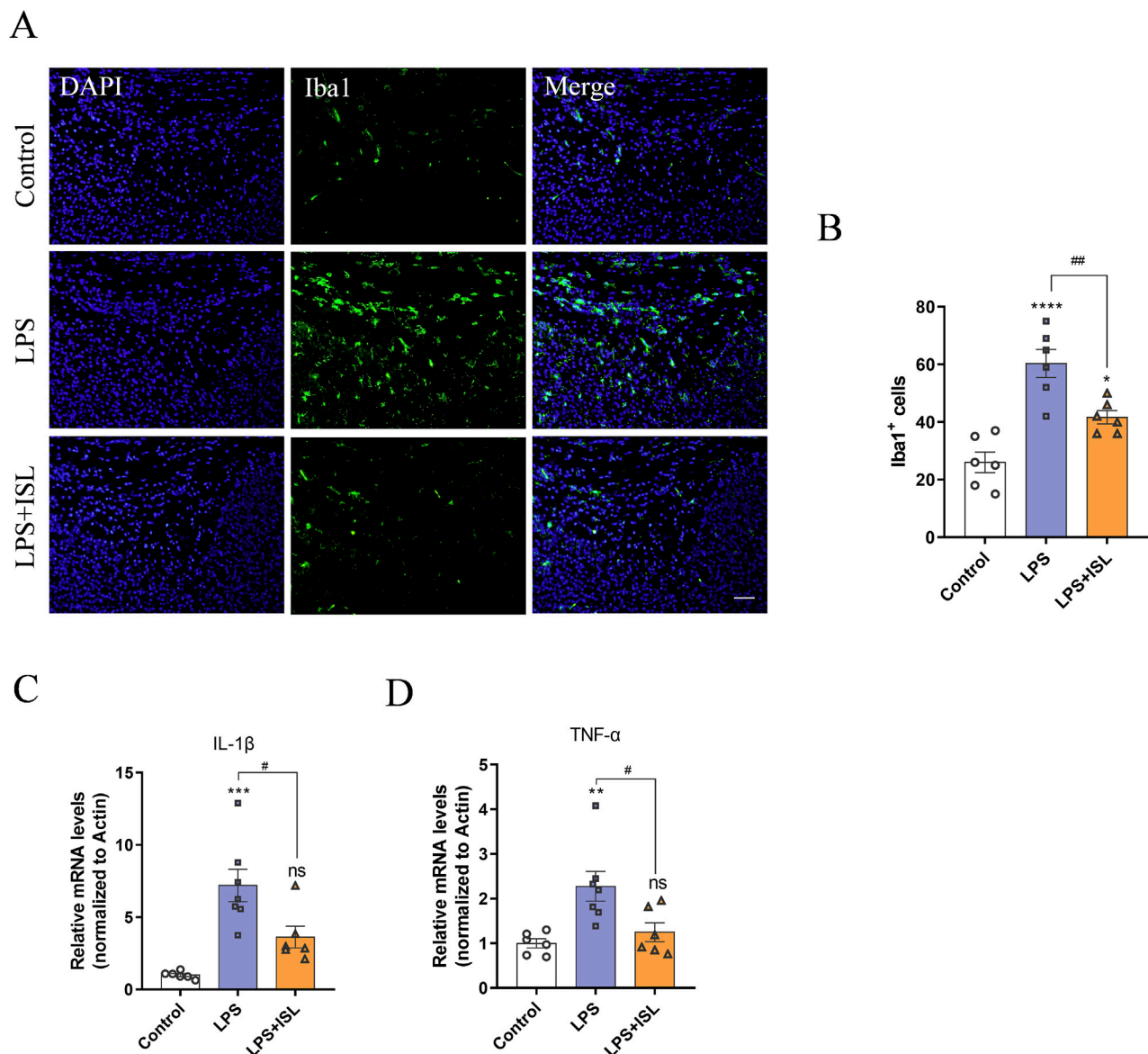


FIGURE 5
Isoliquiritigenin inhibits LPS-induced microglial activation and pro-inflammatory gene expression. (A,B) Representative images and quantification of immunofluorescence analysis of Iba1 (green) expression level from different groups ($n = 6$). (C,D) Quantification of the mRNA level of IL-1 β and TNF- α in the brain ($n = 6-7$). Scale bar = 50 μ m. The results are shown as the mean \pm SEM, and analyzed by one-way ANOVA followed by *post hoc* Turkey test. * $p < 0.05$, ** $p < 0.01$, *** $p < 0.001$, **** $p < 0.0001$ compared with the control group. # $p < 0.05$, ## $p < 0.01$, ### $p < 0.001$, #### $p < 0.0001$ compared with the LPS group. "ns" indicates not significant.

demonstrated that the expressions of IL-1 β and TNF- α in microglia were significantly downregulated in the ISL treatment group compared to the LPS group (Supplementary Figures 2C, D). These findings suggest that ISL may inhibit microglia activation and suppresses proinflammatory gene expression.

3.6 ISL rescues oligodendrocyte development disorder

According to the biological process results of GO enrichment analysis, ISL treatment is related to myelination process. White matter injury primarily arises from a developmental disorder in

oligodendrocyte precursor cells, resulting in defects in myelination and subsequent behavioral changes. In this study, we sought to investigate how ISL affects oligodendrocyte precursor cells. Immunofluorescence staining targeting PDGFR- α revealed an increase in the number of PDGFR- α ⁺ cells in the LPS group. However, ISL treatment was found to restore the number of PDGFR- α ⁺ cells reduced by LPS exposure (Figures 6A, B). Additionally, compared to the control group, the LPS group exhibited a decrease in the number of mature oligodendrocyte APC⁺ cells. However, in the LPS + ISL group, more APC⁺ cells were observed compared to the LPS group (Figures 6C, D). The development of oligodendrocytes involves numerous transcription factors and epigenetic regulation. To further investigate this, we

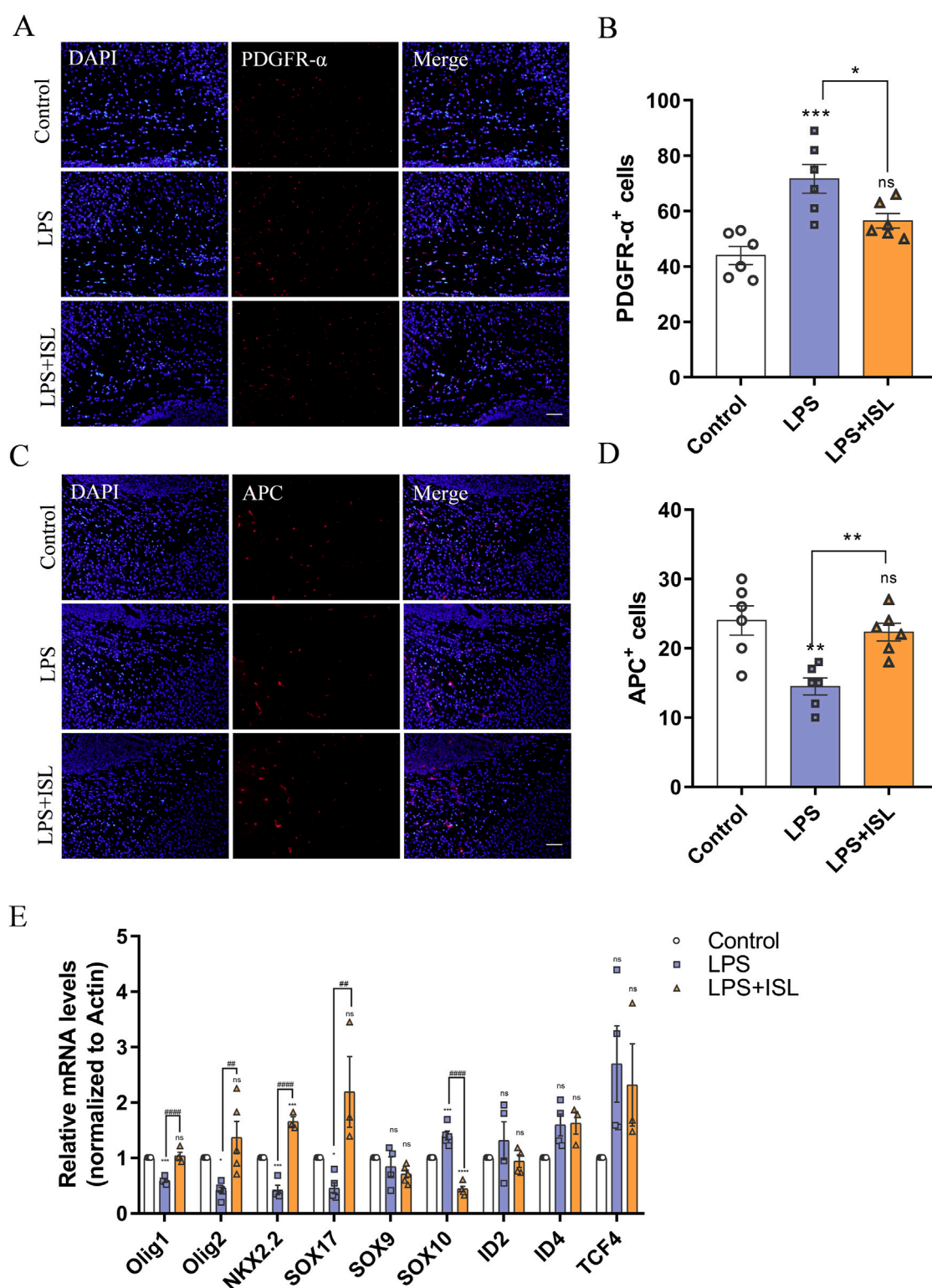


FIGURE 6

Isoliquiritigenin rescues oligodendrocyte dysplasia. **(A)** Representative PDGFR- α stained (red) brain sections of the callosum. Scale bar = 50 μ m. **(B)** Quantitative analysis of the percentage of PDGFR- α $^{+}$ cells in the callosum ($n = 6$). **(C)** Representative APC stained (red) brain sections of the callosum. Scale bar = 50 μ m. **(D)** Quantitative analysis of the percentage of APC $^{+}$ cells in the callosum ($n = 6$). **(E)** Statistical analysis of the expression of Olig1, Olig2, NKX2.2, SOX17, SOX9, SOX10, ID2, ID4 and TCF4 at mRNA level of each group ($n = 3-6$). The results are shown as the mean \pm SEM, and analyzed by one-way ANOVA followed by *post hoc* Turkey test. * $p < 0.05$, ** $p < 0.01$, *** $p < 0.001$, **** $p < 0.0001$ compared with the control group. # $p < 0.05$, ## $p < 0.01$, ### $p < 0.001$, #### $p < 0.0001$ compared with the LPS group. "ns" indicates not significant.

conducted qPCR to examine changes in transcription factors known to play a role in oligodendrocyte maturation and differentiation. Our findings indicate an increase in the expression of SOX10 and a decrease in the expression of Olig1, Olig2, and NKX2.2 in the LPS group. However, treatment with ISL reversed these changes (Figure 6E). These results suggest that ISL may exert a beneficial effect on oligodendrocyte maturation by reducing the population of immature oligodendrocytes and increasing the population of mature oligodendrocytes. It is plausible that this effect is mediated through the influence of ISL on transcription factors involved in oligodendrocyte development.

3.7 ISL protects white matter by inhibiting HDAC3

Class I HDACs play a crucial role in neuroinflammation and the development of oligodendrocytes. Several studies have reported that ISL is capable of inhibiting class I HDACs. Therefore, we investigated the potential of ISL to ameliorate white matter injury through the regulation of class I HDACs. Expression levels of HDAC1, HDAC2, HDAC3, and HDAC8 were measured, demonstrating that ISL could suppress the upregulation of HDAC3 mRNA and protein expression following LPS induction (Figures 7A–C). HDACs are known to regulate histone acetylation; therefore, we assessed changes in histone acetylation. Western blot analysis revealed a decrease in total acetylation of histone H3 following LPS treatment, whereas ISL treatment significantly increased its acetylation (Figures 7D, E). Additionally, we assessed histone acetylation at key sites. Our findings demonstrated a significant decrease in H3K27ac levels in the LPS group, while no significant changes were observed in H3K9/14ac and H3K18ac. Treatment with ISL significantly increased H3K27ac levels (Figures 7F–I). Furthermore, chromatin immunoprecipitation (ChIP) results demonstrated that ISL effectively inhibited the LPS-induced upregulation of HDAC3 binding to the promoter regions of essential transcription factors involved in oligodendrocyte pro-differentiation, such as Olig1, Olig2, SOX17, and NKX2.2 (Figure 7J). Our findings indicate that ISL is capable of modulating histone acetylation levels and the expression of transcription factors involved in oligodendrocyte development through its interaction with HDAC3.

4 Discussion

White matter consists of myelin nerve fibers surrounded by oligodendrocytes and plays a crucial role in various brain functions such as signal transmission, interregional communication, learning and memory, emotional regulation, and motor coordination (Filley and Fields, 2016; Chen et al., 2021). Among survivors of preterm birth, white matter injury stands as the primary form of brain damage (Volpe, 2009). The period of highest risk for white matter injury falls between approximately 23–32 weeks after conception (Back, 2017). During this critical window period, oligodendrocyte progenitors are particularly vulnerable to infection and inflammation, which impede their maturation and myelination processes, which in turn affect the structure and function of

white matter (Segovia et al., 2008). Early intervention significantly mitigates oligodendrocyte development impairment, thereby preserving myelination and reducing associated sequelae (McClendon et al., 2014). LPS is a Gram-negative bacterial endotoxin that triggers an inflammatory response (Wang et al., 2006). Studies have found that in rodents, early exposure to LPS increases the risk of behavioral changes in adulthood (Dinel et al., 2014). Previous studies have shown that LPS stimulation can also induce oligodendrocyte apoptosis and abnormal differentiation in premature mice (Favrais et al., 2011). Therefore, we intraperitoneally injected mice aged 3–5 days with LPS to induce systemic and brain tissue inflammation, simulating perinatal infection-induced white matter injury in preterm infants. Building upon this, we explore the therapeutic potential of ISL in mitigating white matter damage and associated behavioral deficits in mice. In this study, a drug-target network of 336 targets of ISL for WMI was constructed using network pharmacological analysis. These targets were analyzed and corresponding to GO and KEGG enrichment items, and then verified by experiments. The results suggest that ISL treatment can reduce weight loss and early neuroreflex disorders in mice with LPS-induced white matter injury. It can inhibit the inflammatory response of microglia, improve the brain microenvironment of newborn mice, prevent oligodendrocyte dysplasia and myelin formation defects, and improve the motor coordination ability and anxiety- and depression-like behaviors of adult mice with white matter injury. From the perspective of potential mechanisms, we demonstrated that isoliquiritin can downregulate the expression of HDAC3 and regulate oligodendrocyte pro-differentiation factors through epigenetic modification, thus influencing the development of oligodendrocytes.

ISL has a wide range of pharmacological effects, including anti-inflammatory, antioxidant and anti-tumor properties (Peng et al., 2015; Liu et al., 2020; Liu et al., 2022; Bai et al., 2023). In the nervous system, studies have shown that it can inhibit the release of mitochondrial apoptotic factors Bcl-2 and Bax into the cytoplasm, suppress the production of glutamate-induced reactive oxygen species (ROS), alleviate glutamate-induced mitochondrial damage, and prevent hippocampal neuron death (Yang et al., 2012). However, the impact of ISL on oligodendrocytes has remained unknown. The maturation process of oligodendrocytes is complex, involving differentiation from neural stem cells into oligodendrocyte progenitor cells (OPCs), which proliferate and differentiate into pre-oligodendrocytes before becoming mature oligodendrocytes (Zou et al., 2023). During this process, oligodendrocytes gradually contact axons and generate myelin sheaths (Takebayashi and Ikenaka, 2015). In the GO_BP analysis, the target is related to the myelination process. Consistent with the GO results, our research suggests that the protective effect of ISL on oligodendrocyte development and white matter structure restoration may be an important mechanism for treating white matter injuries. Through specific analysis of the corpus callosum region in mouse brains, we demonstrate that ISL treatment can promote oligodendrocyte maturation and increase myelination. Transcription factors Nkx2.2, Olig1/2, Sox10, and MYRF promote the expression of genes related to oligodendrocyte differentiation and myelination (van Tilborg et al., 2016). Our research findings indicate that perinatal infection inhibits oligodendrocyte differentiation and leads to abnormal expression

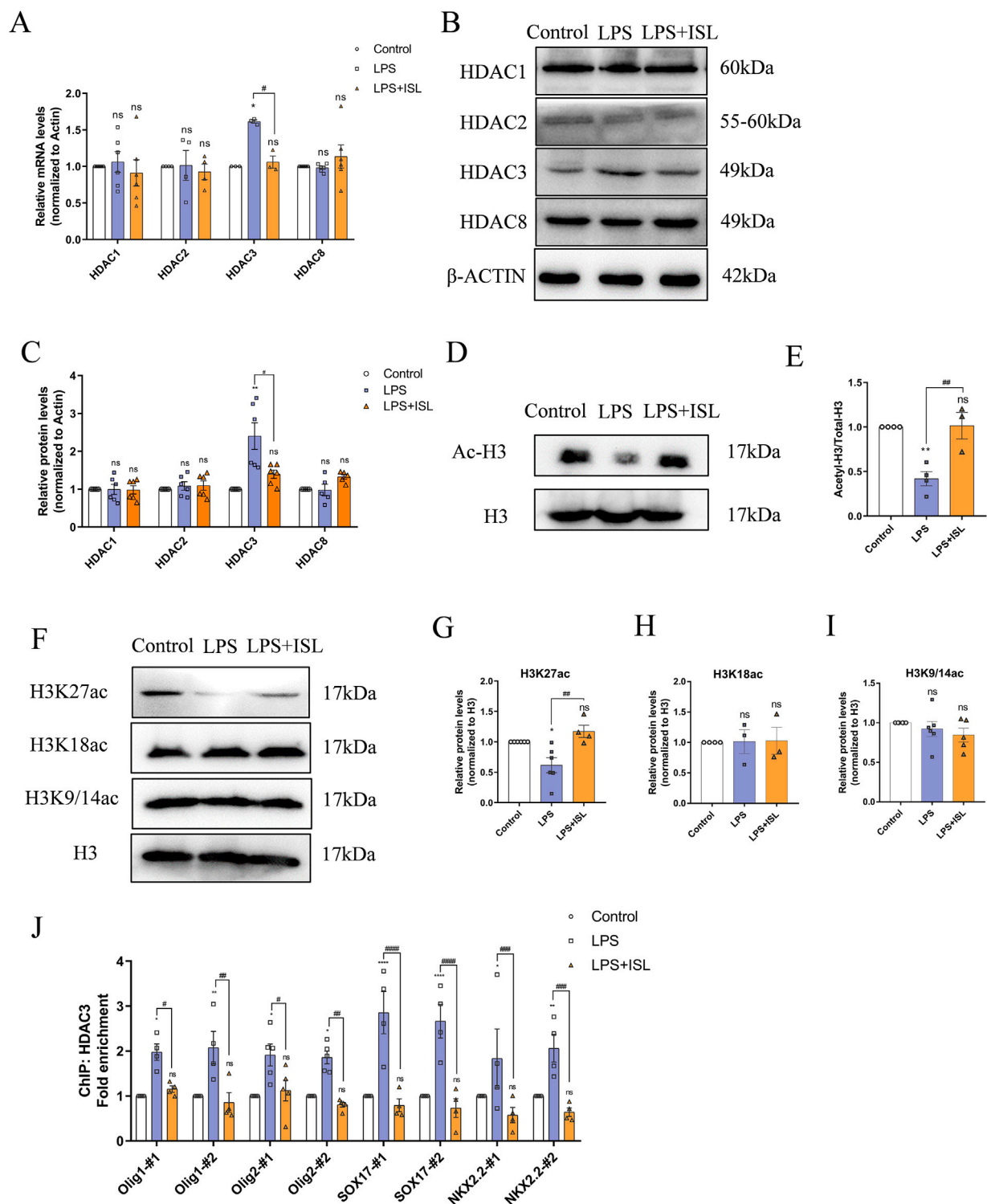


FIGURE 7 Isoliquiritigenin regulates histone acetylation and the expression of oligodendrocyte development related genes through HDAC3. **(A)** Statistical analysis of the expression of HDAC1, HDAC2, HDAC3 and HDAC8 at mRNA level of each group. **(B,C)** Representative Western blot images and relative quantification of HDAC1, HDAC2, HDAC3 and HDAC8. **(D,E)** Representative Western blot images and relative quantification of Ac-H3. **(G–I)** Representative Western blot images and quantification of histone acetylation expression in the brain. **(J)** ChIP-qPCR results showed the localization changes of HDAC3 at the promoters of transcription factors related to oligodendrocyte development. $n = 3–6$ for each group. The results are shown as the mean \pm SEM, and analyzed by one-way ANOVA followed by *post hoc* Turkey test. * $p < 0.05$, ** $p < 0.01$, *** $p < 0.001$, **** $p < 0.0001$ compared with the control group. # $p < 0.05$, ## $p < 0.01$, ### $p < 0.001$, #### $p < 0.0001$ compared with the LPS group. “ns” indicates not significant.

of oligodendrocyte differentiation-related transcription factors. Treatment with ISL can rescue abnormal differentiation of OPCs and increase the expression of pro-differentiation factors (Nkx2.2, Olig1/2, and Sox10), while reducing the expression of differentiation inhibitors (ID2 and ID4).

Microglia are inherent immune cells of the central nervous system and play a crucial role in initiating and maintaining the neuroinflammatory response (Wolf et al., 2017). When exposed to environmental cues, microglia proliferate and transition into either a pro-inflammatory or anti-inflammatory state, thereby adjusting the secretion of factors released into the brain environment. Under physiological conditions, microglia can support oligodendrocyte lineage cell development and myelination (Rahimian et al., 2022). Histological analysis of the brain tissue of preterm infants with diffuse white matter injury revealed the presence of active and pro-inflammatory microglia (Van Steenwinckel et al., 2024). High levels of pro-inflammatory cytokines, such as TNF- α and IL-1 β , have also been observed in the brains of preterm infants with white matter injury, negatively affecting the proliferation, differentiation, and survival of immature oligodendrocytes *in vivo* and *in vitro* (Xie et al., 2016; Bonora et al., 2014). Previous studies have attributed the neuroprotective effect of ISL to its immunomodulatory effects. For example, studies have found that ISL regulates microglia activation by activating the Nrf2-HO-1 antioxidant axis (Foresti et al., 2013). Similarly, in the GO and KEGG analyses, changes in signaling pathways related to microglia activation and inflammation regulation were revealed. Our study also found that ISL effectively reduced microglia activation and the release of inflammatory factors in the corpus callosum region of mice with white matter injury. These results suggest that ISL may reduce disorders of oligodendrocyte differentiation and myelination by improving the microenvironment of the brain by improving the microglial inflammatory response.

Finally, we have demonstrated for the first time that ISL exerts neuroprotective effects in neonatal mice with white matter injury through epigenetic regulation. Previous studies have shown that ISL inhibits the activity of HDAC3 (Orlikova et al., 2012). Chromatin remodeling is a critical epigenetic process that plays a crucial role in oligodendrocyte development. Chromatin remodeling enzymes regulate gene expression by altering the accessibility of DNA to transcription factors (Yuan et al., 2020). HDACs are histone deacetylases. Among them, HDAC3 is upregulated during oligodendrocyte lineage development, and its expression is associated with oligodendrocyte differentiation (Zhang et al., 2016). Our results support these findings, suggesting that LPS treatment upregulates HDAC3 expression, while ISL significantly inhibits LPS-induced HDAC3 expression. Further molecular experiments demonstrate that ISL reduces the binding of HDAC3 to the promoter regions of pro-differentiation transcription factors in oligodendrocytes. Therefore, we suggest that ISL may regulate oligodendrocyte development by regulating HDAC3 activity. In epigenetic studies, histone modification is an important component of epigenetic regulation (Berson et al., 2018). Thus, we analyzed changes in relevant histone modifications. The experiments show that ISL increases the overall acetylation levels of histone H3, with the

H3K27ac3 modification showing the most significant changes, but its specific regulatory targets need to be further studied.

While our findings emphasize the neuroprotective role of ISL in white matter injury, it is crucial to consider other drugs that modulate immune responses and protect white matter, particularly dimethyl fumarate (DMF). DMF has been extensively studied in multiple sclerosis (MS) and other neurodegenerative conditions, demonstrating its ability to activate the Nrf2 pathway, which enhances antioxidant responses and inhibits the production of pro-inflammatory cytokines (Linker and Haghikia, 2016; Yan et al., 2021). Furthermore, recent studies indicate that DMF modifies the expression of histone deacetylases (HDACs) in astrocytes, crucial for regulating inflammatory responses (Kalinin et al., 2013). DMF also reduces the density of microglia associated with white matter dysfunction, supporting its potential clinical value (Fowler et al., 2018). In contrast, our study reveals that ISL downregulates HDAC3 expression, enhances histone acetylation, and promotes oligodendrocyte differentiation, highlighting its unique mechanisms. Notably, ISL's ability to modulate microglial activity and reduce inflammation presents a distinct advantage in treating white matter injury, especially in preterm infants, where inflammation plays a critical role in pathogenesis. This suggests that ISL may not only share epigenetic regulatory pathways with DMF but may also offer additional therapeutic benefits specifically tailored to the needs of vulnerable populations. Given the similarities and differences between ISL and DMF, further exploration of these mechanisms is warranted to better understand their respective therapeutic potentials. Future research could investigate whether the combined use of ISL and DMF might provide synergistic benefits, leading to the development of more effective treatment strategies for white matter injury in preterm infants and other at-risk populations.

In conclusion, our study demonstrates that ISL effectively ameliorates white matter injury and restores neurobehavioral function in preterm infants by inhibiting neuroinflammation and regulating oligodendrocyte development. These findings provide insights into the potential clinical application of ISL for treating white matter injury and related neurological disorders in preterm infants. Future research should focus on elucidating the precise molecular pathways mediating the effects of ISL and optimizing its therapeutic potential in clinical settings.

Data availability statement

The original contributions presented in the study are included in the [supplementary material](#); further inquiries can be directed to the corresponding authors.

Ethics statement

The animal study was reviewed and approved by the National Institutes of Health Guide for the Care and Use of Laboratory Animals and the Institutional Animal Care and Use Committees of Shandong University. The study was conducted in accordance with the local legislation and institutional requirements.

Author contributions

DW: Conceptualization, Software, Validation, Writing–original draft. WZ: Conceptualization, Software, Validation, Writing–original draft, Investigation. JD: Investigation, Validation, Writing–original draft, Supervision. TZ: Writing–original draft, Conceptualization, Formal Analysis, Methodology. NL: Writing–original draft, Investigation, Resources, Visualization. FP: Investigation, Resources, Writing–original draft, Validation. AL: Writing–original draft, Data curation, Formal Analysis. XZ: Writing–original draft, Investigation, Methodology, Software. MZ: Funding acquisition, Visualization, Writing–review and editing. AH: Funding acquisition, Writing–review and editing.

Funding

The author(s) declare that financial support was received for the research, authorship, and/or publication of this article. This work was supported by funding from the National Natural Science Foundation of China (Nos 81771219 and 82071267), and Foundation of Jinan (No. 2021GXRC103).

Conflict of interest

The authors declare that the research was conducted in the absence of any commercial or financial relationships that could be construed as a potential conflict of interest.

References

- Back, S. A. (2017). White matter injury in the preterm infant: pathology and mechanisms. *Acta Neuropathol.* 134 (3), 331–349. doi:10.1007/s00401-017-1718-6
- Bai, Y., Zhou, J., Zhu, H., Tao, Y., Wang, L., Yang, L., et al. (2023). Isoliquiritigenin inhibits microglia-mediated neuroinflammation in models of Parkinson's disease via JNK/AKT/NFκB signaling pathway. *Phytother. Res.* 37 (3), 848–859. doi:10.1002/ptr.7665
- Berson, A., Nativio, R., Berger, S. L., and Bonini, N. M. (2018). Epigenetic regulation in neurodegenerative diseases. *Trends Neurosci.* 41 (9), 587–598. doi:10.1016/j.tins.2018.05.005
- Bonora, M., De Marchi, E., Patergnani, S., Suski, J. M., Celsi, F., Bononi, A., et al. (2014). Tumor necrosis factor-α impairs oligodendroglial differentiation through a mitochondria-dependent process. *Cell Death Differ.* 21 (8), 1198–1208. doi:10.1038/cdd.2014.35
- Chen, T., Chen, Z., and Gong, Q. (2021). White matter-based structural brain network of major depression. *Adv. Exp. Med. Biol.* 1305, 35–55. doi:10.1007/978-981-33-6044-0_3
- Dinel, A.-L., Joffre, C., Trifileff, P., Aubert, A., Foury, A., Le Ruyet, P., et al. (2014). Inflammation early in life is a vulnerability factor for emotional behavior at adolescence and for lipopolysaccharide-induced spatial memory and neurogenesis alteration at adulthood. *J. Neuroinflammation* 11, 155. doi:10.1186/s12974-014-0155-x
- Edwards, A. D., and Tan, S. (2006). Perinatal infections, prematurity and brain injury. *Curr. Opin. Pediatr.* 18 (2), 119–124. doi:10.1097/01.mop.0000193290.02270.30
- Fan, L. W., Kaizaki, A., Tien, L. T., Pang, Y., Tanaka, S., Numazawa, S., et al. (2013). Celecoxib attenuates systemic lipopolysaccharide-induced brain inflammation and white matter injury in the neonatal rats. *Neuroscience* 240, 27–38. doi:10.1016/j.neuroscience.2013.02.041
- Favrais, G., van de Looij, Y., Fleiss, B., Ramanantsoa, N., Bonnin, P., Stoltenburg-Diding, G., et al. (2011). Systemic inflammation disrupts the developmental program of white matter. *Ann. Neurol.* 70 (4), 550–565. doi:10.1002/ana.22489
- Filley, C. M., and Fields, R. D. (2016). White matter and cognition: making the connection. *J. Neurophysiol.* 116 (5), 2093–2104. doi:10.1152/jn.00221.2016
- Foresti, R., Bains, S. K., Pitchumony, T. S., de Castro Brás, L. E., Drago, F., Dubois-Randé, J.-L., et al. (2013). Small molecule activators of the Nrf2-HO-1 antioxidant axis modulate heme metabolism and inflammation in BV2 microglia cells. *Pharmacol. Res.* 76, 132–148. doi:10.1016/j.phrs.2013.07.010
- Fowler, J. H., McQueen, J., Holland, P. R., Manso, Y., Marangoni, M., Scott, F., et al. (2018). Dimethyl fumarate improves white matter function following severe hypoperfusion: involvement of microglia/macrophages and inflammatory mediators. *J. Cereb. Blood Flow. Metab.* 38 (8), 1354–1370. doi:10.1177/0271678X17713105
- Kalinin, S., Polak, P. E., Lin, S. X., Braun, D., Guizzetti, M., Zhang, X., et al. (2013). Dimethyl fumarate regulates histone deacetylase expression in astrocytes. *J. Neuroimmunol.* 263 (1–2), 13–19. doi:10.1016/j.jneuroim.2013.07.007
- Kruse, M., Michelsen, S. I., Flachs, E. M., Brønnum-Hansen, H., Madsen, M., and Uldall, P. (2009). Lifetime costs of cerebral palsy. *Dev. Med. Child. Neurol.* 51 (8), 622–628. doi:10.1111/j.1469-8749.2008.03190.x
- Kuypers, E., Ophelders, D., Jellema, R. K., Kunzmann, S., Gavilanes, A. W., and Kramer, B. W. (2012). White matter injury following fetal inflammatory response syndrome induced by chorioamnionitis and fetal sepsis: lessons from experimental ovine models. *Early Hum. Dev.* 88 (12), 931–936. doi:10.1016/j.earlhumdev.2012.09.011
- Ledger, W. J. (2008). Perinatal infections and fetal/neonatal brain injury. *Curr. Opin. Obstet. Gynecol.* 20 (2), 120–124. doi:10.1097/GCO.0b013e3282f734db
- Linker, R. A., and Haghighi, A. (2016). Dimethyl fumarate in multiple sclerosis: latest developments, evidence and place in therapy. *Ther. Adv. Chronic Dis.* 7 (4), 198–207. doi:10.1177/2040622316653307
- Liu, A., Jiang, B., Song, C., Zhong, Q., Mo, Y., Yang, R., et al. (2020/2023). Isoliquiritigenin inhibits circ0030018 to suppress glioma tumorigenesis via the miR-1236/HER2 signaling pathway. *MedComm* 4 (3), e282. doi:10.1002/mco.2282
- Liu, J., Xiong, X., and Sui, Y. (2019). Isoliquiritigenin attenuates neuroinflammation in traumatic brain injury in young rats. *Neuroimmunomodulation* 26 (2), 102–110. doi:10.1159/000495467
- Liu, J. Q., Zhao, X. T., Qin, F. Y., Zhou, J. W., Ding, F., Zhou, G., et al. (2022). Isoliquiritigenin mitigates oxidative damage after subarachnoid hemorrhage *in vivo* and

Publisher's note

All claims expressed in this article are solely those of the authors and do not necessarily represent those of their affiliated organizations, or those of the publisher, the editors and the reviewers. Any product that may be evaluated in this article, or claim that may be made by its manufacturer, is not guaranteed or endorsed by the publisher.

Supplementary material

The Supplementary Material for this article can be found online at: <https://www.frontiersin.org/articles/10.3389/fphar.2024.1473019/full#supplementary-material>

SUPPLEMENTARY FIGURE 1

Effect of different concentrations of ISL on LPS-induced systemic inflammation (A,B) Quantification of the mRNA level of IL-1β and TNF-α in the brain. n = 3–5 for each group. The results are shown as the mean ± SEM, and analyzed by one-way ANOVA followed by post-hoc Turkey test. *p < 0.05, **p < 0.01, ***p < 0.001, ****p < 0.0001 compared with the control group. #p < 0.05, ##p < 0.01, ###p < 0.001, ####p < 0.0001 compared with the LPS group. "ns" indicates not significant.

SUPPLEMENTARY FIGURE 2

ISL inhibits microglial activation and pro-inflammatory gene expression in vitro (A) Effects of different concentrations of ISL on microglial cell viability (n = 6). (B) Primary microglia were treated with LPS and ISL for 24 h, and Iba1 were stained (green). (C,D) Quantification of the mRNA level of IL-1β and TNF-α (n = 3–4). Scale bar = 20 μm. The results are shown as the mean ± SEM, and analyzed by one-way ANOVA followed by post-hoc Turkey test. *p < 0.05, **p < 0.01, ***p < 0.001, ****p < 0.0001 compared with the control group. #p < 0.05, ##p < 0.01, ###p < 0.001, ####p < 0.0001 compared with the LPS group. "ns" indicates not significant.

- in vitro* by regulating Nrf2-dependent Signaling Pathway via Targeting of SIRT1. *Phytomedicine* 105, 154262. doi:10.1016/j.phymed.2022.154262
- Liu, L., Oza, S., Hogan, D., Chu, Y., Perin, J., Zhu, J., et al. (2016). Global, regional, and national causes of under-5 mortality in 2000-15: an updated systematic analysis with implications for the Sustainable Development Goals. *Lancet* 388 (10063), 3027-3035. doi:10.1016/S0140-6736(16)31593-8
- Malaeb, S., and Dammann, O. (2009). Fetal inflammatory response and brain injury in the preterm newborn. *J. Child. Neurol.* 24 (9), 1119-1126. doi:10.1177/0883073809338066
- McClendon, E., Chen, K., Gong, X., Sharifnia, E., Hagen, M., Cai, V., et al. (2014). Prenatal cerebral ischemia triggers dysmaturation of caudate projection neurons. *Ann. Neurol.* 75 (4), 508-524. doi:10.1002/ana.24100
- Orlikova, B., Schnekenburger, M., Zloh, M., Golais, F., Diederich, M., and Tasdemir, D. (2012). Natural chalcones as dual inhibitors of HDACs and NF- κ B. *Oncol. Rep.* 28 (3), 797-805. doi:10.3892/or.2012.1870
- Pang, Y., Fan, L.-W., Zheng, B., Campbell, L. R., Cai, Z., and Rhodes, P. G. (2012). Dexamethasone and betamethasone protect against lipopolysaccharide-induced brain damage in neonatal rats. *Pediatr. Res.* 71 (5), 552-558. doi:10.1038/pr.2012.9
- Peng, F., Du, Q., Peng, C., Wang, N., Tang, H., Xie, X., et al. (2015). A review: the pharmacology of isoliquiritigenin. *Phytother. Res.* 29 (7), 969-977. doi:10.1002/ptr.5348
- Rahimian, R., Perlman, K., Canonne, C., and Mechawar, N. (2022). Targeting microglia-oligodendrocyte crosstalk in neurodegenerative and psychiatric disorders. *Drug Discov. Today* 27 (9), 2562-2573. doi:10.1016/j.drudis.2022.06.015
- Segovia, K. N., McClure, M., Moravec, M., Luo, N. L., Wan, Y., Gong, X., et al. (2008). Arrested oligodendrocyte lineage maturation in chronic perinatal white matter injury. *Ann. Neurol.* 63 (4), 520-530. doi:10.1002/ana.21359
- Shi, D., Yang, J., Jiang, Y., Wen, L., Wang, Z., and Yang, B. (2020). The antioxidant activity and neuroprotective mechanism of isoliquiritigenin. *Free Radic. Biol. Med.* 152, 207-215. doi:10.1016/j.freeradbiomed.2020.03.016
- Soria-Pastor, S., Gimenez, M., Narberhaus, A., Falcon, C., Botet, F., Bargallo, N., et al. (2008). Patterns of cerebral white matter damage and cognitive impairment in adolescents born very preterm. *Int. J. Dev. Neurosci.* 26 (7), 647-654. doi:10.1016/j.ijdevneu.2008.08.001
- Takebayashi, H., and Ikenaka, K. (2015). Oligodendrocyte generation during mouse development. *Glia* 63 (8), 1350-1356. doi:10.1002/glia.22863
- Van Steenwinckel, J., Bokobza, C., Laforge, M., Shearer, I. K., Miron, V. E., Rua, R., et al. (2024). Key roles of glial cells in the encephalopathy of prematurity. *Glia* 72 (3), 475-503. doi:10.1002/glia.24474
- van Tilborg, E., Heijnen, C. J., Benders, M. J., van Bel, F., Fleiss, B., Gressens, P., et al. (2016). Impaired oligodendrocyte maturation in preterm infants: potential therapeutic targets. *Prog. Neurobiol.* 136, 28-49. doi:10.1016/j.pneurobio.2015.11.002
- Volpe, J. J. (2009). Brain injury in premature infants: a complex amalgam of destructive and developmental disturbances. *Lancet Neurol.* 8 (1), 110-124. doi:10.1016/S1474-4422(08)70294-1
- Volpe, J. J., Kinney, H. C., Jensen, F. E., and Rosenberg, P. A. (2011). The developing oligodendrocyte: key cellular target in brain injury in the premature infant. *Int. J. Dev. Neurosci.* 29 (4), 423-440. doi:10.1016/j.ijdevneu.2011.02.012
- Wang, X., Rousset, C. I., Hagberg, H., and Mallard, C. (2006). Lipopolysaccharide-induced inflammation and perinatal brain injury. *Semin. Fetal Neonatal Med.* 11 (5), 343-353. doi:10.1016/j.siny.2006.04.002
- Wang, Y., Kim, S. C., Wu, T., Jiao, Y., Jin, H., Hyo Lee, B., et al. (2020). Isoliquiritigenin attenuates anxiety-like behavior and locomotor sensitization in rats after repeated exposure to nicotine. *Evid. Based Complement. Altern. Med.* 2020, 9692321. doi:10.1155/2020/9692321
- Wilson-Costello, D., Friedman, H., Minich, N., Fanaroff, A. A., and Hack, M. (2005). Improved survival rates with increased neurodevelopmental disability for extremely low birth weight infants in the 1990s. *Pediatrics* 115 (4), 997-1003. doi:10.1542/peds.2004-0221
- Wolf, S. A., Boddeke, H. W. G., and Kettenmann, H. (2017). Microglia in Physiology and Disease. *Annu. Rev. Physiol.* 79, 619-643. doi:10.1146/annurev-physiol-022516-034406
- Xie, D., Shen, F., He, S., Chen, M., Han, Q., Fang, M., et al. (2016). IL-1 β induces hypomyelination in the periventricular white matter through inhibition of oligodendrocyte progenitor cell maturation via FYN/MEK/ERK signaling pathway in septic neonatal rats. *Glia* 64 (4), 583-602. doi:10.1002/glia.22950
- Yadav, V. R., Prasad, S., Sung, B., and Aggarwal, B. B. (2011). The role of chalcones in suppression of NF- κ B-mediated inflammation and cancer. *Int. Immunopharmacol.* 11 (3), 295-309. doi:10.1016/j.intimp.2010.12.006
- Yan, N., Xu, Z., Qu, C., and Zhang, J. (2021). Dimethyl fumarate improves cognitive deficits in chronic cerebral hypoperfusion rats by alleviating inflammation, oxidative stress, and ferroptosis via NRF2/ARE/NF- κ B signal pathway. *Int. Immunopharmacol.* 98, 107844. doi:10.1016/j.intimp.2021.107844
- Yang, E.-J., Min, J. S., Ku, H.-Y., Choi, H.-S., Park, M.-k., Kim, M. K., et al. (2012). Isoliquiritigenin isolated from *Glycyrrhiza uralensis* protects neuronal cells against glutamate-induced mitochondrial dysfunction. *Biochem. Biophys. Res. Commun.* 421 (4), 658-664. doi:10.1016/j.bbrc.2012.04.053
- Yuan, Z., Xu, P., Yu, F., Zhang, D., Zhao, Q., Yu, W., et al. (2020). An electroosmotic flow-free two-direction migration strategy enables fast affinity capillary electrophoresis to study the weak interactions between basic peptides and RNA. *Anal. Methods* 12 (48), 5833-5838. doi:10.1039/d0ay01515f
- Zhang, L., He, X., Liu, L., Jiang, M., Zhao, C., Wang, H., et al. (2016). Hdac3 interaction with p300 histone acetyltransferase regulates the oligodendrocyte and astrocyte lineage fate switch. *Dev. Cell* 36 (3), 316-330. doi:10.1016/j.devcel.2016.01.002
- Zhu, X., Liu, J., Chen, S., Xue, J., Huang, S., Wang, Y., et al. (2019). Isoliquiritigenin attenuates lipopolysaccharide-induced cognitive impairment through antioxidant and anti-inflammatory activity. *BMC Neurosci.* 20 (1), 41. doi:10.1186/s12868-019-0520-x
- Zou, P., Wu, C., Liu, T. C., Duan, R., and Yang, L. (2023). Oligodendrocyte progenitor cells in Alzheimer's disease: from physiology to pathology. *Transl. Neurodegener.* 12 (1), 52. doi:10.1186/s40035-023-00385-7



OPEN ACCESS

EDITED BY

Jian Hao,
The Second Affiliated Hospital of Guangzhou
Medical University, China

REVIEWED BY

Zheng Yuan,
China Academy of Chinese Medical Sciences,
China
Ruiheng Wang,
Cedars Sinai Medical Center, United States

*CORRESPONDENCE

Lu-Shiun Her,
✉ lsher@mail.ncku.edu.tw

†These authors have contributed equally to this work and share first authorship

RECEIVED 05 July 2024

ACCEPTED 30 August 2024

PUBLISHED 13 September 2024

CITATION

Huang Z-N, Lee S-Y, Chen J-M, Huang Z-T and Her L-S (2024) Oleuropein enhances proteasomal activity and reduces mutant huntingtin-induced cytotoxicity. *Front. Pharmacol.* 15:1459909. doi: 10.3389/fphar.2024.1459909

COPYRIGHT

© 2024 Huang, Lee, Chen, Huang and Her. This is an open-access article distributed under the terms of the [Creative Commons Attribution License \(CC BY\)](#). The use, distribution or reproduction in other forums is permitted, provided the original author(s) and the copyright owner(s) are credited and that the original publication in this journal is cited, in accordance with accepted academic practice. No use, distribution or reproduction is permitted which does not comply with these terms.

Oleuropein enhances proteasomal activity and reduces mutant huntingtin-induced cytotoxicity

Zih-Ning Huang[†], Sin-Yi Lee[†], Jie-Mao Chen, Zih-Ting Huang and Lu-Shiun Her^{*}

Department of Life Sciences, National Cheng Kung University, Tainan, Taiwan

Introduction: Huntington's disease (HD) is a hereditary neurodegenerative disorder that primarily affects the striatum, a brain region responsible for movement control. The disease is characterized by the mutant huntingtin (mHtt) proteins with an extended polyQ stretch, which are prone to aggregation. These mHtt aggregates accumulate in neurons and are the primary cause of the neuropathology associated with HD. To date, no effective cure for HD has been developed.

Methods: The immortalized *STHdh*^{Q111/Q111} striatal cell line, the mHtt-transfected wild-type *STHdh*^{Q7/Q7} striatal cell line, and N2a cells were used as Huntington's disease cell models. Flow cytometry was used to assess cellular reactive oxygen species and transfection efficiency. The CCK-8 assay was used to measure cell viability, while fluorescence microscopy was used to quantify aggregates. Immunoblotting analyses were used to evaluate the effects on protein expression.

Results: Polyphenols are natural antioxidants that offer neuroprotection in neurological disorders. In this study, we provide evidence that oleuropein, the primary polyphenol in olive leaves and olive oil, enhances cell viability in HD cell models, including *STHdh*^{Q7/Q7}/*STHdh*^{Q7/Q7} striatal cells, N2a cells ectopically expressing the truncated mHtt, and *STHdh*^{Q111/Q111} striatal cells expressing the full-length mHtt. Oleuropein effectively reduced both soluble and aggregated forms of mHtt protein in these HD model cells. Notably, the reduction of mHtt aggregates associated with oleuropein was linked to increased proteasome activity rather than changes in autophagic flux. Oleuropein seems to modulate proteasome activity through an unidentified pathway, as it did not affect the 20S proteasome catalytic β subunits, the proteasome regulator PA28 γ , or multiple MAPK pathways.

Abbreviations: AMC, 7-amino-4-methylcoumarin; Baf, Bafilomycin A1; β 1, proteasome 20S core caspase-like protease subunit; β 2, proteasome 20S core trypsin-like protease subunit; β 5, proteasome 20S core chymotrypsin-like protease subunit; CCK8, cell counting kit eight assay; CHX, cycloheximide; DMF, Dimethylformamide; Erk1/2 MAPK, extracellular signal-regulated mitogen-activated protein kinases 1/2; HD, Huntington's disease; Htt, huntingtin; JNK MAPK, c-Jun N-terminal mitogen-activated protein kinases; LC3, Microtubule-associated protein 1A/1B-light chain 3; mHtt, mutant huntingtin; Nrf2, Nuclear factor-erythroid 2 (NF-E2)-related factor 2; Oleu, oleuropein; p38 MAPK, p38 mitogen-activated protein kinases; p62, Sequestosome-1; PA28 γ , proteasome activator subunit 3 (PSME3, Ki); PBS, Phosphate-buffered saline; Q7, *STHdh*^{Q7/Q7} striatal cells; Q111, *STHdh*^{Q111/Q111} striatal cells; ROCK, rho-associated kinases; ROS, reactive oxidative species; SO, superoxide; SEM, standard error of the mean; tBHP, tert-Butyl Hydroperoxide.

Discussion: We demonstrated that oleuropein enhances the degradation of mHtt by increasing proteasomal protease activities and alleviates mHtt-induced cytotoxicity. Hence, we propose that oleuropein and potentially other polyphenols hold promise as a candidate for alleviating Huntington's disease.

KEYWORDS

Huntington's disease, mutant huntingtin aggregates, oleuropein, proteasome, ROS

1 Introduction

Huntington's disease (HD), an autosomal dominant neurodegenerative disorder, is caused by an expansion of the CAG trinucleotide repeats in the exon one of the huntingtin (Htt) gene (MacDonald et al., 1993). The expression of mutant Htt (mHtt) induces cell death in neuronal predisposing mHtt to misfolding and subsequent aggregation. Compelling evidence has linked aggregation of mHtt to striatal neuronal death, and this is recognized as one of the main pathogenic factors in HD (Davies et al., 1997; DiFiglia et al., 1997; Martín-Aparicio et al., 2001; Intihar et al., 2019; Layburn et al., 2022). The cellular dysfunctions associated with mHtt aggregates include proteasomal and mitochondrial dysfunctions and decreased cell viability (Yin et al., 2016; Soares et al., 2019; Fão and Rego, 2021). Hence, neuroprotective treatments such as anti-aggregation compounds, aggregate clearance strategies, and gene-silencing approaches to remove mHtt aggregates have been developed as potential therapeutic strategies for HD patients (Martín-Aparicio et al., 2001; Soares et al., 2019; Huang et al., 2021; Rippin et al., 2021; Zhang et al., 2021; Hommen et al., 2022; Ferlazzo et al., 2023; Jain and Roy, 2023; Yang et al., 2023; Jain et al., 2024).

Recently, microRNA (miRNA) administration has been reported to reduce mHtt aggregates and slow the disease progression of HD model mice (Cheng et al., 2013a; Ban et al., 2017; Chang et al., 2021; Spronck et al., 2021; Kotowska-Zimmer et al., 2022; Chan et al., 2023). However, delivery of the miRNA requires injection into the central nervous system, which is challenging for practical purposes and has ethical concerns. In addition, it is difficult to assess the efficacy because miRNAs are generally unstable. Therefore, whether miRNAs can be used as therapeutic agents remains debatable.

The autophagy-lysosome pathway and the Ubiquitin Proteasome System are the two major cellular proteolytic pathways (Watanabe et al., 2020; Rusilowicz-Jones et al., 2022). Inhibition of either the autophagy or proteasome impairs the degradation of mHtt protein and leads to the accumulation of mHtt aggregates (Koyuncu et al., 2017; Valionyte et al., 2020; Folger and Wang, 2021). For example, activation of the UPS activity by inhibiting the p38 MAPK pathway reduces both the soluble and aggregated forms of mHtt and increases cell viability in the *STHdh* striatal HD model cells (Huang et al., 2021). Also, activation of the autophagy pathway promotes clearance of mHtt aggregates and increases cell viability in human neuroblastoma SH-SY5Y cells, mouse embryonic fibroblast, and the HdH140Q knock-in HD model mice [(Sarkar et al., 2007; Chaudhary et al., 2021; Long et al., 2022) and reviewed in Valionyte et al. (2020); Folger and Wang (2021)]. Therefore, seeking small molecules that can enhance autophagy and/or proteasome activities is a logical strategy to

achieve clearance of the mHtt protein and ameliorate HD phenotype.

Oleuropein is the major phenolic compound present in olive oil and olive leaves (Omar, 2010). Oleuropein is highly antioxidative and has been demonstrated to protect against neurodegenerative diseases and cardiovascular and metabolic disorders [(Rigacci et al., 2015; Achour et al., 2016; Brunetti et al., 2020; Butt et al., 2021; Leri et al., 2021) and review in Micheli et al. (2023)]. In addition to its antioxidative properties, oleuropein increases autophagy and proteasomal activity (Katsiki et al., 2007; Huang and Chen, 2009; El Demerdash et al., 2021). Here, we explored the potential of oleuropein to improve cell viability and its effect on reducing mHtt aggregates in HD model cells. We also investigated whether oleuropein affects HD model cells' proteasome and autophagy activities. Our data provided evidence to show that oleuropein has neuroprotective effects.

2 Materials and methods

2.1 Cell line, cell culture, and drug treatments

The immortalized wild-type *STHdh*^{Q7/Q7} striatal cell line (RRID: CVCL_M590, Coriell ID: CH00097) and the mutant *STHdh*^{Q111/Q111} striatal cell line (RRID: CVCL_M591, Coriell ID: CH00095) were obtained from Coriell (United States of America) (Trettel et al., 2000). Mouse neuroblastoma Neuro-2a (N2a) cell line was purchased from Bioresource Collection and Research Center, Taiwan (RRID: CVCL_0470, BCRC, Cat#60026). Cell culture of the immortalized *STHdh* striatal cells and N2a was carried out as described previously (Huang et al., 2017; Huang and Her, 2017; Huang et al., 2021). Oleuropein (Cat#12247, Sigma, United States of America) was dissolved in DMF to make a 50 mg/mL stock solution. The cells were incubated with oleuropein at 0.5 µg/mL, 2 µg/mL, or 5 µg/mL for 24 or 48 h, as described in Figure legends. Before treatment, the 50 mg/mL oleuropein stock was first diluted in 1:1,000 in cell medium to generate a 50 µg/mL working solution. The 50 µg/mL oleuropein working solution was further diluted in a cell medium to achieve the desired concentration. The DMF concentration in the cell medium was kept at 0.1% throughout the oleuropein experiments. To assess autophagic flux, N2a cells and *STHdh* striatal cells were treated with 200 nM Bafilomycin A1 (Cat#B1793, Sigma, United States of America) for 6 h to block the fusion of the autophagosome with a lysosome (Klionsky et al., 2021). To assess the stability of soluble Htt, N2a cells and *STHdh*^{Q7/Q7} striatal cells were incubated with 100 µg/mL cycloheximide (Cat#C4859, Sigma, United States of America) for 24 h to block protein synthesis (Schneider-Poetsch et al., 2010; #298767).

2.2 DNA constructs and transfection

The pHttQP25-GFP and pHttQP72-GFP expression vectors, containing the exon one of human huntingtin and GFP fusion proteins with 25 or 72 CAG repeats, respectively, were obtained from the CHDI/High Q Foundation (United States of America). The pcDNA3.1-mCherry vector, containing the mCherry fluorescent protein coding sequence, was provided by Dr. Roger Y. Tsien of the University of California, San Diego. The p3xFLAG-QP25 and p3xFLAG-QP103 expression vectors were constructed by inserting the exon one of human huntingtin with 25 and 103 CAG repeats, respectively, into the p3xFLAG-CMV-10 expression vector to generate the FLAG-tagged truncated human huntingtin with 25 or 103 glutamines, respectively (Sigma). The pEBV-HttQ120F expression vector, containing the full-length human huntingtin with 120 CAG repeat coding sequence, was kindly provided by Dr. Xiao-Jiang Li of Jinan University in Guangzhou, China (Zhou et al., 2003). For transfection of the indicated plasmids, the immortalized *STHdh* striatal cells and N2a cells were incubated with Lipofectamine 3,000 (Cat#L3000015, Invitrogen, United States of America) according to the manufacturer's protocol.

2.3 Transfection efficiency assessment

Forty-eight hours after transfection of *STHdh*^{Q71/Q7} striatal cells with HttQP25-GFP or HttQP72-GFP plasmid, the cells were collected for GFP fluorescence analysis using Attune NxT flow cytometry (Thermo Fisher Scientific, United States of America). The cell population was gated by FSC and SSC channels, and the GFP signals were detected in the BL1 channel. The GFP positive signal was gated by the fluorescence intensity over 10³. The transfection efficiency was calculated by analyzing the percentage of GFP-positive cells out of the total number of cells (set as 100%).

2.4 CCK-8 cell viability assay

Cells were pre-incubated with DMF or oleuropein at the concentration of 0.5 µg/mL, 2 µg/mL or 5 µg/mL for 24 h before treatment with 100 µM tBHP (Cat#B2633, Sigma, United States of America) for 4 h. CCK-8 cell viability assays were carried out as described before (Huang et al., 2021).

2.5 Analysis of cellular reactive oxygen species (ROS) and superoxide (SO) levels

For ROS and SO detection, the immortalized *STHdh* striatal cells and N2a cells were seeded in a 6 cm petri dish as described before (Huang et al., 2017). The levels of ROS and SO were determined by Flow cytometry, the BD Biosciences FACS Caliber system (San Jose, CA), with Total ROS/SO detection kit (Cat#ENZ-51010, Enzo, United States of America) as suggested by the manufacturer's instructions. Briefly, cells were washed with 1X phosphate buffered saline (PBS, pH7.4) and incubated with the ROS and SO detection solutions at 37°C for 30 min in the dark. ROS (Green) signals were detected in the FL1 channel, and signals produced by

SO (Orange) were detected in the FL2 channel. Detected cells will appear in the upper left and upper right quadrants of a log FL1 (X-axis) versus a log FL2 (Y-axis) dot plot. For each sample, at least 1 × 10⁴ cells were analyzed. The percentage of ROS-positive and SO-positive cells was calculated using the FlowJo (ver.10.7.1) software. Quantification data were derived from three biological replicates.

2.6 Fluorescence microscopy imaging and quantification of aggregate formation

Fluorescence microscopy imaging was carried out as described previously (Huang et al., 2017; Huang et al., 2021). The mutant Htt-GFP aggregates were visualized with Eclipse Ti epifluorescence inverted microscope (Nikon, Japan). Aggregates were defined as a clear region of dense GFP signal as described previously (Juenemann et al., 2011; Cheng et al., 2013b; Huang and Her, 2017). The co-transfected red mCherry fluorescence signal was used to calculate the total number of transfected cells as a control for transfection efficiency. The percentage of cells containing the aggregates was calculated as the ratio of the number of red cells (mCherry transfected control) with mutant Htt-GFP aggregates/total number of red cells counted (set as 100%). More than 100 red mCherry fluorescence signal-positive cells were counted in each experiment. Data were average obtained from three independent experiments.

2.7 Antibodies and immunoblotting analysis

Antibodies used in this study are: anti-Htt (MAB2166, 1:1,000; Millipore Bioscience Research Reagents), anti-Htt (mEM48, MAB5374, 1:500; Millipore Bioscience Research Reagents), anti-p62 (ab56416, 1:1,000; Abcam), anti-LC3B (ab48394, 1:500; Abcam), anti-Proteasome 20S β1 (BML-PW8140, 1:1,000; Enzo), anti-Proteasome 20S β2 (BML-PW8145, 1:1,000; Enzo), anti-Proteasome 20S β5 (BML-PW8895, 1:1,000; Enzo), anti-PA28γ (PSME3) (GTX106722, 1:2000; GeneTex), anti-Phospho-p38 MAPK (Thr80/Tyr182) (#4511, 1:1,000, Cell Signaling), anti-p38 MAPK (#9212, 1:1,000, Cell Signaling), anti-Phospho-Nrf2 (Phospho S40) (ab76026, 1:5,000, Abcam), anti-Nrf2 (ab62352, 1:1,000, Abcam), anti-Phospho-p44/p42 MAPK (Thr202/Tyr204) (#4370, 1:1,000, Cell Signaling), anti-p44/p42 (#4696, 1:1,000, Cell Signaling), anti-Phospho-SAPK/JNK (Thr183/Tyr182) (#4668, 1:1,000, Cell Signaling), anti-SAPK/JNK (#9252, 1:1,000, Cell Signaling), anti-Phospho-ROCK2 (phosphor Ser1366) (GTX122651, 1:1,000, GeneTex), anti-ROCK2 (GTX108247, 1:1,000, GeneTex), anti-Tubulin (T6074, 1:5,000; Sigma), and anti-Actin (MAB1501, 1:1,000; Millipore Bioscience Research Reagents). Immunoblotting assays were carried out as described previously (Huang and Her, 2017; Huang et al., 2021). Proteins were detected using the enhanced chemiluminescence (ECL) assay-Western Lightning® ECL Pro (Cat#NEL105001EA, PerkinElmer, United States of America). The signals were captured by iBright FL1500 Imaging System (Thermo Fisher Scientific) and UVP ChemStudio PLUS Imaging Systems (Analytik Jena), respectively. Proteins quantification and background correction were analyzed using the iBright analysis software (ver.4.0.1, Thermo Fisher

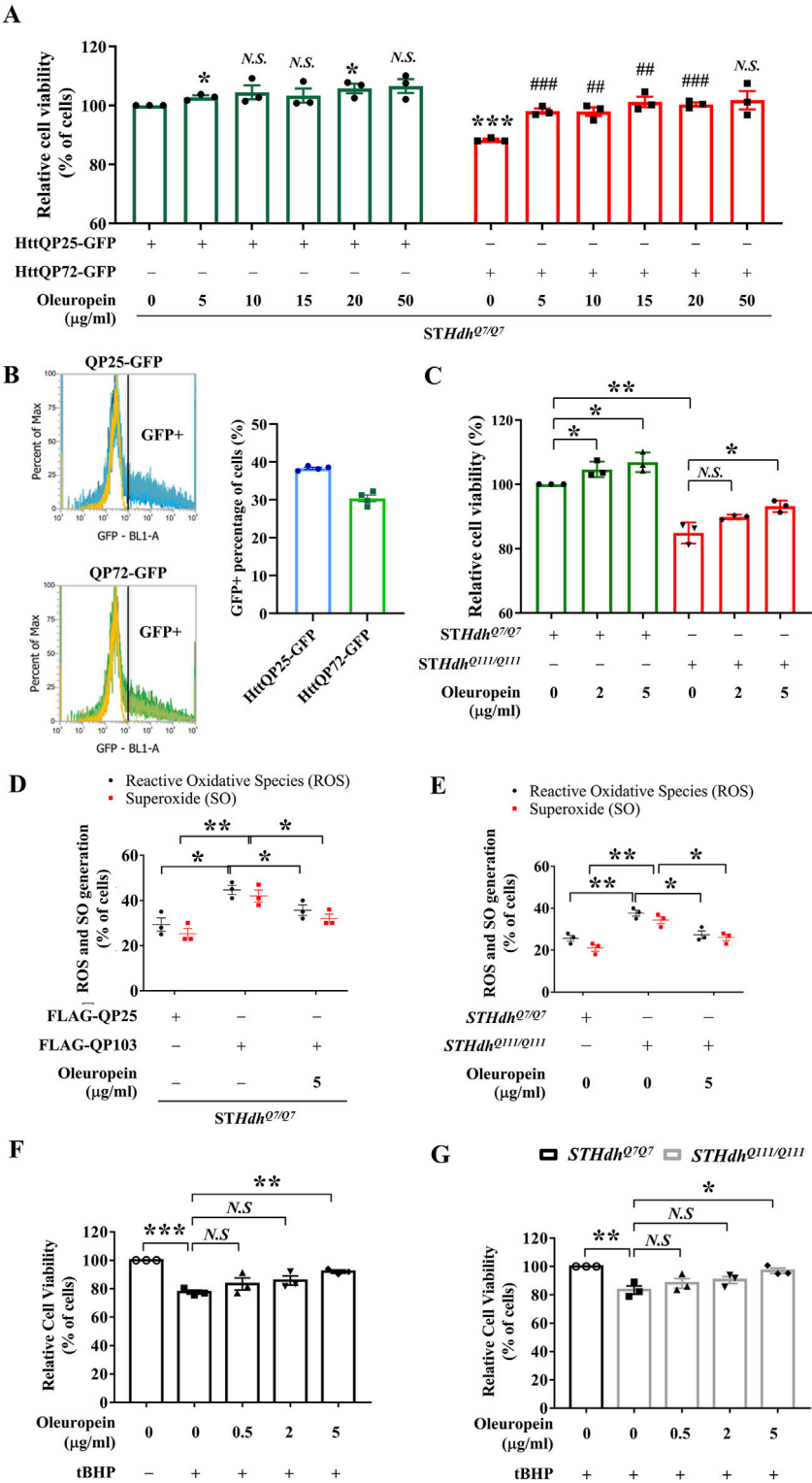


FIGURE 1
Oleuropein ameliorates mHtt-induced cytotoxicity. **(A)** Cell viability analysis of *STHdh*^{Q7/Q7} striatal cells transfected with the HttQP25-GFP or HttQP72-GFP plasmid. 24 h after transfection, cells were incubated with oleuropein at the indicated concentration for another 24 h. Cells without treatment were used as the negative control. Data showing a significant difference compared to the HttQP25-GFP transfected cells treated with 0 µg/ml oleuropein is labeled with an asterisk (*); Data showing a significant difference compared to the HttQP72-GFP transfected cells treated with 0 µg/ml oleuropein is labeled with a pound sign (#). **(B)** Transfection efficiency analysis of the *STHdh*^{Q7/Q7} and *STHdh*^{Q111/Q111} striatal cells transfected with the HttQP25-GFP or HttQP72-GFP plasmid using flow cytometry analysis. **(C)** Cell viability analysis of *STHdh*^{Q7/Q7} and *STHdh*^{Q111/Q111} striatal cells after incubation with oleuropein at the indicated concentration for 24 h. Cells without treatment were used as the negative control. **(D)** Flow cytometric analysis of reactive oxygen species (ROS) and superoxide (SO) levels in *STHdh*^{Q7/Q7} striatal cells transfected with the FLAG-QP25 or FLAG-QP103 plasmid in the presence or absence of oleuropein. The percentage of the cells with positive ROS or SO signal was quantified. Cells were incubated with oleuropein at the indicated concentration for 24 h. **(E)** Flow cytometric analysis of reactive oxygen species (ROS) and superoxide (SO) levels in *STHdh*^{Q7/Q7} and *STHdh*^{Q111/Q111} striatal cells after incubation with oleuropein at the indicated concentration for 24 h. Cells without treatment were used as the negative control. **(F)** Cell viability analysis of *STHdh*^{Q7/Q7} striatal cells transfected with the HttQP25-GFP or HttQP72-GFP plasmid, treated with oleuropein at the indicated concentration for 24 h. Cells without treatment were used as the negative control. Data showing a significant difference compared to the HttQP25-GFP transfected cells treated with 0 µg/ml oleuropein is labeled with an asterisk (*); Data showing a significant difference compared to the HttQP72-GFP transfected cells treated with 0 µg/ml oleuropein is labeled with a pound sign (#). **(G)** Cell viability analysis of *STHdh*^{Q7/Q7} and *STHdh*^{Q111/Q111} striatal cells after incubation with oleuropein at the indicated concentration for 24 h. Cells without treatment were used as the negative control. Data showing a significant difference compared to the *STHdh*^{Q7/Q7} cells treated with 0 µg/ml oleuropein is labeled with an asterisk (*); Data showing a significant difference compared to the *STHdh*^{Q111/Q111} cells treated with 0 µg/ml oleuropein is labeled with a pound sign (#). (Continued)

FIGURE 1 (Continued)

concentration for 24 h. (E) Flow cytometric analysis of ROS and SO levels in *STHdh*^{Q7/Q7} and *STHdh*^{Q111/Q111} striatal cells plasmid in the absence or presence of oleuropein at the indicated concentration for 24 h. (F) Cell viability analysis of tBHP (100 μ M)-treated *STHdh*^{Q7/Q7} striatal cells without or with oleuropein pre-incubation at the indicated concentration for 24 h. (G) Cell viability analysis in tBHP-treated *STHdh*^{Q7/Q7} and *STHdh*^{Q111/Q111} striatal cells in the absence or presence of incubation with oleuropein at the indicated concentration for 24 h. Data from three independent experiments are presented as mean normalized units \pm SEM. Data showing significant differences are labeled as follows: $p < 0.05$ with one asterisk (*), $p < 0.01$ with two asterisks (**), and $p < 0.005$ with three asterisks (***).

Scientific) and the VisionWorks (ver.9.1.20063.7760, UVP ChemStudio PLUS Imaging Systems analysis software, Analytik Jena), respectively.

2.8 Proteasome core protease activity assay

The proteasome core protease activity assay was carried out as described previously (Huang et al., 2021). Cell lysates were prepared with a Tris-based buffer (50 mM Tris pH 7.4, 1 mM EDTA, 2 mM ATP, and 1% Triton). Proteasome activity assay was conducted in a 96-well plate format. For each well, 10 μ g of protein lysate was incubated with the three different fluorogenic substrates separately: 50 μ M of Suc-Leu-Leu-Val-Tyr-7-amino-4-methylcoumarin (Suc-LLVY-AMC, Cat# BML-P802-0,005, Enzo Life Sciences, United States of America) was used for chymotrypsin-like activity assay; 25 μ M of Boc-Leu-Arg-Arg-7-amino-4-methylcoumarin (Boc-LRR-AMC, Cat# BML-BW8515-0,005, Enzo Life Sciences, United States of America) was used for trypsin-like activity assay; and 50 μ M of Z-Leu-Leu-Glu-7-amino-4-methylcoumarin (Z-LLE-AMC, Cat# BML-ZW9345-0,005, Enzo Life Sciences, United States of America) as used for the caspase-like activity assay. To detect free AMC released during the enzymatic reaction, the protease-cleaved fluorogenic products were excited at 360 nm, and the resulting fluorescence emission was detected at 460 nm using a fluorescent plate reader (TECAN Infinite M200 fluorescent plate reader, Tecan Trading AG, Switzerland). The release rate of AMC was measured at 37°C by recording the emitted fluorescence signal every 5 min for a total of 120 min.

2.9 Statistical analysis

Determination of the statistical differences between groups was carried out using the Student's t-test, which was reported as a p -value. Data showed significant differences with $p < 0.05$ are labeled with one asterisk (*); with $p < 0.01$ are labeled with two asterisks (**); with $p < 0.005$ are labeled with three asterisks (***); N.S.: not significant. The experimental results from three independent experiments were calculated and presented as mean \pm standard error of the mean (SEM).

3 Results

3.1 Oleuropein ameliorates mutant htt-induced cytotoxicity

Knowing that oleuropein provides neuroprotection in both cell and animal models of Alzheimer's disease (Leri et al., 2021;

Marianetti et al., 2022), we were interested in asking whether oleuropein could also protect neurons in HD model cells. In this study, we used the *STHdh*^{Q7/Q7} striatal cell as our system because the medium spiny neuron in the striatum is the most affected in HD patients, and the *STHdh*^{Q7/Q7} striatal cells, an immortalized cell line derived from the striatal medium spiny neurons of the wild-type *Hdh*^{Q7/Q7} mice, are commonly used (Trettel et al., 2000; Pal et al., 2006; Jin et al., 2013; Yin et al., 2016; Okada et al., 2021).

To establish an HD cell model, a truncated mutant huntingtin (mHtt)-GFP reporter protein with a 72 polyQ stretch (GFP-QP72) was expressed in *STHdh*^{Q7/Q7} striatal cells. This truncated mHtt protein, encoded by the Htt exon 1 with expanded CAG repeats, is a cleavage product of the full-length mHtt protein and has been shown to form aggregates and induce cytotoxicity (Lunkes et al., 2002; Yang et al., 2020). Ectopic expression of the truncated wild-type Htt (encoded by the Htt exon 1)-GFP reporter (GFP-QP25) was used as a control. The transfection efficiency was assessed by flow cytometry as the percentage of cells displaying a GFP-positive signal. The transfection efficiency of HttQP25-GFP and HttQP72-GFP in *STHdh*^{Q7/Q7} striatal cells was 38.33% and 30.37%, respectively (Figure 1B). Cell viability was measured 24 h after oleuropein incubation. As predicted, ectopic expression of the mutant GFP-QP72 mHtt protein decreased the cell viability of *STHdh*^{Q7/Q7} striatal cells (from 100% to 88%; $p < 0.0001$, Figure 1A). Oleuropein at 5, 10, 15, 20, or 50 μ g/mL was used to treat the *STHdh*^{Q7/Q7} striatal cells expressing the mutant GFP-QP72 mHtt protein. Oleuropein treatment improved the cell viability of the *STHdh*^{Q7/Q7} striatal cells expressing GFP-QP72 mHtt protein at all of the concentrations tested (Figure 1A). However, increasing oleuropein above a concentration of 5 μ g/mL oleuropein (from 88% to 98%, $p = 0.0005$, Figure 1A) did not provide further protection (Figure 1A). Therefore, we used five μ g/mL oleuropein for the rest of the experiments.

To test whether oleuropein-associated neuroprotection is a general or cell line-specific effect, we extended this study to the mouse N2a neuronal cells. Similar to the *STHdh*^{Q7/Q7} striatal cells, treatment of five μ g/mL oleuropein increased the cell viability of N2a cells expressing the mutant GFP-QP72 protein (from 86.41% to 92.41%; $p = 0.034$, Supplementary Figure S1). Oleuropein did not affect the cell viability of the N2a cells expressing the GFP-QP25 protein (from 100% to 101.6%; $p > 0.05$, Supplementary Figure S1C).

Because cellular abnormalities of the mutant *STHdh*^{Q111/Q111} striatal cells that express the endogenous full-length mutant Htt protein resemble damaged neurons reported in HD patients (Trettel et al., 2000; Pal et al., 2006; Jin et al., 2013; Yin et al., 2016; Okada et al., 2021), we tested the effect of oleuropein on the cytotoxicity of mutant *STHdh*^{Q111/Q111} striatal cells. Consistent with previous studies, the mutant *STHdh*^{Q111/Q111} striatal cells had reduced cell viability as compared to the wild-type *STHdh*^{Q7/Q7} striatal cells (from

100% to 84.91%; $p = 0.0013$, Figure 1C). Notably, oleuropein at the 5 $\mu\text{g/mL}$ concentration increased the cell viability of the mutant *STHdh*^{Q111/Q111} striatal cells (from 84.91% to 93.19%; $p = 0.0182$, Figure 1C).

Moreover, extending the duration of oleuropein treatment led to an improved protective effect. Cell viability of *STHdh*^{Q7/Q7} striatal cells transfected with the HttQP72-GFP plasmid was increased by 25% following 48 h of 5 $\mu\text{g/mL}$ oleuropein treatment, starting 48 h post-transfection (from 81.14% to 106%; $p = 0.0009$, Supplementary Figure S1A). Cell viability of mutant *STHdh*^{Q111/Q111} striatal cells was increased by 28% following 48 h of 5 $\mu\text{g/mL}$ oleuropein treatment (from 79.99% to 108.6%; $p = 0.0001$, Supplementary Figure S1B). Taken together, our data demonstrated that oleuropein reduced the cytotoxicity induced by the GFP-QP72 mHtt protein in the *STHdh*^{Q7/Q7} striatal and N2a cells. Moreover, oleuropein also reduced the cytotoxicity in mutant *STHdh*^{Q111/Q111} striatal cells.

3.2 Oleuropein reduces mutant htt-induced ROS accumulation

Increased ROS levels often lead to excess oxidation of cellular macromolecules, such as DNA, lipids, and proteins (Reichmann et al., 2018; Lévy et al., 2019; Yuan et al., 2021; Yu et al., 2024). Knowing that expression of mHtt protein is associated with increased ROS (Trettel et al., 2000; Milakovic et al., 2006) and oleuropein is a potent antioxidant (Kruk et al., 2005; Choi et al., 2021), we asked whether oleuropein affects the cellular redox state that subsequently reduces the cytotoxicity of the mHtt model cells. To test this, the cellular ROS and superoxide (SO) levels were monitored in the *STHdh*^{Q7/Q7} cells expressing the FLAG-tagged truncated mHtt protein with a 103 polyQ stretch (FLAG-QP103). Ectopic expression of the FLAG-QP103 protein caused an increase in ROS levels as compared to the control *STHdh*^{Q7/Q7} striatal cells ectopically expressing the FLAG tagged-truncated wild-type Htt protein (FLAG-QP25) (from 29% to 45%; $p = 0.019$, black bars in Figure 1D) and SO (from 25% to 42%; $p = 0.0091$, red bars in Figure 1D). Furthermore, oleuropein significantly decreased the ROS levels (from 45% to 35%; $p = 0.029$, black bars in Figure 1D) and SO levels (from 42% to 32%; $p = 0.033$, red bars in Figure 1D) in the *STHdh*^{Q7/Q7} striatal cells ectopically expressing the mutant FLAG-QP103 protein. These results suggest that oleuropein may reduce the cytotoxicity of the HD model cells by decreasing the cellular ROS and SO levels.

We then asked whether oleuropein acts on modulating ROS levels to reduce the cytotoxicity of the mutant *STHdh*^{Q111/Q111} striatal cells. As predicted, the mutant *STHdh*^{Q111/Q111} striatal cells had increased ROS signals as compared to those of the wild-type *STHdh*^{Q7/Q7} striatal cells (from 25% to 37%; $p = 0.0062$, black bars in Figure 1E). Consistently, oleuropein treatment significantly reduced the percentage of cells with positive ROS signals in the mutant *STHdh*^{Q111/Q111} striatal cells (from 37% to 27%; $p = 0.017$, black bars in Figure 1E). Oleuropein treatment also significantly reduced the percentage of mutant *STHdh*^{Q111/Q111} striatal cells with SO signals (from 34% to 25%; $p = 0.048$, red bars in Figure 1E). Taken together, our data demonstrated that

cytotoxicity alleviation correlates with the reduction of cellular ROS and SO levels in all mHtt models tested.

3.3 Oleuropein pre-treatment protects against acute oxidative stress in HD model cells

Because of the ability of oleuropein to reduce ROS and SO accumulation in mHtt model cells, we asked whether oleuropein could protect neurons from oxidative stress. To this end, acute oxidative stress was induced in the *STHdh* cells treated with 100 μM tBHP for 4 h. After tBHP treatment, the cell viability of *STHdh*^{Q7/Q7} striatal cells decreased compared to the untreated cells (from 100% to 77.65%; $p = 0.0001$; Figure 1F), indicating cells were under oxidative stress. We then tested the effect of oleuropein on the *STHdh*^{Q7/Q7} striatal cells treated with tBHP. The *STHdh*^{Q7/Q7} striatal cells were preincubated with oleuropein at different concentrations for 24 h before challenging with tBHP. We found that pre-incubation with 5 $\mu\text{g/mL}$ oleuropein increased the viability of tBHP-challenged *STHdh*^{Q7/Q7} striatal cells (from 77.65% to 92.06%; $p = 0.0013$; Figure 1F), suggesting that oleuropein protects neuronal cells from acute oxidative stress.

It is reported that HD striatal neurons are sensitive to oxidative stress (Jalgaonkar et al., 2023). In addition, the accumulation of mHtt aggregates is associated with increased ROS levels, reduced mitochondrial function, and decreased cell viability (Yin et al., 2016; Soares et al., 2019; Fão and Rego, 2021). Knowing that oleuropein protects the *STHdh*^{Q7/Q7} striatal cells from tBHP-induced acute oxidative stress, we were interested in testing whether oleuropein could protect mutant *STHdh*^{Q111/Q111} striatal cells, which already had relatively high ROS levels (Figure 1E), from additional acute oxidative stress. To this end, the mutant *STHdh*^{Q111/Q111} striatal cells were pre-incubated with oleuropein at the concentration of 0.5 $\mu\text{g/mL}$, 2 $\mu\text{g/mL}$, or 5 $\mu\text{g/mL}$ for 24 h before subjecting to 100 μM tBHP treatment. As predicted, the tBHP-treated mutant *STHdh*^{Q111/Q111} striatal cells had lower cell viability as compared to the tBHP-treated *STHdh*^{Q7/Q7} striatal cells (from 100% to 83.41%; $p = 0.005$; Figure 1G). Pre-incubation with 5 $\mu\text{g/mL}$ oleuropein, on the other hand, protected mutant *STHdh*^{Q111/Q111} striatal cells from tBHP-induced oxidative stress (from 83.41 to 96.96; $p = 0.0183$; Figure 1G). Oleuropein at the concentration of 0.5 $\mu\text{g/mL}$ or 2 $\mu\text{g/mL}$ did not have effect. Taken together, our data support that oleuropein at the concentration of 5 $\mu\text{g/mL}$ is capable of protecting *STHdh*^{Q7/Q7} striatal cells and the mutant *STHdh*^{Q111/Q111} striatal cell from acute oxidative stress.

3.4 Oleuropein reduces mutant huntingtin aggregates

Accumulation of mHtt aggregates is a major factor that leads to the death of striatal neurons and is recognized as one of the main pathogenic factors in HD (Davies et al., 1997; DiFiglia et al., 1997; Martín-Aparicio et al., 2001; Intihar et al., 2019; Layburn et al., 2022). Because oleuropein protects the *STHdh*^{Q7/Q7} striatal cells ectopically expressing the truncated mHtt protein and also reduced mHtt-associated ROS accumulation (Figure 1), we asked

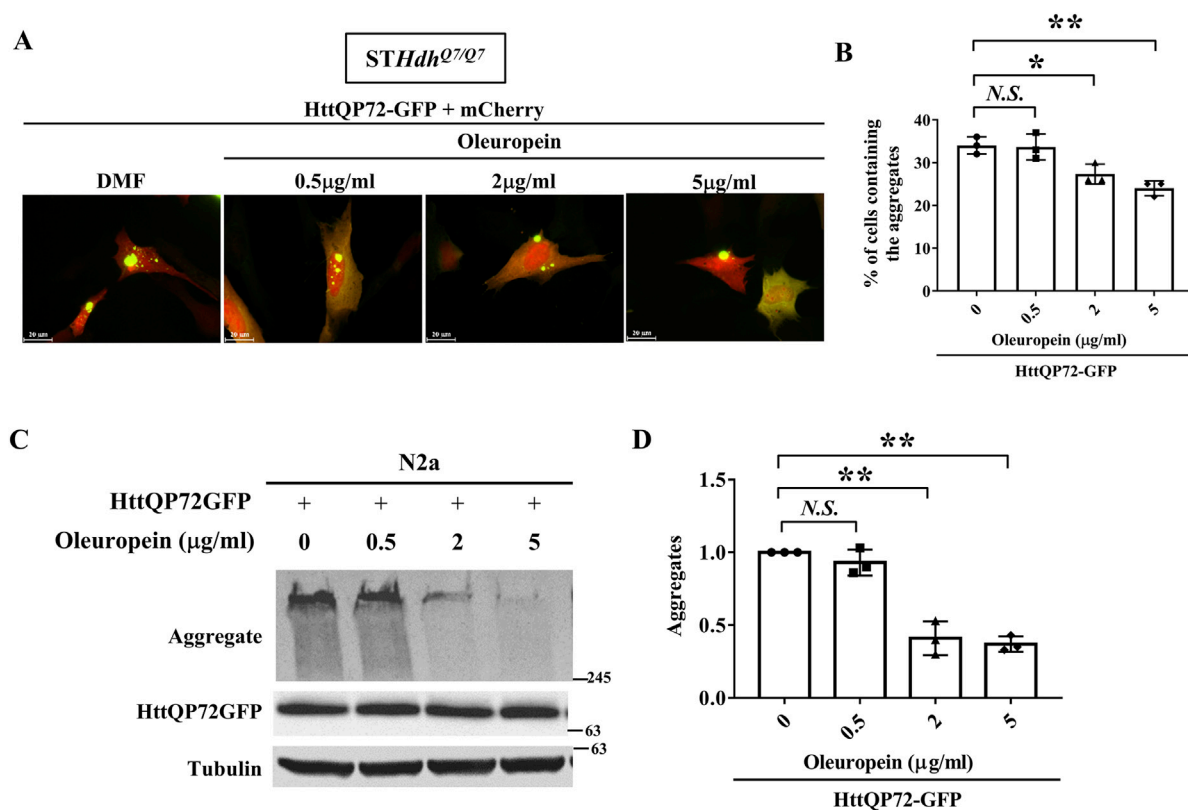


FIGURE 2

Oleuropein reduces mutant huntingtin aggregates. (A) Images showing STHdh^{Q7/Q7} striatal cells co-transfected with the HttQP72-GFP and mCherry plasmids after oleuropein treatment. Cells without treatment were used as the control. (B) Quantification analysis of the percentage of cells containing the aggregates in STHdh^{Q7/Q7} striatal cells transfected with the indicated plasmids in the absence or presence of oleuropein treatment at the indicated concentration for 24 h. (C) Immunoblot detection of the aggregated and soluble forms of HttQP72-GFP in N2a cells transfected with the indicated plasmid incubated in the absence or presence of oleuropein at the indicated concentration for 24 h. Tubulin protein was used as an internal control. (D) Quantification analyses of the normalized HttQP72-GFP aggregates. Tubulin was used as an internal control for normalization in (C). Data from three independent experiments are presented as mean normalized units \pm SEM. Data showing significant differences are labeled as follow: $p < 0.05$ with one asterisk (*), and $p < 0.01$ with two asterisks (**). N.S., no significance.

whether oleuropein-mediated alleviation of HD pathology is linked to decrease in the mHtt aggregates. To test this idea, we monitored the HttQP72-GFP aggregates in the STHdh^{Q7/Q7} striatal cells ectopically expressing the truncated mutant HttQP72-GFP protein in the absence or presence of oleuropein at different concentrations for 24 h. Oleuropein at the concentration of 2 μg/mL and 5 μg/mL caused a visible decrease in the accumulation of HttQP72-GFP aggregates (Figure 2A). Quantification analysis also confirmed that oleuropein treatment significantly reduced the percentage of cells containing the HttQP72-GFP aggregates (from 34% to 27% at the concentration of 2 μg/mL and from 34% to 24% at the concentration of 5 μg/mL); $p = 0.047$ and $p = 0.0072$, respectively, Figure 2B).

Oleuropein-mediated reduction of HttQP72-GFP aggregates was also confirmed in N2a cells by immunoblotting (Figure 2C). Quantification analysis also confirmed oleuropein significantly reduced the amount of HttQP72-GFP aggregates (from one to 0.4 at the concentration of 2 μg/mL and from one to 0.37 at the concentration of 5 μg/mL; $p = 0.0065$ and $p = 0.0053$, respectively, Figure 2D). Taken together, our data indicate that oleuropein reduces the accumulation of HttQP72-GFP aggregates.

3.5 Oleuropein reduces the soluble form of mHtt in mutant huntingtin-expressing cells

Reducing the amount of soluble mHtt is pivotal to preventing the formation of huntingtin oligomers and facilitating the dissolution of mHtt aggregates in HD (Valionyte et al., 2020). Since oleuropein reduces the accumulation of mHtt aggregates, we asked whether oleuropein affects the stability and overall abundance of mHtt protein. To address this, soluble mutant HttQP72-GFP protein was monitored in the N2a cells treated with oleuropein. The N2a cells were treated with cycloheximide to prevent *de novo* protein synthesis. As expected, oleuropein treatment decreased mutant HttQP72-GFP protein aggregation at 24 h (from 1 to 0.83-fold, $p = 0.0404$) and 48 h (from 0.77 to 0.52-fold, $p = 0.0011$) post-treatment (Figures 3A, B). Additionally, the soluble form of mutant HttQP72-GFP protein was also reduced 24 h (from 1 to 0.86-fold; $p = 0.0033$) and 48 h (from 0.81 to 0.6-fold, $p = 0.048$) after oleuropein treatment (Figures 3A, C). The effect of oleuropein on the soluble form of mHtt protein was also tested in STHdh^{Q7/Q7} striatal cells. Consistently, oleuropein reduced the soluble form of the mutant HttQP72-GFP protein 24 h (from

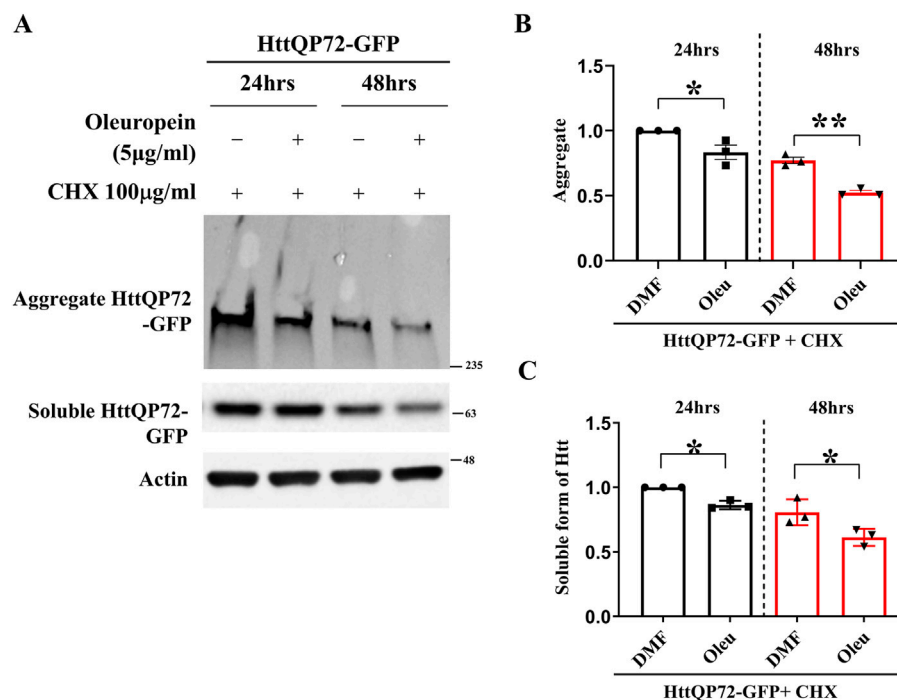


FIGURE 3

Oleuropein decreases the aggregated and soluble forms of truncated mHtt in N2a cells. (A) Immunoblot detection of the aggregated and soluble forms of mutant Htt (HttQP72-GFP) in N2a cells transfected with the HttQP72-GFP plasmid in the absence or presence of oleuropein treatment at the indicated concentration for 24 or 48 h. Cells were treated with 100 µg/ml cycloheximide (CHX) to inhibit protein synthesis. Actin was used as an internal control. (B) Quantification analyses of the aggregated form of HttQP72-GFP protein. (C) Quantification analyses of the soluble form of HttQP72-GFP protein. Actin was used for normalization. Data from three independent experiments are presented as mean normalized units ± SEM. Data showing significant differences are labeled as follows: $p < 0.05$ with one asterisk (*) and $p < 0.01$ with two asterisks (**).

1 to 0.7033-fold; $p = 0.0365$) and 48 h (from 1.05 to 0.6767-fold; $p = 0.0163$) after treatment (Supplementary Figure S2A).

Since oleuropein reduces the soluble form of mutant HttQP72-GFP protein, we asked whether oleuropein has a similar effect on the stability and overall abundance of the full-length mHtt protein. To address this question, the endogenous full-length mHtt protein was monitored in oleuropein-treated *STHdh*^{Q111/Q111} striatal cells. Cycloheximide was added to prevent *de novo* protein synthesis. We found that oleuropein treatment did not affect the level of endogenous full-length mHtt protein (Supplementary Figure S3A). Similarly, oleuropein treatment did not affect the transiently expressed full-length mHtt protein level in *STHdh*^{Q111/Q111} striatal cells (Supplementary Figure S3C). Hence, our results indicated that the effect of oleuropein on the soluble form of truncated mHtt protein appeared to be specific.

3.6 Oleuropein does not affect autophagic flux in the HD model cells

The Autophagy-Lysosome pathway and the Ubiquitin-Proteasome system are the endogenous mechanisms to reduce mutant Htt aggregates (Valionyte et al., 2020). Because oleuropein aglycone, a deglycosylated derivative of oleuropein, has been reported to induce autophagy (Rigacci et al., 2015; Achour et al., 2016; Miceli et al., 2018; Leri et al., 2021), we

tested whether oleuropein activates the autophagy pathway to reduce mHtt aggregates. To do this, the autophagy markers, LC3-II, and p62, were monitored in wild-type *STHdh*^{Q7/Q7} striatal cells and mutant *STHdh*^{Q111/Q111} striatal cells by immunoblotting analysis. Our result showed that oleuropein treatment did not affect the LC3-II and p62 protein levels in wild-type *STHdh*^{Q7/Q7} striatal cells and those in the mutant *STHdh*^{Q111/Q111} striatal cells (Q7: LC3II from 1 to 0.99-fold; $p > 0.05$; p62 from 1 to 0.99-fold; $p > 0.05$, Figures 4A–C, lane 1 and 2. Q111: LC3II from 1.03 to 0.9867-fold; $p > 0.05$; p62 from 1.07 to 1.113-fold; $p > 0.05$; Figures 4A–C, lane 5 and 6). Because the autophagic flux is attributed to both induction and degradation of autophagosome by lysosome that cannot be simply differentiated through examining the steady state of LC3-II and p62 levels [reviewed in Klionsky et al. (2021)]. Alternatively, we used Bafilomycin A1 to block lysosomal degradation and examined whether the accumulation of LC3-II and p62 proteins is affected by oleuropein (Huang et al., 2021; Klionsky et al., 2021). As the control, Bafilomycin A1 treatment increased accumulation of the LC3-II protein in wild-type *STHdh*^{Q7/Q7} striatal cells (from 1 to 2.23-fold; $p = 0.0002$, Figures 4A, B, lanes 1 and 3) and the mutant *STHdh*^{Q111/Q111} striatal cells (from 1.03 to 2.243 folds; $p = 0.0005$, Figures 4A, B, lanes 5 and 7), indicating lysosomal degradation was inhibited. After Bafilomycin A1 treatment, oleuropein did not increase the accumulation of LC3-II protein further in the wild-type *STHdh*^{Q7/Q7} striatal cells (from 2.23 to 2.233 folds; $p > 0.05$, Figures 4A, B, lanes 3 and 4) or mutant *STHdh*^{Q111/Q111} striatal cells

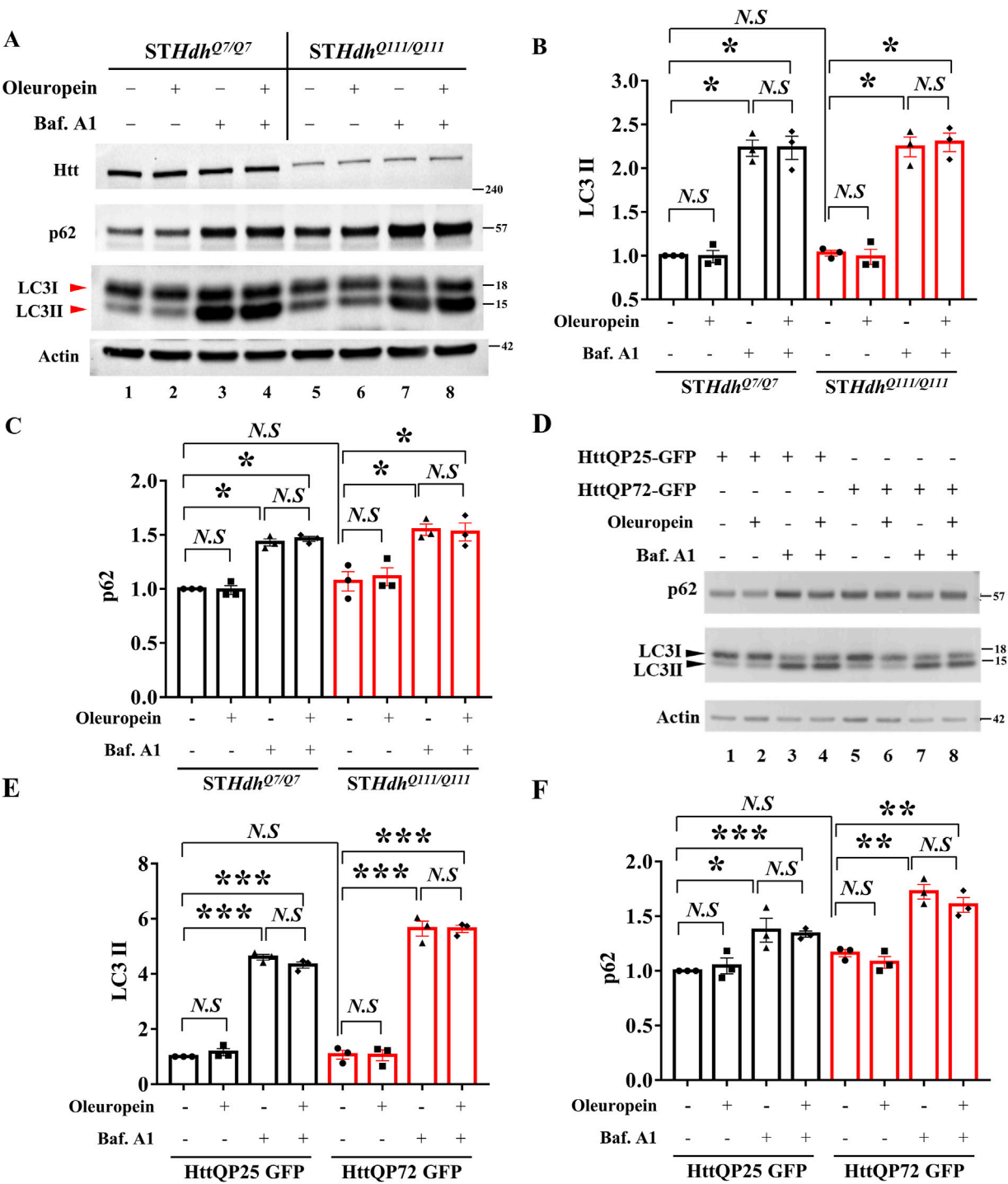


FIGURE 4
Oleuropein does not affect autophagic flux in HD model cells. **(A)** Immunoblotting analysis of the *STHdh*^{Q7/Q7} and *STHdh*^{Q111/Q111} striatal cells treated with 5 μ g/ml oleuropein or 200 nM Bafilomycin A1 or both. Immunoblot detection of Htt, LC3, and p62 proteins in *STHdh*^{Q7/Q7} and *STHdh*^{Q111/Q111} striatal cells. Actin was used as an internal control. Quantitation analyses of **(B)** LC3-II or **(C)** p62 protein normalized to actin. **(D)** Immunoblotting analysis of LC3 and p62 in N2a cells expressing truncated wild-type or mutant Htt after treatment with 5 μ g/ml oleuropein or 200 nM Bafilomycin A1 or both. Actin protein was used as an internal control. Quantitation analysis of **(E)** LC3II or **(F)** p62 protein normalized to actin. Data from three independent experiments are presented as mean normalized units \pm SEM. Data showing significant differences are labeled as follows: $p < 0.05$ with one asterisk (*), $p < 0.005$ with two asterisks (**), and $p < 0.001$ with three asterisks (***). N.S., not significant.

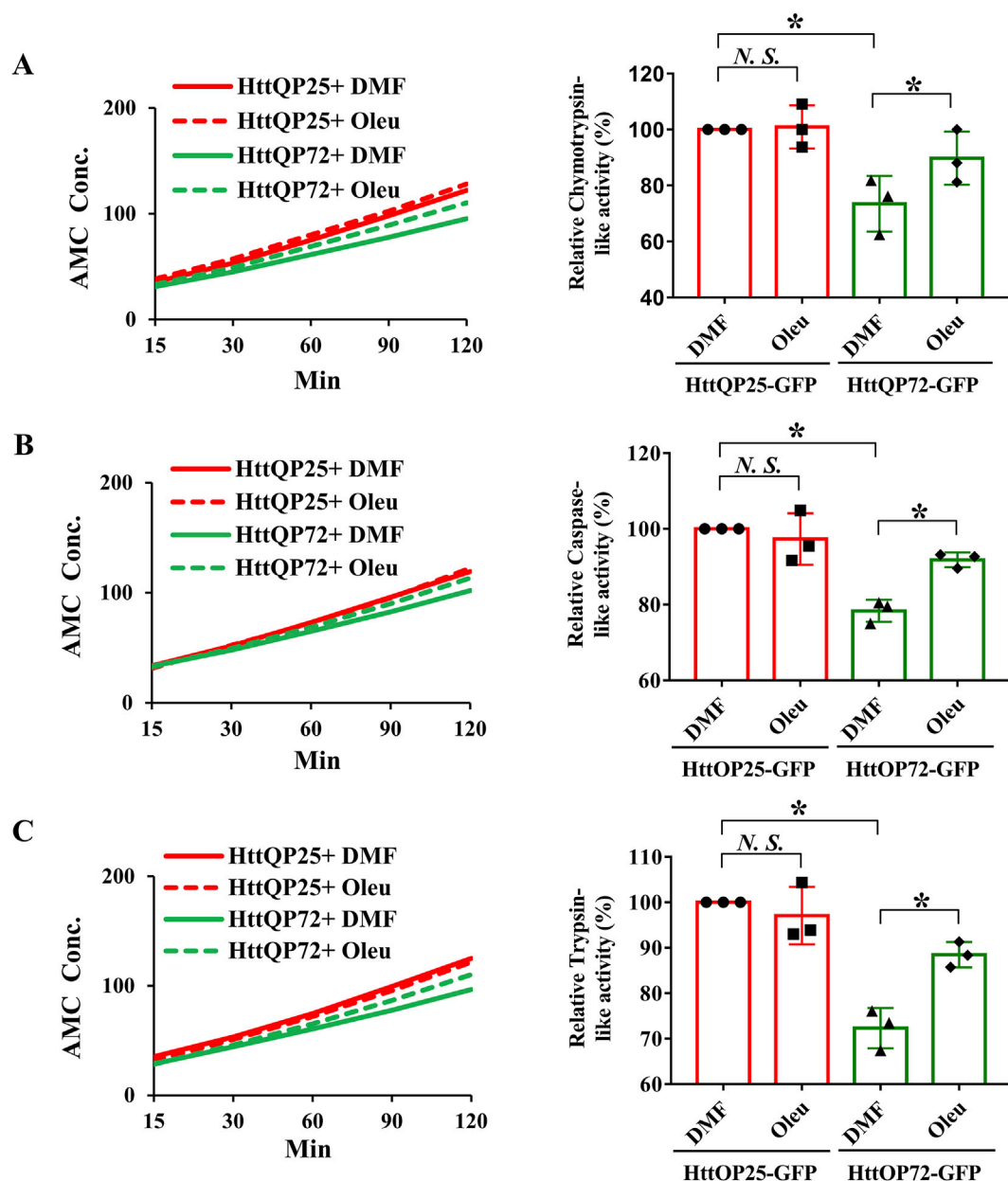


FIGURE 5

Oleuropein increases the proteasome activity in N2a cells expressing the truncated HttQP72-GFP mHtt protein. Oleuropein increases the proteasome activity in N2a cells expressing the truncated HttQP72-GFP mHtt protein. The chymotrypsin-like activity (A), caspase-like activity (B), and trypsin-like activity (C) were examined in N2a cells expressing wild-type or the truncated mHtt in the absence or presence of 5 μ M oleuropein treatment at the indicated concentration for 24 h. Data from three independent experiments are presented as mean normalized units \pm SEM. Data showing a significant difference ($p < 0.05$) is labeled with one asterisk (*). N.S., not significant.

(from 2.243 to 2.297 folds; $p > 0.05$, Figures 4A, B, lanes 7 and 8), indicating oleuropein did not increase the autophagic flux. Consistently, Bafilomycin A1 increased accumulation of the p62 protein in wild-type *STHdh*^{Q7/Q7} striatal cells (from 1 to 1.43 folds; $p = 0.0002$, Figures 4A, C, lanes 1 and 3) and the mutant *STHdh*^{Q111/Q111} striatal cells (from 1.07 to 1.547 folds; $p = 0.0101$, Figures 4A, C, lanes 5 and 7), confirming lysosomal degradation was inhibited. Oleuropein treatment failed to increase the accumulation of p62 protein in the Bafilomycin A1-treated wild-type *STHdh*^{Q7/Q7} striatal cells (from 1.43 to 1.463 folds; $p > 0.05$, Figures 4A, C, lanes 3 and 4) and Bafilomycin A1-treated

mutant *STHdh*^{Q111/Q111} striatal cells (from 1.547 to 1.527 folds; $p > 0.05$, Figures 4A, C, lanes 7 and 8). Hence, our data indicate that oleuropein treatment does not induce autophagy in the *STHdh* HD striatal model cells.

To investigate whether the lack of oleuropein effect on autophagy is cell-specific or a general phenomenon, the effect of oleuropein on the autophagic flux was also examined in the neuronal N2a cells. Similar to the results observed in the *STHdh* striatal model cells, oleuropein did not affect the LC3-II and p62 protein levels in N2a cells ectopically expressing the truncated wild-type HttQP25-GFP or the mutant HttQP72-GFP protein (QP25:LC3II from 1 to 1.165-fold;

$p > 0.05$; p62 from 1 to 1.045-fold; $p > 0.05$, Figures 4D–F, lane 1 and 2. QP72: LC3II from 1.07 to 1.048-fold; $p > 0.05$; p62 from 1.162 to 1.078-fold; $p > 0.05$; Figures 4D–F, lane 5 and 6), indicating that overall autophagy balance was not affected by oleuropein. Bafilomycin A1-dependent increase of the LC3-II protein in the neuronal N2a cells ectopically expressing truncated wild-type HttQP25-GFP (from 1 to 4.607 folds; $p < 0.0001$, Figures 4D, E, lanes 1 and 3) or mutant HttQP72-GFP protein (from 1.07 to 5.642 folds; $p = 0.0001$, Figures 4D, E, lanes 5 and 7). After blocking lysosomal degradation by Bafilomycin A1, oleuropein did not affect the LC3-II protein level in N2a cells overexpressing either the truncated wild-type HttQP25-GFP protein (from 4.6 to 4.32 folds; $p > 0.05$, Figures 4D, E, lanes 3 and 4) or the truncated mutant HttQP72-GFP protein (from 5.64 to 5.63 folds; $p > 0.05$, Figures 4D, E, lanes 7 and 8). Similarly, blocking lysosomal degradation did not affect the p62 protein level in the N2a cells overexpressing either the truncated wild-type HttQP25-GFP protein (from 4.6 to 4.32 folds; $p > 0.05$, Figures 4D, E, lanes 3 and 4) or the truncated mutant HttQP72-GFP protein (from 5.64 to 5.63 folds; $p > 0.05$, Figures 4D, E, lanes 7 and 8). In summary, our data indicate oleuropein did not act through the autophagy pathway to relieve the cytotoxicity of the HD model cells.

3.7 Oleuropein increases the proteolytic activity of the 20S proteasome

Because oleuropein did not affect the autophagy pathway, we tested whether the proteasome system was activated in oleuropein-treated HD model cells. Because the substrate-specific activities of the chymotrypsin-like, trypsin-like and caspase-like proteases are the major proteolytic activity of the 20S core proteasome complex [reviewed in Wang and Le (2019); Wang et al. (2020)], we examined the chymotrypsin-like, caspase-like and trypsin-like activities in neuronal N2a cells ectopically expressing the truncated wild-type HttQP25-GFP protein or truncated mutant HttQP72-GFP protein in the absence or presence of oleuropein treatment. Consistent with the previous report (Huang et al., 2021), ectopic expression of the mutant HttQP72-GFP protein decreased the activities of the chymotrypsin-like protease (from 100% to 73%; $p = 0.043$, Figure 5A), caspase-like protease (from 100% to 78%; $p = 0.037$, Figure 5B) and trypsin-like protease (from 100% to 72%; $p = 0.029$, Figure 5C). Consistent with the previous reports (Katsiki et al., 2007; Trader et al., 2017), oleuropein treatment increased the activities of chymotrypsin-like protease (from 73% to 90%; $p = 0.017$, Figure 5A), caspase-like protease (from 78% to 92%; $p = 0.026$, Figure 5B), and trypsin-like protease (from 72% to 88%; $p = 0.024$, Figure 5C) in cells expressing the mutant HttQP72-GFP protein. In contrast, oleuropein did not alter the activities of chymotrypsin-like protease (100%–101%; $p > 0.05$, Figure 5A), caspase-like protease (from 100% to 97%; $p > 0.05$, Figure 5B), and trypsin-like protease (from 100% to 97%; $p > 0.05$, Figure 5C) in cells expressing the HttQP25-GFP protein.

In addition to the N2a cells, we also tested the effect of oleuropein on proteasome activity in the *STHdh* striatal cells. As compared to the wild-type *STHdh*^{Q7/Q7} striatal cells, the mutant *STHdh*^{Q111/Q111} striatal cells had reduced activities of the chymotrypsin-like protease (from 100% to 68%; $p = 0.028$, Supplementary Figure S4A), caspase-like protease (from 100% to 74%; $p = 0.012$, Supplementary Figure S4B), and trypsin-like protease (from 100% to 76%; $p = 0.014$,

Supplementary Figure S4C). Importantly, oleuropein treatment was able to significantly increase the activities of chymotrypsin-like protease (from 68% to 87%; $p = 0.011$, Supplementary Figure S4A), caspase-like protease (from 74% to 88%; $p = 0.027$, Supplementary Figure S4B), and trypsin-like protease (from 76% to 89%; $p = 0.034$, Supplementary Figure S4C) in the mutant *STHdh*^{Q111/Q111} striatal cells. Similar to the N2a cells, oleuropein did not affect the chymotrypsin-like activity (100%–103%; $p > 0.05$, Supplementary Figure S4A), caspase-like activity (from 100% to 102%; $p > 0.05$, Supplementary Figure S4B), and trypsin-like activity (from 100% to 102%; $p > 0.05$, Supplementary Figure S4C) in the wild-type *STHdh*^{Q7/Q7} striatal cells. Taken together, our data showed that oleuropein could modulate 20S proteasome proteolytic activity in the N2a and *STHdh* HD model cells.

3.8 Oleuropein affects the proteasome pathway via an unidentified mechanism

To investigate how oleuropein affects the proteasome pathway, we used immunoblotting to examine the catalytic subunits of the proteasome pathway. Protein levels of subunits $\beta 1$, $\beta 2$, and $\beta 5$ that represent the respective caspase-like, trypsin-like, and chymotrypsin-like proteases of 20S proteasome were examined in the N2a cells overexpressing the HttQP25-GFP protein or mutant HttQP72-GFP protein in the presence or absence of oleuropein. As the control, oleuropein treatment reduced the accumulation of HttQP72-GFP aggregates (from 18.68 to 12.87 folds; $p = 0.0363$, Figures 6A, B). Even though an ectopic expression of mutant HttQP72-GFP protein decreased activities of all three core proteases of the 20S proteasome (Figure 5), it did not affect the steady-state levels of $\beta 1$ (Figures 6A, C), $\beta 2$ (Figures 6A, D) or $\beta 5$ protein (Figures 6A, E). Moreover, oleuropein treatment did not affect the levels of $\beta 1$ (Figures 6A, C), $\beta 2$ (Figures 6A, D), or $\beta 5$ proteins (Figures 6A, E).

Ectopic expression of the proteasome activator PA28 γ has been shown to improve cellular functions of the *STHdh*^{Q7/Q7} striatal cells and motor behaviors in HD model mice (Seo et al., 2007; Jeon et al., 2016). Since the proteasomal subunits $\beta 1$, $\beta 2$, and $\beta 5$ were not the targets for oleuropein-dependent proteasome activities, we asked whether the 20S proteasome activator, PA28 γ (Cascio, 2021), was the target of oleuropein. Our results showed that neither expression of mutant HttQP72-GFP protein alone nor combination of oleuropein treatment and expression of mutant HttQP72-GFP protein affected PA28 γ protein level in the N2a cells (Figures 6A, F), indicating PA28 γ is not the target of oleuropein. As the control, the expression of HttQP25-GFP protein and its combination with oleuropein treatment did not affect the PA28 γ protein (Figures 6A, F).

Activation of the p38 MAPK pathway has been shown to inhibit proteasome activity (Lee et al., 2010; Leestemaker et al., 2017; Huang et al., 2021). Consequently, we investigated whether oleuropein improved proteasome activity by inhibiting the p38 MAPK pathway. Ectopic expression of mutant HttQP72-GFP protein did not affect the level of phospho-p38 MAPK in the N2a cells (Figures 6A, G). Additionally, oleuropein treatment did not alter the ratio of phospho-p38 MAPK/p38 MAPK in cells expressing the HttQP72-GFP (Figures 6A, G, H), indicating that oleuropein did not affect the p38 MAPK pathway to enhance proteasome activities. The effect of oleuropein on the proteasome and p38 MAPK pathway was further

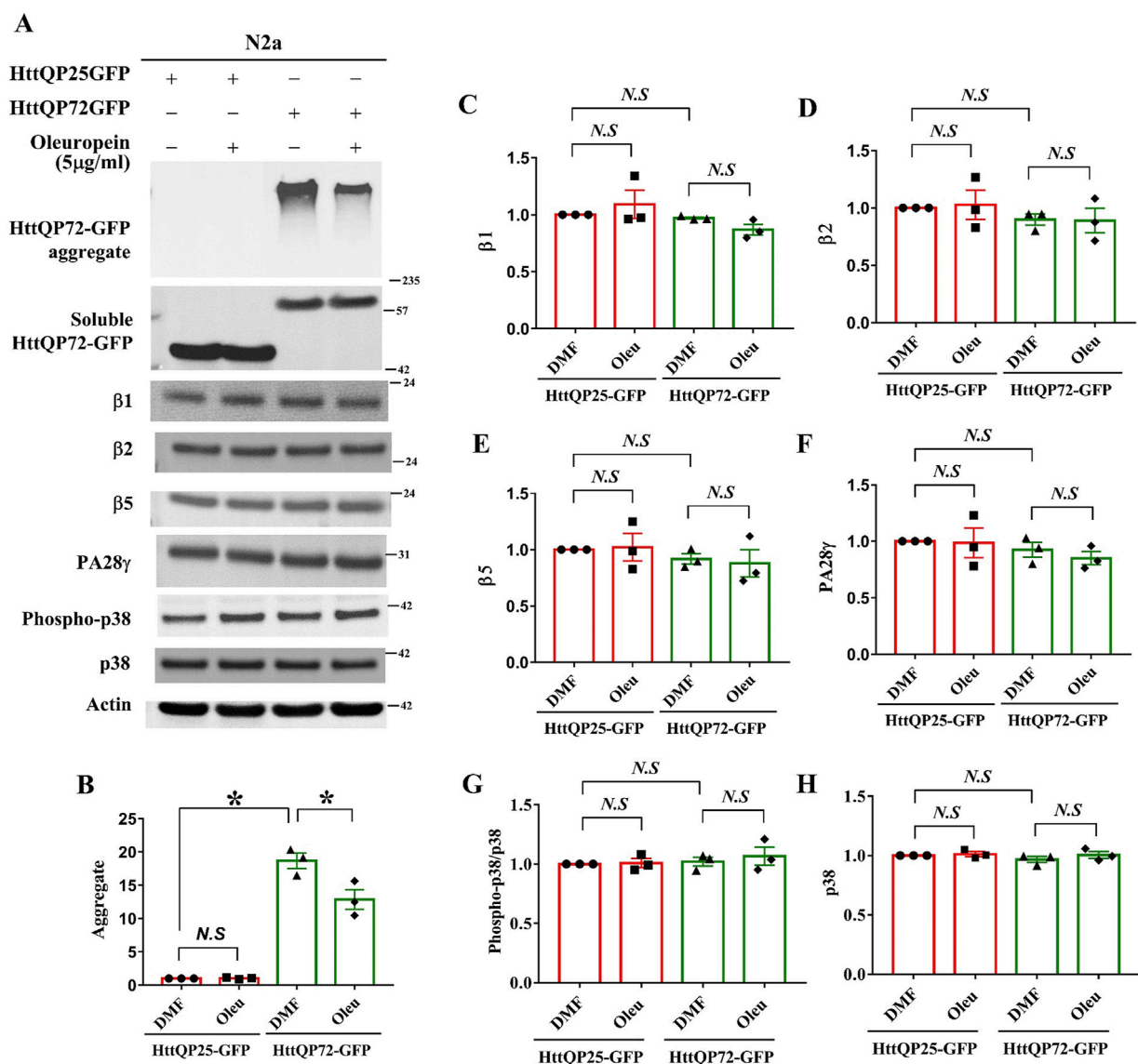


FIGURE 6

Effects of oleuropein on the proteasome-associated proteins in N2a cells expressing the truncated HttQP72-GFP mHtt protein. (A) Immunoblot detection of Htt, β1, β2, β5, PA28γ, phospho-p38, and p38 in N2a cells expressing truncated wild-type or mutant Htt in the absence or presence of oleuropein treatment at the indicated concentration for 24 h. Actin was used as an internal control. (B–H) Quantification analyses of protein levels with the indicated protein normalized to the actin protein. A paired Student's t-test was used for statistical analysis. Data showing significant differences compared to the control are labeled as follows: $p < 0.05$ with one asterisk (*), and $p < 0.01$ with two asterisks (**). N.S., no significance.

tested in the *STHdh*^{Q7/Q7} striatal cells. The catalytic subunits and regulator of the proteasome pathway were examined in *STHdh*^{Q7/Q7} striatal cells expressing the mutant HttQP72-GFP protein. Consistent with the results from the N2a cells, oleuropein did not affect the protein levels of β1, β2, β5, or PA28γ in the *STHdh*^{Q7/Q7} striatal cells expressing mutant HttQP72-GFP protein (Supplementary Figure S5A). Overexpression of mutant HttQP72-GFP protein increased the level of phospho-p38 MAPK in the *STHdh*^{Q7/Q7} striatal cells, however, oleuropein did not affect the levels of unphosphorylated p38 MAPK or alter the p38 MAPK pathway, as indicated by the ratio of phospho-p38 MAPK to p38 MAPK (Supplementary Figure S5A).

We suspected that oleuropein might target other MAPK pathways. It has been shown that the Erk1/2 MAPK pathway

promotes cell survival, while the c-Jun N-terminal kinase (JNK) MAPK pathway inhibits proteasome activity (Mitsiades et al., 2002; Tang et al., 2006; Shah and Orlowski, 2009). However, our experiments showed that oleuropein treatment did not affect either the Erk1/2 or the JNK pathway in the N2a cells expressing HttQP72-GFP (Supplementary Figure S6), suggesting that oleuropein does not act on the MAPK pathways to reduce mHtt aggregates. Consistently, oleuropein did not affect the protein levels of proteasome catalytic subunits β1, β2, and β5, proteasome activator PA28γ, or alter the MAPK pathways in both wild-type *STHdh*^{Q7/Q7} and the mutant *STHdh*^{Q111/Q111} striatal cells (Supplementary Figure S7 and Supplementary Figure S8).

Given that the rho-associated kinases (ROCKs) pathway has been reported to reduce soluble and aggregated forms of mHtt

(Bauer and Nobuyuki, 2009; Bauer et al., 2009), we examined the effect of oleuropein on the ROCKs pathway. Based on our data, oleuropein treatment did not affect the ROCK pathway in N2a cells expressing HttQP25-GFP, as well as in both wild-type *STHdh*^{Q7/Q7} and mutant *STHdh*^{Q111/Q111} striatal cells (Supplementary Figure S9).

Nuclear factor erythroid 2-related factor 2 (Nrf2) is known to coordinate oxidative stress and proteasome functions by enhancing proteasomal activity, degrading oxidized protein, and maintaining proteostasis (Arlt et al., 2009). Since protein aggregation and dysfunction caused by oxidative stress often require 20S proteasome activity (Reichmann et al., 2018; Lévy et al., 2019), oleuropein may modulate the Nrf2 transcription factor to regulate cellular redox balance and proteasome activity. Interestingly, the Nrf2 pathway was activated in the mutant *STHdh*^{Q111/Q111} striatal cells compared to the control *STHdh*^{Q7/Q7} striatal cells, as evidenced by an increase in the ratio of phospho-Nrf2 to Nrf2 from 1 to 1.348-fold ($p = 0.0014$; Supplementary Figure S10). However, oleuropein treatment did not further activate the Nrf2 pathway, as indicated by no additional change in the phospho-Nrf2/Nrf2 ratio in both *STHdh*^{Q111/Q111} and control *STHdh*^{Q7/Q7} striatal cells (Supplementary Figure S10).

In summary, while oleuropein increased the proteolytic activities of the 20S proteasome in all three HD cell models, it did not do so by modulating the major proteasome catalytic subunit and its PA28γ activator, or the MAPK, ROCKS, and the Nrf2 pathways.

4 Discussion

The expression and accumulation of mHtt are crucial for inducing cell cytotoxicity and cell death in neuronal cell cultures (Saudou et al., 1998; Bjørkøy et al., 2005; Raspe et al., 2009). Strategies to reduce the accumulation of mHtt aggregates have been shown to improve cell viability and animal behavior in HD cell and animal models (Hodgson et al., 1999; Bates, 2003; Arrasate and Finkbeiner, 2012; Weiss et al., 2012). In this study, we provided compelling evidence to show that oleuropein reduced cytotoxicity in three HD cell models. Moreover, oleuropein is potent in lowering the soluble form of mHtt protein, mHtt aggregates, and associated ROS. Because the proteolytic activities of the proteasome pathway increased in oleuropein-treated cells, we proposed that oleuropein activates the proteasome pathway to reduce the truncated mHTT protein. However, oleuropein did not affect the core subunits and activator of the 20S proteasome, or the MAPK, ROCKs, and Nrf2 pathways. In addition to the MAPK, ROCKs, and Nrf2 pathways, the cAMP-dependent protein kinase (PKA) pathway has also been shown to inhibit the proteasome activity, specifically targeting the caspase- and trypsin-like proteasome activities (Zhang et al., 2007; Goldberg et al., 2021). Given that oleuropein increased all three protease activities, it is unlikely PKA is the target of oleuropein. This suggests that other regulatory mechanisms of the proteasome pathway are involved.

The question then became how oleuropein enhances proteasome activity. Oxidative stresses have been known to affect the 26S proteasome activity (Ding and Keller, 2001). It is possible that mHtt triggers oxidative stress that inhibits proteasome activities. The primary substrates of 20S proteasome degradation are misfolded proteins, and their accumulation can result in cytotoxicity (Ferrington et al., 2001; David et al., 2002; Shringarpure and Davies, 2002; Liu et al., 2003;

Whittier et al., 2004; Baugh et al., 2009; Raynes et al., 2016). Increasing oxidative stress can lead to the overaccumulation of oxidatively damaged misfolded proteins, which overload the proteasome and inhibit its core protease activity (Pajares et al., 2015; Korovila et al., 2017). Oleuropein may enhance the proteasomal core protease activities through an unidentified mechanism, thereby reducing stress caused by mutant Htt protein. It will be essential to identify the mechanism via an unbiased approach.

Posttranslational modifications (PTMs) have been reported to modulate proteasome activity (Kors et al., 2019; Bi et al., 2021). Oxidative stress has been shown to increase O-GlcNAcylation and S-glutathionylation modification of the proteasome (Zachara and Hart, 2004; Zachara et al., 2004; Dalle-Donne et al., 2009; Xiong et al., 2011; Groves et al., 2013; Reeves et al., 2014). O-linked β-N-acetylglucosamine (O-GlcNAc) modification of the proteasomal 19S regulatory cap Rpt2 protein and S-glutathionylation of the proteasomal 19S regulatory cap RPN1 and RPN2 proteins are reported to reduce proteasome activity and lead to the accumulation of ubiquitylated protein (Zhang et al., 2003; Zmijewski et al., 2009; Keembiyehetty et al., 2011; Liu et al., 2014). Interestingly, upregulated O-GlcNAcylation and S-glutathionylation modified proteins have been reported to impair cell homeostasis and contribute to neuron loss in HD model mice and model cells (Yuzwa et al., 2008; Kumar et al., 2014; Hong et al., 2015; Grima et al., 2017; Lee et al., 2021). Therefore, oleuropein may modulate O-GlcNAcylation or S-glutathionylation modification of the proteasomal proteins to improve proteasome activity and relieve oxidative stress of the mHtt-expressing cells. Further studies are required to address this possibility.

In this study, we did not observe oleuropein's effect on autophagy in three HD cell models. Oleuropein aglycone, the deglycosylated oleuropein, has been shown to activate autophagy in human neuroblastoma SH-SY5Y cells, rat pancreatic epithelial RIN5F cells, and the cortex of TgCRND8 AD mice (Rigacci et al., 2015; Leri et al., 2021). Although both oleuropein and oleuropein aglycone possess anti-oxidative, anti-inflammatory, and lipid-lowering properties, their distinct structures may contribute to different modes of action (Xu et al., 2018). Further experiments are required to elucidate the effects of oleuropein and oleuropein aglycone on autophagy and/or proteasome.

Even though oleuropein has been shown to have neuroprotective functions (Achour et al., 2016; Omar et al., 2018; Brunetti et al., 2020; Leri et al., 2021; Marianetti et al., 2022), identifying the specific targets through which oleuropein reduce cytotoxicity remains challenging. In this study, we showed that oleuropein-mediated protection is linked to reducing ROS levels. Oleuropein may act as a direct ROS scavenger to alleviate oxidative stress in the HD model cells. Since mitochondria are the primary source of ROS production, we speculate that mitochondria-associated ROS balance may be affected by oleuropein. Equally possible is that oleuropein may trigger an endogenous antioxidant response to reduce oxidative stress and protect the HD model cells.

The strategies to reduce soluble and aggregated forms of mHtt have been demonstrated to be essential to alleviate HD pathology (Zhu et al., 2019; Hegde et al., 2020; Valionyte et al., 2020; Srinivasan et al., 2022). Here, we showed that oleuropein potentially decreases the soluble and aggregated forms of truncated mHtt protein and cytotoxicity. Our results suggest that oleuropein can be used as a potential therapeutic remedy.

Moreover, we showed that oleuropein may target the proteasome pathway to improve neuronal health in HD model cells. We propose that the proteasome pathway may serve as the therapeutic target for drug discovery for Huntington's disease.

Data availability statement

The original contributions presented in the study are included in the article/[Supplementary Material](#), further inquiries can be directed to the corresponding author.

Ethics statement

Ethical approval was not required for the study involving humans in accordance with the local legislation and institutional requirements. Written informed consent to participate in this study was not required from the participants or the participants' legal guardians/next of kin in accordance with the national legislation and the institutional requirements. Ethical approval was not required for the studies on animals in accordance with the local legislation and institutional requirements because only commercially available established cell lines were used.

Author contributions

Z-NH: Conceptualization, Formal Analysis, Methodology, Validation, Visualization, Writing-review and editing, Investigation, Writing-original draft. S-YL: Writing-review and editing, Formal Analysis, Investigation, Validation, Visualization, Writing-original draft. J-MC: Writing-review and editing, Formal Analysis, Investigation, Methodology. Z-TH: Writing-review and editing, Formal Analysis, Investigation. L-SH: Conceptualization, Writing-original draft, Writing-review and editing, Data curation, Funding acquisition, Project administration, Supervision.

Funding

The author(s) declare that financial support was received for the research, authorship, and/or publication of this article. This

work was supported by National Science and Technology Council grants (MOST 106-2320-B-006-034, MOST 107-2320-B-006-052-MY3, MOST 110-2320-B-006-016- and MOST 111-2320-B-006-019) to L-SH. Z-NH was supported by post-doctoral fellowship grants.

Acknowledgments

We express our appreciation to Dr. Su-Chiung Fang of the Academia Sinica (Taiwan) for her critical comment on the manuscript. We thank the Confocal Core Facility at Academia Sinica Biotechnology Center in Southern Taiwan for technical assistance. We thank Roger Y. Tsien at the University of San Diego (United States) for his generous gift of the pCDNA3.1-mCherry vector, the CHDI/High Q Foundation (United States) for providing the pHttQP25-GFP and pHttQP72-GFP expression vectors, and Dr. Xiao-Jiang Li at Jinan University for the generous gift of the pEBV-HttQ120F expression vector.

Conflict of interest

The authors declare that the research was conducted in the absence of any commercial or financial relationships that could be construed as a potential conflict of interest.

Publisher's note

All claims expressed in this article are solely those of the authors and do not necessarily represent those of their affiliated organizations, or those of the publisher, the editors and the reviewers. Any product that may be evaluated in this article, or claim that may be made by its manufacturer, is not guaranteed or endorsed by the publisher.

Supplementary material

The Supplementary Material for this article can be found online at: <https://www.frontiersin.org/articles/10.3389/fphar.2024.1459909/full#supplementary-material>

References

- Achour, I., Arel-Dubeau, A. M., Renaud, J., Legrand, M., Attard, E., Germain, M., et al. (2016). Oleuropein prevents neuronal death, mitigates mitochondrial superoxide production and modulates autophagy in a dopaminergic cellular model. *Int. J. Mol. Sci.* 17, 1293. doi:10.3390/ijms17081293
- Arlt, A., Bauer, I., Schafmayer, C., Tepel, J., Muerkoster, S. S., Brosch, M., et al. (2009). Increased proteasome subunit protein expression and proteasome activity in colon cancer relate to an enhanced activation of nuclear factor E2-related factor 2 (Nrf2). *Oncogene* 28, 3983–3996. doi:10.1038/onc.2009.264
- Arrasate, M., and Finkbeiner, S. (2012). Protein aggregates in Huntington's disease. *Exp. Neurol.* 238, 1–11. doi:10.1016/j.expneurol.2011.12.013
- Ban, J. J., Chung, J. Y., Lee, M., Im, W., and Kim, M. (2017). MicroRNA-27a reduces mutant huntingtin aggregation in an *in vitro* model of Huntington's disease. *Biochem. biophysical Res. Commun.* 488, 316–321. doi:10.1016/j.bbrc.2017.05.040
- Bates, G. (2003). Huntingtin aggregation and toxicity in Huntington's disease. *Lancet* 361, 1642–1644. doi:10.1016/S0140-6736(03)13304-1
- Bauer, P. O., and Nobuyuki, N. (2009). Enhanced degradation of mutant huntingtin by rho kinase inhibition is mediated through activation of proteasome and macroautophagy. *Autophagy* 5, 747–748. doi:10.4161/auto.5.5.8704
- Bauer, P. O., Wong, H. K., Oyama, F., Kino, Y., Miyazaki, H., et al. (2009a). Inhibition of Rho kinases enhances the degradation of mutant huntingtin. *J. Biol. Chem.* 284, 13153–13164. doi:10.1074/jbc.M809229200
- Baugh, J. M., Viktorova, E. G., and Pilipenko, E. V. (2009b). Proteasomes can degrade a significant proportion of cellular proteins independent of ubiquitination. *J. Mol. Biol.* 386, 814–827. doi:10.1016/j.jmb.2008.12.081
- Bi, M., Du, X., Jiao, Q., Chen, X., and Jiang, H. (2021). Expanding the role of proteasome homeostasis in Parkinson's disease: beyond protein breakdown. *Cell death and Dis.* 12, 154. doi:10.1038/s41419-021-03441-0

- Bjørkøy, G., Lamark, T., Brech, A., Outzen, H., Perander, M., Overvatn, A., et al. (2005). p62/SQSTM1 forms protein aggregates degraded by autophagy and has a protective effect on huntingtin-induced cell death. *J. Cell Biol.* 171, 603–614. doi:10.1083/jcb.200507002
- Brunetti, G., Di Rosa, G., Scuto, M., Leri, M., Stefani, M., Schmitz-Linneweber, C., et al. (2020). Healthspan maintenance and prevention of Parkinson's-like phenotypes with hydroxytyrosol and oleuropein aglycone in *C. elegans*. *Int. J. Mol. Sci.* 21, 2588. doi:10.3390/ijms21072588
- Butt, M. S., Tariq, U., Iahitisham-Ul-Haq, Naz, A., and Rizwan, M. (2021). Neuroprotective effects of oleuropein: recent developments and contemporary research. *J. Food Biochem.* 45, e13967. doi:10.1111/jfbc.13967
- Cascio, P. (2021). PA28γ: new insights on an ancient proteasome activator. *Biomolecules* 11, 228. doi:10.3390/biom11020228
- Chan, S. C., Tung, C. W., Lin, C. W., Tung, Y. S., Wu, P. M., Cheng, P. H., et al. (2023). miR-196a provides antioxidant neuroprotection via USP15/Nrf2 regulation in Huntington's disease. *Free Radic. Biol. Med.* 209, 292–300. doi:10.1016/j.freeradbiomed.2023.10.407
- Chang, C.-C., Tsou, S. H., Chen, W. J., Ho, Y. J., Hung, H. C., Liu, G. Y., et al. (2021). miR-302 attenuates mutant huntingtin-induced cytotoxicity through restoration of autophagy and insulin sensitivity. *Int. J. Mol. Sci.* 22, 8424. doi:10.3390/ijms22168424
- Chaudhary, S., Dhiman, A., Dilawari, R., Chaubey, G. K., Talukdar, S., Modanwal, R., et al. (2021). Glyceraldehyde-3-Phosphate dehydrogenase facilitates macroautophagic degradation of mutant huntingtin protein aggregates. *Mol. Neurobiol.* 58, 5790–5798. doi:10.1007/s12035-021-02532-5
- Cheng, P.-H., Li, C. L., Chang, Y. F., Tsai, S. J., Lai, Y. Y., Chan, A. W. S., et al. (2013a). miR-196a ameliorates phenotypes of Huntington disease in cell, transgenic mouse, and induced pluripotent stem cell models. *Am. J. Hum. Genet.* 93, 306–312. doi:10.1016/j.ajhg.2013.05.025
- Cheng, P.-H., Li, C. L., Her, L. S., Chang, Y. F., Chan, A. W. S., Chen, C. M., et al. (2013b). Significantly differential diffusion of neuropathological aggregates in the brain of transgenic mice carrying N-terminal mutant huntingtin fused with green fluorescent protein. *Brain Struct. Funct.* 218, 283–294. doi:10.1007/s00429-012-0401-x
- Choi, E. M., Suh, K. S., Yun, S. J., Park, J., Park, S. Y., Chin, S. O., et al. (2021). Oleuropein attenuates the 2, 3, 7, 8-tetrachlorodibenzo-p-dioxin (TCDD)-perturbing effects on pancreatic β-cells. *J. Environ. Sci. Health, Part A* 56, 752–761. doi:10.1080/10934529.2021.1923312
- Dalle-Donne, I., Rossi, R., Colombo, G., Giustarini, D., and Milzani, A. (2009). Protein S-glutathionylation: a regulatory device from bacteria to humans. *Trends Biochem. Sci.* 34, 85–96. doi:10.1016/j.tibs.2008.11.002
- David, D. C., Layfield, R., Serpell, L., Narain, Y., Goedert, M., and Spillantini, M. G. (2002). Proteasomal degradation of tau protein. *J. Neurochem.* 83, 176–185. doi:10.1046/j.1471-4159.2002.01137.x
- Davies, S. W., Turmaine, M., Cozens, B. A., DiFiglia, M., Sharp, A. H., Ross, C. A., et al. (1997). Formation of neuronal intranuclear inclusions underlies the neurological dysfunction in mice transgenic for the HD mutation. *Cell* 90, 537–548. doi:10.1016/s0092-8674(00)80513-9
- DiFiglia, M., Sapp, E., Chase, K. O., Davies, S. W., Bates, G. P., Vonsattel, J. P., et al. (1997). Aggregation of huntingtin in neuronal intranuclear inclusions and dystrophic neurites in brain. *Science* 277, 1990–1993. doi:10.1126/science.277.5334.1990
- Ding, Q., and Keller, J. N. (2001). Proteasome inhibition in oxidative stress neurotoxicity: implications for heat shock proteins. *J. Neurochem.* 77, 1010–1017. doi:10.1046/j.1471-4159.2001.00302.x
- El Demerdash, N., Chen, M. W., O'Brien, C. E., Adams, S., Kulikowicz, E., Martin, L. J., et al. (2021). Oleuropein activates neonatal neocortical proteasomes, but proteasome gene targeting by AAV9 is variable in a clinically relevant piglet model of brain hypoxia-ischemia and hypothermia. *Cells* 10, 2120. doi:10.3390/cells10082120
- Fão, L., and Rego, A. C. (2021). Mitochondrial and redox-based therapeutic strategies in Huntington's disease. *Antioxidants and Redox Signal.* 34, 650–673. doi:10.1089/ars.2019.8004
- Ferlazzo, G. M., Gambetta, A. M., Amato, S., Cannizzaro, N., Angiolillo, S., Arboit, M., et al. (2023). Genome-wide screening in pluripotent cells identifies Mtf1 as a suppressor of mutant huntingtin toxicity. *Nat. Commun.* 14, 3962. doi:10.1038/s41467-023-39552-9
- Ferrington, D. A., Sun, H., Murray, K. K., Costa, J., Williams, T. D., Bigelow, D. J., et al. (2001). Selective degradation of oxidized calmodulin by the 20 S proteasome. *J. Biol. Chem.* 276, 937–943. doi:10.1074/jbc.M005356200
- Folger, A., and Wang, Y. (2021). The cytotoxicity and clearance of mutant huntingtin and other misfolded proteins. *Cells* 10, 2835. doi:10.3390/cells10112835
- Goldberg, A. L., Kim, H. T., Lee, D., and Collins, G. A. (2021). Mechanisms that activate 26S proteasomes and enhance protein degradation. *Biomolecules* 11, 779. doi:10.3390/biom11060779
- Grima, J. C., Daigle, J. G., Arbez, N., Cunningham, K. C., Zhang, K., Ochaba, J., et al. (2017). Mutant huntingtin disrupts the nuclear pore complex. *Neuron* 94, 93–107. doi:10.1016/j.neuron.2017.03.023
- Groves, J. A., Lee, A., Yildirim, G., and Zachara, N. E. (2013). Dynamic O-GlcNAcylation and its roles in the cellular stress response and homeostasis. *Cell Stress Chaperones* 18, 535–558. doi:10.1007/s12192-013-0426-y
- Hegde, R. N., Chiki, A., Petricca, L., Martufi, P., Arbez, N., Mouchiroud, L., et al. (2020). TBK1 phosphorylates mutant Huntingtin and suppresses its aggregation and toxicity in Huntington's disease models. *EMBO J.* 39, e104671. doi:10.15252/embj.2020104671
- Hodgson, J. G., Agopyan, N., Gutekunst, C. A., Leavitt, B. R., LePiane, F., Singaraja, R., et al. (1999). A YAC mouse model for Huntington's disease with full-length mutant huntingtin, cytoplasmic toxicity, and selective striatal neurodegeneration. *Neuron* 23, 181–192. doi:10.1016/s0896-6273(00)80764-3
- Hommen, F., Bilican, S., and Vilchez, D. (2022). Protein clearance strategies for disease intervention. *J. Neural Transm.* 129, 141–172. doi:10.1007/s00702-021-02431-y
- Hong, C., Seo, H., Kwak, M., Jeon, J., Jang, J., Jeong, E. M., et al. (2015). Increased TRPC5 glutathionylation contributes to striatal neuron loss in Huntington's disease. *Brain* 138, 3030–3047. doi:10.1093/brain/awv188
- Huang, L., and Chen, C. H. (2009). Proteasome regulators: activators and inhibitors. *Curr. Med. Chem.* 16, 931–939. doi:10.2174/092986709787581860
- Huang, Z.-N., Chen, J. M., Huang, L. C., Fang, Y. H., and Her, L. S. (2021). Inhibition of p38 mitogen-activated protein kinase ameliorates HAP40 depletion-induced toxicity and proteasomal defect in Huntington's disease model. *Mol. Neurobiol.* 58, 2704–2723. doi:10.1007/s12035-020-02280-y
- Huang, Z.-N., Chung, H.-M., Fang, S.-C., Her, L.-S., et al. (2017). Adhesion regulating molecule 1 mediates HAP40 overexpression-induced mitochondrial defects. *Int. J. Biol. Sci.* 13, 1420–1437. doi:10.7150/ijbs.20742
- Huang, Z. N., and Her, L.-S. (2017). The Ubiquitin receptor ADRM1 modulates HAP40-induced proteasome activity. *Mol. Neurobiol.* 54, 7382–7400. doi:10.1007/s12035-016-0247-y
- Intihar, T. A., Martinez, E. A., and Gomez-Pastor, R. (2019). Mitochondrial dysfunction in huntington's disease; interplay between HSF1, p53 and PGC-1α transcription factors. *Front. Cell Neurosci.* 13, 103. doi:10.3389/fncel.2019.00103
- Jain, G., Lima, M. T., Matlahov, I., Dolga, A., and van der Wel, P. C. (2024). Polyphenol-based modulation of structure and toxicity of huntingtin protein aggregates. *Biophysical J.* 123, 488a–489a. doi:10.1016/j.bpj.2023.11.2955
- Jain, S., and Roy, I. (2023). Aptamer reduces aggregation of mutant huntingtin and rescues proteostasis network in non-neuronal and neuronal cells. *ACS Chem. Neurosci.* 14, 2385–2395. doi:10.1021/acscchemneuro.3c00226
- Jalgaonkar, S., Gajbiye, S., Sayyed, M., Tripathi, R., Khatri, N., Parmar, U., et al. (2023). S-adenosyl methionine improves motor co-ordination with reduced oxidative stress, dopaminergic neuronal loss, and DNA methylation in the brain striatum of 6-hydroxydopamine-induced neurodegeneration in rats. *Anat. Rec. Hob.* 306, 820–830. doi:10.1002/ar.24948
- Jeon, J., Kim, W., Jang, J., Isacson, O., and Seo, H. (2016). Gene therapy by proteasome activator, PA28γ, improves motor coordination and proteasome function in Huntington's disease YAC128 mice. *Neuroscience* 324, 20–28. doi:10.1016/j.neuroscience.2016.02.054
- Jin, Y. N., Yu, Y. V., Gundemir, S., Jo, C., Cui, M., Tieu, K., et al. (2013). Impaired mitochondrial dynamics and Nrf2 signaling contribute to compromised responses to oxidative stress in striatal cells expressing full-length mutant huntingtin. *PLoS One* 8, e57932. doi:10.1371/journal.pone.0057932
- Juenemann, K., Weisse, C., Reichmann, D., Kaether, C., Calkhoven, C. F., and Schilling, G. (2011). Modulation of mutant huntingtin N-terminal cleavage and its effect on aggregation and cell death. *Neurotox. Res.* 20, 120–133. doi:10.1007/s12640-010-9227-6
- Katsiki, M., Chondrogianni, N., Chinou, I., Rivett, A. J., and Gonos, E. S. (2007). The olive constituent oleuropein exhibits proteasome stimulatory properties *in vitro* and confers life span extension of human embryonic fibroblasts. *Rejuvenation Res.* 10, 157–172. doi:10.1089/rej.2006.0513
- Keembiyehetty, C. N., Krzeslak, A., Love, D. C., and Hanover, J. A. (2011). A lipid-droplet-targeted O-GlcNAcase isoform is a key regulator of the proteasome. *J. Cell Sci.* 124, 2851–2860. doi:10.1242/jcs.083287
- Klionsky, D. J., Abdel-Aziz, A. K., Abdelfatah, S., Abdellatif, M., Abdoli, A., Abel, S., et al. (2021). Guidelines for the use and interpretation of assays for monitoring autophagy (4th edition)1. *Autophagy* 17, 1–382. doi:10.1080/15548627.2020.1797280
- Korovila, I., Hugo, M., Castro, J. P., Weber, D., Höhn, A., Grune, T., et al. (2017). Proteostasis, oxidative stress and aging. *Redox Biol.* 13, 550–567. doi:10.1016/j.redox.2017.07.008
- Kors, S., Geijtenbeek, K., Reits, E., and Schipper-Krom, S. (2019). Regulation of proteasome activity by (post-) transcriptional mechanisms. *Front. Mol. Biosci.* 6, 48. doi:10.3389/fmolb.2019.00048
- Kotowska-Zimmer, A., Przybyl, L., Pewinska, M., Suszyska-Zajczyk, J., Wronka, D., Figiel, M., et al. (2022). A CAG repeat-targeting artificial miRNA lowers the mutant huntingtin level in the YAC128 model of Huntington's disease. *Mol. Ther. Nucleic Acids* 28, 702–715. doi:10.1016/j.omtn.2022.04.031

- Koyuncu, S., Fatima, A., Gutierrez-Garcia, R., and Vilchez, D. (2017). Proteostasis of huntingtin in health and disease. *Int. J. Mol. Sci.* 18, 1568. doi:10.3390/ijms18071568
- Kruk, I., Aboul-Enein, H. Y., Michalska, T., Lichszeld, K., and Kladna, A. (2005). Scavenging of reactive oxygen species by the plant phenols genistein and oleuropein. *Luminescence* 20, 81–89. doi:10.1002/bio.808
- Kumar, A., Singh, P. K., Parihar, R., Dwivedi, V., Lakhota, S. C., and Ganesh, S. (2014). Decreased O-linked GlcNAcylation protects from cytotoxicity mediated by huntingtin exon1 protein fragment. *J. Biol. Chem.* 289, 13543–13553. doi:10.1074/jbc.M114.553321
- Layburn, F. E., Tan, A. Y. S., Mehrabi, N. F., Curtis, M. A., Tippet, L. J., Turner, C. P., et al. (2022). N-terminal mutant huntingtin deposition correlates with CAG repeat length and symptom onset, but not neuronal loss in Huntington's disease. *Neurobiol. Dis.* 174, 105884. doi:10.1016/j.nbd.2022.105884
- Lee, B. E., Suh, P. G., and Kim, J. I. (2021). O-GlcNAcylation in health and neurodegenerative diseases. *Exp. and Mol. Med.* 53, 1674–1682. doi:10.1038/s12276-021-00709-5
- Lee, S. H., Park, Y., Yoon, S. K., and Yoon, J. B. (2010). Osmotic stress inhibits proteasome by p38 MAPK-dependent phosphorylation. *J. Biol. Chem.* 285, 41280–41289. doi:10.1074/jbc.M110.182188
- Leestemaker, Y., de Jong, A., Witting, K. F., Penning, R., Schuurman, K., Rodenko, B., et al. (2017). Proteasome activation by small molecules. *Cell Chem. Biol.* 24, 725–736. doi:10.1016/j.chembiol.2017.05.010
- Leri, M., Bertolini, A., Stefani, M., and Bucciantini, M. (2021). EVOO polyphenols relieve synergistically autophagy dysregulation in a cellular model of alzheimer's disease. *Int. J. Mol. Sci.* 22, 7225. doi:10.3390/ijms22137225
- Lévy, E., El Banna, N., Baille, D., Heneman-Masurel, A., Truchet, S., Rezaei, H., et al. (2019). Causative links between protein aggregation and oxidative stress: a review. *Int. J. Mol. Sci.* 20, 3896. doi:10.3390/ijms20163896
- Liu, C.-W., Corboy, M. J., DeMartino, G. N., and Thomas, P. J. (2003). Endoproteolytic activity of the proteasome. *Science* 299, 408–411. doi:10.1126/science.1079293
- Liu, H., Yu, S., Zhang, H., and Xu, J. (2014). Identification of nitric oxide as an endogenous inhibitor of 26S proteasomes in vascular endothelial cells. *PLoS One* 9, e98486. doi:10.1371/journal.pone.0098486
- Long, J., Luo, X., Fang, D., Song, H., Fang, W., Shan, H., et al. (2022). Discovery of an autophagy inducer J3 to lower mutant huntingtin and alleviate Huntington's disease-related phenotype. *Cell Biosci.* 12, 167. doi:10.1186/s13578-022-00906-3
- Lunkes, A., Lindenberg, K. S., Ben-Haïem, L., Weber, C., Devys, D., Landwehrmeyer, G. B., et al. (2002). Proteases acting on mutant huntingtin generate cleaved products that differentially build up cytoplasmic and nuclear inclusions. *Mol. Cell.* 10, 259–269. doi:10.1016/s1097-2765(02)00602-0
- MacDonald, M. E., Ambrose, C. M., Duyao, M. P., Myers, R. H., Lin, C., Srinidhi, L., et al. (1993). A novel gene containing a trinucleotide repeat that is expanded and unstable on Huntington's disease chromosomes. The Huntington's Disease Collaborative Research Group. *Cell* 72, 971–983. doi:10.1016/0092-8674(93)90585-e
- Marianetti, M., Pinna, S., Venuti, A., and Liguri, G. (2022). Olive polyphenols and bioavailable glutathione: promising results in patients diagnosed with mild Alzheimer's disease. *Alzheimers Dement. (N Y)* 8, e12278. doi:10.1002/trc2.12278
- Martin-Aparicio, E., Yamamoto, A., Hernández, F., Hen, R., Avila, J., and Lucas, J. J. (2001). Proteasomal-dependent aggregate reversal and absence of cell death in a conditional mouse model of Huntington's disease. *J. Neurosci.* 21, 8772–8781. doi:10.1523/JNEUROSCI.21-22-00872.2001
- Miceli, C., Santin, Y., Manzella, N., Coppini, R., Berti, A., Stefani, M., et al. (2018). Oleuropein aglycone protects against MAO-A-induced autophagy impairment and cardiomyocyte death through activation of TFEB. *Oxid. Med. Cell Longev.* 2018, 8067592. doi:10.1155/2018/8067592
- Micheli, L., Bertini, L., Bonato, A., Villanova, N., Caruso, C., Caruso, M., et al. (2023). Role of hydroxytyrosol and oleuropein in the prevention of aging and related disorders: focus on neurodegeneration, skeletal muscle dysfunction and gut microbiota. *Nutrients* 15, 1767. doi:10.3390/nu15071767
- Milakovic, T., Quintanilla, R. A., and Johnson, G. V. W. (2006). Mutant huntingtin expression induces mitochondrial calcium handling defects in clonal striatal cells: functional consequences. *J. Biol. Chem.* 281, 34785–34795. doi:10.1074/jbc.M603845200
- Mitsiades, N., Mitsiades, C. S., Poulaki, V., Chauhan, D., Fanourakis, G., Gu, X., et al. (2002). Molecular sequelae of proteasome inhibition in human multiple myeloma cells. *Proc. Natl. Acad. Sci.* 99, 14374–14379. doi:10.1073/pnas.202445099
- Okada, N., Yako, T., Nakamura, S., Shimazawa, M., and Hara, H. (2021). Reduced mitochondrial complex II activity enhances cell death via intracellular reactive oxygen species in STHdhQ111 striatal neurons with mutant huntingtin. *J. Pharmacol. Sci.* 147, 367–375. doi:10.1016/j.jphs.2021.09.001
- Omar, S. H. (2010). Oleuropein in olive and its pharmacological effects. *Sci. Pharm.* 78, 133–154. doi:10.3797/sciparm.0912-18
- Omar, S. H., Scott, C. J., Hamlin, A. S., and Obied, H. K. (2018). Olive biophenols reduces alzheimer's pathology in SH-SY5Y cells and APPsw mice. *Int. J. Mol. Sci.* 20, 125. doi:10.3390/ijms20010125
- Pajares, M., Jiménez-Moreno, N., Dias, I. H. K., Debele, B., Vucetic, M., Fladmark, K. E., et al. (2015). Redox control of protein degradation. *Redox Biol.* 6, 409–420. doi:10.1016/j.redox.2015.07.003
- Pal, A., Severin, F., Lommer, B., Shevchenko, A., and Zerial, M. (2006). Huntingtin-HAP40 complex is a novel Rab5 effector that regulates early endosome motility and is up-regulated in Huntington's disease. *J. Cell Biol.* 172, 605–618. doi:10.1083/jcb.200509091
- Raspe, M., Gillis, J., Krol, H., Krom, S., Bosch, K., van Veen, H., et al. (2009). Mimicking proteasomal release of polyglutamine peptides initiates aggregation and toxicity. *J. Cell Sci.* 122, 3262–3271. doi:10.1042/jcs.045567
- Raynes, R., Pomatto, L. C. D., and Davies, K. J. A. (2016). Degradation of oxidized proteins by the proteasome: distinguishing between the 20S, 26S, and immunoproteasome proteolytic pathways. *Mol. aspects Med.* 50, 41–55. doi:10.1016/j.mam.2016.05.001
- Reeves, R. A., Lee, A., Henry, R., and Zachara, N. E. (2014). Characterization of the specificity of O-GlcNAc reactive antibodies under conditions of starvation and stress. *Anal. Biochem.* 457, 8–18. doi:10.1016/j.ab.2014.04.008
- Reichmann, D., Voith, W., and Jakob, U. (2018). Maintaining a healthy proteome during oxidative stress. *Mol. Cell* 69, 203–213. doi:10.1016/j.molcel.2017.12.021
- Rigacci, S., Miceli, C., Nediani, C., Berti, A., Cascella, R., Pantano, D., et al. (2015). Oleuropein aglycone induces autophagy via the AMPK/mTOR signalling pathway: a mechanistic insight. *Oncotarget* 6, 35344–35357. doi:10.18632/oncotarget.6119
- Rippin, I., Bonder, K., Joseph, S., Sarsor, A., Vaks, L., and Eldar-Finkelman, H. (2021). Inhibition of GSK-3 ameliorates the pathogenesis of Huntington's disease. *Neurobiol. Dis.* 154, 105336. doi:10.1016/j.nbd.2021.105336
- Rusilowicz-Jones, E. V., Urbé, S., and Clague, M. J. (2022). Protein degradation on the global scale. *Mol. Cell* 82, 1414–1423. doi:10.1016/j.molcel.2022.02.027
- Sarkar, S., Davies, J. E., Huang, Z., Tunncliffe, A., and Rubinsztein, D. C. (2007). Trehalose, a novel mTOR-independent autophagy enhancer, accelerates the clearance of mutant huntingtin and alpha-synuclein. *J. Biol. Chem.* 282, 5641–5652. doi:10.1074/jbc.M609532200
- Saudou, F., Finkbeiner, S., Devys, D., and Greenberg, M. E. (1998). Huntingtin acts in the nucleus to induce apoptosis but death does not correlate with the formation of intranuclear inclusions. *Cell* 95, 55–66. doi:10.1016/s0092-8674(00)81782-1
- Seo, H., Sonntag, K. C., Kim, W., Cattaneo, E., and Isacson, O. (2007). Proteasome activator enhances survival of Huntington's disease neuronal model cells. *PLoS One* 2, e238. doi:10.1371/journal.pone.0000238
- Shah, J. J., and Orlowski, R. Z. (2009). Proteasome inhibitors in the treatment of multiple myeloma. *Leukemia* 23, 1964–1979. doi:10.1038/leu.2009.173
- Shringarpure, R., and Davies, K. J. A. (2002). Protein turnover by the proteasome in aging and disease. *Free Radic. Biol. Med.* 32, 1084–1089. doi:10.1016/s0891-5849(02)00824-9
- Soares, T. R., Reis, S. D., Pinho, B. R., Duchon, M. R., and Oliveira, J. M. A. (2019). Targeting the proteostasis network in Huntington's disease. *Ageing Res. Rev.* 49, 92–103. doi:10.1016/j.arr.2018.11.006
- Spronck, E. A., Vallès, A., Lampen, M. H., Montenegro-Miranda, P. S., Keskin, S., Heijink, L., et al. (2021). Intrastriatal administration of AAV5-miHTT in non-human primates and rats is well tolerated and results in miHTT transgene expression in key areas of Huntington disease pathology. *Brain Sci.* 11, 129. doi:10.3390/brainsci11020129
- Srinivasan, E., Ram, V., and Rajasekaran, R. (2022). A review on Huntington protein: insight into protein aggregation and therapeutic interventions. *Curr. Drug Metab.* 23, 260–282. doi:10.2174/1389200223666220321103942
- Tang, G., Xu, Z., and Goldman, J. E. (2006). Synergistic effects of the SAPK/JNK and the proteasome pathway on glial fibrillary acidic protein (GFAP) accumulation in Alexander disease. *J. Biol. Chem.* 281, 38634–38643. doi:10.1074/jbc.M604942200
- Trader, D. J., Simanski, S., Dickson, P., and Kodadek, T. (2017). Establishment of a suite of assays that support the discovery of proteasome stimulators. *Biochim. Biophys. Acta Gen. Subj.* 1861, 892–899. doi:10.1016/j.bbagen.2017.01.003
- Trettel, F., Rigamonti, D., Hilditch-Maguire, P., Wheeler, V. C., Sharp, A. H., Persichetti, F., et al. (2000). Dominant phenotypes produced by the HD mutation in STHdh(Q111) striatal cells. *Hum. Mol. Genet.* 9, 2799–2809. doi:10.1093/hmg/9.19.2799
- Valionyte, E., Yang, Y., Roberts, S. L., Kelly, J., Lu, B., and Luo, S. (2020). Lowering mutant huntingtin levels and toxicity: autophagy-endolysosome pathways in huntington's disease. *J. Mol. Biol.* 432, 2673–2691. doi:10.1016/j.jmb.2019.11.012
- Wang, X., Meul, T., and Meiners, S. (2020). Exploring the proteasome system: a novel concept of proteasome inhibition and regulation. *Pharmacol. Ther.* 211, 107526. doi:10.1016/j.pharmthera.2020.107526
- Wang, Y., and Le, W. D. (2019). Autophagy and ubiquitin-proteasome system. *Adv. Exp. Med. Biol.* 1206, 527–550. doi:10.1007/978-981-15-0602-4_25
- Watanabe, Y., Taguchi, K., and Tanaka, M. (2020). Ubiquitin, autophagy and neurodegenerative diseases. *Cells* 9, 2022. doi:10.3390/cells9092022
- Weiss, K. R., Kimura, Y., Lee, W. C. M., and Littleton, J. T. (2012). Huntingtin aggregation kinetics and their pathological role in a Drosophila Huntington's disease model. *Genetics* 190, 581–600. doi:10.1534/genetics.111.133710

- Whittier, J. E., Xiong, Y., Rechsteiner, M. C., and Squier, T. C. (2004). Hsp90 enhances degradation of oxidized calmodulin by the 20 S proteasome. *J. Biol. Chem.* 279, 46135–46142. doi:10.1074/jbc.M406048200
- Xiong, Y., Uys, J. D., Tew, K. D., and Townsend, D. M. (2011). S-glutathionylation: from molecular mechanisms to health outcomes. *Antioxidants and redox Signal.* 15, 233–270. doi:10.1089/ars.2010.3540
- Xu, F., Li, Y., Zheng, M., Xi, X., Zhang, X., and Han, C. (2018). Structure properties, acquisition protocols, and biological activities of oleuropein aglycone. *Front. Chem.* 6, 239. doi:10.3389/fchem.2018.00239
- Yang, H., Yang, S., Jing, L., Huang, L., Chen, L., Zhao, X., et al. (2020). Truncation of mutant huntingtin in knock-in mice demonstrates exon1 huntingtin is a key pathogenic form. *Nat. Commun.* 11, 2582. doi:10.1038/s41467-020-16318-1
- Yang, J., Xu, H., Zhang, C., Yang, X., Cai, W., and Chen, X. (2023). A prion-like domain of TFEB mediates the co-aggregation of TFEB and mHTT. *Autophagy* 19, 544–550. doi:10.1080/15548627.2022.2083857
- Yin, X., Manczak, M., and Reddy, P. H. (2016). Mitochondria-targeted molecules MitoQ and SS31 reduce mutant huntingtin-induced mitochondrial toxicity and synaptic damage in Huntington's disease. *Hum. Mol. Genet.* 25, 1739–1753. doi:10.1093/hmg/ddw045
- Yu, X., Chen, S., and Wang, H. (2024). Chlorobenzoquinones aggravate RSL3-induced ferroptosis in ROS-dependent manner. *Chem. Res. Toxicol.* 37, 1035–1043. doi:10.1021/acs.chemrestox.4c00100
- Yuan, Z., Yu, F., Zhang, D., and Wang, H. (2021). Profiling of the assembly of RecA nucleofilaments implies a potential target for environmental factors to disturb DNA repair. *J. Environ. Sci.* 102, 283–290. doi:10.1016/j.jes.2020.09.022
- Yuzwa, S. A., Macauley, M. S., Heinonen, J. E., Shan, X., Dennis, R. J., He, Y., et al. (2008). A potent mechanism-inspired O-GlcNAcase inhibitor that blocks phosphorylation of tau *in vivo*. *Nat. Chem. Biol.* 4, 483–490. doi:10.1038/nchembio.96
- Zachara, N. E., and Hart, G. W. (2004). O-GlcNAc a sensor of cellular state: the role of nucleocytoplasmic glycosylation in modulating cellular function in response to nutrition and stress. *Biochimica Biophysica Acta (BBA)-General Subj.* 1673, 13–28. doi:10.1016/j.bbagen.2004.03.016
- Zachara, N. E., Niall, O., Win, D. C., Jessica, J. M., Jamey, D. M., Gerald, W. H., et al. (2004b). Dynamic O-GlcNAc modification of nucleocytoplasmic proteins in response to stress: a survival response of mammalian cells. *J. Biol. Chem.* 279, 30133–30142. doi:10.1074/jbc.M403773200
- Zhang, F., Hu, Y., Huang, P., Toleman, C. A., Paterson, A. J., and Kudlow, J. E. (2007). Proteasome function is regulated by cyclic AMP-dependent protein kinase through phosphorylation of Rpt6. *J. Biol. Chem.* 282, 22460–22471. doi:10.1074/jbc.M702439200
- Zhang, F., Su, K., Yang, X., Bowe, D. B., Paterson, A. J., and Kudlow, J. E. (2003). O-GlcNAc modification is an endogenous inhibitor of the proteasome. *Cell* 115, 715–725. doi:10.1016/s0092-8674(03)00974-7
- Zhang, L., Wu, T., Shan, Y., Li, G., Ni, X., Chen, X., et al. (2021). Therapeutic reversal of Huntington's disease by *in vivo* self-assembled siRNAs. *Brain* 144, 3421–3435. doi:10.1093/brain/awab354
- Zhou, H., Cao, F., Wang, Z., Yu, Z. X., Nguyen, H. P., Evans, J., et al. (2003). Huntingtin forms toxic NH2-terminal fragment complexes that are promoted by the age-dependent decrease in proteasome activity. *J. Cell Biol.* 163, 109–118. doi:10.1083/jcb.200306038
- Zhu, Y., Li, C., Tao, X., Brazill, J. M., Park, J., Diaz-Perez, Z., et al. (2019). Nmnat restores neuronal integrity by neutralizing mutant Huntingtin aggregate-induced progressive toxicity. *Proc. Natl. Acad. Sci. U. S. A.* 116, 19165–19175. doi:10.1073/pnas.1904563116
- Zmijewski, J. W., Banerjee, S., and Abraham, E. (2009). S-glutathionylation of the Rpn2 regulatory subunit inhibits 26 S proteasomal function. *J. Biol. Chem.* 284, 22213–22221. doi:10.1074/jbc.M109.028902



OPEN ACCESS

EDITED BY

Ping Zheng,
The University of Melbourne, Australia

REVIEWED BY

Lourdes Franco,
University of Extremadura, Spain
Xin Zhang,
Zhejiang Chinese Medical University, China

*CORRESPONDENCE

Jie Feng,
✉ fengj@zju.edu.cn

RECEIVED 14 July 2024

ACCEPTED 11 September 2024

PUBLISHED 25 September 2024

CITATION

Li X, Zhang Y, Zhang Q, Cao A and Feng J (2024) Eucalyptus essential oil exerted a sedative-hypnotic effect by influencing brain neurotransmitters and gut microbes via the gut microbiota-brain axis. *Front. Pharmacol.* 15:1464654. doi: 10.3389/fphar.2024.1464654

COPYRIGHT

© 2024 Li, Zhang, Zhang, Cao and Feng. This is an open-access article distributed under the terms of the [Creative Commons Attribution License \(CC BY\)](https://creativecommons.org/licenses/by/4.0/). The use, distribution or reproduction in other forums is permitted, provided the original author(s) and the copyright owner(s) are credited and that the original publication in this journal is cited, in accordance with accepted academic practice. No use, distribution or reproduction is permitted which does not comply with these terms.

Eucalyptus essential oil exerted a sedative-hypnotic effect by influencing brain neurotransmitters and gut microbes via the gut microbiota-brain axis

Xuejiao Li¹, Yuanyi Zhang¹, Qian Zhang¹, Aizhi Cao² and Jie Feng^{1*}

¹Key Laboratory of Animal Feed and Nutrition of Zhejiang Province, College of Animal Sciences, Zhejiang University, Hangzhou, China, ²Biotechnology R&D Center of Shandong Longchang Animal Health Products Co., Ltd., Jinan, China

Sleep disorders are becoming more and more common, leading to many health problems. However, most of current available medications to treat sleep disorders are addictive and even impair cognitive abilities. Therefore, it is important to find a natural and safe alternative to treat sleep disorders. In this study, twenty-four 8-week-old male ICR mice (25 ± 2 g) were equally divided into three groups: the control group (gavage of 0.9% saline), the eucalyptus essential oil (EEO) group (10 mg/kg B.W.), and the diazepam group (1 mg/kg B.W.). Firstly, open field test and sleep induction test were used to determine the sedative-hypnotic effect of EEO. Secondly, the effect of EEO on neurotransmitters in the mice brain was determined. Finally, based on the gut microbiota-brain axis (GMBA), the effect of EEO on the intestinal flora of mice was explored. It was found that EEO significantly reduce the activity and prolong the sleep duration of mice, exhibiting a good sedative-hypnotic effect. In the brain, EEO could increase the levels of sleep-promoting neurotransmitters, such as glutamine, Gamma-aminobutyric acid (GABA), glycine, tryptophan, N-acetylserotonin, and 5-hydroxyindoleacetic acid (5-HIAA). In the intestine, EEO was found to increase the diversity of gut microbes, the abundance of short chain fatty acid (SCFA) producing flora, and the abundance of functional flora synthesizing GABA and glycine neurotransmitters. These studies suggested that EEO exerted a sedative-hypnotic effect by acting on gut microbes and neurotransmitters in the brain. EEO has the potential to become a natural and safe alternative to traditional hypnotic sedative drugs.

KEYWORDS

eucalyptus essential oil, sedative-hypnotic, neurotransmitter, gut microbes, gut microbiota-brain axis

Introduction

Insomnia can seriously influence people quality of life, and recent studies have revealed its association with obesity, diabetes, heart disease, coronary artery disease, depression and other serious problems (Walia and Mehra, 2016; Broussard et al., 2016). It is estimated that 50–70 million American adults suffer from one or more sleep disorders (Harding and Feldman, 2008), so does 31% of Western Europeans and 23% of Japanese (Dasdelen et al., 2022). In recent decades, a large number of medications have appeared on the market for the treatment of various types of sleep disorders such as chloral hydrate, barbiturates, benzodiazepine, benzodiazepine agonists, modafinil, and antidepressants. However, these medications can cause dependence even addiction, and some may even gradually impair cognitive abilities (Matheson and Hainer, 2017). Therefore, it is important to find safe and effective substances to replace existing commercially available medications to treat sleep disorders.

Eucalyptus essential oil (EEO) is extracted from eucalyptus branches and leaves by steam distillation and has a wide range of applications. The main components of EEO are 1,8-eudesmusin and terpineol (Ieri et al., 2019). Many of the components of EEO (Bampidis et al., 2023) and EEO (Regulation (EC) No 1831/2003) are authorized as a food additive and animal feed additive. EEO has been reported to have antibacterial, anti-inflammatory, insecticidal, antioxidant, analgesic, and other excellent biological activities (Caceres et al., 2017; Aziz et al., 2019; Barbosa et al., 2021; Sathantriphop et al., 2014). It has been found that 1,8-eudesmusin can act on the nervous system, affecting the synthesis of neurotransmitters and then exerting analgesic effects (Takaishi et al., 2012). A study has shown that 1,8-eudesmusin can also inhibit locomotion in mice, showing a good sedative effect (Santos and Rao, 2000). However, the sedative-hypnotic effect of EEO has not been studied thoroughly and systematically.

Neurotransmitters in the central nervous system play an important role in the regulation of the sleep-wake cycle as key mediators of neuronal signal (Ngo and Vo, 2019). In recent years, the gut microbiota-brain axis (GMBA) has been a hot topic in biomedical researches and suggested as a potential therapeutic target for central nervous system disorders (Pesarico et al., 2023). Gut microbes not only affect the digestive, metabolic, and immune functions of the host, but also regulate the sleep state of the host through the GMBA (Poroyko et al., 2016; Golubeva et al., 2017; Niu et al., 2022). High-quality sleep has been found to be closely related to the composition of gut microbes, and in addition, gut microbes dysbiosis can exacerbate the cognitive dysfunction in sleep-deprived mice (Torres-Fuentes et al., 2017; Li N. et al., 2023). Gut microbes have been shown to be involved in the production of a variety of neurotransmitters and cytokines (Galland, 2014). Besides, gut microbes and their metabolites may also influence the expression of genes associated with the biological clock in the central nervous system and liver, then affecting sleep quality (Leone et al., 2015). It is necessary to study how EEO works on neurotransmitters and gut microbes for deep understanding the observed improvement in sleep quality. Therefore, the study was conducted to investigate the effects of EEO on brain neurotransmitters and gut microbes in mice through GMBA to find the possible targets of EEO for the treatment of sleep disorders.

Methods

Animals and drugs

All animal testing procedures were conducted in accordance with the guidelines of the Animal Ethics Committee of Zhejiang University (ethical programme code ZJU 20160403). A total of twenty-four 8-week-old male ICR mice (25 ± 2 g) were purchased from Shanghai Lingchang for this study. The 24 mice were equally divided into three groups: the control group (gavage of 0.9% saline), the EEO group (10 mg/kg B.W.), and the diazepam group (1 mg/kg B.W.). Daily gavage was administered at 9:00 a.m. for 14 days. The test environment was controlled at 20°C–25°C and 40%–70% relative humidity. Acclimatisation in the animal house had been carried out for 1 week till the test. EEO was provided by Shandong Longchang Animal Health Products Co. Diazepam was purchased from Shanghai Xudong Haipu Pharmaceutical Co., Ltd., Batch No. H13021864. Pentobarbital sodium salt (CAS no: 57-33-0) was purchased from Sigma-Aldrich, United States.

Preparation of EEO

The method of preparing EEO refers to CN 110558324B. Australian eucalyptus leaves were cleaned, dried at 180°C and then crushed, and the eucalyptus oil was obtained by using water vapour distillation, and finally the eucalyptus oil was added to a vacuum distillation column for distillation to remove impurities, resulting in EEO. Measure out 100 mg of EEO and mix it with 1 mL of Tween 80, then dissolve the mixture in 49 mL of 0.9% saline solution. Shake the mixture thoroughly using a shaker, and store the EEO in a sealed, light-proof container in a refrigerator at 4°C for future experimental use. At this point, the concentration of EEO was 2 mg/mL. The EEO of 2 mg/mL is used for subsequent mice gavage experiment.

Open field test

Thirty min following the final drug administration to the mice in each group, the mice were placed into the open field with a space of $50 \text{ cm}^3 \times 50 \text{ cm}^3 \times 40 \text{ cm}^3$, made of acrylic sheet and aluminium alloy frame, where the photographic equipment (model 550D, Canon digital camera) was suspended at 2 m directly above. After 5 min of acclimatisation, the activities of the mice during the 5 min were recorded. Trajectory analysis was performed by the video analysis system (SANS, SA215).

Sleep induction test

The sleep induction test was referred to the Medeiros study (Medeiros et al., 2018). After the last treatment, all mice were injected intraperitoneally with sodium pentobarbital solution salt according to 50 mg/kg B.W. standard. Sleep onset was determined by the disappearance of reflex for 1 min after administration of pentobarbital sodium salt solution. Sleep latency was the time from the injection of the drug to the disappearance of the reflex, and sleep

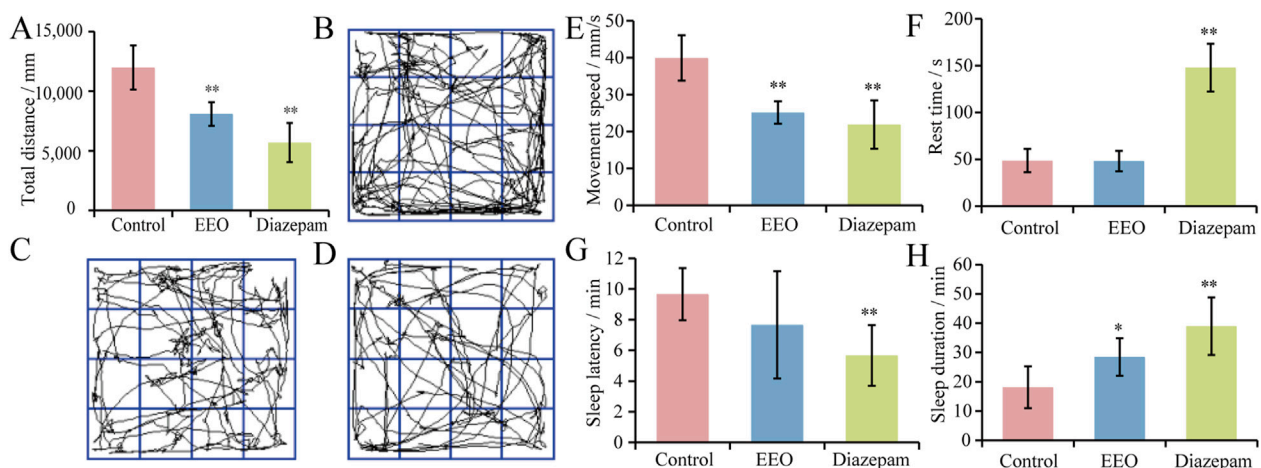


FIGURE 1
Effects of EEO on the behaviors of mice. (A) Total distance. (B–D) The behavioural trajectories of mice in the control group, EEO group, and diazepam group, respectively. (E) Movement speed. (F) Rest time. (G) Sleep latency. (H) Sleep duration. * $p < 0.05$, ** $p < 0.01$; $n = 7–8$.

duration was the time from the disappearance of the reflex to its appearance. The sleep latency and sleep duration were recorded for each group.

Measurement of neurotransmitter levels

Liquid chromatography tandem mass spectrometry (LC-MS/MS) was used to determine the content of neurotransmitters in mouse brain (Horvath et al., 2022). The mouse brain was homogenised and extracted with 20% acetonitrile in methanol for 3 min, then centrifuged ($12,000 \times g$, 4°C , 10 min), and the supernatant was refrigerated at -20°C for 30 min, then centrifuged again, the supernatant was taken as the test solution. The chromatographic column used was a Waters ACQUITY UPLC HSS T3 C18 column ($1.8 \mu\text{m}$, $100 \text{ mm} \times 2.1 \text{ mm i.d.}$), and the column temperature was controlled at 40°C . Mobile phases A and B were ultrapure water (containing 0.1% formic acid) and acetonitrile (containing 0.1% formic acid), respectively, and the control flow rate was 0.35 mL/min. The mass spectrometry conditions were based on the use of an electrospray ionization source, with the mass spectral voltage (MSV) set to 5,500 V in the positive ion mode and to $-4,500 \text{ V}$ in the negative ion mode.

Determination of gut microbes

The mice were dissected at the end of the test and the contents of their cecum were collected in sterile conical tubes. DNA was extracted from the cecal content using the CTAB method according to manufacturer's instructions. The V3 to V4 regions of the microbiota 16S rDNA gene were amplified using 338F/806R primers, then the amplicon was purified using the Qiagen gel extraction kit (Qiagen, Hilden, Germany) and sequenced by the Illumina HiSeq 2500 PE250 platform (Novogene Bioinformatics Technology Co., Ltd., Tianjin, China). Analysis and visualization of

high-throughput sequencing data were collected via the online Novomagic Cloud Platform.

Statistical analysis

Data were tested for significance using one-way ANOVA in SPSS version 22.0 software (IBM, United States), and data were expressed as mean \pm standard deviation ($M \pm SD$), with * $P < 0.05$ being significant and ** $P < 0.01$ being highly significant. Other statistical methods were detailed in the relevant figures.

Results

Effects of EEO on locomotion in mice

The effects of EEO on the total distance, movement speed and rest time of mice were shown in Figures 1A, E, F. Compared with the control group, the total distance travelled and the speed of movement of mice in the EEO group and the diazepam group were highly significantly reduced ($P < 0.01$), with a reduction in the total distance travelled of 32.5% and 52.5%, and the speed of movement was reduced to 25.13 ± 3.01 and $21.88 \pm 6.55 \text{ mm/s}$. Figures 1B–D showed the activity trajectories of mice in the control group, EEO group, and diazepam group, respectively, from which it can also be observed that both EEO and diazepam reduced the activity of mice. In terms of resting time, EEO had no significant effect on the resting time of mice ($P > 0.05$), however, diazepam significantly increased the resting time of mice ($P < 0.01$).

Effects of EEO on sleep in mice

The effects of EEO on sleep latency and sleep duration in mice were shown in Figures 1G, H. Gavage of EEO resulted in a shortening of sleep latency time, but there was no significant

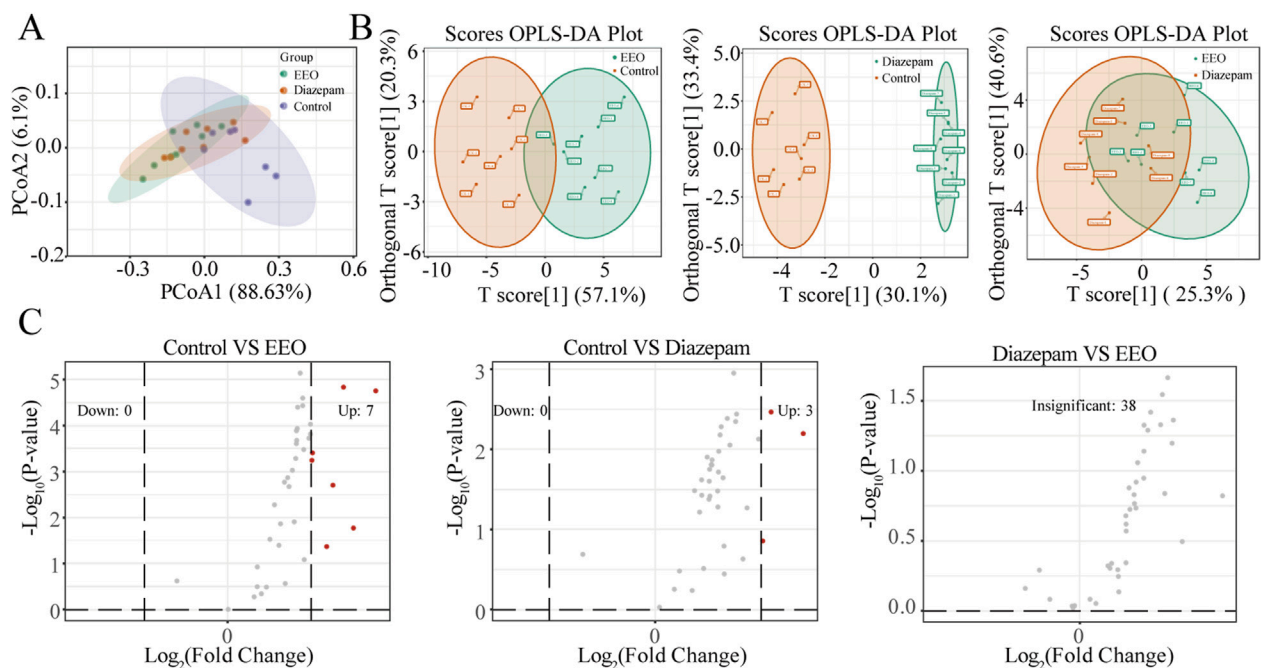


FIGURE 2
Effects of EEO gavage on neurotransmitters diversities of mice. **(A)** Principal coordinate analysis (PCoA) of weighted UniFrac distance. PCoA was performed by statistics function ggplot2 within R (<http://www.r-project.org>). **(B)** Orthogonal Partial Least Squares-Discriminant Analysis (OPLS-DA). After pre-processing the original data in OPLS-DA by $X^* = X - \bar{X}$, the OPLSR. Anal function in the MetaboAnalystR package in R software is used for analysis. **(C)** Volcano plot between different groups. Using fold change analysis, if fold change of a neurotransmitter is ≥ 2 or ≤ 0.5 between the control group and the experimental group, it is considered significantly different. $n = 8$.

difference, and diazepam reduced the sleep latency of mice with a highly significantly ($P < 0.01$). The sleep duration of mice in control, EEO and diazepam groups were 18.17 ± 7.15 , 28.50 ± 6.37 and 39.00 ± 9.85 min, respectively. Compared with the control group, EEO significantly increased the sleep duration of mice ($P < 0.05$), diazepam highly significantly increased the sleep duration of mice ($P < 0.01$). EEO and diazepam prolonged the sleep duration of mice by 56.9% ($P < 0.05$) and 114.7% ($P < 0.01$), respectively.

Effects of EEO on neurotransmitters in the mouse brain

We analysed the effects of EEO on neurotransmitters in the mouse brain. As shown in the PCoA and OPLS-DA score plots, compared with the control group, EEO or diazepam treatment significantly altered neurotransmitters in the mouse brain. The neurotransmitter profile in the brain of mice in the EEO group was similar to that of the diazepam group, with a greater difference from the control group (Figures 2A, B). In addition, volcano plot revealed neurotransmitters that differed significantly between groups (Figure 2C). EEO and diazepam treatments significantly elevated the levels of 7 and 3 neurotransmitters, respectively, compared to the control group. There was no significant difference in neurotransmitter levels between the EEO and diazepam groups.

The changes of neurotransmitters were observed after EEO treatment through a clustering heat map (Figure 3A). Brain levels of Gamma-aminobutyric acid (GABA), glutamine, glycine, tryptophan,

5-hydroxyindoleacetic acid (5-HIAA) and N-acetylserotonin were significantly higher in the EEO-treated and diazepam-treated groups of mice than in the control group (Figure 3B).

Effect of EEO on the diversity of gut microbes

As shown in Figure 4A, the OTUs of mice intestinal flora in the control, EEO and diazepam groups were 2,342, 3,659 and 3,609, EEO and diazepam treatments increased the OTUs of mice intestinal flora, EEO and diazepam groups had more concurrent OTUs (1,114) than the control group duplicated with EEO (812) and diazepam (868) groups, respectively. The α diversity index including shannon, ace and chao1 results were shown in Figures 4B–D. Both EEO and diazepam significantly increased the shannon, ace and chao1 indices of the intestinal microbes in mice compared to the control group ($P < 0.05$). The β diversity index results showed that EEO and diazepam highly significantly increased the intestinal flora of the mouse β diversity (Figure 4E, $P < 0.01$). Based on the weighted UniFrac distance metric, the community composition of each sample was analysed for similarity using principal co-ordinates analysis (PCoA). The microbial communities in the EEO and diazepam groups were altered compared with the control group, and the microbial community species composition was structurally similar in the EEO and diazepam groups (Figure 4F). The similarity between individuals was analysed using the Unweighted UniFrac clustering tree based on the UPGMA method (Figure 4G), and in agreement with the results of the PCoA analysis, the gut microbial

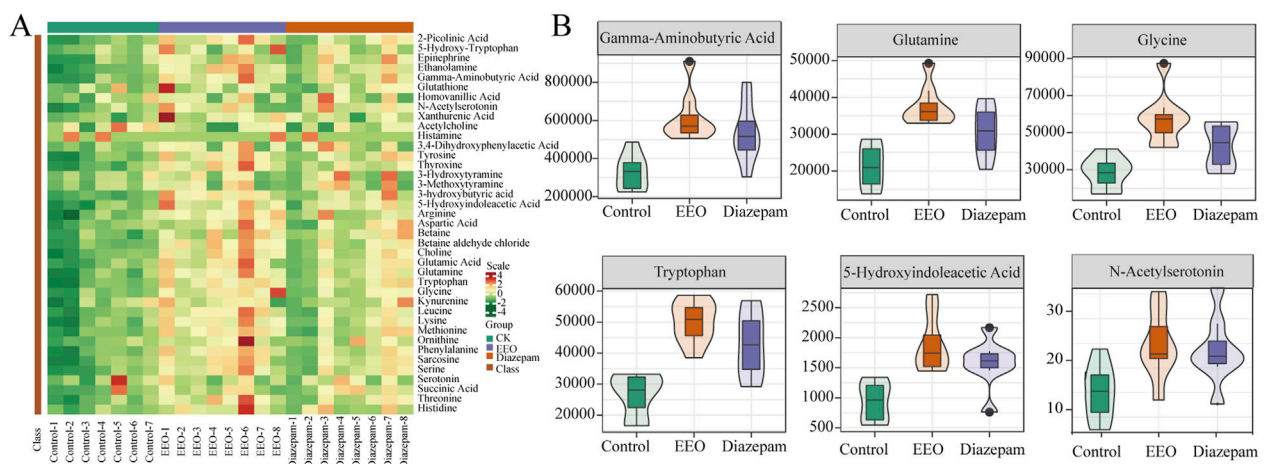


FIGURE 3
Effects of EEO supplementation on the levels of various neurotransmitters in the mice. **(A)** Heat map of neurotransmitter in different groups. The original levels of differential neurotransmitters are normalized using Unit Variance Scaling and heat maps are generated using R software. **(B)** Neurotransmitters with group differences. Using Variable Importance in Projection (VIP) based on the OPLS-DA model for differential testing, and neurotransmitters considered to be significant if VIP > 0.8. n = 8.

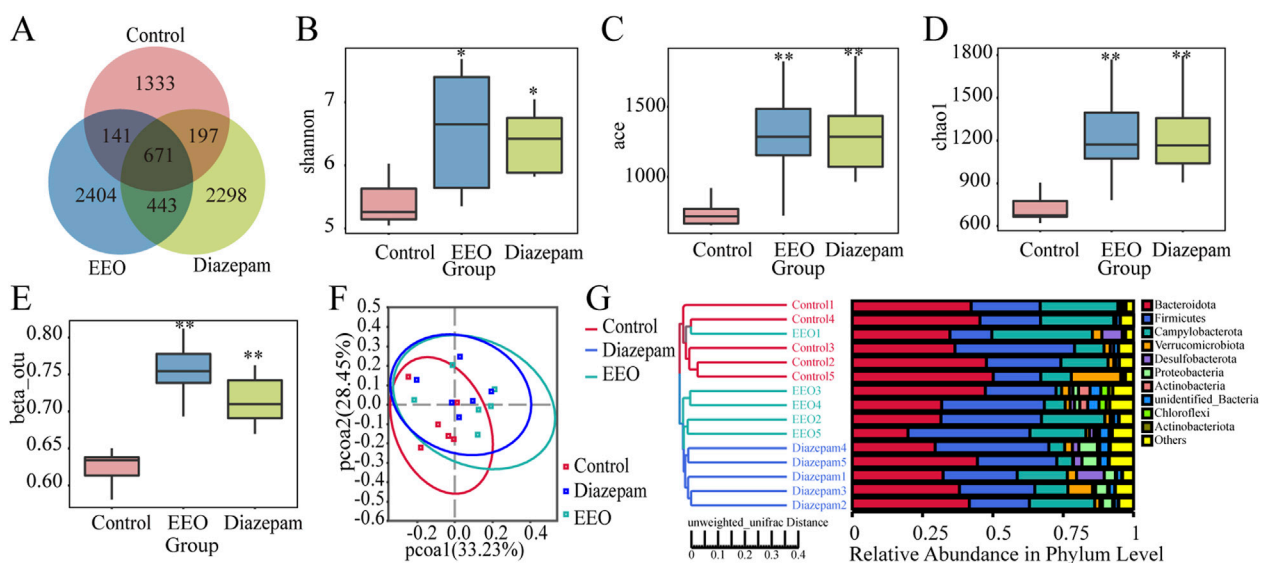


FIGURE 4
Effects of EEO on the diversity of microbial communities in the cecum of mice. **(A)** Wayne plots at ou level. **(B–D)** Box plots of α -diversity indices: Shannon **(B)**, ACE **(C)** and Chao1 **(D)**. **(E)** β -Diversity indices based on otu level. Species diversity difference is analyzed using Tukey and Kruskal–Wallis rank sum tests. * $p < 0.05$, ** $p < 0.01$. **(F)** Scatter plots obtained from PCoA based on the weighted UniFrac distance metric. **(G)** UPGMA clustering tree and community structure map based on unweighted UniFrac distance. n = 5–6.

community composition in the EEO and diazepam groups was dramatically different compared to the control group.

Effect of EEO on the relative abundance of gut microbes

Differences in dominant species among the three groups of samples at the phylum level are shown in Figure 5A, the study found that the

relative abundance of Firmicutes, Proteobacteria, Actinobacteria, and Bacteroidota/Firmicutes differed among the three groups. EEO significantly increased the relative abundance of relative abundance of Firmicutes, Proteobacteria and Actinobacteria ($P < 0.01$) and decreased the abundance ratio of Bacteroidota/Firmicutes (Figure 5B). At the genus level, EEO and diazepam treatment altered the relative abundance of *Bacteroides*, *Dubosiella*, *Prevotella*, 9, and *Lachnospiraceae_NK4A136_groups* in the gut microbial community of mice (Figure 5C). EEO and diazepam significantly

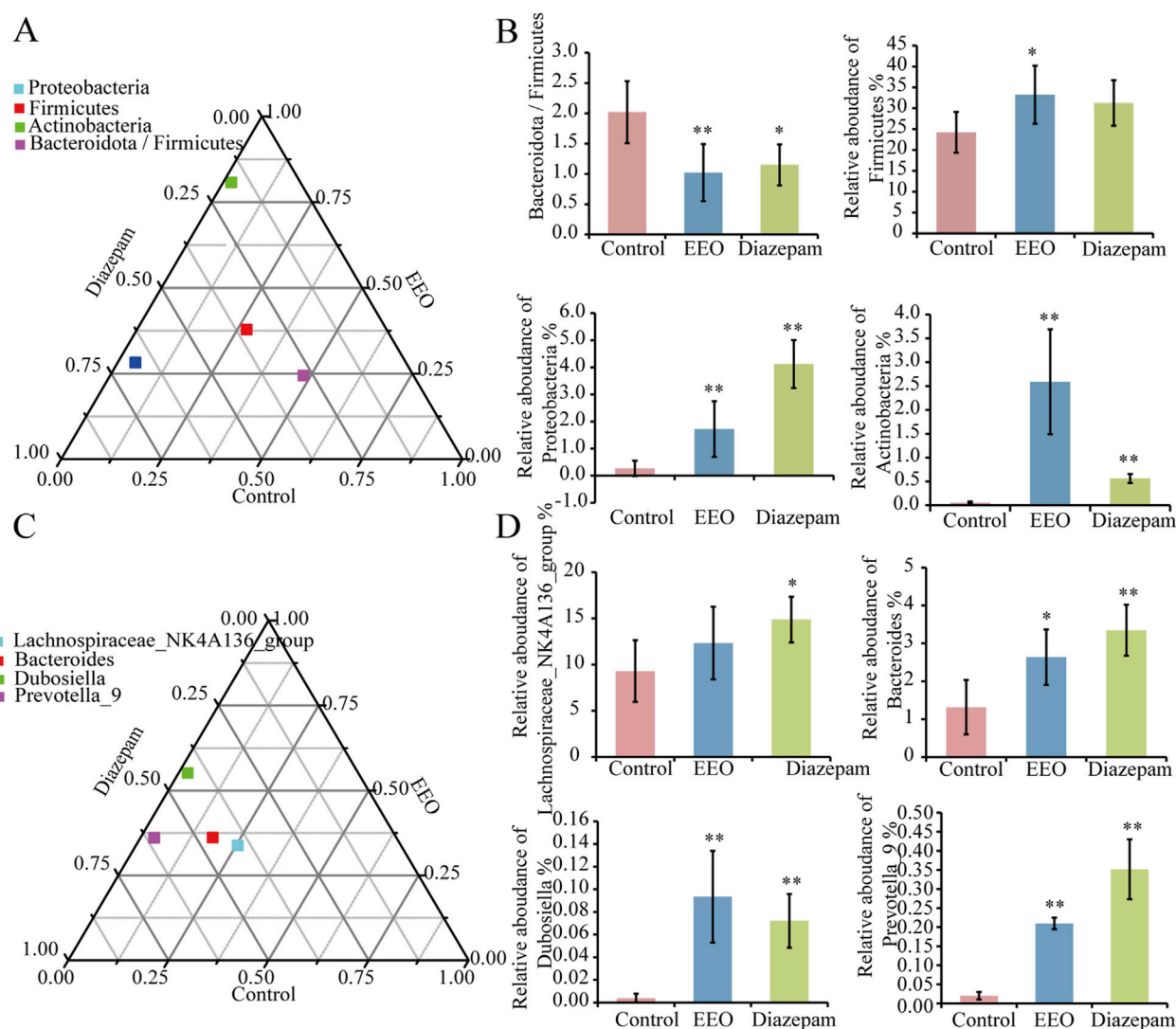


FIGURE 5

Differences in the abundance of intestinal flora in each group at the phylum and genus levels. Ternary phase diagrams of the differences in intestinal flora at the phylum (A) and genus (C) levels. (B) Histograms of the abundance of intestinal flora at the phylum level in each group after treatment with EEO. (D) Histograms of the abundance of intestinal flora at the genus level in each group after eucalyptus essential oils treatment. Find significantly different microbes through t-test analysis. * $p < 0.05$, ** $p < 0.01$; $n = 6$.

increased the elevated relative abundance of *Lachnospiraceae_NK4A136_group*, *Bacteroides*, *Dubosiella*, *Prevotella_9* (Figure 5D).

Linear discriminant analysis of LDA effect size (LEfSe) was used to identify taxa most likely to explain differences in microbiota composition between the control and EEO groups. A comparison of the individuals from both groups revealed that Actinobacteria at phylum level, as well as *Acidothermus*, *Rothia*, *Conexibacter* and *Bacillus* at the genus level exhibited significant influences in the EEO group, while in the control, Bacteroidota in the phylum level made contributions (Figure 6A). A taxonomic cladogram derived from the LEfSe analysis (with the LDA score > 3.0) showed the relationships of the differential microbiota with significant roles (Figure 6B). Altogether, these results suggest that the gut microbes exhibit alterations after EEO treatment.

A KEGG functional prediction was subsequently performed by means of the PICRUST approach. The heat map showed that

the results of KEGG three-level classification enrichment analysis (Figure 6C). The results showed that these differential microbes might be closely related with purine and pyrimidine metabolism, aminoacyl tRNA biosynthesis, energy metabolism and glutamine and glutamate metabolism (Figure 6D).

Correlation analysis between gut microbes and sedation behavior

The correlation and significance between gut microbes and sedation behaviors in mice was investigated by Pearson's correlation analysis (Figure 7A). The observed species, chao1 index showed significantly negative correlation ($P < 0.05$) with total distance and movement speed of mice. Shannon, simpson index showed significantly negative correlation ($P < 0.05$) with

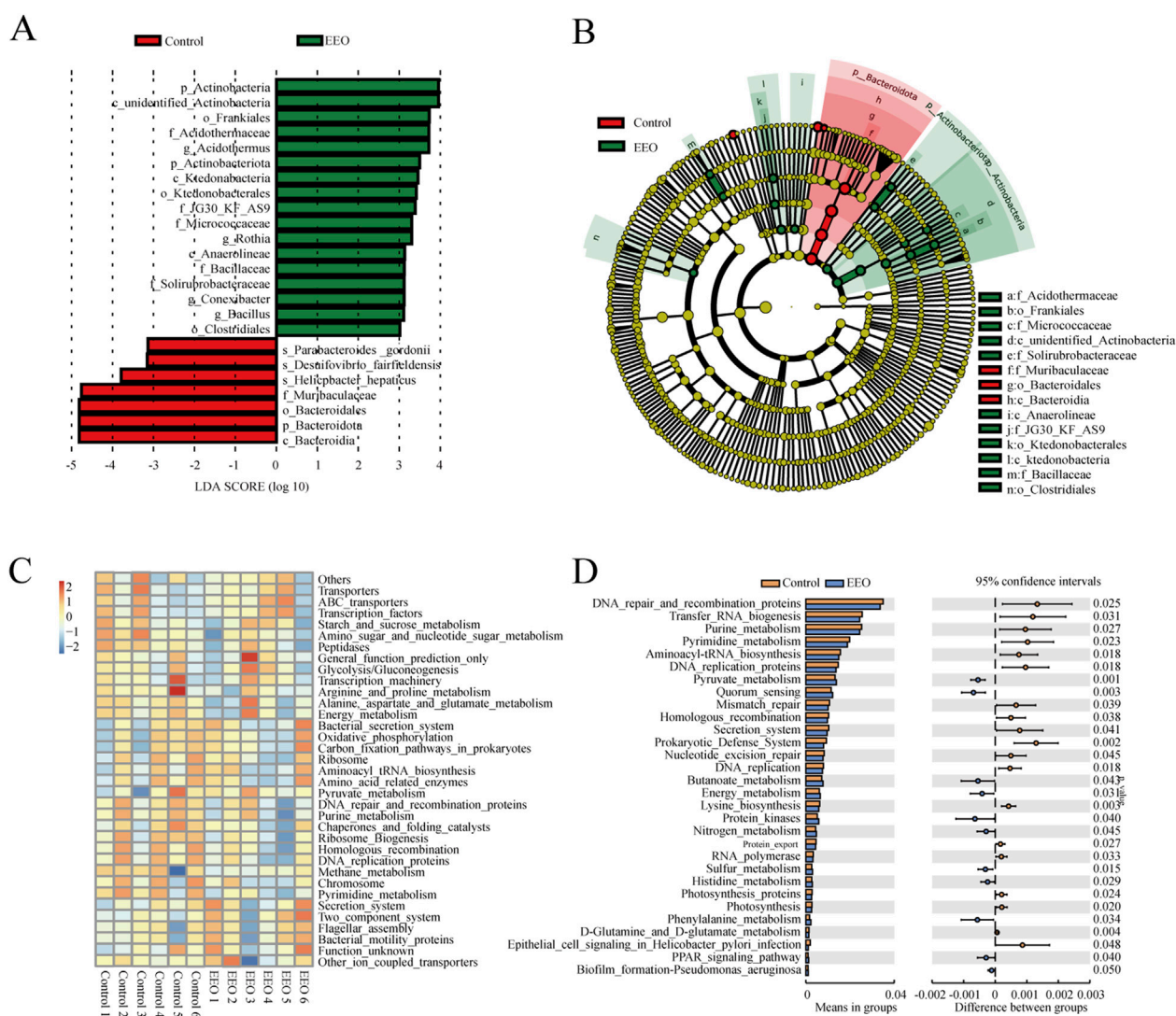


FIGURE 6

Distinct taxa with greater contributions at different taxonomic levels and the predicted functional changes in the gut microbes. (A) Linear discriminant analysis (LDA) effect size (LEfSe) identified microbial biomarkers from phylum to species levels that discriminate the control and EEO groups. (B) Cladogram constructed using the LEfSe method to display the phylogenetic distribution of bacteria that were most highly enriched in the control and EEO groups. (C) For predicting flora function, heat map of PICRUST analysis identified the KEGG pathway among the control and EEO groups. (D) The KEGG analysis showed the potential pathways associated with changes in the intestinal microbes after the EEO treatment. $n = 6$.

movement speed and total distance travelled respectively. Sleep duration was positively correlated with the abundance of Proteobacteria at the phylum level (Figure 7B), and positively correlated with *Enterococcus*, *Pseudomonas*, *Cupriavidus*, *Prevotella_9* and *Ralstonia* at the genus level (Figure 7C). It suggested that the length of sleep duration was related to the composition of the gut microbes.

Effect of EEO on the abundance of neurotransmitter-producing microbes

Through an extensive search, we obtained gut microbes associated with neurotransmitter synthesis (Supplementary Table 1). The total abundance of bacteria associated with dopamine, GABA, glycine,

histamine, and serotonin (5-HT) synthesis were calculated. We found that microbes synthesize dopamine, GABA and glycine were considerably affected by EEO treatment. EEO significantly increased the abundance of GABA- and glycine-synthesize bacteria in the mouse gut (Figures 8B, C, $P < 0.05$), while it had no significant effect on the abundance of bacteria synthesize histamine and 5-HT (Figures 8D, E, $P > 0.05$). Diazepam treatment significantly increased the abundance of bacteria associated with the synthesis of dopamine, GABA and glycine (Figures 8A–C, $P < 0.05$).

Discussion

Sleep disorders can seriously affect people quality of life and increase socio-economic burden (Yuen and Pelayo, 2017; Wickwire

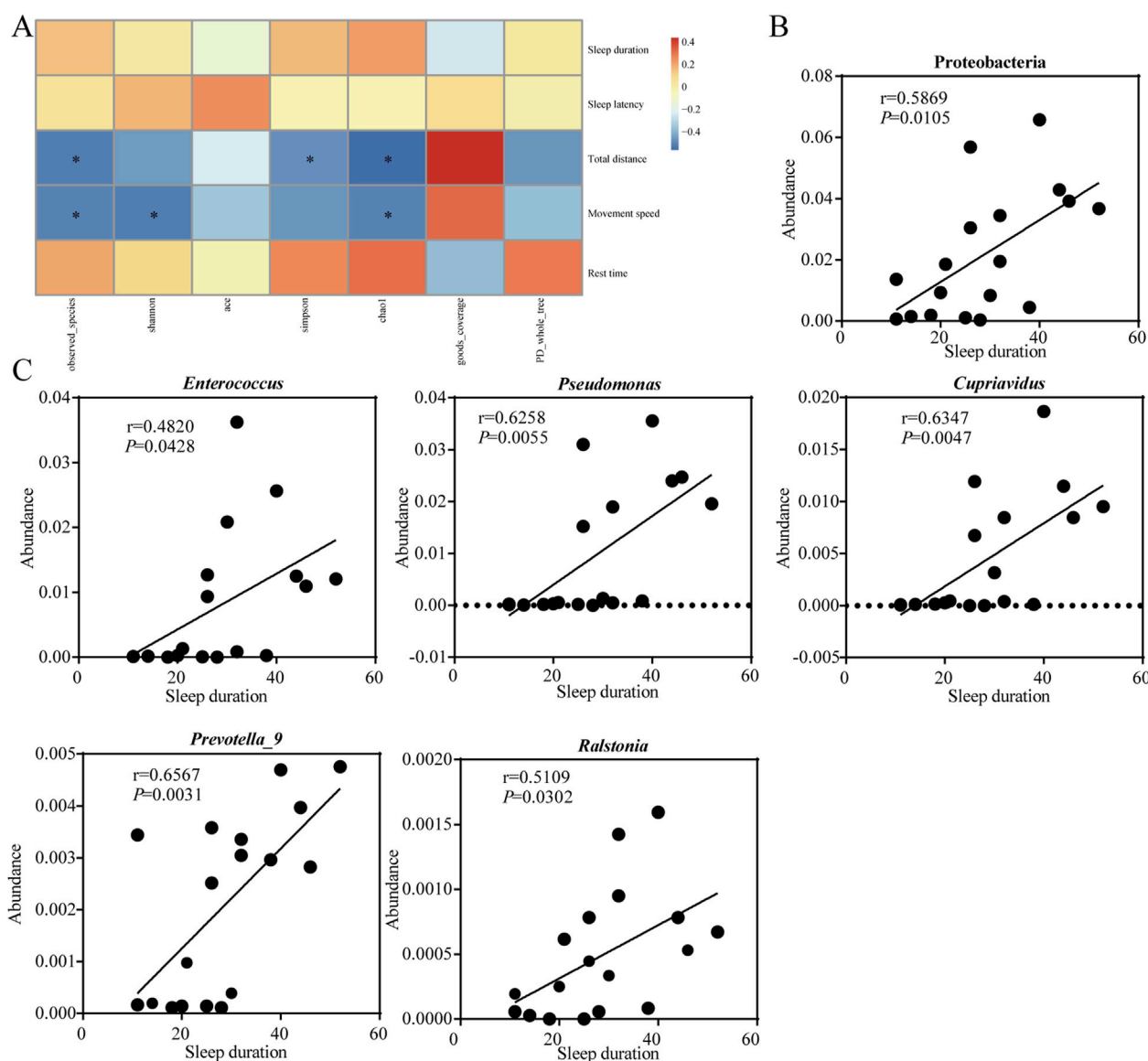


FIGURE 7
Sedative-hypnotic behaviors are associated with occupancy in the intestinal microbes. **(A)** Correlation analysis between mice behaviors with intestinal microbes α diversity. **(B)** Correlation analysis between sleep duration time and the abundance of gut microbes at the phylum level. **(C)** Correlation analysis between sleep duration time and the abundance of gut microbes at the genus level. Statistical significance is evaluated by Pearson correlation coefficient test. * $p < 0.05$; $n = 18$.

et al., 2016). In recent years, many studies have explored the effects of natural products on sleep with a potential to replace conventional hypnotic drugs that may have serious side effects. In this study, we explored the sedative-hypnotic effects of EEO treatment in mice. To our knowledge, this is the first report of a depressant effect of EEO on the central nervous system in mice. The open field test was employed to assess whether EEO affected exploratory activity in mice, after the sleep induction test was performed, which was a specific test to assess sedative-hypnotic drugs. In the open field test, it was found that EEO treatment significantly reduced the total distance travelled and decreased the movement speed in mice, and the results of the barbiturate-induced sleep test also found that EEO significantly increased sleep duration. This was consistent with the effects induced by the positive control diazepam treatment group

(Figure 1). This suggested that EEO had a significant sedative-hypnotic effect. Consistent with our study, one of the EEO constituents, 1,8-eudesmusin, was reported to reduce locomotion in mice with sedative effect (Santos and Rao, 2000). The main components of EEO were shown in Supplementary Table 2, and one of its main components, 1,8-eudesmusin, may be the main functional substance that exerted sedative-hypnotic effects. In terms of the safety of EEO, a study found that mice did not show significant changes in behavior, vital signs, and blood biochemical indicators when orally administered with 833 mg/kg B.W. of EEO (Kapnis et al., 2022). According to the World Health Organization, this may indicate that EEO is classified as “unlikely to cause any acute or subacute hazard.” The good sedative-hypnotic effects of EEO make it a safe natural extract that has the potential to

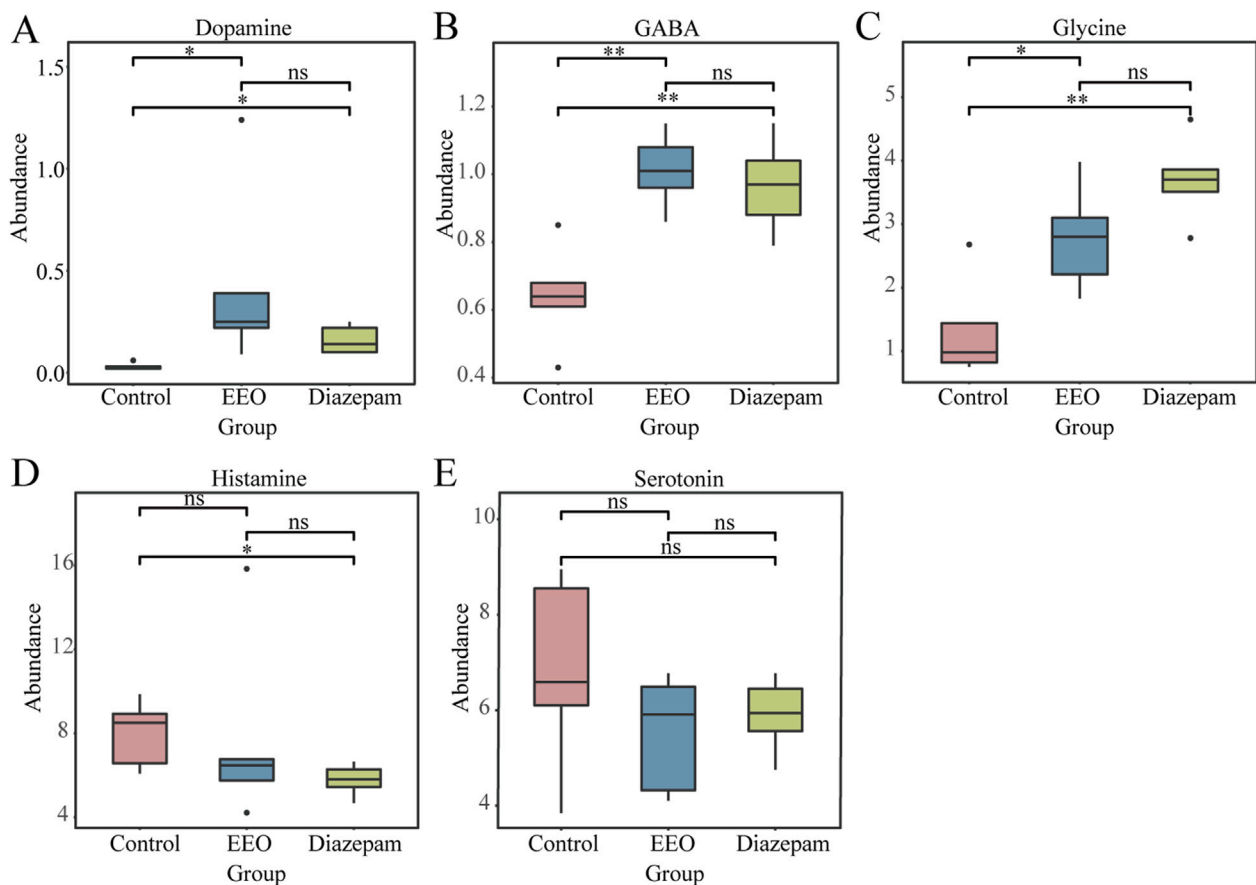


FIGURE 8
Effects of EEO supplementation on the intestinal neurotransmitter-producing flora of mice. The abundance of functional microbes synthesizing dopamine (A), GABA (B), glycine (C), histamine (D), and serotonin (E) neurotransmitters. * $p < 0.05$, ** $p < 0.01$; $n = 6$.

be used as an alternative to traditional hypnotic drugs for improving sleep.

Sleep regulation is a highly complex process that is finely regulated by changes in brain neurochemicals, and many neurotransmitters are involved in sleep regulation. Drugs that interfere or modulate these neurochemical systems can lead to changes in arousal and sleep, which in turn modulate sleep disorders. GABA is produced from glutamate by the enzyme glutamic acid decarboxylase. GABA is the main inhibitory neurotransmitter and it is well established that GABA inhibits nerve conduction and prevents neuronal over-excitation which in turn promotes sleep (Yamatsu et al., 2016; Kim et al., 2019). Glutamate is an excitatory neurotransmitter, and glutamate and glutamine can be interconverted, and glutamate can be inactivated by the glutamate-glutamine cycle, terminating the excitatory effect of glutamate (Chen et al., 2022). The results of our study showed that both EEO and diazepam groups significantly increased the levels of glutamine and GABA in the brain of mice compared to the control group (Figure 3). Similar to our study, many natural products such as *Nelumbo nucifera* Seed Extract and Valerian/Hop Mixture can improve sleep and prolong sleep duration in *Drosophila* by modulating GABA signal (Jo et al., 2018; Choi et al., 2017). Our study also found that EEO significantly increased glycine levels in the mouse brain (Figure 3). In the central nervous system, glycine

acts as an inhibitory neurotransmitter by affecting glycine receptor GlyRs, and glycine has been reported to increase the duration of non-rapid eye movement sleep and reduce the number and mean duration of dark period awakening (Hondo et al., 2011). An increasing number of studies have found that 5-HT promotes sleep (Zhang et al., 2018), and tryptophan, as the sole substrate for 5-HT synthesis, have also been reported to have a hypnotic effect (Roth et al., 2021). N-acetylserotonin and 5-HIAA, as products of 5-HT acetylation and monoamine oxidation, have also been reported to improve sleep. The results of the study found that EEO could upregulate the levels of tryptophan, N-acetylserotonin and 5-HIAA in brain tissues (Figure 3). The study by Wang et al. (2020) found that Schisandrin B could reduce sleep latency in parachlorophenylalanine-induced insomnia in rats by increasing the levels of 5-HIAA and increasing sleep duration. Nyctinastic herbs decoction can also treat insomnia by increasing 5-HIAA levels (Yang et al., 2021). Supplementation with saffron extract increased N-acetylserotonin and tryptophan synthesis and improved sleep quality in rats (Munoz et al., 2023). Our studies illustrated the ability of EEO to affect the levels of sleep-related neurotransmitters in the brain, which in turn affected the sleep state.

Studies in recent years have found a strong association between gut microbes and sleep, and maintaining the homeostasis of the gut microbes is key to improving sleep (Neroni et al., 2021). Intake of

Lactobacillus and *Bacillus longum* has been reported to improve sleep quality preventing sleep disorders (Matsuda et al., 2020). A study by Guo et al. (2019) found that Oolong Tea Polyphenols regulate circadian rhythms by enhancing beneficial gut microbes. All these findings suggested that gut microbes influenced sleep quality through GMBA. In our study, we found that EEO and the positive control diazepam significantly altered the gut microbes of mice and increased the α -diversity and β -diversity of the gut microbes (Figure 4). And observed-species and chao1 index showed significantly negative correlation with both total distance and movement speed. Shannon and simpson index showed significantly negative correlation with movement speed and total distance, respectively (Figure 7A). In addition, the gut microbes of mice in the EEO and diazepam groups possessed a higher number of repetitive OTUs and had a more similar flora structure. It is reported that gut microbial diversity is positively correlated with an increase in sleep efficiency and total sleep time, and that gut microbial diversity promotes healthier sleep (Smith et al., 2019). A study by Ogawa et al. (2020) found that treatment with a broad-spectrum antibiotic significantly reduced the duration of non-rapid eye movement sleep in mice while decreasing their gut microbes. These suggested that the diversity of gut microbes affected sleep quality. The diversity of gut microbes interacted with sleep conditions, and poorer sleep states reduced the diversity of gut microbes, leading to dysbiosis. A good gut microbial ecology promoted better sleep. This might be related to the fact that certain beneficial flora promoted sleep, or it might be due to the fact that gut microbes metabolism affected the synthesis of certain neurotransmitters and certain vitamins associated with sleep (El Aidy et al., 2020).

We found that EEO treatment altered the relative abundance of gut microbes, significantly increased the relative abundance of Firmicutes, Proteobacteria, and Actinobacteria at the phylum level and decreased the Bacteroidota/Firmicutes abundance ratio. At the genus level, EEO treatments increased the abundance of *Bacteroides*, *Dubosiella*, *Prevotella_9*, and *Lachnospiraceae_NK4A136_groups* (Figure 5). Lower Bacteroidota/Firmicutes ratio was beneficial for minimising pathogens and for probiotic colonisation (Ge et al., 2023). It has also been previously found that higher Firmicutes abundance is associated with higher sleep quality in the host (Smith et al., 2019). Therefore, we speculated that EEO may affect the abundance of Firmicutes, promoted probiotic colonisation, maintain intestinal homeostasis and exerted a sedative-hypnotic effect. In addition to this, we found that most of the gut microbes altered by EEO were short-chain fatty acid-producing beneficial bacteria. The members of Firmicutes mainly included beneficial bacteria, and Firmicutes were considered to be the main gate of short-chain fatty acid production in the mouse gut (Li W. T. et al., 2023; Wongsurawat et al., 2023). Proteobacteria promoted propionic acid production, and Actinobacteria mainly produced acetic acid and butyric acid (Zhao et al., 2019; Haenen et al., 2013). *Bacteroides* have been shown to be carbohydrate degraders and short chain fatty acid (SCFA) producers (Fan et al., 2023). SCFA produced by gut microbes were thought to be endogenous circadian signal molecules and were essential for gut-brain axis communication (Fredericks et al., 2020). SCFA interacted with receptors on enteroendocrine cells by inducing the secretion of gut hormones, such as GABA and 5-HT, and facilitating indirect signals to the

brain via the somatic or vagal pathways (Silva et al., 2020), which can in turn alter the organism's sleep state. Therefore, EEO may improve sleep by enriching SCFA-producing microbes and thereby increasing the metabolite SCFA.

Compositions of gut microbes were closely related to sleep quality, and we found that sleep duration time showed a significant correlation with the relative abundance of certain gut microbes using the Pearson correlation coefficient test. At the phylum level, Proteobacteria showed a significantly positive correlation with sleep duration (Figure 7B). Similar to our study, Song et al. (2022) found that the shorter the sleep duration caused by caffeine, the lower the relative abundance of Proteobacteria. At the genus level, *Enterococcus*, *Pseudomonas*, *Cupriavidus*, *Prevotella_9*, and *Ralstonia* showed significantly positive correlation with sleep duration (Figure 7C). Insomnia caused a decrease in *Prevotella* abundance in the gut, while the Radix Ginseng and Semen Ziziphi Spinosae treatment improved insomnia and was able to increase *Prevotella* abundance in the gut (Qiao et al., 2022). All of these studies suggested a strong association between sleep and certain microbes. Although there was insufficient evidence to prove a clear causal relationship between sleep problems and microbiological composition, it is undeniable that modulation of the gut microbes can be a key target for the treatment of sleep disorders.

Studies have now demonstrated that the gut microbes can communicate with the brain through functional metabolites, which in turn control circadian rhythms and sleep quality (Ogawa et al., 2020). Differential microbes in the prediction of KEGG function in gut microbes may be related to glutamine and glutamate metabolism (Figure 6D), associated with this, while there are elevated levels of glutamine in the brain. Therefore, we speculated that there may be gut microbes-induced neurotransmitter differences in the brain. In addition, the effect of EEO on the neurotransmitter-producing flora of the gut microbes was explored. Gut microbes were directly involved in the synthesis of a variety of neurotransmitters and can influence the levels of neurotransmitters in the nervous system through metabolic pathways (Zhao et al., 2022). Olson et al. (2018) found that *Parabacteroides* produced large amounts of GABA. *Oscillibacter*, *Dialister*, and *Coproccoccus* have been reported to be associated with GABA synthesis (Liu and Huang, 2019). *Bacteroides*, *Prevotella*, *Parabacteroides* have been reported to be involved in glycine production (Liu and Huang, 2019; Lynch et al., 2017). GABA and glycine, as the main inhibitory neurotransmitters in the nervous system, played an important role in the regulation of the sleep-wake cycle. There was no direct evidence that gut-produced GABA can cross the blood-brain barrier (BBB), but studies have found that physiological and psychological stress can increase BBB permeability and cause GABA inward flow (Constans et al., 2020; Varanoske et al., 2022). In contrast, glycine readily crossed the BBB via glycine transporter proteins and enters the brain to act on NMDA receptors in the supraoptic nucleus, which in turn affected the sleep cycle (Epping et al., 2022). Our finding that EEO significantly increased the abundance of gut microbes associated with GABA and glycine synthesis (Figures 8B, C), and EEO significantly increased GABA and glycine levels in the mouse brain (Figure 3B). The mechanism by which EEO regulates neurotransmitters in the brain is unclear, whether it acts directly

on the brain to affect neurotransmitter synthesis or regulates neurotransmitter levels via gut microbes will require further studies to elucidate the exact mechanism. However, it is well known that gut microbes produce hormones and neurotransmitters that are transmitted via the afferents of the vagus nervous system, which activate or inhibit the corresponding neurons, thereby promoting sleep (Lyte, 2014; Dinan et al., 2015).

Conclusion

EEO supplementation reduced activity and improved sleep quantity in mice, consistent with the effects of diazepam. Through brain neurotransmitter-targeting histological assays, EEO was shown to increase brain levels of sleep-promoting neurotransmitters such as glutamine, GABA, glycine, tryptophan, N-acetylserotonin and 5-HIAA, and improve sleep in mice. EEO increased the abundance of intestinal flora, short-chain fatty acid-producing flora, and promoted probiotic colonisation, as well as the abundance of functional flora synthesize GABA and glycine neurotransmitters. EEO also increased the abundance of short-chain fatty acid-producing flora and the abundance of functional flora synthesizing GABA and glycine neurotransmitters. EEO may exert sedative-hypnotic effects by improving the gut microbiota and thereby altering brain neurotransmitters. Our findings suggested that gut microbes might serve as a target of action for EEO in the treatment of sleep deprivation, EEO as a natural product alternative for the treatment of insomnia and sleep disorders, and the potential for the development of new drugs for the treatment of sleep disorders.

Data availability statement

The original contributions presented in the study are included in the article/**Supplementary Material**, further inquiries can be directed to the corresponding author.

Ethics statement

The animal study was approved by All animal testing procedures were conducted in accordance with the guidelines of the Animal Ethics Committee of Zhejiang University (ethical programme code ZJU 20160403). The study was conducted in accordance with the local legislation and institutional requirements.

References

- Aziz, Z. A. A., Nasir, H. M., Ahmad, A., Setapar, S. H. M., Ahmad, H., Noor, M. H. M., et al. (2019). Enrichment of eucalyptus oil nanoemulsion by micellar nanotechnology: transdermal analgesic activity using hot plate test in rats' assay. *Sci. Rep.* 9, e13678. doi:10.1038/s41598-019-50134-y
- Bampidis, V., Azimonti, G., Bastos, M. D., Christensen, H., Durjava, M., Kouba, M., et al. (2023). Safety and efficacy of a feed additive consisting of an essential oil derived

Author contributions

XL: Writing–original draft, Writing–review and editing. YZ: Writing–original draft. QZ: Writing–review and editing. AC: Writing–review and editing. JF: Writing–review and editing.

Funding

The authors declare that financial support was received for the research, authorship, and/or publication of this article. This study has been supported by the Zhejiang Province Key R&D Program (grant number 2024C02004) and the National R&D Program of China (grant number 2022YFD1300504).

Acknowledgments

We thank Biotechnology R&D Center of Shandong Longchang Animal Health Products Co., Ltd. for providing reagent raw material support for the experiment. We also thank Wuhan Maiwei Metabolic Biotechnology Co., Ltd. for providing technical support.

Conflict of interest

Author AC was employed by Biotechnology R&D Center of Shandong Longchang Animal Health Products Co., Ltd.

The remaining authors declare that the research was conducted in the absence of any commercial or financial relationships that could be construed as a potential conflict of interest.

Publisher's note

All claims expressed in this article are solely those of the authors and do not necessarily represent those of their affiliated organizations, or those of the publisher, the editors and the reviewers. Any product that may be evaluated in this article, or claim that may be made by its manufacturer, is not guaranteed or endorsed by the publisher.

Supplementary material

The Supplementary Material for this article can be found online at: <https://www.frontiersin.org/articles/10.3389/fphar.2024.1464654/full#supplementary-material>

from *Eucalyptus globulus* Labill. (eucalyptus oil) for all animal species (FEFANA asbl). *Efsa J.* 7 (21), e08178. doi:10.2903/j.efsa.2023.8178

Barbosa, K. T., Acosta, A. P., Schulz, H. R., De Santi, I. I., Delucis, R. D., Beltrame, R., et al. (2021). Biochemical features of organic extractives from eucalyptus and corymbia woods using ethanol as a solvent. *Maderas-Ciencia Y Tecnol.* 23, 58–69. doi:10.4067/s0718-221x2021000100458

- Broussard, J. L., Wroblewski, K., Kilus, J. M., and Tasali, E. (2016). Two nights of recovery sleep reverses the effects of short-term sleep restriction on diabetes risk. *Diabetes Care* 39 (3), 40–e41. doi:10.2337/dc15-2214
- Caceres, A. I., Liu, B. Y., Jabba, S. V., Achanta, S., Morris, J. B., and Jordt, S. E. (2017). Transient receptor potential cation channel subfamily m member 8 channels mediate the anti-inflammatory effects of eucalyptol. *Br. J. Pharmacol.* 174 (9), 867–879. doi:10.1111/bph.13760
- Chen, T. C., Zhang, F. Y., Chen, J. Q., Zhong, Q. G., Hu, Y. X., Wu, R. R., et al. (2022). Effects of alcohol extracts from ganoderma resinaceum on sleep in mice using combined transcriptome and metabolome analysis. *Front. Nutr.* 9, e745624. doi:10.3389/fnut.2022.745624
- Choi, H. S., Ko, B. S., Kim, H. D., Hong, K. B., and Suh, H. J. (2017). Effect of valerian/hop mixture on sleep-related behaviors in *Drosophila melanogaster*. *Biol. Pharm. Bull.* 40 (7), 1101–1110. doi:10.1248/bpb.b17-00262
- Constans, C., Ahnine, H., Santin, M., Lehericy, S., Tanter, M., Pouget, P., et al. (2020). Non-invasive ultrasonic modulation of visual evoked response by GABA delivery through the blood brain barrier. *J. Control. Release.* 318, 223–231. doi:10.1016/j.jconrel.2019.12.006
- Dasdelen, M. F., Er, S., Kaplan, B., Celik, S., Beker, M. C., Orhan, C., et al. (2022). A novel theanine complex, mg-l-theanine improves sleep quality via regulating brain electrochemical activity. *Front. Nutr.* 9, 874254. doi:10.3389/fnut.2022.874254
- Dinan, T. G., Stilling, R. M., Stanton, C., and Cryan, J. F. (2015). Collective unconscious: how gut microbes shape human behavior. *J. Psychiatr. Res.* 63, 1–9. doi:10.1016/j.jpsychires.2015.02.021
- El Aidy, S., Bolsius, Y. G., Raven, F., and Havekes, R. (2020). A brief period of sleep deprivation leads to subtle changes in mouse gut microbiota. *J. Sleep. Res.* 29 (6), e12920. doi:10.1111/jsr.12920
- Epping, L., Schroeter, C. B., Nelke, C., Bock, S., Gola, L., Ritter, N., et al. (2022). Activation of non-classical NMDA receptors by glycine impairs barrier function of brain endothelial cells. *Cell. Mol. Life Sci.* 79 (9), 479–488. doi:10.1007/s00018-022-04502-z
- Fan, Y., Ju, T. T., Bhardwaj, T., Korver, D. R., and Willing, B. P. (2023). Week-old chicks with high bacteroides abundance have increased short-chain fatty acids and reduced markers of gut inflammation. *Microbiol. Spectr.* 11 (2), 345–356. doi:10.1128/spectrum.03616-22
- Fredericks, E., Theunissen, R., and Roux, S. (2020). Short chain fatty acids and monocarboxylate transporters in irritable bowel syndrome. *Turk. J. Gastroenterol.* 31 (12), 840–847. doi:10.5152/tjg.2020.19856
- Galland, L. (2014). The gut microbiome and the brain. *J. Med. Food.* 17 (12), 1261–1272. doi:10.1089/jmf.2014.7000
- Ge, C. Y., Luo, X. Y., Wu, L. C., Lv, Y. J., Hu, Z. Y., Yu, D. Y., et al. (2023). Plant essential oils improve growth performance by increasing antioxidative capacity, enhancing intestinal barrier function, and modulating gut microbiota in Muscovy ducks. *Poult. Sci.* 102 (8), e102813. doi:10.1016/j.psj.2023.102813
- Golubeva, A. V., Joyce, S. A., Moloney, G., Burokas, A., Sherwin, E., Arboleya, S., et al. (2017). Microbiota-related changes in bile acid and tryptophan metabolism are associated with gastrointestinal dysfunction in a mouse model of autism. *Ebiomedicine* 24, 166–178. doi:10.1016/j.ebiom.2017.09.020
- Guo, T. T., Song, D., Ho, C. T., Zhang, X., Zhang, C. D., Cao, J. X., et al. (2019). Omics analyses of gut microbiota in a circadian rhythm disorder mouse model fed with oolong tea polyphenols. *J. Agric. Food Chem.* 67 (32), 8847–8854. doi:10.1021/acs.jafc.9b03000
- Haenen, D., Zhang, J., da Silva, C. S., Bosch, G., van der Meer, I. M., van Arkel, J., et al. (2013). A diet high in resistant starch modulates microbiota composition, scf concentrations, and gene expression in pig intestine. *J. Nutr.* 143, 274–283. doi:10.3945/jn.112.169672
- Harding, K., and Feldman, M. (2008). Sleep disorders and sleep deprivation: an unmet public health problem. *J. Am. Acad. Child. Adolesc. Psychiatry* 47 (4), 473–474. doi:10.1097/01.CHI.0000270812.55636.3b
- Hondo, M., Furutani, N., Yamasaki, M., Watanabe, M., and Sakurai, T. (2011). Orexin neurons receive glycinergic innervations. *PLoS One* 6 (9), e25076. doi:10.1371/journal.pone.0025076
- Horvath, T. D., Ihekweazu, F. D., Haidacher, S. J., Ruan, W., Engevik, K. A., Fultz, R., et al. (2022). Bacteroides ovatus colonization influences the abundance of intestinal short chain fatty acids and neurotransmitters. *IScience* 25 (5), e104158. doi:10.1016/j.isci.2022.104158
- Ieri, F., Cecchi, L., Giannini, E., Clemente, C., and Romani, A. (2019). GC-MS and HS-SPME-GC×GC-TOFMS determination of the volatile composition of essential oils and hydrosols (By-Products) from four Eucalyptus species cultivated in tuscany. *Molecules* 24 (2), 226–239. doi:10.3390/molecules24020226
- Jo, K., Choi, H. S., Jeon, S., Ahn, C. W., and Suh, H. J. (2018). *Nelumbo nucifera* seed extract promotes sleep in drosophila melanogaster. *Biol. Pharm. Bull.* 41 (3), 399–408. doi:10.1248/bpb.b17-00763
- Kapnis, K., Chrysargyris, A., Prokopi, M., Varda, E., Kokkinidou, D., Samourides, A., et al. (2022). Effects on lettuce yield parameters and toxicological safety assessment of a plant-derived formulation based on rosemary and eucalyptus essential oils. *Agronomy-Basel* 12, 2861. doi:10.3390/agronomy12112861
- Kim, S., Jo, K., Hong, K. B., Han, S. H., and Suh, H. J. (2019). GABA and L-theanine mixture decreases sleep latency and improves NREM sleep. *Pharm. Biol.* 57, 65–73. doi:10.1080/13880209.2018.1557698
- Leone, V., Gibbons, S. M., Martinez, K., Hutchison, A. L., Huang, E. Y., Cham, C. M., et al. (2015). Effects of diurnal variation of gut microbes and high-fat feeding on host circadian clock function and metabolism. *Cell Host Microbe* 17 (5), 681–689. doi:10.1016/j.chom.2015.03.006
- Li, N., Tan, S. W., Wang, Y., Deng, J., Wang, N., Zhu, S., et al. (2023). Akkermansia muciniphila supplementation prevents cognitive impairment in sleep-deprived mice by modulating microglial engulfment of synapses. *Gut Microbes* 15 (2), e2252764. doi:10.1080/19490976.2023.2252764
- Li, W. T., Wang, Z. X., Cao, J., Dong, Y. L., and Chen, Y. X. (2023). Melatonin improves skin barrier damage caused by sleep restriction through gut microbiota. *J. Pineal. Res.* 75 (1), e12874. doi:10.1111/jpi.12874
- Liu, T., and Huang, Z. S. (2019). Evidence-based analysis of neurotransmitter modulation by gut microbiota. *Lect. Notes Artif. Intell.* 11837, 238–249. doi:10.1007/978-3-030-32962-4_22
- Lynch, A., Crowley, E., Casey, E., Cano, R., Shanahan, R., McGlacken, G., et al. (2017). The Bacteroidales produce an N-acylated derivative of glycine with both cholesterol-solubilising and hemolytic activity. *Sci. Rep.* 7, e13270. doi:10.1038/s41598-017-13774-6
- Lyte, M. (2014). Microbial endocrinology Host-microbiota neuroendocrine interactions influencing brain and behavior. *Gut Microbes* 5 (3), 381–389. doi:10.4161/gmic.28682
- Matheson, E., and Hainer, B. L. (2017). Insomnia: pharmacologic therapy. *Am. Fam. Physician* 96 (1), 29–35.
- Matsuda, Y., Ozawa, N., Shinozaki, T., Wakabayashi, K., Suzuki, K., Kawano, Y., et al. (2020). Ergothioneine, a metabolite of the gut bacterium *Lactobacillus reuteri*, protects against stress-induced sleep disturbances. *Transl. Psychiatry* 10 (1), 170–179. doi:10.1038/s41398-020-0855-1
- Medeiros, K., Dos Santos, J. R., Melo, T. C. D., De Souza, M. F., Santos, L. D., de Gois, A. M., et al. (2018). Depressant effect of geraniol on the central nervous system of rats: behavior and ecog power spectra. *Biomed. J.* 41 (5), 298–305. doi:10.1016/j.bj.2018.08.008
- Muñoz, M. D., Román-Carmena, M., Amor, S., García-Villalón, A. L., Espinel, A. E., González-Hedström, D., et al. (2023). Effects of supplementation with the standardized extract of saffron (affron™) on the kynurenine pathway and melatonin synthesis in rats. *Antioxidants* 12 (8), 1619–1627. doi:10.3390/antiox12081619
- Neroni, B., Evangelisti, M., Radocchia, G., Di Nardo, G., Pantanella, F., Villa, M. P., et al. (2021). Relationship between sleep disorders and gut dysbiosis: what affects what? *Sleep. Med.* 87, 1–7. doi:10.1016/j.sleep.2021.08.003
- Ngo, D. H., and Vo, T. S. (2019). An updated review on pharmaceutical properties of gamma-aminobutyric acid. *Molecules* 24 (15), 2678. doi:10.3390/molecules24152678
- Niu, Z. F., Wu, L., Kang, J., Bai, J. B., Chen, Y. J., and Xia, H. C. (2022). Regulation of sleep disorders in patients with traumatic brain injury by intestinal flora based on the background of brain-gut axis. *Front. Neurosci.* 16, e934822. doi:10.3389/fnins.2022.934822
- Ogawa, Y., Miyoshi, C., Obana, N., Yajima, K., Hotta-Hirashima, N., Ikkyu, A., et al. (2020). Gut microbiota depletion by chronic antibiotic treatment alters the sleep/wake architecture and sleep EEG power spectra in mice. *Sci. Rep.* 10 (1), e19554. doi:10.1038/s41598-020-76562-9
- Olson, C. A., Vuong, H. E., Yano, J. M., Liang, Q. X. Y., Nusbaum, D. J., and Hsiao, E. Y. (2018). The gut microbiota mediates the anti-seizure effects of the ketogenic diet. *Cell* 174 (2), 497–508. doi:10.1016/j.cell.2018.06.051
- Pesarico, A. P., Vieira, A. T., and Rosa, S. G. (2023). Editorial: gut-microbiota-brain axis in depression: mechanisms and possible therapies. *Front. Behav. Neurosci.* 17, e1221141. doi:10.3389/fnbeh.2023.1221141
- Poroyko, V. A., Carreras, A., Khalyfa, A., Khalyfa, A., Leone, V., Peris, E., et al. (2016). Chronic bacteroides disruption alters gut microbiota, induces systemic and adipose tissue inflammation and insulin resistance in mice. *Sci. Rep.* 6, e35405. doi:10.1038/srep35405
- Qiao, T., Wang, Y., Liang, K., Zheng, B. Y., Ma, J., Li, F. X., et al. (2022). Effects of the Radix Ginseng and Semen Ziziphi Spinosae drug pair on the GLU/GABA-GLN metabolic cycle and the intestinal microflora of insomniac rats based on the brain-gut axis. *Front. Pharmacol.* 13, e1094507. doi:10.3389/fphar.2022.1094507
- Regulation (EC) (2003). No 1831/2003 of the European Parliament and of the council of 22 September 2003 on the additives for use in animal nutrition. *OJ L* 268 (18.10), 29.
- Roth, W., Zadeh, K., Vekariya, R., Ge, Y., and Mohammadzadeh, M. (2021). Tryptophan metabolism and gut-brain homeostasis. *Int. J. Mol. Sci.* 22 (6), e2973. doi:10.3390/ijms22062973
- Santos, F. A., and Rao, V. S. N. (2000). Antiinflammatory and antinociceptive effects of 1,8-cineole a terpenoid oxide present in many plant essential oils. *Phytother. Res.* 14 (4), 240–244. doi:10.1002/1099-1573(200006)14:4<240::aid-pt573>3.0.co;2-x
- Sathantriphop, S., Thanispong, K., Sanguanpong, U., Achee, N. L., Bangs, M. J., and Chareonviriyaphap, T. (2014). Comparative behavioral responses of pyrethroid-susceptible and -resistant aedes aegypti (diptera: culicidae) populations to citronella and eucalyptus oils. *J. Med. Entomol.* 51 (6), 1182–1191. doi:10.1603/ME13191

- Silva, Y. P., Bernardi, A., and Frozza, R. L. (2020). The role of short-chain fatty acids from gut microbiota in gut-brain communication. *Front. Endocrinol.* 11, 25–36. doi:10.3389/fendo.2020.00025
- Smith, R. P., Easson, C., Lyle, S. M., Kapoor, R., Donnelly, C. P., Davidson, E. J., et al. (2019). Gut microbiome diversity is associated with sleep physiology in humans. *Plos One* 14 (10), e0222394. doi:10.1371/journal.pone.0222394
- Song, Z., Liu, L., Xu, Y. Y., Cao, R. F., Lan, X. Y., Pan, C. Y., et al. (2022). Caffeine-induced sleep restriction alters the gut microbiome and fecal metabolic profiles in mice. *Int. J. Mol. Sci.* 23 (23), e14837. doi:10.3390/ijms232314837
- Takaishi, M., Fujita, F., Uchida, K., Yamamoto, S., Sawada, M., Hatai, C., et al. (2012). 1,8-cineole, a TRPM8 agonist, is a novel natural antagonist of human TRPA1. *Mol. Pain.* 8, 86–98. doi:10.1186/1744-8069-8-86
- Torres-Fuentes, C., Schellekens, H., Dinan, T. G., and Cryan, J. F. (2017). The microbiota-gut-brain axis in obesity. *Lancet Gastroenterol. Hepatol.* 2 (10), 747–756. doi:10.1016/S2468-1253(17)30147-4
- Varanoske, A. N., McClung, H. L., Sepowitz, J. J., Halagarda, C. J., Farina, E. K., Berryman, C. E., et al. (2022). Stress and the gut-brain axis: cognitive performance, mood state, and biomarkers of blood-brain barrier and intestinal permeability following severe physical and psychological stress. *Brain Behav. Immun.* 101, 383–393. doi:10.1016/j.bbi.2022.02.002
- Walia, H. K., and Mehra, R. (2016). Overview of common sleep disorders and intersection with dermatologic conditions. *Int. J. Mol. Sci.* 17 (5), 654–663. doi:10.3390/ijms17050654
- Wang, M. Y., Li, N., Jing, S., Wang, C. M., Sun, J. H., Li, H., et al. (2020). Schisandrin B exerts hypnotic effects in pcpa-treated rats by increasing hypothalamic 5-HT and γ -aminobutyric acid levels. *Exp. Ther. Med.* 20 (6), 142–156. doi:10.3892/etm.2020.9271
- Wickwire, E. M., Shaya, F. T., and Scharf, S. M. (2016). Health economics of insomnia treatments: the return on investment for a good night's sleep. *Sleep. Med. Rev.* 30, 72–82. doi:10.1016/j.smrv.2015.11.004
- Wongsurawat, T., Sutheeworapong, S., Jenjaroenpun, P., Charoensiddhi, S., Khoiri, A. N., Topanurak, S., et al. (2023). Microbiome analysis of Thai traditional fermented soybeans reveals short-chain fatty acid-associated bacterial taxa. *Sci. Rep.* 13 (1), 7573–7767. doi:10.1038/s41598-023-34818-0
- Yamatsu, A., Yamashita, Y., Pandharipande, T., Maru, I., and Kim, M. (2016). Effect of oral γ -aminobutyric acid (gaba) administration on sleep and its absorption in humans. *Food Sci. Biotechnol.* 25 (2), 547–551. doi:10.1007/s10068-016-0076-9
- Yang, Y. W., Wu, Y., Xu, P. Q., Guo, F., Guo, F., and Yang, B. C. (2021). Nyctinastic herbs decoction improves para-chlorophenylalanine-induced insomnia by regulating the expression level of neurotransmitters. *Ann. Transl. Med.* 9 (20), 1524–1532. doi:10.21037/atm-21-4462
- Yuen, K. M., and Pelayo, R. (2017). Socioeconomic impact of pediatric sleep disorders. *Sleep. Med. Clin.* 12 (1), 23–30. doi:10.1016/j.jsmc.2016.10.005
- Zhang, X., Yan, H. M., Luo, Y. J., Huang, Z. L., and Rao, Y. (2018). Thermoregulation-independent regulation of sleep by serotonin revealed in mice defective in serotonin synthesis. *Mol. Pharmacol.* 93 (6), 657–664. doi:10.1124/mol.117.111229
- Zhao, C. H., Dong, H. J., Zhang, Y. P., and Li, Y. (2019). Discovery of potential genes contributing to the biosynthesis of short-chain fatty acids and lactate in gut microbiota from systematic investigation in *E. coli*. *Npj Biofilms Microbiomes* 5 (1), 19–28. doi:10.1038/s41522-019-0092-7
- Zhao, N., Shu, Y., Jian, C. X., Zhou, Z. L., Bao, H. J., Li, X. G., et al. (2022). *Lactobacillus* ameliorates sd-induced stress responses and gut dysbiosis by increasing the absorption of gut-derived gaba in rhesus monkeys. *Front. Immunol.* 13, e915393. doi:10.3389/fimmu.2022.915393



OPEN ACCESS

EDITED BY

Jian Hao,
The Second Affiliated Hospital of Guangzhou
Medical University, China

REVIEWED BY

Shi Wenjie,
Carl von Ossietzky University Oldenburg,
Germany
Jindong Xie,
Sun Yat-sen University Cancer Center
(SYSUCC), China

*CORRESPONDENCE

Yingchao Shen,
✉ csfy045@njucm.edu.cn
Hengzhou Zhu,
✉ wxzy082@njucm.edu.cn
Donghua Fan,
✉ 15951922989@163.com

[†]These authors share first authorship

RECEIVED 16 August 2024

ACCEPTED 01 November 2024

PUBLISHED 19 November 2024

CITATION

Chang C, Sun D, Zhang Z, He L, Wang Q, Shen Y,
Zhu H and Fan D (2024) Meta-analysis of the
effect of sophora flavescens on tumor
metastasis-induced bone neuropathic pain.
Front. Pharmacol. 15:1474982.
doi: 10.3389/fphar.2024.1474982

COPYRIGHT

© 2024 Chang, Sun, Zhang, He, Wang, Shen,
Zhu and Fan. This is an open-access article
distributed under the terms of the [Creative
Commons Attribution License \(CC BY\)](#). The use,
distribution or reproduction in other forums is
permitted, provided the original author(s) and
the copyright owner(s) are credited and that the
original publication in this journal is cited, in
accordance with accepted academic practice.
No use, distribution or reproduction is
permitted which does not comply with these
terms.

Meta-analysis of the effect of sophora flavescens on tumor metastasis-induced bone neuropathic pain

Cheng Chang^{1†}, Di Sun^{2†}, Zhilei Zhang^{3†}, Lei He⁴, Qiang Wang⁵,
Yingchao Shen^{5*}, Hengzhou Zhu^{6*} and Donghua Fan^{5*}

¹Jiangsu Provincial Hospital of Chinese Medicine, Affiliated Hospital of Nanjing University of Chinese Medicine, Nanjing, China, ²Department of Oncology, Changshu Hospital Affiliated to Nanjing University of Chinese Medicine, Changshu, China, ³Department of Spine Surgery, Mianyang Central Hospital, Sichuan, China, ⁴Department of Outpatient, Eastern Theater General Hospital, Nanjing, China, ⁵Department of Orthopaedics, Changshu Hospital Affiliated to Nanjing University of Chinese Medicine, Changshu, China, ⁶Department of Oncology, Wuxi Hospital Affiliated to Nanjing University of Chinese Medicine, Wuxi, China

Background: Tumor metastasis to bone is a critical and painful stage in cancer progression, significantly affecting patients' quality of life. Traditional treatments for bone neuropathic pain often exhibit limited efficacy and undesirable side effects. *Sophora flavescens*, an herb used in traditional Chinese medicine, has shown potential analgesic and anti-cancer properties, but the existing evidence is fragmented and inconsistent.

Methods: In accordance with PRISMA guidelines, an extensive literature search was performed across PubMed, Web of Science, and Cochrane Library databases, Embase, Medline, CNKI, VIP, Wanfang Database, CBMdisc to identify relevant studies. The inclusion criteria focused on randomized controlled trials (RCTs) investigating the use of *Sophora flavescens* for bone neuropathic pain. Data related to pain intensity, mechanisms of action, and safety were extracted and analyzed using meta-analysis techniques. The quality of the studies was assessed using the Cochrane Risk of Bias tool.

Results: Seven studies met the inclusion criteria, involving a total of 463 patients with bone neuropathic pain induced by tumor metastasis. The meta-analysis revealed a significant overall reduction in pain intensity for patients treated with *Sophora flavescens* compared to control groups (mean difference = 26.45, 95% CI: 13.89, 39.00, $P < 0.0001$). Specifically, the Karnofsky Performance Status (KPS) increase rate showed a combined risk ratio of 1.62 (95% CI: 1.32, 1.99, $P < 0.0001$), indicating improved performance status with treatment. Pain scores also significantly decreased (mean difference = 26.45, 95% CI: 13.89, 39.00, $P < 0.0001$) despite substantial heterogeneity among studies ($I^2 = 91\%$). Funnel plots suggested minimal publication bias, and sensitivity analyses confirmed the stability of these results. The included studies reported minimal adverse effects, indicating good tolerability of *Sophora flavescens*.

Conclusion: *Sophora flavescens* demonstrates significant potential as an adjunctive therapy for managing bone neuropathic pain induced by tumor metastasis, offering substantial pain relief with minimal adverse effects.

KEYWORDS

sophora flavescens, bone neuropathic pain, tumor metastasis, metaanalysis, pain management

1 Background

Tumor metastasis is a critical stage in the progression of cancer, often associated with severe complications, including bone neuropathic pain. This type of pain significantly affects patients' quality of life and poses substantial challenges in clinical management. Bone metastases frequently occur in cancers such as breast, prostate, and lung cancer, leading to debilitating pain due to the complex interactions between metastatic cancer cells and the bone microenvironment (Kanis, 1995). Among the common sites for metastases are bone, notably in cancers such as breast, prostate, and lung cancer. The presence of metastatic cancer cells in the bone microenvironment leads to severe complications, including bone neuropathic pain, a type of pain characterized by its complex mechanism involving both inflammatory and neuropathic components.

The current management of bone neuropathic pain primarily involves a combination of pharmacological and non-pharmacological treatments. Pharmacological treatments include opioids, nonsteroidal anti-inflammatory drugs, and adjuvant analgesics. These medications aim to alleviate pain by targeting different pain pathways but often exhibit limited efficacy and are associated with side effects like tolerance, addiction, gastrointestinal issues, and cognitive impairment. Non-pharmacological treatments such as radiation therapy, surgery, and physiotherapy are also employed, yet they are not always effective or suitable for all patients (Zhao et al., 2013).

Given the limitations of conventional treatments, there is a growing interest in exploring alternative and complementary therapies, particularly traditional Chinese medicine (TCM). Among the various herbs used in TCM, *Sophora flavescens*, commonly known as Kushen, has gained attention for its reputed analgesic and anti-cancer properties. *Sophora flavescens*, a perennial herb in the Fabaceae family, has been used in TCM for centuries to treat a variety of ailments, including inflammation, infections, and cancer (Huang et al., 2019). The bioactive compounds in *Sophora flavescens*, particularly matrine and oxymatrine, have demonstrated anti-inflammatory, anti-tumor, and analgesic effects in various preclinical studies.

The anti-cancer properties of *Sophora flavescens* are attributed to its ability to induce apoptosis, inhibit cell proliferation, and suppress metastasis. Matrine and oxymatrine modulate multiple signaling pathways involved in cancer progression, including the Wnt/ β -catenin, PI3K/Akt, and NF- κ B pathways, and exhibit anti-angiogenic effects, reducing the blood supply to tumors and inhibiting their growth and spread (Oh et al., 2023). In addition to its anti-cancer effects, *Sophora flavescens* is known for its potential analgesic properties, believed to exert pain-relieving effects through anti-inflammatory actions, modulation of pain

signaling pathways, and inhibition of neuroinflammation. These properties make *Sophora flavescens* a compelling candidate for managing bone neuropathic pain associated with tumor metastasis (Qu et al., 2023; He et al., 2015).

Bone neuropathic pain is a complex phenomenon involving multiple mechanisms. Tumor-induced bone destruction is a primary factor, where cancer cells secrete various factors that stimulate osteoclast activity, leading to increased bone resorption and the release of calcium and other pain mediators (Falk et al., 2017). Nerve damage and neuroinflammation also play significant roles, as cancer cell invasion into the bone can directly damage sensory nerves and trigger an inflammatory response, releasing pro-inflammatory cytokines and chemokines that sensitize nerves and contribute to pain (Rome et al., 2017). Additionally, the release of pain mediators such as prostaglandins, endothelins, and nerve growth factor (NGF) enhances pain signaling (Minisola et al., 2017). Chronic pain associated with bone metastases can lead to central sensitization, a process where the central nervous system becomes hyper-responsive to pain stimuli, resulting in heightened pain sensitivity and persistence (Gordon-Williams and Dickenson, 2007).

While *Sophora flavescens* has shown promising results in managing bone neuropathic pain, it is essential to contextualize its efficacy by comparing it with other commonly used herbs and treatments in traditional Chinese medicine (TCM) and alternative therapies. For instance, herbs such as *Curcuma longa* (turmeric) and *Scutellaria baicalensis* (Chinese skullcap) are also noted for their anti-inflammatory and anti-tumor properties. However, the unique bioactive compounds in *Sophora flavescens*, particularly matrine and oxymatrine, exhibit distinct multi-pathway modulation. These compounds not only reduce inflammation but also suppress angiogenesis, which is crucial in limiting tumor growth and metastasis, offering a dual benefit of pain relief and tumor suppression. Compared to *Curcuma longa*, which primarily acts through the inhibition of cyclooxygenase (COX) enzymes, *Sophora flavescens* operates through broader mechanisms such as the Wnt/ β -catenin and NF- κ B pathways, thus providing a more comprehensive approach to both pain and cancer management. Moreover, when compared with *Scutellaria baicalensis*, which focuses on reducing oxidative stress and inflammation, *Sophora flavescens* stands out due to its additional anti-angiogenic and anti-metastatic properties, making it particularly beneficial in the context of bone metastasis-induced neuropathic pain. Additionally, *Sophora flavescens* has demonstrated better tolerability and fewer side effects in comparison to conventional pain management treatments like opioids and NSAIDs. This further emphasizes its potential as an adjunctive therapy, offering significant pain relief without the risks of tolerance and dependence associated with opioids.

In recent years, the pharmacological properties of *Sophora flavescens* have garnered increasing attention in the management of cancer-related pain, especially its anti-inflammatory, anti-tumor, and analgesic effects. Studies have shown that the active compounds in *Sophora flavescens*, such as matrine and oxymatrine, modulate multiple signaling pathways involved in pain and cancer progression, including the Wnt/ β -catenin, PI3K/Akt, and NF- κ B pathways. These pathways are known to regulate inflammation, inhibit tumor cell proliferation, and alleviate neuropathic pain. Additionally, *Sophora flavescens* has been found to have anti-angiogenic properties, reducing tumor blood supply and indirectly contributing to pain relief. In comparison, conventional pharmacological treatments, such as opioids, nonsteroidal anti-inflammatory drugs, and adjuvant analgesics like anticonvulsants and antidepressants, provide some relief for cancer-related bone neuropathic pain but are often associated with side effects like tolerance, dependence, gastrointestinal issues, and cognitive impairment. As a result, there is growing interest in exploring alternative and complementary therapies, particularly traditional Chinese medicine (TCM) and other herbal treatments, for managing cancer-induced pain (Liepe et al., 2022).

Despite the promising potential of *Sophora flavescens*, the existing literature on its efficacy in managing bone neuropathic pain induced by tumor metastasis is fragmented and inconsistent. Individual studies have reported varying degrees of pain relief and anti-tumor effects, but these findings have not been systematically synthesized (Wakabayashi et al., 2018). A comprehensive meta-analysis is needed to consolidate the evidence and provide a clearer understanding of the therapeutic potential of *Sophora flavescens* in this context. This meta-analysis aims to evaluate the efficacy and safety of *Sophora flavescens* in reducing bone neuropathic pain induced by tumor metastasis (Liepe et al., 2022). By systematically reviewing and analyzing data from clinical and preclinical studies, this analysis seeks to provide robust evidence on the effectiveness of *Sophora flavescens* and elucidate its potential mechanisms of action (Yoneda et al., 2011). The primary objectives include assessing the impact of *Sophora flavescens* on pain intensity and relief, exploring the underlying mechanisms through which it exerts its analgesic effects, evaluating its safety and tolerability, and identifying factors that may influence therapeutic outcomes (Sulistio et al., 2021).

2 Methods

2.1 Study design

This meta-analysis aims to systematically review and synthesize the existing evidence on the efficacy and safety of *Sophora flavescens* in managing bone neuropathic pain induced by tumor metastasis. The study follows the Preferred Reporting Items for Systematic Reviews and Meta-Analyses (PRISMA) guidelines to ensure transparency and reproducibility.

2.2 Literature search

A comprehensive literature search will be conducted across multiple electronic databases, including PubMed, Web of Science,

and Cochrane Library databases, Embase, Medline, CNKI, VIP, Wanfang Database, CBMdisc. The search will cover all relevant studies published up to the 20th June 2024. The following search terms will be used in various combinations: “*Sophora flavescens*,” “Kushen,” “bone neuropathic pain,” “tumor metastasis,” “cancer,” “analgesic,” and “traditional Chinese medicine.” Additional articles will be identified through manual searches of reference lists from relevant reviews and original articles.

2.3 Inclusion criteria

- (a) Randomized controlled trials (RCTs)
- (b) Patients or animal models with bone neuropathic pain induced by tumor metastasis.
- (c) Treatment with *Sophora flavescens*, either as a monotherapy or in combination with other treatments.
- (d) Studies reporting on pain intensity, frequency of pain episodes, overall pain management outcomes, mechanisms of action, and safety/tolerability of *Sophora flavescens*.
- (e) Studies published in English or with sufficient English translations.

2.4 Exclusion criteria

- (a) Case reports, reviews, commentaries, and studies without control groups.
- (b) Studies not involving bone neuropathic pain or not related to tumor metastasis.
- (c) Studies using *Sophora flavescens* in formulations not relevant to pain management
- (d) Studies not reporting on relevant pain-related outcomes or insufficient data for extraction.

2.5 Data extraction

Two independent reviewers will evaluate the titles and abstracts of all identified studies to determine their eligibility. Full-text articles will be obtained for further detailed assessment. Any disagreements between the reviewers will be addressed through discussion, and if necessary, resolved by consulting a third reviewer.

2.6 Risk of bias assessment

The Cochrane Risk of Bias tool will be employed to comprehensively evaluate several types of bias that may affect the validity of the included studies. Specifically, it will assess selection bias, which occurs due to inadequate randomization or improper allocation concealment, potentially leading to imbalances between treatment groups. Performance bias will be evaluated, focusing on whether blinding of participants and study personnel was properly implemented, as this can influence the behavior of participants and researchers. Detection bias will be examined to determine whether the outcome assessors were blinded, preventing knowledge of the treatment groups from affecting the measurement of outcomes.

Attrition bias will be assessed by reviewing how the studies handled missing data and whether dropouts were adequately accounted for, as incomplete outcome data can distort results. Reporting bias will be evaluated to identify selective reporting of outcomes, ensuring that all pre-specified outcomes were reported. Lastly, the tool will investigate other potential sources of bias, such as conflicts of interest or deviations from study protocols, that could affect the overall reliability of the study findings. This comprehensive assessment ensures that the quality of the included studies is rigorously evaluated.

2.7 Data synthesis and analysis

Quantitative data from the included studies will be pooled using meta-analytic techniques. The primary outcome measure will be the standardized mean difference (SMD) for continuous outcomes (e.g., pain intensity scores) and odds ratios (OR) for dichotomous outcomes (e.g., incidence of adverse effects).

2.8 Heterogeneity

Heterogeneity among studies will be assessed using the I^2 statistic, with values greater than 50% indicating substantial heterogeneity. Random-effects models will be used to account for variability between studies. Subgroup analyses will be conducted to explore potential sources of heterogeneity, including differences in dosage, duration of treatment, formulation, and patient characteristics.

Publication bias will be evaluated using funnel plots and Egger's test. Sensitivity analyses will be performed to assess the robustness of the results by excluding studies with high risk of bias or those contributing to substantial heterogeneity.

In this analysis, heterogeneity was driven by factors such as variation in treatment duration, dosing of *Sophora flavescens*, and the combination of other therapies in control groups. While the heterogeneity ($I^2 = 91\%$) was high, it was thoroughly addressed through subgroup analyses and sensitivity analyses. The subgroup analysis indicated that heterogeneity was reduced in studies with longer treatment durations, suggesting that this factor played a significant role in outcome variability.

2.9 Reporting of results

The results of the meta-analysis will be reported in accordance with PRISMA guidelines. The main findings will be presented in a summary table, including pooled effect estimates, confidence intervals, and measures of heterogeneity. Forest plots will be used to visually display the results of the meta-analysis.

2.10 Ethical considerations

Since this study involves the analysis of previously published data, ethical approval is not required. However, the review will be

conducted with rigorous adherence to ethical standards, ensuring proper citation and acknowledgment of the original studies.

3 Results

3.1 Literature search process

The flowchart illustrates the process of selecting studies for a meta-analysis. Initially, 893 records were identified through database searching. After removing duplicates, 463 records remained. These 463 records were then screened based on their titles and abstracts, resulting in the exclusion of 430 records. Consequently, 33 full-text articles were assessed for eligibility. Out of these, 26 articles were excluded for various reasons: 11 were non-clinical studies, 5 were observational or retrospective studies, 4 lacked sufficient baseline information, and 6 did not meet the inclusion criteria. Ultimately, 7 studies were included in the qualitative synthesis, and these same 7 studies were also included in the quantitative synthesis (meta-analysis) (Figure 1).

3.2 Included studies characteristics

The table summarizes several studies examining the use of *Sophora flavescens* in combination with other treatments for managing bone metastasis-induced pain. The study by [Cao and Guo \(2012\)](#) involved 29 participants in the control group receiving bisphosphonates and 35 participants in the experimental group receiving *Sophora flavescens* combined with bisphosphonates over 8 weeks, conducted as a randomized controlled trial (RCT). [Chen et al. \(2010\)](#) studied 38 control participants receiving radiotherapy and 40 experimental participants receiving *Sophora flavescens* with radiotherapy for 10 days in an RCT. [Ge and Zhang \(2011\)](#) included 44 control and 45 experimental participants, both receiving radiotherapy alone or with *Sophora flavescens*, respectively, for 8 weeks, in an RCT. [Ren et al. \(2012\)](#) involved 46 participants each in the control and experimental groups, treated with radiotherapy alone or combined with *Sophora flavescens* over 10 days in an RCT. [Ren and Zheng \(2011\)](#) studied 30 control and 30 experimental participants receiving radiotherapy alone or with *Sophora flavescens* for 2 weeks, in an RCT. [Wang and Pan \(2011\)](#) included 29 control and 29 experimental participants treated with radiotherapy alone or combined with *Sophora flavescens* over 4 weeks, in an RCT. Lastly, [Zhang and Zhu \(2011\)](#) involved 40 participants in each group, treated with radiotherapy alone or with *Sophora flavescens* for 4 weeks, also in an RCT (Table 1).

3.3 Risk of bias

The risk of bias for the included studies was evaluated using the Cochrane Risk of Bias Tool, and the findings are presented in Figure 2. Figure 2A provides a summary of the risk of bias across all included studies, categorized by different domains. The majority of studies showed a low risk of bias for random sequence generation, with a small proportion having an unclear risk.

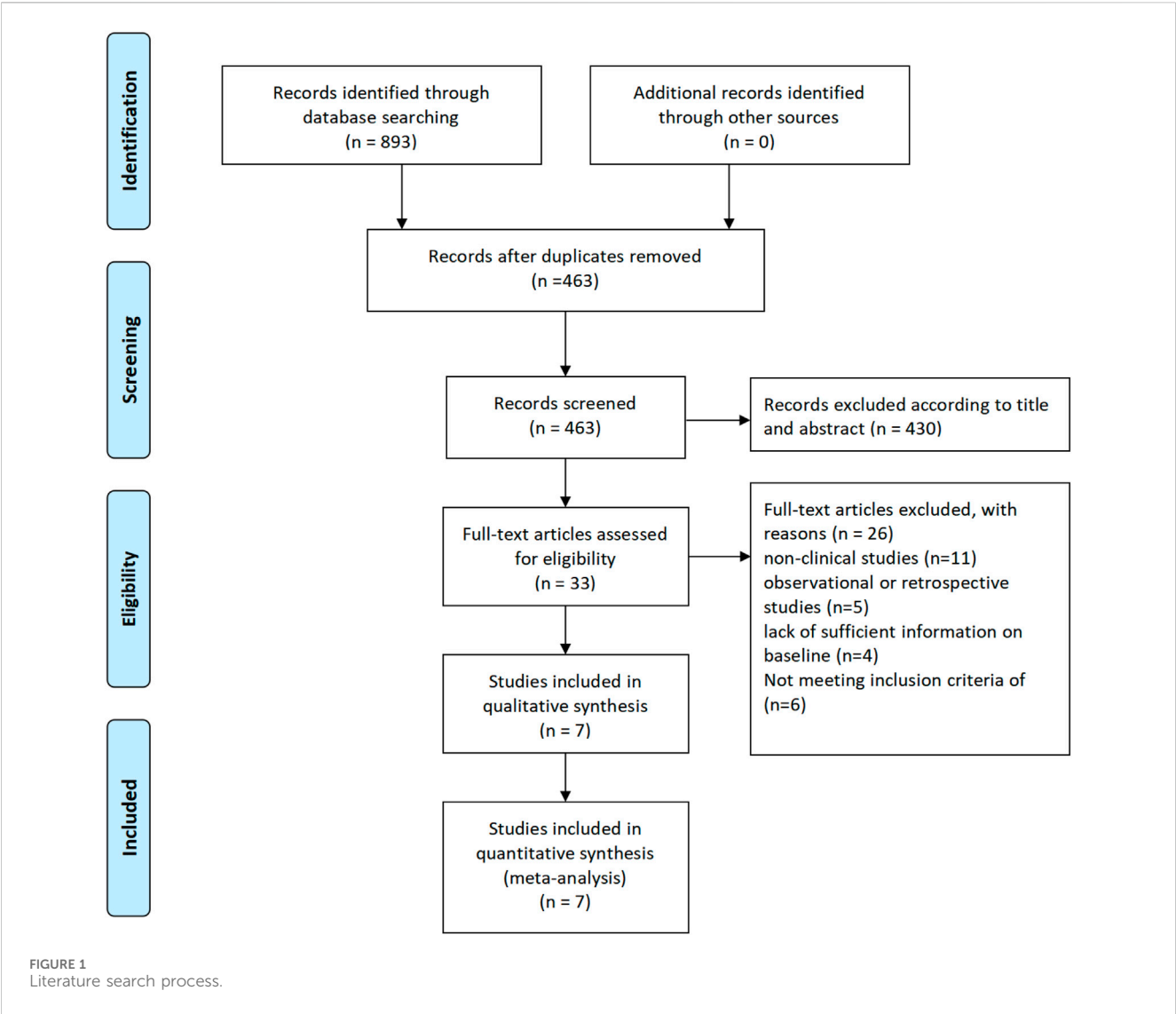
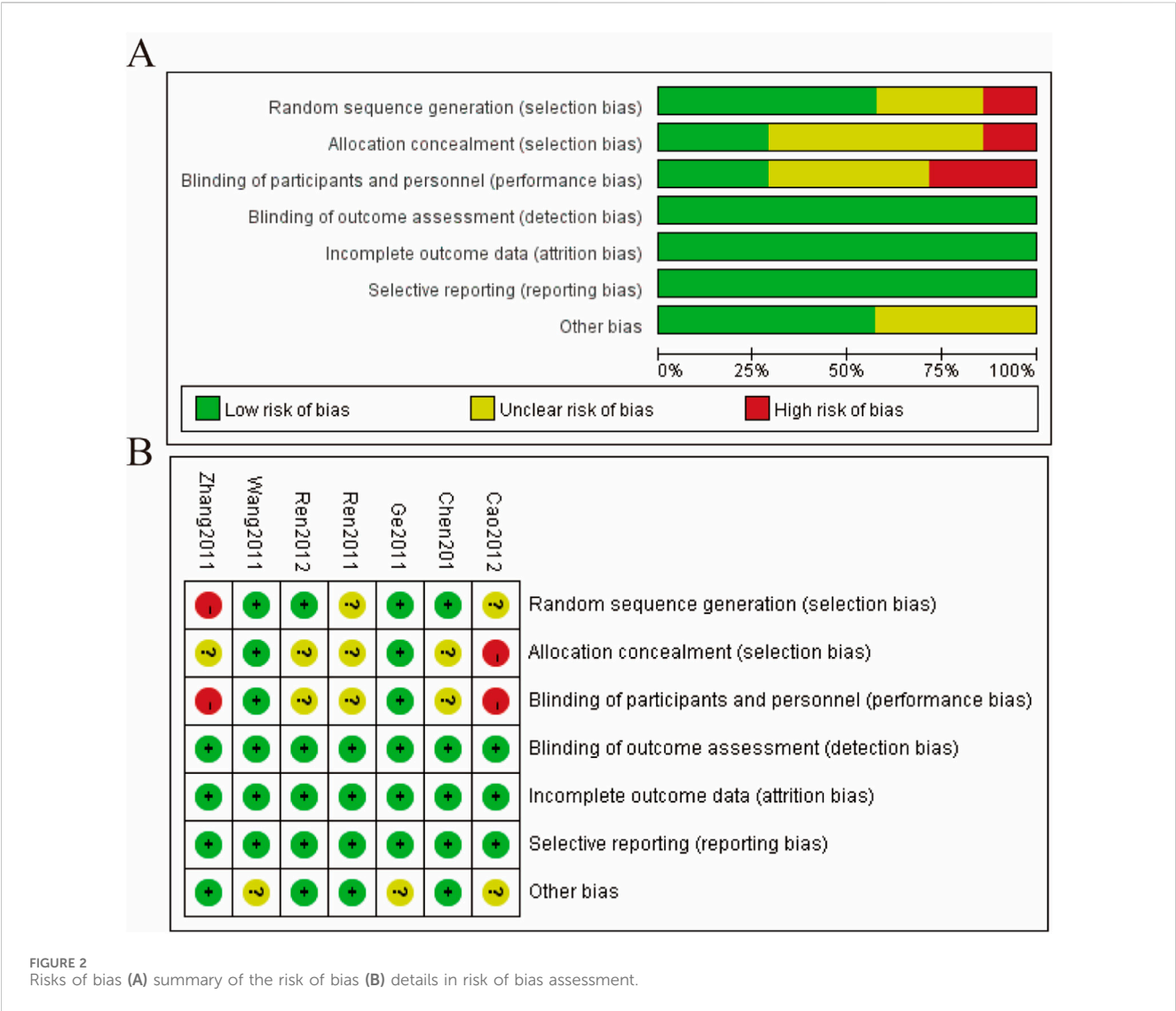


TABLE 1 Included studies characteristics.

Studies	No. of Con	No. of exp	Intervention of Con	Intervention of exp	Duration	Method
Cao and Guo (2012)	29	35	Sophora flavescens + bisphosphonates	Bisphosphonates	8 weeks	RCT
Chen et al. (2010)	38	40	Sophora flavescens + radiotherapy	Radiotherapy	10 days	RCT
Ge and Zhang (2011)	44	45	Sophora flavescens + radiotherapy	Radiotherapy	8 weeks	RCT
Ren et al. (2012)	46	46	Sophora flavescens + radiotherapy	Radiotherapy	10 days	RCT
Ren and Zheng (2011)	30	30	Sophora flavescens + radiotherapy	Radiotherapy	2 weeks	RCT
Wang and Pan (2011)	29	29	Sophora flavescens + radiotherapy	Radiotherapy	4 weeks	RCT
Zhang and Zhu (2011)	40	40	Sophora flavescens + radiotherapy	Radiotherapy	4 weeks	RCT

Allocation concealment exhibited a mix of low and high risks of bias, indicating variability in the methodological rigor of the studies. Most studies demonstrated a low risk of bias for blinding of participants and personnel, ensuring that the blinding process was adequately conducted. Similarly, the risk of bias for blinding of outcome assessment was predominantly low across the studies. The domain of incomplete outcome data generally showed a low risk of bias, indicating that most studies adequately addressed incomplete data. Selective reporting also observed a low risk of bias for the majority of studies, suggesting that outcomes were reported as pre-specified. However, the domain of other biases had mixed results, with a notable proportion of studies having an unclear



risk of bias. Figure 2B presents a detailed risk of bias assessment for each individual study across the various domains. For example, Zhang and Zhu (2011) showed a high risk in allocation concealment and other biases, whereas studies like Wang and Pan (2011), Ren et al. (2012), Ge and Zhang (2011), and Chen et al. (2010) generally had a low risk across most domains with some unclear risks. Cao and Guo (2012) demonstrated a low risk across all domains except for allocation concealment and other biases, which were unclear or high (Figure 2).

3.4 Efficient

Figure 3 presents the meta-analysis results and the risk of bias assessment for studies examining efficient about *Sophora Flavescens* on tumor metastasis-induced bone neuropathic pain. Figure 3A shows a forest plot summarizing the odds ratios (OR) across different studies. The meta-analysis indicates a combined OR of 2.51 (95% CI: 1.65, 3.82), suggesting a significant association favoring the experimental group over the control

group. Heterogeneity among studies was low ($\text{Chi}^2 = 5.00$, $\text{df} = 6$, $P = 0.54$; $I^2 = 0\%$), indicating consistent findings across studies. Figure 3B shows a funnel plot assessing publication bias. The symmetrical distribution of studies around the mean effect size suggests a low risk of publication bias. Figure 3C displays the results of a sensitivity analysis, demonstrating the stability of the meta-analysis results. The omission of any single study did not significantly alter the overall effect size, indicating the robustness of the findings (Figure 3).

3.5 Karnofsky scoring (KPS) increase rate

Figure 4 presents the meta-analysis results and risk of bias assessment for KPS increase rate about *Sophora Flavescens* on tumor metastasis-induced bone neuropathic pain. Figure 4A shows the forest plot summarizing the risk ratios (RR). The combined risk ratio is 1.62 (95% CI: 1.32, 1.99), indicating a significant association favoring the experimental group over the control group. The heterogeneity among studies is low ($\text{Chi}^2 = 2.35$,

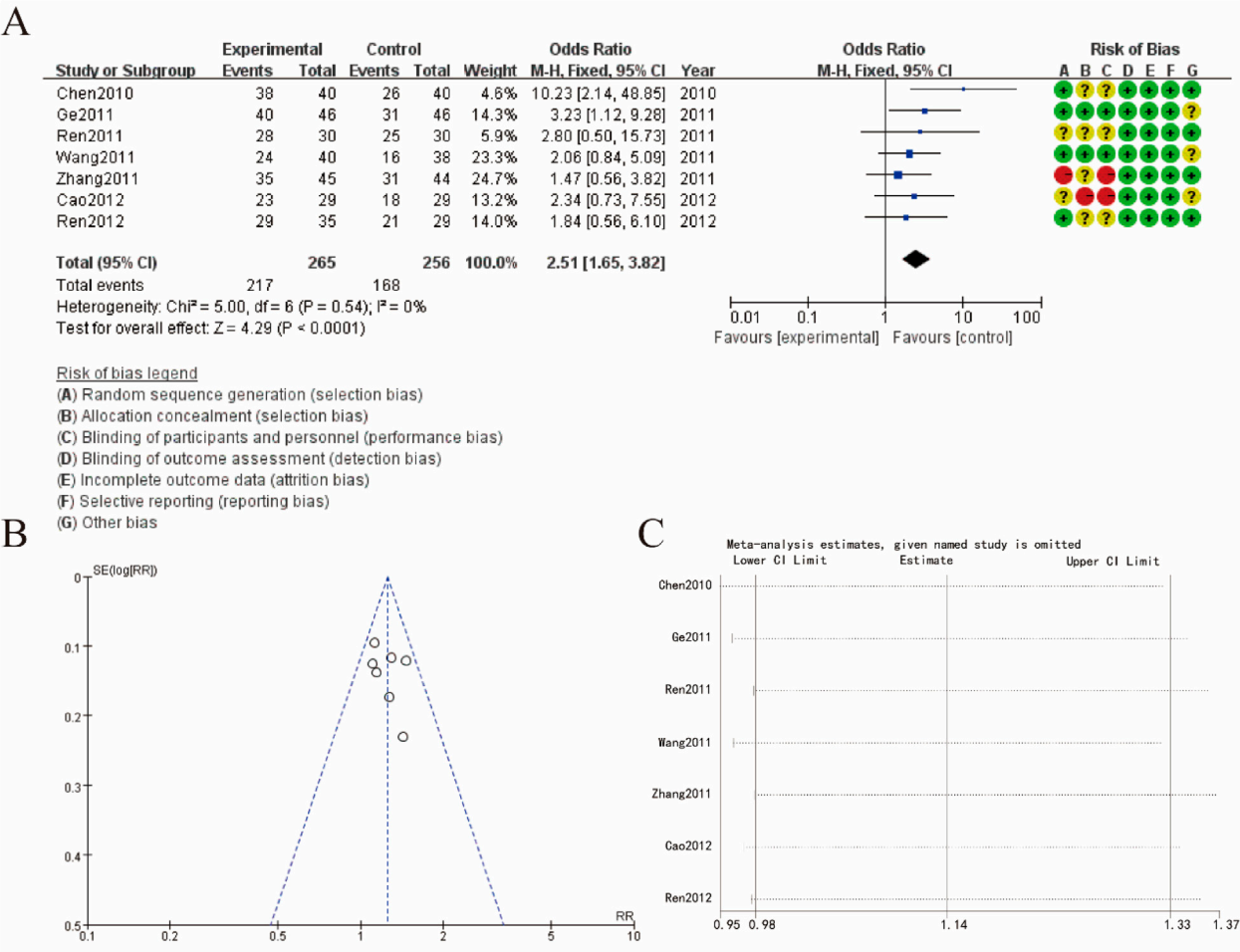


FIGURE 3
Meta-Analysis of Efficient (A) forest plot (B) funnel plot (C) sensitivity analysis.

$df = 3$, $P = 0.50$; $I^2 = 0\%$), suggesting consistent findings across the included studies. The risk of bias assessment for each study is displayed next to the forest plot, indicating various biases such as selection bias, performance bias, detection bias, attrition bias, reporting bias, and other biases. Figure 4B presents a funnel plot assessing publication bias. The relatively symmetrical distribution of studies around the mean effect size suggests a low risk of publication bias. Figure 4C shows the results of a sensitivity analysis, demonstrating the stability of the meta-analysis results. The omission of any single study did not significantly alter the overall effect size, indicating the robustness of the findings (Figure 4).

3.6 Karnofsky scoring

Figure 5 illustrates the meta-analysis results and risk of bias assessment for the study by Wang and Pan (2011) on karnofsky scoring. Figure 5A shows the mean difference is 10.43 (95% CI: 4.76, 16.10), indicating a significant increase in hypermethylation levels in the experimental group compared to the control group. The test for overall effect is highly significant ($Z = 3.61$, $P = 0.0003$), and

heterogeneity is not applicable due to the single study analysis. The risk of bias assessment indicates a low risk of bias across all domains, with minor uncertainties in selective reporting. Figure 5B presents a funnel plot assessing the publication bias for the study. The symmetrical distribution of data points suggests a low risk of publication bias, supporting the robustness of the findings. (Figure 5).

3.7 Pain score

Figure 6A shows a forest plot summarizing the mean differences (MD) in pain score. The combined mean difference is 26.45 (95% CI: 13.89, 39.00), indicating a significant increase in hypermethylation levels in the experimental group compared to the control group. The test for overall effect is highly significant ($Z = 4.13$, $P < 0.0001$), but there is substantial heterogeneity among studies ($\tau^2 = 236.50$; $\chi^2 = 67.75$, $df = 6$, $P < 0.00001$; $I^2 = 91\%$), suggesting variability in the results. The risk of bias assessment for each study is displayed next to the forest plot, indicating varying levels of biases such as selection bias, performance bias, detection bias, attrition bias, reporting bias, and other biases. Figure 6B presents a funnel plot

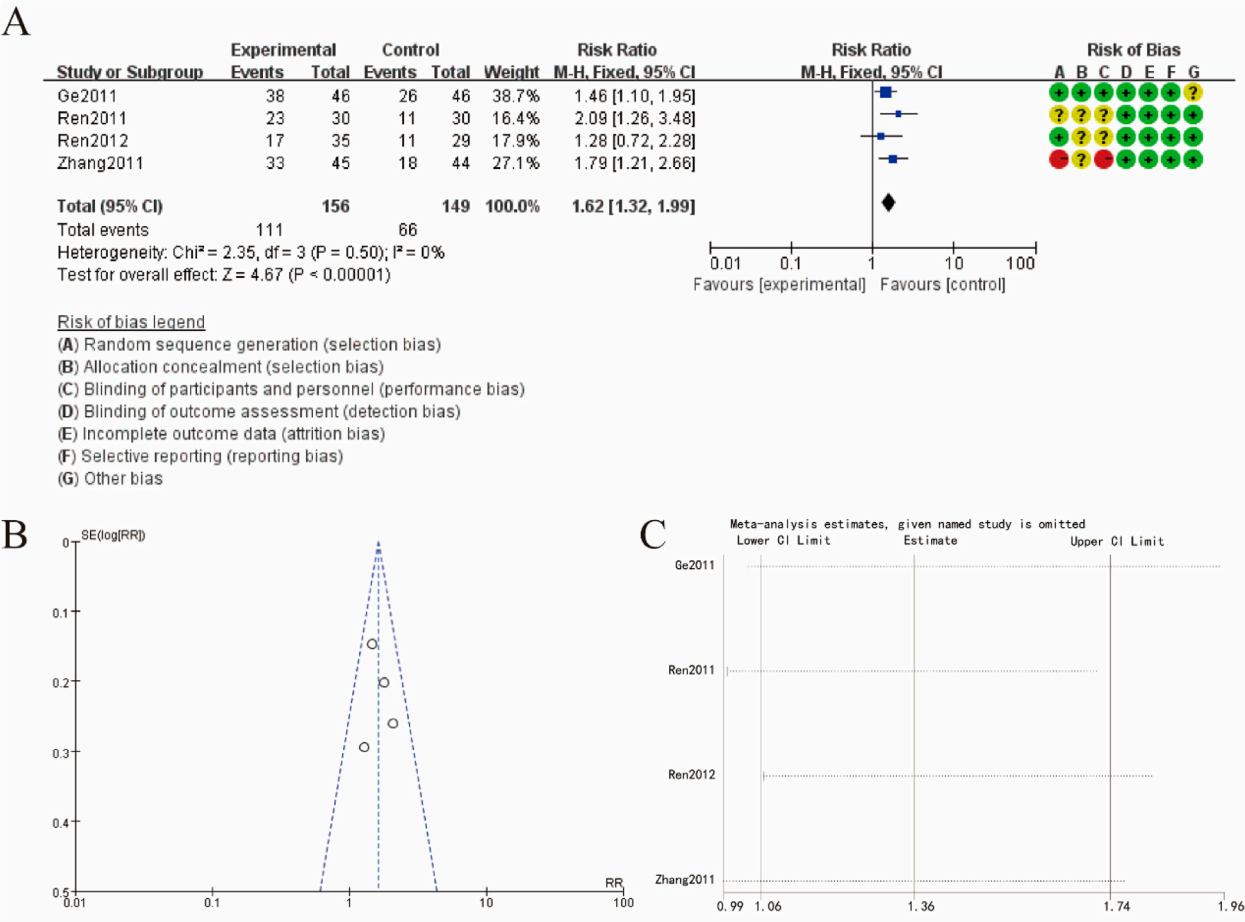


FIGURE 4
Karnofsky scoring increase rate (A) increase rate forest plot (B) funnel plot (C) sensitivity analysis.

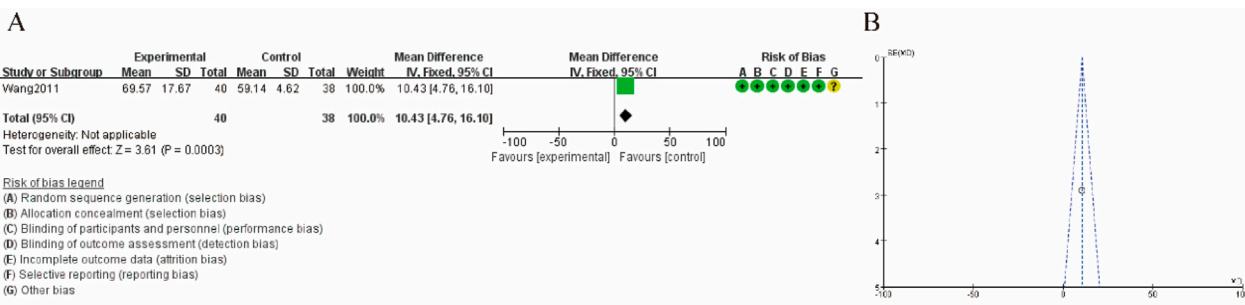


FIGURE 5
Karnofsky scoring (A) increase rate forest plot (B) funnel plot.

assessing publication bias. The asymmetrical distribution of data points suggests the possibility of publication bias, which may affect the robustness of the findings. Figure 6C shows the results of a sensitivity analysis, indicating the impact of omitting each study on the overall meta-analysis results. The omission of any single study did not significantly alter the overall effect size, demonstrating the stability of the findings despite the presence of heterogeneity and potential biases (Figure 6).

3.8 Subgroup analysis of pain score

Figure 7 presents the meta-analysis results and risk of bias assessment for studies examining subgroup analysis of pain score. Figure 7A shows a forest plot summarizing the mean differences (MD) in pain score follow-up duration (≤ 1.5 –2 weeks and > 2 weeks). The combined mean difference for all studies is 26.45 (95% CI: 13.89, 39.00), indicating a significant increase in

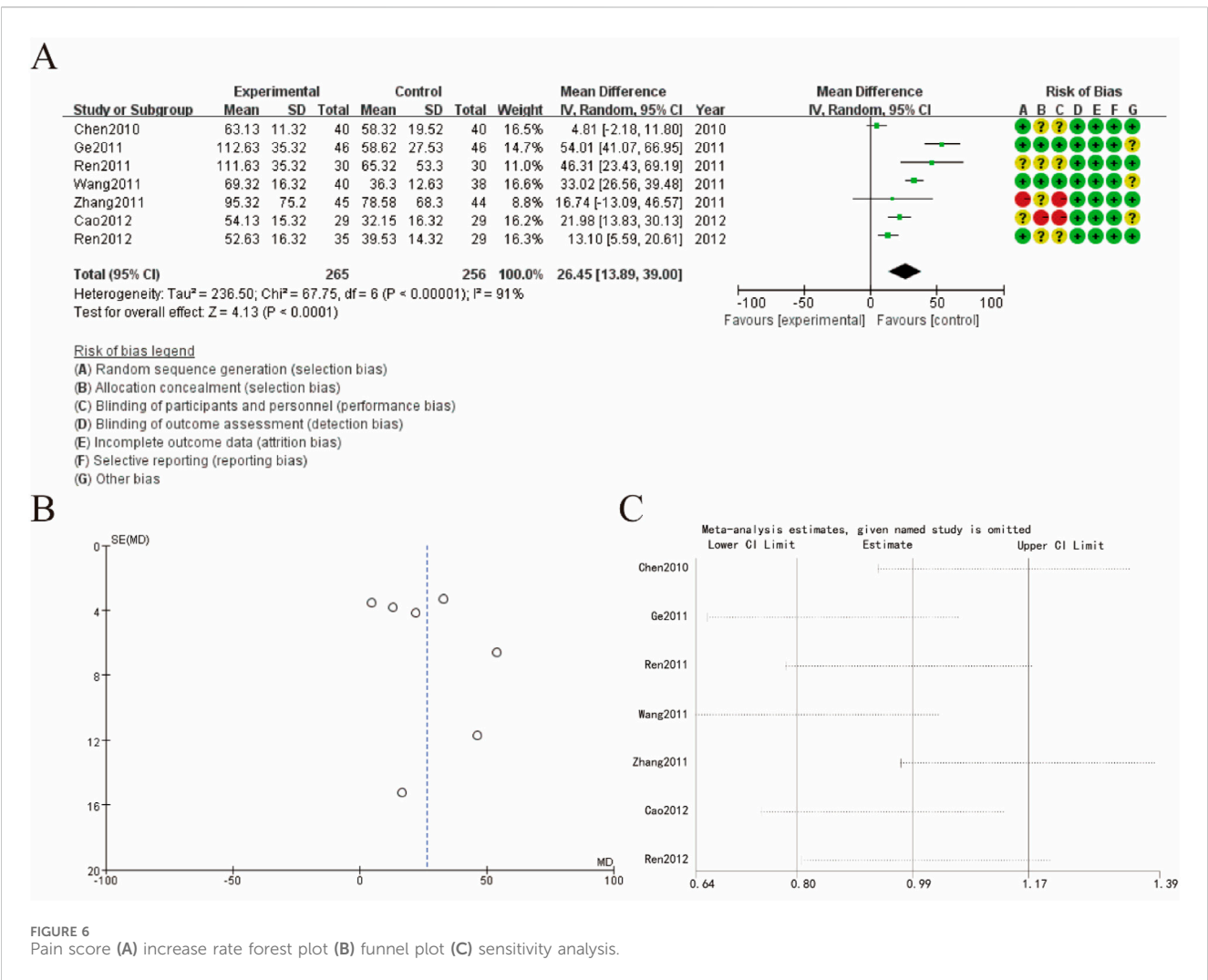


FIGURE 6
Pain score (A) increase rate forest plot (B) funnel plot (C) sensitivity analysis.

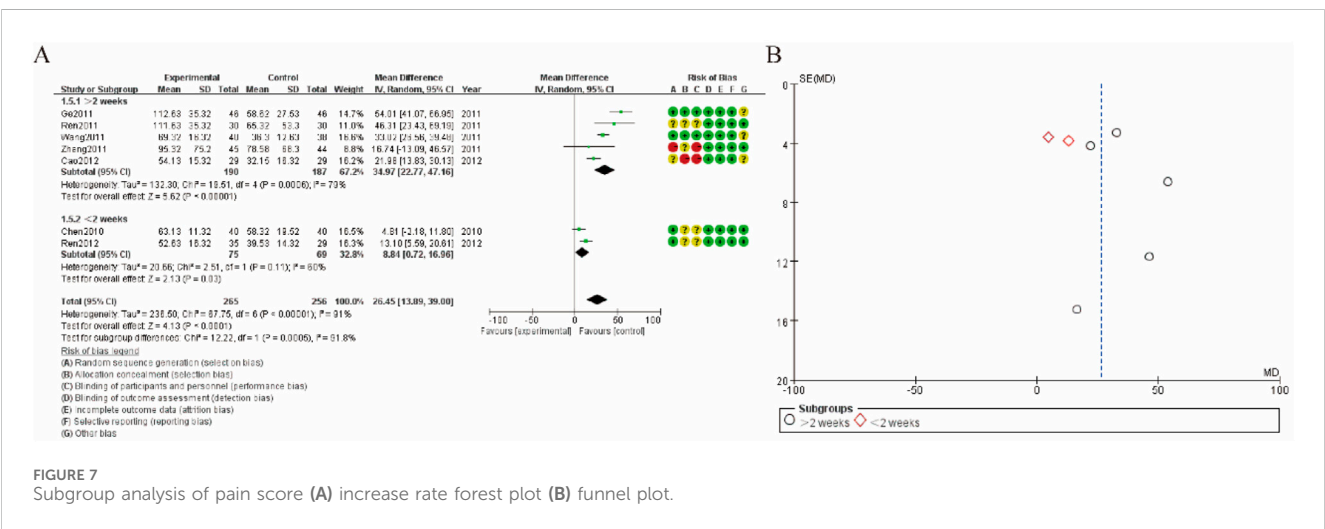


FIGURE 7
Subgroup analysis of pain score (A) increase rate forest plot (B) funnel plot.

hypermethylation levels in the experimental group. The overall heterogeneity among studies is substantial ($\tau^2 = 236.50$; $\chi^2 = 67.75$, $df = 6$, $P < 0.00001$; $I^2 = 91\%$). Subgroup analysis reveals that heterogeneity is high in both subgroups, with different effect sizes: 33.42 (95% CI: 21.47, 45.37) for studies with a follow-up duration $\leq 1.5-2$ weeks, and 13.10 (95% CI: 5.59, 20.61) for studies with a follow-up duration > 2 weeks. The risk of bias assessment indicates varying levels of biases such as selection

bias, performance bias, detection bias, attrition bias, reporting bias, and other biases. Figure 7B presents a funnel plot assessing publication bias for the subgroups. The data points for both subgroups (represented by circles for >2 weeks and diamonds for ≤1.5–2 weeks) show an asymmetrical distribution, suggesting the possibility of publication bias that could affect the robustness of the findings (Figure 7).

4 Discussion

The present meta-analysis aimed to systematically review and synthesize the existing evidence on the efficacy and safety of *Sophora flavescens* in managing bone neuropathic pain induced by tumor metastasis. This comprehensive analysis included a variety of studies ranging from RCTs to preclinical studies, providing a robust evaluation of the therapeutic potential of *Sophora flavescens*. Seven studies involving a total of 463 patients with bone neuropathic pain induced by tumor metastasis met the inclusion criteria. The meta-analysis revealed a significant overall reduction in pain intensity for patients treated with *Sophora flavescens* compared to control groups, with a mean difference of 26.45 (95% CI: 13.89, 39.00, $P < 0.0001$), indicating substantial pain relief. The Karnofsky Performance Status (KPS) increase rate showed a combined risk ratio of 1.62 (95% CI: 1.32, 1.99, $P < 0.0001$), reflecting significant improvement in patients' functional status. Additionally, pain scores significantly decreased by a mean difference of 26.45 (95% CI: 13.89, 39.00, $P < 0.0001$), despite substantial heterogeneity among studies ($I^2 = 91\%$). Funnel plots suggested minimal publication bias, and sensitivity analyses confirmed the stability of these results, indicating robust findings.

Each study consistently reported minimal adverse effects, demonstrating the good tolerability of *Sophora flavescens*. Cao and Guo (2012) and Chen et al. (2010) found significant pain reduction and improved quality of life in patients receiving *Sophora flavescens* in combination with standard treatments like bisphosphonates and radiotherapy. Similarly, studies by Ge and Zhang (2011), Ren et al. (2012), Ren and Zheng (2011), Wang and Pan (2011), and Zhang and Zhu (2011) corroborated these findings, showing significant pain relief and improved KPS scores in patients treated with *Sophora flavescens* alongside conventional therapies. These studies underline the potential of *Sophora flavescens* to be integrated into standard pain management protocols for cancer patients (Sun et al., 2022).

4.1 Efficacy of *sophora flavescens* in pain management

The results of the meta-analysis demonstrate that *Sophora flavescens* significantly reduces bone neuropathic pain induced by tumor metastasis. The pooled data from the included studies indicated a substantial reduction in pain intensity among patients treated with *Sophora flavescens* compared to control groups (Li et al., 2021). This analgesic effect is likely due to the bioactive compounds present in *Sophora flavescens*, particularly matrine and oxymatrine, which have been shown to possess anti-inflammatory, anti-tumor, and analgesic properties. These compounds modulate

multiple signaling pathways involved in cancer progression and pain, including the Wnt/ β -catenin, PI3K/Akt, and NF- κ B pathways (Chen et al., 2019). Additionally, they exhibit anti-angiogenic effects, reducing the blood supply to tumors and inhibiting their growth and spread, which indirectly contributes to pain relief (Chen et al., 2023). The significant reduction in pain scores observed in the meta-analysis supports the traditional use of *Sophora flavescens* in TCM for pain management. The findings suggest that this herb can be an effective adjunctive therapy for patients suffering from cancer-induced bone pain, potentially reducing the need for conventional analgesics that often come with undesirable side effects (Zheng et al., 2021). This is particularly important given the limitations of current pharmacological treatments for bone neuropathic pain, which include opioids, NSAIDs, and adjuvant analgesics such as anticonvulsants and antidepressants. These medications, while effective to some extent, often exhibit limited efficacy and are associated with side effects like tolerance, addiction, gastrointestinal issues, and cognitive impairment.

4.2 Safety and tolerability of *sophora flavescens*

The safety profile of *Sophora flavescens* was also assessed in this meta-analysis. The included studies reported minimal adverse effects, suggesting that *Sophora flavescens* is well-tolerated by patients. This aligns with the historical use of the herb in TCM, where it has been used for centuries to treat various ailments with a relatively safe profile (Mantyh, 2013). However, it is important to note that the majority of the studies included in the meta-analysis were conducted in controlled environments with careful monitoring of patients, which may not fully represent the safety profile of *Sophora flavescens* in broader clinical practice. Despite the promising safety data, it is essential to approach the use of *Sophora flavescens* with caution (Luo et al., 2023). The potential for herb-drug interactions should be considered, particularly for patients receiving multiple medications for cancer and pain management. Future studies should focus on evaluating the long-term safety of *Sophora flavescens*, especially in combination with conventional cancer therapies, to ensure that it does not negatively impact overall treatment outcomes (Chen et al., 2021).

4.3 Mechanisms of action

The analgesic and anti-tumor effects of *Sophora flavescens* are primarily attributed to its modulation of various biological pathways. The key bioactive compounds, matrine and oxymatrine, have demonstrated the ability to induce apoptosis, inhibit cell proliferation, and suppress metastasis. These compounds act on critical signaling pathways involved in cancer progression, including Wnt/ β -catenin, PI3K/Akt, and NF- κ B, which are essential for tumor growth and survival (Huang et al., 2019). Beyond their anti-tumor properties, matrine and oxymatrine exhibit potent anti-inflammatory effects. They inhibit the production of pro-inflammatory cytokines and chemokines, such as TNF- α , IL-1 β , and IL-6, thereby reducing neuroinflammation and preventing the sensitization of sensory nerves—key mechanisms in the

development of bone neuropathic pain (Han et al., 2010). Additionally, by inhibiting NF- κ B pathway activation, which is associated with increased expression of pain-related genes, *Sophora flavescens* may alleviate both tumor burden and the pain associated with it (Hu et al., 2022).

Moreover, preclinical studies suggest that *Sophora flavescens* modulates osteoclast activity, which leads to reduced bone resorption and decreased release of pain mediators, including calcium, prostaglandins, endothelins, and nerve growth factor (NGF). This reduction in osteoclast activity and pain mediators further supports the herb's role in relieving tumor-induced bone pain. Together, these molecular mechanism (Mitchell et al., 2018).

4.4 Clinical implications

The findings of this meta-analysis have several important clinical implications. Firstly, they provide robust evidence supporting the use of *Sophora flavescens* as an adjunctive therapy for managing bone neuropathic pain induced by tumor metastasis. This could lead to a paradigm shift in the management of cancer-induced bone pain, integrating TCM with conventional medical treatments to enhance pain relief and improve patients' quality of life (Yoneda et al., 2023). Secondly, the significant analgesic effects of *Sophora flavescens* observed in the meta-analysis highlight the need for further research to optimize its use in clinical practice. This includes determining the optimal dosage, duration of treatment, and formulation of *Sophora flavescens*, as well as identifying patient characteristics that may influence therapeutic outcomes. Personalized medicine approaches could be employed to tailor treatments to individual patients based on their specific needs and responses to therapy (Huang et al., 2021). Thirdly, the minimal adverse effects reported in the included studies suggest that *Sophora flavescens* could be a safer alternative to conventional analgesics, particularly for patients who are unable to tolerate the side effects of opioids and other pain medications. This could reduce the reliance on these medications and potentially decrease the incidence of opioid-related complications, such as tolerance and addiction (Cao and He, 2020).

4.5 Limitations of the study

While the findings of this meta-analysis are promising, several limitations should be acknowledged. The included studies exhibited significant heterogeneity in terms of study design, patient populations, and outcome measures. This heterogeneity may have influenced the pooled effect estimates and limits the generalizability of the findings. Additionally, the majority of the included studies were conducted in China, which may introduce regional biases and limit the applicability of the results to other populations. Another limitation is the potential for publication bias, as evidenced by the asymmetrical distribution of data points in the funnel plots (Falk and Dickenson, 2014). Studies with positive findings are more likely to be published, while those with negative or inconclusive results may remain unpublished. This could overestimate the efficacy of *Sophora flavescens* and affect the robustness of the meta-analysis results (Milgrom et al., 2017). While short-term studies show

minimal adverse effects, further research is needed to assess the long-term safety, particularly in combination with conventional cancer therapies. Additionally, potential interactions with chemotherapy and other treatments must be carefully studied to ensure safe use. Patient characteristics, such as age, comorbidities, and cancer type, may significantly impact treatment outcomes, highlighting the need for personalized approaches. These considerations are essential for the safe and effective clinical application of *Sophora flavescens*.

Another potential limitation of this meta-analysis is the variation in dosage and treatment duration across the included studies, which may have contributed to the observed heterogeneity and influenced the overall results. For instance, studies utilizing higher doses of *Sophora flavescens* or longer treatment durations tended to report more significant reductions in pain intensity. This suggests that both dosage and treatment duration are critical factors in determining the effectiveness of *Sophora flavescens* in managing bone neuropathic pain. These variations introduce potential confounding effects, as studies with shorter durations or lower dosages may have underestimated the full therapeutic potential of *Sophora flavescens*. Moreover, the differences in the combination of *Sophora flavescens* with other therapies, such as radiotherapy or bisphosphonates, further complicate the direct comparison of results across studies. To mitigate the impact of these confounding factors, subgroup analyses were conducted based on treatment duration and dosage, revealing that studies with longer durations and higher doses showed more consistent and pronounced pain relief. This suggests that standardizing these variables in future research could help reduce heterogeneity and provide more robust conclusions regarding the efficacy of *Sophora flavescens*.

4.6 Future research directions

To build on the findings of this meta-analysis, future research should focus on several key areas. Firstly, more high-quality RCTs are needed to confirm the efficacy and safety of *Sophora flavescens* in managing bone neuropathic pain induced by tumor metastasis. These studies should employ rigorous methodologies, including proper randomization, blinding, and allocation concealment, to minimize bias and enhance the reliability of the results (Li et al., 2023). Secondly, research should explore the mechanisms of action of *Sophora flavescens* in greater detail. Understanding how the bioactive compounds in *Sophora flavescens* interact with various signaling pathways and pain mediators will provide valuable insights into their therapeutic potential and inform the development of more targeted and effective treatments. Thirdly, studies should investigate the long-term safety of *Sophora flavescens*, particularly in combination with conventional cancer therapies (Takei and Tagami, 2023). Evaluating the potential for herb-drug interactions and their impact on overall treatment outcomes is crucial to ensure that *Sophora flavescens* can be safely integrated into clinical practice. Lastly, research should focus on optimizing the use of *Sophora flavescens* in clinical practice (Zhang et al., 2012). This includes determining the optimal dosage, duration of treatment, and formulation of *Sophora flavescens*, as well as identifying patient characteristics that may influence therapeutic

outcomes. Personalized medicine approaches could be employed to tailor treatments to individual patients based on their specific needs and responses to therapy.

5 Conclusion

In conclusion, this meta-analysis provides robust evidence supporting the efficacy and safety of *Sophora flavescens* in managing bone neuropathic pain induced by tumor metastasis. The findings suggest that *Sophora flavescens* can be an effective adjunctive therapy, offering significant pain relief with minimal adverse effects. However, the heterogeneity and potential biases in the included studies highlight the need for more high-quality research to validate these findings and optimize the use of *Sophora flavescens* in clinical practice. Integrating traditional Chinese medicine with conventional medical treatments holds promise for improving pain management and enhancing the quality of life for patients suffering from cancer-induced bone pain.

Data availability statement

The original contributions presented in the study are included in the article/supplementary material, further inquiries can be directed to the corresponding authors.

Author contributions

CC: Writing—original draft, Writing—review and editing. DS: Writing—original draft, Writing—review and editing. ZZ: Writing—original draft, Writing—review and editing. LH: Writing—original draft, Writing—review and editing. QW: Writing—original draft, Writing—review and editing. YS: Writing—original draft, Writing—review and editing. HZ: Writing—original draft, Writing—review and editing. DF: Writing—original draft, Writing—review and editing.

References

- Cao, W., and Guo, R. Y. (2012). Radiotherapy combined with compound Kushen injection in the treatment for 58 cases with malignant bone metastasis. *Chin. Remedies Clin.* 12, 1217–1218.
- Cao, X., and He, Q. (2020). Anti-tumor activities of bioactive phytochemicals in *Sophora flavescens* for breast cancer. *Cancer Manag. Res.* 12, 1457–1467. Published 2020 Feb 27. doi:10.2147/CMAR.S243127
- Chen, H., Yang, J., Hao, J., Lv, Y., Chen, L., Lin, Q., et al. (2019). A novel flavonoid kushenol Z from *Sophora flavescens* mediates mTOR pathway by inhibiting phosphodiesterase and akt activity to induce apoptosis in non-small-cell lung cancer cells. *Molecules* 24 (24), 4425. Published 2019 Dec 4. doi:10.3390/molecules2424425
- Chen, L. A., Gu, H. G., Lu, Y., Wang, X., and Zhang, S. K. (2010). Clinical analysis of treating metastatic bone cancer with radiotherapy plus compound Kushen injection. *China Med. Eng.* 18, 48–50.
- Chen, M. H., Gu, Y. Y., Zhang, A. L., Sze, D. M., Mo, S. L., and May, B. H. (2021). Biological effects and mechanisms of matrine and other constituents of *Sophora flavescens* in colorectal cancer. *Pharmacol. Res.* 171, 105778. doi:10.1016/j.phrs.2021.105778
- Chen, Z., Dong, Y., Yan, Q., Yu, C., Lai, Y., et al. (2023). Liquid chromatography-tandem mass spectrometry analysis of a ratio-optimized drug pair of *Sophora flavescens* Aiton and *Coptis chinensis* Franch and study on the mechanism of anti-colorectal cancer effect of two alkaloids thereof. *Front. Oncol.* 13, 1198467. Published 2023 Jun 19. doi:10.3389/fonc.2023.1198467
- Falk, S., and Dickenson, A. H. (2014). Pain and nociception: mechanisms of cancer-induced bone pain. *J. Clin. Oncol.* 32 (16), 1647–1654. doi:10.1200/JCO.2013.51.7219
- Falk, S., Gallego-Pedersen, S., and Petersen, N. C. (2017). Grid-climbing behaviour as a pain measure for cancer-induced bone pain and neuropathic pain. *Vivo* 31 (4), 619–623. doi:10.21873/in vivo.11102
- Ge, C., and Zhang, D. F. (2011). Clinical observation of compound Kushen injection combined with three-dimensional conformal radiotherapy for advanced metastatic bone pain. *Shandong Med. J.* 51, 72–73.
- Gordon-Williams, R. M., and Dickenson, A. H. (2007). Central neuronal mechanisms in cancer-induced bone pain. *Curr. Opin. Support Palliat. Care* 1 (1), 6–10. doi:10.1097/SPC.0b013e328133f5e9
- Han, Y., Zhang, S., Wu, J., Yu, K., Yin, L., et al. (2010). Matrine induces apoptosis of human multiple myeloma cells via activation of the mitochondrial pathway. *Leuk. Lymphoma* 51 (7), 1337–1346. doi:10.3109/10428194.2010.488708
- He, X., Fang, J., Huang, L., Wang, J., and Huang, X. (2015). *Sophora flavescens* Ait.: traditional usage, phytochemistry and pharmacology of an important traditional Chinese medicine. *J. Ethnopharmacol.* 172, 10–29. doi:10.1016/j.jep.2015.06.010

Funding

The author(s) declare that financial support was received for the research, authorship, and/or publication of this article. Jiangsu Province Wuxi Municipal Science and Technology Bureau, “Taihu Light” Science and Technology Key Project (Medical and Health Technology Research) (NO: Y20212037); Jiangsu Provincial Administration of Traditional Chinese Medicine, 2021 Provincial Traditional Chinese Medicine Science and Technology Development Plan Project (NO: QN202114); Project of Suzhou Health Commission, (LCZX201923); Changshu Science and Technology Bureau Project (CS202001); Project funded by Changshu Municipal Health Commission (CsWs201928).

Acknowledgments

The authors thank AiMi Academic Services (www.aimieditor.com) for English language editing and review services.

Conflict of interest

The authors declare that the research was conducted in the absence of any commercial or financial relationships that could be construed as a potential conflict of interest.

Publisher's note

All claims expressed in this article are solely those of the authors and do not necessarily represent those of their affiliated organizations, or those of the publisher, the editors and the reviewers. Any product that may be evaluated in this article, or claim that may be made by its manufacturer, is not guaranteed or endorsed by the publisher.

- Hu, H. F., Wang, Z., Tang, W. L., Fu, X. M., Kong, X. J., Qiu, Y. K., et al. (2022). Effects of *Sophora flavescens* aiton and the absorbed bioactive metabolite matrine individually and in combination with 5-fluorouracil on proliferation and apoptosis of gastric cancer cells in nude mice. *Front. Pharmacol.* 13, 1047507. Published 2022 Nov 9. doi:10.3389/fphar.2022.1047507
- Huang, W. C., Gu, P. Y., Fang, L. W., Huang, Y. L., Lin, C. F., and Liou, C. J. (2019). Sophoraflavanone G from *Sophora flavescens* induces apoptosis in triple-negative breast cancer cells. *Phytomedicine* 61, 152852. doi:10.1016/j.phymed.2019.152852
- Huang, X. B., Yuan, L. W., Shao, J., Yang, Y., Liu, Y., Lu, J. J., et al. (2021). Cytotoxic effects of flavonoids from root of *Sophora flavescens* in cancer cells. *Nat. Prod. Res.* 35 (22), 4317–4322. doi:10.1080/14786419.2020.1712382
- Kanis, J. A. (1995). Bone and cancer: pathophysiology and treatment of metastases. *Bone* 17 (2 Suppl. 1), 101S–105S. doi:10.1016/8756-3282(95)00194-i
- Li, C., Niu, D., Zhu, R., Yan, X., Qu, H., Zhang, Y., et al. (2023). Adjunctive effect of compound Kushen injection for cancer: an overview of systematic reviews. *J. Ethnopharmacol.* 317, 116778. doi:10.1016/j.jep.2023.116778
- Li, J., Lin, Y., He, L., Ou, R., Chen, T., Zhang, X., et al. (2021). Two new isoprenoid flavonoids from *Sophora flavescens* with antioxidant and cytotoxic activities. *Molecules* 26 (23), 7228. Published 2021 Nov 29. doi:10.3390/molecules26237228
- Liepe, K., Murray, I., and Flux, G. (2022). Dosimetry of bone seeking beta emitters for bone pain palliation metastases. *Semin. Nucl. Med.* 52 (2), 178–190. doi:10.1053/j.semnucmed.2021.11.005
- Luo, D., Dai, X., Tian, H., Fan, C., Xie, H., Chen, N., et al. (2023). Sophoflaurine A, a novel matrine-derived alkaloid from *Sophora flavescens* with therapeutic potential for non-small cell lung cancer through ROS-mediated pyroptosis and autophagy. *Phytomedicine* 116, 154909. doi:10.1016/j.phymed.2023.154909
- Mantyh, P. (2013). Bone cancer pain: causes, consequences, and therapeutic opportunities. *Pain* 154 (Suppl. 1), S54–S62. doi:10.1016/j.pain.2013.07.044
- Milgrom, D. P., Lad, N. L., Koniaris, L. G., and Zimmers, T. A. (2017). Bone pain and muscle weakness in cancer patients. *Curr. Osteoporos. Rep.* 15 (2), 76–87. doi:10.1007/s11914-017-0354-3
- Minisola, S., Peacock, M., Fukumoto, S., Cipriani, C., Pepe, J., Tella, S. H., et al. (2017). Tumour-induced osteomalacia. *Nat. Rev. Dis. Prim.* 3, 17044. Published 2017 Jul 13. doi:10.1038/nrdp.2017.44
- Mitchell, S. A. T., Majuta, L. A., and Mantyh, P. W. (2018). New insights in understanding and treating bone fracture pain. *Curr. Osteoporos. Rep.* 16 (4), 325–332. doi:10.1007/s11914-018-0446-8
- Oh, J., Kim, S. A., Kwon, K. W., Choi, S. R., Lee, C. H., Hossain, M. A., et al. (2023). *Sophora flavescens* Aiton methanol extract exerts anti-inflammatory effects via reduction of Src kinase phosphorylation. *J. Ethnopharmacol.* 305, 116015. doi:10.1016/j.jep.2022.116015
- Qu, Z., Wang, W., and Adelson, D. L. (2023). Chromosomal level genome assembly of medicinal plant *Sophora flavescens*. *Sci. Data* 10 (1), 572. Published 2023 Aug 29. doi:10.1038/s41597-023-02490-8
- Ren, F., Li, S. D., Lin, M. X., Wang, H. M., and Li, M. (2012). Efficacy and safety of compound Kushen injection combined with zoledronic acid for ostealgia in patients with malignant tumor and osseous metastases. *Eval. Anal. Drug-Use Hosp. China* 12, 246–248.
- Ren, S. P., and Zheng, Y. S. (2011). Radiotherapy combined with compound matrine injection in the treatment for 30 cases with malignant bone metastasis. *J. Chin. Oncol.* 17, 795–796.
- Rome, S., Noonan, K., Bertolotti, P., Tariman, J. D., and Miceli, T. (2017). Bone Health, pain, and mobility: evidence-based recommendations for patients with multiple myeloma. *Clin. J. Oncol. Nurs.* 21 (5 Suppl. 1), 47–59. doi:10.1188/17.CJON.S5.47-59
- Sulistio, M., Wojnar, R., Key, S., Kwok, J., Al-Rubaie, Z., and Michael, N. (2021). The role of methadone in cancer-induced bone pain: a retrospective cohort study. *Support Care Cancer* 29 (3), 1327–1335. doi:10.1007/s00520-020-05606-7
- Sun, C. P., Zhou, J. J., Yu, Z. L., Huo, X. K., Zhang, J., Morisseau, C., et al. (2022). Kurarinone alleviated Parkinson's disease via stabilization of epoxyeicosatrienoic acids in animal model. *Proc. Natl. Acad. Sci. U. S. A.* 119 (9), e2118818119. doi:10.1073/pnas.2118818119
- Takei, D., and Tagami, K. (2023). Management of cancer pain due to bone metastasis. *J. Bone Min. Metab.* 41 (3), 327–336. doi:10.1007/s00774-022-01382-y
- Wakabayashi, H., Wakisaka, S., Hiraga, T., Hata, K., Nishimura, R., Tominaga, M., et al. (2018). Decreased sensory nerve excitation and bone pain associated with mouse Lewis lung cancer in TRPV1-deficient mice. *J. Bone Min. Metab.* 36 (3), 274–285. doi:10.1007/s00774-017-0842-7
- Wang, R., and Pan, X. Y. (2011). Clinical observation of compound matrine injection combined with radiotherapy for advanced metastatic bone pain. *China Pharm.* 22, 329–331.
- Yoneda, T., Hata, K., Nakanishi, M., Nagae, M., Nagayama, T., Wakabayashi, H., et al. (2011). Involvement of acidic microenvironment in the pathophysiology of cancer-associated bone pain. *Bone* 48 (1), 100–105. doi:10.1016/j.bone.2010.07.009
- Yoneda, T., Hiasa, M., Okui, T., and Hata, K. (2023). Cancer-nerve interplay in cancer progression and cancer-induced bone pain. *J. Bone Min. Metab.* 41 (3), 415–427. doi:10.1007/s00774-023-01401-6
- Zhang, S., Zhang, Y., Zhuang, Y., Wang, J., Ye, J., et al. (2012). Matrine induces apoptosis in human acute myeloid leukemia cells via the mitochondrial pathway and Akt inactivation. *PLoS One* 7 (10), e46853. doi:10.1371/journal.pone.0046853
- Zhang, Y. K., and Zhu, X. Z. (2011). Clinical observation of compound Kushen injection combined with radiotherapy for advanced metastatic bone pain. *Shandong Med. J.* 51, 84–85.
- Zhao, J., Zhang, H., Liu, S. B., Han, P., Hu, S., Li, Q., et al. (2013). Spinal interleukin-33 and its receptor ST2 contribute to bone cancer-induced pain in mice. *Neuroscience* 253, 172–182. doi:10.1016/j.neuroscience.2013.08.026
- Zheng, X. Q., Wu, Y. H., Huang, J. F., and Wu, A. M. (2021). Neurophysiological mechanisms of cancer-induced bone pain. *J. Adv. Res.* 35, 117–127. Published 2021 Jun 11. doi:10.1016/j.jare.2021.06.006



OPEN ACCESS

EDITED BY

Jian Hao,
The Second Affiliated Hospital of Guangzhou
Medical University, China

REVIEWED BY

Geovanna Nallely Quiñonez-Bastidas,
Autonomous University of Sinaloa, Mexico
Wei Xiong,
MGI Tech Co., Ltd., China

*CORRESPONDENCE

Sajad Fakhri,
✉ pharmacy.sajad@yahoo.com,
✉ sajad.fakhri@kums.ac.ir
Javier Echeverría,
✉ javier.echeverriam@usach.cl

RECEIVED 20 July 2024

ACCEPTED 06 November 2024

PUBLISHED 25 November 2024

CITATION

Hashemi B, Fakhri S, Kiani A, Abbaszadeh F,
Miraghaee S, Mohammadi M and Echeverría J
(2024) Anti-neuropathic effects of astaxanthin
in a rat model of chronic constriction injury:
passing through opioid/benzodiazepine
receptors and relevance to its antioxidant and
anti-inflammatory effects.
Front. Pharmacol. 15:1467788.
doi: 10.3389/fphar.2024.1467788

COPYRIGHT

© 2024 Hashemi, Fakhri, Kiani, Abbaszadeh,
Miraghaee, Mohammadi and Echeverría. This is
an open-access article distributed under the
terms of the [Creative Commons Attribution
License \(CC BY\)](#). The use, distribution or
reproduction in other forums is permitted,
provided the original author(s) and the
copyright owner(s) are credited and that the
original publication in this journal is cited, in
accordance with accepted academic practice.
No use, distribution or reproduction is
permitted which does not comply with these
terms.

Anti-neuropathic effects of astaxanthin in a rat model of chronic constriction injury: passing through opioid/benzodiazepine receptors and relevance to its antioxidant and anti-inflammatory effects

Boshra Hashemi¹, Sajad Fakhri^{2*}, Amir Kiani^{2,3},
Fatemeh Abbaszadeh⁴, Shahram Miraghaee⁵,
Mohammad Mohammadi⁶ and Javier Echeverría^{7*}

¹Student Research Committee, Kermanshah University of Medical Sciences, Kermanshah, Iran,
²Pharmaceutical Sciences Research Center, Health Institute, Kermanshah University of Medical Sciences,
Kermanshah, Iran, ³Regenerative Medicine Research Center (RMRC), Kermanshah University of Medical
Sciences, Kermanshah, Iran, ⁴Neurobiology Research Center, Shahid Beheshti University of Medical
Sciences, Tehran, Iran, ⁵Medical Biology Research Center, Health Technology Institute, Kermanshah
University of Medical Sciences, Kermanshah, Iran, ⁶Department of Radiology and Nuclear Medicine,
School of Paramedical Sciences, Kermanshah University of Medical Sciences, Kermanshah, Iran,
⁷Departamento de Ciencias del Ambiente, Facultad de Química y Biología, Universidad de Santiago de
Chile, Santiago, Chile

Introduction: Neuropathic pain is a debilitating neurological disorder and is on the rise. Since no effective treatment has been so far approved to combat the complex pathological mechanisms behind neuropathic pain, finding new therapeutic candidates is of great importance. Astaxanthin (AST) is a carotenoid with strong antioxidant, and anti-inflammatory activities.

Purpose: The present research aimed to evaluate the ameliorative effects of AST on a rat model of neuropathic pain.

Methods: To induce neuropathic pain, a chronic constriction injury (CCI) model was employed. Accordingly, Wistar rats were divided into nine groups of six including sham, negative control group (CCI), positive control group gabapentin (100 mg/kg), AST (5, 10 mg/kg), flumazenil (0.5 mg/kg), naloxone (0.1 mg/kg), AST (10 mg/kg) + flumazenil (0.5 mg/kg), and AST (10 mg/kg) + naloxone (0.1 mg/kg) were administered intraperitoneally on days 1, 3, 5, 7, 10, and 14. To check the experimental signs of neuropathic pain and motor dysfunction, hot plate, acetone drop, and open field tests were used at the same time points. Additionally, biochemical assay and zymography were done on days 7 and 14 to assess the

Abbreviations: AST, astaxanthin; AUC, area under the curve; CCI, chronic constriction injury; DMSO, dimethylsulfoxide; DTNB, 5,5'-dithio-bis(2-nitrobenzoic acid); FLU, flumazenil; H₂O₂, hydrogen peroxide; MMP, matrix metalloproteinase; NAL, naloxone; NEDD, diamine dihydrochloride; OD, optical density; PWL, paw withdrawal; ROS, reactive oxygen species.

changes in catalase, glutathione and nitrite, as well as matrix metalloproteinases (MMP-2 and MMP-9). Besides, histological evaluations were performed for tissue damages on days 7 and 14.

Results and discussion: Results indicated that intraperitoneal injection of AST improved allodynia, hyperalgesia, and locomotor activity after CCI. AST also increased catalase and glutathione while suppressing nitrite, MMP-2, and MMP-9 activity through opioid/benzodiazepine receptors.

Conclusion: The results highlighted AST as a promising candidate against neuropathic pain with beneficial effects on motor function by suppressing inflammatory mediators, and augmenting antioxidant factors, passing through opioid/benzodiazepine receptors.

KEYWORDS

astaxanthin, chronic constriction injury, inflammation, oxidative stress, opioid receptor, benzodiazepine receptor, neuropathic pain

1 Introduction

Neuropathic pain is a debilitating neural disorder following the disruption of neurons' function and structure, mainly in the somatosensory system (Treede et al., 2008). Neuropathic pain is commonly observed in patients with spinal cord injury, multiple sclerosis, diabetic neuropathy, postherpetic neuralgia, and cancer, which critically reduces life quality (Colloca et al., 2017). Growing studies have been developed to manage neuropathic pain; though, more research is needed to find novel therapeutic agents with higher efficacy and lower side effects (Finnerup et al., 2015).

Chronic constriction injury (CCI) is a model of neuropathic pain, based on nerve damage caused by actual or potential tissue stimuli (Treede et al., 2008). Such pain can be caused by damage to the central or peripheral nervous system, diabetes, metabolic disorders, viral infections, nutritional deficiencies, trauma, and physical injuries (Fonseca-Rodrigues et al., 2021). Neuropathic pain is characterized by signs such as allodynia, hyperalgesia, and dysesthesia (Jensen and Finnerup, 2014). Many drugs have been proposed to control neuropathic pain, including non-steroidal anti-inflammatory drugs (NSAIDs), opiates, tricyclic antidepressants, and anticonvulsant drugs but these drugs suffer from several side effects and have shown low efficacy in the control of neuropathic pain (Muthuraman et al., 2008; Fakhri et al., 2021a). Therefore, many efforts have been made to find a rational and less complicated treatment method for patients with neuropathic pain (Colloca et al., 2017).

Following nerve damage, the signals released from the nerve terminals contribute to microglial activation and propagation of inflammatory cytokines (Soleimani et al., 2019; Zhang et al., 2021) and matrix metalloproteinase 9 (MMP-9) (Fakhri et al., 2021b), which lead to allodynia or hyperalgesia (Kiguchi et al., 2012). Therefore, suppression of inflammatory mediators is believed to relieve neuropathic pain (Kiguchi et al., 2012; Malcangio et al., 2013). On the other hand, oxidative stress factors are also activated following nerve damage; for example, reactive superoxide molecules are increased in the dorsal horn of the spinal cord and dorsal root ganglia as a result of CCI. Also, increased levels of reactive oxygen species (ROS) lead to the initiation and maintenance of central and peripheral sensitization (Bakare and Owoyele, 2020). Previously, the

roles of benzodiazepine receptors (O'Connell et al., 2019; Mir et al., 2020; Lape et al., 2023) and opioid receptors (Jones et al., 2023) have been highlighted in pain management.

Astaxanthin (AST), 3,3'-Dihydroxy-beta,beta-carotene-4,4'-dione, is a natural and red-orange keto-carotenoid that belongs to xanthophylls (Fakhri et al., 2018a). Studies have reported that AST possesses significant effects on the control of neuroinflammation- and oxidative stress-mediated neuronal damages (Zarneshan et al., 2020). The findings of another study showed that treatment with AST significantly reduced neuropathic pain by modulating oxidative stress and mitigating astrocytes activation (Sharma et al., 2018). We have also previously shown the potential of AST in combating spinal cord injury-induced neuropathic pain through different mechanisms (Fakhri et al., 2018b; Fakhri et al., 2019).

Therefore, in this study, we sought to investigate the effects of AST on CCI-induced neuropathic pain and motor dysfunction, highlighting its anti-inflammatory and antioxidant capabilities passing through opioid/benzodiazepine receptors.

2 Materials and methods

2.1 Chemicals and reagents

Astaxanthin (multiple mechanisms; 3,3'-Dihydroxy-β-carotene-4,4'-dione; C₄₀H₅₂O₄) and gabapentin (GABA synthetic enzyme modulator; 1-(Aminomethyl)-cyclohexanecarboxylic acid; C₉H₁₇NO₂) were purchased from Sigma-Aldrich (Sigma Chemical Co., St. Louis, MO, United States). Naloxone [μ-opioid receptor antagonist; (5α)-4,5-Epoxy-3,14-dihydroxy-17-(2-propen-1-yl) morphinan-6-one; C₁₉H₂₁NO₄; Caspian Tamin Pharmaceutical Company, Iran], flumazenil [GABA_A receptor antagonist; 5,6-dihydro-4H-imidazo(1,5-a)(1,4)benzodiazepine; C₁₅H₁₄FN₃O₃; Hameln, Germany], ketamine [NMDA receptor antagonist; 2-(2-Chlorophenyl)-2-(methylamino) cyclohexanone, 2-(2-Chlorophenyl)-2-(methylamino)cyclohexanone hydrochloride; Alfasan IBV, Turkey], and xylazine [α₂ adrenergic receptor agonist; 2-(2,6-Dimethylphenylamino)-5,6-dihydro-4H-thiazine; C₁₂H₁₆N₂S; Alfasan IBV, Turkey] were analytical grade reagents purchased from commercial sources.

2.2 Experimental animals

In this research, 54 adult male Wistar rats (weighing 230–250 g) were selected from the reproductive colony of Kermanshah University of Medical Sciences. They were kept in a suitable situation with access to food and water with a 12-h light/dark cycle, a temperature of $25 \pm 2^\circ\text{C}$, and also at optimum humidity. Also, all the protocols were confirmed by the Ethics Committee in Medical Research of Kermanshah University of Medical Sciences (Ethical code: IR.KUM.REC.1400.431). In the current study lowest numbers of animals and surgeries were done in a clean situation (Soleimani et al., 2019; Zhang et al., 2021).

2.3 Chronic constriction injury

To evaluate the effect of AST on neuropathic pain, the CCI was induced according to the Bennett method (Bennett and Xie, 1988). For this purpose, rats were anesthetized with 50 mg/kg ketamine and 5 mg/kg xylazine. Following disinfection, incision of muscles and skin, and appearing the sciatic nerve on the left side, four loose chromic catgut (4.0) were tied on the sciatic nerve exactly near the trifurcation of the sciatic. Finally, after neuropathy induction, the animals were transferred to the cage for recovery (Amin et al., 2016; Soleimani et al., 2019).

2.4 Experimental groups

In total, 54 rats were divided into nine groups of six, including, the sham group (undergoing surgery without CCI and receiving DMSO 5%), CCI group (undergoing CCI and receiving DMSO 5%), gabapentin (positive control group, 100 mg/kg in DMSO 5%), AST-treated groups (5 and 10 mg/kg in DMSO 5%), flumazenil (FLU) (0.5 mg/kg), naloxone (NAL) (0.1 mg/kg), AST (10 mg/kg) + flumazenil (0.5 mg/kg) (AST + FLU), and AST (10 mg/kg) + naloxone (0.1 mg/kg) (AST + NAL) (Supplementary Figures 1, 2). All groups received intraperitoneal doses on days 1, 3, 5, 7, 10, and 14, about 1 h prior to assessing behavioral tests. Animals were anesthetized on days 7 and 14 with ketamine/xylazine (100/10 mg/kg), and blood samples were obtained from the retro orbital sinus to evaluate the activities of MMP-2 and MMP-9. Besides, glutathione, catalase, and nitrite levels were measured in serum samples. Finally, the sciatic nerve was separated for histopathological analysis (Soleimani et al., 2019). Blood sampling from retro orbital sinus by an expert is a valuable method without animal expiration after sampling. This method allows serial sampling even in different days and researchers can continue performing experiments on the animals until the end of study timeline (e.g., in our study sampling was done on day 7 and rats were studied until day 14 for behavioural analysis and re-sampling). This strategy also minimizes the number of rats as per the National Institutes of Health Guidelines on the care and use of laboratory animals. Once required blood sampling is done, the capillary tube is removed and wiped with sterile cotton. Bleeding can be stopped using gentle finger pressure. Then, rats should be housed individually in large cages and monitored, until the possible

bleeding is stopped. *Ad libitum* intake of water helps replace the lost blood (Sharma et al., 2014; Fakhri et al., 2021b).

2.5 Behavioral tests

Behavioral tests were done on days 1, 3, 5, 7, 10, and 14 after surgery. Open field tests were used for the evaluation of motor activity. In addition, acetone drop and hot plate tests were done to assess cold allodynia and heat hyperalgesia, respectively. All behavioral tests were carried out as per the mentioned order at 30-min intervals.

2.5.1 Acetone drop test

The acetone drop test was used to evaluate cold allodynia. To ensure proper access to the paws, rats were placed on a metal mesh grid during the test. To examine the response to cold stimulation of the hind paw, 100 μL acetone was sprayed on the plantar surface of the paw for 2–3 s from a distance of 2 cm. Response to cold was classified with the following scales: 0: no response; 1: shocking response without paw withdrawal; 2: brief retraction of paw; 3: long-term withdrawal of the paw that lasts between 5–30 s and is often accompanied by flinching and licking the paw; 4: prolonged and frequent withdrawal (30 s) accompanied by shaking, licking and/or vocalization (Kauppila, 2000; Fakhri et al., 2018b).

2.5.2 Hot plate test

In this experiment, we assessed thermal hyperalgesia related to neuropathic pain in rats by measuring their paw withdrawal latency (PWL) using a hot plate apparatus (Harvard Apparatus, Holliston, MA). Briefly, rats were placed within a clear Plexiglas observation chamber on a hot plate analgesia meter. PWL was defined as the time that it took the rat to exhibit pain-related behaviors, such as paw licking, hindlimb withdrawal, or jumping, obtained from three repeats of the experiment (5 min intervals) after being placed on the hot plate surface at $52 \pm 0.5^\circ\text{C}$. A 60-s cut-off time was applied to each animal to prevent damage to the paw tissue (Bakare and Owoyele, 2020; Fakhri et al., 2022).

2.5.3 Open field test

The open field test was conducted to evaluate the overall motor activity of the animals. Briefly, rats were placed individually in an open field ($60 \times 60 \times 40$ cm) with a non-slippery surface. Total distance and velocity were video-recorded in 5 min. The total number of squares crossed by each rat (total crossing), the number of rearing (standing on two hind paws without touching the walls), and grooming were recorded. This experiment was performed in a completely quiet environment with a constant temperature and uniform brightness (Parvardeh and Hosseinzadeh, 2003; Parvardeh et al., 2016). After finalizing each experiment, the entire field was cleaned with ethanol 70%.

2.6 Biochemical analysis

To evaluate serum antioxidant potential, catalase and glutathione activities were measured on days 7 and 14. Serum levels of nitrite were also measured to assess oxidative capacity.

2.6.1 Catalase assay

The activity of catalase was measured according to the Aebi method (Aebi, 1984). Since catalase can convert hydrogen peroxide (H_2O_2) into water and oxygen, to determine the serum level of catalase, we examined changes in the serum levels of H_2O_2 . To do this, first 20 μ L of serum sample and 100 μ L of 65 mM hydrogen peroxide were added to the wells and then incubated for 4 min at 25°C. The reaction was stopped by adding 100 μ L of ammonium molybdate at a concentration of 32.4 mM. Finally, the concentration of yellow molybdate complex and hydrogen peroxide was measured at 405 nm by an ELISA reader.

2.6.2 Glutathione assay

In this test, to assess glutathione, the Ellman method was used. This method is based on the glutathione decline by the Ellman's reagent [5,5'-dithio-bis (2-nitrobenzoic acid) (DTNB)] which leads to the formation of oxidized glutathione-TNB adduct and TNB chromophore. As the rate of DTNB formation is proportional to the amount of glutathione present in the sample, we can estimate the level of plasma glutathione by measuring the amount of TNB formation through spectrophotometry at a wavelength of 412 nm (Tippie and Rogers, 2012; Fakhri et al., 2022). To this aim, 60 μ L of serum was mixed with 100 μ L of DTNB at a concentration of 2 mg/mL in the wells of a 96-well plate and then 50 μ L of phosphate buffer was added and the plate was incubated for 10 min at 37°C. Then, absorbance was read at 412 nm.

Using the following formula, differences of absorbance (%) between sample groups and the sham group was reported in both the glutathione and catalase assays:

$$\{(C_{sham} - C_{sample})/C_{sham}\} \times 100$$

2.6.3 Nitrite assay

The Griess method was employed to measure nitrite levels in the serum (Sun et al., 2003). The serum samples (100 μ L) were combined with a sulfanilamide solution (dissolved in 5% HCl) (50 μ L) in the plate wells and left in darkness for 5 min. Subsequently, 50 μ L of naphthyl ethylene diamine dihydrochloride (NEDD; 0.1% in distilled water) was added, and the plate was incubated in darkness at 37°C for 30 min. The optical density (OD) was then measured at 540 nm using a plate reader. Simultaneously, a standard curve was generated using 100 μ L of sodium nitrite at varying concentrations.

2.7 Gelatin zymography

The gelatin zymography method was used to evaluate the pattern of gelatinases in the serum. Briefly, serum samples with a total protein content of 100 μ g using the Bradford method were loaded on sodium dodecyl sulfate-polyacrylamide gels copolymerized with 0.1% gelatin. Then, electrophoresis was performed at a constant voltage of 150 V using a mini-gel slab device Mini Protean III (Bio-Rad, Hercules, CA). The gel was washed in the renaturation buffer for 1 h on a shaker. The renaturation buffer contained 2.5% Triton X-100 (in 50 mM Tris-HCl). After that, the gel was incubated at 37°C in the incubation buffer for 18 h. The incubation buffer comprises 0.02% NaN_3 , 10 mM $CaCl_2$, and 0.15 NaCl in

Tris-HCl (50 mM). Respectively, Gel staining was done with Coomassie blue, followed by destaining in acetic acid (5%) and methanol (7%). The formed clear bands indicate gelatinolytic activity. ImageJ software (National Institute of Health, United States) was used to quantify the relative intensity of the bands in compare to the sham group (Fakhri et al., 2021b; Fakhri et al., 2022).

2.8 Histological analysis

In this research, rats were anesthetized and sacrificed with a mixture of intraperitoneal xylazine (20 mg/kg) and ketamine (100 mg/kg). Samples from each group were selected on the 7th and 14th day. The close parts of the ligated sciatic nerves were excised and fixed with a 10% formalin solution (Muthuraman et al., 2008). After that, tissues were kept in paraffin. Using hematoxylin and eosin (H&E), consecutive sections of the injury site were stained (Sudoh et al., 2004), and then the sections were qualitatively examined by experts to investigate axonal degeneration under a light microscope ($\times 400$) in accordance with routine histological techniques.

2.9 Statistical analysis

The obtained results were assessed with Prism version 8.0 software and a Two-way ANOVA statistical test and Bonferroni *post hoc* for behavioral analysis. One-way ANOVA statistical test with Tukey *post hoc* test were employed for biochemical analysis. The area under the curve (AUC) was calculated using the linear trapezoidal method. All the data are presented as mean \pm SEM and significant level was set at $p < 0.05$.

3 Results

3.1 Acetone drop test

The results of the acetone drop test indicated that the paw withdrawal reflex in the CCI group had a considerable increase compared to the sham group ($p < 0.01$) (Figure 1A). Moreover, the results indicated that treatment with AST in both doses increased the tolerance threshold of cold stimulus after CCI, with the better result seen in the group receiving AST at the dose 10 mg/kg. This group showed a remarkable decrease in cold allodynia compared to the CCI group on days 7 ($p < 0.01$), 10 and 14 ($p < 0.001$) (Figure 1A). Also, in this group the area under the curve of cold allodynia had a remarkable decrease compared to the CCI group ($p < 0.05$) (Figure 1B).

On the other hand, the paw withdrawal reflex in response to the cold stimulus in the rats receiving flumazenil and naloxone alone was not considerably different from the CCI group (Figure 1C). Nevertheless, the results showed that the intraperitoneal injection of naloxone half an hour before AST (10 mg/kg) remarkably reduced the analgesic activity of AST on day 14 ($p < 0.01$), which led to an increase in cold allodynia in this group (Figure 1C). In addition, in this group,

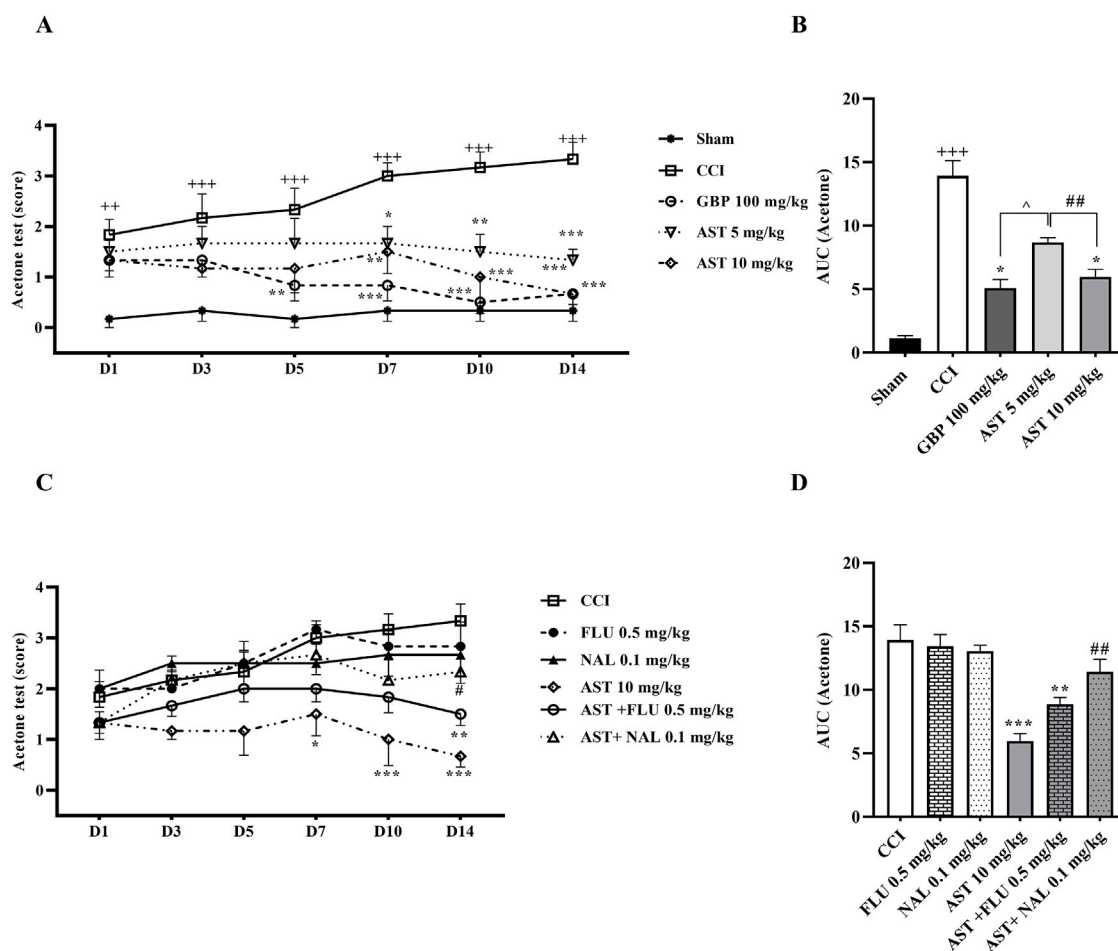


FIGURE 1

Effects of astaxanthin on cold allodynia and its mechanisms after CCI in rats. CCI significantly decreased tolerance threshold of cold stimulus that was reversed by AST (A), and confirmed by AUC analysis (B). While FLU and NAL alone did not affect cold allodynia, those administrations with AST partially reduced AST's effects (C), and the result was confirmed by AUC analysis (D). The data are shown as mean \pm SEM ($n = 6$). $^{**}p < 0.01$, $^{***}p < 0.001$ vs. sham. $^{*}p < 0.05$, $^{**}p < 0.01$, $^{***}p < 0.001$ vs. CCI, $^{##}p < 0.001$ vs. AST 10, $^{#}p < 0.05$ vs. GBP. CCI, chronic constriction injury; GBP, Gabapentin; AST, Astaxanthin; FLU, Flumazenil; NAL, Naloxone.

the area under the curve of cold allodynia also indicated a considerable increase compared to the group treated with AST (10 mg/kg) ($p < 0.01$) (Figure 1D).

3.2 Hot plate test

The data of the hot plate test (Figure 2A) indicated that the time delay of paw withdrawal (PWL) by rats, as the time to reach the pain threshold by heat, was the same in the sham group animals and they were unresponsive. In the CCI group, rats strongly reacted to heat and exhibited a considerable decline in PWL time compared to the first group. The significant differences were seen on the first day with $p < 0.01$ and from days 3–14 with $p < 0.001$. Likewise, the data indicated that treatment with AST caused an increase in PWL delay following CCI, and the better result was related to the group receiving AST at the dose of 10 mg/kg. PWL delay showed a considerable increase in this group compared to the CCI group on days 7 and 14 ($p < 0.01$) and on day 10 ($p < 0.001$) (Figure 2A). In

addition, the area under the PWL curve in the groups treated with AST was significantly increased compared to the CCI group, and this increase was observed in AST 5 mg/kg ($p < 0.05$) and AST 10 mg/kg ($p < 0.001$) groups (Figure 2B). In this study, in rats receiving flumazenil and naloxone, PWL delay did not differ compared to the CCI group (Figure 2C). Besides, the data showed that the area under the PWL curve in the AST + FLU ($p < 0.05$) and AST + NAL ($p < 0.01$) was significantly decreased compared to the AST group (10 mg/kg) indicating a significant increase in thermal hyperalgesia after blocking the opioid and benzodiazepine receptors (Figure 2D).

3.3 Open field test

The data of the open field test showed that all the three components of locomotor activity were the same in the sham group animals and they were unresponsive (Figure 3). The numbers of rearing (Figure 3A), crossing (Figure 3C) and

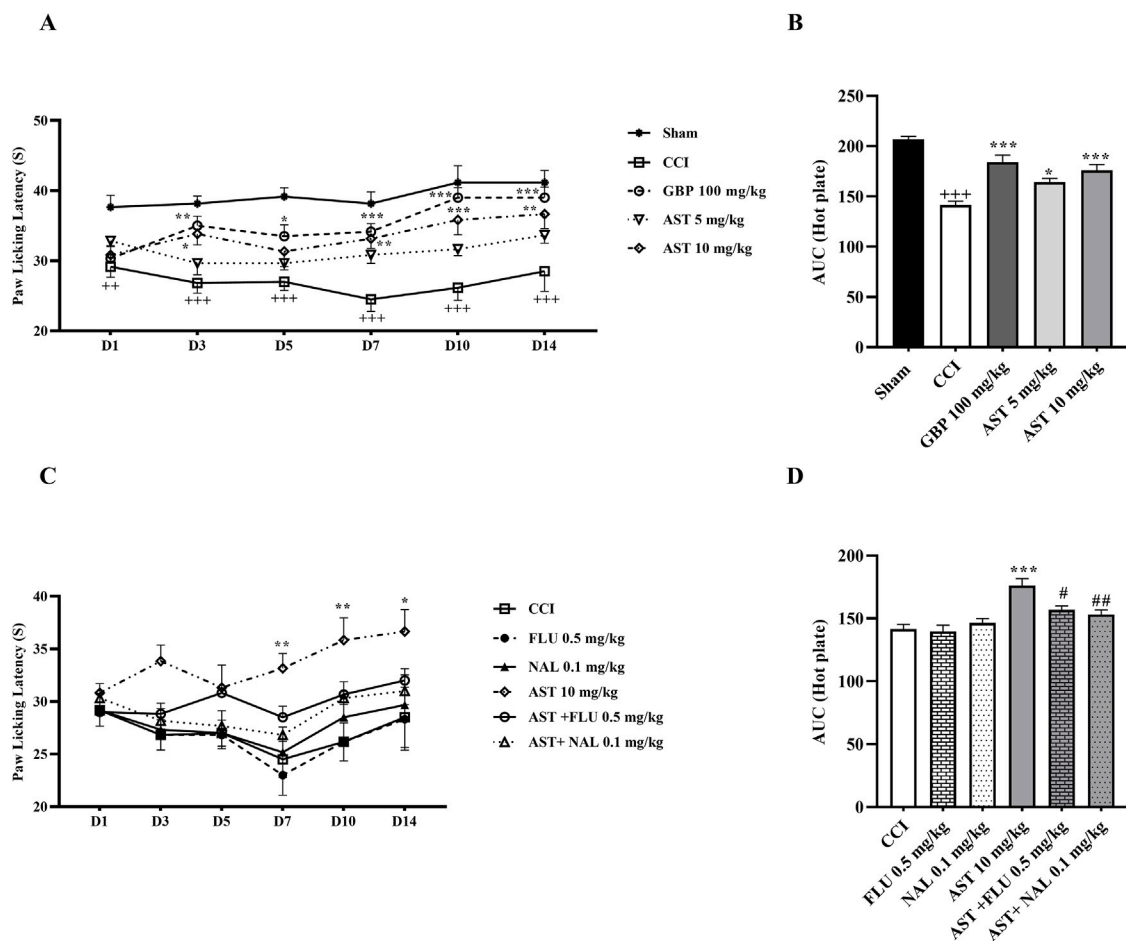


FIGURE 2

Effects of astaxanthin on thermal hyperalgesia and its mechanisms after CCI in rats. CCI significantly decreased paw licking latency during thermal hyperalgesia, that was reversed by AST (A). The result was confirmed by AUC analysis (B). While FLU and NAL alone did not affect thermal hyperalgesia, those administrations with AST partially reduced AST's effect (C), and was confirmed by AUC analysis (D). The data are shown as mean \pm SEM ($n = 6$). $^{++}p < 0.01$, $^{+++}p < 0.001$ vs. sham. $^{*}p < 0.05$, $^{**}p < 0.01$, $^{***}p < 0.001$ vs. CCI, $^{#}p < 0.05$, $^{##}p < 0.01$ vs. AST 10. CCI, chronic constriction injury; GBP, Gabapentin; AST, Astaxanthin; FLU, Flumazenil; NAL, Naloxone.

grooming (Figure 3E) in animals of the CCI group were greatly decreased compared to the sham group ($p < 0.001$).

Results also showed that AST improved all the three motor function parameters compared to the CCI group (Figure 3) ($p < 0.01$). The area under the curve also illustrated the reduction of these three movement parameters following the CCI model ($p < 0.001$), along with the beneficial effect of AST in those parameters (Figures 3B, D, F) ($p < 0.01$).

In the groups receiving flumazenil and naloxone alone, the locomotor activity of rats in all the three components including rearing (Figure 4A), crossing (Figure 4C) and grooming (Figure 4E) did not show any remarkable difference compared to those in the CCI group. However, these parameters were partially reduced in the groups receiving AST + NAL and AST + FLU compared to the AST group (10 mg/kg), which was significant in crossing ($p < 0.05$). The area under the curve clearly showed such changes (Figures 4B, D, F).

In addition to the aforementioned Figures, a Supplementary Figure also provided to refuse the role of solvent volume on neuropathic pain and motor dysfunction (Sham, sham received

v2, CCI, CCI received v2) (Supplementary Figures 1, 2). Since unnecessarily use of different rats is against the National Institutes of Health Guidelines on the care and use of laboratory animals nothing role of solvent volume extrapolated to biochemical and histological analysis.

3.4 Glutathione assay

The serum level of glutathione in CCI group compared to the sham group considerably declined on days 7 and 14, which was related to the antioxidant activity of glutathione ($p < 0.01$) (Figure 5A). The intraperitoneal injection of AST at both doses, especially the dose of 10 mg/kg increased the level of glutathione compared to the CCI group ($p < 0.001$) (Figure 5A). Administration of naloxone and flumazenil alone did not change serum glutathione levels as compared to the CCI group. However, in both AST + NAL and AST + FLU groups, serum levels of glutathione were shown to be significantly decreased compared to the AST group (10 mg/kg) ($p < 0.001$) (Figure 5B).

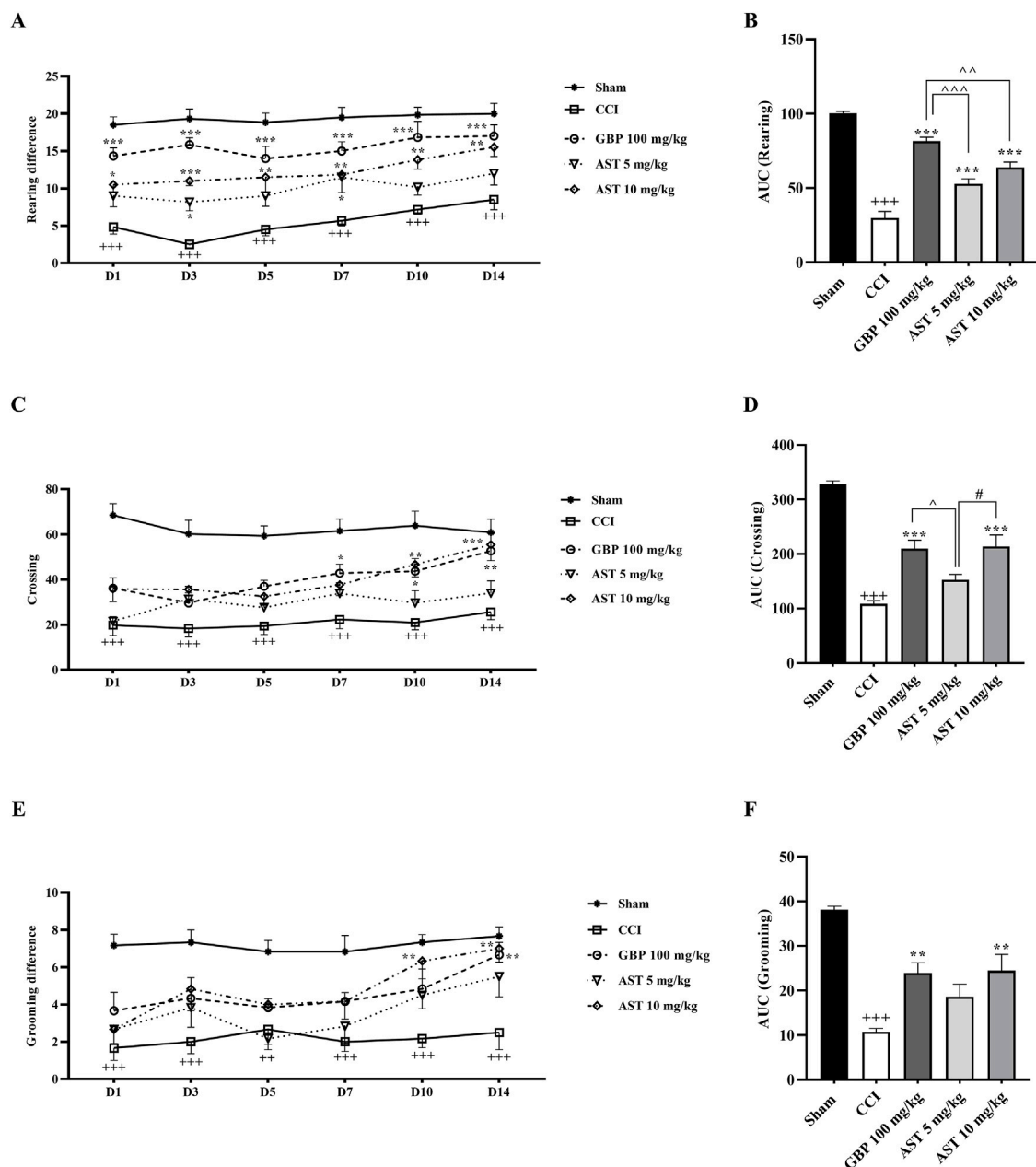


FIGURE 3

Effects of astaxanthin on locomotor activity after CCI in rats. CCI significantly decreased locomotor activity during rearing (A), crossing (C) and grooming (E) evaluations, which was reversed by AST 10 mg/kg. The AUC analysis also confirmed the effect of AST on rearing (B), crossing (D) and grooming (F). The data are shown as mean \pm SEM ($n = 6$). $+++p < 0.001$ vs. sham, $**p < 0.01$, $***p < 0.001$, vs. CCI, $p < 0.05$, $p < 0.01$, $p < 0.001$, vs. GBP, $\#p < 0.05$ vs. AST 10, CCI, chronic constriction injury; GBP, Gabapentin; AST, Astaxanthin; FLU, Flumazenil; NAL, Naloxone.

3.5 Catalase assay

The data showed (Figure 6A) that the serum level of catalase in the CCI group was significantly decreased compared to the sham group ($p < 0.001$). Besides, the serum levels of catalase at both doses of AST, especially the dose of 10 mg/kg ($p < 0.05$), increased significantly compared to the CCI group. Injection of flumazenil and naloxone alone did not affect the serum levels of catalase in rats. The results of flumazenil and naloxone injections on catalase serum

levels were similar to the CCI group. The injection of these two together with AST prevented the positive effect of AST on catalase level ($p < 0.05$) (Figure 6B).

3.6 Nitrite assay

Our findings demonstrated a significant increase in serum nitrite levels in the CCI group compared to the sham group ($p < 0.05$). In

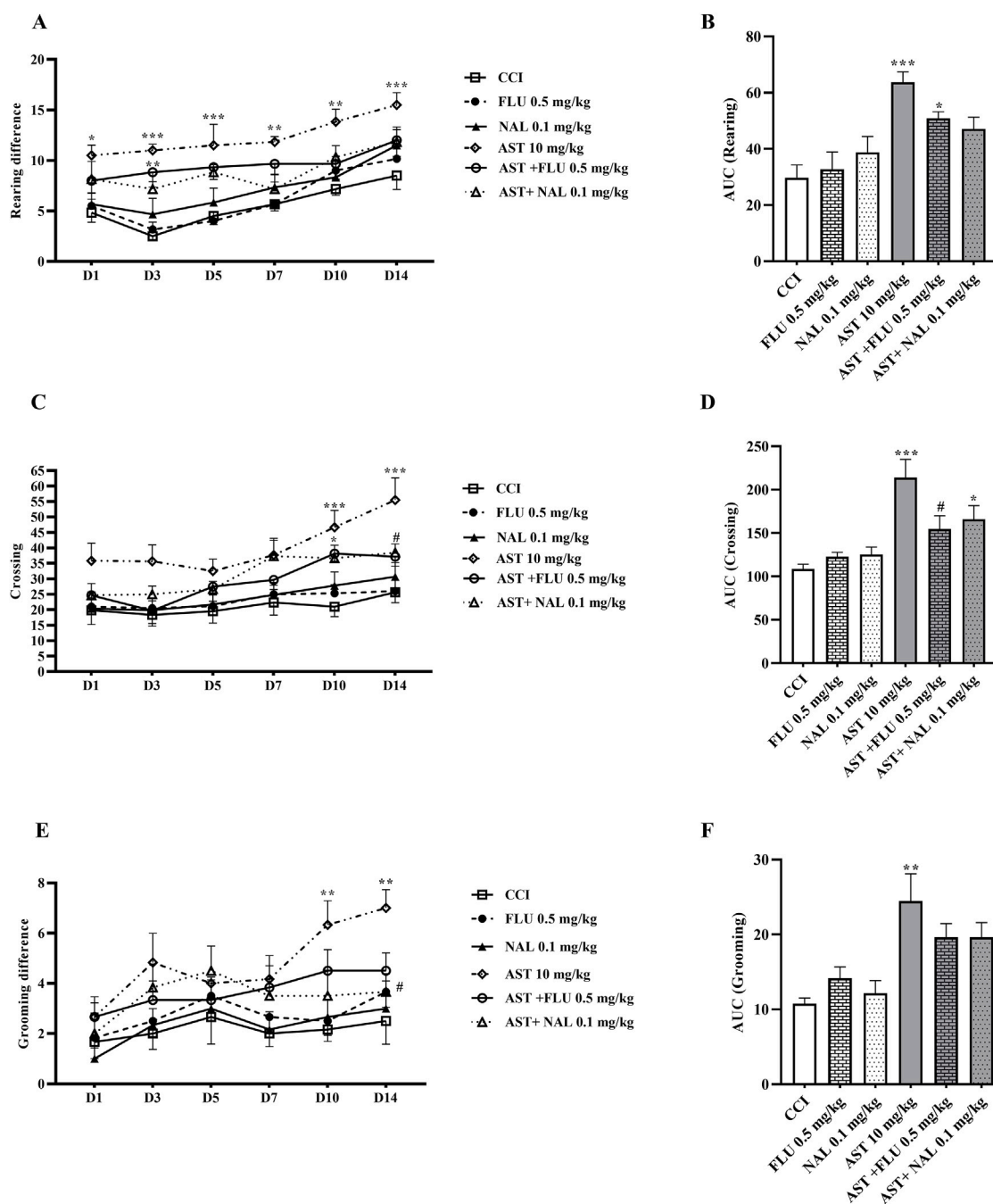


FIGURE 4

Effects of astaxanthin co-administered with FLU and NAL on locomotor activity after CCI in rats. FLU and NAL alone did not affect locomotor activity during rearing (A), crossing (C) and grooming (E), but they reduced AST's effect. AUC analysis confirmed the effect of NAL and FLU on rearing (B), crossing (D) and grooming (F). The data are shown as mean \pm SEM ($n = 6$). * $p < 0.05$, ** $p < 0.01$, *** $p < 0.001$ vs. CCI, # $p < 0.05$ vs. AST 10. CCI, chronic constriction injury; GBP, Gabapentin; AST, Astaxanthin; FLU, Flumazenil; NAL, Naloxone.

addition, AST administration was shown to reduce this increased pattern of nitrite following CCI similar to the positive control group (GBP group) ($p < 0.001$) (Figure 7A). The results of flumazenil and naloxone injections on nitrite serum levels were similar to the CCI group. Their injection with AST did not cause considerable changes in the serum levels of nitrite when compared to the group receiving 10 mg/kg AST on days 7 and 14 (Figure 7B).

3.7 Gelatin zymography

The data showed an increase in the levels of MMP-9 (Figure 8) and MMP-2 (Figure 9) activity following CCI compared to the sham group ($p < 0.001$). Both doses of AST could reverse such increased patterns and had effects close to the effects of GBP (positive control) ($p < 0.01$). Injection of

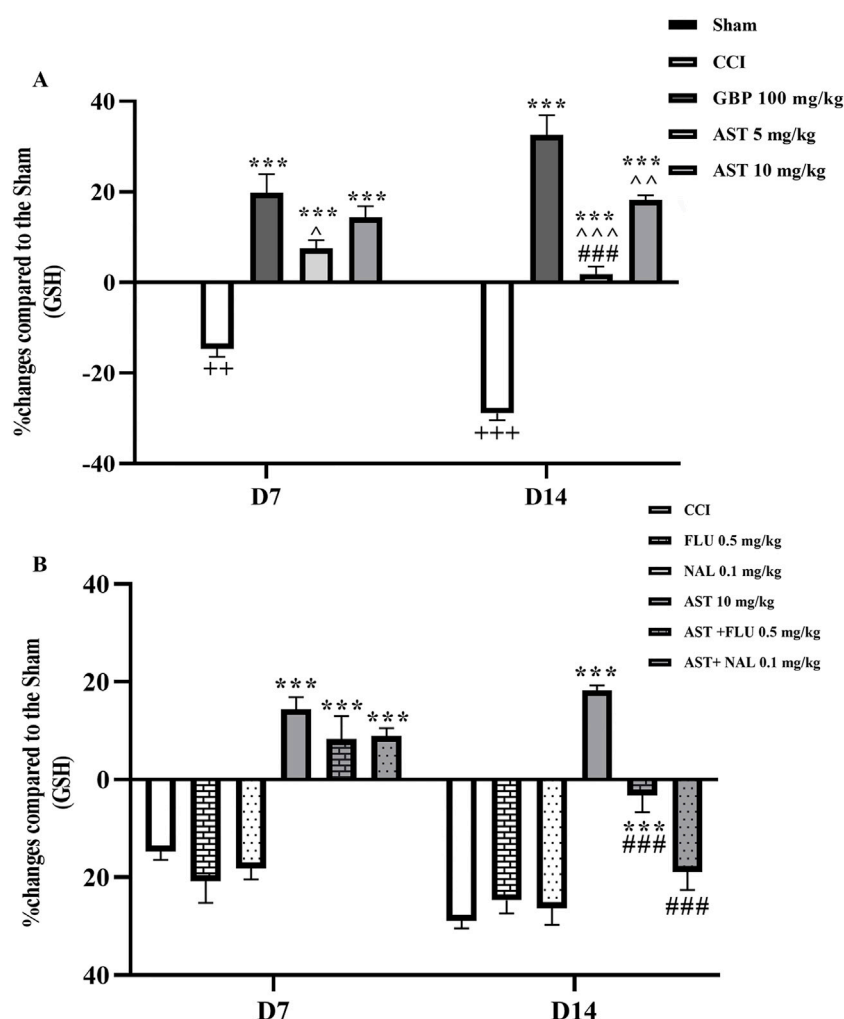


FIGURE 5

Effects of astaxanthin on serum glutathione level and its mechanisms after CCI in rats. CCI significantly decreased glutathione level, which was reversed by AST 10 mg/kg (A). While FLU and NAL alone did not affect serum glutathione level, those administrations with AST partially reduced AST's effects (B). The data are shown as mean \pm SEM ($n = 3$). $^{**}p < 0.01$, $^{***}p < 0.001$ vs. sham, $^{***}p < 0.001$, vs. CCI, $p < 0.05$, $p < 0.01$, $p < 0.001$, vs. GBP, $^{###}p < 0.001$ vs. AST 10. CCI, chronic constriction injury; GBP, Gabapentin; AST, Astaxanthin; FLU, Flumazenil; NAL, Naloxone.

flumazenil and naloxone half an hour before AST administration reduced the positive effects of AST on MMP-2 and MMP-9 activity levels ($p < 0.01$).

3.8 Histopathological analysis

In this study, we utilized H&E staining to assess tissue damage resulting from the CCI model and the impact of AST on it. The sciatic sections of the sham group exhibited well-organized myelin sheaths. Conversely, the stained nerve sections of the CCI group displayed axonal swelling, disrupted myelin sheaths, hemorrhage between cells, and wide separation between nerve fibers. However, CCI rats treated with AST (10 mg/kg) demonstrated a significant improvement in myelin sheath integrity and Schwann cells. These positive effects of AST significantly decreased in the AST + FLU (0.5 mg/kg) and AST + NAL (0.1 mg/kg) groups (Figure 10).

4 Discussion

The present study was designed to investigate the potential of using AST in a CCI model inducing neuropathic pain. Our study yielded several significant findings. Firstly, in rats with CCI, we observed a notable increase in heat hyperalgesia and cold allodynia, accompanied by a decline in motor performance over 14 days. Secondly, CCI rats exhibited elevated levels of MMP-9, MMP-2, and nitrite, while experiencing decreased levels of glutathione, and catalase activity, along with tissue alterations. Thirdly, treatment with AST demonstrated varying degrees of improvement in both behavioral and biochemical parameters. Lastly, the effects of AST appeared to be mediated through the benzodiazepine and opioid receptors, which are known to play roles in the management of neuropathic pain (Figure 11).

The CCI model is widely used to study neuropathic pain caused by nerve damage. This model effectively mimics the symptoms of neuropathic pain experienced by humans, such as allodynia and hyperalgesia, which are caused by peripheral nerve damage and

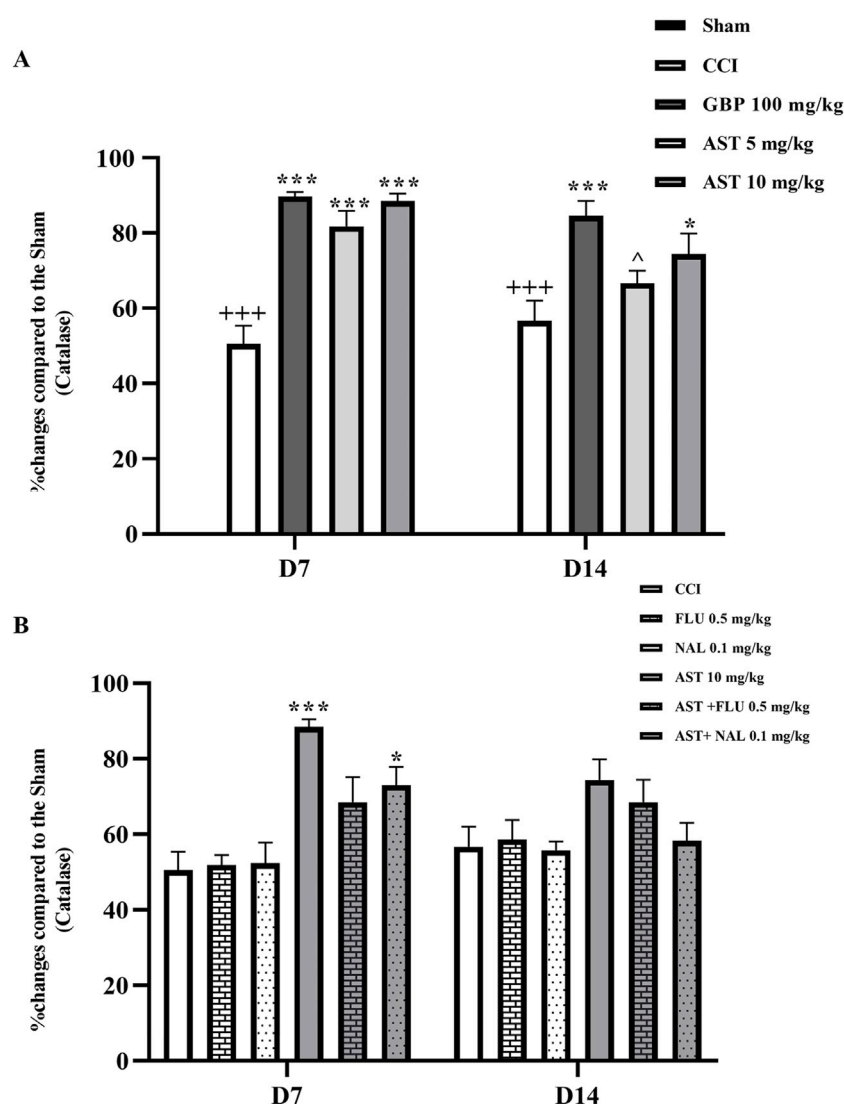


FIGURE 6

Effects of astaxanthin on the serum level of catalase and its mechanisms after CCI in rats. CCI significantly decreased catalase level, which was reversed by AST 10 mg/kg (A). While FLU and NAL alone did not affect serum catalase level, those administrations with AST partially reduced AST's effects (B). The data are shown as mean \pm SEM ($n = 3$). $+++p < 0.001$ vs. sham, $*p < 0.05$, $***p < 0.001$ vs. CCI, $p < 0.05$ vs. GBP. CCI, chronic constriction injury, GBP, Gabapentin, AST, Astaxanthin, FLU, Flumazenil, NAL, Naloxone.

inflammation. Additionally, compared to other peripheral neuropathy models, the CCI model induces long-lasting and widespread behavioral changes (Bennett and Xie, 1988; Austin et al., 2012). CCI-induced neuropathic pain is associated with the release of pro-inflammatory molecules, such as cytokines and chemokines, which activate immune cells and promote oxidative stress. One possible mechanism is the imbalance of the antioxidant defense system. Antioxidant enzymes like superoxide dismutase, glutathione peroxidase, and catalase are impaired, reducing the body's ability to counteract oxidative stress (Naik et al., 2006). The second proposed mechanism is the activation of NADPH oxidase, an enzyme complex that generates ROS in peripheral nerves and the spinal cord following nerve injury. ROS can directly damage nerve tissues and increase the excitability of nociceptive neurons, leading to enhanced pain signaling (Cui et al., 2023). Additionally, nerve injury can disrupt

mitochondrial function, leading to an increase in ROS production (Ilari et al., 2020). In line, other evidence also revealed a relationship between oxidative imbalance and neuropathic pain (Di Cesare Mannelli et al., 2016). Moreover, activation of pro-inflammatory pathways by the activation of glial cells and the release of inflammatory mediators, can induce oxidative stress and contribute to neuropathic pain development. This sustained neuroinflammation further contributes to neuropathic pain by promoting neuronal hyperexcitability and impairing nerve regeneration (Komirishetty et al., 2016; Ilari et al., 2020). Therefore, experimental interventions that can reduce oxidative stress can also reduce neuropathic pain symptoms in CCI models.

AST, a potent antioxidant found in marine organisms, has been proposed as a potential treatment for neuropathic pain due to its antioxidant, anti-inflammatory, and neuroprotective properties. Studies have shown that AST can improve

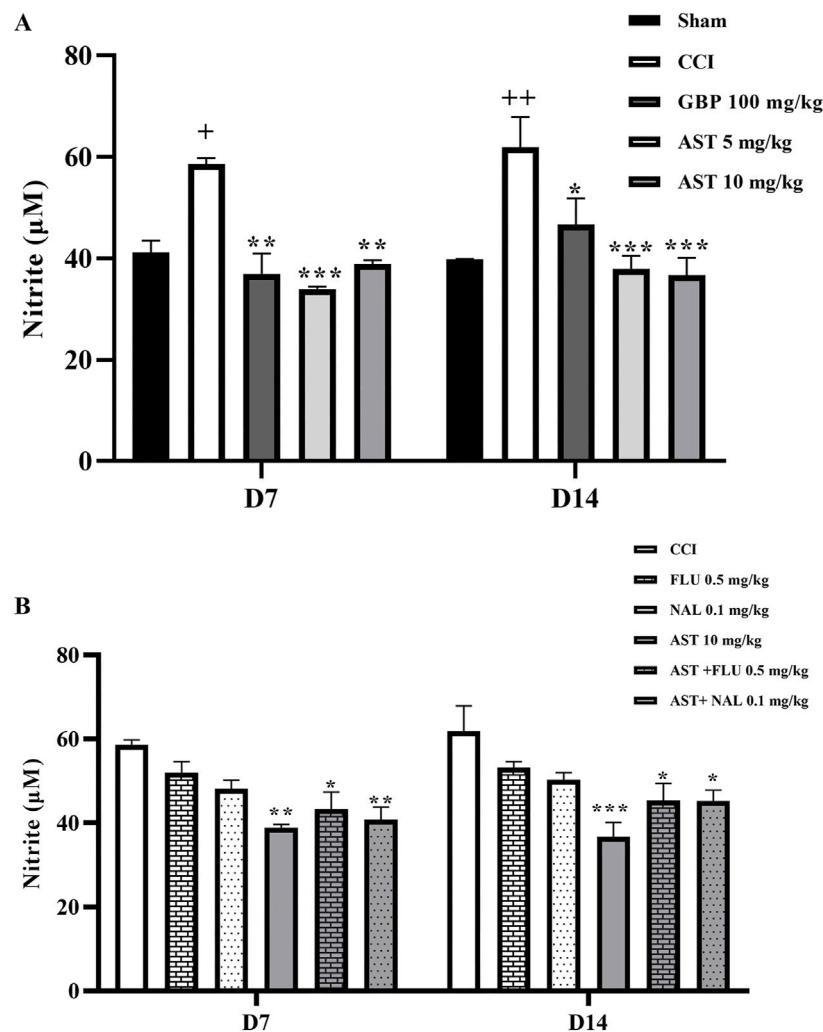


FIGURE 7

Effects of astaxanthin on serum level of nitrite and its mechanisms after CCI in rats. CCI significantly increased nitrite level, which was reversed by AST 10 mg/kg (A). While FLU and NAL alone did not affect serum nitrite level, those administrations with AST partially reduced AST's effects (B). The data are shown as mean \pm SEM ($n = 3$). $^*p < 0.05$, $^{++}p < 0.01$ vs. sham, $^*p < 0.05$, $^{**}p < 0.01$, $^{***}p < 0.001$ vs. CCI. CCI, chronic constriction injury; GBP, Gabapentin; AST, Astaxanthin; FLU, Flumazenil; NAL, Naloxone.

behavioral and biochemical changes under *in vitro* and *in vivo* models of neuropathic pain. During a more related study with intraperitoneal administration of AST, we used 5, 10, and 20 mg/kg doses and found an inverted U-shaped dose-response effectiveness of AST against nociceptive pain (Mohammadi et al., 2021). Our previous results were in line with the quantitative features of the hormetic dose-response models (Calabrese, 2008). In the current study, in line with the findings of others, we showed that AST reduces neuropathic pain and improves motor performance by affecting oxidative stress specially at the dose of 10 mg/kg. This is achieved by the ability of AST to effectively inhibit MAPKs and nuclear factor- κ B pathways, mitigate oxidative stress, and suppress the production of inflammatory cytokines (Zhao et al., 2021; Ciapała et al., 2023).

On the other hand, the upregulation of MMP-9 and MMP-2 in the peripheral nerves contributes to the development and

maintenance of neuropathic pain after CCI. MMP-9 and MMP-2 activate pro-inflammatory pathways such as the release of pro-inflammatory cytokines and chemokines. Such inflammatory mediators can further perpetuate the inflammatory response and contribute to the development and maintenance of neuropathic pain. They can also modulate the activity of ion channels and receptors involved in pain signaling, such as N-methyl-D-aspartate receptors and transient receptor potential channels, leading to increased pain sensitivity. MMP-9 induces early-phase neuropathic pain by activating interleukin (IL)-1 β and microglia in the early phase, while MMP-2 is implicated in the development of late-phase neuropathic pain. Therefore, inhibition of MMP-9 or MMP-2 may help reduce neuropathic pain (Ru-Rong et al., 2008; Lakhan and Avramut, 2012; Gu et al., 2019). In a study by Ciapała et al. (2023), the analgesic effect of a single intrathecal dose of AST in mice during 7 days was shown to be mediated

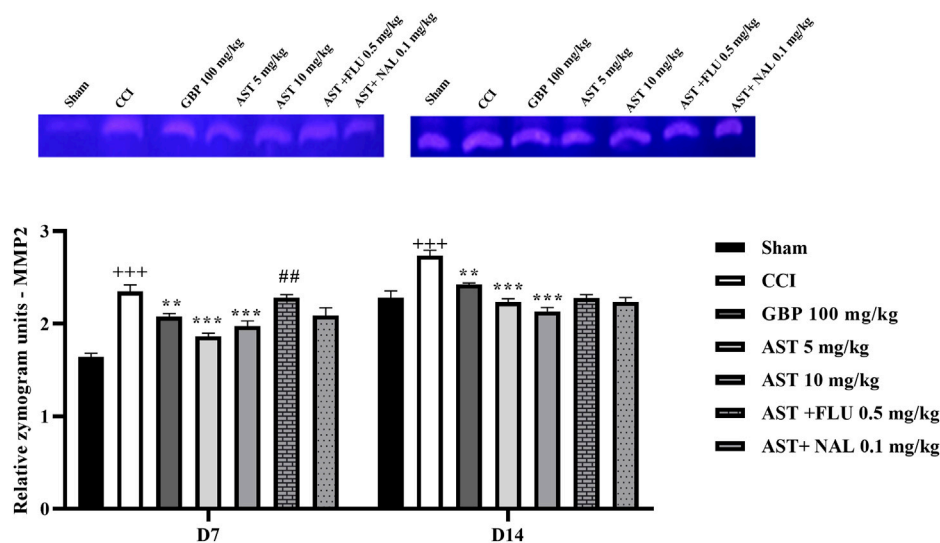


FIGURE 8
Effects of astaxanthin on serum MMP-2 activity after CCI in rats. The data are shown as mean \pm SEM ($n = 3$). ⁺⁺⁺ $p < 0.01$ vs. sham, ^{**} $p < 0.01$, ^{***} $p < 0.001$ vs. CCI, ^{##} $p < 0.01$ vs. AST 10. CCI, chronic constriction injury; GBP, Gabapentin; AST, Astaxanthin; FLU, Flumazenil; MMP, Matrix metalloproteinase; NAL, Naloxone.

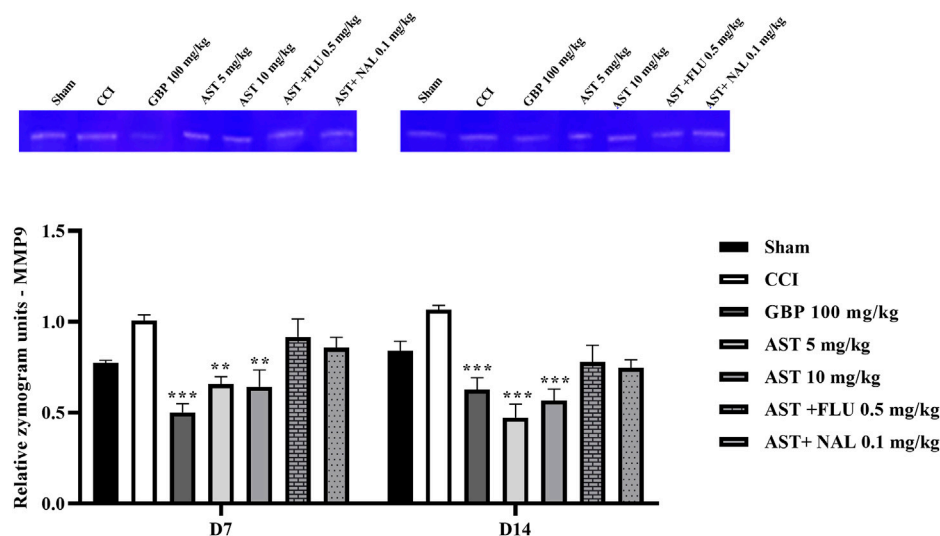


FIGURE 9
Effects of astaxanthin on serum MMP-9 activity after CCI in rats. The data are shown as mean \pm SEM ($n = 3$). ^{**} $p < 0.01$, ^{***} $p < 0.001$ vs. CCI. CCI, chronic constriction injury; GBP, Gabapentin; AST, Astaxanthin; FLU, Flumazenil; MMP, Matrix metalloproteinase; NAL, Naloxone.

through inhibiting mitogen-activated protein kinase and activating nuclear factor erythroid 2-related factor 2. They employed von Frey and cold plate tests for behavioral analysis and found that intrathecal administration of AST with morphine, buprenorphine or oxycodone resulted in greater decreases in tactile and cold allodynia. In our study and in comparison, for the first time we evaluated the anti-neuropathic effects of intraperitoneal AST in rats during 14 days. Additionally, we employed more behavioral tests, including von Frey, hot plate, acetone drop, as well as the motor-related test of open field to assess rearing, crossing, and grooming. From a mechanistic aspect, possible involvement of opioid and benzodiazepine receptors in the anti-neuropathic effects of AST was

examined using the corresponding antagonists, naloxone and flumazenil, respectively. From a molecular point of view, we evaluated oxidative (i.e., nitrite) and antioxidant (i.e., CAT and GSH) mediators, as well as inflammatory ones (e.g., MMP2 and MMP9). Also, in our study histopathological changes were compared in different groups (Ciapala et al., 2023).

Both benzodiazepine receptors (specifically the GABA-A receptor) and opioid receptors (such as mu, delta, and kappa receptors) play roles in pain modulation. They can interact with each other and have synergistic effects in reducing pain perception. Activation of benzodiazepine receptors enhances the analgesic

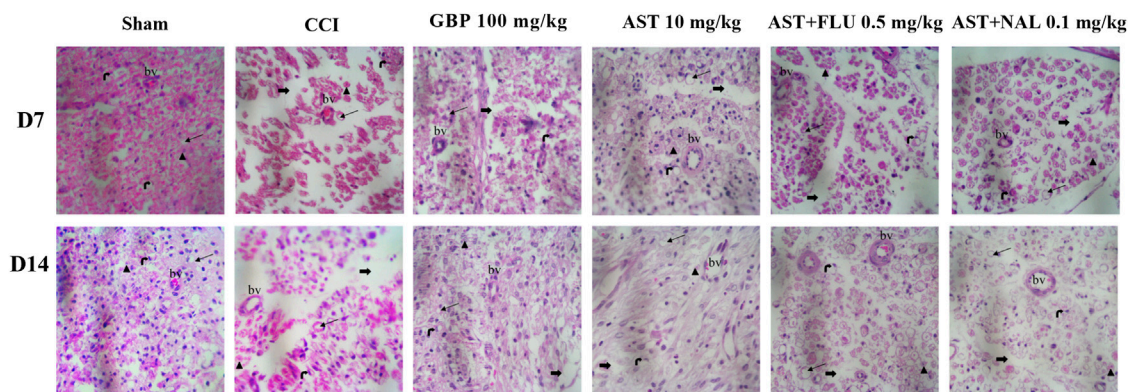


FIGURE 10
Representative photomicrographs (H&E, $\times 400$) of sciatic sections from different groups following CCI in rats ($n = 3$). Thick black arrows indicate neuron gaps (wide separation between the nerve fibers), Thin black arrows indicate the area of axonal swelling, Schwann cell nucleus (right black arrow), Axon (arrow blackhead), bv: blood vessel. CCI, chronic constriction injury; GBP, Gabapentin; AST, Astaxanthin; FLU, Flumazenil; NAL, Naloxone.

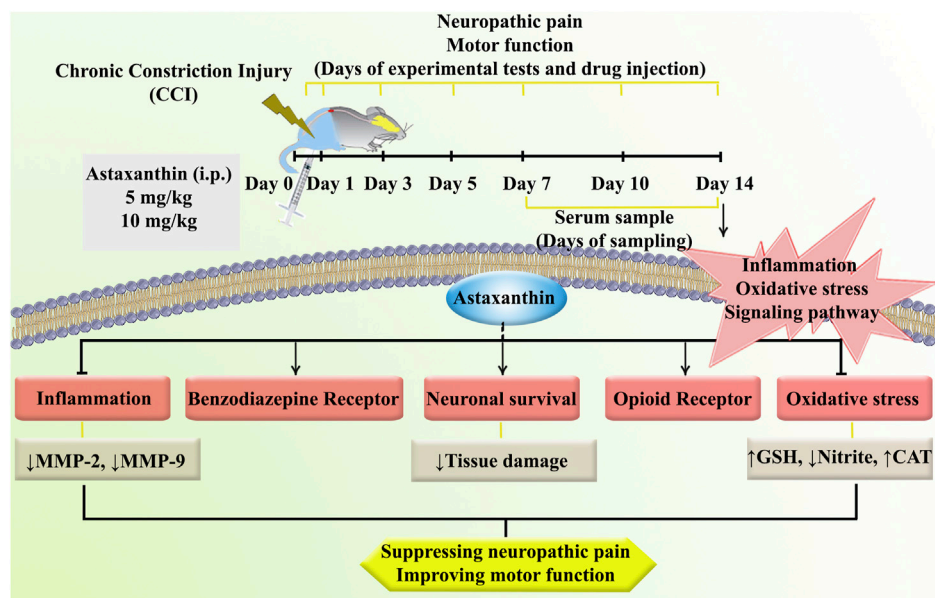


FIGURE 11
A summary of the research protocol and AST effects and mechanisms of action following CCI in rats.

effects of opioids, and vice versa (Gear et al., 1997; Primeaux et al., 2006). CCI has been found to affect the expression and function of benzodiazepine and opioid receptors, thereby impacting inhibitory neurotransmission and playing a role in the modulation of pain processing. Specifically, CCI leads to a decrease in benzodiazepine receptor binding, potentially contributing to the manifestation of anxiety-like behaviors (Shih et al., 2008; Lewis et al., 2012). We also found that AST successfully prevented hyperalgesia and anxiety-like behaviors in the CCI model. Furthermore, when we administered the benzodiazepine antagonist flumazenil or naloxone with AST, the therapeutic effect of AST was suppressed.

According to our tissue analysis, the effect of AST in reducing neuropathic pain is associated with maintaining the structural integrity of the sciatic nerve, regulating myelin sheaths, hemorrhage between cells, and wide separation between nerve fibers. Suppressing

inflammation and oxidative stress could lead to tissue repair during 14 days of AST treatment, which passes through benzodiazepine/opioid receptors. Blocking opioid and benzodiazepine receptors also reduced the therapeutic potential of AST and tissue repair.

5 Conclusion

In conclusion, the findings demonstrated the promising potential of AST as a viable candidate for neuropathic pain treatment and motor function. Through its ability to pass through opioid/benzodiazepine receptors, AST has the potential to suppress inflammatory and oxidative mediators, while enhance antioxidant factors. Further research and clinical trials are warranted to solidify its efficacy and safety profile.

Data availability statement

The datasets generated during and/or analyzed during the current study are available from the corresponding author upon reasonable request.

Ethics statement

The animal study was approved by Dr. Mahmoodreza Moradi, Kermanshah University of Medical Sciences Dr. Reza Khodarahmi, Kermanshah University of Medical Sciences. The study was conducted in accordance with the local legislation and institutional requirements.

Author contributions

BH: Investigation, Writing–original draft. SF: Conceptualization, Formal Analysis, Methodology, Software, Supervision, Writing–original draft, Writing–review and editing. AK: Methodology, Supervision, Writing–original draft. FA: Formal Analysis, Methodology, Writing–original draft. SM: Formal Analysis, Writing–original draft. MM: Formal Analysis, Writing–original draft. JE: Writing–original draft, Writing–review and editing.

Funding

The author(s) declare that financial support was received for the research, authorship, and/or publication of this article.

Acknowledgments

The authors acknowledged the Pharmaceutical Sciences Research Center, Kermanshah University of Medical Sciences, for the special Grant No.4000586.

References

- Aebi, H. (1984). Catalase *in vitro*. *Methods Enzym.* 105, 121–126. doi:10.1016/S0076-6879(84)05016-3
- Amin, B., Poureshagh, E., and Hosseinzadeh, H. (2016). The effect of verbascoside in neuropathic pain induced by chronic constriction injury in rats. *Phyther. Res.* 30, 128–135. doi:10.1002/ptr.5512
- Austin, P. J., Wu, A., and Moalem-Taylor, G. (2012). Chronic constriction of the sciatic nerve and pain hypersensitivity testing in rats. *J. Vis. Exp.* 3393, 3393. doi:10.3791/3393
- Bakare, A. O., and Owoyele, B. V. (2020). Antinociceptive and neuroprotective effects of bromelain in chronic constriction injury-induced neuropathic pain in Wistar rats. *Korean J. Pain* 33, 13–22. doi:10.3344/kjp.2020.33.1.13
- Bennett, G. J., and Xie, Y.-K. (1988). A peripheral mononeuropathy in rat that produces disorders of pain sensation like those seen in man. *Pain* 33, 87–107. doi:10.1016/0304-3959(88)90209-6
- Calabrese, E. J. (2008). Pain and u-shaped dose responses: occurrence, mechanisms, and clinical implications. *Crit. Rev. Toxicol.* 38, 579–590. doi:10.1080/10408440802026281
- Ciapała, K., Rojewska, E., Pawlik, K., Ciechanowska, A., and Mika, J. (2023). Analgesic effects of fisetin, peimine, astaxanthin, artemisinin, bardoxolone methyl and 740 Y-P and their influence on opioid analgesia in a mouse model of neuropathic pain. *Int. J. Mol. Sci.* 24, 9000. doi:10.3390/ijms24109000
- Colloca, L., Ludman, T., Bouhassira, D., Baron, R., Dickenson, A. H., Yarnitsky, D., et al. (2017). Neuropathic pain. *Nat. Rev. Dis. Prim.* 3, 17002. doi:10.1038/nrdp.2017.2
- Cui, C., Liu, H., Yue, N., Du, Y., Che, L., and Yu, J. (2023). Research progress on the mechanism of chronic neuropathic pain. *IBRO Neurosci. Rep.* 14, 80–85. doi:10.1016/j.ibneur.2022.12.007
- Di Cesare Mannelli, L., Zanardelli, M., Landini, I., Pacini, A., Ghelardini, C., Mini, E., et al. (2016). Effect of the SOD mimetic MnL4 on *in vitro* and *in vivo* oxaliplatin toxicity: possible aid in chemotherapy induced neuropathy. *Free Radic. Biol. Med.* 93, 67–76. doi:10.1016/j.freeradbiomed.2016.01.023
- Fakhri, S., Abbaszadeh, F., Dargahi, L., and Jorjani, M. (2018a). Astaxanthin: a mechanistic review on its biological activities and health benefits. *Pharmacol. Res.* 136, 1–20. doi:10.1016/j.phrs.2018.08.012
- Fakhri, S., Abbaszadeh, F., and Jorjani, M. (2021a). On the therapeutic targets and pharmacological treatments for pain relief following spinal cord injury: a mechanistic review. *Biomed. Pharmacother.* 139, 111563. doi:10.1016/j.biopha.2021.111563
- Fakhri, S., Dargahi, L., Abbaszadeh, F., and Jorjani, M. (2018b). Astaxanthin attenuates neuroinflammation contributed to the neuropathic pain and motor

Conflict of interest

The authors declare that the research was conducted in the absence of any commercial or financial relationships that could be construed as a potential conflict of interest.

The author(s) declared that they were an editorial board member of Frontiers, at the time of submission. This had no impact on the peer review process and the final decision.

Publisher's note

All claims expressed in this article are solely those of the authors and do not necessarily represent those of their affiliated organizations, or those of the publisher, the editors and the reviewers. Any product that may be evaluated in this article, or claim that may be made by its manufacturer, is not guaranteed or endorsed by the publisher.

Supplementary material

The Supplementary Material for this article can be found online at: <https://www.frontiersin.org/articles/10.3389/fphar.2024.1467788/full#supplementary-material>

SUPPLEMENTARY FIGURE 1

Refusing the role of intraperitoneal solvent volume on neuropathic pain after CCI. No difference was shown between sham and sham + v2 and also between CCI and CCI + v2 in different days. The data are shown as mean \pm SEM ($n = 6$). $***p < 0.01$ vs. sham, $***p < 0.001$ vs. sham + v2. CCI: chronic constriction injury, DW: distilled water. Sham [Sham receiving DMSO 5% (v1)], Sham + v2 [Sham receiving DMSO 5% (v1) + DW (v2)], CCI [CCI receiving DMSO 5% (v1)], CCI + v2 [CCI receiving DMSO 5% (v1) + DW (v2)].

SUPPLEMENTARY FIGURE 2

Refusing the role of intraperitoneal solvent volume on motor dysfunction after CCI. No difference was shown between sham and sham + v2 and also between CCI and CCI + v2 in different days. The data are shown as mean \pm SEM ($n = 6$). $***p < 0.01$ vs. sham, $***p < 0.001$ vs. sham + v2. CCI: chronic constriction injury, DW: distilled water. Sham [Sham receiving DMSO 5% (v1)], Sham + v2 [Sham receiving DMSO 5% (v1) + DW (v2)], CCI [CCI receiving DMSO 5% (v1)], CCI + v2 [CCI receiving DMSO 5% (v1) + DW (v2)].

dysfunction following compression spinal cord injury. *Brain Res. Bull.* 143, 217–224. doi:10.1016/j.brainresbull.2018.09.011

Fakhri, S., Dargahi, L., Abbaszadeh, F., and Jorjani, M. (2019). Effects of astaxanthin on sensory-motor function in a compression model of spinal cord injury: involvement of ERK and AKT signalling pathway. *Eur. J. Pain* 23, 750–764. doi:10.1002/ejp.1342

Fakhri, S., Kiani, A., Jalili, C., Abbaszadeh, F., Piri, S., Farzaei, M. H., et al. (2021b). Intrathecal administration of melatonin ameliorates the neuroinflammation-mediated sensory and motor dysfunction in A rat model of compression spinal cord injury. *Curr. Mol. Pharmacol.* 14, 646–657. doi:10.2174/1874467213666201230101811

Fakhri, S., Sabouri, S., Kiani, A., Farzaei, M. H., Rashidi, K., Mohammadi-Farani, A., et al. (2022). Intrathecal administration of naringenin improves motor dysfunction and neuropathic pain following compression spinal cord injury in rats: relevance to its antioxidant and anti-inflammatory activities. *Korean J. Pain* 35, 291–302. doi:10.3344/kjp.2022.35.3.291

Finnerup, N. B., Attal, N., Haroutounian, S., McNicol, E., Baron, R., Dworkin, R. H., et al. (2015). Pharmacotherapy for neuropathic pain in adults: a systematic review and meta-analysis. *Lancet Neurol.* 14, 162–173. doi:10.1016/S1474-4422(14)70251-0

Fonseca-Rodrigues, D., Amorim, D., Almeida, A., and Pinto-Ribeiro, F. (2021). Emotional and cognitive impairments in the peripheral nerve chronic constriction injury model (CCI) of neuropathic pain: a systematic review. *Behav. Brain Res.* 399, 113008. doi:10.1016/j.bbr.2020.113008

Gear, R. W., Miaskowski, C., Heller, P. H., Paul, S. M., Gordon, N. C., and Levine, J. D. (1997). Benzodiazepine mediated antagonism of opioid analgesia. *Pain* 71, 25–29. doi:10.1016/S0304-3959(97)03332-0

Gu, H.-W., Xing, F., Jiang, M.-J., Wang, Y., Bai, L., Zhang, J., et al. (2019). Upregulation of matrix metalloproteinase-9/2 in the wounded tissue, dorsal root ganglia, and spinal cord is involved in the development of postoperative pain. *Brain Res.* 1718, 64–74. doi:10.1016/j.brainres.2019.05.007

Ilari, S., Giancotti, L. A., Lauro, F., Gliozzi, M., Malafoglia, V., Palma, E., et al. (2020). Natural antioxidant control of neuropathic pain—exploring the role of mitochondrial SIRT3 pathway. *Antioxidants* 9, 1103. doi:10.3390/antiox9111103

Jensen, T. S., and Finnerup, N. B. (2014). Allodynia and hyperalgesia in neuropathic pain: clinical manifestations and mechanisms. *Lancet Neurol.* 13, 924–935. doi:10.1016/S1474-4422(14)70102-4

Jones, C. M. P., Day, R. O., Koes, B. W., Latimer, J., Maher, C. G., McLachlan, A. J., et al. (2023). Opioid analgesia for acute low back pain and neck pain (the OPAL trial): a randomised placebo-controlled trial. *Lancet* 402, 304–312. doi:10.1016/S0140-6736(23)00404-X

Kauppila, T. (2000). Cold exposure enhances tactile allodynia transiently in mononeuropathic rats. *Exp. Neurol.* 161, 740–744. doi:10.1006/exnr.1999.7287

Kiguchi, N., Kobayashi, Y., and Kishioka, S. (2012). Chemokines and cytokines in neuroinflammation leading to neuropathic pain. *Curr. Opin. Pharmacol.* 12, 55–61. doi:10.1016/j.coph.2011.10.007

Komirishetty, P., Areti, A., Sistla, R., and Kumar, A. (2016). Morin mitigates chronic constriction injury (CCI)-Induced peripheral neuropathy by inhibiting oxidative stress induced PARP over-activation and neuroinflammation. *Neurochem. Res.* 41, 2029–2042. doi:10.1007/s11064-016-1914-0

Lakhan, S. E., and Avramut, M. (2012). Matrix metalloproteinases in neuropathic pain and migraine: friends, enemies, and therapeutic targets. *Pain Res. Treat.* 2012, 952906. doi:10.1155/2012/952906

Lape, E. C., Powers, J. M., Hooker, J. E., Edwards, R. R., and Ditte, J. W. (2023). Benzodiazepine use and dependence in relation to chronic pain intensity and pain catastrophizing. *J. Pain* 24, 345–355. doi:10.1016/j.jpain.2022.09.019

Lewis, S. S., Loram, L. C., Hutchinson, M. R., Li, C.-M., Zhang, Y., Maier, S. F., et al. (2012). (+)-Naloxone, an opioid-inactive toll-like receptor 4 signaling inhibitor, reverses multiple models of chronic neuropathic pain in rats. *J. Pain* 13, 498–506. doi:10.1016/j.jpain.2012.02.005

Malcangio, M., Clark, A. K., and Old, E. A. (2013). Neuropathic pain and cytokines: current perspectives. *J. Pain Res.* 6, 803–814. doi:10.2147/JPR.S53660

Mir, S., Wong, J., Ryan, C. M., Bellingham, G., Singh, M., Waseem, R., et al. (2020). Concomitant benzodiazepine and opioids decrease sleep apnoea risk in chronic pain patients. *ERJ Open Res.* 6, 00093-2020–02020. doi:10.1183/23120541.00093-2020

Mohammadi, S., Fakhri, S., Mohammadi-Farani, A., Farzaei, M. H., and Abbaszadeh, F. (2021). Astaxanthin engages the l-arginine/NO/cGMP/KATP channel signaling

pathway toward antinociceptive effects. *Behav. Pharmacol.* 32, 607–614. doi:10.1097/FBP.0000000000000655

Muthuraman, A., Diwan, V., Jaggi, A. S., Singh, N., and Singh, D. (2008). Ameliorative effects of Ocimum sanctum in sciatic nerve transection-induced neuropathy in rats. *J. Ethnopharmacol.* 120, 56–62. doi:10.1016/j.jep.2008.07.049

Naik, A. K., Tandan, S. K., Dudhgaonkar, S. P., Jadhav, S. H., Kataria, M., Prakash, V. R., et al. (2006). Role of oxidative stress in pathophysiology of peripheral neuropathy and modulation by N-acetyl-L-cysteine in rats. *Eur. J. Pain* 10, 573–579. doi:10.1016/j.ejpain.2005.08.006

O'Connell, M., Sandgren, M., Frantzen, L., Bower, E., and Erickson, B. (2019). Medical cannabis: effects on opioid and benzodiazepine requirements for pain control. *Ann. Pharmacother.* 53, 1081–1086. doi:10.1177/1060028019854221

Parvardeh, S., and Hosseinzadeh, H. (2003). Hypnotic and muscle relaxant activity of thymoquinone, the major active constituent of *Nigella sativa* seeds, and its effects on locomotor activity and motor coordination in mice. *J. Med. Plants* 2, 17–26.

Parvardeh, S., Moghimi, M., Eslami, P., and Masoudi, A. (2016). α -Terpineol attenuates morphine-induced physical dependence and tolerance in mice: role of nitric oxide. *Iran. J. Basic Med. Sci.* 19, 201–208. doi:10.22038/ijbms.2016.6546

Primeaux, S., Wilson, S., McDonald, A., Mascagni, F., and Wilson, M. (2006). The role of delta opioid receptors in the anxiolytic actions of benzodiazepines. *Pharmacol. Biochem. Behav.* 85, 545–554. doi:10.1016/j.pbb.2006.09.025

Ru-Rong, J., Xiaoying, W., and Zhen-Zhong, X. (2008). MMP-2 and MMP-9 investigations in neuropathic pain phases. *U. S. Neurol.* 4, 71–74. doi:10.17925/USN.2008.04.02.71

Sharma, A., Fish, B. L., Moulder, J. E., Medhora, M., Baker, J. E., Mader, M., et al. (2014). Safety and blood sample volume and quality of a refined retro-orbital bleeding technique in rats using a lateral approach. *Lab. Anim. (NY)* 43, 63–66. doi:10.1038/labani.432

Sharma, K., Sharma, D., Sharma, M., Sharma, N., Bidve, P., Prajapati, N., et al. (2018). Astaxanthin ameliorates behavioral and biochemical alterations in *in-vitro* and *in-vivo* model of neuropathic pain. *Neurosci. Lett.* 674, 162–170. doi:10.1016/j.neulet.2018.03.030

Shih, A., Miletic, V., Miletic, G., and Smith, L. J. (2008). Midazolam administration reverses thermal hyperalgesia and prevents γ -aminobutyric acid transporter loss in a rodent model of neuropathic pain. *Anesth. Analg.* 106, 1296–1302. doi:10.1213/ane.0b013e318164f1e9

Soleimani, M., Sheikholeslami, M. A., Ghafghazi, S., Pouriran, R., and Parvardeh, S. (2019). Analgesic effect of α -terpineol on neuropathic pain induced by chronic constriction injury in rat sciatic nerve: involvement of spinal microglial cells and inflammatory cytokines. *Iran. J. Basic Med. Sci.* 22, 1445–1451. doi:10.22038/IJBMS.2019.14028

Sudoh, Y., Desai, S., Haderer, A., Sudoh, S., Gerner, P., Anthony, D., et al. (2004). Neurologic and histopathologic evaluation after high-volume intrathecal amitriptyline. *Reg. Anesth. Pain Med.* 29, 434–440. doi:10.1016/j.rapm.2004.06.008

Sun, J., Zhang, X., Broderick, M., and Fein, H. (2003). Measurement of nitric oxide production in biological systems by using griess reaction assay. *Sensors* 3, 276–284. doi:10.3390/s30800276

Tipple, T. E., and Rogers, L. K. (2012). “Methods for the determination of plasma or tissue glutathione levels,” in *Developmental toxicology*, 315–324. doi:10.1007/978-1-61779-867-2_20

Treede, R.-D., Jensen, T. S., Campbell, J. N., Cruccu, G., Dostrovsky, J. O., Griffin, J. W., et al. (2008). Neuropathic pain: redefinition and a grading system for clinical and research purposes. *Neurology* 70, 1630–1635. doi:10.1212/01.wnl.0000282763.29778.59

Zarneshan, S. N., Fakhri, S., Farzaei, M. H., Khan, H., and Saso, L. (2020). Astaxanthin targets PI3K/Akt signaling pathway toward potential therapeutic applications. *Food Chem. Toxicol.* 145, 111714. doi:10.1016/j.fct.2020.111714

Zhang, X., Wang, J., Sui, A., Zhang, N., Lv, Q., and Liu, Z. (2021). Antinociceptive effect of magnolol in a neuropathic pain model of mouse. *J. Pain Res.* 14, 2083–2093. doi:10.2147/JPR.S317204

Zhao, L., Tao, X., and Song, T. (2021). Astaxanthin alleviates neuropathic pain by inhibiting the MAPKs and NF- κ B pathways. *Eur. J. Pharmacol.* 912, 174575. doi:10.1016/j.ejphar.2021.174575



OPEN ACCESS

EDITED BY

Jian Hao,
The Second Affiliated Hospital of Guangzhou
Medical University, China

REVIEWED BY

Zheng Yuan,
China Academy of Chinese Medical Sciences,
China
Yong Chen,
Affiliated Hospital of Zunyi Medical University,
China

*CORRESPONDENCE

Xiaohua Duan,
✉ 1047896527@qq.com

RECEIVED 27 December 2024

ACCEPTED 04 February 2025

PUBLISHED 25 February 2025

CITATION

Cheng J, Ma X, Tao J, Jiang X, Chen P and
Duan X (2025) Neuroprotective effects of
ethanol extraction from *Rubia yunnanensis*
Diels on chronic cerebral hypoperfusion:
modulation of the System Xc⁻/GSH/GPX4 axis
to alleviate oxidative stress and ferroptosis.
Front. Pharmacol. 16:1552228.
doi: 10.3389/fphar.2025.1552228

COPYRIGHT

© 2025 Cheng, Ma, Tao, Jiang, Chen and Duan.
This is an open-access article distributed under
the terms of the [Creative Commons Attribution
License \(CC BY\)](#). The use, distribution or
reproduction in other forums is permitted,
provided the original author(s) and the
copyright owner(s) are credited and that the
original publication in this journal is cited, in
accordance with accepted academic practice.
No use, distribution or reproduction is
permitted which does not comply with these
terms.

Neuroprotective effects of ethanol extraction from *Rubia yunnanensis* Diels on chronic cerebral hypoperfusion: modulation of the System Xc⁻/GSH/GPX4 axis to alleviate oxidative stress and ferroptosis

Jianghao Cheng, Xiaoxia Ma, Jie Tao, Xiaoli Jiang, Pu Chen and
Xiaohua Duan*

Yunnan Key Laboratory of Dai and Yi Medicines, Yunnan University of Chinese Medicine, Kunming,
Yunnan, China

Introduction: Vascular dementia (VD) is a neurodegenerative disease caused by chronic cerebral hypoperfusion (CCH), which considerably impact patients' quality of life. Ethanol extraction from *Rubia yunnanensis* (RY-A) has gained attention for its potential neuroprotective effects, but its effects and mechanisms of action on CCH are unknown.

Methods: After 30 days of RY-A gavage treatment in a CCH rat model, its effects were evaluated using the Morris water maze test, cerebral blood flow measurements, and HE staining of the brain. These findings, combined with serum medicinal chemistry, RNA-seq, and metabolomics analyses, revealed the active compounds and mechanisms of RY-A in CCH rats. The results were further validated using assay kits and Western blot techniques.

Results: RY-A treatment significantly attenuated neurological damage and improved cognitive function in CCH rats. Ultra-high-performance liquid chromatography high-resolution mass spectrometry identified 511 blood-entry compounds of RY-A. RNA-seq and metabolomic analysis showed that RY-A might help to normalize changes in gene and metabolite expression caused by CCH. RY-A induced neuroprotective effects by increasing the production of key proteins involved in ferroptosis inhibition, such as SLC7A11, SLC3A2, GSS, and GPX4, while increasing antioxidant enzyme activities and alleviating oxidative stress.

Abbreviations: BPC, base peak chromatogram; CCH, chronic cerebral hypoperfusion; CBF, cerebral blood flow; DEGs, differentially expressed genes; DEMs, differentially expressed metabolites; FPKM, fragments per kilobase of transcript per million fragments mapped; GO, Gene Ontology; HE, hematoxylin and eosin; KEGG, Kyoto Encyclopedia of Genes and Genomes; LIP, labile iron pool; MRM, multiple reaction monitoring; OPLS-DA, orthogonal partial least squares discriminant analysis; RY-A, Ethanol extraction from *Rubia yunnanensis*; UHPLC-HRMS, ultra-high-performance liquid chromatography high-resolution mass spectrometry; VD, vascular dementia; XIC, extracted ion chromatograms; 2VO, two-vessel occlusion.

Conclusion: RY-A inhibited oxidative stress and ferroptosis by activating the System Xc-/GSH/GPX4 pathway and balancing iron metabolism, thereby attenuating CCH-induced neurological damage and cognitive deficits.

KEYWORDS

Rubia yunnanensis, chronic cerebral hypoperfusion, System Xc-/GSH/Gpx4, serum pharmacochimistry, metabolomic, transcriptomic

1 Introduction

Vascular dementia (VD) is a neurodegenerative disorder associated with chronic cerebral hypoperfusion (CCH), characterized by memory impairment, cognitive decline, and behavioral changes (Pendlebury et al., 2019). With its prevalence increasing annually, VD has become a major global public health challenge, exerting a growing impact on patients and their families (Gorelick et al., 2011). Although VD is the only form of dementia that may be prevented and treated through early interventions, its complex pathomechanisms, including inflammatory responses, impaired energy metabolism, and oxidative stress, pose substantial challenges to effective treatment (Darweesh et al., 2018; Zhu et al., 2021).

Oxidative stress and lipid peroxidation play central roles in the etiology and progression of VD (Cobley et al., 2018). These processes closely resemble ferroptosis, a type of cell death caused by disruptions in intracellular iron metabolism (Hirschhorn and Stockwell, 2019). Currently, therapeutic options for VD are limited. The primary drugs, edaravone and donepezil, are often associated with side effects, such as drug resistance, liver abnormalities, and cardiac arrhythmias (Liu et al., 2023b). Therefore, the development of new treatments is crucial to improve outcomes for patients with VD.

Rubia yunnanensis Diels, a traditional Chinese medicinal herb, has been included in the Dian Nan Ben Cao. Its rhizomes and roots have been shown to activate the blood circulation, remove blood stasis, and soothe tendons and collaterals, as well as to have antithrombotic, anti-ischemic, and antioxidant pharmacological effects (Lan, 1959; Zhang et al., 2022). Previous studies have shown that RY-A has a protective effect against hypoxia/reoxygenation-induced damage to hippocampal HT22 cells and ameliorates oxidative stress (Cheng et al., 2024). However, the effects of RY-A on CCH and its underlying mechanisms need to be further investigated.

Metabolomics and transcriptomics, powerful tools for the study of neurodegenerative diseases, are capable of identifying and quantifying a wide range of metabolites and differentially expressed genes (DEGs), offering profound insights into the molecular underpinnings of cerebrovascular disease (Horgusluoglu et al., 2022; Arbaizar-Rovirosa et al., 2023; Askew et al., 2024). When combined with serum and plasma pharmacochimical analyses of blood-entry drug compounds, the material basis of pharmacodynamic effects can be further explored (Jin et al., 2022; Zhao et al., 2024).

The possible therapeutic impact of RY-A on CCH and its mechanism of action were examined in this study using an integrated approach involving serum pharmacochimistry, metabolomics, transcriptomics, and verification via animal

experiments. Via these investigations, we aimed to establish a scientific foundation for the pharmacological effects of *Rubia yunnanensis* and offer novel perspectives on alternative preventive and treatment techniques for cerebral ischemia.

2 Materials and methods

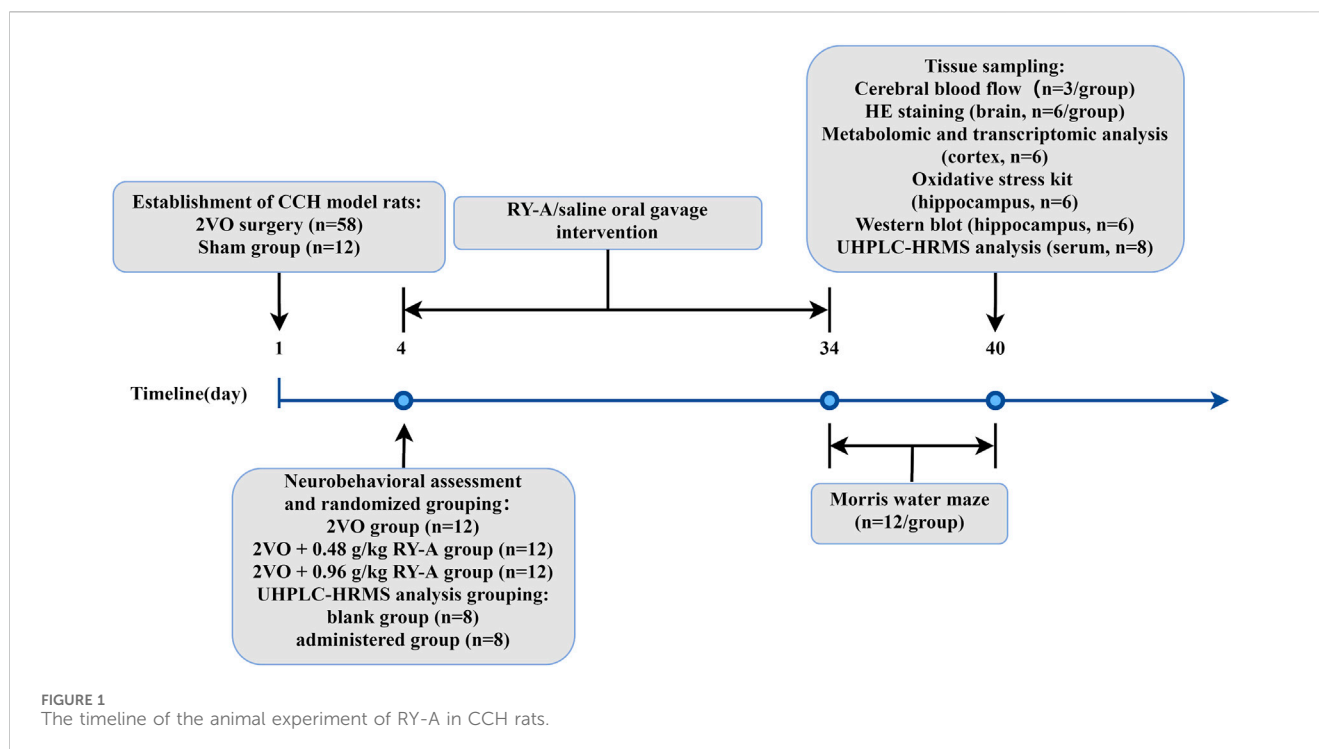
2.1 Drug preparation

The Yunnan Key Laboratory of Dai and Yi Medicines supplied the of *Rubia yunnanensis* Yi medicine powder that was used in this investigation. Prof. Zili Yin of Yunnan University of Chinese Medicine was responsible for the drug's authentication. The preparation process was as follows: First, 500 g of *Rubia yunnanensis* powder was taken and soaked in 95% ethanol for 24 h. Subsequently, the medicinal liquid was separated from the solid residue using a 0.22- μ m polytetrafluoroethylene filter membrane. The collected medicinal liquid was concentrated by heating at 45°C using a rotary evaporator (EYELA, Shanghai, China). To ensure adequate extraction, the entire steeping and concentration process was repeated three times. The final extract obtained was *Rubia yunnanensis* ethanol extraction (RY-A), which was stored at -80°C to maintain its stability and potency.

2.2 Animals and treatment

The 70 male Sprague-Dawley rats, weighing 260 ± 20 g and aged 8 weeks, used in this study were supplied by SiPeiFu (Beijing Biotechnology Co., Ltd.). The rats were acclimatized and fed for 1 week, and 58 of them were operated upon by two-vessel occlusion (2VO) to establish a CCH model, while the remaining 12 served as a control group (Sham group) with bilateral carotid artery exposure only, without ligation. All animals were housed at $21^\circ\text{C} \pm 2^\circ\text{C}$, provided with adequate food and distilled water, and maintained on a 12-hour diurnal schedule. The Yunnan University of Chinese Medicine's Ethics Committee for Animal Experimentation (Approval No. R-062022LH077) gave clearance for the use of animals in this study, and there was strict compliance with the pertinent standards of the National Institute for Animal Research.

On the third day after modeling, the model rats were assessed for neurobehavioral changes using a modified 5-point scale developed by Longa et al. (1989), with model success being marked by a score of 1–3. In this study, 52 model rats were deemed successful in the model construction assessment. Thirty-six of them were randomly divided into three groups according to the random number table method: CCH model group (2VO group), RY-A low-dose group (2VO + 0.48 g/kg RY-A), and RY-A high-dose group (2VO +



0.96 g/kg RY-A). The clinical dose of RY-A was 30 g, with an extraction yield of 17.63%, and the dosages administered to the rats were calculated based on body surface area conversion (Li et al., 2024). Another 16 model rats were randomly divided into two groups of 8 rats, the 2VO group (blank group) and the RY-A high-dose group (administered group), which were used for the qualitative and quantitative analysis of RY-A blood-entry compounds. Starting from the day of scoring, rats in each group received gavage intervention with a dosing volume of 1 mL/100 g of body weight, with equal volumes of 0.9% saline given to the Sham and 2VO groups, and the treatments lasted for 30 days. The timeline of the animal experiment is shown in Figure 1.

2.3 Morris water maze test

The cognitive functions of learning and memory were observed using a Morris water maze after the 30-day pharmacological intervention. The apparatus consisted of a cylindrical pool containing a circular platform 30 cm high and 10 cm in diameter. The pool was filled with tap water, kept at $25^{\circ}\text{C} \pm 0.5^{\circ}\text{C}$, and colored with ink to obscure the platform from the rat's view. Each rat was submerged in the water in the second quadrant of the pool, facing away from the platform, and the platform was placed in the fourth quadrant for testing. The main dependent variable measured was escape latency, i.e., the time a rat took to find and stay on the platform within 90 s. In case a rat failed to find the platform within the pre-specified time, the animal was guided to the platform and allowed to stay there for 10 s. Animals were trained four times a day, and the platform position was rotated clockwise to a new quadrant prior to each training session. The aforementioned training paradigm was executed for five consecutive days. A probe test was performed on the sixth day, during which the

platform was removed. Rats were introduced into the pool from the second quadrant, which was situated opposite to the initial platform location, and permitted to swim freely for a duration of 120 s. Shanghai Xinruan Information Technology's Super Maze System (Shanghai, China) was used to methodically record the behavioral data, encompassing the frequency of occurrences in the prior platform position and the duration spent in the target quadrant. These data provided us with quantitative information about the spatial memory capacity of the rats.

2.4 Cerebral blood flow and histological staining

After the behavioral assessment was completed, cerebral blood flow (CBF) measurements were performed on the rats. Under anesthesia, each rat's head was fixed, and the scalp was incised and cleaned along the median line to fully expose the skull. Using a PeriCam PSI blood flow monitoring video system from Perimed, Sweden, the rat brain was illuminated by a light beam at the location where the sagittal suture meets the coronal suture. The data were processed using PIMsoft 1.5 Operational Analysis Software, which monitored the CBF in rats in a resting state for 20 s and calculated the mean value.

Brain tissue sampling was performed after CBF measurement. The animals were subjected to anesthesia, after which the thoracic cavity was perfused with 250 mL of saline, followed by 100 mL of 4% paraformaldehyde. The brains underwent postfixation for a duration of 48 h in a 4% paraformaldehyde solution, followed by embedding in paraffin. Subsequently, serial coronal sections with a thickness of 3 μm were prepared for further staining analysis. In the interim, surplus hippocampal tissue was promptly cryopreserved in liquid nitrogen and subsequently maintained at -80°C . For

hematoxylin and eosin (HE) staining, paraffin-embedded slices that had been subjected to partial deparaffinization using xylene for 5 min were dehydrated via a step-by-step ethanol series (70%, 95%, and 100%, each for 5 min), and finally stained with HE. Histopathological changes in the hippocampal tissue were observed using CaseViewer 2.4 software, and images were taken at $\times 200$ magnification for further analysis.

2.5 Qualitative identification of RY-A blood-entry compounds

2.5.1 Extraction of RY-A samples

After transferring 600 μL of RY-A solution and 400 μL of pure methanol to a 1.5-mL EP tube, the mixture was vortexed for 10 s. Then, to 200 μL of this mixture, 200 μL of 40% aqueous methanol solution was added and vortexed to mix again for 10 s. At 4°C, after centrifugation at $16,000 \times g$ for 15 min, the supernatant was collected as the extracted sample.

2.5.2 Extraction of serum sample

An appropriate amount of serum sample was taken and vortexed with methanol for 60 s, then left at -20°C for 30 min. Following centrifugation at $16,000 \times g$ for a duration of 20 min at 4°C, the supernatant was collected and subjected to vacuum drying. The residue was subsequently re-dissolved in 100 μL of 40% aqueous methanol, subjected to vortex mixing, and centrifuged once more. The supernatant was collected as the extracted sample ($16,000 \times g$, 4°C, 15 min).

2.5.3 Extraction of blank serum + RY-A sample

An appropriate amount of blank serum sample was obtained, to which RY-A solution and methanol were added. The solution was subjected to vortexing for a duration of 60 s and subsequently permitted to equilibrate at a temperature of -20°C for a period of 30 min. After centrifugation at $16,000 \times g$ for 20 min at 4°C, the supernatant was obtained and subjected to vacuum drying. The dried residue was reconstituted in 100 μL of a 40% aqueous methanol solution. The extracted sample was obtained from the supernatant after further centrifugation at $16,000 \times g$ for 15 min at 4°C. This procedure ensured the thorough extraction and preparation of the samples and the provision of high-quality biological specimens for subsequent analysis.

2.6 Ultra-high-performance liquid chromatography–high-resolution mass spectrometry analysis

2.6.1 UHPLC conditions

Samples were evaluated with a Vanquish ultra-high-performance liquid chromatography–high-resolution mass spectrometry (UHPLC) system manufactured by Thermo Fisher Scientific, Germany, connected to an ACQUITY UPLC HSS T3 column with dimensions of 2.1 mm \times 100 mm and a particle size of 1.8 μm . The column temperature was set at 35°C with a flow rate of 0.3 mL/min. A 0.1% aqueous solution of formic acid (A) and a 0.1% acetonitrile solution (B) were used in the two mobile phases.

The gradient removal procedure below was applied by Thermo Scientific's SII software (version 1.4): the concentration of phase B commenced at 5%, escalating to 25% after 3 min, 45% after 8.5 min, 95% after 14 min, and reaching 98% at 17 min. Between 17 and 17.2 min, the B-phase fraction was decreased to 5% until the 20 min mark.

2.6.2 HRMS conditions

Q-exactive HFX mass spectrometry analysis was conducted to provide primary and secondary spectra for the samples. The mass spectrometer was connected to the UHPLC system, utilizing ESI (+/–) for the acquisition of the mass spectrum. The spray voltage was established at 3800 V (ESI+) and 3500 V (ESI–), the sheath gas pressure was maintained at 45 arb, the auxiliary gas pressure was set to 20 arb, the ion transfer tube temperature was regulated to 320°C, and the nebulization temperature was adjusted to 350°C. Detection occurred in full-MS/data-dependent secondary scanning (full-MS/dd-MS2) modes, with first-order and second-order resolutions of 60,000 and 15,000, respectively. The 10 highest-intensity MS1 ions were chosen for MS/MS spectrum capture, with collision energies set at normalized values of 20, 40, and 60 units. The principal mass-to-charge ratio scanning range was 90 m/z to 1,300 m/z .

2.6.3 Sample detection and analysis

Then, 6 μL of each blank group sample, administered group sample, blank group + RY-A sample, and RY-A solution were injected separately for liquid chromatography–mass spectrometry analysis. One injection of each batch of blank group samples and administered group samples was added, with repeated injections (3 for blank group + RY-A samples, 5 for RY-A samples). The proteoWizard software package was used to import the raw files (.raw) and convert them into the “.mzXML” format. Peak alignment, retention time adjustment, and peak extraction were performed with the XCMS program. The compounds were identified by querying the high-resolution mass spectrometry database of Shanghai Applied Protein Technology, with a primary mass error of less than 25 ppm and a secondary fragmentation spectrum match score exceeding 0.7. A higher score indicates greater spectral similarity, and a score of 0.7 or above is typically regarded as a dependable identification outcome.

2.7 Transcriptomic analysis

Total RNA was extracted from the left cortical region of rats using the Trizol method (Joy et al., 2018). Extracted RNA samples were solubilized in diethylpyrocarbonate-treated water, then analyzed qualitatively and quantitatively using a Qubit fluorescence quantimeter from Thermo Fisher Scientific (MA, USA) and a Qsep400 high-throughput biofragment analyzer from BiOptic Inc. (Taiwan, China). The mRNA with polyA tails were enhanced using Oligo (dT) beads with magnets, then fragmented at the specified temperature. These fragments served as templates for reverse transcription utilizing random hexamer primers to generate the first-strand cDNA, followed by the synthesis of the second-strand cDNA. dUTP was employed instead of dTTP in this process to achieve the doping of the second strand of the cDNA and the repair of the double-stranded cDNA ends. Next, sequencing adapter

ligation was performed, and DNA magnetic bead purification and fragment selection were used to obtain 250-bp to 350-bp insert fragments, then PCR amplification was performed. The constructed libraries were quality checked on the Qubit instrument and Qsep400 instrument and were accurately quantified to assure the effective Q-PCR concentration, which is usually considered to be greater than 2 nM. Metware Biotechnology Co. Ltd. (Wuhan, China) used the Illumina platform to sequence the qualifying libraries. HISAT2 version 2.2.1 software (<https://daehwankimlab.github.io/hisat2/>) was used to match clean reads to the reference genome sequence. Gene comparisons were conducted utilizing the featureCounts tool, while gene expression levels were assessed by the fragments per kilobase of transcript per million fragments mapped (FPKM) methodology. Then, the transcriptomes of the RY-A group and 2VO group were compared with DESeq2, with three biological replicates of each group. Genes were categorized as DEGs if their corrected *p*-value was less than 0.05 and their $|\log_2$ fold change (FC)| was more than 1. Ultimately, the clustering procedure was performed to elucidate the expression patterns of the DEGs across various experimental settings utilizing the R package. The enrichment of DEGs was studied using a hypergeometric test. For KEGG pathway (<http://www.genome.jp/kegg/>) and GO annotation (<http://www.ebi.ac.uk/QuickGO/>), the hypergeometric distribution test and GO term analysis were performed, respectively.

2.8 Metabolomic analysis

To thoroughly examine RY-A's metabolic effects on the CCH rat model, metabolomic analysis was performed on the right cortical region of rats from the RY-A and 2VO groups. Initially, six samples from each group were homogenized for 20 s in a ball mill at a frequency of 30 Hz. Centrifugation was used to sediment the samples for 30 s at 4°C and 3,000 × *g*. Four hundred microliters of a methanol-water internal standard extract were added to the samples, shaken at 2,500 revolutions per minute for 5 min, and allowed to stand on ice for 15 min. Then, at the same temperature as used previously, the samples were centrifuged for 10 min at 12,000 × *g*. After 30 min, 300 µL of the supernatant was removed and kept at −20°C. Following 3 minutes of centrifugation at 12,000 × *g*, 200 µL of the supernatant was taken for analysis by mass spectrometry.

The UPLC parameters were delineated as follows: The column employed was a Waters ACQUITY UPLC HSS T3 C18 (1.8 µm, 2.1 mm × 100 mm); mobile phase A consisted of a water solution containing 0.1% formic acid, whereas mobile phase B comprised acetonitrile with 0.1% formic acid. The flow rate was 0.4 mL/min, and the injection volume was 2 µL. The column temperature was sustained at 40°C. Gradient program: Phase B was begun at 5%, increased to 20% at 2.0 min, reached a maximum of 99% at 6.0 min and continued until the 7.5 min mark, then lowered to 5% at 7.6 min and continued to 10.0 min. This analysis was conducted by Metware Biotechnology Co., Ltd.

In the pre-processing stage, the data underwent unit variance scaling. Orthogonal partial least squares discriminant analysis was conducted using OPLSR, an analytical function within the MetaboAnalystR package of R. Metabolites were designated differentially expressed metabolites (DEMs) when their VIP values were above 1 and their *p*-values were below 0.05, as

determined by Student's *t*-test within the orthogonal partial least squares discriminant analysis (OPLS-DA) model. The expression patterns of DEMs were analyzed by clustering, with heatmaps drawn in the R package. Metabolic pathways were annotated for DEMs by utilizing the KEGG database. These analytical steps provided us with a comprehensive view of the metabolic effects of RY-A on the CCH rat model, revealing the underlying metabolic regulatory mechanisms.

2.9 Joint analysis of the transcriptome and metabolome

Based on the transcriptomic and metabolomic data, the KEGG signaling pathways in which the DEGs and DEMs were co-enriched were further analyzed. The Pearson correlation coefficients for comparisons between gene expression variations and metabolite alterations were computed using the cor function in the R program. Subsequently, relationships with an absolute Pearson correlation coefficient over 0.8 and a *p*-value below 0.05 were identified, and a nine-quadrant plot was constructed.

2.10 Oxidative stress kit assay

The subsequent steps were undertaken to assess the degree of oxidative stress in hippocampal tissue.

2.10.1 Reactive oxygen species level assay

Fifty milligrams of hippocampal tissue samples were mixed thoroughly with 1 mL of homogenization buffer A. Following sediment removal using centrifugation, the supernatant was obtained. Two hundred microliters of the supernatant and 2 µL of the DHE probe were put into a 96-well plate, thoroughly mixed, and incubated at 37°C for 30 min under light protection. The fluorescence intensity was measured by setting the FLIR's excitation and emission wavelengths to 488–535 nm and 610 nm, respectively. After taking out 50 µL of the supernatant, 100 µL was used for protein quantification after 30-fold dilution with PBS. Reactive oxygen species (ROS) levels were expressed as the fluorescence intensity divided by milligrams of protein.

2.10.2 Detection of malondialdehyde, superoxide dismutase and glutathione peroxidase levels

We sampled 50 mg of hippocampal tissue and mixed it thoroughly with 1 mL of homogenization buffer A. The samples were centrifuged and the supernatant collected. The instructions that came with the malondialdehyde (MDA), superoxide dismutase (SOD), and glutathione peroxidase (GSH-Px) kits were followed. A thiobarbituric acid assay was used to measure MDA levels, the WST-8-based colorimetric reaction was applied to measure SOD activity, and the DTNB method was used to measure GSH-Px protein levels.

2.11 Western blot analysis

Western blot was employed to evaluate the proteins in rat hippocampal tissues linked to iron metabolism and the System

Xc-/GSH/GPX4 pathway. Six rats in each group had their hippocampal tissues quickly frozen in liquid nitrogen and kept at -80°C after all animals were sacrificed. The hippocampal tissues were lysed using RIPA lysing solution (KGP702-100; KeyGEN Bio TECH, NanJing, China) containing PMSF (97064-898; Amresco, VWR International, OH, USA), and were thoroughly mixed by an electric homogenizer. The supernatant was obtained using centrifugation at $12,000 \times g$ for 5 min at 4°C , and the protein content was assessed using the BCA Protein Quantification Kit (KGP902; KeyGEN Bio TECH).

Gel electrophoresis was conducted to transfer the proteins onto a PVDF membrane, which was subsequently sealed with a TBST solution containing 5% skim milk powder. After that, the following antibodies were used: transferrin receptor antibody (1:5000; ab269513), anti-SLC7A11 antibody (1:1000; ab307601), anti- β -actin antibody (1:1000; ab8227), goat anti-rabbit IgG H&L (HRP) (1:10000; ab6721), and rabbit anti-mouse IgG H&L (HRP) (1:10000; ab6728), all from Abcam; anti-ferroportin/SLC40A1 antibody (1:500; 26601-1-AP) from Proteintech; and anti-CD98/SLC3A2 antibody (1:200; sc-136139), anti-GPX-4 antibody (1:100; sc-166120), and anti-GSS antibody (1:100; sc-365863) from Santa Cruz Biotechnology. Subsequent to the initial incubation, a further incubation of 1 h at an ambient temperature was conducted utilizing the appropriate secondary antibodies. The software Image Pro Plus 6.0 was used to capture the optical density values of the protein bands. Then, the proteins' relative expression levels were ascertained by dividing the target protein's grayscale values by those of the internal reference protein.

2.12 Molecular docking

Molecular docking experiments were used in this study to explore at how the possible active chemicals in RY-A interacted with the main targets. Initially, the identifiers of the primary targets were retrieved from the UniProt database, and their three-dimensional structures were acquired from the Protein Data Bank (PDB, <https://www.rcsb.org/>). Concurrently, the three-dimensional structures of the prospective active chemicals in RY-A were acquired from the PubChem database and stored in SDF format. These structures underwent pre-processing with PyMOL software (<https://pymol.org/2>), which involved the elimination of water molecules and non-essential small-molecule ligands from the structures. Hydrogen atoms were included, and the charges were allocated to these structures via AutoDock Tools (<https://autodocksuite.scripps.edu/adt/>). The processed structures were then saved in PDBQT format to enable molecular docking simulations.

Molecular docking simulations were conducted utilizing Vina 2.0 software, designating the key target proteins as receptors and the prospective active chemicals in RY-A as ligands. Evaluating the binding energy allowed for the prediction of the interaction intensity between these active molecules and their targets. The analysis of binding energies showed that compounds with binding energies below -4.25 kcal/mol had possible binding activity, those with energies below -5.0 kcal/mol had stronger binding activity, and compounds with energies below -7.0 kcal/mol had considerable binding activity (Hsin et al., 2013). Upon completion of docking, the

findings were visualized and analyzed in three dimensions with PyMOL software, while two-dimensional plots were produced using Discovery Studio 2020 Client software.

2.13 Statistical methods

Statistical analysis of the data in this study was performed using GraphPad Prism 9.0 software, and the results are expressed as the mean \pm standard error of the mean. To examine the differences among the various experimental groups, one-way analysis of variance was employed. In this analysis, differences were deemed statistically significant when the p -value was below 0.05.

3 Results

3.1 Improvements in spatial learning and memory ability in RY-A-treated CCH rats

CCH has been shown to cause impairments to of spatial memory ability (Yuan et al., 2019). This study assessed the possibility of RY-A enhancing the learning and memory capabilities of CCH rats using the Morris water maze test, and the experimental findings are illustrated in Figure 2. In the concealed platform assessment, the mean escape delay was documented for each cohort of rats during a 5-day duration. The findings indicated (Figures 2A, D) that the average escape delay across all groups diminished with training. The 2VO group exhibited a significantly prolonged mean escape latency relative to the Sham group, signifying their compromised learning and memory capabilities ($P < 0.0001$). Following RY-A therapy, rats in the low and high RY-A dosage groups exhibited markedly reduced escape latency in comparison to the 2VO group (0.48 g/kg RY-A: $P < 0.0001$; 0.96 g/kg RY-A: $P < 0.0001$), indicating RY-A substantially enhanced the rats' learning and memory capabilities.

During the probe test, all rats exhibited a tendency to swim in the quadrant where the initial platform was situated. Figures 2B, C illustrate that, after 33 days of chronic ischemia treatment, rats in the 2VO group exhibited a significant reduction in the time spent swimming in the original platform and the frequency of crossing the original platform compared to the Sham group ($P < 0.001$). These results highlight the detrimental effects of CCH on spatial memory capabilities. Conversely, RY-A therapy greatly reversed these changes. Rats in the treatment group spent more time swimming in the original platform quadrant ($P < 0.0001$) and crossed the original platform more often (0.96 g/kg RY-A: $P < 0.01$). These findings indicate that RY-A markedly enhanced spatial learning and memory impairments in CCH rats.

3.2 Effect of RY-A on increasing CBF and improving of neuronal morphology in hippocampal and cortical regions in CCH rats

The CBF of rats was measured in each group using a laser scattering technique to assess the effect of RY-A in

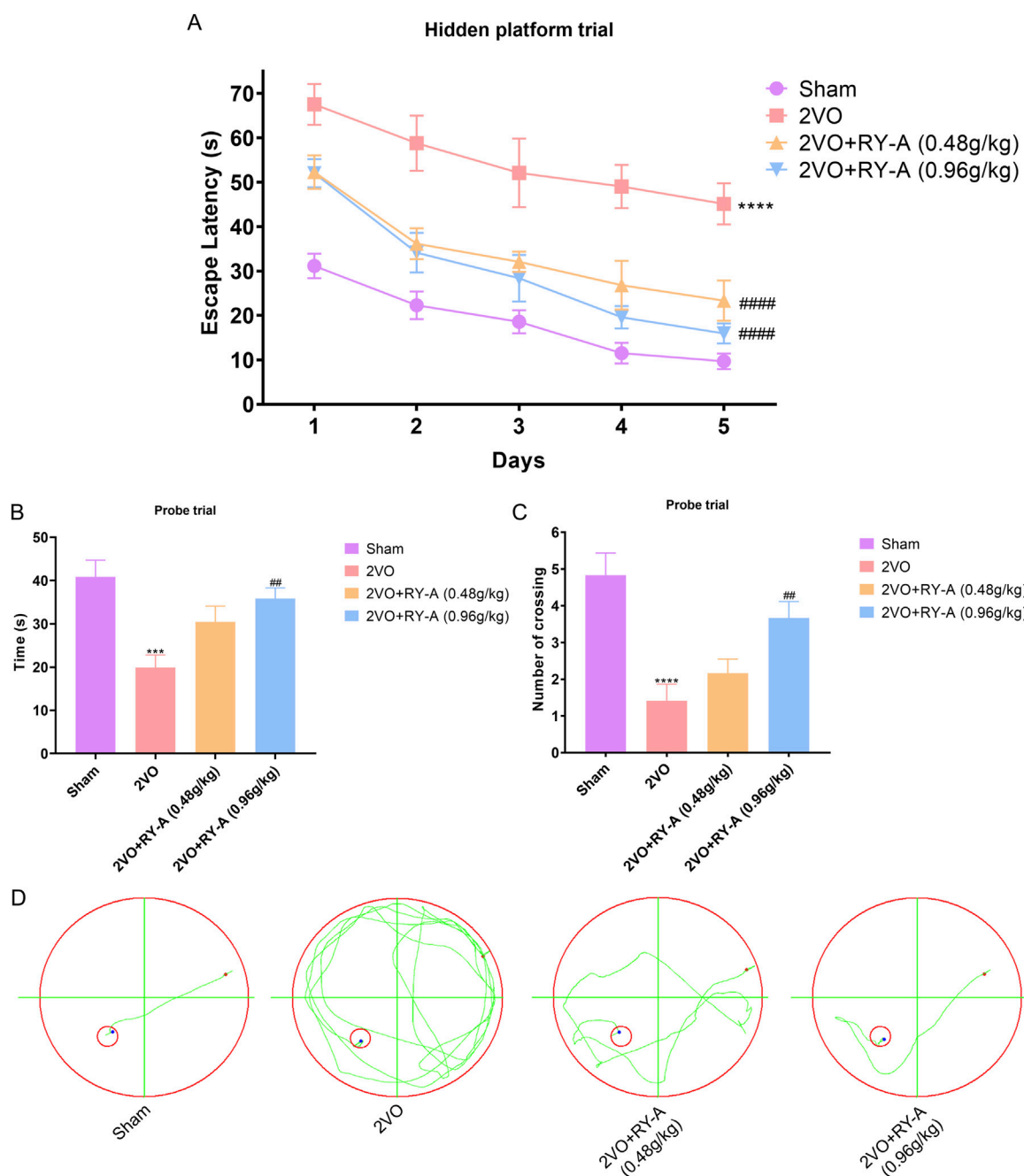
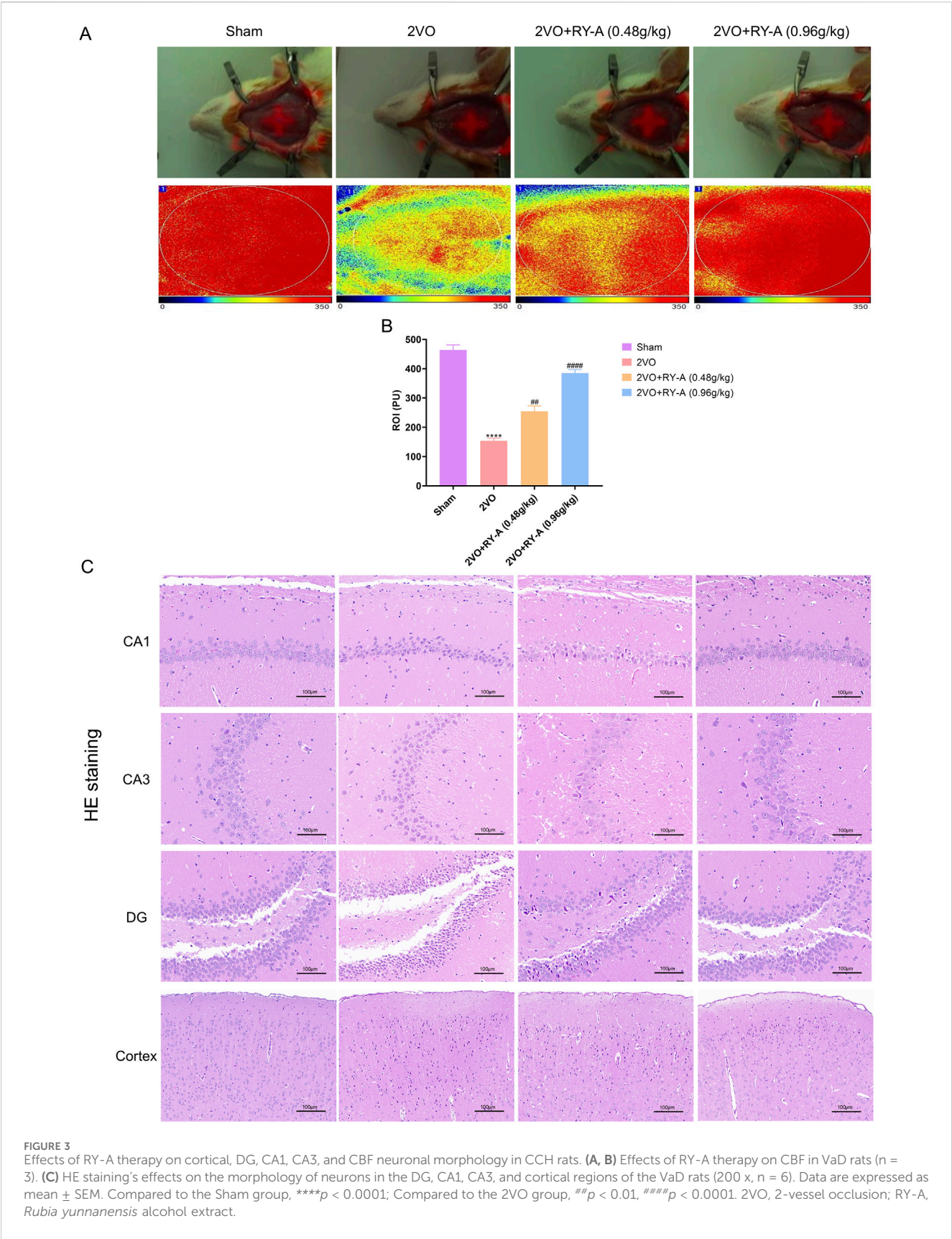


FIGURE 2

RY-A enhances the learning and memory capacities of CCH rats in the Morris water maze test. (A) Average escape latency for every rat group in the concealed platform experiment. (B) Each group's swimming time during the probe trial in the quadrant containing the original platform. (C) The number of times throughout the probe experiment that each group crossed the initial platform. (D) Swim trajectory charts that are representative of each rat group. Data are expressed as mean \pm SEM ($n = 12$). Compared to the Sham group, **** $p < 0.0001$; Compared to the 2VO group, ## $p < 0.01$, ### $p < 0.0001$. 2VO, 2-vessel occlusion; RY-A, *Rubia yunnanensis* alcohol extract.

CCH rats. As shown in Figures 3A, B, CBF was significantly lower in the 2VO group than the Sham group ($p < 0.0001$), suggesting that CCH resulted in reduced CBF. After RY-A treatment, CBF was significantly enhanced, with the most significant effect seen in the RY-A high-dose group (0.48 g/kg RY-A: $p < 0.01$; 0.96 g/kg RY-A: $p < 0.0001$), which suggests that RY-A is effective in ameliorating the reduction in CBF caused by CCH.

Histological examination is a key method for assessing nerve cell damage and drug efficacy (Brun and Englund, 1986). Neuronal abnormalities in CA1, CA3, DG, and cortical areas of the hippocampal region are closely associated with spatial learning disabilities. Using HE staining, the loss of neurons in these regions was observed in the brain tissue of rats after modeling and the degree of recovery after RY-A treatment was recorded. As shown in Figure 3C, the 2VO group's cerebral cortex and



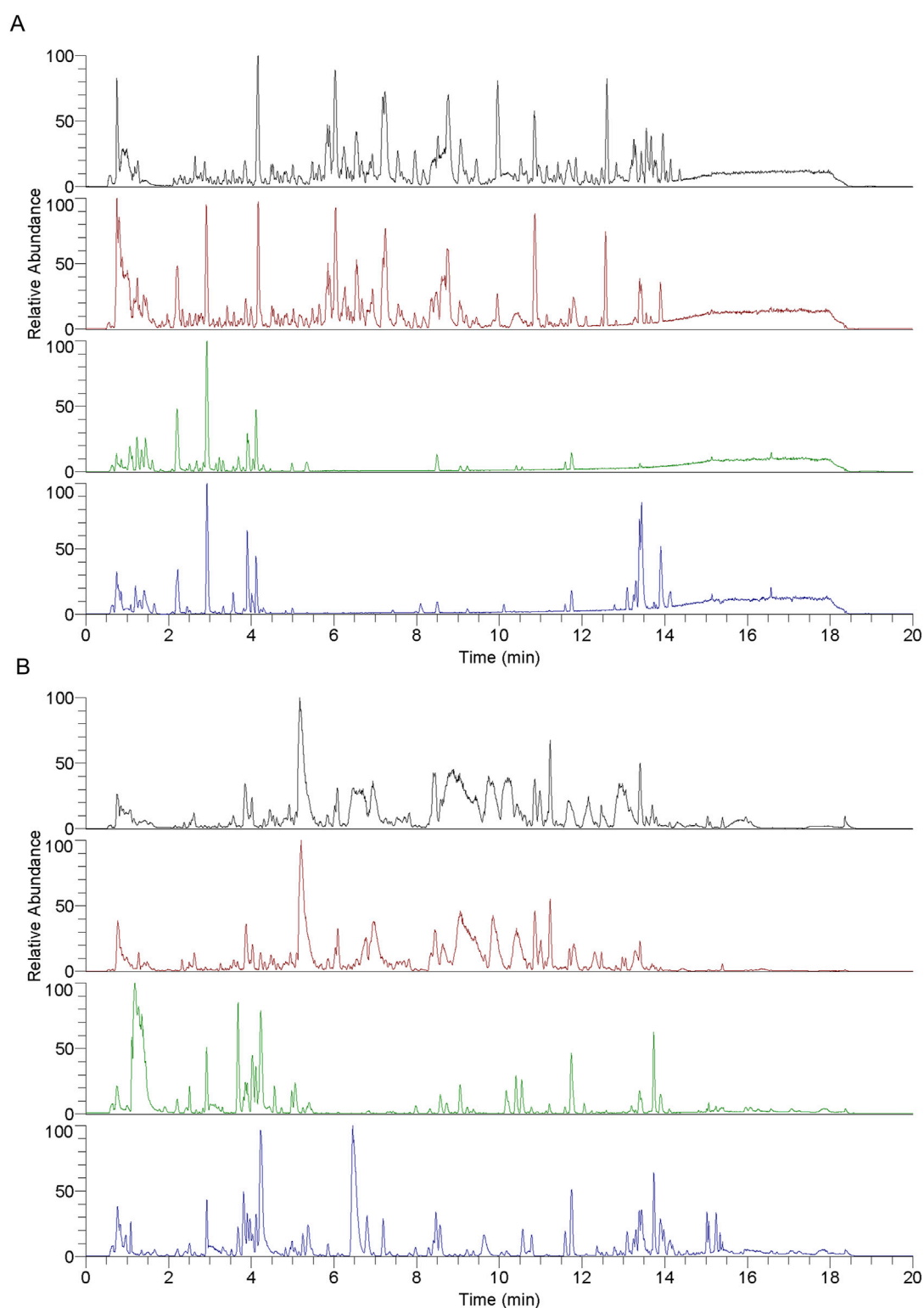


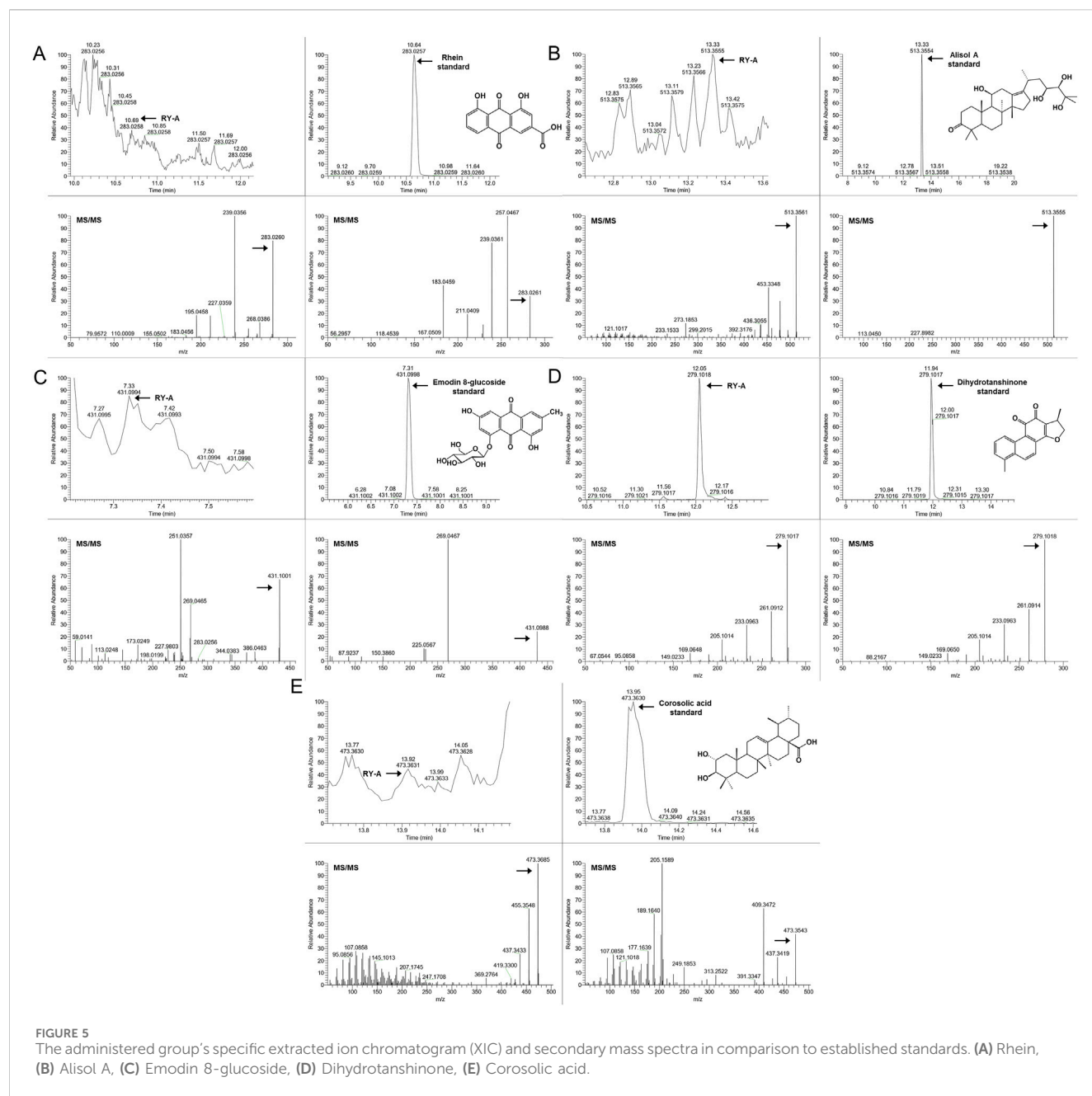
FIGURE 4

Each group of samples' base peak chromatograms (BPC) as determined by UHPLC-HRMS analysis. (A) Positive ion scan and (B) negative ion scan.

Top to bottom, the chromatograms show the following: RY-A sample, blank group (2VO group) + RY-A sample, blank group, and RY-A high-dose group (administered group).

hippocampus had considerably lower numbers of neurons than those of the Sham group, along with larger cell gaps and a disorganized cell layout. Treatment with RY-A significantly

improved these pathological changes and attenuated the CCH-induced neural tissue damage. This is consistent with the trends observed in the behavioral experiments. Therefore, the RY-A high-



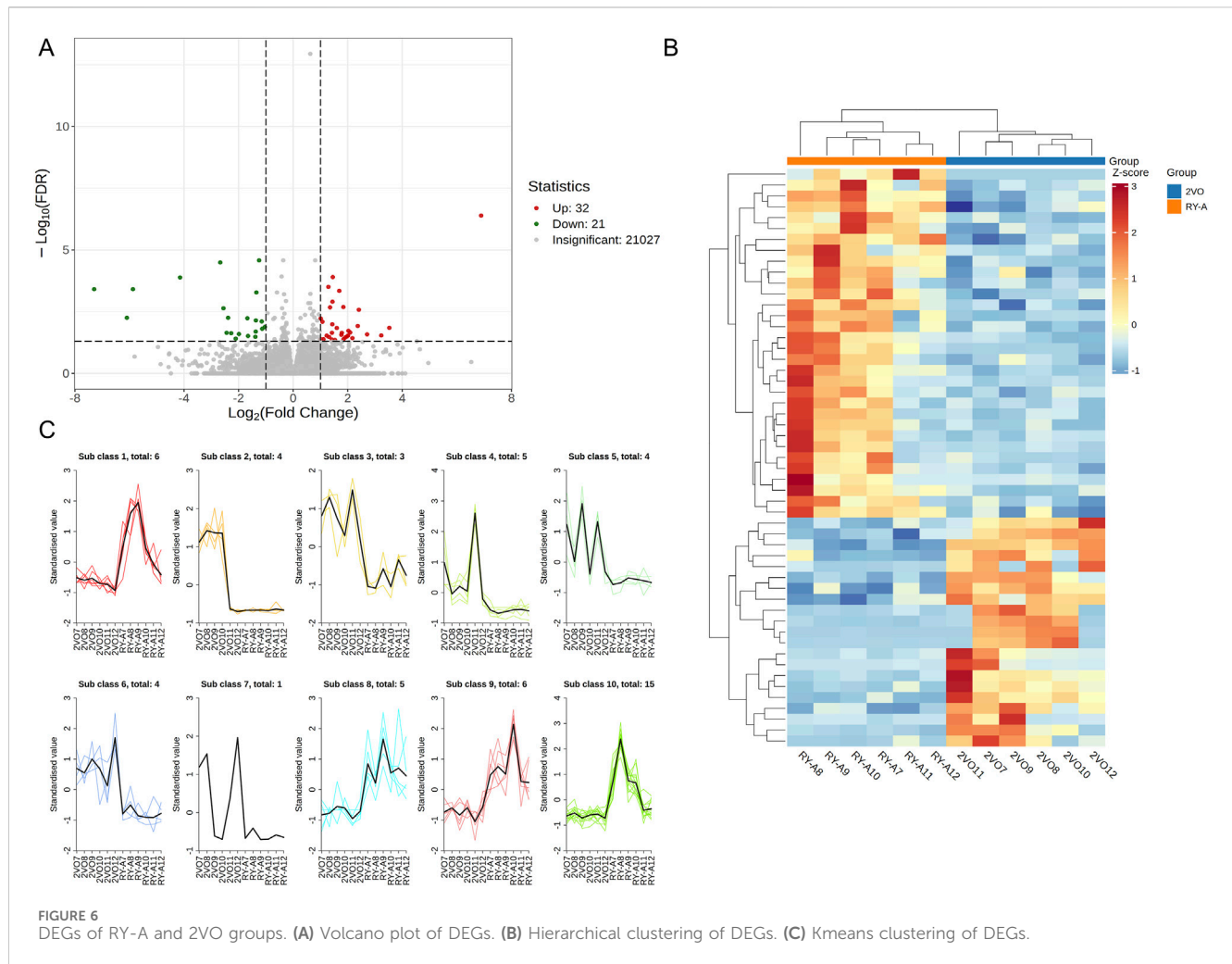
dose group and 2VO group were selected for subsequent transcriptomic and metabolomic studies. In addition, the above data suggest that RY-A has potential therapeutic effects on CCH-induced neurological damage and cognitive deficits by promoting CBF and improving neuronal morphology.

3.3 Identification of blood-entry compounds in RY-A using UHPLC-HRMS technique

A detailed analysis of the blood-entry compounds of RY-A was performed by UHPLC-HRMS. Figure 4 illustrates the base peak chromatogram of each group of samples, while Supplementary Table S1 lists our preliminary identification of 511 blood-entry compounds of RY-A, including 276 compounds identified in the

positive ion mode and 240 compounds identified in the negative ion mode. It has been shown that triterpenoids and quinones are key active *Rubia yunnanensis* compounds against hyperlipidemia, which is one of the key pathological factors of CCH (Gao et al., 2014). Five quinones and triterpenoids were deduced from the literature review, and the known standards rhein (Liu et al., 2023a), emodin 8-glucoside (Wang et al., 2007), alisol A (Li et al., 2023), dihydrotanshinone (Wu et al., 2023), and corosolic acid (Zhang et al., 2024) are potential active compounds in RY-A with neuroprotective effects.

In order to verify the entry of these compounds into the blood, serum samples from the RY-A-administered group were further analyzed and compared using the retention time and MS/MS fragment information of the known standards. This step confirmed the accuracy of our UHPLC-HRMS results. Figure 5 demonstrates the specific extracted ion chromatograms and



secondary mass spectra of these standards, which provide the material basis for the pharmacological effects of RY-A.

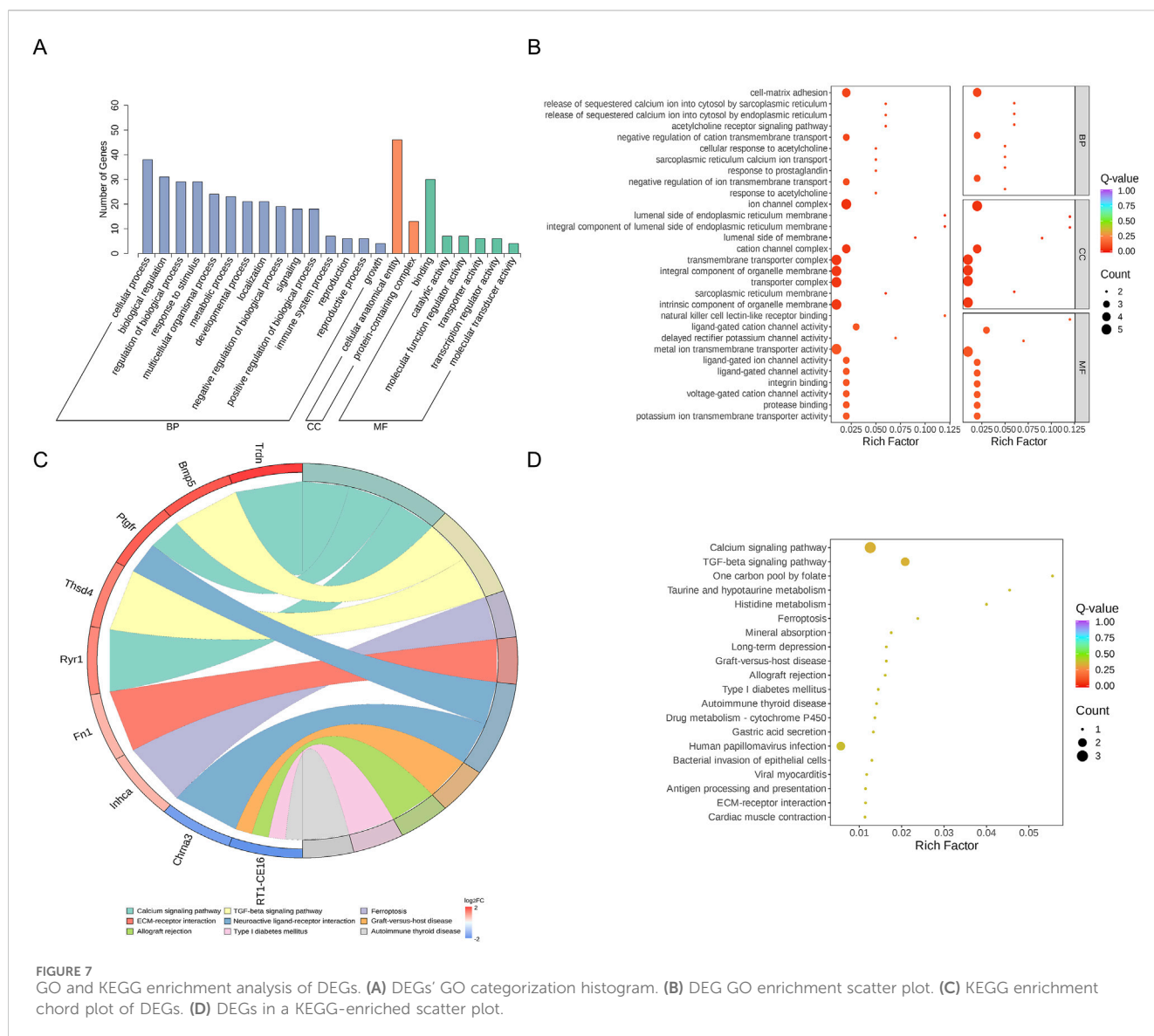
3.4 DEGs screening results

In this study, a total of 50.2 Gb of raw data was obtained by transcriptome sequencing. The amount of sequencing data per sample ranged from 1.61 Gb to 2.33 Gb, of which 97.73%–98.16% met the Q20 standard, indicating high sequencing accuracy. In addition, 93.2%–94.37% of the data quality met the Q30 standard with an average GC content of 50.79%. By comparing the RY-A group with the 2VO group, DEGs were screened with a corrected p -value ≤ 0.05 and $|\log_2 FC| \geq 1$ (Figure 6A). Using FPKM values, hierarchical clustering and Kmeans clustering analyses were performed on the DEGs to analyze differences in the gene expression patterns (Figures 6B, C). A total of 32 genes upregulated and 21 genes downregulated in expression were identified under RY-A treatment (Supplementary Table S2). Among them, ENSRNOG00000031607 gene expression was most significantly downregulated, whereas ENSRNOG00000065367 gene expression was most significantly upregulated, and their $\log_2 FC$ values were -7.29 and 6.89 , respectively.

3.5 DEGs functional and pathway enrichment analysis results

The DEGs were also analyzed using GO and KEGG enrichment analyses. GO enrichment analysis classified the DEGs into three functional categories: biological process (BP), cellular component (CC), and molecular function (MF). Supplementary Table S3 lists the 1,027 BPs, 128 cellular components, and 183 molecular functions that were stronger in the 2VO group than the RY-A group. Most of the expressed genes were allocated to three groups: biological regulation (GO:0065007), control of BP (GO:0050789), and cellular process (GO:0009987) (Figure 7A; Supplementary Table S4). The 10 best categories in BP, CC, and MF were chosen for the bubble plot (Figure 7B), and genes were arranged in order of the Q -value (corrected p -value). The findings indicated that the majority of the genes were enriched in activities that included the negative regulation of cation transmembrane transport (GO:1904063), ion channel complex (GO:0034702), and metal ion transmembrane transporter activity (GO:0046873).

KEGG enrichment analysis revealed the three pathways most significantly altered between the RY-A group and the 2VO group: calcium signaling pathway (rno04020, p -value = 0.0079), TGF-beta signaling pathway (rno04350, p -value = 0.012), and one carbon pool by folate pathway (rno00670, p -value = 0.031) (Figure 7D). In



addition, significant changes were observed in the pathways taurine and hypotaurine metabolism (rno00430, p -value = 0.038), histidine metabolism (rno00340, p -value = 0.043), and ferroptosis (rno04216, p -value = 0.044) (Supplementary Table S5). The chord plot demonstrates the nine pathways with the lowest p -values (Figure 7C), and the upregulated genes with the largest multiplicity of differences on these pathways were Trdn, Bmp5, Ptgrf, Thsd4, Ryr1, Fn1, and Inhca; while the downregulated genes were Chrna3 and RT1-CE16. These enrichment analyses suggested that these pathways and genes may be closely related to the pathogenesis of CCH and the therapeutic efficacy of RY-A.

3.6 Results of metabolomic analysis

Liquid chromatography-quadrupole time-of-flight mass spectrometry was utilized in this investigation to identify metabolites in the samples. The metabolites were measured in

pre-processing via mass spectrometry peak extraction, calibration and annotated for metabolite identification, followed by quantitative analysis utilizing triple quadrupole mass spectrometry in multiple reaction monitoring mode. A total of 1,727 metabolites were identified, comprising 830 in the positive ion mode and 897 in the negative ion mode (616 in the T3 negative ion mode and 281 in the HILIC negative ion mode) (Figures 8A–C). The findings of principal component analysis showed that the two sample groups' metabolites differed significantly (Figure 9A). The score plots and S-plots of the OPLS-DA models further validated the significant variations in metabolomics between the groups and the absence of outlier data points (Figures 9B, C).

Clustering analysis of 107 DEMs based on the Z-score values identified 41 metabolites with downregulated expression between the RY-A and 2VO groups, including L-fucose (VIP = 2.85, p = 0.000047), trolox (VIP = 2.84, p = 0.00092), and 3-(imidazol-4-yl) propionic acid (VIP = 2.81, p = 0.0071), and the upregulation of 66 metabolites, such as 12-oxoETE (VIP = 2.73, p = 0.012), GSH

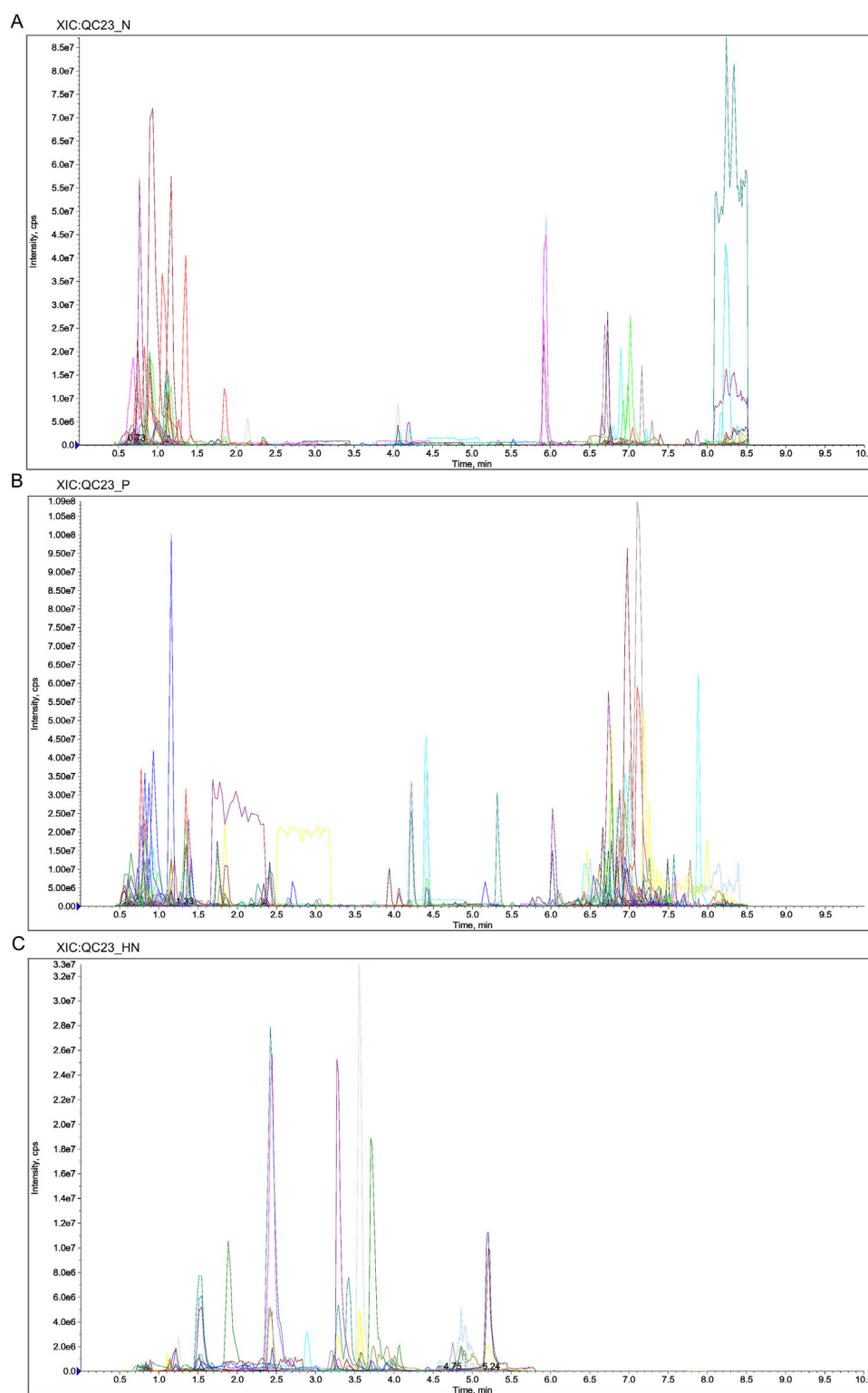


FIGURE 8

Extracted Ion Chromatogram (XIC) of MRM. (A) XIC of N. (B) XIC of P. (C) XIC of HN. Abbreviations: N, T3 negative ion mode; P, T3 positive ion mode; HN, HILIC negative ion mode.

(VIP = 2.65, $p = 0.023$), and adrenic acid (AA, VIP = 1.96, $p = 0.012$) (Figures 9D, E). These DEMs were mostly engaged in ferroptosis (ko04216), glutathione metabolism (ko00480), fatty acid

biosynthesis (ko00061), and unsaturated fatty acid biosynthesis (ko01040), among other BPs, according to the results of the KEGG enrichment studies (Figure 9F; Supplementary Table S6).

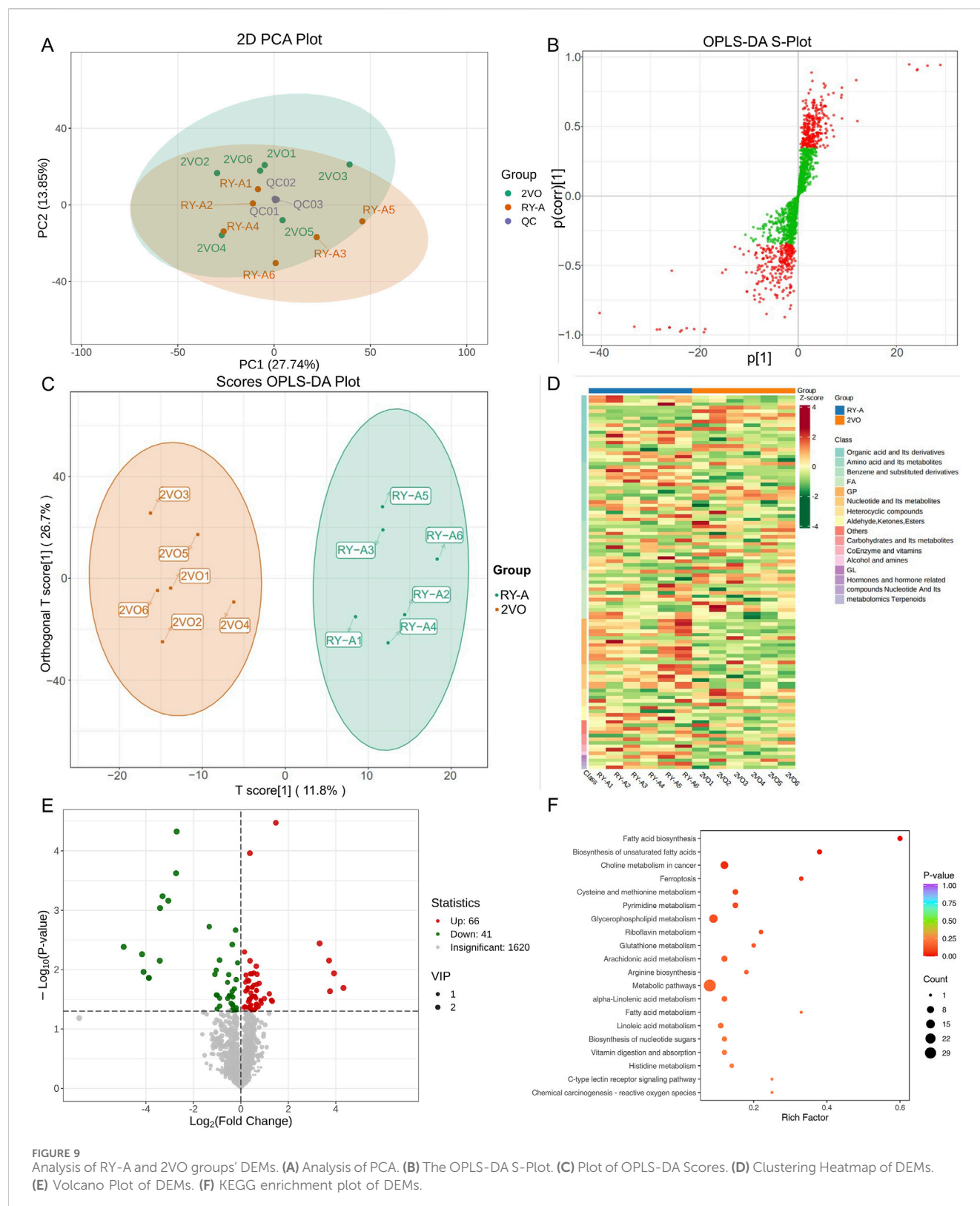
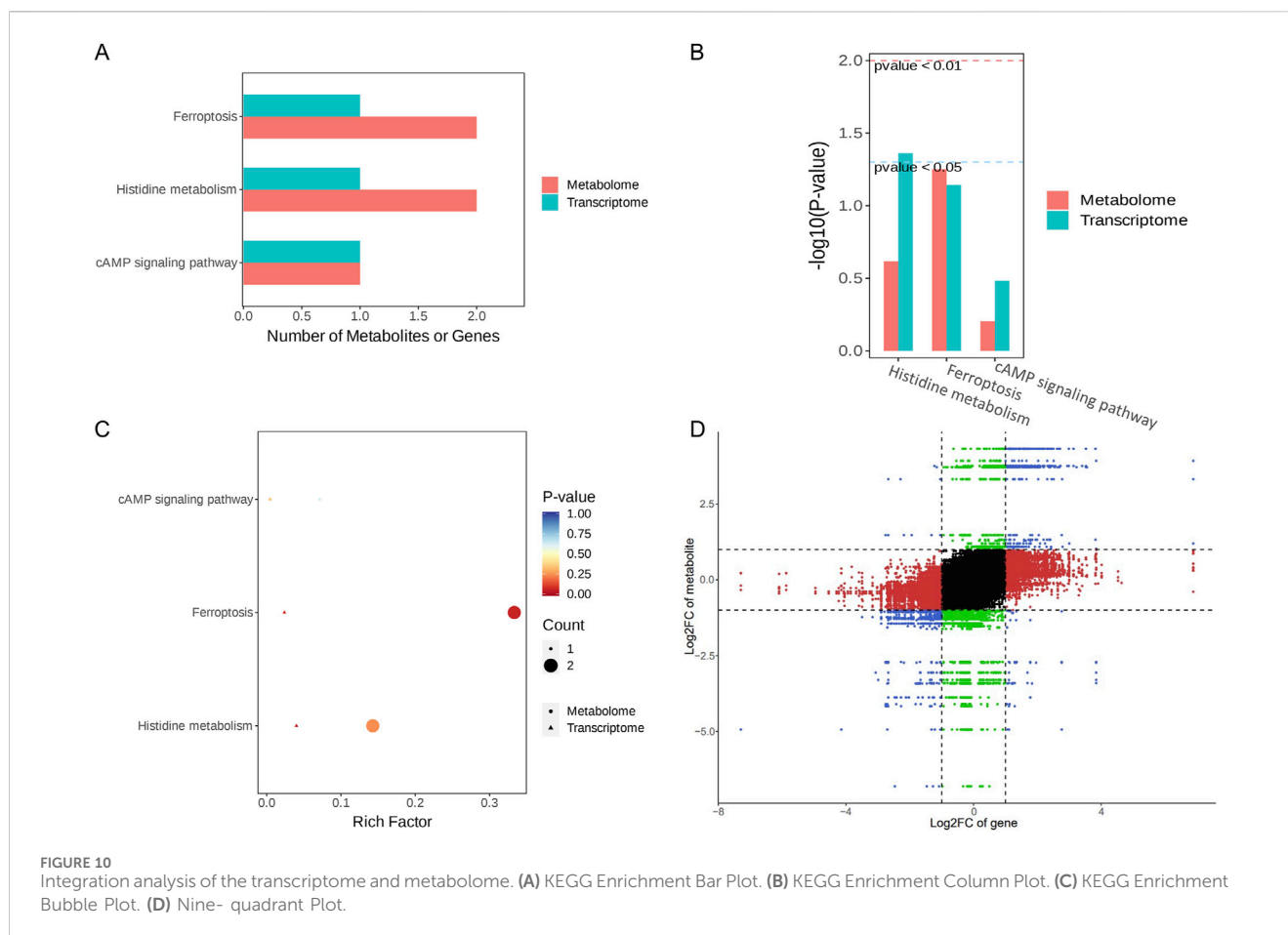


FIGURE 9 Analysis of RY-A and 2VO groups' DEMs. **(A)** Analysis of PCA. **(B)** The OPLS-DA S-Plot. **(C)** Plot of OPLS-DA Scores. **(D)** Clustering Heatmap of DEMs. **(E)** Volcano Plot of DEMs. **(F)** KEGG enrichment plot of DEMs.

3.7 Results of transcriptome and metabolome integration analysis

In a comparison of the RY-A group and 2VO group, 53 DEGs and 107 DEMs were identified. Ferroptosis (ko04216), histidine

metabolism (ko00340), and the cAMP signaling pathway (ko04024) were found to be co-enriched in the integration study of the two omics datasets, according to KEGG pathway analysis (Figures 10A–C). This implies that these routes could be the main mechanisms by which RY-A produces its pharmacological effects.



Genes linked to the integration analysis, including RGD1310507 and Hcar1, showed considerably higher expression in the RY-A group, although Ftcd expression was significantly lower. Similarly, metabolites such as GSH, AA, 3-hydroxybutanoic acid, and [1-(5-phosphoribosyl) imidazol-4-yl] acetic acid were significantly increased in the RY-A group, whereas 3-(imidazol-4-yl) propionic acid 3-(imidazol-4-yl) propionic acid was significantly decreased. The results pertaining to the correlation analysis of these genes and metabolites are shown in Figure 10D.

The ferroptosis pathway occupied first place among the co-enriched pathways, with a *p*-value of less than 0.05, suggesting that this pathway may be significantly altered by RY-A. In particular, GSH levels were significantly elevated in RY-A-containing serum, and GSH expression levels are closely related to oxidative stress. These data suggest that RY-A may act by regulating oxidative stress and the ferroptosis pathway.

3.8 Results of analyzing the effect of RY-A on oxidative stress related indices

A variety of kits were used to measure oxidative-stress-related markers, such as ROS, MDA, SOD, and GSH-Px, to see how well RY-A changes oxidative stress levels. We found that RY-A effectively stopped the production of pro-oxidant substances, such as ROS and MDA (Figures 11A, B), while greatly increasing the activity of

antioxidant enzymes, such as SOD and GSH-Px (Figures 11C, D). Based on these indicators, the RY-A high-dose group demonstrated the best inhibitory effect. These results suggest that RY-A possesses notable antioxidant effects and is able to alleviate oxidative stress by enhancing the antioxidant defense system.

3.9 Western blot analysis for validation

The combined transcriptomic and metabolomic analysis showed that the ferroptosis pathway was significantly upregulated by RY-A treatment, and there is a close link between ferroptosis and CCH-induced VD (Fu et al., 2023). Thus, the presence of key proteins of the System Xc-/GSH/GPX4 pathway, including SLC7A11, SLC3A2, GSS, and GPX4, was validated by Western blot. These proteins play important roles in regulating oxidative stress and iron metabolism in cells.

One of the features of ferroptosis is an imbalance in the intracellular labile iron pool (LIP), which leads to an increase in unstable iron ions. The main regulatory proteins of LIP include transferrin receptor (TFRC) and ferritin (FPN). To verify whether RY-A can regulate ferroptosis and related pathways, the expression levels of TFRC, FPN, and System Xc-/GSH/GPX4 pathway proteins in the rat groups were determined. The experimental results showed that the 2VO procedure significantly increased TFRC (Figures 12A, B) and suppressed FPN expression (Figures 12A, C), SLC7A11

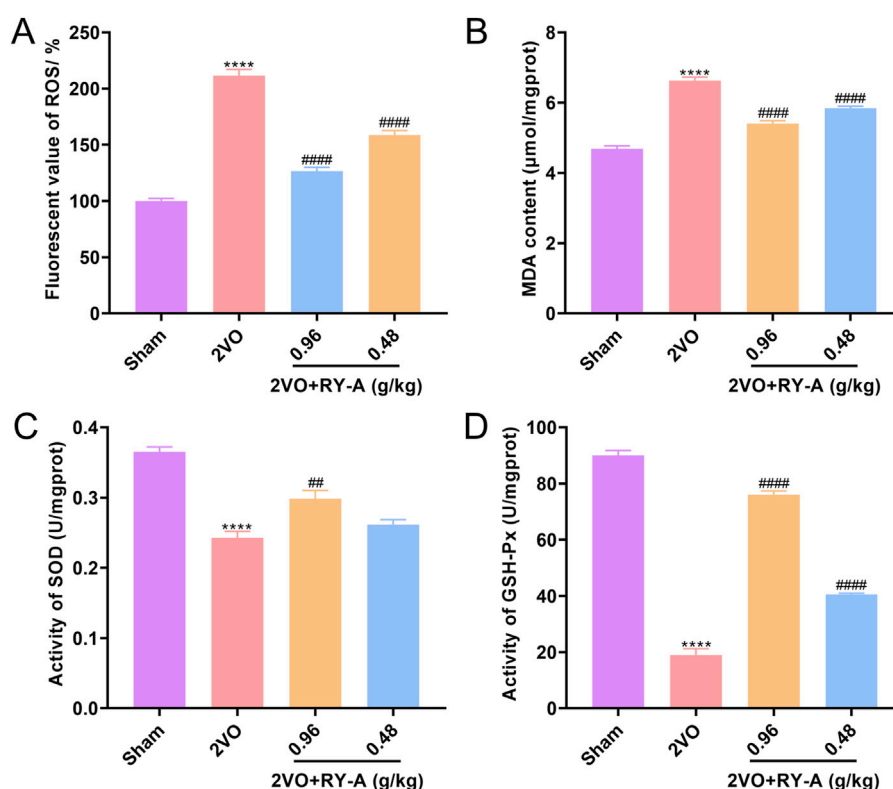


FIGURE 11

Inhibition of oxidative stress by RY-A. (A) ROS fluorescence values for each group of rats. (B) MDA content of rats in each group. (C) SOD activity in each group of rats. (D) GSH-Px activity in each group of rats. Data are expressed as mean \pm SEM (n = 6). Compared to the Sham group, **** p < 0.0001; Compared to the 2VO group, ## p < 0.01, #### p < 0.0001. 2VO, 2-vessel occlusion; RY-A, *Rubia yunnanensis* alcohol extract.

(Figures 12A, D), SLC3A2 (Figures 12A, E), GSS (Figures 12A, F), and GPX4 levels (Figures 12A, G), in contrast to the Sham group. After RY-A treatment, the expression of TFRC was suppressed, whereas the expression of FPN, SLC7A11, SLC3A2, GSS, and GPX4 was activated, suggesting that RY-A promoted LIP homeostasis and activated the System Xc-/GSH/GPX4 pathway. These findings confirmed the role of RY-A in the regulation of the ferroptosis pathway at the molecular level and provided strong evidence for RY-A's capacity as a potential neuroprotective agent.

3.10 Molecular docking analysis for validation

Lastly, this study explored the interactions between the potential active compounds in RY-A and ferroptosis-associated core target proteins using a molecular docking technique, and the relevant binding energy data are detailed in [Supplementary Table S7](#). Dihydrotanshinone was found to have the strongest binding energies with FPN and SLC7A11 at -9.6 and -9.5 kcal/mol, respectively, suggesting that it may have high binding affinity. The binding energy of emodin 8-glucoside with TFRC and GSS followed closely at -9.5 kcal/mol. These results were visualized by two-dimensional and three-dimensional binding diagrams (Figure 13). In terms of intermolecular interactions, dihydrotanshinone partook in alkyl and Pi-alkyl interactions with

ALA-69, ALA-62, LEU-66, ILE-512, and LEU-505 of FPN; and Pi-Pi stacked and amide-Pi stacked interactions with GLY-65 and PHE-508. Dihydrotanshinone partook in Pi-alkyl interactions with PRO-352 and TRP-128 of SLC7A11, Pi-Sigma and Pi-Pi stacked interactions with PHE-467, and a Pi-cation interaction with LYS-473. Whereas emodin 8-glucoside was involved in conventional hydrogen bond interactions with ASP-457, PHE-264, ASP-538, and LEU-566 of TFRC, Pi-anion interactions with ASP-562, and alkyl and Pi-alkyl interactions with LEU-489. Emodin 8-glucoside participated in conventional hydrogen bond interactions with ARG-125 and ASN-216 of GSS, van der Waals interactions with ALA-463, and amide-Pi stacked and Pi-alkyl interactions with ALA-462. These results suggest that these compounds inhibit oxidative stress and ferroptosis by interacting with specific amino acid residues of key target proteins, thereby modulating the System Xc-/GSH/GPX4 pathway and consequently attenuating the neurological damage and cognitive impairment in the CCH model (Figure 14).

4 Discussion

Rubia yunnanensis has a long history of use as an intervention in cardiovascular and cerebrovascular diseases, but its effects and mechanisms of action on CCH have not yet been reported. In the present study, it was demonstrated for the first time that RY-A

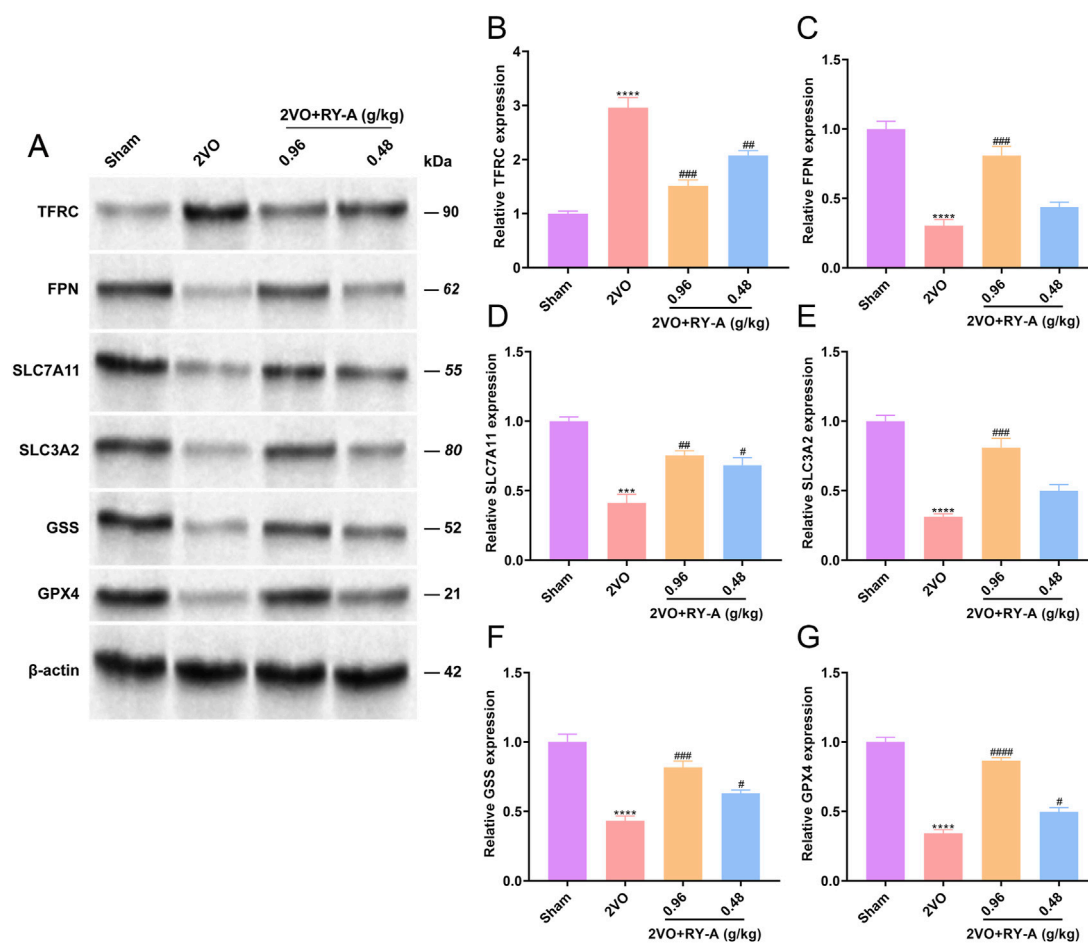


FIGURE 12

Regulation of intracellular iron ion homeostasis and System Xc-/GSH/GPX4 pathway by RY-A. Expression of (A, B) TFRC, (A, C) FPN, (A, D) SLC7A11, (A, E) SLC3A2, (A, F) GSS, (A, G) GPX4 in rat hippocampal tissues was detected by Western blot. Data are expressed as mean \pm SEM (n = 3). Compared to the Sham group, ****p < 0.0001; Compared to the 2VO group, ##p < 0.01, ###p < 0.0001. 2VO, 2-vessel occlusion; RY-A, *Rubia yunnanensis* alcohol extract.

has a therapeutic effect on CCH, as it ameliorated cortical and hippocampal neuronal damage and increased CBF, as well as improved spatial learning and memory ability in CCH rats. In the brain tissue of CCH rats, neuronal cells in the CA1, CA3, DG, and cortical regions were damaged to different degrees, and the morphology of these neuronal cells was improved after RY-A treatment. These observations were consistent with the results of the Morris water maze experiments, suggesting the ameliorative effect of RY-A on neuronal damage.

RY-A is a natural multi-component extract, thus the identification of its active compounds is challenging. Our previous work identified two compounds in RY-A, *Rubia yunnanensis* naphthoquinones A and *Rubia yunnanensis* quinone B, by HPLC analysis (Li et al., 2024). In this study, the UHPLC-HRMS technique was used to improve the specificity of the identification and characterize for the first time 511 blood-entry compounds of RY-A released into the blood (Supplementary Table S1). The reliability of these results was further verified by comparison with several standards, which included potentially active compounds such as rhein, emodin 8-glucoside, alisol A, dihydrotanshinone, and corosolic acid. Of these compounds,

rhein has multiple anti-inflammatory, antioxidant, and anti-cancer effects. Reportedly, rhein is able to inhibit ferroptosis through the NRF2/SLC7A11/GPX4 signaling pathway, attenuate the damage caused by cerebral ischemia/reperfusion, and induce dose-dependent neuroprotective effects (Liu et al., 2023a). Emodin 8-glucoside has considerable antibacterial and anti-inflammatory activities. Wang et al. showed the protective effect of emodin 8-glucoside against ischemia-reperfusion-induced brain injury and glutamate-induced neuronal damage, as well as its high antioxidant properties (Wang et al., 2007). Alisol A was shown to lead to neurovascular protection in cerebral ischemic mice through the activation of the AKT/GSK3 β signaling pathway; the compound attenuated the neurological deficits and cognitive deficits and inhibited IL-6 and IL-1 β expression, in addition to promoting neuronal survival (Li et al., 2023). Wu et al. (2023) concluded that dihydrotanshinone is able to prevent ischemic stroke by activating Nrf2 and inhibiting ferroptosis. Their study revealed that dihydrotanshinone reduced ferroptosis through the activation of the Nrf2 signaling pathway, reduced the neurological damage in cerebral ischemic rats, and improved CBF and brain tissue microstructure. According to Zhang et al.

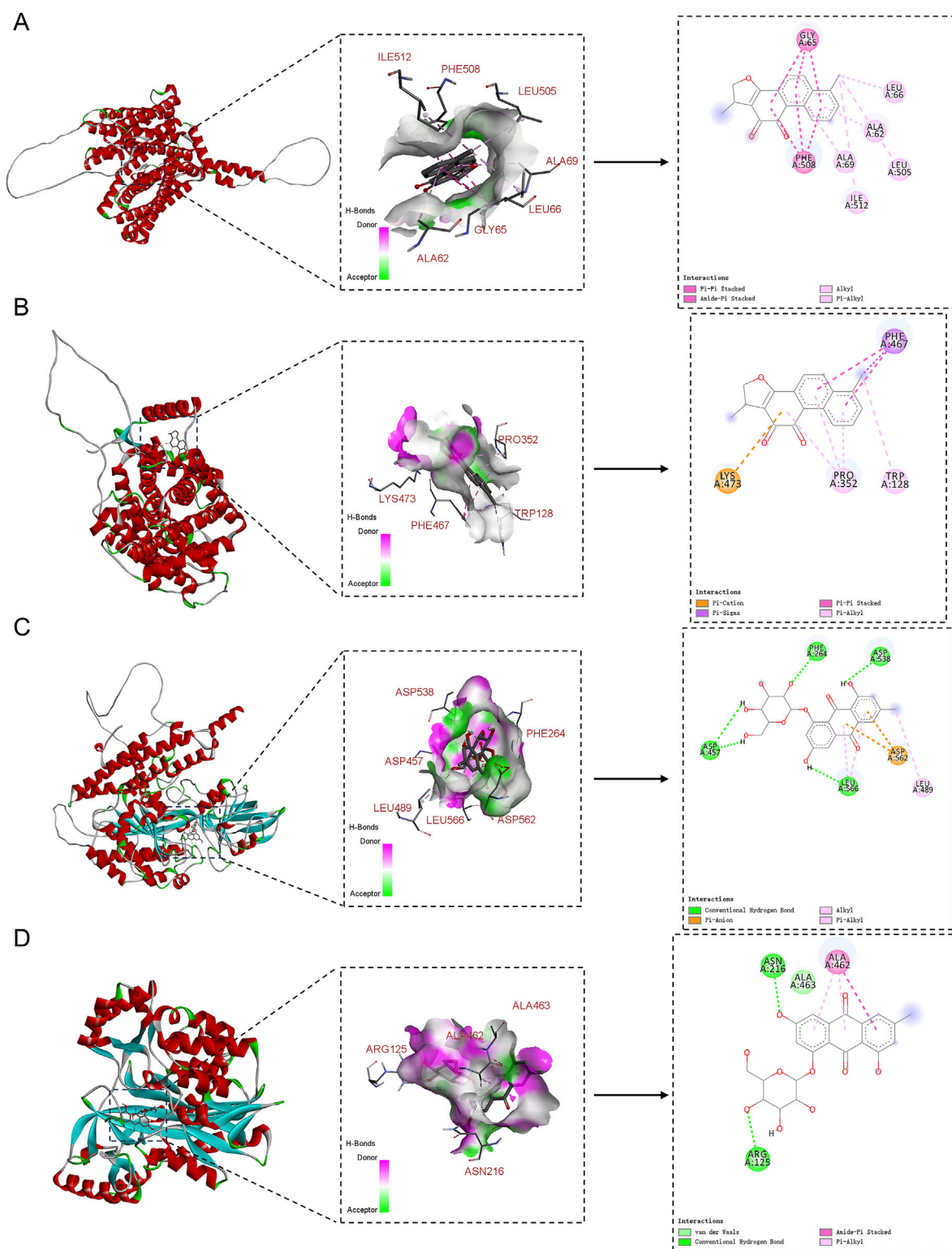


FIGURE 13
2D and 3D binding diagrams of molecular docking. (A) Dihydrotanshinone binding to FPN; (B) Dihydrotanshinone binding to SLC7A11; (C) Emodin 8-glucoside binding to TFRC; (D) Emodin 8-glucoside binding to GSS.

(2024), corosolic acid can effectively protect the heart from cerebral ischemia-reperfusion injury in rat experiments. It functions by stifling oxidative stress and fostering mitochondrial autophagy, two processes intimately associated with ferroptosis. The effects

of these compounds suggest that RY-A has the potential to treat cerebral ischemia.

In recent years, network pharmacology has provided a networked technical tool for research related to Traditional

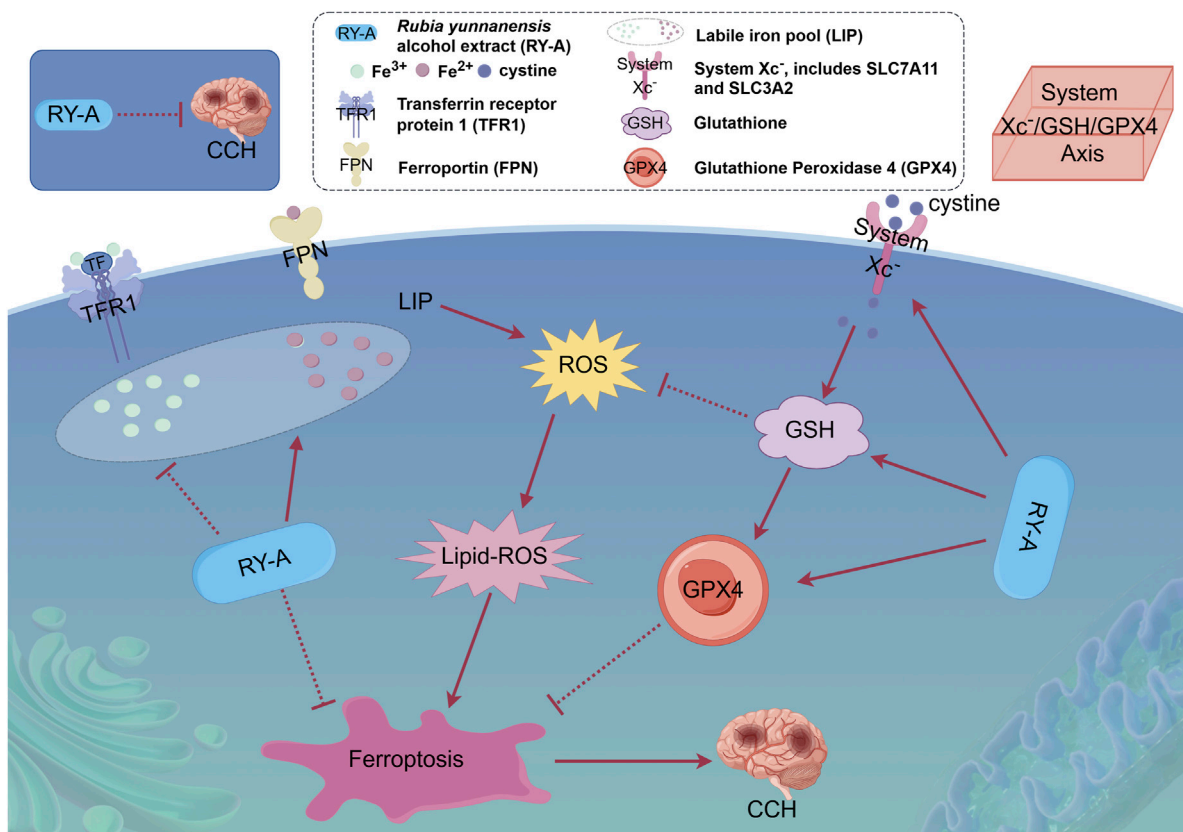


FIGURE 14
Overview of the mechanism of neuroprotective effects of RY-A in CCH rats. The protective effect of RY-A may be related to oxidative stress, labile iron pool, and regulation of the System Xc⁻/GSH/GPX4 pathway [By: Figdraw (www.figdraw.com)].

Chinese Medicine (Nam et al., 2024; Zhao et al., 2024). However, considering the limitations of incomplete databases and homogeneous substances, and the infeasibility of quantitative studies (Pohjala and Tammela, 2012; Luo et al., 2020), metabolomics and transcriptomics were selected in the present study to conduct a more reliable and quantitative analysis of the rat cortical tissues. The results more visually reflected the metabolites and genes that were significantly different before and after RY-A treatment. Between the two groups, a total of 53 DEGs and 107 DEMs were found in the current study. Transcriptomic analysis showed that, compared with 2VO group gene expression, most of the DEGs in the RY-A group were enriched in the calcium, TGF- β , one carbon pool by folate, and ferroptosis signaling pathways. Calcium signaling is an important pathway that affects Ca^{2+} transport inside and outside neuronal cells and the normal physiological activities of neuronal cells. When excessive intracellular Ca^{2+} causes overloading, a series of Ca^{2+} -dependent biochemical reactions, such as mitochondrial dysfunction, are induced, causing hypoxic neuronal injury and diminished memory and learning capacity (Tanovic and Alfaro, 2006). TGF- β signaling is an important cytokine pathway associated with various pathological processes, including endothelial cell death, microglia activation, and neuronal loss. It also plays a role in tissue repair, which contributes to the improvement of vascular-related lesions and the enhancement of learning and memory

abilities in patients with VD (Kandasamy et al., 2020). One carbon pool by folate pathway is associated with the biosynthesis of folic acid, a compound commonly used clinically as an adjunctive therapy for patients with dementia. This pathway exhibits neurotrophic effects and has been associated with CBF (Tu et al., 2023). Ferroptosis, a recently identified ferroptosis-dependent pathological process characterized by peroxidation and the inactivation of GSH and GPX4, has been shown to be induced by the CCH-mediated inactivation of System Xc⁻-associated transporter proteins (Fu et al., 2023). Clearly, these pathways play key roles in neuronal function and tissue repair and are closely related to the pathophysiological process of CCH.

Our metabolomic analysis showed that, when compared to 2VO group expression, most of the DEMs in RY-A were enriched in fatty acid biosynthesis (ko00061), biosynthesis of unsaturated fatty acids (ko01040), ferroptosis (ko04216), and glutathione metabolism (ko00480). The role of fatty acids is like a double-edged sword, with the biosynthesis of fatty acids, especially unsaturated fatty acids, being one of the key causes of ferroptosis production (She et al., 2020). Thus, omega-3 polyunsaturated fatty acids for dietary use have been suggested as a non-medical alternative for improving brain function and dementia (Burckhardt et al., 2016). Furthermore, a study by Mukamal (2020) found that circulating levels of nonesterified fatty acids can contribute to the development of cardiovascular diseases and can be used as a preventive indicator

f of cardiovascular disease in healthy populations. Glutathione metabolism maintains the normal immune system of the body; GSH is considered the most abundant antioxidant, and a decrease in its level marks the generation of oxidative stress (Detteverry et al., 2023). In turn, activation of GPX4 prevents lipid peroxidation and ferroptosis while inhibiting tumor growth (Xu et al., 2021). These metabolites play important roles in brain cell function and oxidative stress, with the regulation of glutathione metabolism being critical for maintaining redox homeostasis.

In the integrated transcriptomics and metabolomics investigations, the ferroptosis pathway ranked first among the co-enriched pathways, and the level of GSH was significantly increased after RY-A treatment. GSH is strongly linked to the progression of several neurodegenerative disorders, including Alzheimer's and Parkinson's diseases, and is regarded as a potential therapeutic target (Aoyama, 2021; Shi et al., 2022). Our prior research showed the inhibitory impact of RY-A on the oxidative stress generated by oxygen-glucose deprivation/reoxygenation (OGD/R) in HT22 neural cells (Cheng et al., 2024). Our examination of the combined omics data suggested that RY-A may function by mitigating oxidative stress and ferroptosis.

The results of the oxidative stress-related kit assay showed that the antioxidant enzymes SOD and GSH-Px were inhibited and ROS and MDA levels were elevated in CCH rats compared to Sham rats. These indices were reversed by RY-A treatment of CCH rats compared to untreated CCH rats, with the results converging toward those of the Sham group and optimal effects seen in the high-dose RY-A group. The results were clear in suggesting that RY-A treatment inhibited the occurrence of oxidative stress.

An imbalance in intracellular LIP is one of the most important reasons for the emergence of ferroptosis, and two key ferric ion transport proteins that regulate the balance of the iron pool are TFRC and FPN (Rochette et al., 2015; Zheng and Conrad, 2020). The System Xc-/GSH/GHX4 pathway, an important pathway linking GSH to ferroptosis, has been shown to ameliorate the neuronal loss induced by cerebral ischemia-reperfusion injury in previous reports (Xu et al., 2023). The main proteins of System Xc- are SLC7A11 and SLC3A2 (Wu et al., 2024). Therefore, the effects of RY-A on the iron-metabolizing proteins within the System Xc-/GSH/GHX4 pathway were further explored. The results of Western blot experiments showed that the expression of TFRC was suppressed after RY-A treatment. The relevant literature demonstrates that TFRC is a signature protein for the uptake of ferric ions into cells, and inhibition of its expression prevents ferroptosis production (Xu et al., 2023). Furthermore, we found that RY-A activated the expression of FPN, which is considered to be a major intracellular iron storage protein. In addition, ferroptosis production involves the autophagic degradation of FPN, hence blocking its degradation could be used to resist ferroptosis (Chen et al., 2020). Our research additionally showed that giving rats RY-A increased the levels of SLC7A11, SLC3A2, GSS, and GPX4 proteins in the System Xc-/GSH/GHX4 pathway. SLC7A11 and SLC3A2 are the principal proteins of System Xc-, a cystine/glutamate reverse transporter essential for the cellular uptake of cystine. Cystine is subsequently reduced to cysteine, facilitating the synthesis of GSH (Ishii et al., 1992). Liu et al. (2019) showed that increasing the expression of SLC7A11 by inducing the expression of the deubiquitinating enzyme OTUB1 protected cells from ferroptosis. The expression of GSS was also activated by RY-A treatment in this study;

GSS is a major synthase of GSH, and increasing the expression of GSH was observed to inhibit ferroptosis (Rochette et al., 2022). The dysfunction of GPX4, a glutathione peroxidase that degrades intracellular lipid peroxides into non-toxic alcohols, is considered a key feature of ferroptosis (Cao and Dixon, 2016; Chen et al., 2021). Research found that the occurrence of ferroptosis in mice was closely linked to the deletion of SLC7A11 and GPX4 expression, which further led to cognitive impairment and early embryonic death (Koppula et al., 2021).

Clearly, the above evidence supports our conjecture that RY-A inhibits oxidative stress, promotes intracellular LIP homeostasis and activates the System Xc-/GSH/GHX4 pathway.

However, there are several limitations to this study. Initially, the study primarily relied on animal models and was lacking clinical validation, and thus its translational application requires further confirmation. Additionally, although multiple active compounds in RY-A were identified, their relative contribution to the overall therapeutic effect remains unclear. Future research should aim to further clarify the roles and interactions of these compounds.

5 Conclusion

The potential therapeutic impact of RY-A on CCH and its mechanism was examined using an integrated approach combining serum pharmacochimistry, metabolomics, and transcriptomics, with verification through animal experiments. The findings of this provide a scientific foundation for the pharmacological effects of *Rubia yunnanensis* and offer novel perspectives on advanced preventive and treatment techniques for cerebral ischemia.

Data availability statement

The original contribution presented in this study is included in the article/Supplementary Material, and the raw RNA-seq data are freely available in the NCBI database under accession no. PRJNA1174397.

Ethics statement

The animal study was approved by Yunnan University of Chinese Medicine's Ethics Committee. The study was conducted in accordance with the local legislation and institutional requirements.

Author contributions

JC: Conceptualization, Formal Analysis, Funding acquisition, Investigation, Methodology, Validation, Visualization, Writing—original draft. XM: Formal Analysis, Funding acquisition, Methodology, Writing—review and editing. JT: Formal Analysis, Methodology, Supervision, Validation, Writing—review and editing. XJ: Software, Validation, Writing—review and editing. PC: Conceptualization, Investigation, Resources, Writing—review and editing. XD: Conceptualization, Funding acquisition, Investigation, Writing—review and editing.

Funding

The author(s) declare that financial support was received for the research, authorship, and/or publication of this article. The present study was supported by the Xingdian Talent Support Program -Special for Young Talent (grant no. XDYC-QNRC-2022-0284), the High-level Talents Projects of Yunnan University of Chinese Medicine-Fifth Level Talents (grant no. 2023-05-007), the National Administration of Traditional Chinese Medicine High-level Key Discipline Construction Project “Minority medicine (Dai Medicine)” (grant no. Zyyzdxk-2023193), Yunnan Key laboratory of Dai and Yi medicines open project (grant no. 2024ZD2403) and the Scientific Research Foundation of The Education Department of Yunnan Province (grant no. 2024Y372).

Conflict of interest

The authors declare that the research was conducted in the absence of any commercial or financial relationships that could be construed as a potential conflict of interest.

References

- Aoyama, K. (2021). Glutathione in the brain. *Int. J. Mol. Sci.* 22 (9), 5010. doi:10.3390/ijms22095010
- Arbaizar-Roviro, M., Gallizioli, M., Lozano, J. J., Sidorova, J., Pedragosa, J., Figuerola, S., et al. (2023). Transcriptomics and translomics identify a robust inflammatory gene signature in brain endothelial cells after ischemic stroke. *J. Neuroinflammation* 20 (1), 207. doi:10.1186/s12974-023-02888-6
- Askev, K. E., Beverley, J., Sigfridsson, E., Szymkowiak, S., Emelianova, K., Dando, O., et al. (2024). Inhibiting CSF1R alleviates cerebrovascular white matter disease and cognitive impairment. *Glia* 72 (2), 375–395. doi:10.1002/glia.24481
- Brun, A., and Englund, E. (1986). A white matter disorder in dementia of the Alzheimer type: a pathoanatomical study. *Ann. Neurol.* 19 (3), 253–262. doi:10.1002/ana.410190306
- Burckhardt, M., Herke, M., Wustmann, T., Watzke, S., Langer, G., and Fink, A. (2016). Omega-3 fatty acids for the treatment of dementia. *Cochrane Database Syst. Rev.* 4 (4), CD009002. doi:10.1002/14651858.CD009002.pub3
- Cao, J. Y., and Dixon, S. J. (2016). Mechanisms of ferroptosis. *Cell Mol. Life Sci.* 73 (11–12), 2195–2209. doi:10.1007/s00018-016-2194-1
- Chen, P. H., Wu, J., Ding, C. C., Lin, C. C., Pan, S., Bossa, N., et al. (2020). Kinome screen of ferroptosis reveals a novel role of ATM in regulating iron metabolism. *Cell Death Differ.* 27 (3), 1008–1022. doi:10.1038/s41418-019-0393-7
- Chen, X., Li, J., Kang, R., Klionsky, D. J., and Tang, D. (2021). Ferroptosis: machinery and regulation. *Autophagy* 17 (9), 2054–2081. doi:10.1080/15548627.2020.1810918
- Cheng, J., Li, G., Yang, L., Chen, P., and Duan, X. (2024). Alcohol extract of Rubia yunnanensis: metabolic alterations and preventive effects against OGD/R-induced oxidative damage in HT22 cells. *Biomed. Rep.* 20 (5), 75. doi:10.3892/br.2024.1763
- Coble, J. N., Fiorello, M. L., and Bailey, D. M. (2018). 13 reasons why the brain is susceptible to oxidative stress. *Redox Biol.* 15, 490–503. doi:10.1016/j.redox.2018.01.008
- Darweesh, S. K. L., Wolters, F. J., Ikram, M. A., Bos, D., and Hofman, A. (2018). Broadening the scope of epidemiologic dementia research. *Eur. J. Epidemiol.* 33 (7), 617–620. doi:10.1007/s10654-018-0421-9
- Detcheverry, F., Senthil, S., Narayanan, S., and Badhwar, A. (2023). Changes in levels of the antioxidant glutathione in brain and blood across the age span of healthy adults: a systematic review. *Neuroimage Clin.* 40, 103503. doi:10.1016/j.nicl.2023.103503
- Fu, P., Chen, Y., Wu, M., Bao, B., Yin, X., Chen, Z., et al. (2023). Effect of ferroptosis on chronic cerebral hypoperfusion in vascular dementia. *Exp. Neurol.* 370, 114538. doi:10.1016/j.expneurol.2023.114538
- Gao, Y., Su, Y., Huo, Y., Mi, J., Wang, X., Wang, Z., et al. (2014). Identification of antihyperlipidemic constituents from the roots of Rubia yunnanensis Diels. *J. Ethnopharmacol.* 155 (2), 1315–1321. doi:10.1016/j.jep.2014.07.027
- Gorelick, P. B., Scuteri, A., Black, S. E., Decarli, C., Greenberg, S. M., Iadecola, C., et al. (2011). Vascular contributions to cognitive impairment and dementia: a statement for

Generative AI statement

The author(s) declare that no Generative AI was used in the creation of this manuscript.

Publisher's note

All claims expressed in this article are solely those of the authors and do not necessarily represent those of their affiliated organizations, or those of the publisher, the editors and the reviewers. Any product that may be evaluated in this article, or claim that may be made by its manufacturer, is not guaranteed or endorsed by the publisher.

Supplementary material

The Supplementary Material for this article can be found online at: <https://www.frontiersin.org/articles/10.3389/fphar.2025.1552228/full#supplementary-material>

healthcare professionals from the american heart association/american stroke association. *Stroke* 42 (9), 2672–2713. doi:10.1161/STR.0b013e3182299496

Hirschhorn, T., and Stockwell, B. R. (2019). The development of the concept of ferroptosis. *Free Radic. Biol. Med.* 133, 130–143. doi:10.1016/j.freeradbiomed.2018.09.043

Horgusluoglu, E., Neff, R., Song, W. M., Wang, M., Wang, Q., Arnold, M., et al. (2022). Integrative metabolomics-genomics approach reveals key metabolic pathways and regulators of Alzheimer's disease. *Alzheimers Dement.* 18 (6), 1260–1278. doi:10.1002/alz.12468

Hsin, K. Y., Ghosh, S., and Kitano, H. (2013). Combining machine learning systems and multiple docking simulation packages to improve docking prediction reliability for network pharmacology. *PLoS One* 8 (12), e83922. doi:10.1371/journal.pone.0083922

Ishii, T., Sato, H., Miura, K., Sagara, J., and Bannai, S. (1992). Induction of cystine transport activity by stress. *Ann. N. Y. Acad. Sci.* 663, 497–498. doi:10.1111/j.1749-6632.1992.tb38714.x

Jin, Y., Cheng, S., Liu, R., Yu, C., Zhang, L., Li, X. L., et al. (2022). Comprehensive characterization of the chemical composition of Lurong dabu decoction and its absorbed prototypes and metabolites in rat plasma using UHPLC-Q Exactive Orbitrap-HRMS. *Food Res. Int.* 161, 111852. doi:10.1016/j.foodres.2022.111852

Joy, A. P., Ayre, D. C., Chute, I. C., Beauregard, A. P., Wajnberg, G., Ghosh, A., et al. (2018). Proteome profiling of extracellular vesicles captured with the affinity peptide Vn96: comparison of Laemmli and TRIzol® protein-extraction methods. *J. Extracell. Vesicles* 7 (1), 1438727. doi:10.1080/20013078.2018.1438727

Kandasamy, M., Anusuyadevi, M., Aigner, K. M., Unger, M. S., Kniwallner, K. M., de Sousa, D. M. B., et al. (2020). TGF-beta signaling: a therapeutic target to reinstate regenerative plasticity in vascular dementia? *Aging Dis.* 11 (4), 828–850. doi:10.14336/AD.2020.0222

Koppula, P., Zhuang, L., and Gan, B. (2021). Cystine transporter SLC7A11/xCT in cancer: ferroptosis, nutrient dependency, and cancer therapy. *Protein Cell* 12 (8), 599–620. doi:10.1007/s13238-020-00789-5

Lan, M. (1959). *Dian nan ben cao*. Kunming, China: yun nan ren min chu ban she

Li, G., Cheng, J., Yang, L., Chen, P., and Duan, X. (2024). Ethanol extract of Rubia yunnanensis inhibits carotid atherosclerosis via the PI3K/AKT signaling pathway. *Biomed. Rep.* 20 (2), 19. doi:10.3892/br.2023.1707

Li, H., Zhang, C., Zhou, Y., Deng, Y., Zheng, X., and Xue, X. (2023). Neurovascular protection of alisol A on cerebral ischemia mice through activating the AKT/GSK3β pathway. *Aging (Albany NY)* 15 (20), 11639–11653. doi:10.18632/aging.205151

Liu, H., Zhang, T. A., Zhang, W. Y., Huang, S. R., Hu, Y., and Sun, J. (2023a). Rhein attenuates cerebral ischemia-reperfusion injury via inhibition of ferroptosis through NRF2/SLC7A11/GPX4 pathway. *Exp. Neurol.* 369, 114541. doi:10.1016/j.expneurol.2023.114541

- Liu, S., Chen, W., Zhao, Y., Zong, Y., Li, J., and He, Z. (2023b). Research progress on effects of ginsenoside Rg2 and Rh1 on nervous system and related mechanisms. *Molecules* 28 (23), 7935. doi:10.3390/molecules28237935
- Liu, T., Jiang, L., Tavara, O., and Gu, W. (2019). The deubiquitylase OTUB1 mediates ferroptosis via stabilization of SLC7A11. *Cancer Res.* 79 (8), 1913–1924. doi:10.1158/0008-5472.CAN-18-3037
- Longa, E. Z., Weinstein, P. R., Carlson, S., and Cummins, R. (1989). Reversible middle cerebral artery occlusion without craniectomy in rats. *Stroke* 20 (1), 84–91. doi:10.1161/01.str.20.1.84
- Luo, T. T., Lu, Y., Yan, S. K., Xiao, X., Rong, X. L., and Guo, J. (2020). Network pharmacology in research of Chinese medicine formula: methodology, application and prospective. *Chin. J. Integr. Med.* 26 (1), 72–80. doi:10.1007/s11655-019-3064-0
- Mukamal, K. J. (2020). Nonesterified fatty acids, cognitive decline, and dementia. *Curr. Opin. Lipidol.* 31 (1), 1–7. doi:10.1097/MOL.0000000000000656
- Nam, D. G., Kim, M., Choi, A. J., and Choe, J. S. (2024). Health benefits of antioxidant bioactive compounds in ginger (zingiber officinale) leaves by network pharmacology analysis combined with experimental validation. *Antioxidants (Basel)* 13 (6), 652. doi:10.3390/antiox13060652
- Pendlebury, S. T., Rothwell, P. M., and Oxford Vascular, S. (2019). Incidence and prevalence of dementia associated with transient ischaemic attack and stroke: analysis of the population-based Oxford Vascular Study. *Lancet Neurol.* 18 (3), 248–258. doi:10.1016/S1474-4422(18)30442-3
- Pohjala, L., and Tammela, P. (2012). Aggregating behavior of phenolic compounds--a source of false bioassay results? *Molecules* 17 (9), 10774–10790. doi:10.3390/molecules170910774
- Rochette, L., Dogon, G., Rigal, E., Zeller, M., Cottin, Y., and Vergely, C. (2022). Lipid peroxidation and iron metabolism: two corner stones in the homeostasis control of ferroptosis. *Int. J. Mol. Sci.* 24 (1), 449. doi:10.3390/ijms24010449
- Rochette, L., Gudjoncik, A., Guenancia, C., Zeller, M., Cottin, Y., and Vergely, C. (2015). The iron-regulatory hormone hepcidin: a possible therapeutic target? *Pharmacol. Ther.* 146, 35–52. doi:10.1016/j.pharmthera.2014.09.004
- She, X., Lan, B., Tian, H., and Tang, B. (2020). Cross talk between ferroptosis and cerebral ischemia. *Front. Neurosci.* 14, 776. doi:10.3389/fnins.2020.00776
- Shi, Y., Han, L., Zhang, X., Xie, L., Pan, P., and Chen, F. (2022). Selenium alleviates cerebral ischemia/reperfusion injury by regulating oxidative stress, mitochondrial fusion and ferroptosis. *Neurochem. Res.* 47 (10), 2992–3002. doi:10.1007/s11064-022-03643-8
- Tanovic, A., and Alfaro, V. (2006). Glutamate-related excitotoxicity neuroprotection with memantine, an uncompetitive antagonist of NMDA-glutamate receptor, in Alzheimer's disease and vascular dementia. *Rev. Neurol.* 42 (10), 607–616. doi:10.33588/rn.4210.2005252
- Tu, M. C., Chung, H. W., Hsu, Y. H., Yang, J. J., and Wu, W. C. (2023). Neurovascular correlates of cobalamin, folate, and homocysteine in dementia. *J. Alzheimers Dis.* 96 (3), 1329–1338. doi:10.3233/JAD-230763
- Wang, C., Zhang, D., Ma, H., and Liu, J. (2007). Neuroprotective effects of emodin-8-O-beta-D-glucoside *in vivo* and *in vitro*. *Eur. J. Pharmacol.* 577 (1-3), 58–63. doi:10.1016/j.ejphar.2007.08.033
- Wu, C., Duan, F., Yang, R., Dai, Y., Chen, X., and Li, S. (2023). 15, 16-Dihydrotanshinone I protects against ischemic stroke by inhibiting ferroptosis via the activation of nuclear factor erythroid 2-related factor 2. *Phytomedicine* 114, 154790. doi:10.1016/j.phymed.2023.154790
- Wu, Y., Jia, Q., Tang, Q., Deng, H., He, Y., and Tang, F. (2024). Berberine-mediated ferroptosis through system Xc(-)/GSH/GPX4 Axis inhibits metastasis of nasopharyngeal carcinoma. *J. Cancer* 15 (3), 685–698. doi:10.7150/jca.90574
- Wu, C., Sun, S., Johnson, T., Qi, R., Zhang, S., Zhang, J., et al. (2021). The glutathione peroxidase Gpx4 prevents lipid peroxidation and ferroptosis to sustain Treg cell activation and suppression of antitumor immunity. *Cell Rep.* 35 (11), 109235. doi:10.1016/j.celrep.2021.109235
- Xu, S., Li, X., Li, Y., Li, X., Lv, E., Zhang, X., et al. (2023). Neuroprotective effect of DI-3-n-butylphthalide against ischemia-reperfusion injury is mediated by ferroptosis regulation via the SLC7A11/GSH/GPX4 pathway and the attenuation of blood-brain barrier disruption. *Front. Aging Neurosci.* 15, 1028178. doi:10.3389/fnagi.2023.1028178
- Yuan, Z., Zhou, H., Zhou, N., Dong, D., Chu, Y., Shen, J., et al. (2019). Dynamic evaluation indices in spatial learning and memory of rat vascular dementia in the Morris water maze. *Sci. Rep.* 9 (1), 7224. doi:10.1038/s41598-019-43738-x
- Zhang, J., Zhao, Y., Yan, L., Tan, M., Jin, Y., Yin, Y., et al. (2024). Corosolic acid attenuates cardiac ischemia/reperfusion injury through the PHB2/PINK1/parkin/mitophagy pathway. *iScience* 27 (8), 110448. doi:10.1016/j.isci.2024.110448
- Zhang, R., Miao, Y., Chen, L., Yi, S., and Tan, N. (2022). De novo transcriptome analysis reveals putative genes involved in anthraquinone biosynthesis in Rubia yunnanensis. *Genes (Basel)* 13 (3), 521. doi:10.3390/genes13030521
- Zhao, L., Yu, X., Wu, S., Xia, K., Wang, Y., Qin, P., et al. (2024). Pharmacokinetic profiling and network pharmacology of honey-fried Licorice: an Integrative workflow to study traditional Chinese medicines (TCMs). *J. Chromatogr. B Anal. Technol. Biomed. Life Sci.* 1248, 124353. doi:10.1016/j.jchromb.2024.124353
- Zheng, J., and Conrad, M. (2020). The metabolic underpinnings of ferroptosis. *Cell Metab.* 32 (6), 920–937. doi:10.1016/j.cmet.2020.10.011
- Zhu, T., Wang, L., Feng, Y., Sun, G., and Sun, X. (2021). Classical active ingredients and extracts of Chinese herbal medicines: pharmacokinetics, pharmacodynamics, and molecular mechanisms for ischemic stroke. *Oxid. Med. Cell Longev.* 2021, 8868941. doi:10.1155/2021/8868941



OPEN ACCESS

EDITED BY

Jawed A. Siddiqui,
New York University, United States

REVIEWED BY

Jian Hao,
The Second Affiliated Hospital of Guangzhou
Medical University, China
Nihar Ranjan Jana,
Indian Institute of Technology Kharagpur, India
Anjan Thakurta,
University of Oxford, United Kingdom

*CORRESPONDENCE

Sanghamitra Bandyopadhyay,
✉ sanghmitra@iitr.res.in,
✉ bandyo12@gmail.com
Jimut Kanti Ghosh,
✉ jk_ghosh@cdri.res.in

RECEIVED 12 October 2024

ACCEPTED 13 January 2025

PUBLISHED 25 February 2025



CITATION

Garg A, Saroj J, Tiwari S, Das U, Shukla N,
Ghosh JK and Bandyopadhyay S (2025)
Exploring the potential anti-senescence effects
of soybean-derived peptide Soymetide in mice
hippocampal neurons via the Wnt/ β -
catenin pathway.
Front. Pharmacol. 16:1510337.
doi: 10.3389/fphar.2025.1510337

COPYRIGHT

© 2025 Garg, Saroj, Tiwari, Das, Shukla, Ghosh
and Bandyopadhyay. This is an open-access
article distributed under the terms of the
[Creative Commons Attribution License \(CC BY\)](https://creativecommons.org/licenses/by/4.0/).
The use, distribution or reproduction in other
forums is permitted, provided the original
author(s) and the copyright owner(s) are
credited and that the original publication in this
journal is cited, in accordance with accepted
academic practice. No use, distribution or
reproduction is permitted which does not
comply with these terms.

Exploring the potential anti-senescence effects of soybean-derived peptide Soymetide in mice hippocampal neurons via the Wnt/ β -catenin pathway

Asmita Garg^{1,2}, Jyotshana Saroj^{2,3}, Saurabh Tiwari^{1,2},
Uttara Das^{1,2}, Neetu Shukla^{1,2}, Jimut Kanti Ghosh ^{2,3*} and
Sanghamitra Bandyopadhyay ^{1,2*}

¹Systems Toxicology Group, Food, Drug and Chemical, Environment and Systems Toxicology Division, CSIR-Indian Institute of Toxicology Research (CSIR-IITR), Lucknow, Uttar Pradesh, India, ²Academy of Scientific and Innovative Research (AcSIR), Ghaziabad, India, ³Biochemistry and Structural Biology Division, CSIR-Central Drug Research Institute, Lucknow, India

Soybean-based foods enhance cognitive functions by influencing hippocampal mechanisms. These salutary effects have so far been attributed to isoflavones present in soybeans. Considering cellular senescence contributes to cognitive decline and that no specific soy-derived peptides are known for their potential to mitigate senescence, we examined the efficacy of a thirteen amino acid soy-derived peptide, Soymetide, on a doxorubicin-induced senescence mice model. Soymetide pretreatment lowered the senescence markers p53, p21 and p16, pro-inflammatory cytokines, and Senescence β -Galactosidase staining while enhancing the mature neuronal marker NeuN in the hippocampus. This anti-senescent effect was comparable with that of a well-known senolytic combination (dasatinib and quercetin). Research indicates that Wnt signaling influences cellular senescence, and our findings here demonstrate that doxorubicin decreased hippocampal Wnt3a, p-LRP6, Frizzled, Dishevelled, Axin1, and β -catenin levels and increased GSK-3 β , while Soymetide mitigated these effects. Additionally, upon inhibition of the Wnt/ β -catenin pathway, Soymetide's ability to reduce senescence markers and restore NeuN expression was reduced. We validated the anti-senescence impact on hippocampal neurons by co-immunostaining Wnt/ β -catenin and senescence indicators alongside NeuN in mice and assessed it in primary hippocampal neurons. Further examining the neuronal survival and functions revealed that Soymetide blocked the doxorubicin-induced loss in Nissl-stained surviving neurons and learning-memory performances, measured by Y-Maze and Passive Avoidance tests, which Wnt/ β -catenin inhibitors could counteract. In conclusion, our study identifies a novel Wnt/ β -catenin-linked mechanism of doxorubicin-induced senescence in the hippocampal neurons and

demonstrates Soymetide's effectiveness in reversing this process. Hence, this suggests Soymetide's potential therapeutic application in addressing cognitive decline associated with cellular aging.

KEYWORDS

Soymetide, senescence, doxorubicin, Wnt/ β -catenin pathway, hippocampus, neuroprotection

Introduction

Cellular senescence, characterized by irreversible cell cycle arrest, is increasingly recognized for its role in hippocampal decline (Lin et al., 2021). Senescence affects hippocampal neurons by diminishing their functionality and plasticity, leading to a decline in cognitive abilities such as learning and memory (Miyamoto et al., 1986). The senescent neurons express markers like p53, p21, p16, and β -Galactosidase and morphological alterations (Mijit et al., 2020; Wang et al., 2024). This may promote the generation of senescence-associated secretory phenotype (SASP) cytokines, exacerbating neuroinflammation (Saito et al., 2021). Hence, while cellular senescence is a physiological process, its aberrant accumulation adversely affects neuronal health, causing age-associated hippocampal dysfunction (Piechota et al., 2016; Wissler Gerdes et al., 2020).

The Wnt signaling pathway, particularly involving Wnt3a, plays a crucial role in hippocampal neuronal processes and functions (Fortress and Frick, 2016; Arrazola et al., 2017). An activated Wnt pathway has been linked to enhanced neurogenesis and neuronal survival within the hippocampus (Inestrosa et al., 2004; Avila et al., 2010; Wei et al., 2012; Zhang et al., 2022a; Tao et al., 2023). Additionally, reduced Wnt3a expression or aberrant downstream signaling events may contribute to cognitive decline (Oliva et al., 2013; Palomer et al., 2019). Wnt3a interacts with cell-surface receptor Frizzled (Fz) and Low-density lipoprotein receptor-related protein 6 (LRP6), triggering downstream events involving Dishevelled (Dvl) and Axin1 (Huang and Klein, 2004; Garg and Bandyopadhyay, 2024). Notably, Glycogen Synthase Kinase-3 β (GSK-3 β) serves as a key player in the Wnt pathway, where an inhibited GSK-3 β may lead to cytoplasmic accumulation of β -catenin, affecting hippocampal functions and neuronal health (Beurel et al., 2015; Li et al., 2024).

Emerging evidence suggests a link between the Wnt/ β -catenin signaling pathway and cell senescence or aging in the brain (Jia et al., 2019; Chen et al., 2020). A dysregulated Wnt signaling associated with senescence involving morphological changes in brain cells, cell cycle alterations, β -Galactosidase staining, and decline in cognitive functions (Li et al., 2018; Swarbrick et al., 2019; Xiang et al., 2019; Zhang et al., 2019; Prud'homme et al., 2022). Cellular senescence demonstrated a connection with Wnt signaling in the hippocampus as well, involving the participation of altered Dickkopf-1 (a secreted inhibitor of β -catenin-dependent Wnt signaling), GSK-3 β activation, β -catenin, along with neuronal loss and dysregulated expression of apoptosis-related proteins (Bayod et al., 2015). Hence, targeting Wnt pathway components and reducing senescence could hold promise as a therapeutic strategy for mitigating neurodegeneration and cognitive decline.

The beneficial effects of soy-based foods in mitigating cognitive decline are primarily attributed to phytoestrogen isoflavones (Kim, 2021). Although largely uncharacterized, research has shown promising outcomes in animal models of cognitive decline and behavioral deficits with soy protein isolates/peptide mixture (Dong et al., 2023; Zheng et al., 2023; Tamura et al., 2024). These protein isolates/peptide mixtures/soy food demonstrated protection against neuronal damage, promoted neurogenesis, regulated neurotransmitter synthesis and metabolism, increased neurotrophin signaling, induced anti-inflammatory and antioxidant effects in the brain, modulated neuronal apoptosis, and mitigated cognitive decline (Jeong et al., 2021; Dong et al., 2023; Zheng et al., 2023; Tamura et al., 2024). Human studies also indicate a lower risk of dementia and significant improvements in cognition and neurotrophin levels associated with consuming soy products (Hwang et al., 2019; Deng et al., 2023).

Building on this evidence, our study aims to investigate the therapeutic potential of a short-length soy-derived bioactive peptide, Soymetide (Schuler et al., 1982; Tsuruki et al., 2003) in preventing age-related senescence. Utilizing a doxorubicin-induced senescent mouse model, we explored the effects of Soymetide on the senescence markers in the hippocampus. We investigated the participation of the Wnt/ β -catenin pathway in the process. Our study aimed to examine the anti-senescence and cognitive improvement capabilities, as well as the underlying mechanisms of Soymetide for potential therapeutic applications in senescence-related neurological disorders of which memory impairment is the dominant type. Through the investigation of these mechanisms, we seek to evaluate Soymetide's efficacy in improving cognitive function and its therapeutic role in addressing age-related neurological conditions, especially those associated with memory deficits.

Materials and methods

Reagents, chemicals and antibodies

Doxorubicin hydrochloride (cat no. PHR1789), dasatinib (cat no. SML2589), quercetin (cat no. Q4951), β -Catenin/Tcf Inhibitor III, iCRT3 (cat no. 219332) and cresyl violet acetate (cat no. C5042) were bought from Sigma-Aldrich (St. Louis, Missouri). Human Dkk-1 Recombinant Protein (cat no. PHC9214) and Mouse ProcartaPlex Mix&Match 9-plex kit (cat no. PPX-09-MX2XAC3) were purchased from Thermo Fisher Scientific (Waltham, Massachusetts). Senescence β -Galactosidase Staining Kit (cat no. 9860) was purchased from Cell Signaling Technology (Danvers, Massachusetts). Polyvinylidene difluoride membrane (cat no. IPVH00010) and Immobilon Western Chemiluminescent HRP Substrate (cat no. WBKLS0500) were bought from MilliporeSigma

(Burlington, Massachusetts). The prestained protein ladders (cat no. PG-PMT2922 and cat no. 786419) were procured from Genetix Biotech Asia Pvt Ltd. (New Delhi, India) and G-Biosciences (St. Louis, Missouri), respectively. Vectashield mounting medium with DAPI was purchased from Vector Laboratories (Newark, California). Mouse monoclonal p53 (cat no. 2524), rabbit polyclonal p21 (cat no. 64016), phospho-LRP6 (cat no. 2568), β -catenin (cat no. 9562), rabbit monoclonal NeuN (cat no. 24307), LRP6 (cat no. 3395), Dvl2 (cat no. 3224), Axin1 (cat no. 2087), GSK-3 β (cat no. 12456) and TCF3/TCF7L1 (cat no. 2883) antibodies were purchased from Cell Signaling Technology. Rabbit polyclonal p16INK4a (cat no. PA5-20379) antibody was purchased from Thermo Fisher Scientific. Rabbit polyclonal Wnt3a (cat no. 09162), HRP-conjugated secondary anti-rabbit IgG (cat no. A0545), and anti-mouse IgG (cat no. A9044) antibodies were purchased from Sigma-Aldrich. Rabbit polyclonal Frizzled-7 (cat no. ab64636) antibody was purchased from Abcam (Cambridge, Massachusetts). Horseradish peroxidase (HRP)-conjugated mouse monoclonal β -actin (cat no. sc-47778) antibody was procured from Santa Cruz Biotechnology (Dallas, Texas). Mouse monoclonal NeuN (cat no. 66836-1-Ig) and rabbit polyclonal NeuN (cat no. 26975-1-AP) antibodies were procured from Proteintech (Rosemond, Illinois). Alexa Fluor[®] 546 goat anti-rabbit IgG (cat no. A11010), Alexa Fluor[®] 488 goat anti-mouse IgG (cat no. A11001), Alexa Fluor[®] 546 goat anti-mouse IgG (cat no. A11030) and Alexa Fluor[®] 488 goat anti-rabbit IgG (cat no. A11008) were procured from Invitrogen (Carlsbad, California). *In Situ* Cell Death Detection Kit, Fluorescein (cat no. 11684795910) was purchased from Roche (Mannheim, Germany).

Peptide synthesis

Soymetide (Soym; MITLAIPVNKPGR) (Schuler et al., 1982; Tsuruki et al., 2003) was synthesized (98.27% purity (HPLC), -20°C storage in the dark) by GL Biochem Shanghai Ltd. (Shanghai, China). We designed the Scrambled peptide (Scr; MVNLGIPITKPAR), which was subsequently synthesized by GL Biochem Shanghai Ltd.

Animal treatments

C57BL/6 male mice were kept under a 12-h light/dark cycle condition with *ad libitum* availability of chow diet and R. O water. The treatment and assessment timeline of mice is as shown in [Supplementary Material 1](#). To generate a senescence mice model, mice (≈ 22 –25 gm) were intraperitoneally injected with doxorubicin hydrochloride (DOX; 1, 5 and 10 mg/kg in PBS), once a week for 4 weeks, closely following the reported protocol (Sun et al., 2022). To examine whether Soymetide had anti-senescence properties, it was once injected bilaterally (2 $\mu\text{L}/\text{min}$) into the hippocampus of mice through stereotaxic surgery (coordinates: AP -1.7 , ML $+1.6$, DV -1.9 to bregma) (Sierra et al., 2015; Garg and Bandyopadhyay, 2024) at doses of 10, 50, and 100 $\mu\text{g}/\text{kg}$ in PBS (4 μL), 7 days before the doxorubicin treatment. To specifically identify the effect of Soymetide, scrambled peptide (50 $\mu\text{g}/\text{kg}$ in PBS) was given to the mice in the same method and schedule. A senolytic combination of dasatinib (D) (5 mg/kg) plus quercetin (Q) (50 mg/kg) (D + Q) (Wang et al., 2023) was orally administered

to the doxorubicin-treated mice once a week for 4 weeks as a positive control. To assess the role of Wnt in the doxorubicin and Soymetide-induced effects, recombinant Dickkopf-1 (rDkk1) protein [200 ng in 2 μL sterile saline (Garg and Bandyopadhyay, 2024)] was injected into the hippocampus of Soymetide- and doxorubicin-treated mice through stereotaxic surgery, 7 days before the assessment. To assess the role of β -catenin, inhibitor of β -catenin responsive transcription-3 (iCRT3) protein [5 mg/kg in sterile saline with 5% DMSO (Sharma et al., 2017)] was injected intraperitoneally into the Soymetide- and doxorubicin-treated mice. Vehicle-only-treated sets were included for every treatment. Animal treatment and behavioral analyses were randomized to ensure an unbiased approach.

Western blotting

The hippocampal tissue was isolated from the mice brain, and the proteins (30–50 μg) were separated using SDS-PAGE (8%–15%) and transferred onto a PVDF membrane, as we reported (Garg and Bandyopadhyay, 2024). The blots were probed with p53, p21, p16, NeuN, Wnt3a, p-LRP6, LRP6, Fz, Dishevelled, Axin1, GSK-3 β , β -catenin and TCF3 antibodies for overnight (1:1000 dilution; 4°C), and HRP-conjugated β -actin antibody (loading control) for 2 h (1:5000; room temperature). Except for the β -actin-probing, the blots were incubated with HRP-conjugated secondary antibody for 2 h (1:5000 dilution; room temperature) and developed using Immobilon Western Chemiluminescent HRP Substrate in Amersham Imager 600 (GE Healthcare Life Sciences, Pittsburgh, Pennsylvania). Relative protein levels were determined by densitometric quantification by applying the Quantity One software (Bio-Rad Laboratories, Hercules, California).

Cytokine multiplexing

Blood samples of mice were collected and serum was isolated (Pandey et al., 2022). The quantitative determination of cytokine levels in serum was performed using the Mouse ProcartaPlex Mix&Match 9-plex kit as per its manufacturer's protocol. The cytokine levels were measured using Luminex MAGPIX[®] instrument (Bio-Rad Laboratories) and expressed as the mean Magnetic Fluorescence Intensity (MFI).

Senescence β -galactosidase staining

The whole brain was isolated from mice after transcardial perfusion with PBS, cryoprotected (on dry ice) in OCT and stored at -80°C (Das et al., 2016), and subsequently cut into 30- μm thick coronal sections using a cryomicrotome (Microm HM 520, Labcon, Germany). Following the manufacturer's protocol of the Senescence β -Galactosidase staining kit, the sections were fixed (using the fixative solution) for 15 min at room temperature, stained with β -Galactosidase staining solution (pH 6.0) that contained 0.2% X-Gal, and incubated for 18 h at 37°C in a dry incubator (Sarkar et al., 2011). The sections were then mounted with 70% glycerol solution, and images of the hippocampus were captured under a 20 \times objective [Leica DMi1 microscope (Leica

Microsystems, Wetzlar, Germany)]. The results were quantified using ImageJ software (Wayne Rasband, NIH).

Immunofluorescence

The whole brain was isolated from mice after perfusion with PFA (4%), cryoprotected, and 10- μ m thick sections were prepared using a cryomicrotome, as previously described by us (Gupta et al., 2022). Sections were then probed with the Wnt3a, β -catenin, p53, p16, and NeuN primary antibodies overnight (1:250 dilution; 4°C), incubated with Alexa Fluor secondary antibodies for 2 h (1:500 dilution; room temperature), and mounted using VECTASHEILD anti-fade mounting media containing DAPI. Fluorescence photomicrography of the hippocampus was conducted in these sections under 20 \times objective (NIS-Elements software, Nikon Instech Co. Ltd., Kawasaki, Kanagawa, Japan), and the images were processed using the ImageJ software.

Nissl staining

Cryosections of 30- μ m thickness were made and processed for Cresyl violet acetate staining following our previously described protocol (Mishra et al., 2021). Images of the hippocampus were captured in these sections with 20 \times and 40 \times objectives [Leica DMi1 microscope (Leica Microsystems)] and imported into the ImageJ software. The surviving neurons (%) were then manually counted from five different fields using the Cell Counter plugin.

Terminal deoxynucleotidyl transferase dUTP nick-end labeling (TUNEL) assay

Hippocampal neuronal apoptosis was assessed as reported earlier (Pandey et al., 2017). Briefly, 10- μ m brain sections were treated with TdT and fluorescein-labeled dUTP, immunostained with anti-rabbit NeuN, and then mounted. The images of the hippocampus were captured (20 \times) and TUNEL-positive neurons were counted in five random areas using ImageJ, expressed as TUNEL-positive cells per 100 DAPI-stained nuclei.

Learning and memory assays

Mice were subjected to Y-maze and Passive Avoidance tests to assess learning and memory functions, as we previously reported (Pandey et al., 2020). For the Y-Maze test, the learning trials (training) were conducted on mice in a Y-Maze apparatus, where running to the unsafe arms (dark arms with foot shock) from the safe arm (bright and shock-free) was considered an error. The % number of errors (E) was calculated for learning trials. Further, the % Saving Memory was assessed in the Y-Maze apparatus at 24 h, 48 h, and 7th day post-learning, and calculated as (Etraining–Etest) \times 100/Etraining. During the Passive Avoidance test, mice were subjected to acquisition trials in a gated two-compartment apparatus. One compartment was bright and free of shocks, while the other was dark and delivered an electrical shock. After 24 h (R1), 48 h (R2), and 72 h (R3) of acquisition trials, three

shock-free retention trials of 300 s each were conducted. The time taken by the mice to move from the bright to the dark compartment was considered as transfer latency time (TLT) for learning-memory performance.

Primary neuronal culture and treatments

Embryos were collected at embryonic day 16 (E-16), and the hippocampus was dissected in Hank's Balanced Salt Solution (HBSS), followed by mechanical digestion in serum-free neurobasal media, as previously reported (Pandey et al., 2020). The suspension was digested using 0.05% trypsin-EDTA and incubated for 15 min at 37°C in a CO₂ incubator, and treated with trypsin inhibitor to neutralize the effect of trypsin. The remaining suspension was centrifuged at 1500 rpm for 10 min and the pellet was suspended in the complete neurobasal medium containing N2 supplement (1%), B-27 supplement (2%), 2 mM L-glutamine, penicillin (100 units/mL), streptomycin (100 μ g/mL) and amphotericin (0.25 μ g/mL). Cells were plated on poly-L-lysine-coated 25 cm² flask or 4-well culture plates and grown in a humidified incubator at 37°C with 5% CO₂. Doxorubicin at 50 nM (Marques et al., 2020) was then added to the neurons for 18 h to induce senescence. For standardizing the treatment dose of Soymetide, neurons were pre-treated for 2 h with Soymetide at doses of 1, 10, and 100 nM followed by co-treatment with doxorubicin and assessed for the lowest dose affecting p53 levels (Supplementary Material 2). To analyze the role of Wnt and β -catenin, rDkk1 2.38 nM (Wei et al., 2019) and iCRT3 20 μ M (Lee et al., 2013) were given to the cells, respectively, 2 h before the assessment time.

Protein extraction and western blotting (*in vitro*)

Primary neurons were first lysed with cell lysis reagent and Western blotting was carried out as above using the Wnt3a, β -catenin, p53, p16, NeuN and β -actin antibodies.

Senescence β -galactosidase staining (*in vitro*)

Primary hippocampal neurons were plated onto poly-L-lysine-coated chamber slides. Following the treatment and washing with PBS, fixation, and staining of the cells were performed as per the manufacturer's protocol of the Senescence β -Galactosidase staining kit. Briefly, the cells were fixed in the fixative solution for 10–15 min at room temperature, washed with PBS, and incubated in a no CO₂ incubator with the staining solution overnight at 37°C. 70% glycerol solution was used to mount the slides. Images of the cells were captured with a 40 \times objective [Leica DMi1 microscope (Leica Microsystems)].

Statistics

One-way ANOVA for comparisons involving a single parameter across multiple groups (Figures 1A–7C) or two-way ANOVA for multiple parameters and groups (Figures 7D, E), with subsequent

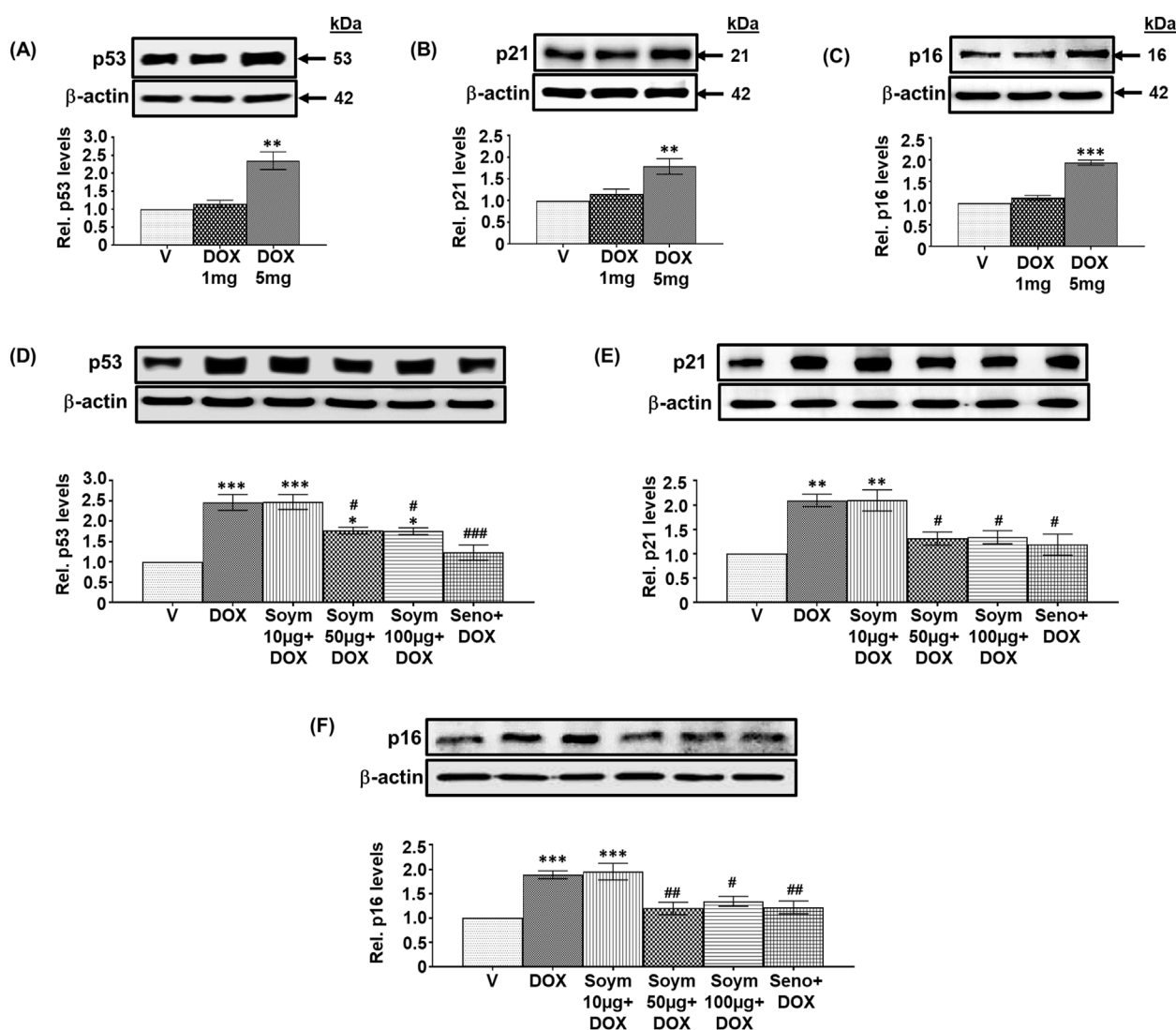


FIGURE 1

Soymetide prevents doxorubicin-induced senescence in the hippocampus of mice. Hippocampal tissues were isolated from vehicle (V), doxorubicin (DOX), Soymetide (Soym)+DOX and senolytic combination (Seno)+DOX-treated mice. (A–F) Representative Western blots and corresponding densitometry (relative to (Rel.) vehicle) of p53 (A, D), p21 (B, E), and p16 (C, F) normalized with β -actin in the hippocampal tissues. Data represent means \pm Standard Error (SE) of three mice/group. *** $p < 0.001$, ** $p < 0.01$ and * $p < 0.05$ compared to V. ### $p < 0.001$, ## $p < 0.01$ and # $p < 0.05$ compared to DOX.

Tukey's posthoc tests for detailed comparisons, was conducted (GraphPad Software, Inc., San Diego, California).

Results

Effect of Soymetide and doxorubicin on senescence markers in the hippocampus of mice

We conducted a screening study to investigate how different doses of doxorubicin (1 mg/kg, 5 mg/kg, and 10 mg/kg) affect senescence in the hippocampus of mice. Specifically, we measured the levels of senescence markers p53, p21 and p16. Our observation indicated that 1 mg/kg had no effect, while 5 mg/kg elevated the

hippocampal p53 (Figure 1A), p21 (Figure 1B), and p16 (Figure 1C) levels, and 10 mg/kg was lethal (data not shown). Therefore, we continued our study using a 5 mg/kg dose of doxorubicin. Next, we investigated whether Soymetide pretreatment (10, 50, and 100 μ g/kg) affected the doxorubicin-induced senescence in the hippocampus of mice. Our findings indicated that 10 μ g/kg of Soymetide had no effect. However, doses of 50 and 100 μ g/kg caused a reduction in the doxorubicin-induced hippocampal p53 (Figure 1D), p21 (Figure 1E) and p16 (Figure 1F) levels, which were comparable to that of a previously demonstrated senolytic combination, D + Q (referred to Seno in Figure) (Krzystyniak et al., 2022) (Figures 1D–F). (The scrambled peptide did not affect the doxorubicin-induced senescence in the hippocampus (Supplementary Material 3). We conducted further analysis of the other features of senescence. We found that doxorubicin

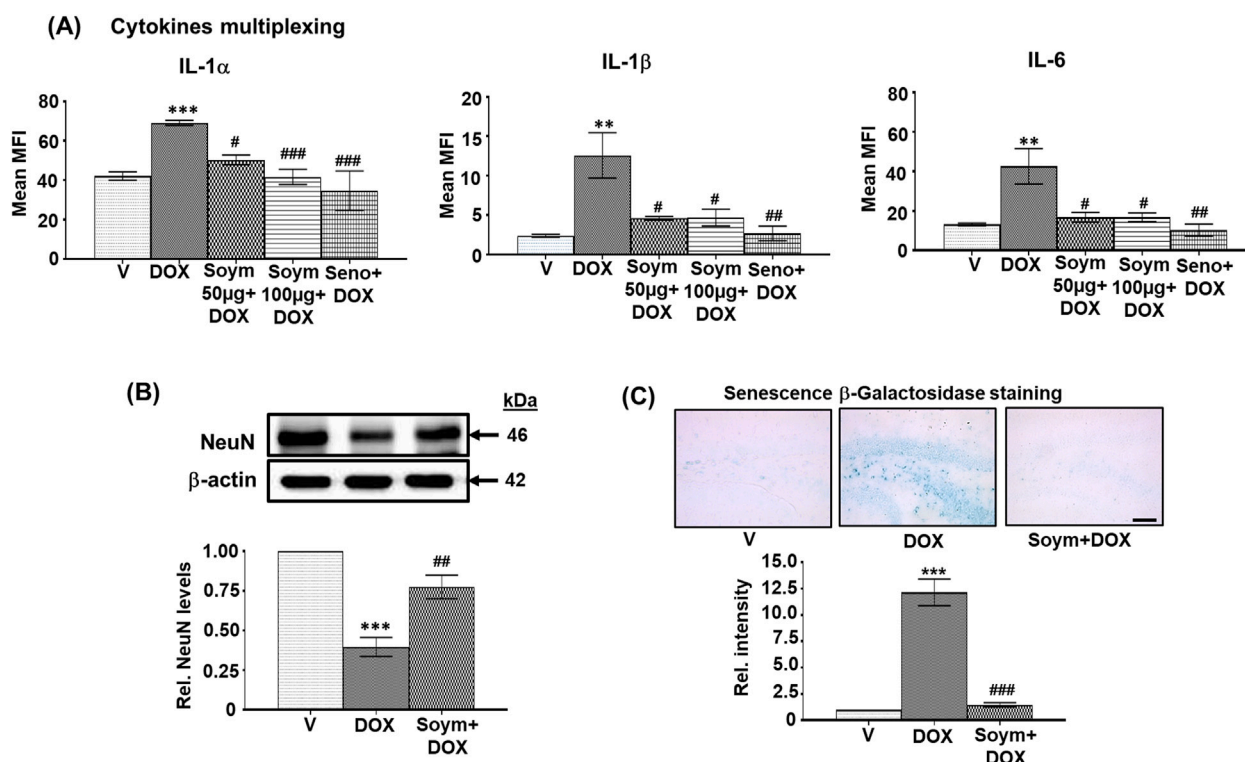


FIGURE 2

Soymetide prevents doxorubicin-induced rise in serum cytokine levels and hippocampal β -Galactosidase staining and the loss of hippocampal NeuN levels in mice. Serum was isolated from the blood of vehicle (V), doxorubicin (DOX), Soymetide (Soym)+DOX, and senolytic combination (Seno)+DOX-treated mice. (A) Representative densitometry of serum IL-1 α , IL-1 β and IL-6 levels. Hippocampal tissues and whole brain were isolated from vehicle (V), doxorubicin (DOX), and Soymetide (Soym)+DOX-treated mice. (B) Representative Western blots and corresponding densitometry (relative to vehicle) of NeuN normalized with β -actin in the hippocampal tissues. (C) Representative photomicrographs and corresponding bar graph (relative to vehicle) of Senescence β -Galactosidase-stained hippocampus. Scale bar: 100 μ m. Data represent means \pm SE of three mice/group. ***p < 0.001 and **p < 0.01 compared to V. ###p < 0.001, ##p < 0.01 and #p < 0.05 compared to DOX.

increased the expression of SASP inflammatory factors, such as IL-1 α , IL-1 β and IL-6, while Soymetide (50 and 100 μ g/kg) and senolytic combination, D + Q reduced SASP levels (Figure 2A). We proceeded with our study using 50 μ g/kg of Soymetide, i.e., the lower dose of Soymetide showing anti-senescence activity.

We further found that doxorubicin reduced the matured neuronal marker, NeuN (Figure 2B), and increased the Senescence β -Galactosidase staining in neurons (Figure 2C). These effects were inhibited by Soymetide (Figures 2B, C).

Effect of Soymetide and doxorubicin on Wnt pathway and its link with anti-senescence effects in the hippocampus

We explored the effects of doxorubicin on the Wnt pathway (known to participate in neuronal functioning (Garg and Bandyopadhyay, 2024) and its involvement in the anti-senescence activity induced by Soymetide. Our initial findings demonstrated a reduction in the levels of hippocampal Wnt3a (Figure 3A), along with decreases in Wnt receptors, p-LRP6 (Figure 3B) and Fz (Figure 3C), and Wnt pathway components, Dvl (Figure 3D) and Axin1 (Figure 3E), following administration of doxorubicin. This treatment caused an increase in GSK-3 β levels (Figure 3F) and a

decrease in β -catenin (Figure 3G). However, pre-treatment with Soymetide appeared to counteract these effects, suggesting a restoration of the Wnt/ β -catenin pathway (Figures 3A–G). Upon investigating the interplay between the Wnt/ β -catenin pathway components and anti-senescence mechanism, our findings demonstrated that blocking Wnt and β -catenin with rDkk1 and iCRT3, respectively, prevented the Soymetide-induced decreases in p53 (Figure 4A), p21 (Figure 4B) and p16 (Figure 4C) and Senescence β -Galactosidase staining (Figure 4D), and increase in NeuN levels (Figure 4E). These findings suggested the participation of the components of Wnt3a/ β -catenin pathway in the senescence mechanism of the hippocampus, which Soymetide can inhibit.

Effect of Soymetide and doxorubicin on senescence and Wnt signaling in the hippocampal neurons

We verified the involvement of Wnt3a/ β -catenin signaling in the hippocampal neuronal senescence. Our co-immunolabeling experiment with NeuN revealed a decrease in Wnt3a (Figure 5A) and β -catenin (Figure 5B), and an increase in p53 (Figure 5C) and p16 (Figure 5D) in the hippocampal neurons of mice following doxorubicin treatment. However, these changes were counteracted

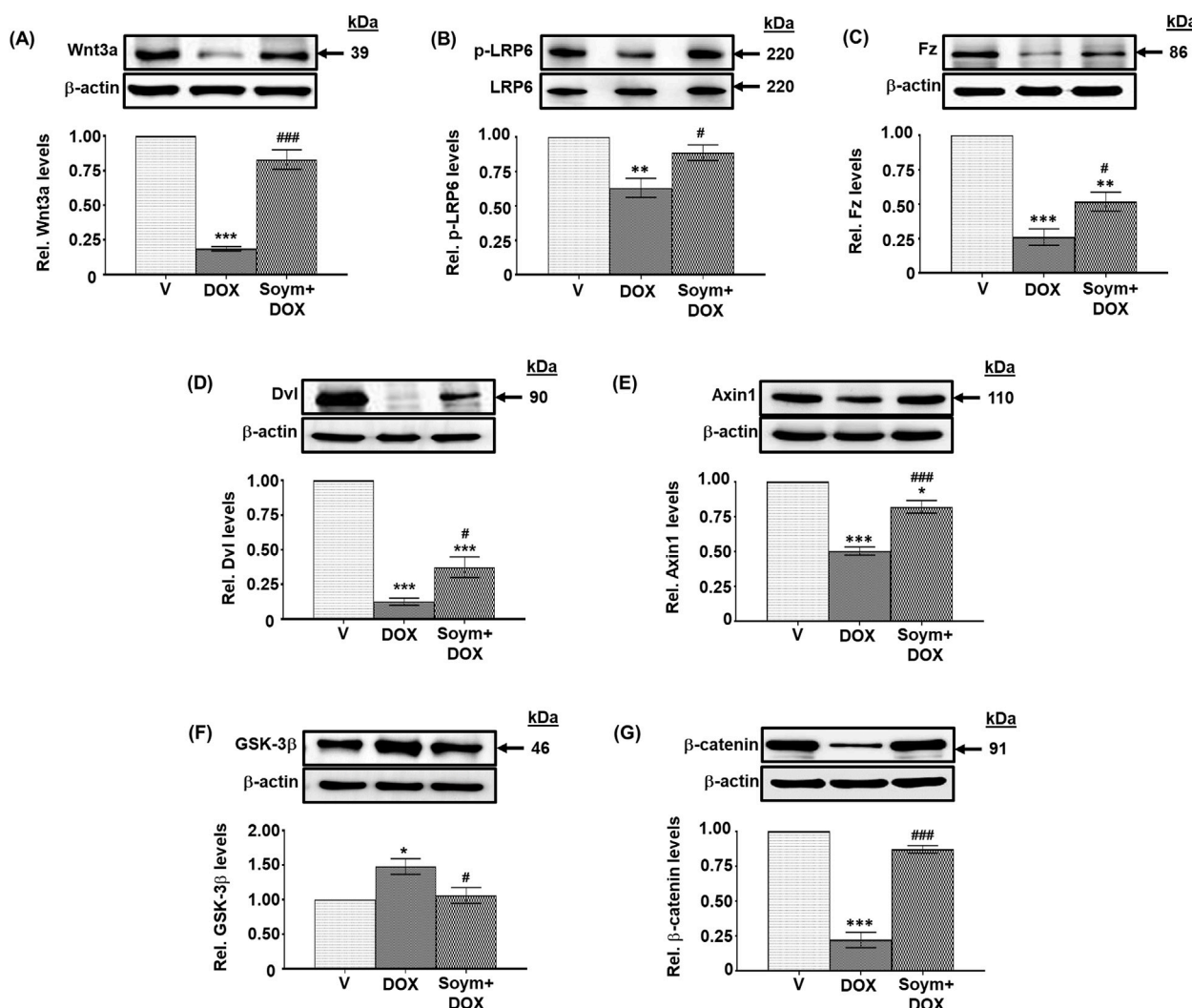


FIGURE 3

Soymetide inhibits doxorubicin-induced attenuation of hippocampal Wnt3a/β-catenin pathway in mice. Hippocampal tissues were isolated from vehicle (V), doxorubicin (DOX) and Soymetide (Soym)+DOX-treated mice. (A–G) Representative Western blots and corresponding densitometry (relative to vehicle) of Wnt3a (A), p-LRP6 (B), Frizzled (Fz) (C), Dishevelled (Dvl) (D), Axin1 (E), GSK-3β (F) and β-catenin (G) normalized with β-actin (A, C–G) or LRP6 (B) in the hippocampal tissues. Data represent means ± SE of three mice/group. ***p < 0.001, **p < 0.01 and *p < 0.05 compared to V. ###p < 0.001 and #p < 0.05 compared to DOX.

by Soymetide (Figures 5A–D). Moreover, rDkk1 and iCRT3 inhibited the Soymetide-induced decrease in p53 (Figure 5C) and p16 (Figure 5D), thereby verifying that Soymetide exerts its anti-senescence effects by modulating the Wnt3a/β-catenin pathway in the hippocampal neurons.

We conducted *in vitro* validation of the anti-senescence mechanism of Soymetide (10 nM, Supplementary Material 2) in primary cultures of mouse hippocampal neurons. Consistent with the *in vivo* observations, our findings showed that doxorubicin treatment led to a decrease in the Wnt3a (Figure 6A) and β-catenin levels (Figure 6B), while elevating p53 (Figure 6C), p16 (Figure 6D) and Senescence β-Galactosidase staining (Figure 6E), and decreasing NeuN levels (Figure 6F). However, the doxorubicin-induced changes in Wnt3a, β-catenin and senescent markers were mitigated by Soymetide (Figures 6A–F). (The scrambled peptide failed to affect the doxorubicin-

induced senescence (Supplementary Material 4). Additionally, these Soymetide-induced effects were blocked by rDkk1 and iCRT3 (Figures 6C–F). Hence, our findings verified the involvement of components of Wnt3a/β-catenin pathway in the hippocampal neuronal senescence and demonstrated the anti-senescence effect of Soymetide.

Effect of Soymetide and doxorubicin on the hippocampal neuronal survival and learning-memory performance of mice

Wnt pathway and senescence are linked with neuronal survival and subsequent cognitive functions (Garg and Bandyopadhyay, 2024). Hence, we assessed the effect of doxorubicin and Soymetide on hippocampal Nissl staining

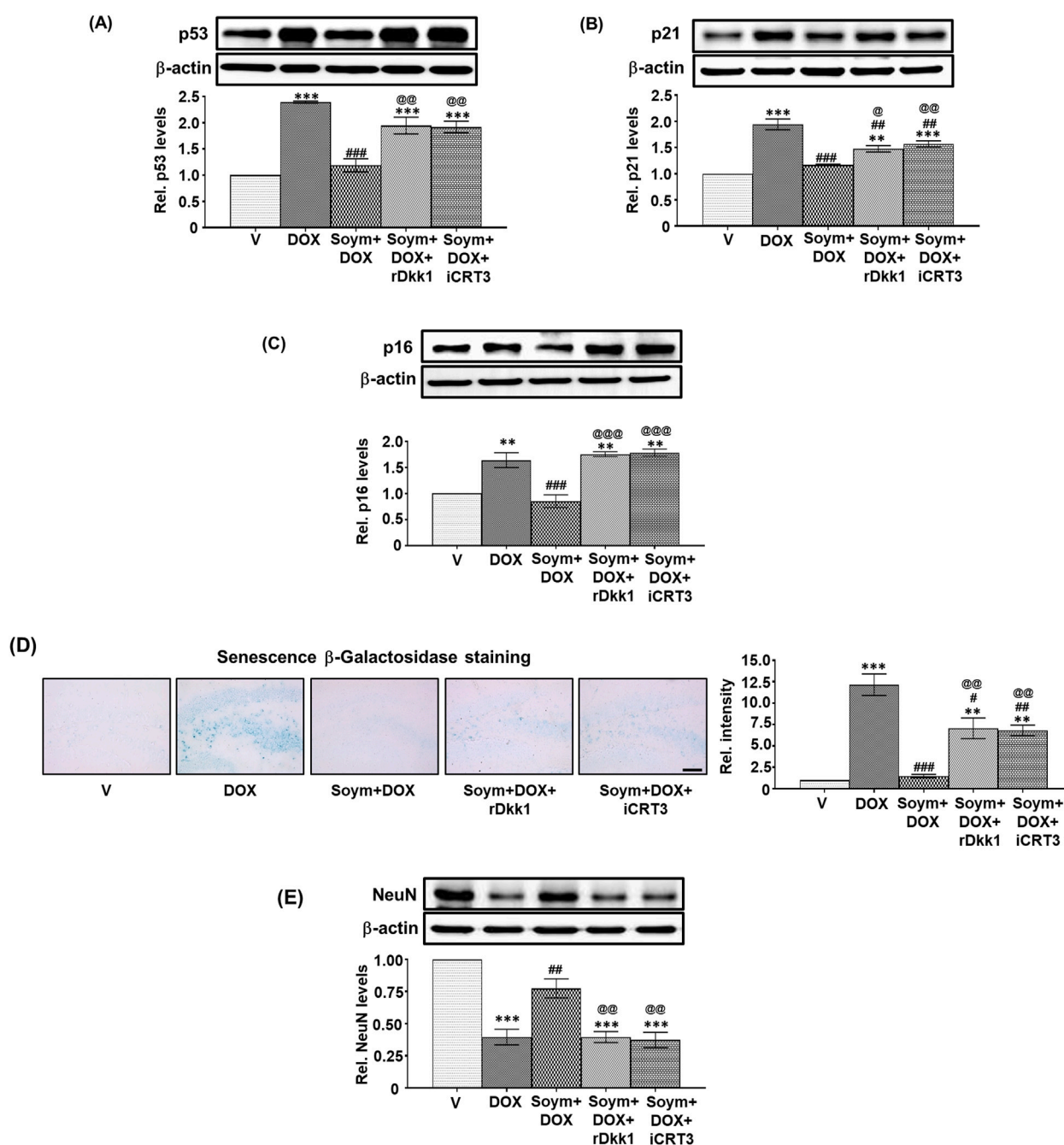


FIGURE 4

The Soymetide-induced reduction in senescence markers and increase in NeuN levels are *Wnt3a/β-catenin*-dependent in the hippocampus of doxorubicin-treated mice. Hippocampal tissues and the whole brain were isolated from vehicle (V), doxorubicin (DOX), Soymetide (Soym)+DOX, Soym + DOX + rDkk1, and Soym + DOX + iCRT3-treated mice. (A–C, E) Representative Western blots and corresponding densitometry (relative to vehicle) of p53 (A), p21 (B), p16 (C) and NeuN (E) normalized with β-actin in the hippocampal tissues. (D) Representative photomicrographs and corresponding bar graph (relative to vehicle) of Senescence β-Galactosidase-stained hippocampus in brain sections. Scale bar: 100 μm. Data represent means ± SE of three mice/group. The quantification of the first three groups in (D) and (E) are based on the same data sets as in Figures 2B, C. ***p < 0.001 and **p < 0.01 compared to V. ###p < 0.001, ##p < 0.01 and #p < 0.05 compared to DOX. @@@p < 0.001, @@p < 0.01 and @p < 0.05 compared to Soym + DOX.

for neuronal count, TUNEL staining for neuronal apoptosis, and learning-memory performance of mice. We found that doxorubicin led to a reduction in Nissl staining (Figure 7A) and increase in TUNEL positive neuronal apoptotic index (Figure 7B) in the hippocampus, indicating neuronal loss. However, Soymetide counteracted these effects (Figures 7A,

B). Additionally, we observed that doxorubicin impaired learning and memory abilities, as demonstrated by an increased number of errors during learning trials (Figure 7C) and diminished memory retention in the Y-Maze test at various intervals post-learning (Figure 7D). Conversely, Soymetide treatment facilitated a notable improvement in these

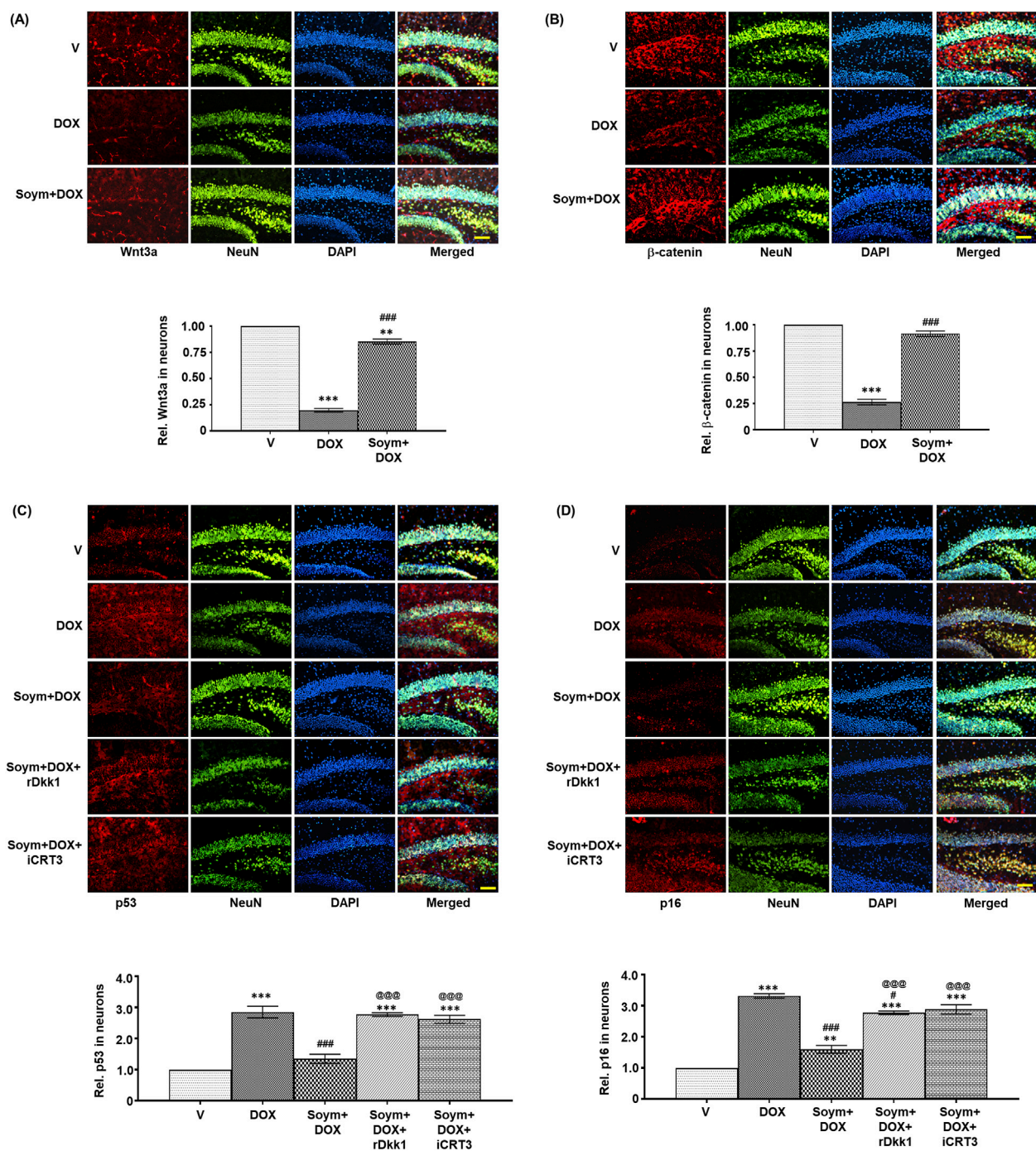


FIGURE 5

Soymetide increases Wnt3a and β-catenin and decreases p53 and p16 levels in the hippocampal neurons of doxorubicin-treated mice.

Fluorescence immunohistochemistry was performed on brain sections of vehicle (V), doxorubicin (DOX), Soymetide (Soym)+DOX, Soym + DOX + rDkk1 and Soym + DOX + iCRT3-treated mice. (A–D) Representative fluorescence photomicrographs of Wnt3a (A), β-catenin (B), p53 (C) and p16 (D) co-immunolabeled with NeuN and counter-stained with DAPI in the hippocampus of brain sections. Bar diagrams represent corresponding quantification relative to vehicle. Scale bar: 100 μm. Data represent means ± SE of three mice/group. ***p < 0.001 and **p < 0.01 compared to V. ###p < 0.001 and #p < 0.05 compared to DOX. @@@p < 0.001 compared to Soym + DOX.

cognitive functions (Figures 7C, D). This was further supported by results from the Passive Avoidance test, where Soymetide enhanced the TLT across the retention trials in doxorubicin-treated mice (Figure 7E). The beneficial outcomes associated

with Soymetide administration were counteracted by rDkk1 and iCRT3 (Figures 7A–E), suggesting that the neuroprotective and cognitive-enhancing effects of Soymetide are mediated through the components of the Wnt3a/β-catenin pathway.

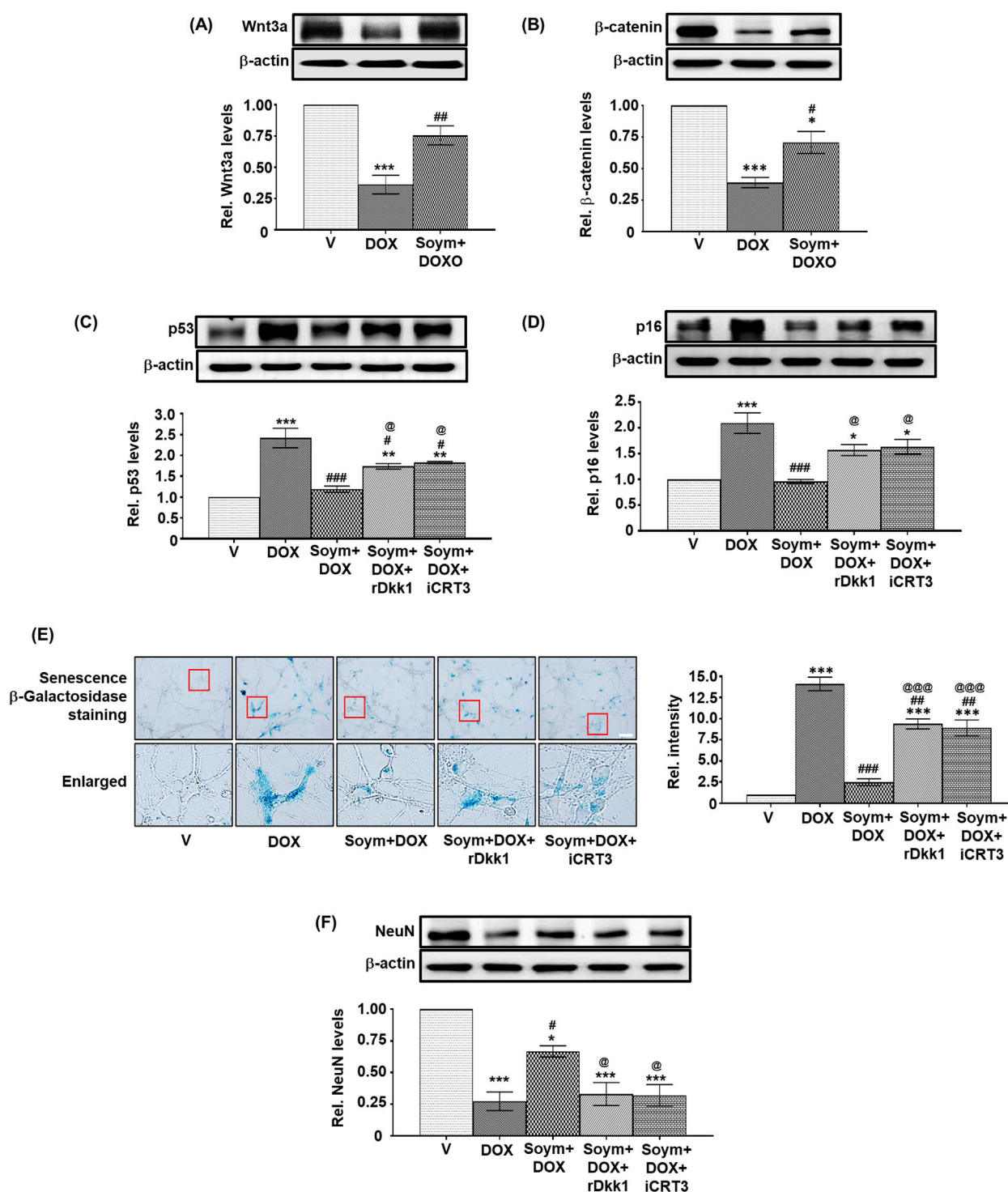


FIGURE 6

Soymetide inhibits the doxorubicin-induced reduction in Wnt3a, β-catenin, and NeuN and the increase in senescence of primary mice hippocampal neurons. Primary hippocampal neurons treated with vehicle (V), doxorubicin (DOX), Soymetide (Soym)+DOX, Soym + DOX + rDkk1 and Soym + DOX + iCRT3 were harvested. **(A–D, F)** Representative Western blots and corresponding densitometry (relative to vehicle) of Wnt3a **(A)**, β-catenin **(B)**, p53 **(C)**, p16 **(D)** and NeuN **(F)** normalized with β-actin in primary hippocampal neurons. **(E)** Representative photomicrographs and corresponding bar graph (relative to vehicle) of Senescence β-Galactosidase-stained primary hippocampal neurons. Scale bar: 20 μm. Data represent means ± SE of three independent experiments. ****p* < 0.001, ***p* < 0.01 and **p* < 0.05 compared to V. ###*p* < 0.001, ##*p* < 0.01 and #*p* < 0.05 compared to DOX. @@@*p* < 0.001 and @*p* < 0.05 compared to Soym + DOX.

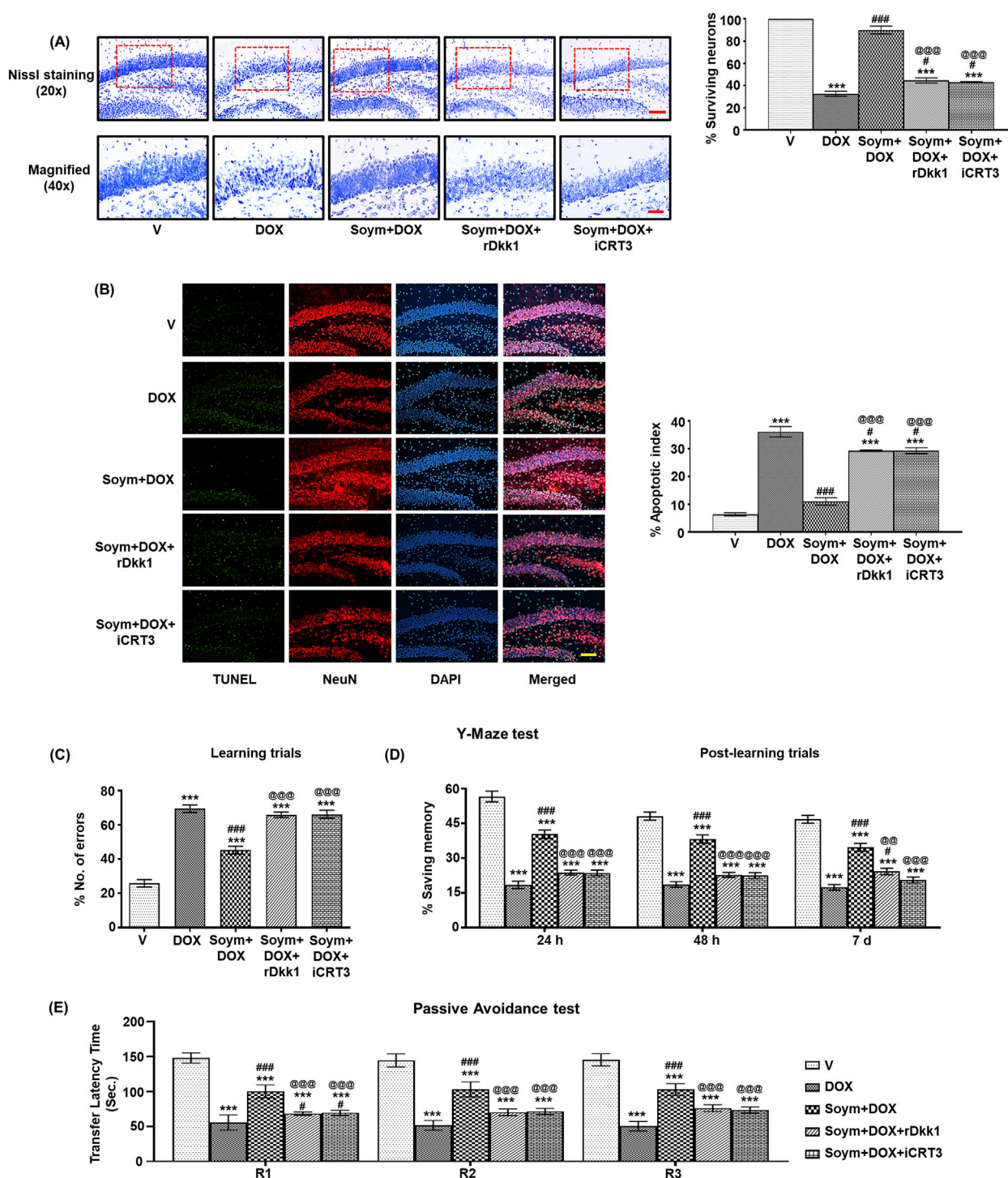
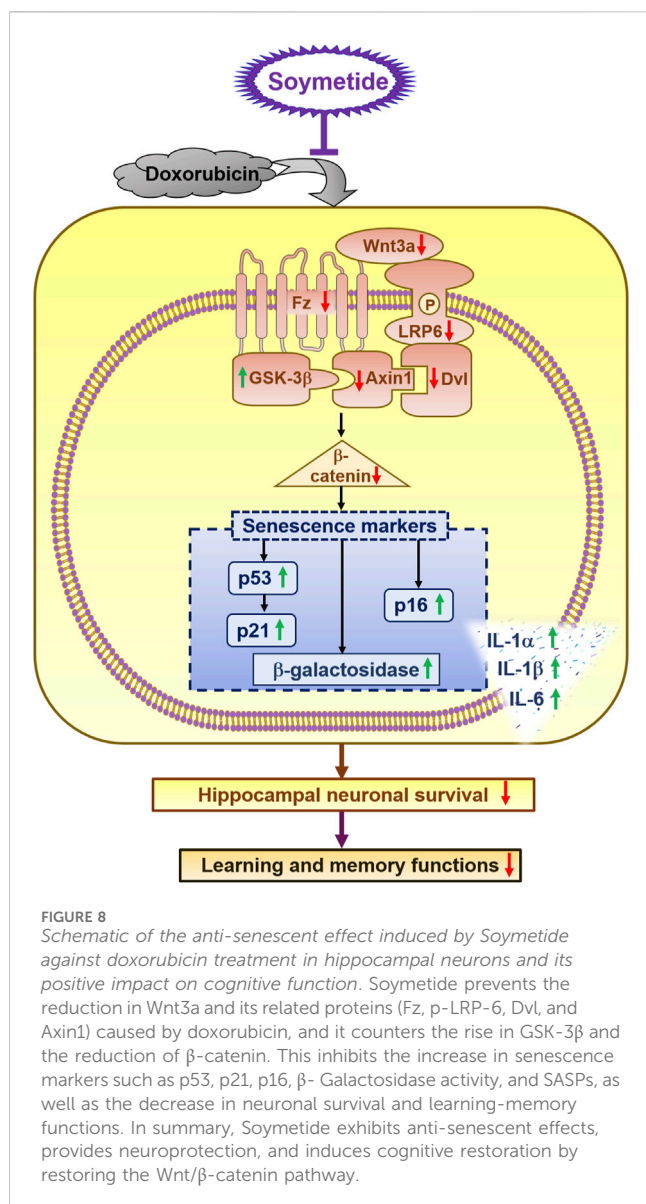


FIGURE 7

Soymetide protects against doxorubicin-induced hippocampal neuronal loss and learning-memory impairment via the Wnt/β-catenin pathway in mice. Brain sections were made from vehicle (V), doxorubicin (DOX), Soymetide (Soym)+DOX, Soym + DOX + rDkk1 and Soym + DOX + iCRT3-treated mice. (A) Upper panel-20x (with quantification, %) and lower panel-40x represent photomicrographs of Nissl-stained hippocampal neurons. Scale bar: 100 μm (20X) and 30 μm (40X). (B) Representative fluorescence photomicrographs of TUNEL, immunolabeled with NeuN and counter-stained with DAPI in the hippocampus. Bar diagrams represent corresponding quantification relative to the vehicle. Scale bar: 100 μm. Y-Maze and Passive Avoidance tests were performed in vehicle (V), doxorubicin (DOX), Soymetide (Soym)+ DOX, Soym + DOX + rDkk1 and Soym + DOX + iCRT3-treated mice. (C, D) Representative bar graphs for the number of errors (%) during learning trials (C) and the memory retained (% saving memory) at 24 h, 48 h and 7-day post-learning (D) in Y-Maze test. (E) Representative bar graphs for TLT for first (R1), second (R2), and third (R3) retention trials (24 h, 48 h, and 72 h, respectively) in Passive Avoidance test. Data represent means ± SE of three mice/group (A, B) and seven mice/group (C–E). ***p < 0.001 compared to V. ###p < 0.001 and #p < 0.05 compared to DOX. @@@p < 0.001 and @@p < 0.01 compared to Soym + DOX.



Discussion

The current study unravels novel neuroprotective properties of Soymetide, with a specific focus on: 1. Reduction of senescence in the hippocampus, with effects comparable to a known senolytic combination (D + Q). 2. Beneficial impact involving the Wnt/ β -catenin pathway. The reduction of key components in the Wnt3a/ β -catenin pathway accelerates neuronal senescence. However, Soymetide's ability to restore Wnt/ β -catenin signaling helped counteract this senescence process. 3. Improvement in neuronal survival and enhancement of learning and memory functions. The study overall introduces a soy peptide that shows promise for improving hippocampal health and cognitive functions by targeting the interlinked senescence pathways and Wnt/ β -catenin mechanism, offering a potential therapeutic approach against cognitive decline (Figure 8).

Studies suggest that fermented soy food products like cheonggukjang and doenjang offer neuroprotection by inhibiting

neuronal death, inflammation, and susceptibility to ischemic injury (Ko et al., 2019; Jeong et al., 2020; Jang et al., 2021). Nattō, a fermented whole soybean improves age-related cognitive decline and associated deregulated hippocampal neuronal signaling in senescence-accelerated mouse-prone eight mice (Zheng et al., 2023). Additionally, soy isoflavones (genistein and daidzein) and their metabolites (equol), and soyasaponin I (a triterpenoid compound) prevent neuronal apoptosis, promote neuroregeneration, synaptic plasticity, neurotransmission, and antioxidative effects (Ma et al., 2010; Hong et al., 2013; Lu et al., 2021; Shi et al., 2023). However, the soy-derived compounds may face limitations regarding their “drug-likeness” due to concerns about metabolic stability restricting potential therapeutic applications, as reported for phytochemicals (Sharan et al., 2009). Reports further indicate that soy peptides, VHVV and Tyr-Pro, enzymatic and fungal hydrolysates of soy proteins, respectively, maintain neuronal survival and reduce memory loss (Ju et al., 2019; Tanaka et al., 2020). However, while hydrolyzed proteins and peptides show promise as food and potential nutraceutical applications, standardizing them as therapeutic products may pose challenges. In this context, Soymetide, a well-characterized small/short soy-derived peptide can serve as a promising biologic/peptide drug, marking a considerable advancement in this field. Our findings identify Soymetide as a neuroprotectant that promotes a wide range of anti-senescence features in the hippocampal neurons, comparable with broad-target senolytic drugs (D + Q). The small peptide is proposed to hold potential for advancing peptide drug design and development, based on probable advantages such as improved absorption, enhanced cell targeting, reduced immunogenicity, and increased cost-effectiveness (Fosgerau and Hoffmann, 2015). These features may position Soymetide as a potential candidate for therapies aimed at anti-senescence and neuroprotection. Besides, this novel pro-cognitive role adds a notable new dimension to the functional profile of Soymetide, reported for immunostimulating and anti-cancer activities (Schuler et al., 1982; Tsuruki et al., 2003), offering fresh insights into its potential mechanism of action. The selected dose of 50 μ g/kg of Soymetide was identified for its effective anti-senescence properties, offering a cost-effective alternative to the higher 100 μ g/kg dose. While safety data was not specifically assessed in this study, the lower dose presents a promising approach that warrants further investigation to determine the best balance of safety and therapeutic benefits.

Prior studies show that eliminating p16-expressing senescent cells and lowering the p53 stress protein can prevent mild cognitive impairment, neuronal death, and synaptic issues (Bussian et al., 2018; Zhang et al., 2022b). This process minimizes p53-triggered p21 activation and DNA damage, averting cell cycle arrest and senescence (de Carne Treccesson et al., 2011; Tajima et al., 2019; Tufekci et al., 2021). Our research suggests that Soymetide influences these communications involving p16, p21, p53, and SASPs, leading to healthier neuronal expression, reduced cellular damage, and improved brain repair, benefiting the central nervous system (CNS). Specifically, regarding soy peptides, previous research has mainly focused on their roles in preventing and suppressing tumors by engaging pathways such as p53, p16, p21, and cytokines, and growth arrest and apoptosis in various cancer cells (Lin et al., 1998; Payton-Stewart et al., 2009). Studies in osteoblasts did show

the involvement of p53/p21 pathway in bone development following soy peptide treatment (Zhang et al., 2014; Chen et al., 2015). However, the lack of research on the impact of soy peptides on the brain, specifically its anti-senescent effects on the hippocampus, underscores the importance and promise of our study on these soy-based peptides for future exploration.

Our research enriches the current understanding of senescence in the hippocampal neurons and extends upon earlier work (Bayod et al., 2015; Su et al., 2018), which showed a link between the upregulation of the Wnt pathway inhibitor, Dickkopf-1, and the perturbation of essential elements within the Wnt/ β -catenin signaling cascade. Our findings further detail that the senescence process is associated with precise alterations in Wnt signaling markers in the hippocampal neurons, which correspond with an apparent decline in neuronal viability, as evidenced by a diminished reduction in Nissl bodies, along with NeuN expression. In a notable progression from past research (Fortress and Frick, 2016; Arredondo et al., 2020), which predominantly focused on the broader aspects of Wnt signaling, our study also identifies a decrease in both the Wnt ligands and its corresponding Frizzled receptor during senescence. Moreover, while prior reports only noted changes in Wnt signaling during hippocampal senescence (Bayod et al., 2015; Fortress and Frick, 2016), our investigation additionally sheds light on how these modifications in Wnt pathway actively played a key role in controlling neuronal senescence and the impact on its essential molecules, such as p53, p21, p16, SASP, β -Galactosidase, etc. Our research explicitly linked these observations with Soymetide treatment, demonstrating its restoration in the levels of the Wnt ligand and Frizzled receptor in the senescent neurons. Moreover, it unraveled that Soymetide's anti-senescent effects are highly dependent on regulated Wnt signaling, demonstrated by the use of the Wnt antagonist rDkk1 and the β -catenin inhibitor iCRT3, which blocked the reduction of senescent markers in the hippocampal neurons. In this context, in terms of soy-based protein and Wnt signaling (as such), there have been several contradictory reports. On the one hand, soy proteins (predominantly genistein) reduced β -catenin signaling (via the participation of altered IGF-1 and E-cadherin production) leading to a decreased T-cell factor/lymphoid enhancer factor (TCF/LEF) activity and resulting prostate cancer cell growth, development of hepatocellular carcinoma, intestinal tumorigenesis, and proliferation in cancer cells (Liss et al., 2010; Mahmoud et al., 2014; Mercer et al., 2017). Other studies indicated that genistein and soy isoflavones enhanced Wnt/ β -catenin signaling and led to osteoblast formation, improved bone health, and prevented non-alcoholic fatty liver disease (NAFLD) and pathological adiposity (Kim and Kang, 2012; Mannino et al., 2024). In line with the latter, results from our study demonstrated the neuroprotective effects of Soymetide through the enhancement of the components of the Wnt/ β -catenin pathway, verifying a protective role of soy peptides in increasing Wnt/ β -catenin pathway for normal cells as opposed to the tumorous and cancerous cells. As a supportive observation, Soymetide inhibits the reduction of Transcription Factor 3 (TCF3) levels

caused by doxorubicin (Supplementary Material 5), which emphasize the involvement of the Wnt/ β -catenin pathway. This effect could be linked to the regulation of p53, p21, p16, and β -galactosidase, laying the groundwork for future studies to investigate its mechanisms of action. Hence, it may be said that in terms of the Wnt pathway, the importance of our study for hippocampal neurons is two-fold. It offers new insights into the senescence pathway and emphasizes the potential of Soymetide in mitigating the adverse effects of senescence.

Research indicates that soy proteins, isoflavone extracts, and peptides can enhance cognitive performance in adults, postmenopausal women, and the aged by activating brain pathways such as Brain-Derived Neurotrophic Factor (BDNF)-Tropomyosin-related kinase receptor B (TrkB)/cAMP response element-binding protein (CREB) signaling, N-methyl-D-aspartate receptor (NMDAR)-calcium/calmodulin-dependent protein kinase II (CaMKII) cascade (NMDAR-CaMKII), as well as Phosphatidylinositol-3 Kinase (PI3K)/Akt signaling, and through antioxidant and cholinergic properties (Kreijkamp-Kaspers et al., 2004; Geller and Studee, 2006; Katayama et al., 2014; Unno and Konishi, 2015; Yoo et al., 2022; Zheng et al., 2023). Earlier individual studies have also shown a connection between Wnt/ β -catenin signaling with the BDNF (TrkB)/CREB signaling, NMDAR-CaMKII, PI3K/Akt, antioxidant, and cholinergic properties (Arrazola et al., 2009; Sinha et al., 2015; Xu et al., 2015; Hu et al., 2019; Ishidori et al., 2022; Nachtigall et al., 2023; Lou et al., 2024). Hence, in continuation, our research highlights the importance of investigating the relationships between neurotrophins, neurotransmitters, antioxidants, and specific signaling pathways in Soymetide-treated hippocampal neurons. Our work points to the need to explore Soymetide's impact on aging, specifically concerning hippocampal Wnt signaling. Moreover, while our study demonstrated Soymetide's anti-senescence effects when directly applied to the hippocampus, proving its potential to protect against neuronal aging, this method is infeasible for human use. Therefore, there is a need for further research to develop a brain-transportable Soymetide formulation for systemic administration.

Hence, our research suggests that Soymetide has the potential to diminish cellular senescence in hippocampal neurons, which may improve cognitive performance and maintain neuronal health through modulation of senescence markers. Additionally, we propose that Soymetide might possess anti-inflammatory properties through its impact on macrophages and monocytes, offering neuroprotection against age-related diseases. The observed reduction in serum pro-inflammatory cytokines suggests an immune modulation mechanism that warrants further exploration.

We recognize few limitations in this study. The primary focus has been on investigating the effectiveness of Soymetide as a single-agent treatment. Additionally, while the potential for immune modulation has not been thoroughly examined, and the use of combination therapies (pairing Soymetide with dasatinib or quercetin) has yet to be explored, these aspects are crucial for future research aimed at improving treatment efficacy and minimizing toxicity. Furthermore, it is vital to determine optimal dosages, study the pharmacokinetics of Soymetide in various biological settings, and develop more effective peptide variants through *in vitro* assays, with the goal of extending these findings

to *in vivo* applications. These efforts will enhance our understanding and optimize the therapeutic outcomes when utilizing Soymetide.

Data availability statement

The raw data supporting the conclusions of this article will be made available by the authors, without undue reservation.

Ethics statement

The animal study was approved by the Institutional Animal Ethics Committee-Indian Institute of Toxicology Research. IAEC reference numbers are IITR/IAEC/53/20 and IITR/IAEC/10/24. The study was conducted in accordance with the local legislation and institutional requirements.

Author contributions

AG: Conceptualization, Data curation, Formal Analysis, Investigation, Methodology, Visualization, Writing—original draft, Writing—review and editing. JS: Writing—review and editing, Data curation. ST: Data curation, Writing—review and editing. UD: Methodology, Writing—review and editing. NS: Data curation, Writing—review and editing. JG: Conceptualization, Methodology, Supervision, Writing—review and editing. SB: Conceptualization, Methodology, Supervision, Funding acquisition, Project administration, Resources, Software, Validation, Writing—original draft, Writing—review and editing.

Funding

The author(s) declare that financial support was received for the research, authorship, and/or publication of this article. This study was supported by the Science and Engineering Research Board-Scientific and Useful Profound Research Advancement, Govt. of India (SPR/2019/000346), Indian Council of Medical Research, Govt. of India (5/8-4/2/Env/2020-NCD-II) and CSIR-IITR Institutional fund (MLP005).

References

- Arrazola, M. S., Ramos-Fernandez, E., Cisternas, P., Ordenes, D., and Inestrosa, N. C. (2017). Wnt signaling prevents the $\alpha\beta$ oligomer-induced mitochondrial permeability transition pore opening preserving mitochondrial structure in hippocampal neurons. *PLoS One* 12 (1), e0168840. doi:10.1371/journal.pone.0168840
- Arrazola, M. S., Varela-Nallar, L., Colombres, M., Toledo, E. M., Cruzat, F., Pavez, L., et al. (2009). Calcium/calmodulin-dependent protein kinase type IV is a target gene of the Wnt/beta-catenin signaling pathway. *J. Cell Physiol.* 221 (3), 658–667. doi:10.1002/jcp.21902
- Arredondo, S. B., Valenzuela-Bezanilla, D., Mardones, M. D., and Varela-Nallar, L. (2020). Role of Wnt signaling in adult hippocampal neurogenesis in health and disease. *Front. Cell Dev. Biol.* 8, 860. doi:10.3389/fcell.2020.00860
- Avila, M. E., Sepulveda, F. J., Burgos, C. F., Moraga-Cid, G., Parodi, J., Moon, R. T., et al. (2010). Canonical Wnt3a modulates intracellular calcium and enhances excitatory neurotransmission in hippocampal neurons. *J. Biol. Chem.* 285 (24), 18939–18947. doi:10.1074/jbc.M110.103028
- Bayod, S., Felice, P., Andres, P., Rosa, P., Camins, A., Pallas, M., et al. (2015). Downregulation of canonical Wnt signaling in hippocampus of SAMP8 mice. *Neurobiol. Aging* 36 (2), 720–729. doi:10.1016/j.neurobiolaging.2014.09.017
- Beurel, E., Grieco, S. F., and Jope, R. S. (2015). Glycogen synthase kinase-3 (GSK3): regulation, actions, and diseases. *Pharmacol. Ther.* 148, 114–131. doi:10.1016/j.pharmthera.2014.11.016
- Bussian, T. J., Aziz, A., Meyer, C. F., Swenson, B. L., van Deursen, J. M., and Baker, D. J. (2018). Clearance of senescent glial cells prevents tau-dependent pathology and cognitive decline. *Nature* 562 (7728), 578–582. doi:10.1038/s41586-018-0543-y
- Chen, D., Zhang, Y., Zhang, M., Chang, J., Zeng, Z., Kou, X., et al. (2020). Exercise attenuates brain aging by rescuing down-regulated wnt/ β -catenin signaling in aged rats. *Front. Aging Neurosci.* 12, 105. doi:10.3389/fnagi.2020.00105
- Chen, J. R., Lazarenko, O. P., Blackburn, M. L., Badger, T. M., and Ronis, M. J. (2015). Soy protein isolate inhibits high-fat diet-induced senescence pathways in osteoblasts to maintain bone acquisition in male rats. *Endocrinology* 156 (2), 475–487. doi:10.1210/en.2014-1427
- Das, G., Yu, Q., Hui, R., Reuhl, K., Gale, N. W., and Zhou, R. (2016). EphA5 and EphA6: regulation of neuronal and spine morphology. *Cell Biosci.* 6, 48. doi:10.1186/s13578-016-0115-5
- de Carne Trecesson, S., Guillemin, Y., Belanger, A., Bernard, A. C., Preisser, L., Ravon, E., et al. (2011). Escape from p21-mediated oncogene-induced senescence leads to cell

Acknowledgments

AG received her fellowship from UGC, Govt. of India. JS, ST, and UD received their fellowship from CSIR, Govt. of India. NS received her fellowship from ICMR, Govt. of India. The CSIR-IITR communication number of this article is IITR/SEC/MS/2024/55.

Conflict of interest

The authors declare that the research was conducted in the absence of any commercial or financial relationships that could be construed as a potential conflict of interest.

Generative AI statement

The author(s) declare that Generative AI was used in the creation of this manuscript. During the preparation of this work the author(s) used Grammarly in order to improve readability of the manuscript. After using this tool/service, the author(s) reviewed and edited the content as needed and take(s) full responsibility for the content of the publication.

Publisher's note

All claims expressed in this article are solely those of the authors and do not necessarily represent those of their affiliated organizations, or those of the publisher, the editors and the reviewers. Any product that may be evaluated in this article, or claim that may be made by its manufacturer, is not guaranteed or endorsed by the publisher.

Supplementary material

The Supplementary Material for this article can be found online at: <https://www.frontiersin.org/articles/10.3389/fphar.2025.1510337/full#supplementary-material>

- dedifferentiation and dependence on anti-apoptotic Bcl-xL and MCL1 proteins. *J. Biol. Chem.* 286 (15), 12825–12838. doi:10.1074/jbc.M110.186437
- Deng, Z., Xie, D., Cai, J., Jiang, J., Pan, D., Liao, H., et al. (2023). Different types of milk consumption and the risk of dementia: analysis from a large-scale cohort study. *Clin. Nutr.* 42 (10), 2058–2067. doi:10.1016/j.clnu.2023.08.019
- Dong, B., Qi, Y., Sundas, H., Yang, R., Zhou, J., and Li, Z. (2023). Soy protein increases cognitive level in mice by modifying hippocampal nerve growth, oxidative stress, and intestinal microbiota. *J. Sci. Food Agric.* 103 (8), 4085–4094. doi:10.1002/jsfa.12388
- Fortress, A. M., and Frick, K. M. (2016). Hippocampal Wnt signaling: memory regulation and hormone interactions. *Neuroscientist* 22 (3), 278–294. doi:10.1177/1073858415574728
- Fosgerau, K., and Hoffmann, T. (2015). Peptide therapeutics: current status and future directions. *Drug Discov. Today* 20 (1), 122–128. doi:10.1016/j.drudis.2014.10.003
- Garg, A., and Bandyopadhyay, S. (2024). Role of an interdependent Wnt, GSK3- β /catenin and HB-EGF/EGFR mechanism in arsenic-induced hippocampal neurotoxicity in adult mice. *Chemosphere* 352, 141375. doi:10.1016/j.chemosphere.2024.141375
- Geller, S. E., and Studee, L. (2006). Soy and red clover for mid-life and aging. *Climacteric* 9 (4), 245–263. doi:10.1080/13697130600736934
- Gupta, K., Vishwakarma, J., Garg, A., Pandey, R., Jain, V., Gupta, R., et al. (2022). Arsenic induces gsk3 β -dependent p-tau, neuronal apoptosis, and cognitive impairment via an interdependent hippocampal ER α and IL-1/IL-1R1 mechanism in female rats. *Toxicol. Sci.* 190 (1), 79–98. doi:10.1093/toxsci/kfac087
- Hong, S. W., Heo, H., Yang, J. H., Han, M., Kim, D. H., and Kwon, Y. K. (2013). Soyasaponin I improved neuroprotection and regeneration in memory deficient model rats. *PLoS One* 8 (12), e81556. doi:10.1371/journal.pone.0081556
- Hu, Y., Chen, W., Wu, L., Jiang, L., Liang, N., Tan, L., et al. (2019). TGF- β 1 restores hippocampal synaptic plasticity and memory in alzheimer model via the PI3K/Akt/Wnt/ β -Catenin signaling pathway. *J. Mol. Neurosci.* 67 (1), 142–149. doi:10.1007/s12031-018-1219-7
- Huang, H. C., and Klein, P. S. (2004). The Frizzled family: receptors for multiple signal transduction pathways. *Genome Biol.* 5 (7), 234. doi:10.1186/gb-2004-5-7-234
- Hwang, Y. H., Park, S., Paik, J. W., Chae, S. W., Kim, D. H., Jeong, D. G., et al. (2019). Efficacy and safety of lactobacillus plantarum C29-fermented soybean (DW2009) in individuals with mild cognitive impairment: a 12-week, multi-center, randomized, double-blind, placebo-controlled clinical trial. *Nutrients* 11 (2), 305. doi:10.3390/nu11020305
- Inestrosa, N. C., Urrea, S., and Colombres, M. (2004). Acetylcholinesterase (AChE)-amyloid-beta-peptide complexes in Alzheimer's disease. the Wnt signaling pathway. *Curr. Alzheimer Res.* 1 (4), 249–254. doi:10.2174/1567205043332063
- Ishidori, H., Okihara, H., Ogawa, T., Abe, Y., Kato, C., Aung, P. T., et al. (2022). Nasal obstruction during the growth period modulates the Wnt/ β -catenin pathway and brain-derived neurotrophic factor production in association with tyrosine kinase receptor B mRNA reduction in mouse hippocampus. *Eur. J. Neurosci.* 55 (1), 5–17. doi:10.1111/ejn.15547
- Jang, C. H., Oh, J., Lim, J. S., Kim, H. J., and Kim, J. S. (2021). Fermented soy products: beneficial potential in neurodegenerative diseases. *Foods* 10 (3), 636. doi:10.3390/foods10030636
- Jeong, D. Y., Jeong, S. Y., Zhang, T., Wu, X., Qiu, J. Y., and Park, S. (2020). Chungkookjang, a soy food, fermented with *Bacillus amyloliquefaciens* protects gerbils against ischemic stroke injury, and post-stroke hyperglycemia. *Food Res. Int.* 128, 108769. doi:10.1016/j.foodres.2019.108769
- Jeong, D. Y., Ryu, M. S., Yang, H. J., and Park, S. (2021). γ -PGA-Rich chungkookjang, short-term fermented soybeans: prevents memory impairment by modulating brain insulin sensitivity, neuro-inflammation, and the gut-microbiome-brain Axis. *Foods* 10 (2), 221. doi:10.3390/foods10020221
- Jia, L., Pina-Crespo, J., and Li, Y. (2019). Restoring Wnt/ β -catenin signaling is a promising therapeutic strategy for Alzheimer's disease. *Mol. Brain* 12 (1), 104. doi:10.1186/s13041-019-0525-5
- Ju, D. T., K, A. K., Kuo, W. W., Ho, T. J., Chang, R. L., Lin, W. T., et al. (2019). Bioactive peptide VHVH upregulates the long-term memory-related biomarkers in adult spontaneously hypertensive rats. *Int. J. Mol. Sci.* 20 (12), 3069. doi:10.3390/ijms20123069
- Katayama, S., Imai, R., Sugiyama, H., and Nakamura, S. (2014). Oral administration of soy peptides suppresses cognitive decline by induction of neurotrophic factors in SAMP8 mice. *J. Agric. Food Chem.* 62 (16), 3563–3569. doi:10.1021/jf405416s
- Kim, I. S. (2021). Current perspectives on the beneficial effects of soybean isoflavones and their metabolites for humans. *Antioxidants (Basel)* 10 (7), 1064. doi:10.3390/antiox10071064
- Kim, M. H., and Kang, K. S. (2012). Isoflavones as a smart curer for non-alcoholic fatty liver disease and pathological adiposity via ChREBP and Wnt signaling. *Prev. Med.* 54 (Suppl. 1), S57–S63. doi:10.1016/j.ypmed.2011.12.018
- Ko, J. W., Chung, Y. S., Kwak, C. S., and Kwon, Y. H. (2019). Doenjang, A Korean traditional fermented soybean paste, ameliorates neuroinflammation and neurodegeneration in mice fed a high-fat diet. *Nutrients* 11 (8), 1702. doi:10.3390/nu11081702
- Kreijkamp-Kaspers, S., Kok, L., Grobbee, D. E., de Haan, E. H., Aleman, A., Lampe, J. W., et al. (2004). Effect of soy protein containing isoflavones on cognitive function, bone mineral density, and plasma lipids in postmenopausal women: a randomized controlled trial. *JAMA* 292 (1), 65–74. doi:10.1001/jama.292.1.65
- Krzyszyniak, A., Wesierska, M., Petrazzo, G., Gadecka, A., Dudkowska, M., Bielak-Zmijewska, A., et al. (2022). Combination of dasatinib and quercetin improves cognitive abilities in aged male Wistar rats, alleviates inflammation and changes hippocampal synaptic plasticity and histone H3 methylation profile. *Aging (Albany NY)* 14 (2), 572–595. doi:10.18632/aging.203835
- Lee, E., Madar, A., David, G., Garabedian, M. J., Dasgupta, R., and Logan, S. K. (2013). Inhibition of androgen receptor and β -catenin activity in prostate cancer. *Proc. Natl. Acad. Sci. U. S. A.* 110 (39), 15710–15715. doi:10.1073/pnas.1218168110
- Li, T., Wan, Y. C., Sun, L. J., Tao, S. J., Chen, P., Liu, C. H., et al. (2018). DIXDC1 prevents oxygen-glucose deprivation/reoxygenation-induced injury in hippocampal neurons *in vitro* by promoting Wnt/ β -catenin signaling. *Eur. Rev. Med. Pharmacol. Sci.* 22 (17), 5678–5687. doi:10.26355/eurrev_201809_15835
- Li, W., Gan, C., Yu, S., Xu, J., Tang, L., and Cheng, H. (2024). Wnt3a/GSK3 β / β -catenin signaling modulates doxorubicin-associated memory deficits in breast cancer. *Mol. Neurobiol.* 61, 5441–5458. doi:10.1007/s12035-023-03910-x
- Lin, A. W., Barradas, M., Stone, J. C., van Aelst, L., Serrano, M., and Lowe, S. W. (1998). Premature senescence involving p53 and p16 is activated in response to constitutive MEK/MAPK mitogenic signaling. *Genes Dev.* 12 (19), 3008–3019. doi:10.1101/gad.12.19.3008
- Lin, Y. F., Wang, L. Y., Chen, C. S., Li, C. C., and Hsiao, Y. H. (2021). Cellular senescence as a driver of cognitive decline triggered by chronic unpredictable stress. *Neurobiol. Stress* 15, 100341. doi:10.1016/j.ynstr.2021.100341
- Liss, M. A., Schlicht, M., Kahler, A., Fitzgerald, R., Thomassi, T., Degueme, A., et al. (2010). Characterization of soy-based changes in Wnt-frizzled signaling in prostate cancer. *Cancer Genomics Proteomics* 7 (5), 245–252.
- Lou, S., Gong, D., Yang, M., Qiu, Q., Luo, J., and Chen, T. (2024). Curcumin improves neurogenesis in alzheimer's disease mice via the upregulation of wnt/ β -catenin and BDNF. *Int. J. Mol. Sci.* 25 (10), 5123. doi:10.3390/ijms25105123
- Lu, C., Gao, R., Zhang, Y., Jiang, N., Chen, Y., Sun, J., et al. (2021). S-equol, a metabolite of dietary soy isoflavones, alleviates lipopolysaccharide-induced depressive-like behavior in mice by inhibiting neuroinflammation and enhancing synaptic plasticity. *Food Funct.* 12 (13), 5770–5778. doi:10.1039/d1fo00547b
- Ma, T. C., Campana, A., Lange, P. S., Lee, H. H., Banerjee, K., Bryson, J. B., et al. (2010). A large-scale chemical screen for regulators of the arginase 1 promoter identifies the soy isoflavone daidzein as a clinically approved small molecule that can promote neuronal protection or regeneration via a cAMP-independent pathway. *J. Neurosci.* 30 (2), 739–748. doi:10.1523/JNEUROSCI.5266-09.2010
- Mahmoud, A. M., Yang, W., and Bosland, M. C. (2014). Soy isoflavones and prostate cancer: a review of molecular mechanisms. *J. Steroid Biochem. Mol. Biol.* 140, 116–132. doi:10.1016/j.jsmb.2013.12.010
- Mannino, F., Imbesi, C., Irrera, N., Pallio, G., Squadrito, F., and Bitto, A. (2024). Insights into the antiosteoporotic mechanism of the soy-derived isoflavone genistein: modulation of the Wnt/beta-catenin signaling. *Biofactors* 50 (2), 347–359. doi:10.1002/biof.2008
- Marques, L., Johnson, A. A., and Stolzinger, A. (2020). Doxorubicin generates senescent microglia that exhibit altered proteomes, higher levels of cytokine secretion, and a decreased ability to internalize amyloid β . *Exp. Cell Res.* 395 (2), 112203. doi:10.1016/j.yexcr.2020.112203
- Mercer, K. E., Pulliam, C. F., Pedersen, K. B., Hennings, L., and Ronis, M. J. (2017). Soy protein isolate inhibits hepatic tumor promotion in mice fed a high-fat liquid diet. *Exp. Biol. Med. (Maywood)* 242 (6), 635–644. doi:10.1177/1535370216685436
- Mijit, M., Caracciolo, V., Melillo, A., Amicarelli, F., and Giordano, A. (2020). Role of p53 in the regulation of cellular senescence. *Biomolecules* 10 (3), 420. doi:10.3390/biom10030420
- Mishra, J., Vishwakarma, J., Malik, R., Gupta, K., Pandey, R., Maurya, S. K., et al. (2021). Hypothyroidism induces interleukin-1-dependent autophagy mechanism as a key mediator of hippocampal neuronal apoptosis and cognitive decline in postnatal rats. *Mol. Neurobiol.* 58 (3), 1196–1211. doi:10.1007/s12035-020-02178-9
- Miyamoto, M., Kiyota, Y., Yamazaki, N., Nagaoka, A., Matsuo, T., Nagawa, Y., et al. (1986). Age-related changes in learning and memory in the senescence-accelerated mouse (SAM). *Physiol. Behav.* 38 (3), 399–406. doi:10.1016/0031-9384(86)90112-5
- Nachtigall, E. G., de Freitas, J. D. R., de, C. M. J., and Furini, C. R. G. (2023). Role of hippocampal Wnt signaling pathways on contextual fear memory reconsolidation. *Neuroscience* 524, 108–119. doi:10.1016/j.neuroscience.2023.05.028
- Oliva, C. A., Vargas, J. Y., and Inestrosa, N. C. (2013). Wnt signaling: role in LTP, neural networks and memory. *Ageing Res. Rev.* 12 (3), 786–800. doi:10.1016/j.arr.2013.03.006
- Palomer, E., Buechler, J., and Salinas, P. C. (2019). Wnt signaling deregulation in the aging and alzheimer's brain. *Front. Cell Neurosci.* 13, 227. doi:10.3389/fncel.2019.00227
- Pandey, R., Garg, A., Gupta, K., Shukla, P., Mandrah, K., Roy, S., et al. (2022). Arsenic induces differential neurotoxicity in male, female, and E2-deficient females:

- comparative effects on hippocampal neurons and cognition in adult rats. *Mol. Neurobiol.* 59 (5), 2729–2744. doi:10.1007/s12035-022-02770-1
- Pandey, R., Rai, V., Mishra, J., Mandrah, K., Kumar Roy, S., and Bandyopadhyay, S. (2017). From the cover: arsenic induces hippocampal neuronal apoptosis and cognitive impairments via an up-regulated BMP2/smud-dependent reduced BDNF/TrkB signaling in rats. *Toxicol. Sci.* 159 (1), 137–158. doi:10.1093/toxsci/kfx124
- Pandey, R., Shukla, P., Anjum, B., Gupta, H. P., Pal, S., Arjaria, N., et al. (2020). Estrogen deficiency induces memory loss via altered hippocampal HB-EGF and autophagy. *J. Endocrinol.* 244 (1), 53–70. doi:10.1530/JOE-19-0197
- Payton-Stewart, F., Schoene, N. W., Kim, Y. S., Burow, M. E., Cleveland, T. E., Boue, S. M., et al. (2009). Molecular effects of soy phytoalexin glyceollins in human prostate cancer cells LNCaP. *Mol. Carcinog.* 48 (9), 862–871. doi:10.1002/mc.20532
- Piechota, M., Sunderland, P., Wysocka, A., Nalberczak, M., Sliwinska, M. A., Radwanska, K., et al. (2016). Is senescence-associated beta-galactosidase a marker of neuronal senescence? *Oncotarget* 7 (49), 81099–81109. doi:10.18632/oncotarget.12752
- Prud'homme, G. J., Kurt, M., and Wang, Q. (2022). Pathobiology of the klotho antiaging protein and therapeutic considerations. *Front. Aging* 3, 931331. doi:10.3389/fagi.2022.931331
- Saito, Y., Miyajima, M., Yamamoto, S., Sato, T., Miura, N., Fujimiya, M., et al. (2021). Accumulation of senescent neural cells in murine lupus with depression-like behavior. *Front. Immunol.* 12, 692321. doi:10.3389/fimmu.2021.692321
- Sarkar, G., Curran, G. L., Mahlum, E., Decklever, T., Wengenack, T. M., Blahnik, A., et al. (2011). A carrier for non-covalent delivery of functional beta-galactosidase and antibodies against amyloid plaques and IgM to the brain. *PLoS One* 6 (12), e28881. doi:10.1371/journal.pone.0028881
- Schuler, M. A., Schmitt, E. S., and Beachy, R. N. (1982). Closely related families of genes code for the alpha and alpha' subunits of the soybean 7S storage protein complex. *Nucleic Acids Res.* 10 (24), 8225–8244. doi:10.1093/nar/10.24.8225
- Sharan, K., Siddiqui, J. A., Swarnkar, G., Maurya, R., and Chattopadhyay, N. (2009). Role of phytochemicals in the prevention of menopausal bone loss: evidence from *in vitro* and *in vivo*, human interventional and pharmacokinetic studies. *Curr. Med. Chem.* 16 (9), 1138–1157. doi:10.2174/092986709787581806
- Sharma, A., Yang, W. L., Ochani, M., and Wang, P. (2017). Mitigation of sepsis-induced inflammatory responses and organ injury through targeting Wnt/ β -catenin signaling. *Sci. Rep.* 7 (1), 9235. doi:10.1038/s41598-017-08711-6
- Shi, B., Chen, M., Xia, Z., Tang, W., Li, Y., Qin, C., et al. (2023). Genistein attenuates neuroinflammation and oxidative stress and improves cognitive impairment in a rat model of sepsis-associated encephalopathy: potential role of the Nrf2 signaling pathway. *Metab. Brain Dis.* 38 (1), 339–347. doi:10.1007/s11011-022-01076-4
- Sierra, A., Martin-Suarez, S., Valcarcel-Martin, R., Pascual-Brazo, J., Aelvoet, S. A., Abiega, O., et al. (2015). Neuronal hyperactivity accelerates depletion of neural stem cells and impairs hippocampal neurogenesis. *Cell Stem Cell* 16 (5), 488–503. doi:10.1016/j.stem.2015.04.003
- Sinha, A., Tamboli, R. S., Seth, B., Kanhed, A. M., Tiwari, S. K., Agarwal, S., et al. (2015). Neuroprotective role of novel triazine derivatives by activating wnt/ β catenin signaling pathway in rodent models of alzheimer's disease. *Mol. Neurobiol.* 52 (1), 638–652. doi:10.1007/s12035-014-8899-y
- Su, D., Li, W., She, X., Chen, X., Zhai, Q., Cui, B., et al. (2018). Chronic noise exposure exacerbates AD-like neuropathology in SAMP8 mice in relation to Wnt signaling in the PFC and hippocampus. *Sci. Rep.* 8 (1), 14622. doi:10.1038/s41598-018-32948-4
- Sun, T., Zhang, L., Feng, J., Bao, L., Wang, J., Song, Z., et al. (2022). Characterization of cellular senescence in doxorubicin-induced aging mice. *Exp. Gerontol.* 163, 111800. doi:10.1016/j.exger.2022.111800
- Swarbrick, S., Wragg, N., Ghosh, S., and Stolzing, A. (2019). Systematic review of miRNA as biomarkers in alzheimer's disease. *Mol. Neurobiol.* 56 (9), 6156–6167. doi:10.1007/s12035-019-1500-y
- Tajima, K., Matsuda, S., Yae, T., Drapkin, B. J., Morris, R., Boukhali, M., et al. (2019). SETD1A protects from senescence through regulation of the mitotic gene expression program. *Nat. Commun.* 10 (1), 2854. doi:10.1038/s41467-019-10786-w
- Tamura, H., Miyazaki, A., Kawamura, T., Gotoh, H., Yamamoto, N., and Narita, M. (2024). Chronic ingestion of soy peptide supplementation reduces aggressive behavior and abnormal fear memory caused by juvenile social isolation. *Sci. Rep.* 14 (1), 11557. doi:10.1038/s41598-024-62534-w
- Tanaka, M., Kiyohara, H., Yoshino, A., Nakano, A., Takata, F., Dohgu, S., et al. (2020). Brain-transportable soy dipeptide, Tyr-Pro, attenuates amyloid β peptide₂₅₋₃₅-induced memory impairment in mice. *NPJ Sci. Food* 4, 7. doi:10.1038/s41538-020-0067-3
- Tao, W., Ruan, J., Wu, R., Zhao, M., Zhao, T., Qi, M., et al. (2023). A natural carotenoid crocin exerts antidepressant action by promoting adult hippocampal neurogenesis through Wnt/ β -catenin signaling. *J. Adv. Res.* 43, 219–231. doi:10.1016/j.jare.2022.02.015
- Tsuruki, T., Kishi, K., Takahashi, M., Tanaka, M., Matsukawa, T., and Yoshikawa, M. (2003). Soymetide, an immunostimulating peptide derived from soybean beta-conglycinin, is an fMLP agonist. *FEBS Lett.* 540 (1-3), 206–210. doi:10.1016/s0014-5793(03)00265-5
- Tufekci, K. U., Alural, B., Tarakcioglu, E., San, T., and Genc, S. (2021). Lithium inhibits oxidative stress-induced neuronal senescence through miR-34a. *Mol. Biol. Rep.* 48 (5), 4171–4180. doi:10.1007/s11033-021-06430-w
- Unno, K., and Konishi, T. (2015). Preventive effect of soybean on brain aging and amyloid- β accumulation: comprehensive analysis of brain gene expression. *Recent Pat. Food Nutr. Agric.* 7 (2), 83–91. doi:10.2174/2212798407666150629140132
- Wang, C., Kang, Y., Liu, P., Liu, W., Chen, W., Hayashi, T., et al. (2023). Combined use of dasatinib and quercetin alleviates overtraining-induced deficits in learning and memory through eliminating senescent cells and reducing apoptotic cells in rat hippocampus. *Behav. Brain Res.* 440, 114260. doi:10.1016/j.bbr.2022.114260
- Wang, Y., Kuca, K., You, L., Nepovimova, E., Heger, Z., Valko, M., et al. (2024). The role of cellular senescence in neurodegenerative diseases. *Arch. Toxicol.* 98, 2393–2408. doi:10.1007/s00204-024-03768-5
- Wei, L., Chen, C., Ding, L., Mo, M., Zou, J., Lu, Z., et al. (2019). Wnt1 promotes EAAT2 expression and mediates the protective effects of astrocytes on dopaminergic cells in Parkinson's disease. *Neural Plast.* 2019, 1247276. doi:10.1155/2019/1247276
- Wei, L. C., Ding, Y. X., Liu, Y. H., Duan, L., Bai, Y., Shi, M., et al. (2012). Low-dose radiation stimulates Wnt/ β -catenin signaling, neural stem cell proliferation and neurogenesis of the mouse hippocampus *in vitro* and *in vivo*. *Curr. Alzheimer Res.* 9 (3), 278–289. doi:10.2174/156720512800107627
- Wissler Gerdes, E. O., Zhu, Y., Weigand, B. M., Tripathi, U., Burns, T. C., Tchkonja, T., et al. (2020). Cellular senescence in aging and age-related diseases: implications for neurodegenerative diseases. *Int. Rev. Neurobiol.* 155, 203–234. doi:10.1016/bs.irn.2020.03.019
- Xiang, Y., Wang, S. H., Wang, L., Wang, Z. L., Yao, H., Chen, L. B., et al. (2019). Effects of ginsenoside Rg1 regulating wnt/ β -catenin signaling on neural stem cells to delay brain senescence. *Stem Cells Int.* 2019, 5010184. doi:10.1155/2019/5010184
- Xu, N., Zhou, W. J., Wang, Y., Huang, S. H., Li, X., and Chen, Z. Y. (2015). Hippocampal Wnt3a is necessary and sufficient for contextual fear memory acquisition and consolidation. *Cereb. Cortex* 25 (11), 4062–4075. doi:10.1093/cercor/bhu121
- Yoo, D. Y., Jung, S., Kang, J. S., Baek, J. H., Park, K. H., Lee, D. H., et al. (2022). Isoflavone-enriched soybean leaves (Glycine max) alleviate cognitive impairment induced by ovariectomy and modulate PI3K/akt signaling in the Hippocampus of C57BL6 mice. *Nutrients* 14 (22), 4753. doi:10.3390/nu14224753
- Zhang, J., Lazarenko, O. P., Blackburn, M. L., Badger, T. M., Ronis, M. J., and Chen, J. R. (2014). Soy protein isolate down-regulates caveolin-1 expression to suppress osteoblastic cell senescence pathways. *FASEB J.* 28 (7), 3134–3145. doi:10.1096/fj.13-243659
- Zhang, L., Cheng, F., Wei, Y., Zhang, L., Guo, D., Wang, B., et al. (2019). Inhibition of TAZ contributes radiation-induced senescence and growth arrest in glioma cells. *Oncogene* 38 (15), 2788–2799. doi:10.1038/s41388-018-0626-0
- Zhang, S., Kong, D. W., Ma, G. D., Liu, C. D., Yang, Y. J., Liu, S., et al. (2022a). Long-term administration of salvianolic acid A promotes endogenous neurogenesis in ischemic stroke rats through activating Wnt3a/GSK3 β / β -catenin signaling pathway. *Acta Pharmacol. Sin.* 43 (9), 2212–2225. doi:10.1038/s41401-021-00844-9
- Zhang, X., Pearsall, V. M., Carver, C. M., Atkinson, E. J., Clarkson, B. D. S., Grund, E. M., et al. (2022b). Rejuvenation of the aged brain immune cell landscape in mice through p16-positive senescent cell clearance. *Nat. Commun.* 13 (1), 5671. doi:10.1038/s41467-022-33226-8
- Zheng, Y., Yasuda, M., Yamao, M., Gokan, T., Sejima, Y., Nishikawa, T., et al. (2023). Fermented soybean foods (natto) ameliorate age-related cognitive decline by hippocampal TAAR1-mediated activation of the CaMKII/CREB/BDNF signaling pathway in senescence-accelerated mouse prone 8 (SAMP8). *Food Funct.* 14 (22), 10097–10106. doi:10.1039/d3fo03987k



OPEN ACCESS

EDITED BY

Jian Hao,
The Second Affiliated Hospital of Guangzhou
Medical University, China

REVIEWED BY

Junhui Li,
University of Massachusetts Medical School,
United States
Zheng Yuan,
China Academy of Chinese Medical Sciences,
China

*CORRESPONDENCE

Jiandong Yu,
✉ yujiandongjnu@163.com
Jianhong Liu,
✉ jianhong.liu304@163.com

†These authors have contributed equally to
this work

RECEIVED 11 December 2024

ACCEPTED 12 February 2025

PUBLISHED 11 March 2025

CITATION

Wang Y, Dong L, Han S, You Y, Zhang M, Sun B,
Ni H, Ge R, Liu J and Yu J (2025) Zingerone
alleviates inflammatory pain by reducing the
intrinsic excitability of anterior cingulate cortex
neurons in a mice model.
Front. Pharmacol. 16:1543594.
doi: 10.3389/fphar.2025.1543594

COPYRIGHT

© 2025 Wang, Dong, Han, You, Zhang, Sun, Ni,
Ge, Liu and Yu. This is an open-access article
distributed under the terms of the [Creative
Commons Attribution License \(CC BY\)](#). The use,
distribution or reproduction in other forums is
permitted, provided the original author(s) and
the copyright owner(s) are credited and that the
original publication in this journal is cited, in
accordance with accepted academic practice.
No use, distribution or reproduction is
permitted which does not comply with these
terms.

Zingerone alleviates inflammatory pain by reducing the intrinsic excitability of anterior cingulate cortex neurons in a mice model

Yuanyuan Wang ^{1,2,3†}, Lang Dong ^{1,2†}, Shu Han ^{2†}, Yuehan You ^{2†},
Mingrui Zhang ², Bingjing Sun ^{2,3}, Hong Ni ^{2,3}, Rongjing Ge ^{2,3},
Jianhong Liu ^{2,4*} and Jiandong Yu ^{1,2,5*}

¹Department of Neurosurgery, the First Affiliated Hospital of Bengbu Medical University, Bengbu, Anhui, China, ²Laboratory of Brain and Psychiatric Disease, Bengbu Medical University, Bengbu, Anhui, China, ³School of Basic Medicine, Bengbu Medical University, Bengbu, Anhui, China, ⁴Department of Biochemistry and Molecular biology, School of Laboratory Medicine, Bengbu Medical University, Bengbu, Anhui, China, ⁵Anhui Engineering Research Center for Neural Regeneration Technology and Medical New Materials, Bengbu Medical University, Bengbu, Anhui, China

Background: *Zingiber officinale Roscoe* has been shown to possess analgesic properties. Zingerone (ZO), a bioactive compound derived from *Zingiber officinale Roscoe*, exhibits a range of pharmacological effects, including anti-inflammatory, anti-cancer, antioxidant, antibacterial, and anti-apoptotic activities. However, the analgesic properties of zingerone remain unclear.

Methods: Complete Freund's adjuvant (CFA) was administered to the left hind paw of C57BL/6 mice to induce a model of inflammatory pain. The analgesic effects of zingerone were assessed using the Von Frey and Hargreaves tests. *In vivo* fiber photometry and whole-cell patch clamp techniques were employed to investigate the potential mechanisms.

Results: Both acute and long-term treatment with zingerone resulted in a significant increase in mechanical and thermal pain thresholds in mice experiencing CFA-induced inflammatory pain. Mechanical stimulation led to a pronounced increase in calcium levels within the anterior cingulate cortex (ACC) neurons of the inflammatory pain model, which was alleviated by zingerone administration. Furthermore, zingerone was found to modify synaptic transmission to ACC neurons and decrease their intrinsic excitability by prolonging the refractory period of these neurons.

Conclusion: Zingerone demonstrates potential for alleviating CFA-induced inflammatory pain by reducing the intrinsic excitability of ACC neurons in a mouse model.

KEYWORDS

Zingiber officinale roscoe, analgesic, intrinsic excitability, complete Freund's adjuvant (CFA), refractory period, electrophysiological, synaptic transmission

1 Introduction

Pain is defined as an aversive sensory and emotional experience that is linked to actual or potential damage to bodily tissues. It is recognized as the fifth vital sign in human health and represents a significant challenge of global health (Raja et al., 2020). Inflammatory pain represents the most prevalent form of pain observed in clinical practice (Barr et al., 2015). Inflammatory pain significantly impacts patients' quality of life and their capacity to work. Furthermore, the progression of acute inflammatory pain to chronic pain is likely to impose a substantial economic burden on both the patients' families and society at large (Patnaik et al., 2017).

The ACC plays a crucial role in the integration of nociceptive perception and emotional responses associated with chronic pain (Baliki and Apkarian, 2015; Bliss et al., 2016; Rainville et al., 1997). In chronic pain, the ACC is identified as the most significantly activated region within the brain (Bushnell et al., 2013). The suppression of neuronal activity in the ACC has been shown to induce analgesic effects in the context of inflammatory pain (Pan et al., 2022). In chronic pain, there exist presynaptic and postsynaptic forms of long-term potentiation in the neurons of the ACC. A reduction in such potentiation is associated with the manifestation of analgesic effects (Koga et al., 2015; Zhuo, 2014). The enhancement of intrinsic excitability observed in chronic pain conditions is characterized by an increased input-output gain, as well as a reduction in spike threshold and refractory period (Yang et al., 2018). Both synaptic plasticity and intrinsic excitability plasticity play crucial roles in the hyperactivity of ACC neurons associated with chronic pain.

Zingiber officinale Roscoe has been shown to possess analgesic properties (Kim et al., 2022a). Among the 400 compounds identified in *Zingiber officinale Roscoe*, the primary bioactive components include gingerols, shogaols, and paradols (Mao et al., 2019). Recent studies have highlighted the analgesic effects of specific sub-components, particularly [6]-Shogaol and [6]-Gingerol (Kim et al., 2022a). These compounds exert their pain-relieving properties primarily through their anti-inflammatory actions in brain regions and the colon (Santos et al., 2024; Özdemir et al., 2023). For instance, [6]-Shogaol has been shown to significantly alleviate oxaliplatin-induced cold allodynia and mechanical hyperalgesia by modulating the serotonin system in the spinal cord (Kim et al., 2022b). However, current research has predominantly focused on the spinal cord, while chronic pain is often closely associated with emotional responses mediated by central brain regions. Whether other sub-components of *Z. officinale Roscoe* and central brain regions, particularly the ACC, play a role in its analgesic effects remains to be elucidated. Further investigation into the involvement of central brain mechanisms could provide a more comprehensive understanding of their therapeutic potential.

Zingerone exhibits a range of pharmacological properties, including anti-inflammatory, anti-cancer, antioxidant, antibacterial, and anti-apoptotic effects (Choi et al., 2018; Mahomoodally et al., 2021). Recent research has demonstrated that zingerone influences the electrophysiological properties of neurons. Specifically, zingerone has been shown to inhibit the amplitude of sodium and calcium currents, thereby modulating the functional activities of mouse

pituitary cell lines (GH3 cells) and hippocampal neurons (Lai et al., 2022). Zingerone has the capacity to inhibit the pacemaker potential in a concentration-dependent manner through the modulation of ATP-sensitive potassium channels in gastrointestinal interstitial cells of Cajal (ICCs) (Kim et al., 2018). Zingerone has been shown to have the capacity to inhibit neuronal excitability. However, its potential analgesic effects through modulation of the ACC neuronal excitability remain to be elucidated. To investigate this, we employed a mouse model of inflammatory pain induced by complete Freund's adjuvant, utilizing a combination of pain behavior assessments, calcium imaging, and patch-clamp techniques to evaluate the impact of zingerone on inflammatory pain and to explore the underlying mechanisms involved.

2 Method

2.1 Animals

110 male C57BL/6 mice, aged between 6 and 8 weeks, were procured from Henan Scobes Biotechnology Co., Ltd. (License No.: SCXK 2020-0005). The mice were maintained under a controlled environment with a 12-h light/dark cycle, temperature regulated between 20 and 26°C, and humidity levels maintained at 50% ± 20%. They were provided with *ad libitum* access to food and water and were acclimatized for a minimum of 1 week prior to the commencement of experimental procedures. All animal experimentation protocols adhered to the guidelines established by the Laboratory Animal Ethics Committee of Bengbu Medical University.

2.2 Inflammatory pain model

To induce inflammatory pain, 20 µL of CFA was administered subcutaneously to the plantar surface of the left hind paw of 66 mice (Alotaibi et al., 2023; Zhou et al., 2021). The control group (26 mice) received an equivalent volume of normal saline instead of CFA. After the induction of inflammatory pain, the affected mice were randomly divided into several treatment groups: 6 mice did not receive saline injection and served as the CFA group (Figure 1A); 10 mice received a saline injection 3 days after CFA administration and were designated as the CFA + vehicle group (Figure 1D); 10 mice received daily saline injections and were also labeled as the CFA + vehicle group (Figure 2A); and 40 mice were assigned to the CFA + ZO group. Within the CFA + ZO group, 10 mice were administered each of the differing doses of zingerone (Mani et al., 2017; Chopra et al., 2023; Mehrzadi et al., 2021) (as shown in Figure 1D), while another 10 mice received daily intraperitoneal injections of 20 mg/kg zingerone for 14 days (as shown in Figure 2A). The vehicle group received saline injections as a control. All behavioral assessments were conducted by an investigator blinded to the treatment allocations to ensure unbiased results.

2.3 von Frey test

The von Frey test was utilized to evaluate mechanical allodynia by determining the paw withdrawal threshold in response to

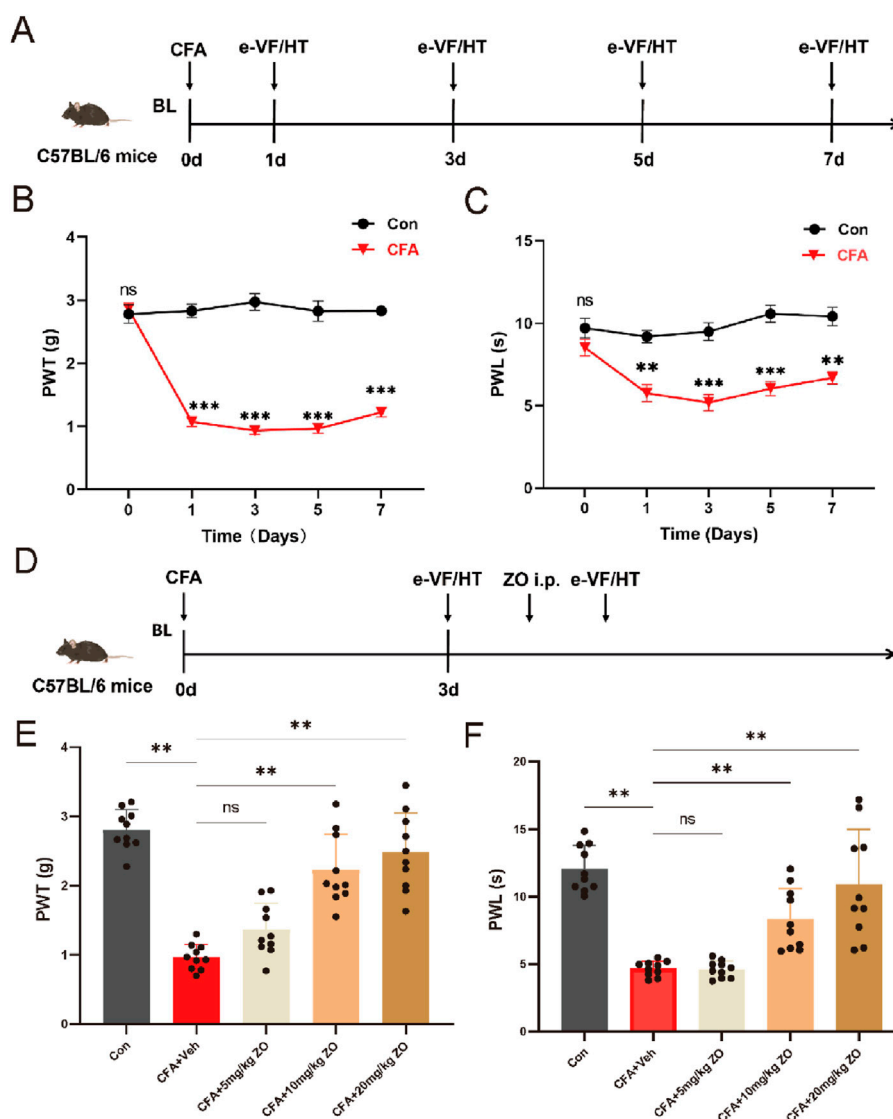


FIGURE 1

The acute administration of zingerone and its effects on hyperalgesia in a model of inflammatory pain induced by CFA. (A) The experimental timeline outlines the procedures employed in this study. (B) The paw withdrawal threshold (PWT) was assessed to evaluate mechanical allodynia following CFA injection (repeated measures two-way ANOVA with Bonferroni *post hoc* test, $F(4,40) = 5.507$, the p-values were calculated for the control and CFA groups on specified days). (C) The paw withdrawal latency (PWL) was measured to assess thermal hyperalgesia post-CFA administration (repeated measures two-way ANOVA with Bonferroni *post hoc* test, $F(4,40) = 38.11$, the p-values were calculated for the control and CFA groups on the specified days). (D) The timeline for evaluating the analgesic effects of zingerone is presented. (E) The PWT was utilized to assess the potential analgesic properties of zingerone in relation to mechanical allodynia (one-way ANOVA with Bonferroni *post hoc* test, $F(4,45) = 35.16$, $P < 0.001$). (F) The PWL was employed to evaluate the potential analgesic effects of zingerone on thermal hyperalgesia (one-way ANOVA with Bonferroni *post hoc* test, $F(4,45) = 23.42$, $P < 0.001$). All data are expressed as mean \pm standard error of the mean (SEM). Statistical significance is indicated as * $P < 0.05$, ** $P < 0.01$, and *** $P < 0.001$. The abbreviations used are: ns: not significant; i.p.: intraperitoneal injection; e-VF: electric Von Frey; HT: Hargreaves Test; Con: control; Veh: vehicle; ZO: zingerone.

mechanical stimuli, employing von Frey filaments (Zhongshi, Beijing, China). Prior to testing, mice were acclimatized in transparent plastic chambers equipped with a wire mesh floor for a minimum duration of 30 min. During the assessment, the measuring filament was positioned to penetrate the mesh and contact the plantar surface of the hind paw, with the force being gradually increased until a withdrawal response was elicited from the mice.

2.4 Hargreaves test

The Hargreaves test was employed to assess hyperalgesia by measuring the paw withdrawal latency, defined as the interval between the initiation of a light beam and the subsequent withdrawal of the paw. Mice were acclimatized in a manner identical to that used in the von Frey test. The thermal radiation source (Zhongshi, Beijing, China) was positioned beneath the center

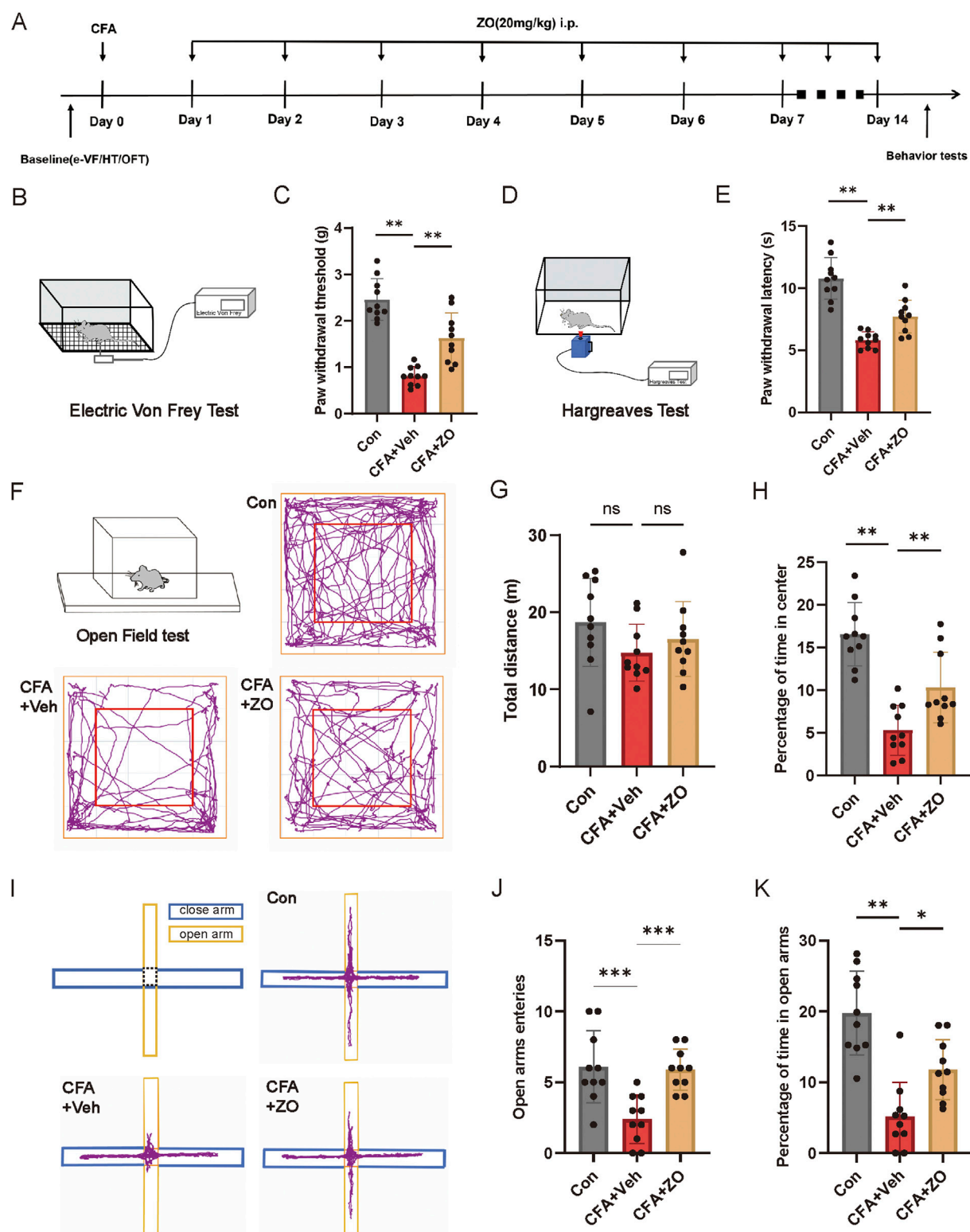


FIGURE 2

The prolonged administration of zingerone has been shown to mitigate chronic inflammatory pain and associated anxiety-like behaviors. (A) The experimental timeline is outlined. (B, C) The PWT was assessed to determine the long-term analgesic effects of zingerone on mechanical allodynia (one-way ANOVA with Bonferroni *post hoc* test, $F(2,27) = 38.35$, $P < 0.001$). (D, E) The PWL was evaluated to assess the long-term analgesic effects of zingerone on thermal hyperalgesia (one-way ANOVA with Bonferroni *post hoc* test, $F(2,27) = 37.65$, $P < 0.001$). (F) Locomotion patterns of mice subjected to control, CFA, and CFA combined with zingerone were recorded during an open field test. (G, H) Group data illustrating the total distance traveled (G, one-way ANOVA with Bonferroni *post hoc* test, $F(2,27) = 1.696$, $P = 0.2$) and the percentage of time spent in the center of the arena (H, one-way ANOVA with Bonferroni *post hoc* test, $F(2,27) = 24.36$, $P < 0.001$) during the open field test for the three experimental groups are presented. (I) Representative locomotion traces of mice injected with control, CFA, and CFA + zingerone in the elevated plus maze test are shown. (J, K) Group data (Continued)

FIGURE 2 (Continued)

reflecting the number of entries into the open arms (J, one-way ANOVA with Bonferroni *post hoc* test, $F(2,27) = 11.22$, $P < 0.001$) and the percentage of time spent in the open arms (K, one-way ANOVA with Bonferroni *post hoc* test, $F(2,27) = 20.85$, $P < 0.001$) during the elevated plus maze test for the three groups are provided. Data are expressed as mean \pm SEM, with significance levels indicated as * $P < 0.05$, ** $P < 0.01$, and *** $P < 0.001$. The abbreviations used ns: not significant; i.p.: intraperitoneal injection; e-VF: electric Von Frey; HT: Hargreaves Test; OFT: open field test; Con: control; Veh: vehicle; ZO: zingerone.

of the paw until a withdrawal response was observed from the animal.

2.5 Open-field test

Prior to the commencement of testing, the mice underwent a habituation period of 1 hour within the testing environment. Subsequently, each mouse was positioned in the center of a chamber measuring $50 \times 50 \times 30$ cm. The mice were carefully placed in the chamber and observed via a camera for 5 minutes. The time spent by each mouse in the central area, defined as a 30×30 cm square, as well as the total distance traveled by the mice within the open field arena, were recorded. Additionally, a 75% ethanol solution was utilized to sanitize the open field arena between each trial.

2.6 Elevated plus maze test

The elevated plus maze apparatus was positioned 50 cm above the ground. It comprised two open arms measuring $25 \times 8 \times 0.5$ cm and two closed arms measuring $25 \times 8 \times 12$ cm, all extending from a central platform of dimensions 8×8 cm. The closed arms were enclosed by transparent walls that were 12 cm in height, while the open arms featured a 0.5 cm ledge. Each mouse was introduced into the center of the maze, oriented towards a closed arm. A camera mounted above the maze recorded the mouse's movements during a 5-min observation period. The duration of time spent by the mice in both the open and closed arms was subsequently quantified. The maze was sanitized with 75% ethanol between each trial to ensure cleanliness. All behavioral assessments were conducted using ANY-maze (stoelting, United States) software for analysis.

2.7 Fiber photometry

The mice were subjected to anesthesia using pentobarbital administered intraperitoneally at a dosage of 75 mg/kg (Wang et al., 2023) and subsequently positioned on a stereotaxic apparatus (RWD, China). AAV vectors (rAAV-hSyn-GCaMp6s-WPRE, BrainVTA) were injected unilaterally into the ACC at the following coordinates: anteroposterior (AP) +0.98 mm, mediolateral (ML) ± 0.30 mm, and dorsoventral (DV) -1.70 mm, at a rate of 20 nL/min. A ferrule fiber-optic cannula with a core diameter of 200 μ m (RWD, China) was implanted above the site of viral injection and affixed to the skull using dental cement. Three weeks post-implantation, a multi-channel fiber photometry system (R811/821, RWD, China) was employed to monitor changes in calcium signaling during von Frey filaments

(NC12775-99, North Coast, United States) stimuli. The change in fluorescence, denoted as $\Delta F/F$, was calculated using the formula $(F_{\text{signal}} - F_0)/F_0$, with F_0 representing the baseline fluorescence, utilizing the data analysis module of the OFRS software (RWD, China).

2.8 Immunohistochemistry staining

Mice that received AVV injections were euthanized using pentobarbital administered intraperitoneally at a dosage of 75 mg/kg. Following euthanasia, the animals were subjected to a sequential perfusion process involving normal saline followed by 4% paraformaldehyde (PFA) in phosphate-buffered saline (PBS, at pH 7.2–7.4). The brains were subsequently harvested and post-fixed in 4% PFA overnight at a temperature of 4°C. After post-fixation, the brains underwent cryoprotection in a 10%–30% sucrose solution in PBS for a duration of 3 days. Staining of the 20 μ m sections of mouse brain was conducted using DAPI (P24000042957, biosharp). Imaging was performed utilizing eclipse software (Nikon) on a D-Eclipse-C1 confocal microscope (Nikon).

2.9 Acute ACC slice preparation

Following administration of isoflurane anesthesia, the mice were promptly decapitated, and their brains were swiftly excised and immersed in ice-cold artificial cerebrospinal fluid (ACSF) (Zheng et al., 2022; Shao et al., 2023; Zhang et al., 2021), which comprised the following components: NaCl (124 mM), Glucose (12.5 mM), NaHCO_3 (24 mM), KCl (2.5 mM), NaH_2PO_4 (1.2 mM), CaCl_2 (2 mM), MgCl_2 (2 mM), and HEPES (5 mM), adjusted to a pH of 7.35–7.45 and an osmolality of 310–330 mOsm/L. 300 μ m coronal brain slices containing the ACC, were prepared using a vibrating microtome (Leica VT1000S). The slices were then rapidly transferred to oxygen-saturated ACSF at 33°C for a 30-min incubation period, after which they were maintained at room temperature until recording commenced.

2.10 Whole-cell patch-clamp recordings

Brain slices were recorded within a submersion chamber (Warner RC-26 G) that was perfused with oxygenated ACSF at ambient temperature (22°C–25°C). Whole-cell patch clamp recordings were performed on layer II/III pyramidal neurons in the ACC using infrared differential interference contrast (IR-DIC) optics (Nikon FN1). All whole-cell recordings were executed with a Multiclamp 700B amplifier (Molecular Devices, CA, United States) and sampled at a frequency of 10 kHz using a Digidata

1550 interface (Molecular Devices, CA, United States). The action potentials and spontaneous excitatory postsynaptic currents (sEPSCs) of ACC pyramidal neurons were recorded using a solution composed of: HEPES (10 mM), K-gluconate (140 mM), phosphocreatine (5 mM), EGTA (0.5 mM), Mg-ATP (4 mM), TrisGTP (1 mM), and NaCl (4 mM) at pH 7.40 and an osmolality of 290 mOsm. sEPSCs were recorded at a holding potential of -70 mV in the presence of SR 95531 (10 μ M), a GABA_A receptor antagonist, within the ACSF. Additionally, spontaneous inhibitory postsynaptic currents (sIPSCs) of ACC pyramidal neurons were recorded using a solution containing: HEPES (10 mM), KCl (40 mM), K-gluconate (110 mM), phosphocreatine (5 mM), EGTA (0.5 mM), Mg-ATP (4 mM), TrisGTP (1 mM), and NaCl (4 mM) at pH 7.40 and an osmolality of 290 mOsm, also at -70 mV, in the presence of kynurenic acid (3 mM), an antagonist of ionotropic glutamate receptors, within the ACSF. Data analysis was conducted using Clampfit 10.7 software (Molecular Devices, CA, United States).

2.11 Statistical analysis

Statistical analyses and graphical representations were performed utilizing OriginPro 2019 (OriginLab Corporation, United States) and GraphPad Prism 8 (GraphPad Software, Inc., United States). Comparisons between two groups were executed using either paired or unpaired Student's *t*-tests. For experiments involving multiple groups, after passed Shapiro-Wilk test, one-way or two-way analysis of variance (ANOVA) was employed, accompanied by Bonferroni or Tukey's *post hoc* analyses. The data are presented as mean \pm standard error of the mean (SEM), with differences deemed statistically significant at a threshold of $*p < 0.05$.

3 Result

3.1 Zingerone has been shown to mitigate inflammatory pain and associated anxiety-like behaviors

To establish a model of inflammatory pain in mice, CFA was administered via injection into the left hind paws (Figure 1A). Following the injection, mechanical allodynia (Figure 1B) and thermal hyperalgesia (Figure 1C) were observed, beginning 1 day post-injection and persisting for a minimum of 1 week. To assess the analgesic properties of zingerone on inflammatory pain, various doses of zingerone were administered intraperitoneally to the mice 3 days after the CFA injection (Figure 1D). A single administration of zingerone at doses of 10 mg/kg or 20 mg/kg led to a rapid reduction in both mechanical allodynia (Figure 1E) and thermal hyperalgesia (Figure 1F). To evaluate the long-term effects of zingerone (20 mg/kg), administration commenced 1 day post-CFA injection and continued for 14 days (Figure 2A). This treatment led to a significant decrease in both mechanical allodynia (Figure 2C) and thermal hyperalgesia (Figure 2E). Given that chronic pain can induce anxiety symptoms (Baliki and Apkarian, 2015), we further

examined the impact of zingerone treatment on anxiety in CFA-injected mice. In the open field test, both control and CFA mice exhibited similar distances traveled (Figure 2G). However, CFA mice spent significantly less time in the center of the arena compared to control mice, a behavior that was reversed by zingerone treatment (Figure 2H). In the elevated plus maze test, CFA mice demonstrated reduced time spent in the open arms and infrequent entries into these areas compared to controls, with zingerone treatment also reversing this behavior (Figure 2J, K). Collectively, these findings indicate that zingerone effectively alleviates CFA-induced inflammatory pain and anxiety-like behaviors.

3.2 The neurons located in the ACC play a significant role in the analgesic effects of zingerone

The ACC plays a pivotal role in the perception of pain, with heightened neuronal activity in this region being closely associated with pain experiences (Pan et al., 2022). To assess the involvement of the ACC in the analgesic effects of zingerone, we conducted an investigation into the dynamics of neuronal activity within the ACC through fiber photometry recordings of calcium (Ca^{2+}) signals (Figure 3A). An adeno-associated virus (AAV) encoding the fluorescent calcium indicator GCaMP6s (AAV-hSyn-GCaMP6s) was administered into the ACC of mice (Figure 3B). Three weeks post-injection, a notable increase in the fluorescence intensity of GCaMP6s-labeled neurons in the ACC was observed following stimulation of the ipsilateral hind limb using von Frey filaments in CFA mice. Following treatment with zingerone (20 mg/kg), this increase in fluorescence intensity was significantly diminished (Figures 3C–E). These findings indicate that zingerone treatment effectively mitigates alterations in neuronal activity within ACC neurons in a model of CFA-induced inflammatory pain.

3.3 Zingerone modifies synaptic transmission within the ACC

To elucidate the mechanisms by which zingerone modulates the activity of the ACC neurons, we employed whole-cell patch clamp techniques to assess the synaptic inputs to these neuronal cells. Our findings indicate that zingerone (10 μ M) administration (Lai et al., 2022) resulted in an increased frequency of excitatory postsynaptic currents (EPSCs) in ACC neurons (Figure 4A, B, control: 1.14 ± 0.09 Hz, ZO: 1.66 ± 0.16 Hz, 13 cells from three mice, paired T-test, $P = 0.012$), while the amplitude of EPSCs remained constant (Figure 4C, control: 9.21 ± 0.71 pA, ZO: 8.81 ± 0.65 pA, 13 cells from three mice, paired T-test, $P = 0.32$). Conversely, we observed a decrease in the frequency of inhibitory postsynaptic currents (IPSCs) following zingerone (10 μ M) treatment (Figure 4D, E, control: 1.03 ± 0.06 Hz, ZO: 0.91 ± 0.09 Hz, 13 cells from three mice, paired T-test, $P = 0.032$), with the amplitude of IPSCs showing no significant change (Figure 4F, control: 11.86 ± 1.53 pA, ZO: 10.70 ± 1.19 pA, 13 cells from three mice, paired T-test, $P = 0.21$). These results suggest that zingerone has the capacity to modulate the frequency of both EPSCs and IPSCs in ACC neurons.

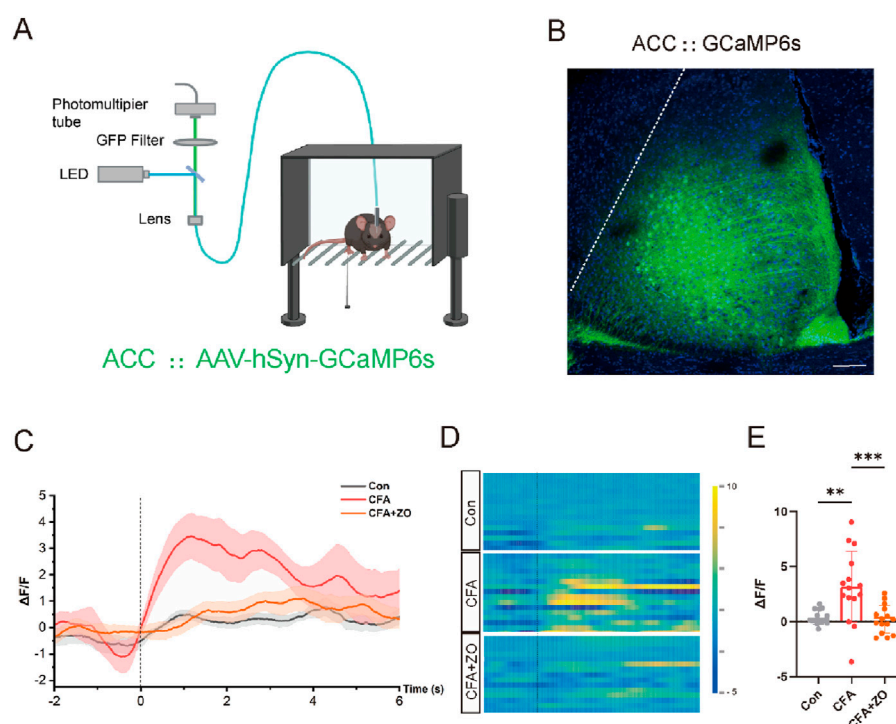


FIGURE 3
Zingerone reduces neuronal activity linked to pain in the ACC. **(A)** A schematic representation of the real-time fiber photometry assay is provided. Image was created with [BioRender.com](https://www.biorender.com), with permission. **(B)** A representative image illustrating the expression of AAV-hSyn-GCaMP6s in the ACC is shown, with a scale bar of 100 μ m. **(C, D)** The average calcium activity (C, “-2” refers to 2 s prior to stimulation) and corresponding heat maps (D) depicting calcium signals in response to 0.07g von Frey stimuli in control, CFA and CFA + zingerone mice are presented. **(E)** Statistics on the change in mean Ca²⁺ fluorescence signal in mice following stimulation (analyzed by one-way ANOVA with Tukey’s *post hoc* test, $F(2, 42) = 9.961$, ** $P < 0.01$, *** $P < 0.001$). All data are expressed as mean \pm SEM, with a sample size of $n = 3$ mice in each group.

3.4 Zingerone has been shown to prolong the refractory period and reduce the intrinsic excitability of neurons within the ACC

Neuronal intrinsic excitability plays a critical role in modulating neuronal activity. Consequently, we examined the impact of zingerone on the intrinsic excitability of ACC neurons. Our findings indicated a significant reduction in firing frequencies of ACC neurons in response to incrementally injected currents following zingerone (10 μ M) perfusion (Figures 5A, B). Further analysis revealed that zingerone primarily prolonged the interval between the first and the second action potentials in response to 40 pA stimulation in ACC neurons (Figure 5C, control: 37.59 ± 4.21 ms, ZO: 62.18 ± 2.11 ms, 11 cells from five mice, paired T-test, $P < 0.05$). The refractory period, defined as the minimum interval between action potentials elicited by a specific testing stimulus, is a key determinant of neuronal firing rates. To further elucidate the effects of zingerone on the refractory period of ACC neurons, we varied the inter-pulse interval of depolarizing pulses. Our results demonstrated that zingerone (10 μ M) significantly extended the refractory period of ACC neurons across various stimulus intensities (Figures 5D, E). These findings suggest that zingerone diminishes the intrinsic excitability of ACC neurons by prolonging their refractory period.

4 Discussion

In the current investigation, we present novel findings indicating that zingerone exhibits analgesic effect in a model of inflammatory pain induced by CFA. This analgesic effect is attributed to zingerone’s modulation of synaptic transmission and the intrinsic excitability of neurons in the ACC (Figure 6).

Given the issues of tolerance, dependence, and withdrawal symptoms associated with commonly used clinical opioid analgesics like morphine, researchers have been actively seeking safer alternatives for pain management (Badshah et al., 2024; Lane et al., 2004; Little et al., 2013). Recent findings indicate that the naturally bioactive compound zingerone exhibits analgesic effect on inflammatory pain. Notably, zingerone has been documented to mitigate the development of antinociceptive tolerance and physical dependence associated with morphine, potentially through its capacity to reduce oxidative stress (Molavinia et al., 2024). Zingerone demonstrates anti-epileptic and neuroprotective properties through its various pharmacological activities, which encompass anti-inflammatory, antioxidant, and anti-apoptotic effects (Rashid et al., 2021). In our model, the analgesic effect is observed 30 min following the administration of zingerone, even in the absence of anti-apoptotic and anti-inflammatory mechanisms.

The ACC is a pivotal area involved in the perception of nociception, and the activity of pyramidal neurons within the

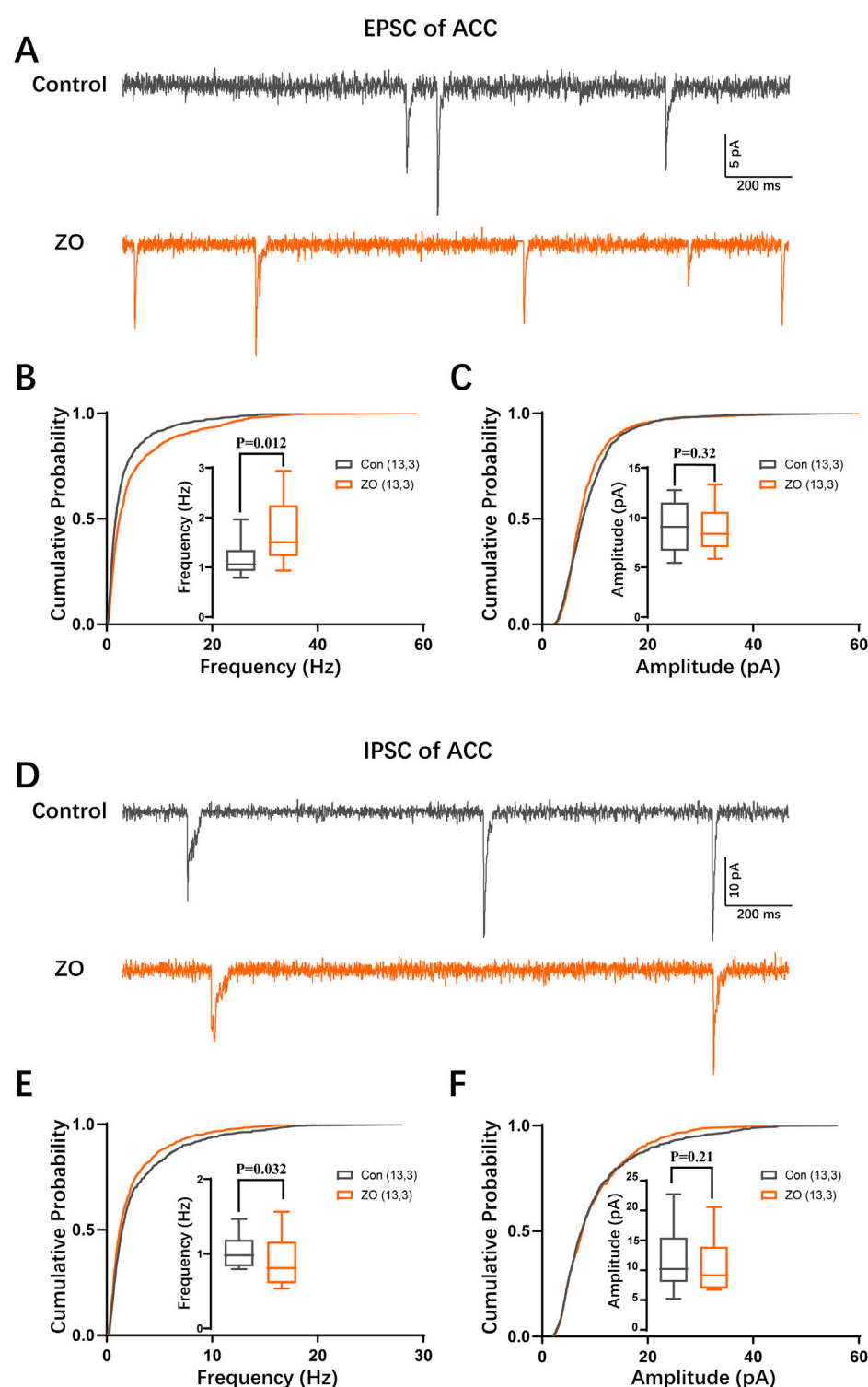


FIGURE 4

Zingerone modulates synaptic transmission in ACC neurons. (A) Representative traces of excitatory postsynaptic currents (EPSCs) recorded from ACC pyramidal neurons, both in the absence and presence of zingerone. (B) The cumulative frequency distribution and mean frequency of EPSCs in ACC pyramidal neurons are presented, comparing measurements taken prior to and following zingerone (10 μ M) administration. (C) The cumulative amplitude distribution and mean amplitude of EPSCs in ACC pyramidal neurons are also analyzed before and after the application of zingerone. (D) Representative traces of inhibitory postsynaptic currents (IPSCs) are shown for ACC pyramidal neurons, recorded without and with zingerone. (E) The cumulative frequency distribution and mean frequency of IPSCs in ACC pyramidal neurons are evaluated before and after zingerone (10 μ M) treatment. (F) The cumulative amplitude distribution and mean amplitude of IPSCs in ACC pyramidal neurons are assessed in relation to zingerone application.

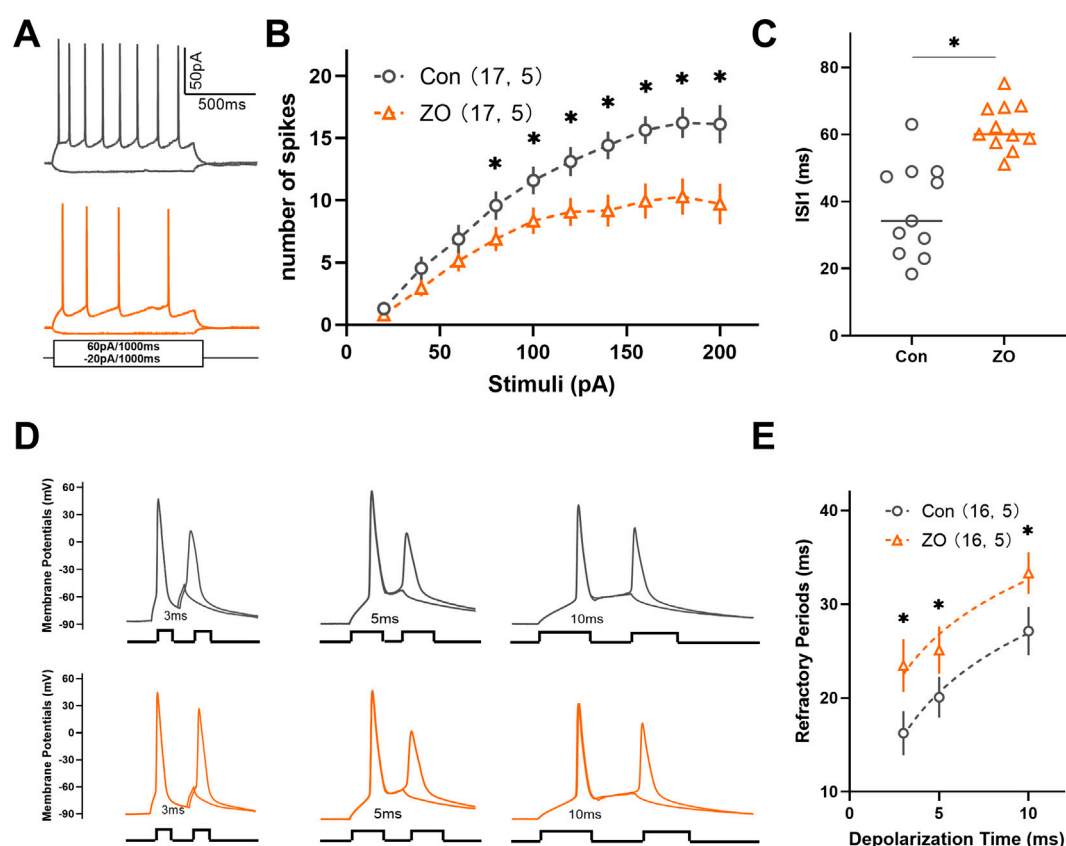


FIGURE 5

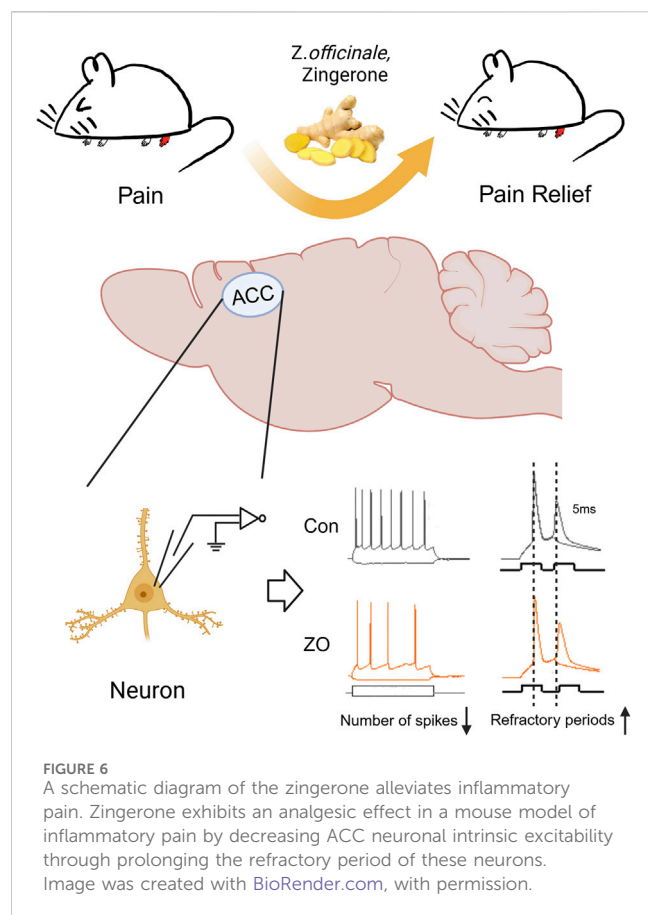
Zingerone has been shown to prolong the refractory period of action potentials and diminish the firing capacity of ACC neurons. (A) The representative firing patterns of neurons are depicted without zingerone (black, top) and with zingerone (orange, middle) in response to the stimulus waveform (black, bottom). (B) The application of zingerone (10 μ M) resulted in a reduced gain in the input-output curve (repeated measures two-way ANOVA with Bonferroni *post hoc* test between groups, $F(1, 320) = 53.3$, $P < 0.0001$). (C) Furthermore, zingerone was found to increase the inter-spike interval (ISI) of ACC neurons (paired T-test, $P < 0.05$). (D) A comparison of the spike refractory periods of ACC neurons is illustrated, showing the absence of zingerone (black, top) versus its presence (orange, bottom). (E) Zingerone significantly decreased the spike refractory period in ACC pyramidal neurons (repeated measures two-way ANOVA with Bonferroni *post hoc* test between groups, $F(1, 90) = 9.42$, $P = 0.003$). Data are expressed as mean \pm SEM, with significance levels indicated as $*P < 0.05$.

ACC is elevated in both acute and chronic pain (Koga et al., 2010; Shyu et al., 2008). In this study, we utilized fiber photometry to monitor the activity of ACC neurons prior to and following the administration of zingerone during mechanical pain stimuli. This advanced technology allows for the real-time recording of calcium dynamics within neuronal populations in the ACC of awake mice while nociceptive behavioral tests are being conducted (Legaria et al., 2022; Gunaydin et al., 2014). Utilizing advanced technology, we have determined that zingerone diminishes the activity of ACC neurons in response to stimuli. Our findings align with those of a previous study, which demonstrated that targeted inhibition of pyramidal neuron activity in the ACC through optogenetic methods led to a rapid and significant reduction in hypersensitivity (Kang et al., 2015).

The excitability of a neuron is influenced by both synaptic inputs and its intrinsic properties. Prior research has demonstrated that inflammatory pain increases excitatory synaptic transmission while simultaneously decreasing inhibitory synaptic transmission in neurons of the ACC (Zhao et al., 2006; Gong et al., 2010). A separate investigation has demonstrated that the heightened intrinsic excitability of pyramidal neurons in the ACC is

associated with neuropathic pain (Yang et al., 2018). In the current investigation, we performed a comprehensive analysis of the impact of zingerone on synaptic transmission and the intrinsic excitability of pyramidal neurons in the ACC utilizing the whole-cell patch-clamp methodology. Our research indicates that zingerone enhances the frequency of glutamatergic spontaneous excitatory transmission in pyramidal neurons of the ACC. Our findings are consistent with that zingerone has the potential to augment glutamatergic spontaneous excitatory transmission in neurons located in the spinal substantia gelatinosa of rats (Yue et al., 2013). Furthermore, zingerone appears to decrease the frequency of GABAergic spontaneous inhibitory transmission. Notably, our *in vivo* calcium dynamics recordings reveal that zingerone significantly inhibits neuronal activity in the ACC. Consequently, we hypothesize that the analgesic properties of zingerone may be attributed to its influence on intrinsic neuronal excitability rather than on synaptic transmission.

Following the administration of zingerone, there is an observed increase in the refractory period of pyramidal neurons in the ACC. This suggests that zingerone may play a role in modulating the activity of voltage-gated sodium channels (VGSCs). Notably, two constituents of



ginger extract, namely [6]-gingerol and [6]-shogaol, have also been shown to inhibit VGSCs and exhibit analgesic properties (Hitomi et al., 2017). The VGSC has consistently served as a focal point for the development of analgesic pharmaceuticals, particularly those targeting subtypes expressed within the peripheral nervous system, including NaV1.7, NaV1.8, and NaV1.9 (Goodwin and McMahon, 2021). A new selective inhibitor of NaV1.8, designated as VX-548, is presently in phase III clinical trials aimed at further assessing its safety and efficacy for the management of post-surgical pain (Kaye et al., 2024). Zingerone has the potential to function as a natural inhibitor of VGSC for the purpose of analgesia. However, additional research is required to substantiate this claim.

Emerging evidence indicates temporal specificity in Notch signaling activation during neuropathic pain progression. In rodent models of neuropathic pain, the Notch pathway shows transient activation in the ACC during the early phase (7 days post-surgery) (Duan et al., 2021). Paradoxically, recent pharmacological studies demonstrate that both zingerone and its structural analog acetyl zingerone upregulate Notch pathway components (NOTCH1 and MAML3) in dermal fibroblasts (Swindell et al., 2020), suggesting potential tissue-specific regulation of this pathway. The molecular mechanisms underlying ACC neuronal sensitization appear predominantly mediated through the MAPK signaling cascade (Lin et al., 2021; Xiao et al., 2021). This critical pathway exhibits three principal therapeutic targets - p38, ERK, and JNK kinases - whose pharmacological inhibition in both neuronal and glial populations produces significant antinociceptive

effects across various pain models (Deng et al., 2025; Li et al., 2023; Sanna et al., 2015). Of particular relevance, zingerone demonstrates multimodal regulation of MAPK signaling: mechanistic studies reveal its capacity to suppress NF- κ B activation through concurrent inhibition of ERK, p38, and JNK phosphorylation in inflammatory models (Kim et al., 2010). Further research is needed to elucidate the precise molecular interactions and downstream effects associated with these pathways.

5 Limitations of the study

Despite the significance of our findings, this study has several limitations that should be acknowledged. First, the selection of the ACC as the focus was based on previous studies, but other brain regions, such as the ventrolateral periaqueductal gray (vPAG) (Liu et al., 2020; Baptista-de-Souza et al., 2020) and prelimbic cortex (PrL) (Gao et al., 2023; Wang et al., 2015), may also play a role in the antinociceptive effects of zingerone. Second, the conclusions drawn in this study are based solely on experiments conducted in male C57BL/6 mice. Given potential sex differences in pain processing and drug responses (Ram et al., 2021), the antinociceptive effects of zingerone in female mice, as well as in other animal models and humans, require further investigation. Third, the study lacks a detailed exploration of the molecular mechanisms underlying zingerone's antinociceptive effects, as the analysis was limited to the cellular level. Elucidating the molecular mechanisms responsible for ACC neuronal hyperactivity could pave the way for the development of targeted therapies for chronic inflammatory pain.

6 Conclusion

The current investigation demonstrates that zingerone produces antinociceptive effects by inhibiting the activity of ACC neurons. The findings indicate that zingerone may represent a safe and promising therapeutic option for the treatment of migraines.

Data availability statement

The raw data supporting the conclusions of this article will be made available by the authors, without undue reservation.

Ethics statement

The animal study was approved by Laboratory Animal Ethics Committee of Bengbu Medical University. The study was conducted in accordance with the local legislation and institutional requirements.

Author contributions

YW: Data curation, Writing—original draft, Investigation, Methodology, Visualization. LD: Data curation, Investigation,

Methodology, Visualization, Writing—original draft. SH: Investigation, Methodology, Visualization, Writing—original draft. YY: Investigation, Methodology, Visualization, Writing—original draft. MZ: Investigation, Methodology, Writing—review and editing. BS: Investigation, Methodology, Writing—review and editing, Visualization. HN: Investigation, Writing—review and editing, Project administration. RG: Project administration, Writing—review and editing, Conceptualization. JL: Project administration, Writing—review and editing, Data curation, Writing—original draft. JY: Data curation, Project administration, Writing—original draft, Writing—review and editing, Conceptualization, Funding acquisition, Resources, Supervision.

Funding

The author(s) declare that financial support was received for the research, authorship, and/or publication of this article. The work was supported by the National Natural Science Foundation of China (Grant No. 82171446 and 81671288).

References

- Alotaibi, G., Khan, A., Ronan, P. J., Lutfy, K., and Rahman, S. (2023). Glial glutamate transporter modulation prevents development of complete Freund's adjuvant-induced hyperalgesia and allodynia in mice. *Brain Sci.* 13 (5), 807. doi:10.3390/brainsci13050807
- Badshah, I., Anwar, M., Murtaza, B., and Khan, M. I. (2024). Molecular mechanisms of morphine tolerance and dependence: novel insights and future perspectives. *Mol. Cell. Biochem.* 479 (6), 1457–1485. doi:10.1007/s11010-023-04810-3
- Baliki, M. N., and Apkarian, A. V. (2015). Nociception, pain, negative moods, and behavior selection. *Neuron* 87 (3), 474–491. doi:10.1016/j.neuron.2015.06.005
- Baptista-de-Souza, D., Tavares, L. R. R., Furuya-da-Cunha, E. M., Carneiro de Oliveira, P. E., Canto-de-Souza, L., Nunes-de-Souza, R. L., et al. (2020). Chronic fluoxetine impairs the effects of 5-HT(1A) and 5-HT(2C) receptors activation in the PAG and amygdala on antinociception induced by aversive situation in mice. *Front. Pharmacol.* 11, 260. doi:10.3389/fphar.2020.00260
- Barr, A. J., Campbell, T. M., Hopkinson, D., Kingsbury, S. R., Bowes, M. A., and Conaghan, P. G. (2015). A systematic review of the relationship between subchondral bone features, pain and structural pathology in peripheral joint osteoarthritis. *Arthritis Res. and Ther.* 17 (1), 228. doi:10.1186/s13075-015-0735-x
- Bliss, T. V., Collingridge, G. L., Kaang, B. K., and Zhuo, M. (2016). Synaptic plasticity in the anterior cingulate cortex in acute and chronic pain. *Nat. Rev. Neurosci.* 17 (8), 485–496. doi:10.1038/nrn.2016.68
- Bushnell, M. C., Ceko, M., and Low, L. A. (2013). Cognitive and emotional control of pain and its disruption in chronic pain. *Nat. Rev. Neurosci.* 14 (7), 502–511. doi:10.1038/nrn3516
- Choi, J. G., Kim, S. Y., Jeong, M., and Oh, M. S. (2018). Pharmacotherapeutic potential of ginger and its compounds in age-related neurological disorders. *Pharmacol. and Ther.* 182, 56–69. doi:10.1016/j.pharmthera.2017.08.010
- Chopra, D., Chadha, V. D., and Dhawan, D. K. (2023). Understanding the role of zingerone on biochemical and behavioral changes in rat brain inflicted with C6 glioma cells. *J. Biochem. Mol. Toxicol.* 37 (11), e23477. doi:10.1002/jbt.23477
- Deng, Y., Xuan, R., Qiu, Z., Xiang, P., Guo, Y., Xu, L., et al. (2025). Nuclear receptor 4A1 facilitates complete Freund's adjuvant-induced inflammatory pain in rats by promoting ferroptosis in spinal glial cells. *Brain, Behav. Immun.* 125, 92–109. doi:10.1016/j.bbi.2024.12.152
- Duan, H., Shen, F., Li, L., Tu, Z., Chen, P., Chen, P., et al. (2021). Activation of the Notch signaling pathway in the anterior cingulate cortex is involved in the pathological process of neuropathic pain. *Pain* 162 (1), 263–274. doi:10.1097/j.pain.0000000000002014
- Gao, F., Huang, J., Huang, G. B., You, Q. L., Yao, S., Zhao, S. T., et al. (2023). Elevated prelimbic cortex-to-basolateral amygdala circuit activity mediates comorbid anxiety-like behaviors associated with chronic pain. *J. Clin. Invest* 133 (9), e166356. doi:10.1172/jci166356
- Gong, K. R., Cao, F. L., He, Y., Gao, C. Y., Wang, D. D., Li, H., et al. (2010). Enhanced excitatory and reduced inhibitory synaptic transmission contribute to persistent pain-

Conflict of interest

The authors declare that the research was conducted in the absence of any commercial or financial relationships that could be construed as a potential conflict of interest.

Generative AI statement

The author(s) declare that no Generative AI was used in the creation of this manuscript.

Publisher's note

All claims expressed in this article are solely those of the authors and do not necessarily represent those of their affiliated organizations, or those of the publisher, the editors and the reviewers. Any product that may be evaluated in this article, or claim that may be made by its manufacturer, is not guaranteed or endorsed by the publisher.

induced neuronal hyper-responsiveness in anterior cingulate cortex. *Neuroscience* 171 (4), 1314–1325. doi:10.1016/j.neuroscience.2010.10.028

Goodwin, G., and McMahon, S. B. (2021). The physiological function of different voltage-gated sodium channels in pain. *Nat. Rev. Neurosci.* 22 (5), 263–274. doi:10.1038/s41583-021-00444-w

Gunaydin, L. A., Grosenick, L., Finkelstein, J. C., Kauvar, I. V., Fenno, L. E., Adhikari, A., et al. (2014). Natural neural projection dynamics underlying social behavior. *Cell* 157 (7), 1535–1551. doi:10.1016/j.cell.2014.05.017

Hitomi, S., Ono, K., Terawaki, K., Matsumoto, C., Mizuno, K., Yamaguchi, K., et al. (2017). [6]-gingerol and [6]-shogaol, active ingredients of the traditional Japanese medicine hangeshashinto, relief oral ulcerative mucositis-induced pain via action on Na(+) channels. *Pharmacol. Res.* 117, 288–302. doi:10.1016/j.phrs.2016.12.026

Kang, S. J., Kwak, C., Lee, J., Sim, S. E., Shim, J., Choi, T., et al. (2015). Bidirectional modulation of hyperalgesia via the specific control of excitatory and inhibitory neuronal activity in the ACC. *Mol. Brain* 8 (1), 81. doi:10.1186/s13041-015-0170-6

Kaye, A. D., Everett, E. S., Lehuquet, A. M., Mason, J. W., Maitski, R., Plessala, M. J., et al. (2024). Frontiers in acute pain management: emerging concepts in pain pathways and the role of VX-548 as a novel NaV1.8 inhibitor: a narrative review. *Curr. pain headache Rep.* 28 (11), 1135–1143. doi:10.1007/s11916-024-01295-7

Kim, J. N., Kim, H. J., Kim, I., Kim, Y. T., and Kim, B. J. (2018). The mechanism of action of zingerone in the pacemaker potentials of interstitial cells of cajal isolated from murine small intestine. *Cell. physiology Biochem. Int. J. Exp. Cell. physiology, Biochem. Pharmacol.* 46 (5), 2127–2137. doi:10.1159/000489453

Kim, M. K., Chung, S. W., Kim, D. H., Kim, J. M., Lee, E. K., Kim, J. Y., et al. (2010). Modulation of age-related NF-kappaB activation by dietary zingerone via MAPK pathway. *Exp. Gerontol.* 45 (6), 419–426. doi:10.1016/j.exger.2010.03.005

Kim, S., Cheon, C., Kim, B., and Kim, W. (2022a). The effect of ginger and its sub-components on pain. *Plants (Basel, Switz.)* 11 (17), 2296. doi:10.3390/plants11172296

Kim, S., Gang, J., Lee, J. H., Yang, H., Cheon, C., Ko, S. G., et al. (2022b). [6]-Shogaol attenuates oxaliplatin-induced allodynia through serotonergic receptors and GABA in the spinal cord in mice. *Pharm. (Basel, Switz.)* 15 (6), 726. doi:10.3390/ph15060726

Koga, K., Descalzi, G., Chen, T., Ko, H. G., Lu, J., Li, S., et al. (2015). Coexistence of two forms of LTP in ACC provides a synaptic mechanism for the interactions between anxiety and chronic pain. *Neuron* 85 (2), 377–389. doi:10.1016/j.neuron.2014.12.021

Koga, K., Li, X., Chen, T., Steenland, H. W., Descalzi, G., and Zhuo, M. (2010). *In vivo* whole-cell patch-clamp recording of sensory synaptic responses of cingulate pyramidal neurons to noxious mechanical stimuli in adult mice. *Mol. pain* 6, 62. doi:10.1186/1744-8069-6-62

Lai, M. C., Wu, S. N., and Huang, C. W. (2022). Zingerone modulates neuronal voltage-gated Na(+) and L-type Ca(2+) currents. *Int. J. Mol. Sci.* 23 (6), 3123. doi:10.3390/ijms23063123

Lane, D. A., Tortorici, V., and Morgan, M. M. (2004). Behavioral and electrophysiological evidence for tolerance to continuous morphine administration

- into the ventrolateral periaqueductal gray. *Neuroscience* 125 (1), 63–69. doi:10.1016/j.neuroscience.2004.01.023
- Legaria, A. A., Matikainen-Ankney, B. A., Yang, B., Ahanonu, B., Licholai, J. A., Parker, J. G., et al. (2022). Fiber photometry in striatum reflects primarily nonsomatic changes in calcium. *Nat. Neurosci.* 25 (9), 1124–1128. doi:10.1038/s41593-022-01152-z
- Li, X., Shi, H., Zhang, D., Jing, B., Chen, Z., Zheng, Y., et al. (2023). Paeonol alleviates neuropathic pain by modulating microglial M1 and M2 polarization via the RhoA/p38MAPK signaling pathway. *CNS Neurosci. and Ther.* 29 (9), 2666–2679. doi:10.1111/cns.14211
- Lin, F.-Y., Huang, K.-F., Chen, J.-C., Lai, M.-F., Ma, K.-H., and Yeh, C.-C. (2021). The clinical application of pulsed radiofrequency induces inflammatory pain via MAPKs activation: a novel hint for pulsed radiofrequency treatment. *Int. J. Mol. Sci.* 22 (21), 11865. doi:10.3390/ijms222111865
- Little, J. W., Cuzzocrea, S., Bryant, L., Esposito, E., Doyle, T., Rausaria, S., et al. (2013). Spinal mitochondrial-derived peroxynitrite enhances neuroimmune activation during morphine hyperalgesia and antinociceptive tolerance. *Pain* 154 (7), 978–986. doi:10.1016/j.pain.2013.02.018
- Liu, C., Zhou, X., Zhu, Q., Fu, B., Cao, S., Zhang, Y., et al. (2020). Dopamine neurons in the ventral periaqueductal gray modulate isoflurane anesthesia in rats. *CNS Neurosci. and Ther.* 26 (11), 1121–1133. doi:10.1111/cns.13447
- Mahmoodally, M. F., Aumeeruddy, M. Z., Rengasamy, K. R. R., Roshan, S., Hamad, S., Pandohee, J., et al. (2021). Ginger and its active compounds in cancer therapy: from folk uses to nano-therapeutic applications. *Seminars cancer Biol.* 69, 140–149. doi:10.1016/j.semcancer.2019.08.009
- Mani, V., Arivalagan, S., Islam Siddique, A., and Namasivayam, N. (2017). Antihyperlipidemic and antiapoptotic potential of zingerone on alcohol induced hepatotoxicity in experimental rats. *Chemico-Biological Interact.* 272, 197–206. doi:10.1016/j.cbi.2017.04.019
- Mao, Q.-Q., Xu, X.-Y., Cao, S.-Y., Gan, R.-Y., Corke, H., Beta, T., et al. (2019). Bioactive compounds and bioactivities of ginger (*Zingiber officinale* Roscoe). *Foods* 8 (6), 185. doi:10.3390/foods8060185
- Mehrzi, S., Khalili, H., Fatemi, I., Malayeri, A., Siahpoosh, A., and Goudarzi, M. (2021). Zingerone mitigates carrageenan-induced inflammation through antioxidant and anti-inflammatory activities. *Inflammation* 44 (1), 186–193. doi:10.1007/s10753-020-01320-y
- Molavinia, S., Nikraves, M., Pashmforoosh, M., Vardanjani, H. R., and Khodayar, M. J. (2024). Zingerone alleviates morphine tolerance and dependence in mice by reducing oxidative stress-mediated NLRP3 inflammasome activation. *Neurochem. Res.* 49 (2), 415–426. doi:10.1007/s11064-023-04043-2
- Özdemir, F., Akçay, G., Özkinali, S., and Çelik, Ç. (2023). [6]-Shogaol and [6]-Gingerol active ingredients may improve neuropathic pain by suppressing cytokine levels in an experimental model. *Türk J. Med. Sci.* 53 (6), 1593–1604. doi:10.55730/1300-0144.5728
- Pan, T. T., Gao, W., Song, Z. H., Long, D. D., Cao, P., Hu, R., et al. (2022). Glutamatergic neurons and myeloid cells in the anterior cingulate cortex mediate secondary hyperalgesia in chronic joint inflammatory pain. *Brain, Behav. Immun.* 101, 62–77. doi:10.1016/j.bbi.2021.12.021
- Patnaik, S. S., Lagana, A. S., Vitale, S. G., Buttice, S., Noventa, M., Gizzo, S., et al. (2017). Etiology, pathophysiology and biomarkers of interstitial cystitis/painful bladder syndrome. *Archives Gynecol. obstetrics* 295 (6), 1341–1359. doi:10.1007/s00404-017-4364-2
- Rainville, P., Duncan, G. H., Price, D. D., Carrier, B., and Bushnell, M. C. (1997). Pain affect encoded in human anterior cingulate but not somatosensory cortex. *Sci. (New York, NY)* 277 (5328), 968–971. doi:10.1126/science.277.5328.968
- Raja, S. N., Carr, D. B., Cohen, M., Finnerup, N. B., Flor, H., Gibson, S., et al. (2020). The revised International Association for the Study of Pain definition of pain: concepts, challenges, and compromises. *Pain* 161 (9), 1976–1982. doi:10.1097/j.pain.0000000000001939
- Ram, A., Edwards, T., McCarty, A., Afrose, L., McDermott, M. V., and Bobeck, E. N. (2021). GPR171 agonist reduces chronic neuropathic and inflammatory pain in male, but not female mice. *Front. pain Res. (Lausanne, Switz.)* 2, 695396. doi:10.3389/fpain.2021.695396
- Rashid, S., Wali, A. F., Rashid, S. M., Alsaffar, R. M., Ahmad, A., Jan, B. L., et al. (2021). Zingerone targets status epilepticus by blocking hippocampal neurodegeneration via regulation of redox imbalance, inflammation and apoptosis. *Pharm. (Basel, Switz.)* 14 (2), 146. doi:10.3390/ph14020146
- Sanna, M. D., Stark, H., Lucarini, L., Ghelardini, C., Masini, E., and Galeotti, N. (2015). Histamine H4 receptor activation alleviates neuropathic pain through differential regulation of ERK, JNK, and P38 MAPK phosphorylation. *Pain* 156 (12), 2492–2504. doi:10.1097/j.pain.0000000000000319
- Santos, J. M., Deshmukh, H., Elmassry, M. M., Yakhnitsa, V., Ji, G., Kiritoshi, T., et al. (2024). Beneficial effects of ginger root extract on pain behaviors, inflammation, and mitochondrial function in the colon and different brain regions of male and female neuropathic rats: a gut-brain Axis study. *Nutrients* 16 (20), 3563. doi:10.3390/nu16203563
- Shao, M., Yu, H., Santhakumar, V., and Yu, J. (2023). Antiepileptogenic and neuroprotective effect of mefloquine after experimental status epilepticus. *Epilepsy Res.* 198, 107257. doi:10.1016/j.eplepsyres.2023.107257
- Shyu, B. C., Chen, W. F., and Shih, H. C. (2008). Electrically and mechanically evoked nociceptive neuronal responses in the rat anterior cingulate cortex. *Acta Neurochir. Suppl.* 101, 23–25. doi:10.1007/978-3-211-78205-7_4
- Swindell, W. R., Bojanowski, K., and Chaudhuri, R. K. (2020). A zingerone analog, acetyl zingerone, bolsters matrix synthesis, inhibits matrix metalloproteinases, and represses IL-17a target gene expression. *J. Investigative Dermatology* 140 (3), 602–614.e15. doi:10.1016/j.jid.2019.07.715
- Wang, D., Pan, X., Zhou, Y., Wu, Z., Ren, K., Liu, H., et al. (2023). Lateral septum-lateral hypothalamus circuit dysfunction in comorbid pain and anxiety. *Mol. Psychiatry* 28 (3), 1090–1100. doi:10.1038/s41380-022-01922-y
- Wang, G. Q., Cen, C., Li, C., Cao, S., Wang, N., Zhou, Z., et al. (2015). Deactivation of excitatory neurons in the prefrontal cortex via Cdk5 promotes pain sensation and anxiety. *Nat. Commun.* 6, 7660. doi:10.1038/ncomms8660
- Xiao, C., Liu, D., Du, J., Guo, Y., Deng, Y., Hei, Z., et al. (2021). Early molecular alterations in anterior cingulate cortex and hippocampus in a rodent model of neuropathic pain. *Brain Res. Bull.* 166, 82–91. doi:10.1016/j.brainresbull.2020.11.020
- Yang, Z., Tan, Q., Cheng, D., Zhang, L., Zhang, J., Gu, E. W., et al. (2018). The changes of intrinsic excitability of pyramidal neurons in anterior cingulate cortex in neuropathic pain. *Front. Cell. Neurosci.* 12, 436. doi:10.3389/fncel.2018.00436
- Yue, H. Y., Jiang, C. Y., Fujita, T., and Kumamoto, E. (2013). Zingerone enhances glutamatergic spontaneous excitatory transmission by activating TRPA1 but not TRPV1 channels in the adult rat substantia gelatinosa. *J. neurophysiology* 110 (3), 658–671. doi:10.1152/jn.00754.2012
- Zhang, T., Yu, F., Xu, H., Chen, M., Chen, X., Guo, L., et al. (2021). Dysregulation of REV-ERBa impairs GABAergic function and promotes epileptic seizures in preclinical models. *Nat. Commun.* 12 (1), 1216. doi:10.1038/s41467-021-21477-w
- Zhao, M. G., Ko, S. W., Wu, L. J., Toyoda, H., Xu, H., Quan, J., et al. (2006). Enhanced presynaptic neurotransmitter release in the anterior cingulate cortex of mice with chronic pain. *J. Neurosci. official J. Soc. Neurosci.* 26 (35), 8923–8930. doi:10.1523/jneurosci.2103-06.2006
- Zheng, J., Li, T., Qi, S., Qin, B., Yu, J., and Chen, G. (2022). Neuroregenerative gene therapy to treat temporal lobe epilepsy in a rat model. *Prog. Neurobiol.* 208, 102198. doi:10.1016/j.pneurobio.2021.102198
- Zhou, Z., Qiu, N., Ou, Y., Wei, Q., Tang, W., Zheng, M., et al. (2021). N-Demethylsinomenine, an active metabolite of sinomenine, attenuates chronic neuropathic and inflammatory pain in mice. *Sci. Rep.* 11 (1), 9300. doi:10.1038/s41598-021-88521-z
- Zhuo, M. (2014). Long-term potentiation in the anterior cingulate cortex and chronic pain. *Philosophical Trans. R. Soc. Lond. Ser. B, Biol. Sci.* 369 (1633), 20130146. doi:10.1098/rstb.2013.0146



OPEN ACCESS

EDITED BY

Jian Hao,
The Second Affiliated Hospital of Guangzhou
Medical University, China

REVIEWED BY

Zheng Yuan,
China Academy of Chinese Medical Sciences,
China
Zhongqi Yang,
University of California, Irvine, United States

*CORRESPONDENCE

Sajad Fakhri,
✉ pharmacy.sajad@yahoo.com,
✉ sajad.fakhri@kums.ac.ir
Javier Echeverría,
✉ javier.echeverriam@usach.cl

[†]These authors have contributed equally to this work and share first authorship

RECEIVED 17 December 2024

ACCEPTED 05 March 2025

PUBLISHED 24 March 2025

CITATION

Kooshki L, Fakhri S, Abbaszadeh F, Kiani A, Farzaei MH, Mohammadi-Noori E and Echeverría J (2025) Pelargonidin improves functional recovery and attenuates neuropathic pain following spinal cord injury in rats: relevance to its neuroprotective, antioxidant, and anti-inflammatory effects. *Front. Pharmacol.* 16:1547187. doi: 10.3389/fphar.2025.1547187

COPYRIGHT

© 2025 Kooshki, Fakhri, Abbaszadeh, Kiani, Farzaei, Mohammadi-Noori and Echeverría. This is an open-access article distributed under the terms of the [Creative Commons Attribution License \(CC BY\)](https://creativecommons.org/licenses/by/4.0/). The use, distribution or reproduction in other forums is permitted, provided the original author(s) and the copyright owner(s) are credited and that the original publication in this journal is cited, in accordance with accepted academic practice. No use, distribution or reproduction is permitted which does not comply with these terms.

Pelargonidin improves functional recovery and attenuates neuropathic pain following spinal cord injury in rats: relevance to its neuroprotective, antioxidant, and anti-inflammatory effects

Leila Kooshki^{1†}, Sajad Fakhri^{2*†}, Fatemeh Abbaszadeh³, Amir Kiani^{2,4}, Mohammad Hosein Farzaei², Ehsan Mohammadi-Noori² and Javier Echeverría^{5*}

¹Student Research Committee, Kermanshah University of Medical Sciences, Kermanshah, Iran, ²Pharmaceutical Sciences Research Center, Health Institute, Kermanshah University of Medical Sciences, Kermanshah, Iran, ³Neurobiology Research Center, Institute of Neuroscience and Cognition, Shahid Beheshti University of Medical Sciences, Tehran, Iran, ⁴Regenerative Medicine Research Center, Health Technology Institute, Kermanshah University of Medical Sciences, Kermanshah, Iran, ⁵Departamento de Ciencias del Ambiente, Facultad de Química y Biología, Universidad de Santiago de Chile, Santiago, Chile

Background: Spinal cord injury (SCI) significantly impairs individuals' sensorimotor functions, hindering daily activities. Current therapeutic options often demonstrate limited efficacy and lead to undesirable side effects. Emerging research highlights the potential of anthocyanins, especially pelargonidin, which possess neuroprotective, anti-inflammatory, and antioxidant properties beneficial for neurological conditions.

Purpose: This study sought to explore the impact of intrathecal administration of pelargonidin on the recovery of sensory-motor functions and associated disorders in a rat model of SCI through neuroprotective effects and regulating inflammatory/oxidative stress mediators.

Materials and methods: In total, 35 male Wistar rats were divided into five groups: sham, SCI, and three treatment groups receiving different intrathecal concentrations of pelargonidin (1, 2, and 4 mM) once on day 0 after surgery/injury. Weight changes were assessed and behavioral analyses were done, including hot plate tests, acetone drop tests, von Frey tests, inclined plane tests, as well as Basso, Beattie, and Bresnahan (BBB) scores, weekly up to day 28 post-injury. On day 28, serum levels of nitrite, catalase, and glutathione as well as matrix metalloproteinase (MMP) assays and histological evaluations were done.

Results and discussion: Pelargonidin significantly attenuated neuropathic pain, improved motor performance, and reduced weight loss in rats with SCI. Biochemical assays demonstrated increased serum catalase/glutathione level, and MMP2 activity, while decreased serum nitrite level and MMP9 activity. Histological analyses showed an enhancement in the number of motor neurons in the ventral horn of the spinal cord after treatment with pelargonidin, highlighting its neuroprotective and neurogenic effects.

Conclusion: Pelargonidin makes substantial therapeutic benefits following SCI by accelerating sensorimotor recovery. This effect is likely due to its strong antioxidant, anti-inflammatory, and neuroprotective properties.

KEYWORDS

spinal cord injury, pelargonidin, motor activity, neuropathic pain, neuroinflammation, neuroprotection, oxidative stress

1 Introduction

Spinal cord injury (SCI) is a multifaceted medical condition that profoundly affects individuals' healthcare systems. This condition results from spinal cord damage and can be triggered by both traumatic and non-traumatic events (Diop and Epstein, 2024). The World Health Organization (WHO) reports that the global incidence of SCI varies between 8 and 246 cases per million people each year (Kumar et al., 2018). Beyond the immediate physical consequences, SCI is associated with various secondary complications encompassing a cascade of biological events such as inflammation, oxidative stress, and neuronal apoptosis. These secondary processes can exacerbate initial damages, leading to further loss of function and complicating recovery efforts (Anjum et al., 2020).

Currently, available treatments for SCI are limited, primarily focusing on symptom management and the prevention of secondary complications. Surgical interventions can stabilize the spine or decompress neural structures, but they do not guarantee functional recovery. Pharmacological approaches, such as analgesics and anti-inflammatory medications, help manage pain but often come with adverse effects that complicate the clinical picture (Alvi et al., 2024). Notably, there is no Food and Drug Administration (FDA)-approved medication against SCI. While some studies suggested that high doses of methylprednisolone may offer neuroprotective benefits, many investigations indicated that this treatment may be ineffective in reducing neurological impairment and could even worsen spinal tissue injury, leading to severe side effects (Evaniew et al., 2015; Jeong et al., 2021). Consequently, there is a pressing need for innovative therapeutic strategies to enhance recovery and improve functional outcomes for individuals with SCI.

In recent years, there has been increasing interest in the potential of natural compounds, particularly those derived from plants, to provide neuroprotective benefits and improve recovery after SCI (Coyoy-Salgado et al., 2019; Abbaszadeh et al., 2020). Among these phytochemicals, anthocyanins are water-soluble pigments found in a variety of fruits, vegetables, and plants that have garnered attention for their therapeutic properties (Mohammadi Pour et al., 2019; S; Jaiswal et al., 2020; Chen et al., 2024). As a notable anthocyanin, pelargonidin is commonly found in strawberries, raspberries, and other red fruits. Research suggests that pelargonidin exhibits potent anti-inflammatory, antioxidant, and neuroprotective effects (Roghani et al., 2010; Sohanaki et al., 2016; Duarte et al., 2018), making it a promising candidate for addressing the oxidative stress and inflammation associated with SCI.

Oxidative stress significantly contributes to SCI by increasing reactive oxygen species (ROS) production, which worsens neuronal damage and triggers secondary injury mechanisms like apoptosis (programmed cell death) (Yu et al., 2023). As another dysregulated cross-talk pathway to oxidative stress and apoptosis, inflammation also plays a critical role in SCI complications leading to further

complications (Chan, 2008). Therefore, the use of antioxidant/anti-inflammatory pelargonidin could provide a dual benefit in promoting sensory-motor recovery and protection of neural tissues.

This study sought to investigate the effects of pelargonidin on motor function recovery and neuropathic pain in a rat model of SCI through antioxidant, anti-inflammatory, and neuroprotective effects.

2 Material and methods

2.1 Animals

In total, 35 adult male Wistar rats, weighing 230–250 g, were kept in a light/dark (12-h) cycle. This study was conducted following the guidelines of the animal care committee at Kermanshah University of Medical Sciences (IR.KUMS.AEC.1401.017). The rats were assigned to five groups at random: Sham (laminectomy with no injury then receiving 10 μ L intrathecal distilled water), SCI (laminectomy + injury, then receiving 10 μ L intrathecal distilled water), and three treatment groups receiving three doses (1, 2, and 4 mM) of pelargonidin (purchased from Sigma-Aldrich). Thirty minutes following the compression injury, the SCI group received an intrathecal injection of distilled water as a vehicle for sham and SCI groups, while the three pelargonidin groups were given 10 μ L of pelargonidin at concentrations of 1, 2, and 4 mM.

2.1.1 Spinal cord injury

The rats were given a combination of ketamine/xylazine (80/10 mg/kg, intraperitoneal, purchased from Alfasan, Netherlands) to achieve deep anesthesia. A laminectomy was then carried out at the thoracic 8-9 (T8-T9) level a Micro Rongeur (Fine Science Tools, United States). Following the surgery, an aneurysm clamp made a force of 90 g (Aesculap, Tuttlingen, Germany) for 1 minute to induce severe SCI in the SCI and pelargonidin groups. After the surgical procedure, the tissue and skin were sutured. Daily administrations of cefazolin (40 mg/kg) and 2 mL of normal saline were provided, along with manual bladder massage, until normal bladder function was regained.

2.1.2 Intrathecal drug injection

For the intrathecal injection, a 25-G needle connected to a Hamilton syringe was utilized. The needle was inserted at a 45° angle into the subarachnoid space between the lumbar 6 (L6) and L5 vertebrae. The confirmation of needle placement in the subarachnoid space was based on the immediate lateral tail movement observed upon penetrating the ligamentum flavum. Once the needle was correctly positioned, a dosage of either pelargonidin or distilled water (10 μ L) was gradually injected over 10 s. To prevent the backflow of medication, the syringe was left in place for an additional 10 s after the injection (Mestre et al., 1994).

2.2 Behavioral test

The animals underwent behavioral testing on day 0 and on days 7, 14, 21, and 28 post-surgeries. All behavioral assessments were conducted in a blinded manner.

2.2.1 Assessment of motor performance

The Basso, Beattie, and Bresnahan (BBB) locomotor rating scale was employed to evaluate locomotor recovery in rats following SCI. The scale ranges from 0 to 21, with 0 indicating no hindlimb movement and 21 representing normal, coordinated locomotion. The final score was calculated by averaging the scores of both hind paws (Abbaszadeh et al., 2018; Fakhri et al., 2022c).

In addition, the ability of rats to bear their body weight and maintain a standing position on an inclined surface serves as a critical metric for evaluating their recovery post-SCI. For this assessment, a wooden plane measuring 60 × 40 cm was employed, which could be inclined at angles from 0° (horizontal) to 60°. The maximum angle at which the rats were able to sustain their position for 5 s was recorded (Fakhri et al., 2018; Zhang et al., 2023).

2.2.2 Assessment of neuropathic pain; cold allodynia, heat hyperalgesia, and mechanical pain

Acetone was utilized to assess pain sensitivity and behavioral responses to cold stimuli, called cold allodynia. During the test, 0.1 mL of acetone was applied from a distance of 2 cm to assess the rats' reactions, which were categorized and scored based on their hind paw withdrawal behavior. (0) no paw withdrawal, (1) the rat exhibited a startled reaction but did not withdraw its paw, (2) the rat slightly withdrew its paw in response to the cold sensation, (3) the rat withdrew its paw for an extended period, indicating discomfort, (4) the rat licked or flinched its paw, demonstrating a heightened sensitivity to the cold stimulus (Allchorne et al., 2005).

In the hot plate test, rats were positioned on a heated surface with a temperature of 50 ± 2°C. The duration until they displayed signs of discomfort, such as licking or biting their hind limbs, was measured and documented as the latency of paw withdrawal (PWL) (Xu et al., 2024).

Mechanical allodynia was evaluated using the von Frey test, which involved applying filaments exerting forces of 10, 15, 26, 60, and 100 g to the plantar surface of the rat's paw. The application of each filament was repeated five times, with a brief 5-s interval separating each application. A positive response was defined as any nocifensive behavior, including hindpaw withdrawal, flinching, licking, or biting. To determine the allodynia threshold, the criterion required was a minimum of three positive responses out of the five applications (Alimoradian et al., 2024).

2.2.3 Weight change measurement

The weights of the rats were recorded every week. Weight changes for each group were calculated as follows:

$$\text{Weight difference} = (\text{weight on days 7, 14, 21, and 28 post-surgery} - \text{weight on day 0})$$

2.3 Zymography

On day 28 of the study, a gelatin zymography assay was performed to analyze the activity of MMP2 and MMP9. This

technique utilized 7.5% SDS-PAGE gels that were copolymerized with 0.1% gelatin. Samples were collected from the aorta of rats, loaded onto the gels, and subjected to electrophoresis at a constant voltage of 150 V, which facilitates the separation of proteins based on size. The gels were washed with a buffer containing Triton X-100 (purchased from ACROS) and Tris-HCl (Tris Base purchased from Merck Company, Germany) to remove the SDS (purchased from Merck Company, Germany), allowing the gelatin to retain its structure for enzyme activity. The gels were then incubated for 18 h at 37°C in a buffer containing 10 mM CaCl₂ (purchased from Merck Co, Germany), 0.15 M NaCl, and 0.02% NaN₃ in 50 mM Tris-HCl (pH 7.5), which provided the necessary conditions for the MMPs to degrade the gelatin. At this stage, the gels were stained using Coomassie Blue (Sigma-Aldrich), a dye that binds to proteins, creating a blue background. The areas where enzymatic activity occurred, where the MMPs had degraded the gelatin, appeared as clear bands against this blue background. These clear bands indicate the presence and activity of MMP2 and MMP9. Finally, ImageJ software was used to quantify band intensity (Bagheri Bavandpouri et al., 2024).

2.4 Biochemical test

2.4.1 Catalase and glutathione activity assay

Catalase activity was determined using the Aebi method (Aebi, 1984). 20 µL of rat serum was incubated with 100 µL of a 65 mM hydrogen peroxide solution at 25°C for 4 min. The reaction was stopped with 100 µL of ammonium molybdate and measured at 405 nm using an ELISA reader.

Glutathione activity was assessed via Ellman's method (Eyer and Podhradský, 1986). In this procedure, 20 µL of rat serum was added to the wells, followed by the addition of 50 µL of phosphate buffer at pH 7. Then, 40 µL of dithiobisnitrobenzoic acid (DTNB) was included, and the plate was incubated at 37°C for 10 min. The absorbance was subsequently read at 412 nm using an ELISA reader. Finally, the percentage difference in absorbance for both catalase and glutathione was calculated between the other groups and sham groups.

2.4.2 Nitrite assay

Nitrite levels were assessed using the Griess reaction assay. To prepare the serum samples, protein removal was achieved by adding zinc sulfate, followed by centrifugation of the samples obtained from rats on day 28. The supernatant was then mixed with vanadium chloride solution at a 1:1 ratio. A Griess solution containing 2% sulfanilamide and 0.1% diamide dihydrochloride was added, and the samples were incubated at 37°C for 30 min. The resulting color was measured at 540 nm using a spectrophotometer, and nitrite concentration in the samples was determined by comparing the absorbance to that of a standard reference (Sun et al., 2003).

2.5 Histological analysis

On day 28, the animals were perfused with normal saline and 4% paraformaldehyde. Subsequently, a 1-cm segment of spinal cord tissue

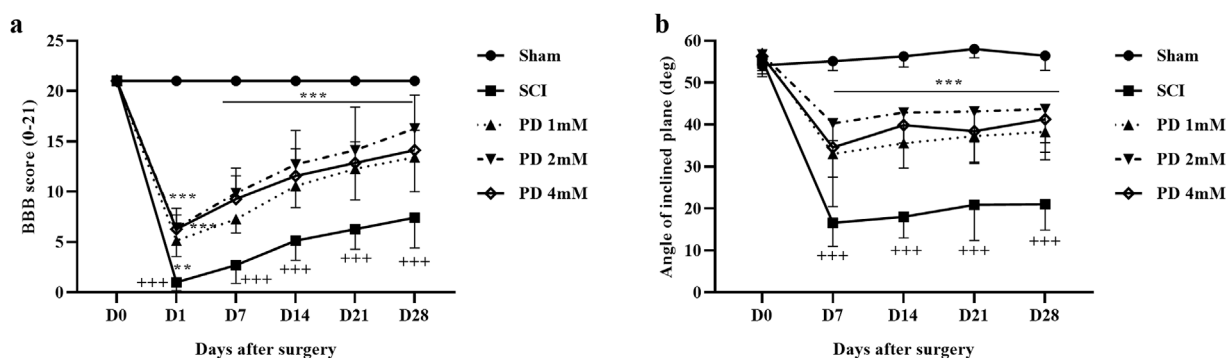


FIGURE 1

The impact of pelargonidin on motor activity after SCI. BBB score (a), and inclined-plane (b) test. Data are expressed as mean \pm SD ($n = 7$). The statistical analysis was done using repeated measures of two-way ANOVA. $+++p < 0.001$ vs. sham group; $**p < 0.01$, $***p < 0.001$ vs. SCI group. SCI: spinal cord injury; PD: pelargonidin.

centered on the injury was excised. The spinal cord tissue was embedded in paraffin, sliced into 7- μ m sections, and stained with hematoxylin and eosin (H&E). For lesion size, 4X magnification was used to calculate the ratio of damaged tissue to the total cross-sectional area from images taken across all study groups, expressing this ratio as a percentage relative to the sham group. This method enabled a detailed comparison of tissue damage among the experimental groups. For neuron counting, we captured images from the ventral horn region of the spinal cord tissue sections from each sample at 40X magnification. Using ImageJ software, we determined the average number of neurons in each section of the ventral horn across different groups and compared these numbers (Li et al., 2014).

2.6 Statistical analysis

GraphPad Prism, Version 8.0, was utilized for data analysis. The results are shown as mean \pm SD. To compare the groups, a repeated measures one-way or two-way analysis of variance ANOVA was conducted, followed by Tukey's or Bonferroni's *post hoc* tests as appropriate. A significance threshold of $p < 0.05$ was established for all statistical evaluations.

3 Results

3.1 Behavioral result

3.1.1 Pelargonidin significantly enhanced motor function in rats with SCI

We evaluated the motor performance of rats following SCI using the BBB scale and the inclined plane test. The sham group, which underwent a laminectomy without injury, consistently scored 21 on the BBB scale, indicating no functional deficits. In contrast, SCI rats exhibited significantly lower scores of 2 on the first day post-injury, which remained substantially below the sham group's average score of approximately 8 until day 28 ($p < 0.001$). Importantly, treatment with pelargonidin at various doses led to significant improvements

in motor function starting from day 1, compared to the SCI group ($p < 0.001$, Figure 1a).

In terms of balance, the sham group was able to maintain their balance on an incline of up to 55°. However, the SCI group exhibited a significant decrease in their average angle of balance, dropping by about 25° ($p < 0.001$) compared to the sham group. Conversely, rats treated with pelargonidin showed considerable enhancements in balance from the first week, achieving angles between 30° and 40° ($p < 0.001$, Figure 1b).

3.1.2 Pelargonidin significantly alleviated neuropathic pain in rats with SCI

Throughout the 4 weeks, the sham group maintained typical sensitivity to cold pain stimuli, whereas the SCI group demonstrated marked hypersensitivity ($p < 0.001$). Treatment with various doses of pelargonidin, especially at 2 mM, resulted in a notable improvement in response to cold stimulation from the first week ($p < 0.05$, Figure 2a).

In the current study and during the hot plate test, rats in the sham group displayed a stable paw-licking latency across all testing days and no significant changes in pain perception or response. When rats experienced SCI, there was a marked decrease in their response threshold to thermal stimuli starting from day 7 of the study, meaning they were more sensitive to the thermal stimulus ($p < 0.001$). In the following, treatment with different doses of pelargonidin led to a significant decrease in sensitivity to thermal stimuli as evidenced by an increased paw-licking latency ($p < 0.001$, Figure 2b).

Also, the sham group demonstrated consistent responses to mechanical stimuli throughout the 28-day follow-up period, and they did not exhibit any significant changes in pain perception or withdrawal behavior. In contrast, rats in SCI groups showed a significant increase in sensitivity to mechanical stimuli, as indicated by a decrease in the paw withdrawal threshold ($p < 0.001$). Notably, administration of pelargonidin, particularly at a dose of 2 mM, effectively alleviated the sensitivity of the response to the stimulus and symptoms of mechanical allodynia beginning from day 7 post-treatment ($p < 0.05$, Figure 2c).

3.1.3 Pelargonidin effectively regulated weight changes in rats with SCI

Rats in the sham group displayed a normal weight gain pattern, indicating their physiological condition remained unchanged. In contrast, the SCI group experienced notable

weight loss, underscoring the considerable effects of the injury on their overall health and metabolic function. Notably, the administration of different doses of pelargonidin resulted in a significant enhancement in weight gain for the injured animals ($p < 0.001$, Figure 3).

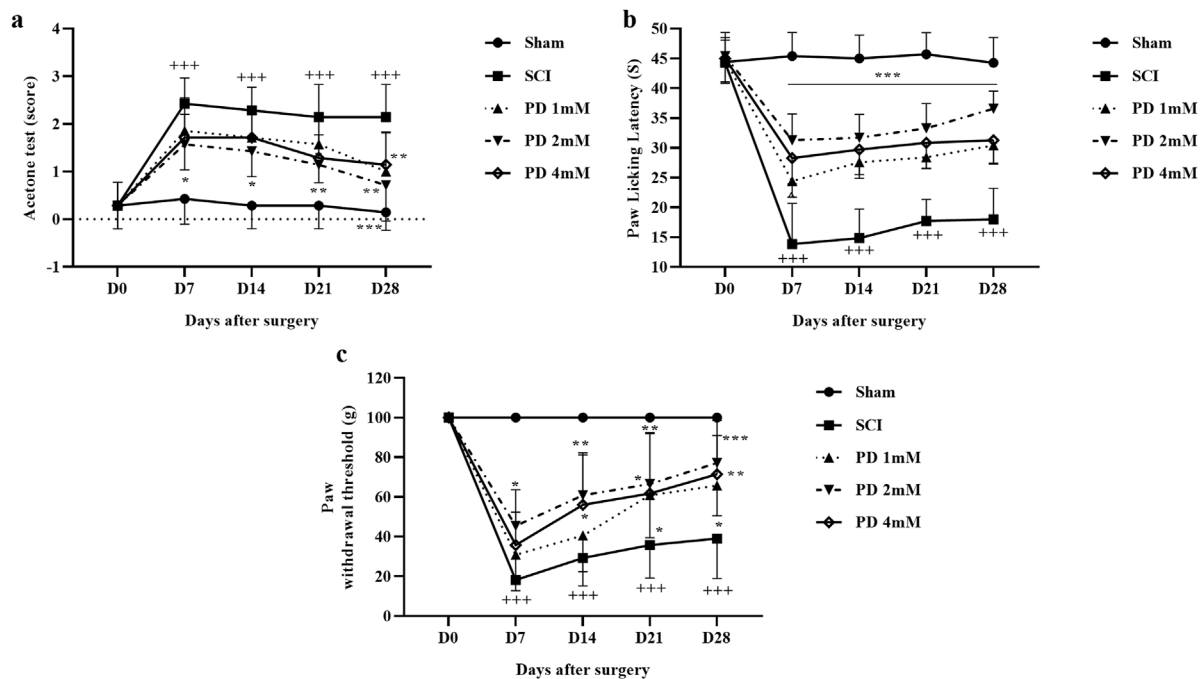


FIGURE 2

The impact of pelargonidin on neuropathic pain after SCI. Acetone (a), hot plate (b), and von Frey (c) test. Data are expressed as mean \pm SD ($n = 7$).

The statistical analysis was done using repeated measures of two-way ANOVA. $+++p < 0.001$ vs. sham group; $*p < 0.05$, $**p < 0.01$, $***p < 0.001$ vs. SCI group. SCI: spinal cord injury; PD: pelargonidin.

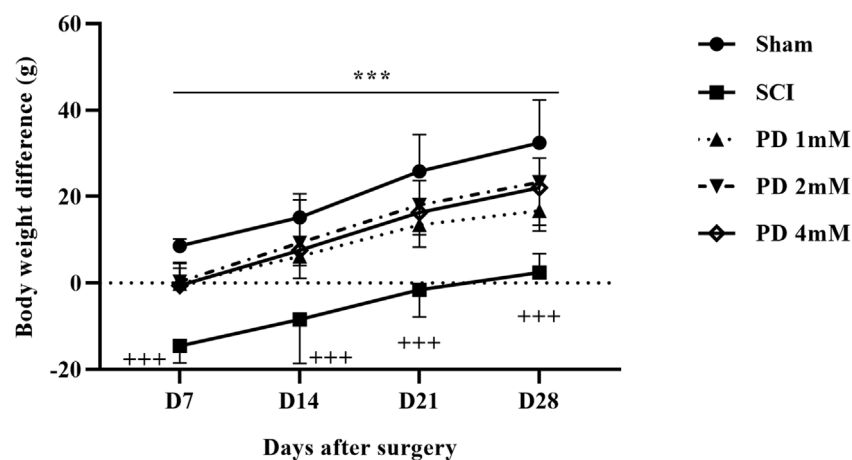


FIGURE 3

Effects of pelargonidin on body weight changes after SCI. Data are expressed as mean \pm SD ($n = 7$). The statistical analysis was done using repeated measures of two-way ANOVA. $+++p < 0.001$ vs. sham group; $***p < 0.05$ vs. SCI group. SCI: spinal cord injury; PD: pelargonidin.

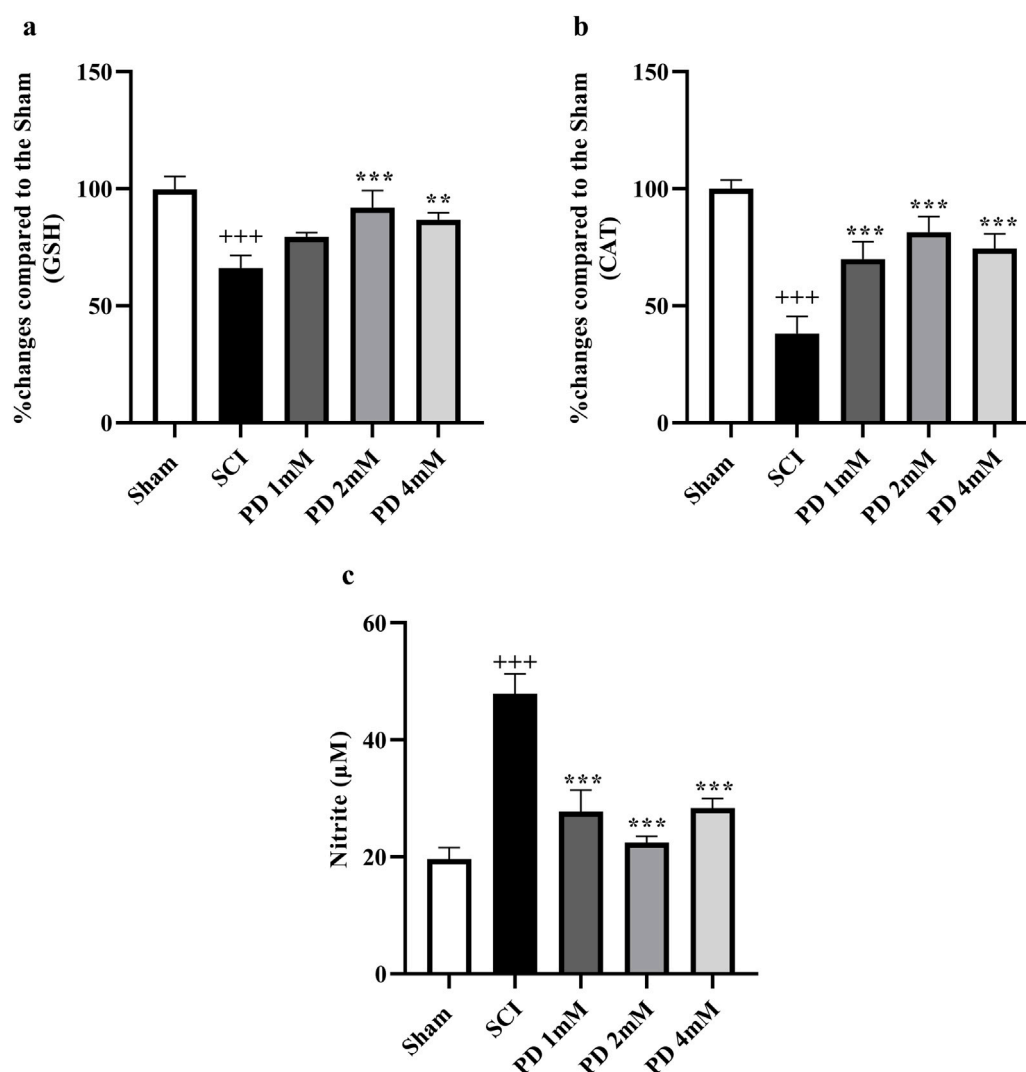


FIGURE 4
Effect of pelargonidin on changes of oxidative stress after SCI. Percentage of activity changes of glutathione (a), catalase (b), and level of nitrite (c). Data are expressed as mean \pm SD. The statistical analysis was done using repeated measures of one-way ANOVA. *** $p < 0.001$ vs. sham group; ** $p < 0.001$, *** $p < 0.001$ vs. SCI group. SCI: spinal cord injury; PD: pelargonidin.

3.2 Pelargonidin modulated oxidative stress markers in rats with SCI

Our study findings revealed that compared to the sham group, SCI significantly reduced serum levels of glutathione (Figure 4a) and catalase (Figure 4b), key antioxidants, indicating increased oxidative stress ($p < 0.001$). Treatment with pelargonidin effectively restored these antioxidant levels ($p < 0.05$). In addition to the changes in antioxidant levels, SCI was associated with an increase in serum nitrite levels (Figure 4c), which can be indicative of heightened nitrite production and further oxidative stress. However, treatment with pelargonidin also resulted in a significant reduction of these elevated nitrite levels ($p < 0.001$).

3.3 Pelargonidin effectively modulated MMP levels in rats with SCI

After SCI, the analysis showed a significant reduction in MMP2 levels ($p < 0.001$, Figure 5a), indicating a potential loss of its protective anti-inflammatory function. Concurrently, MMP9 levels were significantly elevated ($p < 0.001$, Figure 5b), which could suggest a heightened inflammatory response and contribute to secondary injury processes. However, treatment with varying doses of pelargonidin, particularly at a concentration of 2 mM, resulted in a remarkable reversal of these trends. Pelargonidin administration not only restored MMP2 levels ($p < 0.05$) to more favorable values, enhancing its anti-inflammatory effect but also significantly lowered MMP9 levels ($p < 0.05$).

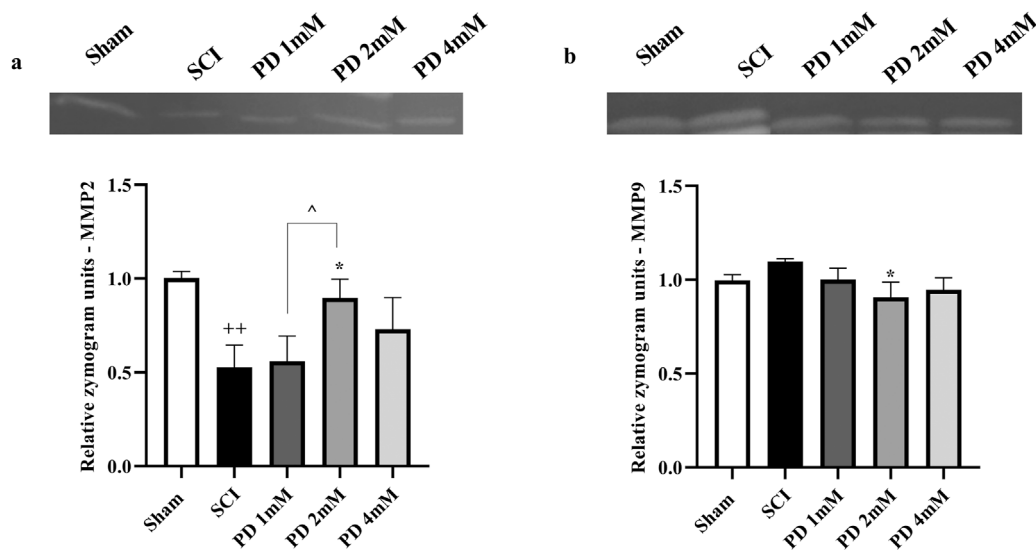


FIGURE 5

Effects of pelargonidin on MMPs level after SCI. MMP2 (a) and MMP9 (b). Data are expressed as mean \pm SD. The statistical analysis was done using repeated measures of one-way ANOVA. ^{*} $p < 0.05$, ⁺⁺⁺ $p < 0.001$ vs. sham group; ^{*} $p < 0.05$, ^{**} $p < 0.01$ vs. SCI group; [^] $p < 0.05$ vs. PD 2 mM group. SCI: spinal cord injury; PD: pelargonidin. MMP: Matrix metalloproteinase.

3.4 Pelargonidin mitigated histological alterations in rats with SCI

Following SCI, a significant amount of spinal cord tissue was damaged, with lesions occurring more frequently in the SCI group compared to the sham group ($p < 0.001$, Figure 6a). Histological analysis indicated specific characteristics of these lesions, including increased cavitation and neuronal loss. Treatment with pelargonidin, especially at a concentration of 2 mM, was associated with a reduction in both the severity and size of the lesions ($p < 0.05$).

Histopathological analysis demonstrated a substantial decrease of neurons in the spinal cord of the SCI group compared to the sham group ($p < 0.001$, Figure 6b). In contrast, the groups receiving pelargonidin, especially at the 2 mM dose, experienced a significant increase in spinal cord neuron counts ($p < 0.01$).

4 Discussion

The current study showed that pelargonidin significantly improved motor function and alleviated neuropathic pain (e.g., cold allodynia, heat hyperalgesia, and mechanical pain). Mechanistically, pelargonidin increased the level of glutathione and catalase, as well as MMP2 activity while reducing MMP9 activity and nitrite levels. Additionally, pelargonidin supports motor neuron survival in the spinal cord's ventral horn, protecting against secondary damage from oxidative stress/inflammation. In almost the whole experiments of the current study, the dose of 2 mM shows better results than 1 mM and 4 mM. Such a method of dose-responsiveness refers to a reverse u-shaped dose-response effectiveness and the concept of hormesis (Peper, 2009; Fakhri et al., 2020; Fakhri et al., 2022c).

The initial trauma of SCI initiates a complex cascade of biological responses that further complicate recovery. One of the key consequences of SCI is the increase in ROS, which occurs as a result of disrupted cellular homeostasis. This elevation in ROS can be attributed to several factors, including mitochondrial dysfunction, inflammatory responses, and the activation of various enzymatic pathways, these processes contribute to oxidative stress and exacerbate neuronal damage (Yu et al., 2023). Elevated ROS levels cause oxidative stress by disrupting the balance between ROS production and detoxification (Yuan et al., 2021). Oxidative stress poses a significant threat to cellular wellbeing by causing damage to essential cellular components such as lipids, proteins, and DNA and can further intensify neuronal injury (Khatri et al., 2018; Singh et al., 2019). SCI initiates an inflammatory response that activates resident immune cells and recruits peripheral immune cells, releasing pro-inflammatory cytokines and chemokines that enhance oxidative stress and neuronal damage (Freyermuth-Trujillo et al., 2022). The relationship between oxidative stress and inflammation is bidirectional. On one hand, oxidative stress can activate signaling pathways that enhance the inflammatory response, while on the other hand, inflammatory mediators can increase ROS production. The combined effects of oxidative stress and inflammation can lead to programmed cell death, or apoptosis, in neurons. This process is characterized by specific morphological and biochemical changes, ultimately resulting in neuronal loss (Zhang et al., 2012; Behl et al., 2021). These changes and loss can lead to impaired motor and sensory functions, as well as other complications associated with SCI (Anjum et al., 2020).

Understanding and targeting these mechanisms is crucial for developing potential therapeutic strategies aimed at mitigating oxidative stress and inflammation, promoting neuronal survival, and enhancing recovery after SCIs. In this study, we provided evidence for the neuroprotective effects of intrathecal injection of

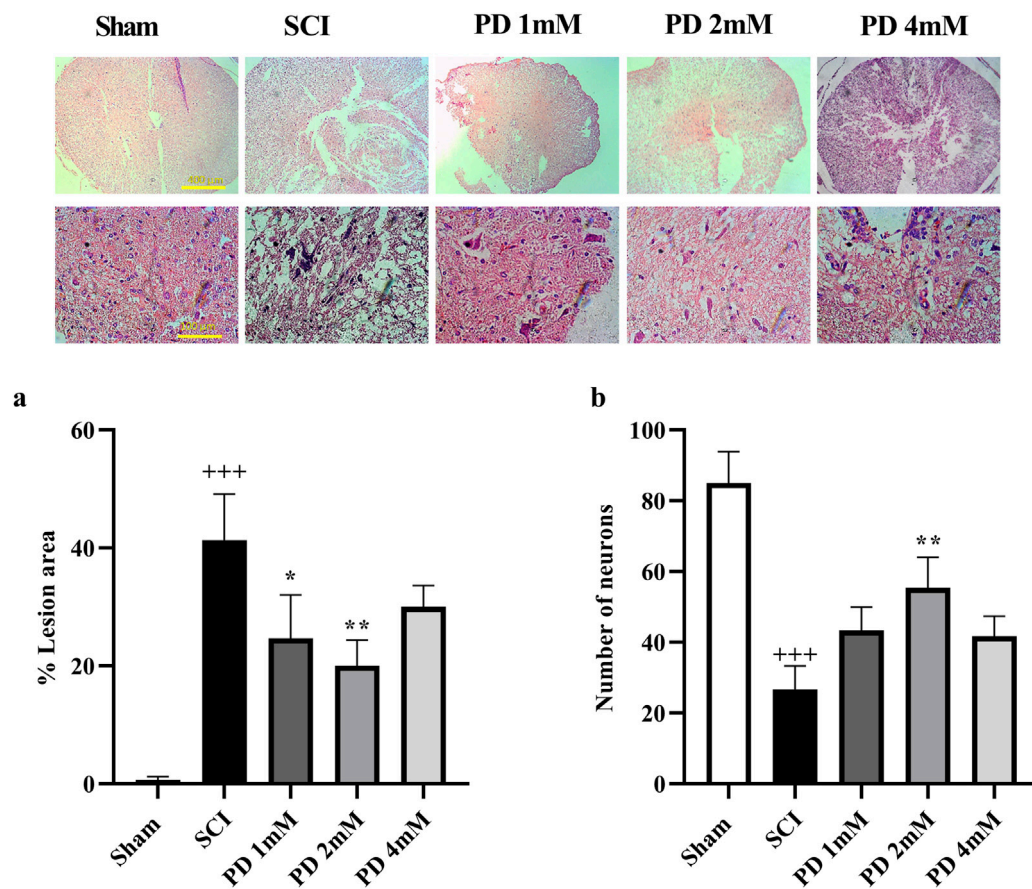


FIGURE 6

The impact of pelargonidin on the tissue change after SCI. Lesion area with 4X magnification (a) and the number of neurons with 40X magnification (b). Data are expressed as mean \pm SD. The statistical analysis was done using repeated measures of two-way ANOVA. +++ p < 0.001 vs. sham group; * p < 0.05, ** p < 0.01 vs. SCI group. SCI: spinal cord injury; PD: pelargonidin.

pelargonidin administered 30 min after SCI. Intrathecal delivery is commonly used in SCI research as it allows for the direct delivery of therapeutic agents into the cerebrospinal fluid (CSF) and removes pharmacokinetic limitations. This method ensures higher localized concentrations of the drug at the site of injury while reducing systemic side effects. Employing such a methodology of intrathecal administration paves the road for the identification of the real efficacy of therapeutic agents (without pharmacokinetic limitations) towards developing novel formulations and other routes of administration. Intrathecal drug administration is also particularly beneficial for compounds that have difficulty crossing the blood-brain barrier or require rapid action within the central nervous system (Vaquero et al., 2018; Hu et al., 2023). The choice of administering pelargonidin 30 min' post-injury is based on the understanding of the pathophysiological processes occurring immediately after SCI. The initial phase of injury involves primary mechanical damage, followed by a secondary phase characterized by inflammatory responses, oxidative stress, and excitotoxicity, which can exacerbate neuronal damage. Early intervention during this critical window aims to mitigate these secondary injuries, potentially improving recovery outcomes (Anjum et al., 2020; Jeong et al., 2021). Research indicates

that interventions initiated shortly after injury can significantly influence long-term functional recovery (Zu et al., 2014).

Pelargonidin, 3,5,7-trihydroxy-2-(4-hydroxyphenyl)-1-benzopyrylium, is part of a larger group of secondary metabolites known as anthocyanins, which are widely recognized for their antioxidant properties and potential health benefits (Li et al., 2022). In the current study, we have shown that pelargonidin plays both direct (suppressing serum nitrite) and indirect (increasing antioxidant agents, catalase, and glutathione) effects on the modulation of oxidative stress. Previous reports also showed that pelargonidin functions as a potent antioxidant by scavenging free radicals and reducing oxidative damage at the cellular level. Numerous studies supported this property, demonstrating its capacity to neutralize ROS, which effectively lowers oxidative stress within cells (Sharath Babu et al., 2017; Xu et al., 2018; Li et al., 2022). Beyond its direct antioxidant actions, pelargonidin has the potential to bolster the body's natural antioxidant defenses by increasing the expression of endogenous antioxidant enzymes. A key player in this process is the Keap1/nuclear factor erythroid 2-related factor 2 (Nrf2) signaling pathway, which mediates cellular responses to oxidative

stress. By activating this pathway, pelargonidin facilitated the upregulation of protective enzymes, thereby enhancing overall cellular health. Research has shown that pelargonidin modulates gene expression within the Keap1/Nrf2 pathway and effectively mitigates citrinin-induced oxidative stress in HepG2 cells, highlighting its therapeutic potential in combating oxidative damage (Sharath Babu et al., 2017). This adaptive response can mitigate secondary injury in tissues affected by oxidative stress, thereby contributing to overall recovery. Our findings confirmed that pelargonidin indirectly modulates oxidative stress by acting as an antioxidant, as evidenced by the restoration of key antioxidant levels (glutathione and catalase) in the serum of SCI rats. Additionally, the observed decrease in serum nitrite levels after pelargonidin treatment reinforces its involvement in modulating oxidative stress. This is particularly noteworthy given the role of oxidative stress in exacerbating neuronal damage following SCI.

The neuroprotective effects of pelargonidin pass through a multifaceted approach that encompasses direct modulation of oxidative stress, reduction of inflammatory responses, and support for neuronal regeneration which all are interconnected. We have also previously shown a near interconnection between inflammation, oxidative stress, and apoptosis. This means that suppressing inflammation and oxidative stress could affect the apoptotic signaling pathways toward neuroprotection and neuronal regeneration (Fakhri et al., 2022a; Fakhri et al., 2022b). In line with our report, pelargonidin previously exhibited notable anti-inflammatory properties (Soleimani Asl et al., 2019; Henriques et al., 2020). MMP9 is often associated with increased inflammation and tissue damage, while MMP2 is linked to tissue remodeling and repair (Gravandi et al., 2024). Mechanical stimuli, ROS, and inflammatory mediators such as tumor necrosis factor- α can directly elevate MMP expression. MMP2 and MMP9 contribute to the breakdown of the blood-spinal cord barrier, increasing oxidative stress, demyelination, leukocyte trafficking, edema, and hemorrhage (Noble et al., 2002; Zhang et al., 2011). In injured tissue, MMP2 and MMP9 play a role in the inflammatory response by modulating the development of neuropathic pain. MMP9 is associated with microglia activation, while MMP2 is related to astrocyte activation (Schomberg et al., 2012). Our findings indicated that treatment with pelargonidin resulted in a notable modulation of MMPs, particularly the reduction of MMP9 and the restoration of MMP2 levels. The favorable shift in the balance of these MMPs suggested that pelargonidin may reduce the inflammatory response, thereby mitigating secondary injury processes that could hinder recovery.

Furthermore, a key finding of this study is the notable improvement in motor function and reduction of neuropathic pain in rats treated with pelargonidin. Supporting this, a study involving middle cerebral artery occlusion (MCAO) demonstrated that treatment with pelargonidin significantly improved neurological functions, as evidenced by reduced neurological severity scores compared to untreated MCAO rats (Fu et al., 2021). In models of diabetic neuropathy, pelargonidin treatment also led to a significant decrease in hyperalgesia, indicating its potential effectiveness in alleviating neuropathic pain associated with diabetes. Specifically, diabetic rats treated with pelargonidin showed improvements in both chemical and thermal hyperalgesia, which were linked to the compound's antioxidant and anti-

inflammatory properties, further underscoring its neuroprotective effects (Mirshekar et al., 2010). Also, studies have highlighted pelargonidin's role in mitigating oxidative stress by reducing lipid peroxidation and enhancing the efficacy of endogenous antioxidant enzymes such as superoxide dismutase and catalase (Kowalczyk et al., 2024). *In vitro* studies have demonstrated that pelargonidin can inhibit the activation of nuclear factor kappa B (NF- κ B), a key transcription factor involved in the inflammatory response. By modulating this pathway, pelargonidin can help reduce the expression of pro-inflammatory genes and enzymes such as inducible nitric oxide synthase (iNOS) and cyclooxygenase-2 (COX-2) (Kowalczyk et al., 2024; Scarpa et al., 2024). On the other hand, in studies involving 6-hydroxydopamine (6-OHDA)-induced toxicity, pelargonidin administration was effective in preserving dopaminergic neurons and improving behavioral outcomes in rats (Roghani et al., 2010). Our findings also were aligned with the neuroprotective effects of pelargonidin. The positive correlation between pelargonidin treatment and neuronal count highlights the compound's neuroprotective properties.

Weight loss following SCI is indicative of metabolic dysfunction and can complicate recovery (Gorgey et al., 2014). The notable weight recovery observed in pelargonidin-treated rats further emphasizes the compound's positive influence on overall health post-SCI. In a model of metabolic syndrome induced by a high-fat diet, pelargonidin 3-glucoside (P3G) enriched strawberries were shown to reduce abdominal fat and body weight gain in rats. This effect was associated with improvements in cardiovascular and liver health, suggesting that pelargonidin can positively influence body composition and metabolic parameters (Ghattamaneni et al., 2020). Moreover, a separate study indicated that daily administration of pelargonidin to mice over a month did not result in weight loss compared to control groups. This finding suggests that pelargonidin may not negatively impact body weight during treatment, highlighting its potential safety for regular use without adverse effects on weight recovery (Lamson et al., 2022). In previous studies, we found that compounds with antioxidant properties can effectively promote weight recovery in rats after SCI (Fakhri et al., 2019; Fakhri et al., 2021).

At the level of histopathological results, we showed herein that SCI made neuronal loss in ventral horn of spinal cord, which are responsible for motor activity. In the current report, we also confirmed that SCI caused demyelination of spinal cord. We further showed that pelargonidin improved compression SCI-induced degeneration by increasing motor neuron survival in ventral horn, while decreasing lesion size of spinal cord.

5 Conclusion

In conclusion, pelargonidin offers notable advantages in various areas, such as motor function recovery, pain relief, and metabolic health, through a multifaceted approach that includes direct/indirect modulation of oxidative stress, reduction of inflammation, and promotion of neuronal regeneration. Further research is crucial to fully understand the specific mechanisms and highlights the need for more rigorous mechanistic studies (e.g., apoptotic and neurogenesis pathways) by which pelargonidin exerts its beneficial effects in the

context of SCI. Evaluating the effects of multiple doses of pelargonidin and in different routes of administration for a long period (e.g., 56–84 days) would be also valuable in future works.

Data availability statement

The raw data supporting the conclusions of this article will be made available by the authors, without undue reservation.

Ethics statement

The animal study was approved by Dr. Leila Hosseinzadeh, Committee Director, Laboratory Animals, Kermanshah University of Medical Sciences. Dr. Keivan Moradi, Committee Secretary, Laboratory Animals, Kermanshah University of Medical Sciences. The study was conducted in accordance with the local legislation and institutional requirements.

Author contributions

LK: Investigation, Writing–original draft, Data curation. SF: Formal Analysis, Investigation, Software, Writing–original draft, Writing–review and editing. FA: Writing–original draft, Formal Analysis. AK: Investigation, Methodology, Supervision, Writing–original draft. MF: Supervision, Writing–original draft. EM-N: Writing–original draft, Investigation. JE: Writing–original draft, Writing–review and editing.

Funding

The author(s) declare that financial support was received for the research, authorship, and/or publication of this article. The research

is supported by the Pharmaceutical Sciences Research Center, Kermanshah University of Medical Sciences, for the special Grant No. 4010532.

Acknowledgments

The authors acknowledged the Pharmaceutical Sciences Research Center, Kermanshah University of Medical Sciences, for the special Grant No. 4010532.

Conflict of interest

The authors declare that the research was conducted in the absence of any commercial or financial relationships that could be construed as a potential conflict of interest.

The author(s) declared that they were an editorial board member of Frontiers, at the time of submission. This had no impact on the peer review process and the final decision.

Generative AI statement

The authors declare that no Generative AI was used in the creation of this manuscript.

Publisher's note

All claims expressed in this article are solely those of the authors and do not necessarily represent those of their affiliated organizations, or those of the publisher, the editors and the reviewers. Any product that may be evaluated in this article, or claim that may be made by its manufacturer, is not guaranteed or endorsed by the publisher.

References

- Abbaszadeh, F., Fakhri, S., and Khan, H. (2020). Targeting apoptosis and autophagy following spinal cord injury: therapeutic approaches to polyphenols and candidate phytochemicals. *Pharmacol. Res.* 160, 105069. doi:10.1016/j.phrs.2020.105069
- Abbaszadeh, H. A., Tiraihi, T., Sadeghi, Y., Delshad, A. R., Sadeghizadeh, M., Taheri, T., et al. (2018). Decrease in cavity size and oligodendrocyte cell death using neurosphere-derived oligodendrocyte-like cells in spinal cord contusion model. *Iran. Biomed. J.* 22, 246–257. doi:10.22034/ibj.22.4.246
- Aebi, H. (1984). Catalase *in vitro*. *Methods Enzym.* 105, 121–126. doi:10.1016/S0076-6879(84)05016-3
- Alimoradian, A., Abbaszadeh, F., and Jorjani, M. (2024). Testosterone signaling pathways for reducing neuropathic pain in a rat model of spinothalamic tract lesion. *Iran. J. Basic Med. Sci.* 27, 1417–1422. doi:10.22038/ijbms.2024.78491.16968
- Alchorne, A. J., Broom, D. C., and Woolf, C. J. (2005). Detection of cold pain, cold allodynia and cold hyperalgesia in freely behaving rats. *Mol. Pain* 1, 36. doi:10.1186/1744-8069-1-36
- Alvi, M. A., Pedro, K. M., Quddusi, A. I., and Fehlings, M. G. (2024). Advances and challenges in spinal cord injury treatments. *J. Clin. Med.* 13, 4101. doi:10.3390/jcm13144101
- Anjum, A., Yazid, M. D., Fauzi Daud, M., Idris, J., Ng, A. M. H., Selvi Naicker, A., et al. (2020). Spinal cord injury: pathophysiology, multimolecular interactions, and underlying recovery mechanisms. *Int. J. Mol. Sci.* 21, 7533. doi:10.3390/ijms21207533
- Bagheri Bavandpour, F. S., Azizi, A., Abbaszadeh, F., Kiani, A., Farzaei, M. H., Mohammadi-Noori, E., et al. (2024). Polydatin attenuated neuropathic pain and motor dysfunction following spinal cord injury in rats by employing its anti-inflammatory and antioxidant effects. *Front. Pharmacol.* 15, 1452989. doi:10.3389/fphar.2024.1452989
- Behl, T., Makkar, R., Sehgal, A., Singh, S., Sharma, N., Zengin, G., et al. (2021). Current trends in neurodegeneration: cross talks between oxidative stress, cell death, and inflammation. *Int. J. Mol. Sci.* 22, 7432. doi:10.3390/ijms22147432
- Chan, C. (2008). Inflammation: beneficial or detrimental after spinal cord injury? *Recent Pat. CNS Drug Discov.* 3, 189–199. doi:10.2174/157488908786242434
- Chen, S., Jia, Y., Wu, Y., and Ren, F. (2024). Anthocyanin and its bioavailability, health benefits, and applications: a comprehensive review. *Food Rev. Int.* 40, 3666–3689. doi:10.1080/87559129.2024.2369696
- Coyoy-Salgado, A., Segura-Urbe, J. J., Guerra-Araiza, C., Orozco-Suárez, S., Salgado-Ceballos, H., Feria-Romero, I. A., et al. (2019). The importance of natural antioxidants in the treatment of spinal cord injury in animal models: an overview. *Oxid. Med. Cell. Longev.* 2019, 3642491. doi:10.1155/2019/3642491
- Diop, M., and Epstein, D. (2024). A systematic review of the impact of spinal cord injury on costs and health-related quality of life. *Pharmacoeconomics - Open* 8, 793–808. doi:10.1007/s41669-024-00517-3
- Duarte, L. J., Chaves, V. C., Dos Santo Nascimento, M. V. P., Calvete, E., Li, M., Ciralo, E., et al. (2018). Molecular mechanism of action of Pelargonidin-3-O-glucoside, the main anthocyanin responsible for the anti-inflammatory effect of strawberry fruits. *Food Chem.* 247, 56–65. doi:10.1016/j.foodchem.2017.12.015
- Evaniew, N., Noonan, V. K., Fallah, N., Kwon, B. K., Rivers, C. S., Ahn, H., et al. (2015). Methylprednisolone for the treatment of patients with acute spinal cord injuries: a propensity score-matched cohort study from a Canadian multi-center spinal cord injury registry. *J. Neurotrauma* 32, 1674–1683. doi:10.1089/neu.2015.3963

- Eyer, P., and Podhradský, D. (1986). Evaluation of the micromethod for determination of glutathione using enzymatic cycling and Ellman's reagent. *Anal. Biochem.* 153, 57–66. doi:10.1016/0003-2697(86)90061-8
- Fakhri, S., Abbaszadeh, F., Moradi, S. Z., Cao, H., Khan, H., and Xiao, J. (2022a). Effects of polyphenols on oxidative stress, inflammation, and interconnected pathways during spinal cord injury. *Oxid. Med. Cell. Longev.* 2022, 8100195. doi:10.1155/2022/8100195
- Fakhri, S., Ahmadpour, Y., Rezaei, H., Kooshki, L., Moradi, S. Z., Iranpanah, A., et al. (2020). The antinociceptive mechanisms of melatonin: role of L-arginine/nitric oxide/cyclic GMP/KATP channel signaling pathway. *Behav. Pharmacol.* 31, 728–737. doi:10.1097/FBP.0000000000000579
- Fakhri, S., Dargahi, L., Abbaszadeh, F., and Jorjani, M. (2018). Astaxanthin attenuates neuroinflammation contributed to the neuropathic pain and motor dysfunction following compression spinal cord injury. *Brain Res. Bull.* 143, 217–224. doi:10.1016/j.brainresbull.2018.09.011
- Fakhri, S., Dargahi, L., Abbaszadeh, F., and Jorjani, M. (2019). Effects of astaxanthin on sensory-motor function in a compression model of spinal cord injury: involvement of ERK and AKT signalling pathway. *Eur. J. Pain* 23, 750–764. doi:10.1002/ejp.1342
- Fakhri, S., Kiani, A., Jalili, C., Abbaszadeh, F., Piri, S., Farzaei, M. H., et al. (2021). Intrathecal administration of melatonin ameliorates the neuroinflammation-mediated sensory and motor dysfunction in A rat model of compression spinal cord injury. *Curr. Mol. Pharmacol.* 14, 646–657. doi:10.2174/1874467213666201230101811
- Fakhri, S., Piri, S., Moradi, S. Z., and Khan, H. (2022b). Phytochemicals targeting oxidative stress, interconnected neuroinflammatory, and neuroapoptotic pathways following radiation. *Curr. Neuropharmacol.* 20, 836–856. doi:10.2174/1570159X19666210809103346
- Fakhri, S., Sabouri, S., Kiani, A., Farzaei, M. H., Rashidi, K., Mohammadi-Farani, A., et al. (2022c). Intrathecal administration of naringenin improves motor dysfunction and neuropathic pain following compression spinal cord injury in rats: relevance to its antioxidant and anti-inflammatory activities. *Korean J. Pain* 35, 291–302. doi:10.3344/kjp.2022.35.291
- Freyermuth-Trujillo, X., Segura-Urbe, J. J., Salgado-Ceballos, H., Orozco-Barrios, C. E., and Coyoy-Salgado, A. (2022). Inflammation: a target for treatment in spinal cord injury. *Cells* 11, 2692. doi:10.3390/cells11172692
- Fu, K., Chen, M., Zheng, H., Li, C., Yang, F., and Niu, Q. (2021). Pelargonidin ameliorates MCAO-induced cerebral ischemia/reperfusion injury in rats by the action on the Nrf2/HO-1 pathway. *Transl. Neurosci.* 12, 020–031. doi:10.1515/tnsci-2021-0006
- Ghattamaneni, N. K., Sharma, A., Panchal, S. K., and Brown, L. (2020). Pelargonidin 3-glucoside-enriched strawberry attenuates symptoms of DSS-induced inflammatory bowel disease and diet-induced metabolic syndrome in rats. *Eur. J. Nutr.* 59, 2905–2918. doi:10.1007/s00394-019-02130-1
- Gorgey, A. S., Dolbow, D. R., Dolbow, J. D., Khalil, R. K., Castillo, C., and Gater, D. R. (2014). Effects of spinal cord injury on body composition and metabolic profile – Part I. *J. Spinal Cord. Med.* 37, 693–702. doi:10.1179/2045772314Y.00000000245
- Gravandi, M. M., Pourmanouchehri, Z., Behbood, L., Fakhri, S., Mohammadi-Noori, E., Zhalah, M., et al. (2024). Rutin-loaded chitosan nanoparticles alleviated Freund's adjuvant induced rheumatoid arthritis via modulating oxidative stress and inflammatory parameters in Wistar rats. *Naunyn. Schmiedeberg. Arch. Pharmacol.* 397, 4771–4790. doi:10.1007/s00210-023-02902-x
- Henriques, J. F., Serra, D., Dinis, T. C. P., and Almeida, L. M. (2020). The anti-neuroinflammatory role of anthocyanins and their metabolites for the prevention and treatment of brain disorders. *Int. J. Mol. Sci.* 21, 8653. doi:10.3390/ijms21228653
- Hu, X., Xu, W., Ren, Y., Wang, Z., He, X., Huang, R., et al. (2023). Spinal cord injury: molecular mechanisms and therapeutic interventions. *Signal Transduct. Target. Ther.* 8, 245. doi:10.1038/s41392-023-01477-6
- Jaiswal, S., Guan, Y., Hwan Moon, K., and Williams, L. (2020). "Anthocyanins: natural sources and traditional therapeutic uses," in *Flavonoids - a coloring model for cheering up life*, London, United Kingdom: IntechOpen. doi:10.5772/intechopen.86888
- Jeong, H.-J., Yun, Y., Lee, S.-J., Ha, Y., and Gwak, S.-J. (2021). Biomaterials and strategies for repairing spinal cord lesions. *Neurochem. Int.* 144, 104973. doi:10.1016/j.neuint.2021.104973
- Khatri, N., Thakur, M., Pareek, V., Kumar, S., Sharma, S., and Datusalia, A. K. (2018). Oxidative stress: major threat in traumatic brain injury. *CNS Neurol. Disord. - Drug Targets* 17, 689–695. doi:10.2174/1871527317666180627120501
- Kowalczyk, T., Muskała, M., Merez-Sadowska, A., Sikora, J., Picot, L., and Sitarek, P. (2024). Anti-inflammatory and anticancer effects of anthocyanins in *in vitro* and *in vivo* studies. *Antioxidants* 13, 1143. doi:10.3390/antiox13091143
- Kumar, R., Lim, J., Mekary, R. A., Rattani, A., Dewan, M. C., Sharif, S. Y., et al. (2018). Traumatic spinal injury: global epidemiology and worldwide volume. *World Neurosurg.* 113, e345–e363. doi:10.1016/j.wneu.2018.02.033
- Lamson, N. G., Fein, K. C., Gleeson, J. P., Newby, A. N., Xian, S., Cochran, K., et al. (2022). The strawberry-derived permeation enhancer pelargonidin enables oral protein delivery. *Proc. Natl. Acad. Sci.* 119, e2207829119. doi:10.1073/pnas.2207829119
- Li, H., Zhang, C., Deng, Z., Zhang, B., and Li, H. (2022). Antioxidant activity of delphinidin and pelargonidin: theory and practice. *J. Food Biochem.* 46, e14192. doi:10.1111/jfbc.14192
- Li, Z.-W., Li, J.-J., Wang, L., Zhang, J.-P., Wu, J.-J., Mao, X.-Q., et al. (2014). Epidermal growth factor receptor inhibitor ameliorates excessive astrogliosis and improves the regeneration microenvironment and functional recovery in adult rats following spinal cord injury. *J. Neuroinflammation* 11, 71. doi:10.1186/1742-2094-11-71
- Mestre, C., Pélissier, T., Fialip, J., Wilcox, G., and Eschaliere, A. (1994). A method to perform direct transcutaneous intrathecal injection in rats. *J. Pharmacol. Toxicol. Methods* 32, 197–200. doi:10.1016/1056-8719(94)90087-6
- Mirshakar, M., Roghani, M., Khalili, M., Baluchnejadmojarad, T., and Arab Moazzen, S. (2010). Chronic oral pelargonidin alleviates streptozotocin-induced diabetic neuropathic hyperalgesia in rat: involvement of oxidative stress. *Iran. Biomed. J.* 14, 33–39.
- Mohammadi Pour, P., Fakhri, S., Asgari, S., Farzaei, M. H., and Echeverría, J. (2019). The signaling pathways, and therapeutic targets of antiviral agents: focusing on the antiviral approaches and clinical perspectives of anthocyanins in the management of viral diseases. *Front. Pharmacol.* 10, 1207. doi:10.3389/fphar.2019.01207
- Noble, L. J., Donovan, F., Igarashi, T., Goussev, S., and Werb, Z. (2002). Matrix metalloproteinases limit functional recovery after spinal cord injury by modulation of early vascular events. *J. Neurosci.* 22, 7526–7535. doi:10.1523/JNEUROSCI.22-17-07526.2002
- Peper, A. (2009). Aspects of the relationship between drug dose and drug effect. *Dose. Response* 7, 172–192. doi:10.2203/dose-response.08-019.Peper
- Roghani, M., Niknam, A., Jalali-Nadoushan, M.-R., Kiasalari, Z., Khalili, M., and Baluchnejadmojarad, T. (2010). Oral pelargonidin exerts dose-dependent neuroprotection in 6-hydroxydopamine rat model of hemi-parkinsonism. *Brain Res. Bull.* 82, 279–283. doi:10.1016/j.brainresbull.2010.06.004
- Scarpa, E.-S., Antonelli, A., Balercia, G., Sabatelli, S., Maggi, F., Caprioli, G., et al. (2024). Antioxidant, anti-inflammatory, anti-diabetic, and pro-osteogenic activities of polyphenols for the treatment of two different chronic diseases: type 2 diabetes mellitus and osteoporosis. *Biomolecules* 14, 836. doi:10.3390/biom14070836
- Schomberg, D., Ahmed, M., Miranpuri, G., Olson, J., and Resnick, D. K. (2012). Neuropathic pain: role of inflammation, immune response, and ion channel activity in central injury mechanisms. *Ann. Neurosci.* 19, 125–132. doi:10.5214/ans.0972.7531.190309
- Sharath Babu, G. R., Anand, T., Ilaiyaraja, N., Khanum, F., and Gopalan, N. (2017). Pelargonidin modulates keap1/nrf2 pathway gene expression and ameliorates citrinin-induced oxidative stress in HepG2 cells. *Front. Pharmacol.* 8, 868. doi:10.3389/fphar.2017.00868
- Singh, A., Kukreti, R., Saso, L., and Kukreti, S. (2019). Oxidative stress: a key modulator in neurodegenerative diseases. *Molecules* 24, 1583. doi:10.3390/molecules24081583
- Sohanaki, H., Baluchnejadmojarad, T., Nikbakht, F., and Roghani, M. (2016). Pelargonidin improves memory deficit in amyloid β 25-35 rat model of Alzheimer's disease by inhibition of glial activation, cholinesterase, and oxidative stress. *Biomed. Pharmacother.* 83, 85–91. doi:10.1016/j.biopha.2016.06.021
- Soleimani Asl, S., Bergen, H., Ashtari, N., Amiri, S., Los, M. J., and Mehdizadeh, M. (2019). Pelargonidin exhibits restoring effects against amyloid β -induced deficits in the hippocampus of male rats. *Med. J. Islam. Repub. Iran.* 33, 135. doi:10.34171/mjiri.33.135
- Sun, J., Zhang, X., Broderick, M., and Fein, H. (2003). Measurement of nitric oxide production in biological systems by using griess reaction assay. *Sensors* 3, 276–284. doi:10.3390/s30800276
- Vaquero, J., Zurita, M., Rico, M. A., Aguayo, C., Bonilla, C., Marin, E., et al. (2018). Intrathecal administration of autologous mesenchymal stromal cells for spinal cord injury: safety and efficacy of the 100/3 guideline. *Cytotherapy* 20, 806–819. doi:10.1016/j.jcyt.2018.03.032
- Xu, X., Zhang, C.-J., Talifu, Z., Liu, W.-B., Li, Z.-H., Wang, X.-X., et al. (2024). The effect of Glycine and N-acetylcysteine on oxidative stress in the spinal cord and skeletal muscle after spinal cord injury. *Inflammation* 47, 557–571. doi:10.1007/s10753-023-01929-9
- Xu, Y., Hu, D., Li, Y., Sun, C., and Chen, W. (2018). An effective method for preparation of high-purity pelargonidin-3-O-glucoside from strawberry and its protective effect on cellular oxidative stress. *J. Chromatogr. B* 1072, 211–220. doi:10.1016/j.jchromb.2017.11.025
- Yu, M., Wang, Z., Wang, D., Aierxi, M., Ma, Z., and Wang, Y. (2023). Oxidative stress following spinal cord injury: from molecular mechanisms to therapeutic targets. *J. Neurosci. Res.* 101, 1538–1554. doi:10.1002/jnr.25221
- Yuan, Z., Yu, F., Zhang, D., and Wang, H. (2021). Profiling of the assembly of RecA nucleofilaments implies a potential target for environmental factors to disturb DNA repair. *J. Environ. Sci.* 102, 283–290. doi:10.1016/j.jes.2020.09.022
- Zhang, H., Chang, M., Hansen, C. N., Basso, D. M., and Noble-Haeusslein, L. J. (2011). Role of matrix metalloproteinases and therapeutic benefits of their inhibition in spinal cord injury. *Neurotherapeutics* 8, 206–220. doi:10.1007/s13311-011-0038-0
- Zhang, H., Wu, C., Yu, D., Su, H., Chen, Y., and Ni, W. (2023). Piperine attenuates the inflammation, oxidative stress, and pyroptosis to facilitate recovery from spinal cord injury via autophagy enhancement. *Phyther. Res.* 37, 438–451. doi:10.1002/ptr.7625
- Zhang, N., Yin, Y., Xu, S.-J., Wu, Y.-P., and Chen, W.-S. (2012). Inflammation and apoptosis in spinal cord injury. *Indian J. Med. Res.* 135, 287–296. Available online at: <http://www.ncbi.nlm.nih.gov/pubmed/22561613>.
- Zu, J., Wang, Y., Xu, G., Zhuang, J., Gong, H., and Yan, J. (2014). Curcumin improves the recovery of motor function and reduces spinal cord edema in a rat acute spinal cord injury model by inhibiting the JAK/STAT signaling pathway. *Acta Histochem.* 116, 1331–1336. doi:10.1016/j.acthis.2014.08.004

Frontiers in Pharmacology

Explores the interactions between chemicals and living beings

The most cited journal in its field, which advances access to pharmacological discoveries to prevent and treat human disease.

Discover the latest Research Topics

[See more →](#)

Frontiers

Avenue du Tribunal-Fédéral 34
1005 Lausanne, Switzerland
frontiersin.org

Contact us

+41 (0)21 510 17 00
frontiersin.org/about/contact



Frontiers in Pharmacology

